



# FORM

---

## **From Orogens to Rifted Margins and Back**

The formation and deformation of continental margins through Wilson Cycles

6<sup>th</sup>-9<sup>th</sup> June 2017  
Saint Florent, Corsica

Eds. Gaina, C., Magni, V., Gørbitz T.-L., Jakob, J.



UiO : **The Centre for Earth Evolution and Dynamics**  
University of Oslo



The Centre for Earth Evolution and Dynamics  
is funded by CoE-grant 223272 from the Research Council of Norway.



A conference to celebrate Torgeir's 65<sup>th</sup> anniversary  
...and to talk about the Wilson cycle.



# Contents

<b>Conference Programme</b>	<b>7</b>
<b>Posters</b>	<b>8</b>
<b>Abstracts</b>	<b>11</b>
<u>ALSAIF, M., GUEYDAN, F., GAREL, F., Modelling upper plate deformation with increasing trench retreat velocity . . . . .</u>	11
<u>ASHWAL, L.D., WIEDENBECK, M., and TORSVIK, T.H., Hidden continents . . . . .</u>	11
<u>AUSTRHEIM, H., and JAMTVEIT, B., Intermediate depth earthquakes and high grade metamorphism . . . . .</u>	12
<u>VAN DEN BROEK, J.M., GAINA, C., BUTER, S., ANDERSEN, T., Microcontinent formation associated with subduction zones, clues to their formation . . . . .</u>	12
<u>BRUN, J.-P., Rollover-type basins controlled by ramp-flat extension following exhumation of metamorphic rocks . . . . .</u>	12
<u>CORFU, F., The Jotun Nappe Complex and its relations to surrounding allochthons . . . . .</u>	12
<u>FACCENNA, C. and BECKER, T., Orogeny, the Wilson cycle and the scale of mantle convection . . . . .</u>	13
<u>FALEIDE, J.I., Comparing rifted margins in the South and North Atlantic with focus on along-margin structural and magmatic segmentation . . . . .</u>	13
<u>GAINA, C., Microcontinents: Stories about complexities in the Wilson tectonic cycles . . . . .</u>	14
<u>GUEYDAN, F., Oligo-miocene sequential extension as a record of Corsica rotation during Apennines slab roll-back . . . . .</u>	15
<u>HACKER, B., KELEMEN, P. and BEHN, M., Relamination . . . . .</u>	15
<u>JAKOB J., Transitional crust in the fossil ocean-continent transition zone of the pre-Caledonian rifted margin of Baltica and its link to the Scandinavian Dyke Complex . . . . .</u>	15
<u>LABROUSSE, L., Experimental insights on mechanic impacts of metamorphic reactions: torturing Norwegian and Corsican rocks . . . . .</u>	16
<u>LEROY, S. and NONN, C., Formation and structural evolution of young continental margins: Insights from the Gulf of Aden . . . . .</u>	16
<u>MAGNI, V., On the importance of along-trench variations on subduction dynamics: from back-arc basins to underplating of continental lithosphere . . . . .</u>	17
<u>MANATSCHAL, G., TUGEND, J., CHENIN, P., EPIN, M.E., DECARLIS, A., LESCOUTRE, R. and MOHN, G., Formation and reactivation of rifted margins and implications for the interpretation of orogenic processes . . . . .</u>	17
<u>MEDVEDEV, S., Self-localizing thermal runaway as a mechanism for intermediate and deep earthquakes: numerical studies and comparison with field observations . . . . .</u>	18
<u>OSMUNDSEN, P.T., What's reactivated at rifted margins? Examples from onshore and offshore Norway . . . . .</u>	18
<u>DI ROSA, M., and MARRONI, M., The tectono-metamorphic history of the Corte slices (Alpine Corsica): An example of continental subduction and polyphased exhumation . . . . .</u>	18
<u>DI ROSA, M., MARRONI, M. and PANDOLFI, L., Geological and structural map of the area between Golo and Tavignano Valleys (Central Corsica) . . . . .</u>	19
<u>TEGNER, C., ANDERSEN, T.B., BROWN, E.L., CORFU, F., PLANKE, S., KJØLL, H. J. and TORSVIK, T.H., The pre-Caledonian Scandinavian Dyke Complex and 600 Ma plate reconstructions of Baltica . . . . .</u>	20
<u>TORSVIK, T.H., The Iapetus Ocean and Torgeir Andersen: From the mysterious Opening to the dramatic Closure . . . . .</u>	20
<u>WERNER, S.C., PT versus T: Shaping of a planetary body . . . . .</u>	21
<u>YAMATO, P., Catastrophic pressure drops in subduction zones: an unsuspected process recorded in metamorphic rocks . . . . .</u>	21
<b>Participant list with contact information</b>	<b>22</b>
<b>Selected contributions of Torgeir's to the geology of Corsica and the Wilson cycle</b>	<b>23</b>
Andersen, T. B., H. Austrheim, N. Deseta, P. Silkoset, and L. D. Ashwal. 2014. "Large Subduction Earthquakes along the Fossil Moho in Alpine Corsica." <i>Geology</i> 42 (5): 395–98. doi:10.1130/G35345.1. . . . .	25
Andersen, Torgeir B. 1998. "Extensional Tectonics in the Caledonides of Southern Norway, an Overview." <i>Tectonophysics</i> 285: 333–351. . . . .	30
Andersen, Torgeir B., and Håkon Austrheim. 2006. "Fossil Earthquakes Recorded by Pseudotachylytes in Mantle Peridotite from the Alpine Subduction Complex of Corsica." <i>Earth and Planetary Science Letters</i> 242 (1–2): 58–72. . . . .	49
Andersen, Torgeir B., Fernando Corfu, Loic Labrousse, and Per-Terje Osmundsen. 2012. "Evidence for Hyperextension along the Pre-Caledonian Margin of Baltica." <i>Journal of the Geological Society, London</i> 169 (5): 601–12. doi:10.1144/0016-76492012-011. . . . .	64
Andersen, Torgeir B., and Bjørn Jamtveit. 1990. "Uplift of Deep Crust during Orogenic Extensional Collapse: A Model Based on Field Studies in the Sogn-Sunnfjord Region of Western Norway." <i>Tectonics</i> 9 (5): 1097–1111. doi:10.1029/TC009i005p01097. . . . .	76

Andersen, Torgeir B., Bjørn Jamtveit, John F. Dewey, and Eivind Swensson. 1991. "Subduction and Eduction of Continental Crust: Major Mechanisms during Continent-Continent Collision and Orogenic Extensional Collapse, a Model Based on the South Norwegian Caledonides" <i>Terra Nova</i> 3: 303–10. . . . .	91
Andersen, Torgeir B., Karen Mair, Håkon Austrheim, Yuri Y. Podladchikov, and Johannes C. Vrijmoed. 2008. "Stress Release in Exhumed Intermediate and Deep Earthquakes Determined from Ultramafic Pseudotachylyte." <i>Geology</i> 36 (12): 995–98. doi:10.1130/G25230A.1. . . . .	99
Austrheim, Håkon, and Torgeir B. Andersen. 2004. "Pseudotachylytes from Corsica: Fossil Earthquakes from a Subduction Complex." <i>Terra Nova</i> 16 (4): 193–97. doi:10.1111/j.1365-3121.2004.00551.x. . . . .	103
Deseta, N., T. B. Andersen, and L. D. Ashwal. 2014. "A Weakening Mechanism for Intermediate-Depth Seismicity? Detailed Petrographic and Microtextural Observations from Blueschist Facies Pseudotachylytes, Cape Corse, Corsica." <i>Tectonophysics</i> 610. Elsevier B.V.: 138–49. doi:10.1016/j.tecto.2013.11.007. . . . .	108
Hacker, B. R., T. B. Andersen, D. B. Root, L. Mehl, J. M. Mattinson, and J. L. Wooden. 2003. "Exhumation of High-Pressure Rocks beneath the Solund Basin, Western Gneiss Region of Norway." <i>Journal of Metamorphic Geology</i> 21 (6): 613–29. doi:10.1046/j.1525-1314.2003.00468.x. . . . .	120
John, Timm, Sergei Medvedev, Lars H. Rüpke, Torgeir B. Andersen, Yuri Y. Podladchikov, and Håkon Austrheim. 2009. "Generation of Intermediate-Depth Earthquakes by Self-Localizing Thermal Runaway." <i>Nature Geoscience</i> 2 (2). Nature Publishing Group: 137–40. doi:10.1038/ngeo419. . . . .	137
Maggi, M., F. Rossetti, F. Corfu, T. Theye, T. B. Andersen, and C. Faccenna. 2012. "Clinopyroxene-Rutile Phyllonites from the East Tenda Shear Zone (Alpine Corsica, France): Pressure-Temperature-Time Constraints to the Alpine Reworking of Variscan Corsica." <i>Journal of the Geological Society</i> 169 (6): 723–32. doi:10.1144/jgs2011-120. . . .	141
Osmundsen, P.T., T.B. Andersen, and S. Markussen. 1998. "Tectonics and Sedimentation in the Hangingwall of a Major Extensional Detachment: The Devonian Kvamshesten Basin, Western Norway." <i>Basin Research</i> 10 (2): 213–34. doi:10.1046/j.1365-2117.1998.00064.x. . . . .	151
Ravna, E. J K, T. B. Andersen, L. Jolivet, and C. de Capitani. 2010. "Cold Subduction and the Formation of Lawsonite Eclogite - Constraints from Prograde Evolution of Eclogitized Pillow Lava from Corsica." <i>Journal of Metamorphic Geology</i> 28 (4): 381–95. doi:10.1111/j.1525-1314.2010.00870.x. . . . .	173
Torsvik, T. H., T. B. Andersen, E. A. Eide, and H. J. Walderhaug. 1997. "The Age and Tectonic Significance of Dolerite Dykes in Western Norway." <i>Journal of the Geological Society</i> 154 (6): 961–73. doi:10.1144/gsjgs.154.6.0961. . . .	188

# Conference Programme

## Tuesday, June 6<sup>th</sup>

### Ice Breaker

16:00 Ice breaker in the small meeting room at *Hotel Madame Mere*

## Wednesday, June 7<sup>th</sup>

09:00-09:10 Opening Ceremony and Welcome Speech by Carmen Gaina

### “The Wilson Cycle”: pre-Atlantic stories

Chair: Carmen Gaina

- 09:10-09:40 The Iapetus Ocean and Torgeir Andersen: From the mysterious Opening to the dramatic Closure (Invited), TORSVIK, T.H.
- 09:50-10:10 The pre-Caledonian Scandinavian Dyke Complex and 600 Ma plate reconstructions of Baltica, TEGNER, C., ANDERSEN, T.B., BROWN, E.L., CORFU, F., PLANKE, S., KJØLL, H.J. AND TORSVIK, T.H.
- 10:10-10:30 Transitional crust in the fossil ocean-continent transition zone of the pre-Caledonian rifted margin of Baltica and its link to the Scandinavian Dyke Complex, JOHANNES JAKOB, PHILIPPE BOULVAIS, OLIVIER BEYSSAC, FERNANDO CORFU, MANAR ALSAIF, TORGEIR B. ANDERSEN
- 10:30-11:00 Coffee break

### Passing the torch though the Wilson Cycle – The role of inheritance

Chair: Manar Alsaif

- 11:00-11:30 Formation and reactivation of rifted margins and implications for the interpretation of orogenic processes (Invited), GIANRETO MANATSCHAL, TUGEND, J., CHENIN, P., EPIN, M.E., DECARLIS, A., LESCOUTRE, R. and MOHN, G.
- 11:40-12:00 The Jotun Nappe Complex and its relations to surrounding allochthons, CORFU, F.
- 12:00-12:20 Hidden continents, ASHWAL, L.D., WIEDENBECK, M., TORSVIK, T.H.
- 12:12-12:40 What's inherited at rifetd margins? Examples from the Norwegian margin, OSMUNDSSEN, P.T.
- 12:40-14:00 Lunch at *Madame Mere*

### Rifting and Passive margin formation

Chair: Joost M. van den Broek

- 14:00-14:30 Formation and structural evolution of young continental margins: Insights from the Gulf of Aden (Invited), LEROY, S., NONN, C.
- 14:40-15:00 Comparing rifted margins in the South and North Atlantic with focus on along-margin structural and magmatic segmentation, FALÉIDE, J.I.
- 15:00-15:20 Microcontinents: Stories about complexities in the Wilson tectonic cycles, GAINA, C.
- 15:20-15:40 *Two-minutes madness*: Poster presentations
- 15:40-16:10 The geology of Corsica, OSMUNDSSEN, P.T. and GUEYDAN, F.
- 16:10 Drinks/posters at *Madame Mere*

## Thursday, June 8<sup>th</sup>

### A full day field trip

Guides: Per Terje Osmundsen and Frederic Gueydan.

The mini vans leave hotel Madame Mere at 9:00 in the morning. CEED brings lunch bags for the participants. Note that the excursion ends with a visit to the wine yard *Clos Santini* from 17:00 to 18:30. **Hiking shoes are recommended.**

## Friday, June 9<sup>th</sup>

### Subduction, Collision and Orogeny

Chair: Johannes Jakob

- 09:00-09:30 Oligo-miocene sequential extension as a record of Corsica rotation during Apennines slab roll-back (Invited), GUEYDAN, F.
- 09:40-10:00 Rollover-type basins controlled by ramp-flat extension following exhumation of metamorphic rocks, BRUN, J.-P.
- 10:00-10:20 The tectono-metamorphic history of the Corte slices (Alpine Corsica): An example of continental subduction and polyphased exhumation, DI ROSA, M., and MARRONI, M.
- 10:20-10:40 Experimental insights on mechanic impacts of metamorphic reactions: torturing Norwegian and Corsican rocks, LABROUSSE, L.
- 14:00-11:00 Modelling upper plate deformation with increasing trench retreat velocity, ALSAIE, M., GUEYDAN, F., GAREL, F.
- 11:00-11:30 Coffee break

### Subduction, Collision and Orogeny (continued)

Chair: Hans Jørgen Kjøll

- 11:30-12:00 Relamination (Invited), HACKER, B.
- 12:00-12:20 Catastrophic pressure drops in subduction zones: an unsuspected process recorded in metamorphic rocks, JAMATO, P.
- 12:20-12:40 Intermediate depth earthquakes and high grade metamorphism, AUSTRHEIM, H. and JAMTVEIT, B.
- 12:40-13:00 Self-localizing thermal runaway as a mechanism for intermediate and deep earthquakes: numerical studies and comparison with field observations, MEDVEDEV, S.
- 13:00-14:30 Lunch at *Madame Mere*

### Mantle Dynamics and the Wilson Cycle

Chair: Pavel Dubrovin

- 14:30-15:10 Orogeny, Wilson cycle and the scale of mantle convection (Invited), FACCENNA C. and BECKER, T.
- 15:10-15:40 On the importance of along-trench variations on subduction dynamics: from back-arc basins to underplating of continental lithosphere, MAGNI, V.
- 15:40-16:00 Concluding remarks, TORGEIR B. ANDERSEN

### Conference Dinner

- 19:00 Conference dinner in restaurant La Crique, Address: La Plage de la Cirque, 20217 Saint-Florent, France (East of the Port, by the sea)

Phone: +33 495 37 04 30

## Posters

1. Microcontinent formation associated with subduction zones, clues to their formation, VAN DEN BROEK, J.M., GAINA, C., BUITER, S., ANDERSEN, T.
2. Tracing the pre-Caledonian ocean-continent transition zone of Baltica across Gudbrandsdalen, central and northern South Norway, JAKOB, J.
3. Observations from deep crustal levels of a magma-rich passive margin, KJØLL, H.J.
4. Geological and structural map of the area between Golo and Tavignano Valleys (Central Corsica), DI ROSA, M., MARRONI, M. and PANDOLFI, L.
5. Slab dehydration and deep water recycling through time, MAGNI, V., P. BOUILHOL, J. VAN HUNEN
6. An attempt to grasp the 4 billion years old Martian atmosphere: weathering profiles mimicked by column experiments, VIENNET, J.-C.
7. PT versus T: Shaping of a planetary body, WERNER, S.C.



## Abstracts

### Modeling upper plate deformation with increasing trench retreat velocity

MANAR ALSAIF, FRÉDÉRIC GUEYDAN, FANNY GAREL

Géosciences Montpellier, Université de Montpellier, France

The Mediterranean shows complex subduction systems with strongly segmented slabs. In the Aegean subduction zone, trench retreat started around 30 Ma ago and accelerated from 1 cm/yr to 3 cm/yr in the last 15 Ma, which was likely related to slab tearing and subsequent narrowing. This study aims at quantifying the effect of this increase in the rate of trench retreat on deformation patterns in the upper plate.

We first present 2D numerical results obtained using the code Fluidity. The code simulates viscous fluids with an adaptive mesh and allows a real upper plate in the subduction setup. The model in this study simulates subduction of oceanic crust beneath a rheologically continental upper plate. The trench retreat rate is varied artificially by imposing lithospheric blocks of varying density in the subducting plate.

We then present preliminary field data from Syros, Cyclades, which documents changes in the styles of deformation in the Cyclades related to changes in the rate of trench retreat.

### Hidden continents

LEWIS D. ASHWAL<sup>1</sup>, M. WIEDENBECK<sup>1,2</sup>, and TROND H. TORSVIK<sup>1,4</sup>

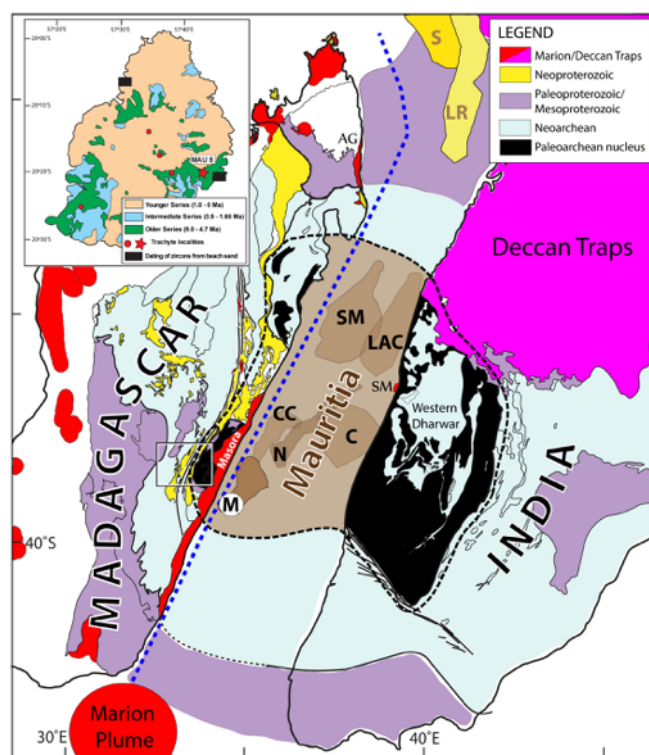
<sup>1</sup>University of the Witwatersrand, Johannesburg, South Africa

<sup>2</sup>Deutsches GeoForschungsZentrum (GFZ), Telegrafenberg, D14473, Potsdam, Germany

<sup>3</sup>The Center for Earth Evolution and Dynamics (CEED), University of Oslo, 0316 Oslo, Norway

<sup>4</sup>Geodynamics, Norges Geologiske Undersøkelse (NGU), N-7491 Trondheim, Norway

A fragment of continental crust has been postulated to underlie the young plume-related lavas of the Indian Ocean island of Mauritius, on both the basis of inversion of gravity anomaly data (crustal thickness) and the recovery of Proterozoic zircons (660-1971 Ma) from basaltic beach sands (Torsvik et al., 2013, *Nature Geosci.* 6, 227). We recovered 13 zircon grains from a trachyte associated with the Older Series basalts (9.0-4.7 Ma) of Mauritius, the second youngest member of a hot-spot track extending from the contamination during sample processing. Ten of the 13 grains are featureless, with no internal structures, and SIMS analyses (Cameca 1280-HR instrument) yield 49 spots with Miocene U-Pb systematics and a mean age of  $5.7 \pm 0.2$  Ma (1 sd), constraining the magmatic crystallization age of the trachyte. Three grains with partially resorbed magmatic zoning, partial metamictization and mineral inclusions (quartz, K-feldspar, monazite) show uniquely



**Simplified geology of Madagascar and India reconstructed to 90-85 Ma.** Mauritius (M) is reconstructed in a likely location near Archaean-Neoproterozoic rocks in central-east Madagascar just prior to break-up. The exact size and geometries of Mauritius and other potential Mauritian continental fragments (SM Saya de Malha; N, Nazareth; CC, Cargados-Carajos Banks; LAC, Laccadives; C, Chagos) are unknown. We propose that Mauritius was dominantly composed of Archaean continental crust, and represented part of the ancient nucleus of Madagascar and India (stippled black line). AG, Analava gabbro (91.6 Ma); LR, Laxmi Ridge; S, Seychelles; SM, St. Mary rhyolites (91.2 Ma). The black-white box shows a region of Madagascar that could correspond to the age spectrum of Mauritian zircons. Inset map shows simplified geology of Mauritius, including trachyte plugs. Star symbol marked MAU-8 is the sampling area for the present study and black bars indicate locations of zircons recovered from beach sand samples. Originally published in Ashwal et al., 2017, *Nature Communications* (<http://rdcu.be/oVJ5>).

mid- to late-Archaean systematics: 20 spot analyses give concordant to near-concordant ages of  $3030 \pm 5$  Ma to  $2552 \pm 11$  Ma. This suggests that during ascent, the trachytic magmas incorporated silicic continental crustal material that preserves a record of several hundred m.y. of Archaean evolution. This is consistent with Sr-Nd isotope systematics of the Mauritian trachytes, which can be modelled as having been contaminated with 0.4-3.5% of ancient granitoid crustal components. Our new age results, combined with the Proterozoic ages of zircons recovered from Mauritian beach sands, are best correlated with continental crust of east-central Madagascar, presently  $\sim 700$  km west of Mauritius, where Archaean gneisses and Neoproterozoic intrusive rocks are juxtaposed such that a 2000 km<sup>2</sup> area could correspond to a fragment of continent presently underlying Mauritius.

This, and other continental fragments now scattered across the western Indian Ocean, once constituted a Precambrian microcontinent called Mauritius, which occupied a position between Madagascar and India prior to the late Cretaceous break-up of Gondwana (Fig. 1). Some of these Precambrian continen-

tal fragments were later blanketed, and in the case of Mauritius, sampled, by much younger plume-related volcanics. Our results allow a more precise continental reconstruction of parts of Gondwana, and suggest that continental break-up processes may be more complex than previously appreciated. Fragments of ancient continental crust, of various sizes and shapes, can become isolated within, and transferred between newly-forming oceanic plates, by successive mid-ocean-ridge relocations (or “jumps”). Another example has been documented beneath SE Iceland (Torsvik et al., 2015, PNAS 112, E1818), and we suggest that the ancient continental fragments might also be found beneath the young volcanoes of the Galapagos, Cape Verdes and Canary Islands.

## Intermediate depth earthquakes and high grade metamorphism

HÅKON AUSTRHEIM and BJØRN JAMTVEIT

Physics of Geological Processes, Department of Geosciences, University of Oslo

Earthquakes riddle the Earth’s lithosphere with fractures and faults on all scales and have significant effects on its petrological and structural evolution. We document here through structures and micro textures how eclogite and amphibolite facies metamorphism is induced through seismic faulting in granulites of the Bergen Arcs, Western Norway. Metamorphism in the wall rock is enhanced through massive formation of dislocations and fragmentation of wall rock minerals interpreted to have developed during the seismic loading. Numerous inclusion including omphacite, amphibole and sulfides in the damaged granulite facies garnet is a consequent of seismic event and may have formed during the dilatational stage. The wall rock and the pseudotachylyte contains abundant hydrous minerals and carbonates documenting fluid transport during the seismic period which was essential to a convert the “dry” granulite facies lower crust to hydrous eclogites and amphibolites.

The classical eclogites facies shear zones of the Bergen Arcs (Austrheim and Griffin 1985) locally nucleated on the pseudotachylytes implying the earthquakes not only was a precursor to the ductile deformation of the area, but also that intermediate depth earthquakes influence the structural evolution of the crust.

### References:

Austrheim, H and Griffin, W.L. 1985. Shear deformation and eclogite formation within granulite- facies anorthosites of the Bergen Arcs, western Norway. *Chemical Geology*, 50, 267-281.

## Microcontinent formation associated with subduction zones, clues to their formation

JOOS M. VAN DEN BROEK, CARMEN GAINA, SUSANNE BUTTER, TORGEIR B. ANDERSEN

Centre for Earth Evolution and Dynamics, Univ. of Oslo, Norway

Microcontinents are defined as fragments of continental crust that are rifted of the parent continent and are surrounded by oceanic lithosphere. Proposed mechanisms for microcontinent formation relate to continental rifting followed by seafloor spreading and mid-ocean-ridge relocation resulting in isolation of continental blocks and thus the formation of microcontinents. However, several generations of microcontinents have been formed by processes associated with subduction processes such as slab pull and trench relocation. Examples of such settings include, but are not limited to, the Corsica – Sardinia block in the Mediterranean and continental fragments around NE Australia. It is difficult to explain the formation of microcontinents in these subduction settings with the aforementioned mechanism of mid-ocean-ridge relocation. By characterising several microcontinents associated with these subduction zones we search for clues to unravel the relationship between inherited structures and microcontinent formation and gain better understanding of their evolution.

## Rollover-type basins controlled by ramp-flat extension following exhumation of metamorphic rocks

JEAN-PIERRE BRUN

Géosciences Rennes, Université de Rennes 1, France

The development of rollover-type sedimentary basins is observed on top of pile of metamorphic rocks recently exhumed, either high pressure or high temperature (e.g. Southwest Norwegian Caledonides; North Aegean). Rollover-type geometry results from ramp-flat extensional systems that require the presence of layers weak enough to be activated as décollement between stronger rocks units. We illustrate the development of this type of extensional structures using: i) the example of the Neogene basins that emplaced on top of the Southern Rhodope Core Complex in North Aegean and ii) laboratory experiments. The physical parameters that have likely controlled the activation of low-angle extensional décollements (i.e. flats) in a metamorphic pile recently exhumed are discussed in terms of lithology, thermal conditions and rate of extension.

## The Jotun Nappe Complex and its relations to surrounding allochthons

FERNANDO CORFU

Department of Geosciences and CEED, University of Oslo

The Jotun Nappe Complex is the largest allochthon in southern Norway. It is dominated by Meso- to Neoproterozoic meta-plutonic rocks which have been metamorphosed at conditions varying from relatively low to high grades, and with variable but in part very intensive deformation. The complex can be divided in different nappe sheets. The Upper Jotun Nappe (UJN) comprises a main central body making up the mountains in central Jotunheimen and consisting of felsic to ultramafic plutonic rock formed at 1700-1600 Ma, with local mafic intrusives formed at 1450 and 1250 Ma. The southwestern part of the UJN is dominated instead by the Inner Sogn anorthosite intruded at about 970 Ma. All these rocks were affected by multistage high grade metamorphism between 950 and 900 Ma, and were intruded by granitic to trondhjemitic dyke complexes in the Silurian at 430-425 Ma, in the early stages of Caledonian thrusting. The lower Jotun Nappe (LJN) in general exhibits very strong deformation and amphibolite facies metamorphism, with similar protoliths and timing of metamorphism as the UJN. The persistence of conglomerate at the interface between LJN and underlying sparagmite (Neoproterozoic arkoses) suggests an original depositional relationship, implying that the whole complex is now upside-down. Smaller marginal thrust sheets consist in part of supracrustal rocks and have uncertain relationships to the main unit of the Jotun Nappe Complex. Regional correlations can link the Jotun Nappe Complex to specific thrust sheets in the southwest and the Lindås and Bergsdalen nappes, but other such allochthons have a very distinct, Telemarkian instead of Gothian, origin. Among these there is also the mainly anorthositic Espedalen Nappe in the east. In the Heidal area to the northeast, the complex is separated by a steep shear zone from the high grade Rudihø Complex, which in turn is overlain by the metasedimentary Heidal group, itself overlain by the southern outlier of the Paleozoic Meråker Nappe. The presence of serpentinite bodies with serpentinite conglomerates typical of hyperextended lithosphere both in the Meråker Nappe, above the Jotun Nappe Complex, and the Bøverdalen Melange, below it, presents an interesting paradox that has yet to be resolved.

## Orogeny, the Wilson cycle and the scale of mantle convection

CLAUDIO FACCENNA<sup>1</sup> and THORSTEN BECKER<sup>2</sup>

<sup>1</sup>Università Roma Tre, Dip. Scienze, Roma Italy

<sup>2</sup>Institute for Geophysics, Jackson School of Geosciences, The University of at Austin, USA

Orogenic belt show difference in size, style and geometry. Most of them show an asymmetry, forming wedge tapering towards the lower plate and crustal thickness not exceeding 50 km. Few of them exceeds crustal thickness of 50 km, up to 80 km, and show a doubly-vergent geometry forming orogenic

plateaux. Here we surmise that subduction in the upper mantle may result in the convergent margin controlling the style of orogeny throughout the Wilson cycle.

A situation where the slab is confined to the upper mantle is likely to result in trench rollback and formation of back arc extension. However, if after transient slab ponding, the slab penetrates into the lower mantle it may generate a surge of compression in the upper plate because trench migration slows down after anchoring, and because the upper plate is dragged against the subduction zone by large-scale return flow. This vigorous surge of mantle convection drags plates against each other, generating the necessary protracted compressional forces to sustain orogeny, for example producing the Himalayan-Tibetan belt and the Andes.

Accordingly, we classify those two types of mountain belts as end members of a wide range of orogens. On one side, we have the "slab pull" type of orogen, where subduction is mainly confined to the upper mantle, and rollback leads to moderately thick crustal stacks and reduced topographic signal, such as in the Mediterranean. On the other side, the "slab suction" orogen would correspond to whole-mantle convection cells ("conveyor belts") leading to the more extreme expressions of orogeny, such as the largely thickened crust and high plateaus of present-day Tibet. For the slab suction type, deep mantle convection produces the unique conditions to drag plates toward each other, irrespective of their nature and other boundary conditions.

If this "bottom-up" tectonic model is correct, the geological records of orogenic cycles and of the topographic evolution along mobile belts can be used to decipher time-dependent mantle convection. Our main conclusion is that beneath the Tethyan belt we should imagine a multi-scale style of convection operating at different time and length scales, with a small-scale convection style in the upper most part of the upper mantle embedded within a larger/slower and intermittent large scale whole mantle convection.

## Comparing rifted margins in the South and North Atlantic with focus on along-margin structural and magmatic segmentation

JAN INGE FALÉIDE

Centre for Earth Evolution and Dynamics, Univ. of Oslo, Norway

The structure and evolution of conjugate rifted margins in the South and North Atlantic have been studied mainly based on seismic reflection and refraction profiles, complemented by potential field data and plate reconstructions. All margins exhibit distinct along-margin structural and magmatic changes reflecting both structural inheritance extending back to a complex pre-breakup geological history and the final breakup processes. Spatially related conjugate transfer systems have been identified on several margins. A series of conjugate crustal transects reveal tectono-magmatic asymmetry, both along-strike and across the conjugate margin systems.

The continent-ocean transitional domain along the magma-dominated margin segments is characterized by a large volume of flood basalts and high-velocity/high-density lower crust emplaced during and after continental breakup. Both the volume

and duration of excess magmatism varies. The extrusive and intrusive complexes make it difficult to pin down a COB to be used in plate reconstructions. The continent-ocean transition is usually well defined as a rapid increase of P-wave velocities at mid- to lower crustal levels. The transition is further constrained by comparing the mean P-wave velocity to the thickness of the crystalline crust. By this comparison we can also address the magmatic processes associated with breakup, whether they are convection dominated or temperature dominated.

In the NE Atlantic there is a strong correlation between magma productivity and early plate spreading rate, suggesting a common cause. A model for the breakup-related magmatism should be able to explain this correlation, but also the magma production peak at breakup, the along-margin magmatic segmentation, and the active mantle upwelling.

It is likely that mantle plumes (Iceland in the NE Atlantic, Tristan da Cunha in the South Atlantic) may have influenced the volume of magmatism but they did not necessarily alter the process of rifted margin formation, implying that parts of the volcanic margins may have much in common with more magma-poor margins.

The South Atlantic also comprises magma-poor margin segments characterized by a hyperextended continent-ocean transitional domain that shows evidence of rotated fault blocks and a detachment surface active during rifting. The central segment (Brazil-Angola) is not a magma-poor end-member. Increase of volcanic activity during the late stages of rifting may have "interrupted" the extensional system implying a failed exhumation phase that was replaced instead by continental breakup and emplacement of fully igneous crust. This resulted in an initial asymmetric thinning domain followed by a symmetric transitional domain.

Conjugate margin segments from the North and South Atlantic will be compared and discussed with particular focus on the tectono-magmatic processes associated with continental breakup.

## Microcontinents: Stories about complexities in the Wilson tectonic cycles

CARMEN GAINA

Centre for Earth Evolution and Dynamics, Univ. of Oslo, Norway

Microcontinents are small continental slivers surrounded by oceanic crust, which are detached from large continental masses by rifting and subsequent seafloor spreading. They are common in the accreted continental geological record, and also described in modern tectonic settings. Many of today's microcontinents are found scattered in large oceanic basins like the North Atlantic and Indian oceans, but also in smaller basins like in the Tasman and Coral seas or in the High Arctic.

In this contribution I will describe the present day crustal architecture of several microcontinents found in the North Atlantic, Indian Ocean, the Arctic realm and east and northeast of Australia. Based on geophysical data and sometimes rock samples recovered from these small continental slivers, one can establish the crustal thickness, sedimentary cover and the amount of volcanic material. For example, in the case of the Jan Mayen microcontinent, situated in the NE Atlantic midway

between the Eurasian and Greenland margins, it has been established that the crustal thickness is decreasing from north to south, volcanic extrusive layers (sea dipping reflectors) are observed only in the northeastern part, but the southern part was affected by later volcanic flows due to the proximity to the Iceland plume (e.g. Gudlaugsson et al., 1988; Peron-Pinvidic et al., 2013a, b). In other cases, the original continental crust was completely covered by the magmatic material supposedly generated by a mantle plume, but geochemical signature of surface rocks can reveal the continental signature of deeper layers (as it has been suggested for the Mauritius Island from the Indian Ocean by Torsvik et al., 2013, 2015).

In the Arctic Ocean, there are many microcontinents dispersed within a confined space; some of them have undisputed continental nature (like in the case of the Lomosov Ridge), in other areas – like the Alpha-Mendeleev ridges – their nature is controversial due to thick volcanic layers which may hinder evidences of continental origin. However, new seismic data and dredged samples may hint to the presence of small continental fragments within these igneous plateaus (Døssing et al., 2013), a situation observed in other Large Igneous Provinces (LIPs) – like the Kerguelan Plateau, south Indian Ocean, e.g. Gaina et al., 2007).

Several studies aimed to build conceptual models for the formation of microcontinents based on present day examples, especially the ones in the Indian Ocean, North Atlantic and around Australia (e.g. Mueller et al., 2001; Gaina et al., 2003 and Gaina et al., 2009). The succession of tectonic events leading to the isolation of microcontinents include: (1) rifting of a passive margin, (2) possible volcanism (sometimes LIP formation) due to the presence of a mantle plume, and (3) ridge jumps which will relocate rifting and seafloor spreading few hundred or thousands kilometres away from the previous plate boundary and complete isolation of the microcontinent. Other possible mechanisms for microcontinent formation will be also briefly discussed.

## References:

- Døssing, A., Jackson, H.R., Matzka, J., Einarsson, I., Rasmussen, T.M., Olesen, A., and J.M. Brozena, 2013, On the origin of the Amerasia Basin and the High Arctic Large Igneous Province-Results of new aeromagnetic data. *Earth and Planetary Science Letters*, Vol. 363, 2013, p. 219-230.
- Gaina, C., Müller, R.D. Brown, B., and Ishihara, T., 2003, Microcontinent formation around Australia, In: *The Evolution and Dynamics of the Australian Plate*, Geological Society of Australia Special Paper 22 and Geological Society of America Special Paper 372, ed. by Hillis R. and Müller, R.D., 405-417.
- Gaina, C., Müller, R.D. Brown, B., Ishihara, T. and S. Ivanov, 2007, Breakup and early seafloor spreading between India and Antarctica, 2007, *Geophysical Journal International*, 170, 151-169.
- Gaina, C., Gernigon, L., and P. Ball, 2009, Paleocene-Recent Plate Boundaries in the NE Atlantic and the formation of Jan Mayen microcontinent, *Journal of Geological Society*, 166, 601-616, doi:10.1144/0016-76492008-112.
- Gudlaugsson, S.T., Gunnarsson, K., Sand, M. and J. Skogseid, 1988. Tectonic and volcanic events at the Jan Mayen Ridge microcontinent. In: Morton, A.C. and Parson, L.M. (eds),

*Early Tertiary Volcanism and the Opening of the NE Atlantic.* Geological Society, London, Special Publications, 39, 85–93.

Müller, R.D., Gaina, C., W.Roest, and D. L. Hansen, 2001. A recipe for microcontinent formation, *Geology*, 29, 203–206.

Peron-Pinvidic, G., Gernigon, L., Gaina, C. and P. Ball, Insights from the Jan Mayen system in the Norwegian-Greenland Sea: Mapping of a microcontinent, 2012, *Geophysical Journal International*, doi:10.1111/j.1365-246X.2012.05639.x.

Peron-Pinvidic, G., Gernigon, L., Gaina, C. and P. Ball, Insights from the Jan Mayen system in the Norwegian-Greenland Sea: Architecture of a microcontinent, 2012, *Geophysical Journal International*, doi:10.1111/j.1365-246X.2012.05623.x.

Torsvik, T. H., Amundsen, H., Hartz, E. H., Corfu, F., Kuznir, N., Gaina, C., Doubrovine, P.V., Steinberger, B., Ashwal, L., Jamtveit, B., 2013. A Precambrian microcontinent in the Indian Ocean. *Nature Geoscience*, doi:10.1038/ngeo1736.

Torsvik, T.H., H. E.F. Amundsen, F. Corfu, R. G. Trønnes, P. V. Doubrovine, C. Gaina, N. Kuznir, B. Steinberger, L. D. Ashwal, W. L. Griffin, S. C. Werner, B. Jamtveit, 2015, Continental crust beneath Iceland, *Proceeding of National Academy of Sciences*, doi:10.1073/pnas.1423099112.

## Oligo-miocene sequential extension as a record of Corsica rotation during Apennines slab roll-back

FRÉDÉRIC GUEYDAN

Université Montpellier 2, France

Corsica is a key locality that recorded the Alpine subduction-collision history followed by 30 Ma of the Apennines slab rollback, responsible for the successive opening of the Liguro-Provençal basin and Tyrrhenian Sea. The overall strain pattern of the Alpine metamorphic units of Alpine Corsica is studied through a synthesis of i) available geological maps, ii) geochronological data and iii) new structural data relative to successive extensional deformations, both ductile and brittle. Three successive stages of extension are recorded: 1) Synmetamorphic Oligocene extension accommodated by N140° trending ductile faults, that correspond to the reactivation of a major Alpine thrust; 2) Burdigalian ramp-flat extension with N60°-70° trending fault zones that controlled the deposition of onshore piggy-back basins, and 3) Serravalian N-S trending fault zones. From a geodynamical point of view, these successive extensional deformations in Alpine Corsica can be correlated to the history Apennine slab rollback. The two first stages are related to a southeastward rollback of the Apennines slab that successively triggered: 1) Continental rifting in Oligocene leading to the opening of the Liguro-Provençal basin and 2) Burdigalian extension with N60°-70° trending fault zones, oblique to the Alpine thrust no more able to accommodate extension because of counter clockwise rotation of Corso-Sardinian block. Finally, NS-trending fault zones developed in Serravalian, at the onset of Tyrrhenian sea opening, related to an eastward rollback of the Apennines slab, as a response of slab tearing in Sicily.

## Relamination

BRADLEY HACKER<sup>1</sup>, PETER KELEMEN and MARK BEHN

<sup>1</sup>Earth Research Institute, University of California, Santa Barbara, CA 93106-9630

Most immature crust must be refined to attain the composition of mature continental crust. This refining may take the form of weathering, delamination, or relamination. Delamination and relamination both call upon gravity-driven separation of low-density felsic rock into the crust and high-density mafic rock into the mantle. Delamination involves foundering of rock from the base of active magmatic arcs. Relamination involves subduction (erosion) of sediment, arc crust, and continent crust in any convergence zone. Heating of the subducted material reduces viscosity, speeds metamorphic reactions, drives devolatilization, and causes melting. Melt separation and compression of the subducted material creates composition-dependent density differences. Some rocks—most obviously, mafic rocks, but also some pelites—become denser than the mantle. Other—even refractory—rocks reach a range of lower densities. If conditions permit, dense, low-SiO<sub>2</sub> material is returned to the mantle with the subducting slab, and buoyant, high-SiO<sub>2</sub> material is relaminated to the base of the upper plate. Different compositions may ascend to different crustal levels, depending on buoyancy and rheology. Relamination may be more efficient than lower crustal foundering at generating large volumes of material with the major- and trace-element composition of continental crust, and may have operated rapidly enough to have refined the composition of the entire continental crust over the lifetime of Earth. If so, felsic rocks could form much of the lower crust, and the bulk continental crust may be more silica rich than generally considered.

## Transitional crust in the fossil ocean-continent transition zone of the pre-Caledonian rifted margin of Baltica and its link to the Scandinavian Dyke Complex

JOHANNES JAKOB<sup>1</sup>, PHILIPPE BOULVAIS<sup>2</sup>, OLIVIER BEYSSAC<sup>3</sup>, FERNANDO CORFU<sup>1</sup>, MANAR ALSAIF<sup>4</sup>, TORGEIR B. ANDERSEN<sup>1</sup>

<sup>1</sup>The Centre for Earth Evolution and Dynamics, University of Oslo, Norway

<sup>2</sup>Géosciences Rennes, Université de Rennes 1, France

<sup>3</sup>Institut de Minéralogie, de Physique des Matériaux et de Cosmochimie IMPMC UMR 7590 CNRS-UMPC-MNHN-IRD, France

<sup>4</sup>Géosciences Montpellier, Université de Montpellier, France

Part of the pre-Caledonian passive margin of Baltica is preserved in the nappes of the Scandinavian Caledonides. On a first order, the passive margin can be divided into: 1) a magma-rich segment, where mafic intrusives abound in metasediments and which is referred to as the Scandinavian Dyke Complex; 2) and a magma-poor segment, that is characterised by a lithostratigraphy typical for transitional crust as well as a paucity of rift-related intrusives.

Crystallisation ages of metamorphosed gabbro, dolerite, and basalt in the metasediments of the magma-rich segment have been dated at  $\sim 616$ - $596$  Ma and are interpreted to have been emplaced as part of the Central Iapetus Magmatic Province during opening of the Iapetus ocean. Vestiges of magma-poor hyperextended crust in central South Norway are structurally below large crystalline nappes of Baltican origin, including the Jotun, Lindås, Dalsfjord, and upper Bergsdalen nappe complexes. The fossil transitional crust of the magma-poor hyperextended margin is preserved as a lithological mixed unit, including detrital and solitary metaperidotites with a complex hydration and carbonation history, originally fine-grained metasediments, continent-derived sandstones/conglomerates, thin slivers of Proterozoic gneisses, and minor late Cambrian-Middle Ordovician and late Silurian metamorphosed felsic and mafic intrusive rocks. The mixed unit is characterised by a consistent along strike Scandian metamorphic overprint, which is estimated at  $500 \pm 50$  °C and  $\sim 7 \pm 2$  kbar, as well as by homogeneous oxygen isotope compositions of the (ophi-)carbonates of about 11.5-15 ‰ (SMOW). The depositional age of the mixed unit is apparently early Middle Ordovician in age (Dapingian detrital zircon and fossil ages), suggesting that the magma-poor segment may have been reworked and redeposited during a poorly-understood orogenic event in the late Cambrian-Middle Ordovician.

Because of the young depositional ages of the metasediments and the paucity of rift-related intrusives in the mixed unit, a direct link of the magma-poor with the magma-rich segment is difficult. Moreover, associated with the change in lithology of the mixed unit from a magma-poor to a magma-rich passive margin is a major structural break in the architecture of the Scandinavian Caledonides. In the vicinity of Vågåmo and Otta across Gudbrandsdalen, the large, crystalline, Baltican nappes terminate and the fossil ocean-continent transition zone is directly overlain by the exotic Trondheim Nappe Complex. However, the lithostratigraphic association of the magma-poor hyperextended segment continues across the structural break into the nappes structurally below the Trondheim Nappe Complex. In contrast to the fossil transitional crust below the Jotun Nappe Complex, the mixed unit structurally underlying the Trondheim Nappe Complex additionally comprises a progressively increasing number of yet undated elongate bodies of metamorphosed gabbro, dolerite, and basalt towards the north and northeast. These units may represent the vestiges of a transition zone from the magma-poor to the magma-rich segments of the pre-Caledonian passive margin. Therefore, the mixed unit between Gudbrandsdalen and Essandsjøen may link the reworked, fossil, transitional crust that was originally formed in a narrow oceanic basin between the proximal Baltican margin and an outboard lying microcontinent with the Ediacaran Scandinavian Dyke Complex.

## Experimental insights on mechanic impacts of metamorphic reactions: torturing Norwegian and Corsican rocks

LOIC LABROUSSE

Sorbonne Universités, UPMC Paris 06, France, Institut des Sciences de la Terre de Paris (ISTEP)

Among all metamorphic reactions, partial melting and eclogitization are the most often taken into account in comprehensive understanding of force balance within convergence systems. In the Norwegian Caledonides, both are linked to crucial stages in the orogenic wedge evolution. Eclogitization of granulites within the Bergen Arcs Lindås nappe is associated to pseudotachylytes and the development of an intricate network of eclogite facies shear zone prone to localize strain at peak conditions. In the Western Gneiss Region, younger eclogites are exhumed in an amphibolite facies migmatitic gneiss matrix, whose partial melting initiated so close to peak conditions, that it has been proposed as the actual mechanism triggering exhumation.

Original deformation experiments presented here were designed in the Griggs and D-DIA apparatus, to (1) estimate the amplitude of the rheological impact of partial melting in realistic pressure conditions, relative to the weakening or softening due to the presence of weak phases such as micas, and (2) estimate the mechanical effect and seismogenic potentials of different eclogitization processes such as the glaucophane-out reaction expected in subduction zones (exemplified in Corsican rocks) and the albite-out reaction expected at the base of thickening collision wedges (exemplified in the Bergen Arcs).

Preliminary results emphasize that partial melting is more a weakening than a softening process, therefore not expected to localize strain. The values of steady state strength in large shear strain experiments also yield much more limited weakening than previously deduced from peak strengths measurements. Regarding eclogitization, both wet (gl-out) and dry (alb-out) eclogitization reactions produce acoustic emissions, ie, earthquakes, in the lab, suggesting that fluid production is not the first order parameter controlling the seismic potential of a metamorphic reaction. Gl-out also seems a more relevant and realistic earthquake trigger in subduction zones, compared to the fashionable and spectacular lawsonite breakdown reaction.

## Formation and structural evolution of young continental margins: insights from the Gulf of Aden

SYLVIE LEROY and C. NONN

ISTEP, Sorbonne Universités, CNRS, UPMC, 4 place Jussieu, 75 252 Paris

In this study, we present the yet unexplored conjugate passive margins between the Socotra-Hadbeen (SHFZ) and the eastern Gulf of Aden fracture zone in the eastern Gulf of Aden. We map the crustal domains (proximal, necking, hyper-extended, exhumed mantle, proto-oceanic and oceanic domains) and structures using seismic reflection data. The most striking result is that the magma-poor conjugate margins exhibit a

long-term asymmetrical architecture with sharp necking domains and narrow hyper-extended domains. We suggest that this asymmetry is related to the migration of the rift center producing significant lower crustal flow and sequential faulting in the hyper-extended domain. Multiple generations of detachment faults exhuming serpentinized subcontinental mantle in the ocean-continent transition is associated with significant decompression melting and final detachment fault may have triggered the formation of a proto-oceanic crust. Finally, the stable oceanic spreading center occurs at ~17 Ma.

Two reconstructed cross-sections show that (1) symmetric structures lead to the necking of the lithosphere (Upper Chattian–Aquitainian). Then, the crustal deformation becomes asymmetrical and triggers the southward upwelling of the asthenosphere. The northward migration of the rift center (Aquitainian–Burdigalian) may have induced lower crustal flow that accommodates most of the extension and triggers the asymmetry of margins with a sequential faulting; (2) the formation of the Ocean-Continent Transition (OCT) is associated with a northward-dipping detachment fault at the beginning of the exhumation phase (Burdigalien). It separates the northern upper plate (Oman) from southern lower plate (Socotra island) and may have generated rift-induced decompression melting and magmatism affecting the upper plate (Omani margin). (3) mantle convections along the main fracture zones may be responsible of change in fault polarity in the Omani hyper-extended domain and of the propagation of the eastern Sheba ridge towards the Socotra-Sharbitat segment.

## On the importance of along-trench variations on subduction dynamics: from back-arc basins to underplating of continental lithosphere

VALENTINA MAGNI

Centre for Earth Evolution and Dynamics (CEED), University of Oslo, Norway

The understanding of the regional tectonic evolution of a specific subduction zone is often very challenging due to the many complexities involved in the subduction process. It is unlikely that a system would remain in a steady-state condition for long time; instead, it is much more common to see clear changes in the tectonic and magmatic evolution because of variations within the subducting plate, the overriding plate, the far-field stress regime, and/or the mantle flow. These variations include, for instance, changes in the lithosphere strength, in the plate age, in the presence of continental and oceanic lithosphere, in the composition, in the plate thermal structure, in the far-field velocities and forces, in the presence of neighbouring subductions and/or plumes, and many other features. Here, I focus on the important effects that these type of variations within the subducting plate can have on the evolution of a subduction zone by using three-dimensional finite element models. I will present two different model setups.

In the first case, the subducting plate is oceanic in the middle and has two continental blocks colliding at the sides. Interestingly, results from these models show that the collision happening at the sides is crucial to trigger the formation of a back-arc basin in the centre. Moreover, the formation of slab windows at depth due to the retreat of the oceanic slab is nec-

essary to have an episodic style of extension in the overriding plate, as well as episodes of more intense melt production at the back-arc. These results are applied to investigate the Central Mediterranean subduction zone.

In the second type of setup, collision occurs in the centre. If the oceanic sides are wide enough or if a far-field velocity is imposed to the subducting plate, the previously subducted continental lithosphere rises back towards the surface after the slab breaks off at depth and can flatten below the overriding plate. This process of underplating after slab break-off results in a thick horizontal layer of continental crust that extends for about 200 km beyond the suture. These models can be used to explain the dynamics that led to the present-day crustal configuration of the India-Eurasia collision zone.

## Formation and reactivation of rifted margins and implications for the interpretation of orogenic processes

GIANRETO MANATSCHAL<sup>1</sup>, TUGEND, J.<sup>1</sup>, CHENIN, P.<sup>1</sup>, EPIN, M.E.<sup>1</sup>, DECARLIS, A.<sup>1</sup>, LESCOUTRE, R.<sup>1</sup> and MOHN, G.<sup>2</sup>

<sup>1</sup>IPGS-CNRS-EOST, Université de Strasbourg, Strasbourg, France (manat@unistra.fr)

<sup>2</sup>Géoscience Environnement Cergy, Université Cergy-Pontoise, F-95000 Cergy, France. (Geoffroy.Mohn@u-cergy.fr)

A long-standing question in Earth Sciences is related to the role of inheritance in controlling the rheology, deformation and magmatic history of tectonic systems. In contrast to physical processes that are generally applicable, the role of inheritance is difficult to assess without having insights into the history of a geological system. Moreover, inherited features are not always reactivated, which makes it difficult to include them in generic models. In order to identify the role of inheritance and define its relative control on the deformation and rheological evolution of a geological system, we define inheritance as the difference between an "ideal" layer-cake type lithosphere and a "real" lithosphere containing heterogeneities. In this sense, three types of inheritance can be defined: structural, compositional and thermal inheritance. The aim of the presentation is to discuss, using these definitions and examples from Western Europe, how inheritance may control the architecture and evolution of extensional and compressional systems within the Wilson cycle.

In the presentation, we will focus on three well-studied systems that are the Iberia-Newfoundland, the Pyrenean-Bay of Biscay and the Alpine Tethys rift systems. All these rift systems went through a stage of hyperextension and show variable amounts of reactivation ranging from incipient to complete. For these examples, we are able to show that the strain evolution and localization of deformation during the early stages of rifting are controlled to a first order by the distribution and thickness variations of ductile and brittle layers, inherited from the initial composition and thermal structure of the lithosphere. However, at more advanced stages of rifting, once the crust is less than 10 km thick, deformation seems to be mainly controlled by the presence of fluids and the breakdown reactions of feldspar and olivine into weaker hydrated minerals (e.g. clay, serpentine), and/or by the presence of magma. How these processes can modify the rheology and control the final stages of rifting remains, however, unclear. In addition, it is important

to note that the location of final lithospheric breakup is not always controlled by inherited structures. This seems to contrast with the onset of reactivation, which appears to be controlled by the presence of weak decoupling horizons that are inherited from the formation of the rifted margins and are preferentially reactivated during subsequent convergence.

Understanding how far the new ideas and concepts derived from the southern North Atlantic and Alpine Tethys can be translated to other less explored rift systems and mountain belts will be one of the challenges of future research.

## Self-localizing thermal runaway as a mechanism for intermediate and deep earthquakes: numerical studies and comparison with field observations

SERGEI MEDVEDEV

Centre for Earth Evolution and Dynamics, Univ. of Oslo, Norway

Convergent margins are characterized by strong seismic activity with earthquakes occurring at depths of up to 700 km. Shallow earthquakes (<60 km) are explainable by the brittle failure of rocks. At greater depths, the increased ambient pressure should inhibit brittle failure. We present a self-localising thermal runaway (SLTR) as a possible mechanism for intermediate to deep earthquakes. Recently discovered, this phenomenon presents an ultimate failure mechanism for viscoelastic materials. Irreversible ductile deformation dissipates mechanical work into heat that can lead to thermal softening and failure by progressively self-localizing deformation, SLTR. This failure mechanism, in contrast to brittle failure, is independent from ambient pressure. We present the results of an analytical, numerical and petrological study that evaluates SLTR as a failure mechanism for intermediate to deep earthquakes. Our numerical experiments compare well to field evidence from the Krakenes Gabbro in Western Norway. Particularly, our experiments show possible coexistence of ductile (shear zones) and brittle-like (pseudotachylyte veins) deformation and catastrophic failure with seismogenic strain rates and active melting in the deep-earth conditions. We show that weakening by hydration also plays a key role in shear zone formation and ultimately seismic failure. We also compare differential stresses required for SLTR and compare them to brittle yield stresses according to Byerlee's law. This study shows that at depths greater than 60-80 km failure by SLTR is more likely than brittle failure, and that SLTR is a viable mechanism for earthquakes in subducting slabs and continental root zones.

## What's reactivated at rifted margins? Examples from onshore and offshore Norway

PER TERJE OSMUNDSEN

The Geological Survey of Norway

The opening of oceans along ancient mountain belts was stated as fundamental in the Wilson cycle and implies reactivation of pre-existing geological features. The question of what is actually reactivated appears as much more difficult. From orogen to rifted margin, each evolutionary stage leaves a series of structural and rheological templates to be inherited into the next. For the Norwegian margin, we consider the following aspects: 1) inheritance of the orogenic template into a phase of post-orogenic extension; 2) inheritance of post-orogenic rheological and structural template into the main stages of rifting; 3) inheritance of the early rift configuration into the stage of crustal necking and 4) inheritance of the entire post-rift template into the 'passive' margin phase. The outline of the Norwegian margin follows structural trends that were important during Devonian, post-Caledonian extension. Thus inheritance from this phase appears to have been particularly important. But which structures were actually inherited, how did inheritance occur and how long into the rifting process was it important? The post-orogenic extension involved large-magnitude extensional and strike-slip faults. In Svalbard, strike-slip faults that had developed along the flanks of extension-parallel folds in the Devonian were reactivated with normal sense during formation of Carboniferous half-graben. Later, both transpressional orogeny and transtensional margin formation appears to have followed the same trend. Offshore SW Norway, deflected detachment zones partly controlled lateral changes in the Permo-Triassic and younger rift architecture. Along the Møre segment of the Mid-Norwegian margin, reactivation was followed by the successive incision of the large-magnitude faults that facilitated deformation coupling in Late Jurassic-Early Cretaceous time. Incision into a variable crustal template, inherited from the earliest phases of rifting, led to significant variations in the geometry of the large-magnitude faults that facilitated deformation coupling and to variations between 'core complex' and other types of fault geometries along the necking domains of the Møre and Vøring margins. Coupling deformation froze in the crustal taper, which served as a template in the post-rift phase. Offshore Norway, the taper break remains seismically active below thick Neogene deposits, indicating a long-term weakness in the margin architecture. Variations in onshore topography correlate with the crustal taper, as does late-stage fault reactivation and the width of the strandflat, an erosional surface that is presently forming along coastal Norway. Older incised surfaces became rotated and buried offshore, but became templates for landscape evolution onshore. Thus, inheritance is complex at rifted margins and involves structures, rheology and bulk crustal/lithospheric templates that, in turn, control many aspects of the subsequent margin evolution.

## The tectono-metamorphic history of the Corte slices (Alpine Corsica): An example of continental subduction and polyphased exhumation

MARIA DI ROSA<sup>1,2</sup> and M. MARRONI<sup>2,3</sup>

<sup>1</sup>Dipartimento di Scienze della Terra, Università di Firenze (Italia)

<sup>2</sup>Dipartimento di Scienze della Terra, Università di Pisa (Italia)

<sup>3</sup>Istituto di Geoscienze e Georisorse, IGG-CNR, Pisa (Italia)

The role of the ductile deformation observed in the Corte Slices (Central Corsica) is critical for the study of the behaviour of the European continental crust involved in the Alpine processes of subduction and exhumation. The Corte Slices consist in a set of tectonic units affected by a polyphased penetrative deformation and characterized by a well-preserved HP-LT metamorphism with a complex retrograde path (Di Rosa et al., 2017). Therefore the relationships between the structural and the metamorphic data allow to constrain their tectonic history and thus to frame them out within the geodynamic evolution of the Alpine Corsica.

The Corte Slices belong to the Lower Units (i.e. Parautochthonous), that, together with the Schistes Lustrés Complex and the Upper Units, compose the Alpine Domain of the Corsica island (Molli 2008); they crop out in the central Corsica, where are delimited to the east by the Schistes Lustrés Complex and to the west by the Autochthonous (i.e. Variscan Domain). From the meso- and microstructural analysis a three-steps ductile deformation history emerged, that has similar features but different in intensity for each of the Corte Slices (i.e. Castiglione-Popolasca, Croce d'Arbitro and Piedigriggio-Prato Unit). The D1 phase, rarely observed at the meso-scale (F1 sheath folds) and well preserved at the micro-scale (S1 foliation within the S2 microlithons), is almost completely transposed by the D2 phase, that produces the main meso- and micro-structures (F2 isoclinal folds with a sub-vertical AP2 axial plane foliation and sub-horizontal A2 fold axes, L2 stretching lineation); conversely the D3 phase is well observed at the meso-scale (F3 open folds with a sub-horizontal AP3 axial plane foliation gently dipping to west), but rarely observable at the micro-scale (weak crenulation cleavage). Furthermore, the D1 and D2 phases produce, in the politic lithotypes, the metamorphic recrystallization of chlorite-phengite-albite-quartz assemblage, that allows to constrain the P-T conditions at the time of their (de)formation. Although there are slight differences in the P- and T-peak values, what is came out is that the Corte Slices reached the deepest position in the tectonic wedge (12,2-7,5 kbar/250-365 °C) during the D1 phase, as testified by the oldest metamorphic assemblage. A second set of chlorite-phengite contained in the S1 foliation and in equilibrium at 8,2-5,6 kbar/280-435 °C confirms that the exhumation of the Corte Slices already started during the D1 phase. Finally, a third metamorphic assemblage that constitute the S2 foliation testifies that the D2 phase occurred only when the units are parked at 4,5-2,1 kbar/310-180 °C. The absence of a metamorphic assemblage related to the D3 phase suggests that at that time the position of the Corte Slices is next to the surface.

## References:

Molli G. 2008. Northern Apennine-Corsica orogenic system: an update overview. In: S. Siegesmund, B. Gugenstuh and N. Froitzheim (eds.) Tectonic aspects of the Alpine-Dinaride-Carpathian System. London: Geological Society, special publications, 298, 413-442.

Di Rosa M., De Giorgi A., Marroni M. and Vidal O. 2017. Syn-convergence exhumation of continental crust: evidence from structural and metaorphic analysis of the Monte Cecu area, Alpine Corsica (Northern Corsica, France). *Geol.J.*, in press.

## The tectono-metamorphic history of the Corte slices (Alpine Corsica): An example of continental subduction and polyphased exhumation

MARIA DI ROSA<sup>1,2</sup>, M. MARRONI,<sup>2,3</sup> and L. PANDOLFI<sup>2,3</sup>

<sup>1</sup>Dipartimento di Scienze della Terra, Università di Firenze (Italia)

<sup>2</sup>Dipartimento di Scienze della Terra, Università di Pisa (Italia)

<sup>3</sup>Istituto di Geoscienze e Georisorse, IGG-CNR, Pisa (Italia)

The area between Golo and Tavignano valleys (Lat.: 42°20'N, Long.: 9°10'E) in Central Corsica is characterized by the occurrence of continental metamorphic units belonging to the Lower Units of the Alpine Corsica. These units, also known as Corte Slices, represent the fragments of the European continental margin involved in the continental subduction and the subsequent collision, both resulting from the closure of the Ligure-Piemontese Oceanic Basin. These units are thus characterized by a complex, polyphased deformation history developed under blueschists to greenschists metamorphic facies conditions during the Late Eocene-Early Miocene time span.

In the study area, the Corte Slices have been investigated by a multidisciplinary approach consisting of a detailed mapping associated to meso- and microstructural analyses and estimate of the P-T conditions of the metamorphic events. The 1:10 000 scale geological map illustrates the results of this approach that provided a detailed snapshot of the stratigraphic and structural analysis of the Corte Slices (Di Rosa et al., 2017).

The structural setting of the area is characterized by a polyphased deformation history: within the Corte Slices, three folding phases are recognized at all the scale of observation (D1, D2 and D3). The D1 produces F1 sheath folds and a S1 foliation, almost completely transposed by the D2 phase that is characterized by F2 isoclinal folds with a subvertical axial plane foliation, a S2 and a L2 stretching lineation. The D3 phase is associated to F3 folds with a subhorizontal axial plane foliation. A post-D3 brittle deformation phase is associated to the Central Corsica Shear Zone (ccsz), a strike-slip faults system that cuts all the previous structures.

## References:

Di Rosa M., De Giorgi A., Marroni M. and Pandolfi L. 2017. Geology of the area between Golo and Tavignano Valleys

(Central Corsica): a snapshot of the continental metamorphic units of Alpine Corsica. Journal of Maps, submitted.

## The pre-Caledonian Scandinavian Dyke Complex and 600 Ma plate reconstructions of Baltica

CHRISTIAN TEGNER<sup>1</sup>, TORGEIR B. ANDERSEN<sup>2</sup>, ERIC L. BROWN<sup>1</sup>, FERNANDO CORFU<sup>2</sup>, SVERRE PLANKE<sup>2</sup>, HANS JØRGEN KJØLL<sup>2</sup> and TROND H. TORSVIK<sup>2</sup>

<sup>1</sup>Centre of Earth System Petrology, Department of Geoscience, Aarhus University, Denmark (christian.tegner@geo.au.dk)

<sup>2</sup>Centre for Earth Evolution and Dynamics, University of Oslo, Norway

Magmatism of the first known rifting phase of the North Atlantic Wilson cycle is surprisingly well preserved in the Caledonian nappes of central and northern Scandinavia. Along c. 1000 km the Särsv and Seve Nappes are characterised by spectacular dyke complexes and other intrusive forms originally emplaced into continental sedimentary basins along the rifted margin of Iapetus. We refer to this as the magma-rich segment of the pre-Caledonian margin of Baltica, in contrast to the hyper-extended and magma-poor segment exposed in southern Norway (Andersen et al., Jakob et al., this meeting). In the larger picture the Scandinavian Dyke Complex is part of the Central Iapetus Magmatic Province (CIMP). The intensity, volume and structure of the Scandinavian Dyke Complex is comparable to that of the present passive margins of the North Atlantic large igneous province (Kjøll et al., this meeting) and U-Pb ages suggest magmatism was short-lived at 610-590 Ma.

To constrain the origin of the Scandinavian Dyke Complex and to potentially guide plate reconstructions of Baltica we: (1) re-visited the dyke complexes of the Särsv, Sarek, Kebnekaise, Tornetrask and Indre Troms mountains of Sweden and Norway; (2) compiled new and published geochemical data for the entire dyke complex; (3) modeled mantle sources and melting dynamics; and (4) extended reconstructions of the paleo-position of Baltica back to 600 Ma. Although the appearance of the dykes ranges from garnet amphibolite gneiss to pristine mag-

matic intrusions, all bulk rock compositions largely reflect the original magmatic rock. The compiled dataset includes c. 600 analyses that essentially forms a coherent suite dominated by tholeiitic ferrobasalt akin to the North Atlantic large igneous province, but including alkali basalts in the central portion where meta-carbonatite is also reported. A few samples (<30) are significantly contaminated with crust, but most are largely uncontaminated.

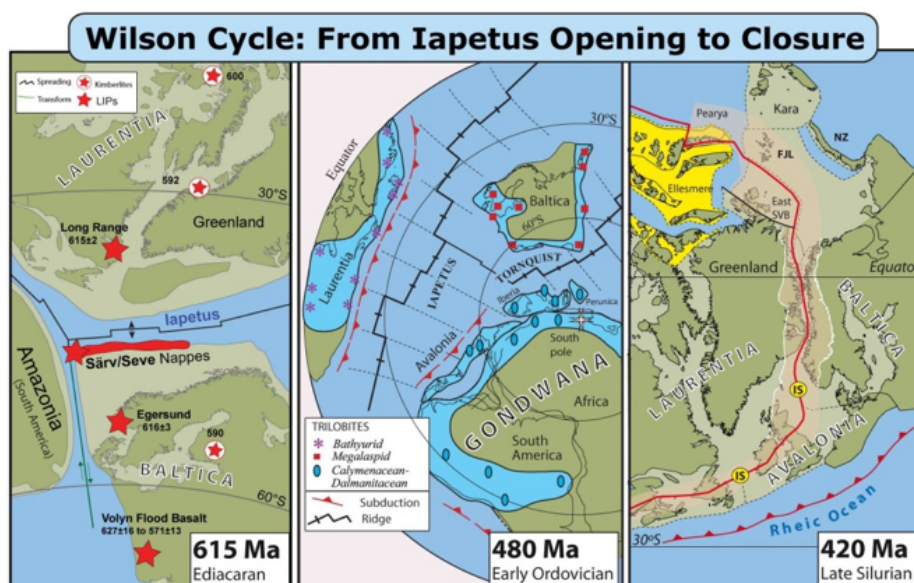
The tholeiitic dykes display systematic lateral variations over c. 1000 km in trace element compositions suggesting geochemical enrichment (e.g. delta-Nb and La/Sm(N) relative to mid-ocean ridge basalt) in the southern and central portions, grading to more depleted compositions in the north. The most enriched tholeiites occur in the central portion that also includes alkali basalts. The lateral geochemical zoning is comparable to e.g. the North Atlantic large igneous province and around Iceland today. Our petrological modeling suggests melting of asthenospheric mantle involving at least two source compositions at temperatures elevated above ambient mantle. We therefore speculate that the Scandinavian Dyke Complex formed by melting of a zoned mantle plume originating from a plume generation zone (margins of large low shear-wave velocity provinces) at the core-mantle boundary. If the position of the present plume generation zone in the Pacific can be viewed as stationary back to 600 Ma, we entertain the idea that the Scandinavian Dyke Complex may be used to guide plate reconstructions.

## The Iapetus Ocean and Torgeir Andersen: From the mysterious Opening to the dramatic Closure

TROND HELGE TORSVIK

The Centre for Earth Evolution and Dynamics (CEED), University of Oslo, 0315 Oslo, Norway.

The understanding and application of plate tectonic theory, integrated with Tuzo Wilson's principles of its effect on rifting, crustal subsidence and ocean opening, subduction



initiation and ocean closure, and finally continent-continent collision (the Wilson Cycle) are essential when modelling past geographies. The Norwegian and Greenland conjugate margins are probably the best example of Wilson Cycle tectonics on our Planet. Subsequent to Late Precambrian hyperextension and large igneous province volcanism, Norway (Baltica) drifted away from Greenland (Laurentia) at around 600 Ma and opened the Iapetus Ocean between them. The Iapetus Ocean was at its largest in the Early Ordovician and the distance between Norway and Greenland was ~4000 km. Large Ordovician oceans are also witnessed by distinctive provinces of shallow-shelf benthos, including most trilobites and nearly all brachiopods. For example, the Baltic (megistaspimid) Province occupied temperate southerly latitudes whilst the bathyurid Province in Greenland colonised equatorial latitudes.

The waning stages of a Wilson Cycle involve oceanic subduction, closure and continental collisions which are recorded in the geological record. Avalonia (including England) rifted off the margin of Gondwana in the Early Ordovician and by the Late Ordovician it had drifted to palaeolatitudes comparable with those of Baltica with subduction beneath Avalonia. That is clearly reflected in the geological record by Andean-type calc-alkaline magmatism in Avalonia, and explosive vents associated with that subduction were the source for gigantic Late Ordovician ash falls in Baltica (the Kinnekulle bentonite). The Caledonian Orogeny is a prime example of the final stage of a Wilson Cycle: Avalonia first docked softly with Baltica in the Late Ordovician but the combined landmasses shortly thereafter collided much more aggressively with Laurentia during Mid-Silurian times. Subduction and continent-continent collision caused the calc-alkaline magmatism in Scotland/East Greenland and the ultra-high pressure terranes in western Norway, which demonstrate subduction of Baltic continental crust beneath East Greenland to depths of 100 km or more. Those ultra-high pressure terranes were subsequently exhumed rapidly during the Early Devonian.

## PT versus T: Shaping of a planetary body

STEPHANIE C. WERNER

The Centre for Earth Evolution and Dynamics (CEED), University of Oslo, 0315 Oslo, Norway.

Planetary bodies show diverse morphology at global scale. The shape and the surface roughness can be interpreted to be caused by tectonic processes. This requires interior dynamical processes driving the breaking and redistribution of plates. Earth in this sense is peculiar, as these broken plates not only get rearranged horizontally, but also vertically. Thus, Earth is unique, at least currently. I will show other examples of tectonic surface expressions and basic observations, which suggest that all tectonic processes on other planetary bodies can be explained without plate tectonics.

## Catastrophic pressure drops in subduction zones: an unsuspected process recorded in metamorphic rocks

PHILIPPE YAMATO

Géosciences Rennes, Université de Rennes 1, France

When deeply buried in subduction zones, rocks undergo mineral transformations that record the increase of pressure and temperature. The fact that high-pressure metamorphic parageneses are found at the Earth's surface proves that rock burial is followed by exhumation. The analysis of available data sets from high-pressure metamorphic rocks worldwide shows that the peak pressure is proportional to the subsequent decompression occurring during the initial stage of retrogression. I propose, using a simple mechanical analysis, that this linear relationship can be explained by the transition from burial-related compression to extension at the onset of exhumation. This major switch in orientation and magnitude of principal tectonic stresses leads to a catastrophic pressure drop prior to actual rock ascent. Therefore, peak pressures are not necessarily, as commonly believed, directly dependent on the maximum burial depth, but can also reflect a change of tectonic regime. These results, which are in agreement with natural data, have significant implications for rock rheology, subduction zone seismicity, and the magnitudes of tectonic pressures sustained by rocks at the subduction interface. These implications for subduction dynamics will be discussed.



## Participant list with contact information

1. Alsaif, Manar - PhD student, University of Montpellier, [alsaif@gm.univ-montp2.fr](mailto:alsaif@gm.univ-montp2.fr)
2. Andersen, Torgeir - Professor University of Oslo, [t.b.andersen@geo.uio.no](mailto:t.b.andersen@geo.uio.no)
3. Ashwal, Lewis - Professor University of Witwatersrand, [Lewis.Ashwal@wits.ac.za](mailto:Lewis.Ashwal@wits.ac.za)
4. Austrheim, Håkon - Professor University of Oslo, [h.o.austrheim@geo.uio.no](mailto:h.o.austrheim@geo.uio.no)
5. Brun, Jean-Pierre - Professor University of Rennes, [Jean-Pierre.Brun@univ-rennes1.fr](mailto:Jean-Pierre.Brun@univ-rennes1.fr)
6. Corfu, Fernando -, Professor University of Oslo, [fernando.corfu@geo.uio.no](mailto:fernando.corfu@geo.uio.no)
7. Di Rosa, Maria - PhD student University of Pisa, [maria.dirosa@unifi.it](mailto:maria.dirosa@unifi.it)
8. Dubrovin, Pavel - Researcher University of Oslo, [pavel.dubrovin@geo.uio.no](mailto:pavel.dubrovin@geo.uio.no)
9. Faccenna, Claudio - Professor University of Roma Tre, [claudio.faccenna@uniroma3.it](mailto:claudio.faccenna@uniroma3.it)
10. Faleide, Jan Inge - Professor University of Oslo, [j.i.faleide@geo.uio.no](mailto:j.i.faleide@geo.uio.no)
11. Gaina, Carmen - Professor University of Oslo, [carmen.gaina@geo.uio.no](mailto:carmen.gaina@geo.uio.no)
12. Gørbitz, Trine-Lise – Admin .leader CEED, Univ. of Oslo, [t.l.k.gorbitz@geo.uio.no](mailto:t.l.k.gorbitz@geo.uio.no)
13. Gueydan, Frederic - Professor University of Montpellier, [frederic.gueydan@umontpellier.fr](mailto:frederic.gueydan@umontpellier.fr)
14. Hacker, Bradley - Professor University of California, [hacker@geol.ucsb.edu](mailto:hacker@geol.ucsb.edu)
15. Jakob, Johannes - Postdoc University of Oslo, [johannes.jakob@geo.uio.no](mailto:johannes.jakob@geo.uio.no)
16. Kjøll, Hans Jørgen - PhD student University of Oslo, [h.j.kjoll@geo.uio.no](mailto:h.j.kjoll@geo.uio.no)
17. Labrousse, Loic - Professor Univ, Pierre at Marie Curie Paris 6, [loic.labrousse@upmc.fr](mailto:loic.labrousse@upmc.fr)
18. Leroy, Sylvie - Professor CNRS Paris, [sylvie.leroy@upmc.fr](mailto:sylvie.leroy@upmc.fr)
19. Magni, Valentina - Postdoc University of Oslo, [valentina.magni@geo.uio.no](mailto:valentina.magni@geo.uio.no)
20. Manatschal, Gianreto - Professor University of Strasbourg, [manat@unistra.fr](mailto:manat@unistra.fr)
21. Medvedev, Sergei - Researcher University of Oslo, [sergei.medvedev@geo.uio.no](mailto:sergei.medvedev@geo.uio.no)
22. Osmundsen, Per Terje - Researcher Geol. Survey of Norway, [p.t.osmundsen@ngu.no](mailto:p.t.osmundsen@ngu.no)
23. Sleveland, Marie
24. Tegner, Christian - Professor University of Aarhus, [christian.tegner@geo.au.dk](mailto:christian.tegner@geo.au.dk)
25. Torsvik, Trond H. - Professor University of Oslo, [t.h.torsvik@geo.uio.no](mailto:t.h.torsvik@geo.uio.no)
26. van den Broek, Joost M. - PhD student University of Oslo, [j.v.d.broek@geo.uio.no](mailto:j.v.d.broek@geo.uio.no)
27. Viennet, Jean-Christophe - Postdoc University of Oslo, [j.c.viennet@geo.uio.no](mailto:j.c.viennet@geo.uio.no)
28. Werner, Stephanie - Associate Prof., University of Oslo, [stephanie.werner@geo.uio.no](mailto:stephanie.werner@geo.uio.no)
29. Yamato, Philippe – Professor University of Rennes, [philippe.yamato@univ-rennes1.fr](mailto:philippe.yamato@univ-rennes1.fr)



## **Selected contributions of Torgeir's to the geology of Corsica and the Wilson cycle**

Downloaded from [geology.gsapubs.org](http://geology.gsapubs.org) on April 25, 2014

## Large subduction earthquakes along the fossil Moho in Alpine Corsica

T.B. Andersen<sup>1\*</sup>, H. Austrheim<sup>1</sup>, N. Deseta<sup>2</sup>, P. Silkose<sup>1</sup>, and L.D. Ashwal<sup>2</sup><sup>1</sup>Centre of Earth Evolution and Dynamics, Department of Geosciences, University of Oslo, P.O. Box 1047, Blindern 0316 Oslo, Norway<sup>2</sup>School of Geosciences, University of Witwatersrand, Wits 2050 Johannesburg, South Africa

## ABSTRACT

Subduction earthquakes release vast amounts of energy to crust and mantle lithosphere. The products of such drastic events are rarely observed in the field because they are mostly lost by subduction. We present new observations of deformation products formed by a few very large and numerous small intermediate-depth Alpine subduction earthquakes that are preserved along the exhumed gabbro–mantle peridotite contact of the Piemont-Liguria oceanic basin in Corsica. The abrupt release of energy resulted in shear heating events that completely melted both gabbro and peridotite. The large volumes of melt that were generated can be studied in the fault and injection vein breccia complex along the fault zone. The energy required for wholesale melting of a large volume of peridotite along the fault combined with previous estimates of stress drops show that very large earthquakes took place along the Moho of the subducting plate. Because these fault rocks formed by intraplate seismicity, we suggest, by analogy with present-day subduction, that they represent a proxy for the lower seismogenic zone.

## INTRODUCTION

Pseudotachyrites (PSTs) are melt rocks formed by earthquake faulting or by shock events such as extraterrestrial impacts. Such sudden release of strain energy may generate very high temperatures and may melt rocks regardless of bulk composition (e.g., Spray, 1995). Wadati-Benioff zones are the most seismically active domains on Earth and host the largest known earthquakes. Exhumed high-pressure (HP) and low-temperature (LT) provinces are regions recording low geotherms characteristic of subduction and collision; therefore, ancient HP-LT terrains may provide opportunities to make direct observations of phenomena produced by collision and subduction earthquakes (Austrheim and Boundy, 1994). Field examples of PST produced by intermediate depth earthquakes (~50–300 km; Frohlich, 2006) are rare (Austrheim and Boundy, 1994; John and

Schenk, 2006), not because the processes they record are rare, but because the likelihood of exhumation of such fault rocks to the surface, enabling direct observation, is very small. Such rocks will normally be lost permanently by subduction (Bjørnerud et al., 2002) or be restructured and recrystallized during exhumation. Only a few occurrences worldwide are known (Sibson and Toy, 2006).

Previous studies in the HP-LT terrains of Alpine Corsica (Ravna et al., 2010; Vitale Brovarone et al., 2011a) documented coseismic slip evinced by numerous, mostly small PST fault and injection veins (Andersen and Austrheim, 2006; Deseta et al., 2014). These studies demonstrated that complete melting and high-*P* quenching of gabbro and peridotite took place and that large stress drops (>570 MPa) were caused by small (<5 cm) slip events in the peridotite (Andersen et al., 2008). Here we present

new observations of PSTs that formed by much larger earthquakes than described previously. The gabbro–mantle peridotite contact exposed at Cima di Gratera (Fig. 1) formed in the slow-spreading Piemont-Liguria Ocean or in distal parts of its hyperextended passive margin. It represents the fossil crust–mantle boundary (Moho) in the vestiges of the oceanic basin that closed during Alpine subduction (Vitale Brovarone et al., 2011b, 2013). In this study, the exposed gabbro–mantle peridotite contact in Cape Corse (Fig. 1) and its evidence for HP-LT coseismic faulting are taken to represent a proxy for an oceanic lithosphere Moho during subduction.

## FIELD OBSERVATIONS

Earthquakes along the paleo-Moho in the study area (Corsica; Fig. 1) caused melting of large volumes of spinel- and plagioclase-bearing mantle peridotite (Fig. 2) as well as the gabbro of the lower crust (e.g., Austrheim and Andersen, 2004; Deseta et al., 2014). The exposed crust–mantle interface is a sharp, gently dipping contact between serpentinitized to well-preserved mantle peridotite and the overlying layered to variably textured metagabbro. Evidence for dramatic PST generation events can be studied within both gabbro and mantle peridotite lenses, which are as much as 140 m thick and 850 m long and preserved for ~2.5 km along the exposed crust–mantle contact (Fig. 1). The contact is offset by later normal faults that also truncate the nonmetamorphic Miocene Saint Florent Basin (Fig. 1). The PST faulting

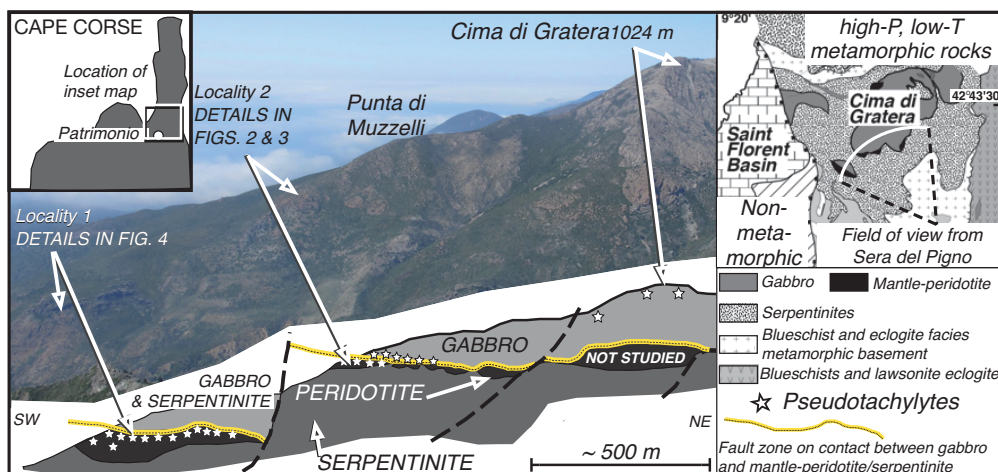
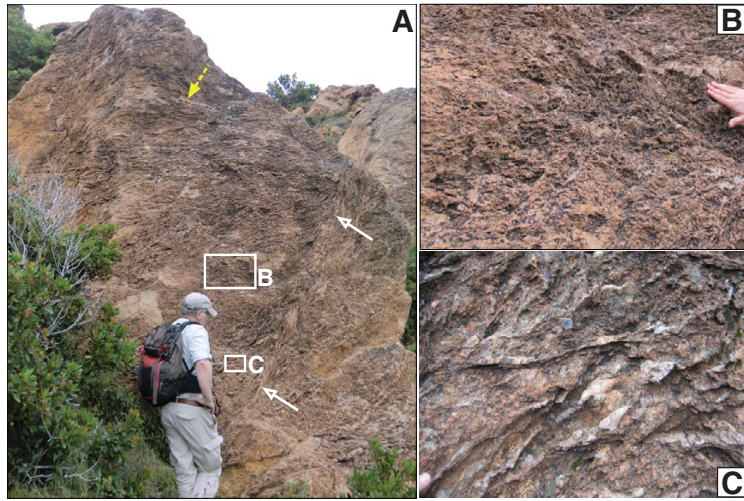


Figure 1. View and sketch of south face of Cima di Gratera, Cape Corse, Corsica. Fossil crust–mantle boundary of Piemont-Liguria ocean basin (yellow line) is preserved along distance of ~2.5 km. Best-preserved pseudotachyrites (PST) in peridotite are found at locality 2; for details see Figures 2 and 3. All visited outcrops have large volumes of ultramafic PST. Inset maps show location (left) and view with local geology (from Ravna et al., 2010). *P*—pressure; *T*—temperature.

\*E-mail: [t.b.andersen@geo.uio.no](mailto:t.b.andersen@geo.uio.no).

Downloaded from [geology.gsapubs.org](http://geology.gsapubs.org) on April 25, 2014



**Figure 2. A:** View toward northeast of main melt vein complex with >6-m-thick damage zone in peridotite at locality 2 (Fig. 1). Cliff face constitutes net veined, sponge-like breccia with dominantly subparallel, but mutually crosscutting, ultramafic pseudotachylyte (PST) veins dipping gently to left. PST veins and pockets form positive topography on weathered surface. Some veins coalesce into massive injection veins, to 15 cm thick (at dotted arrow). Vein complex is truncated by later steeply (~60°) dipping fault also decorated by PST (2–4-cm-wide fault veins at arrows). Main vein complex is without obvious temporal vein hierarchy. **B:** Detail showing intensity of sponge-like net veining with >50% melt. Positive surface features are mostly formed by hair-thin to centimeter-wide melt accumulations and PST matrix also without obvious sequence of emplacement. Lichen-covered (darker) negative surface features are disintegrating host-peridotite fragments. Note thicker veins to 8 cm wide above hand and lack of later faults cutting vein complex. This part of vein complex formed by only one event. **C:** Detail of glassy bifurcating and coalescing net veins making positive topography on weathered surface with ~40% melt (fingertip on extreme lower left for scale). With exception of late steep fault seen in A, there is no suggestion that this vein complex was formed by multiple, distinctly time separated and crosscutting events, as would be the case if fault vein complex was formed by number of individual fault episodes.

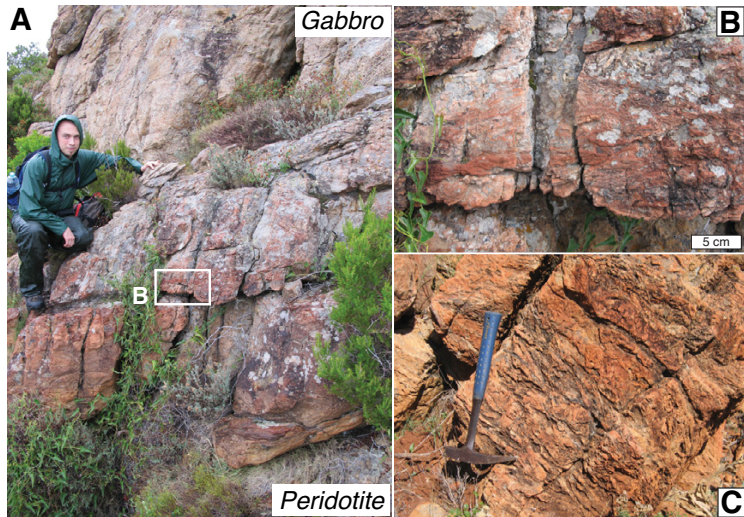


**Figure 3. Moho fault. A:** Close up of fault at locality 2. Gabbro-peridotite contact is sharp (at person's left hand). Both lithologies have pseudotachylytes (PSTs). Damage zone in peridotite is >2 m wide (limited by outcrop) and consists mostly of PST as intensely net veined material with as much as 80% melt as shown in the detail of A in B. **B:** Detail of A. **C:** Detail from Moho fault damage zone at locality 1 showing lack of vein hierarchy. PST thickness (>0.8 m) corresponding to ~2.4 tons of mantle melt per square meter fault surface occurred in single event. Hammer is 32 cm.

occurred along two main fault systems, a steep and a more gently dipping (~30°) set of faults parallel to the Moho fault zone (Andersen and Austrheim, 2006; Silkoset, 2013).

The PSTs are pristine in the least hydrated parts, and occur as relicts in areas with more hydration. Evidence for prograde dehydration of serpentinites near PST faults has not been observed (Deseta et al., 2014). The crust-mantle contact is mostly overprinted by ductile shearing at locality 1 (Fig. 1), but evidence for the former presence of PSTs is found as porphyroclasts in the mylonitic rocks along the contact (Fig. DR3 in the GSA Data Repository<sup>1</sup>). The PST veins increase in abundance at the paleo-Moho at localities 1 and 2. In the best preserved areas (locality 2) the upper ~6 m of the mantle consists of a PST network breccia, which may contain ~50% ultramafic PST (Fig. 2). The largest melt volumes form a dense network of mutually intruding veins (Figs. 2 and 3C; Figs. DR1a, DR1d, and DR1f in the Data Repository). Locally, this produces a breccia with a PST matrix without an obvious temporal hierarchy of individual veins (Figs. 2 and 3C). A number of minor faults with PST postdate the large vein breccia (Fig. 2; Fig. DR1). Other localities along the Moho have massive and thicker fault veins that may be >1 m in cumulative thickness (Fig. 3; Fig. DR1). These were formed by at most a few major ruptures succeeded by several minor events, as shown by reinjection of younger PST (Fig. DR2b). The fault veins and dense vein network constitute a several-meter-wide damage zone along the Moho fault. The distribution of PST along the fault zone varies considerably; there is an apparent maximum in areas where the vein network is thickest (locality 2). From the lateral thickness variation it is obvious that redistribution by flow of ultramafic melt along the fault took place after generation, but before complete solidification. The partial solidification, remobilization, and back veining are interpreted to have produced the sponge-like network where PST occupies space in veins and between fragments (Fig. 2; Fig. DR1). The network breccia in Figure 2 is >6 m thick, and is composed of as much as 50% ultramafic PST. It is truncated by several minor faults with PST, which also remelted older PST (Fig. DR2b). These faults may represent aftershocks succeeding the main earthquakes.

<sup>1</sup>GSA Data Repository item 2014145, Figure DR1 (photo documentation of macroscopic features of the PST along the Moho fault zone), Figure DR2 (microtextures and electron backscattered diffraction data from the Moho fault zone), and Figure DR3 (photo documentation showing remnants of PST veins along the Moho fault zone where it is overprinted by ductile blueschist facies deformation), is available online at [www.geosociety.org/pubs/ft2014.htm](http://www.geosociety.org/pubs/ft2014.htm), or on request from [editing@geosociety.org](mailto:editing@geosociety.org) or Documents Secretary, GSA, P.O. Box 9140, Boulder, CO 80301, USA.

Downloaded from [geology.gsapubs.org](http://geology.gsapubs.org) on April 25, 2014**MELT VOLUMES, ENERGY BUDGET, AND EARTHQUAKE MAGNITUDE**

Locality 2 provides excellent evidence that rapid release of energy accompanied by melting has intensely fractured the wall rocks. Wall-rock fragments and deformed xenocrysts were incorporated and progressively assimilated in the PST, producing domains of variable composition and banding at a millimeter scale (Deseta et al., 2014). Thin melt channels remained open and the bifurcating and coalescing network could effectively funnel cubic meters of melt from the generation zone in the fault core several meters into the wall rocks (Fig. 2). In order to transport PST melts several meters in thin channels and sheets, the melt must have had a low viscosity (Suzuki et al., 2001), or it would have solidified toward the wall rocks. The melts may have been superheated, even supercritical (Kanamori et al., 1998) during their explosive formation and drainage from the generation zone, in which case additional melt may have been produced within the vein complex during injection. The presence of a melt zone as much as 3 m thick (Fig. 2A) shows that as much as ~9500 kg of the peridotite may have melted per square meter of the fault plane.

Most of the net vein complex is without an obvious crosscutting vein hierarchy, and it is likely that most of it may have formed in just one major event. Even after careful examination it is difficult to ascertain if the thick breccia formed by a single or by a few major events, in addition to the many smaller ones described previously (e.g., Andersen et al., 2008; Deseta et al., 2014). There are some rootless, crosscutting injection veins in the main fault zone, suggesting that more than one major melting event took place (Fig. DR1a). Because veins of different generations have different weathering (Fig. DR1e) and textural characteristics (Fig. DR2), our interpretation is that the main melt zone (Figs. 2 and 3) may have formed by at most a few (2–3) large events and a number of associated aftershocks. In the calculation of earthquake magnitude we assume that most of the melt breccia with a cumulative melt thickness of as much as 3 m formed by a few large melt-generating events. It is not yet possible to quantitatively deduce more specifics about relative importance and magnitude of these large events.

Using standard values for heat capacity and heat of fusion for an olivine-rich peridotite (Weatherley and Katz, 2012), the release of energy must have been  $>1.9 \times 10^{10}$  J m<sup>-2</sup> along the fault plane in order to melt the observed volumes of ultramafic PST (Fig. 2A). Along strike the PST is more concentrated in thicker veins and the cumulative thickness is less, commonly 1–1.5 m (Fig. 3). We also observed smaller branching vein patterns with a three-dimensional star shape (Fig. DR1g); we interpret these to reflect local explosive production and injection

of melts on a smaller scale but similar to the thick sponge-like melt breccia described herein. Both structures demonstrate that melt volumes stored on generation surfaces are much smaller than the total volume generated, and that in most cases melt volumes will be underestimated.

In calculating earthquake magnitude we use mantle strength  $\Delta\sigma = 500$  MPa (Andersen et al., 2008; Obata and Karato, 1995), mantle density  $\rho = 3200$  kg m<sup>-3</sup>, heat capacity  $C_p = 1200$  J kg<sup>-1</sup> °C<sup>-1</sup>, temperature change  $\delta T = 1250$  °C (regional  $T$  of 420 °C to melting  $T$  of 1670 °C; Katz et al., 2003), and heat of fusion  $H = 5 \times 10^5$  J kg<sup>-1</sup> ( $C_p$  and  $H$ , Weatherley and Katz, 2012). We assume that >95% of the total energy of the earthquake is dissipated as heat (McGarr, 1999). It is possible to make an estimate of the shear strain ( $\gamma - d/h$ , where  $d$  is displacement and  $h$  is thickness of fault core) if we assume that a single earthquake produced the melt. From the equation for 100% melting:

$$\Delta\sigma = \rho(C_p \delta T + H)\gamma^{-1}, \quad (1)$$

(e.g., Di Toro et al., 2005), we obtain  $\gamma \approx 12.8$ . Provided that the movement took place across a 1.5-m-wide slip zone, as indicated by massive PST fault veins, cogenetic fault vein ladder networks, and breccias (Sibson, 1977) (Fig. 3), the displacement along the Moho fault may have been >19 m. If this was a single slip event, the earthquake must have had a moment magnitude ( $M_w$ ) of ~8. Generation by 2–3 successive large events would reduce the displacement for the individual earthquakes by as much as 1/3, which still suggest displacements of >6 m displacement and magnitude ~7.5 earthquakes.

**DISCUSSION**

The rupture length associated with the largest magnitude estimates may have been as much as several hundred kilometers (e.g., Bonilla et al., 1984), and so the fossil earthquakes in Corsica may have affected a large part of the early Alpine subduction zone and been effective almost on a basin scale in the relatively small Piemont-Liguria oceanic basin (Handy et al., 2010). Therefore, the subduction earthquakes exposed in Corsica may have been cogenetic with the deeper HP-LT coseismic events described from the western Alps (Angiboust et al., 2012).

A point of contention concerning intermediate-depth earthquakes is the weakening mechanism for the seismic events. The main hypothesis used to explain the weakening (Rice, 2006) involves high pore-fluid pressures (Green and Houston, 1995; Kirby, 1996). Fluid pressure reduces effective stress and may cause failure and a runaway stress drop of the system. High fluid pressures in this model are nourished by prograde metamorphic dehydration of subducted sediments and serpentinized mantle (Hacker et al., 2003). There may also be a close

link between metamorphism and seismicity in subduction zones (Rondenay et al., 2008). Our initial work in Corsica was strongly influenced by the dehydration embrittlement hypothesis, but we found no mineralogical or textural evidence suggesting that prerupture dehydration reactions occurred in the fault zones (Austreheim and Andersen, 2004), and formation of secondary anhydrous minerals produced by dehydration of serpentine, talc, clinocllore, or amphiboles in the gabbro and peridotite has not been observed. Secondary anhydrous minerals within the PST veins are very common, but it is the shear heating, melting, and crystallization, and not prograde metamorphism, that formed them.

Consequently, alternative weakening mechanisms have been explored based on textural and mineralogical evidence. Localized ductile precursors to the faulting along smaller faults from Corsica have been described by Deseta et al. (2014). Evidence for viscous precursor deformation has also been documented by dislocation slip systems in olivine (Silkose, 2013). The deformation studied by electron backscatter diffraction analyses (Fig. DR3d) is characteristic of intermediate to high water contents and high stresses (200–340 MPa in experiments at ~1250 °C, type E, by Jung et al., 2006). We therefore infer shear heating as the most likely weakening mechanism (Kelemen and Hirth, 2007). Viscous dissipation of heat resulted in thermal runaway and earthquake faulting. Theoretical investigations (Braeck and Podladchikov, 2007) and numerical simulations (John et al., 2009) of thermal runaway show that it requires lower differential stresses than frictional faulting at the ambient conditions of intermediate and deep earthquakes in the absence of a free fluid. A recent seismological study of 253 intermediate-depth earthquakes recorded in the Andean subduction zone also support the suggestions that such earthquakes are triggered by a thermal runaway mechanism rather than by brittle faulting (Prieto et al., 2013).

**CONCLUSIONS**

The observations presented here show that at most a few very large earthquakes produced a thick PST melt zone along the crust-mantle boundary of the Piemont-Liguria basin during the Alpine subduction. The commonly used mechanism for explaining subduction earthquakes is embrittlement by dehydration of seawater-altered rocks (e.g., Green and Houston, 1995). Our current and previous work provides no evidence for prerupture prograde metamorphic dehydration, and we therefore support previous interpretations (John et al., 2009; Kelemen and Hirth, 2007) that shear heating was the most likely weakening mechanism for large subduction earthquakes in the HP-LT metamorphic rocks in Corsica.

Downloaded from [geology.gsapubs.org](http://geology.gsapubs.org) on April 25, 2014

## ACKNOWLEDGMENTS

Constructive reviews by A. Vitale Brovarone, M. Steltenpohl, and an anonymous reviewer are greatly acknowledged. We also acknowledge the South African National Research Foundation (NRF) for grants to Ashwal, and the Mellon Foundation for support to Deseta. The Norwegian Research Council Centre of Excellence [grants 223272 to CEED and PGP] funded this work.

## REFERENCES CITED

- Andersen, T.B., and Austrheim, H., 2006, Fossil earthquakes recorded by pseudotachylytes in mantle peridotite from the Alpine subduction complex of Corsica: *Earth and Planetary Science Letters*, v. 242, p. 58–72, doi:10.1016/j.epsl.2005.11.058.
- Andersen, T.B., Mair, K., Austrheim, H., Podladchikov, Y.Y., and Vrijmoed, J.C., 2008, Stress release in exhumed intermediate and deep earthquakes determined from ultramafic pseudotachylyte: *Geology*, v. 36, p. 995–998, doi:10.1130/G25230A.1.
- Angiboust, S., Agard, P., Yamato, P., and Raimbourg, H., 2012, Eclogite breccias in a subducted ophiolite. A record of intermediate-depth earthquakes?: *Geology*, v. 40, p. 707–710, doi:10.1130/G32925.1.
- Austrheim, H., and Andersen, T.B., 2004, Pseudotachylytes from Corsica: Fossil earthquakes from a subduction complex: *Terra Nova*, v. 16, p. 193–197, doi:10.1111/j.1365-3121.2004.00551.x.
- Austrheim, H., and Boundy, T.M., 1994, Pseudotachylytes generated during seismic faulting and eclogitization of the deep crust: *Science*, v. 265, p. 82–83, doi:10.1126/science.265.5168.82.
- Bjørnerud, M.G., Austrheim, H., and Lund, M.G., 2002, Processes leading to eclogitization (densification) of subducted and tectonically buried crust: *Journal of Geophysical Research*, v. 107, no. B10, p. 1–18, doi:10.1029/2001JB000527.
- Bonilla, M.G., Mark, R.K., and Lienkaemper, J.J., 1984, Statistical relations among earthquake magnitude, surface rupture length and surface fault displacement: U.S. Geological Survey Open-File Report 84–256, 46 p.
- Braeck, S., and Podladchikov, Y.Y., 2007, Spontaneous thermal runaway as an ultimate failure mechanism of materials: *Physical Review Letters*, v. 98, doi:10.1103/PhysRevLett.98.095504.
- Deseta, N., Andersen, T.B., and Ashwal, L.D., 2014, A weakening mechanism for intermediate-depth seismicity? Detailed petrographic and microtextural observations from blueschist facies pseudotachylytes, Cape Corse, Corsica: *Tectonophysics*, v. 610, p. 138–149, doi:10.1016/j.tecto.2013.11.007.
- Di Toro, G., Pennacchioni, G., and Teza, G., 2005, Can pseudotachylytes be used to infer earthquake source parameters? An example of limitations on the study of exhumed faults: *Tectonophysics*, v. 402, p. 3–20, doi:10.1016/j.tecto.2004.10.014.
- Frohlich, C., 2006, *Deep earthquakes*: Cambridge, UK, Cambridge University Press, 573 p.
- Green, H.W., and Houston, H., 1995, The mechanics of deep earthquakes: *Annual Review of Earth and Planetary Sciences*, v. 23, p. 169–213, doi:10.1146/annurev.earth.23.050195.001125.
- Hacker, B.R., Peacock, S.M., Abers, G.A., and Hollaway, S.D., 2003, Subduction factory: 2. Are intermediate-depth earthquakes in subducting slabs linked to metamorphic dehydration reactions: *Journal of Geophysical Research*, v. 108, p. 1–8, doi:10.1029/2001JB001129.
- Handy, M.R., Schmid, S.M., Bousquet, R., Kissling, E., and Bernoulli, D., 2010, Reconciling plate-tectonic reconstructions of Alpine Tethys with the geological-geophysical record of spreading and subduction in the Alps: *Earth-Science Reviews*, v. 102, p. 121–158, doi:10.1016/j.earscirev.2010.06.002.
- John, T., and Schenk, V., 2006, Interrelations between intermediate-depth earthquakes and fluid flow within subducting oceanic plates: Constraints from eclogite facies pseudotachylytes: *Geology*, v. 34, p. 557–560, doi:10.1130/G22411.1.
- John, T., Medvedev, S., Rüpke, L.H., Andersen, T.B., Podladchikov, Y.Y., and Austrheim, H., 2009, Generation of intermediate-depth earthquakes by self-localizing thermal runaway: *Nature Geoscience*, v. 2, p. 137–140, doi:10.1038/ngeo419.
- Jung, H., Katayama, I., Jiang, Z., Hirago, T., and Karato, S.I., 2006, Effect of water and stress on the lattice-preferred orientation of olivine: *Tectonophysics*, v. 421, p. 1–22, doi:10.1016/j.tecto.2006.02.011.
- Kanamori, H., Anderson, D.L., and Heaton, T.H., 1998, Frictional melting during the rupture of the 1994 Bolivian earthquake: *Science*, v. 279, p. 839–842, doi:10.1126/science.279.5352.839.
- Katz, R.F., Spiegelman, M., and Langmuir, C.H., 2003, A new parameterization of hydrous mantle melting: *Geochemistry Geophysics Geosystems*, v. 4, p. 1–19, doi:10.1029/2002GC000433.
- Kelemen, P.B., and Hirth, G., 2007, A periodic shear-heating mechanism for intermediate-depth earthquakes in the mantle: *Nature*, v. 446, p. 787–790, doi:10.1038/nature05717.
- Kirby, S.H., 1996, Intermediate-depth intraslab earthquakes and arc volcanism as physical expressions of crustal and uppermost mantle metamorphism in subducting slabs, *in* Bebout, G.E., et al., eds., *Subduction top to bottom*: American Geophysical Union Geophysical Monograph 96, p. 195–213, doi:10.1029/GM096p0195.
- McGarr, A., 1999, On relating apparent stress to the stress causing earthquake fault slip: *Journal of Geophysical Research*, v. 104, p. 3003–3012, doi:10.1029/1998JB900083.
- Obata, M., and Karato, S.I., 1995, Ultramafic pseudotachylyte from the Balmuccia peridotite, Ivrea-Verbano zone, northern Italy: *Tectonophysics*, v. 242, p. 313–328, doi:10.1016/0040-1951(94)00228-2.
- Prieto, G.A., Florez, M., Barrett, S.A., Beroza, G.C., Pedraza, P., Blanco, J.F., and Poveda, E., 2013, Seismic evidence for thermal runaway during intermediate-depth earthquake rupture: *Geophysical Research Letters*, v. 40, p. 1–5, doi:10.1002/2013GL058109.
- Ravna, E.J.K., Andersen, T.B., Jolivet, L., and Capitani, C., 2010, Cold subduction and the formation of lawsonite eclogites—Constraints from prograde evolution of eclogitized pillow lava from Corsica: *Journal of Metamorphic Geology*, v. 28, p. 381–395, doi:10.1111/j.1525-1314.2010.00870.x.
- Rice, J.R., 2006, Heating and weakening of faults during earthquake slip: *Journal of Geophysical Research*, v. 111, B05311, doi:10.1029/2005JB004006.
- Rondenay, S., Abers, G.A., and van Keken, P.E., 2008, Seismic imaging of subduction zone metamorphism: *Geology*, v. 36, p. 275–278, doi:10.1130/G24112A.1.
- Sibson, R.H., 1977, Fault rocks and fault mechanisms: *Geological Society of London Journal*, v. 133, p. 191–213, doi:10.1144/gsjgs.133.3.0191.
- Sibson, R.H., and Toy, V.G., 2006, The habitat of fault-generated pseudotachylyte: Presence vs. absence of friction-melts, *in* Abercrombie, R., et al., eds., *Earthquakes: Radiated energy and the physics of faulting*: American Geophysical Union Geophysical Monograph 170, p. 153–166, doi:10.1029/170GM16.
- Silkoset, P., 2013, *Microtexture of ultramafic pseudotachylyte fault veins from Corsica, an SEM-EBSD analysis* [M.S. thesis]: Oslo, University of Oslo, 196 p.
- Spray, J.G., 1995, Pseudotachylyte controversy: Fact or friction?: *Geology*, v. 23, p. 1119–1122, doi:10.1130/0091-7613(1995)023<1119:PCF>2.3.CO;2.
- Suzuki, A., Ohtani, E., Urakawa, S., Terasaki, H., and Kato, T., 2001, Viscosity of komatiite magma at high pressure: Bayerisches Forschungsinstitut für Experimentelle Geochemie und Geophysik, Universität Bayreuth Annual Report, v. 2001, p. 105.
- Vitale Brovarone, A., Groppo, C., Hetenyi, G., Compagnoni, R., and Malavieille, J., 2011a, Coexistence of lawsonite-eclogite and blueschist: Phase equilibria modeling of Alpine Corsica metabasalts and petrological evolution of subduction slabs: *Journal of Metamorphic Geology*, v. 29, p. 583–600, doi:10.1111/j.1525-1314.2011.00931.x.
- Vitale Brovarone, A., Beltrando, M., Malavieille, J., Giuntoli, F., Tondella, E., Groppo, C., Beysac, O., and Compagnoni, R., 2011b, Inherited ocean-continent transition zones in deeply subducted terranes: Insights from Alpine Corsica: *Lithos*, v. 124, p. 273–290, doi:10.1016/j.lithos.2011.02.013.
- Vitale Brovarone, A., Beysac, O., Malavieille, J., Molli, G., Beltrando, M., and Compagnoni, R., 2013, Stacking and metamorphism of continuous segments of subducted lithosphere in a high-pressure wedge: The example of Alpine Corsica (France): *Earth-Science Reviews*, v. 116, p. 35–56, doi:10.1016/j.earscirev.2012.10.003.
- Weatherley, S.M., and Katz, R.F., 2012, Melting and channelized magmatic flow in chemically heterogeneous, upwelling mantle: *Geochemistry Geophysics Geosystems*, v. 13, p. 1–23, doi:10.1029/2011GC003989.

Manuscript received 29 November 2013

Revised manuscript received 14 January 2014

Manuscript accepted 17 February 2014

Printed in USA



ELSEVIER

Tectonophysics 285 (1998) 333–351

TECTONOPHYSICS

## Extensional tectonics in the Caledonides of southern Norway, an overview

Torgeir B. Andersen \*

*Institutt for Geologi, Universitetet i Oslo, P.O. Box 1047, Blindern, N-0316 Oslo, Norway*

Received 24 October 1995; accepted 30 July 1996

### Abstract

The extensional collapse of the Scandinavian Caledonides resulted in rapid tectonic denudation of the orogen, exhumation of high- and ultra-high-pressure metamorphic rocks and provided a structural template for the formation of Devonian supra-detachment sedimentary basins. The geometry and intensity of the extensional deformation show considerable variation vertically in the crustal section as well as horizontally from east to west across the orogen. The most prominent structural feature related to the extension in central-south Norway is the change in the direction of tectonic transport, from the easterly directed nappe translation during the Silurian Scandian Orogeny, to top-westerly directed sense of shear during the extension. The Fennoscandian basement was little affected by extension in the eastern Caledonides. In the west, however, top-to-the-west shear zones are commonly observed in basement windows. Deformation affecting the Cambrian to Late Silurian rocks in the Caledonian foreland developed a typical of foreland fold and thrust belt geometry. Deformation in the foreland was apparently contemporaneous with the extension-related decompression of the high-pressure rocks in the hinterland. Thrusting in the foreland may thus have been driven by gravitational collapse, and as such have important similarities to the foreland–hinterland relationships of the Himalayan–Tibetan region. The basal contacts of the Jotun and other major nappes constitute prominent shear zones in which fabrics related to thrusting have been mostly destroyed by extensional shearing. The high structural levels of the Western Gneiss Region, adjacent to the western margin of the Jotun Nappe, were only moderately affected by the extensional deformation. Consequently, the Proterozoic orthogneiss complexes are generally well preserved in this area. The westernmost and structurally lowermost parts of the Western Gneiss Region have, however, been subjected to extreme overburden during the Caledonian continental collision. Initial, near-isothermal decompression of the high-pressure rocks occurred by non-rotational vertical shortening–horizontal stretching at eclogite- to amphibolite-facies conditions; at a later stage, decompression and cooling from amphibolite to greenschist facies occurred by rotational deformation associated with the large-scale extensional detachments. The initial extensional deformation in the hanging wall of the detachments in western Norway commenced at greenschist-facies conditions, and became progressively more brittle and localised as the complexes were exhumed in the Late Silurian to Middle Devonian. Major syn-depositional normal faults in the hanging wall of the extensional detachments eventually controlled sedimentation in the Devonian supra-detachment basins. © 1998 Elsevier Science B.V. All rights reserved.

*Keywords:* extension; eclogites; exhumation; Caledonides; Norway

\* Tel.: +47 (22) 856-664; Fax: +47 (22) 854-215; E-mail: t.b.andersen@geologi.uio.no

## 1. Introduction

The lower Palaeozoic Caledonian mountain belt in Scandinavia is one of the classical terrains in the study of orogenic products and processes. From the trace of the Tornquist line in the North Sea to the Trollfjord–Komagelv Fault on the Porsanger Peninsula in the northeast, the Scandinavian Caledonides form an approximately 2000-km-long curvilinear belt, broadly comparable in length to the Himalayan mountain belt between the eastern and western syntaxes (Fig. 1). The lower Palaeozoic plate reconstruction, summarised by Torsvik et al. (1996), shows that the Scandinavian Caledonides were facing the similar-sized East Greenland Caledonides after the collision between Laurentia and

Baltica. The preserved width of the Caledonides on-shore south Norway and eastern Greenland is approximately 500 km and 350 km, respectively. In addition large parts of the hinterland of the orogen occur on the attenuated basement of the shelf areas and continental crust fragments within the North Atlantic (Skogseid, 1994). Although lacking precise Late Silurian palaeogeographical reconstruction, it is clear that the Caledonides of the North Atlantic region including the submerged hinterland regions of the shelves areas, constituted a very large mountain belt similar in size to the present Himalayan–Tibetan region from the frontal thrust in the south to the Tarim basin in the north.

In spite of the widespread extensional deformation affecting the thickened crust in the hinterland of

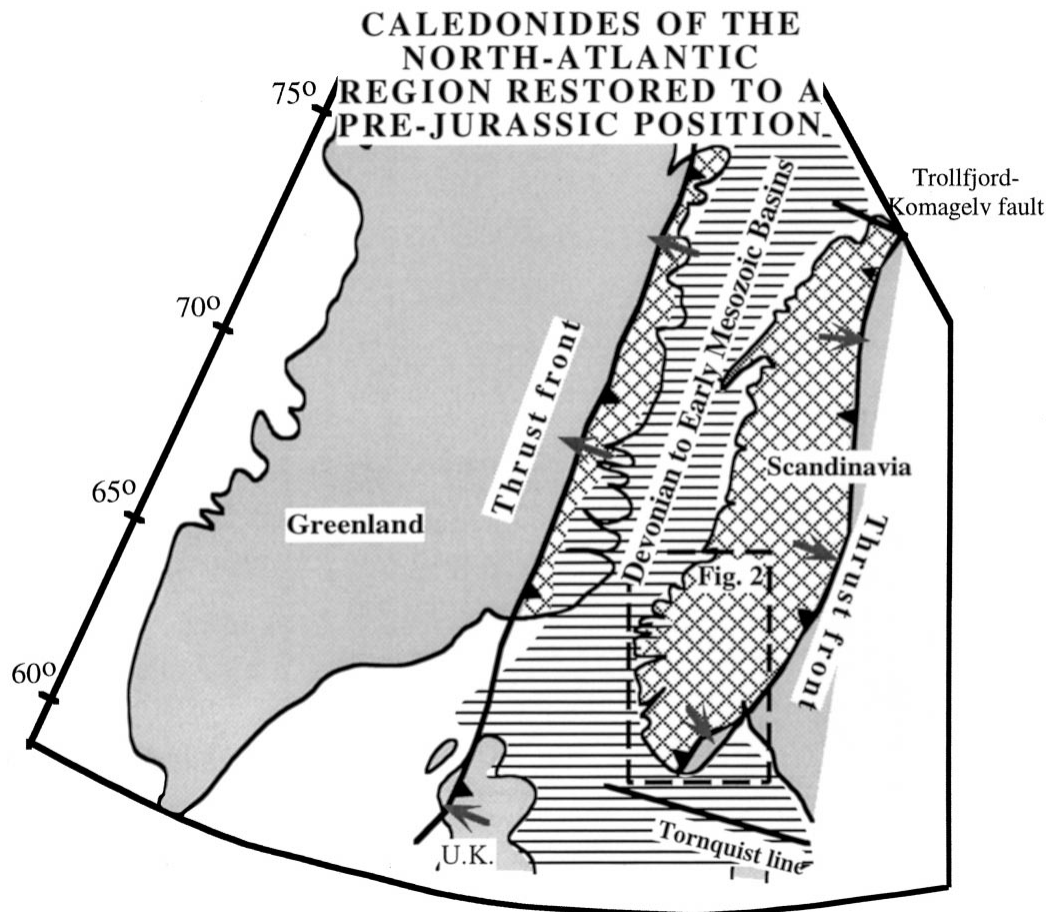


Fig. 1. Pre-Jurassic reconstruction (modified after Skogseid, 1994) of the Caledonides (square pattern) in the North Atlantic region. The map shows location of the study area in southern Norway. Note that the shelf areas and major parts of the onshore regions have been subjected to pre-Jurassic extension.

the mountain chain during the extensional collapse and throughout the late Palaeozoic, the Caledonides of the North Atlantic region essentially remained a positive topographic element throughout the late Palaeozoic and early Mesozoic (Ziegler, 1988).

Historically, the Scandinavian Caledonides have been particularly important because of the spectacular development of thin, far-travelled and aerial very extensive thrust nappes. Although the product of a polyphase orogenic development, it is generally agreed that the present 'layer-cake' tectonostratigraphy (Roberts and Gee, 1985) was finally assembled and emplaced onto the Fennoscandian Shield basement and cover rocks during the continental collision between Baltica and Laurentia in the middle to Late Silurian referred to as the Scandian phase of the Caledonian Orogeny. Extensional structures in southern Norway are primarily identified by a general reversal in polarity of deformation. The Scandian contraction was associated with south-east-directed structures and nappe transport, whereas the extension is generally characterised by west and northwesterly directed structures thinning the nappe stack. The ductile to brittle extensional structures were superimposed on the tectonostratigraphy established during the Scandian phase (Fig. 2), comprising five main units (Roberts and Gee, 1985):

(1) The *Autochthon–Parautochthon* consist of the Fennoscandian Shield basement and the sedimentary cover of Neoproterozoic and early Palaeozoic age.

(2) The *Lower Allochthon* consists mainly of low-grade sedimentary sequences of Neoproterozoic to early Palaeozoic age and some Fennoscandian Shield basement rocks are involved in the thrust sheets.

(3) The *Middle Allochthon* is dominated by large crystalline nappe complexes and thick psammitic sequences, locally overlain by Vendian to lower Palaeozoic metasediments.

(4) The *Upper Allochthon* contains mainly ophiolites and island-arc complexes and some parts which are believed to have constituted the transitional continental–oceanic crust segments of the rifted margin of Baltica.

(5) The *Uppermost Allochthon* is present only in northern Norway and will not be discussed further here.

Since Bjørlykke's and Hossack's suggestions (Bjørlykke, 1983; Hossack, 1984) that large-scale

listric normal faults controlled formation of the Devonian basins in western Norway, considerable attention has been paid to the late- to post-orogenic extensional modification of the orogen in Scandinavia. Structures formed at various upper to lower crustal levels related to the extensional collapse have been identified in several on-shore cross-sectional traverses along-strike of the orogen (e.g., Norton, 1986; Séranne and Séguret, 1987; Andersen and Jamtveit, 1990; Fossen, 1992; Rykkelid and Andresen, 1994). The late- to post-orogenic extension in southern Norway resulted in penetrative reworking and decompression of Caledonian high-pressure metamorphic rocks, formation of large extensional detachments and the Devonian supra-detachment basins (Andersen et al., 1994; Osmundsen, 1996; Osmundsen et al., 1998). Similarly, exhumed Caledonian high-pressure rocks (Gilotti, 1994), extensional detachments and associated Devonian basin formation have recently been identified in the East Greenland Caledonides (Strachan, 1994; Hartz and Andresen, 1995; Andresen and Hartz, 1998), documenting a belt-wide late- to post-orogenic extension of the North Atlantic Caledonides. This paper attempts a review of the geometry, regional distribution and relative age of the extensional structures across the south Norwegian Caledonides.

## 2. Extensional domains and structures in south Norway

Papers presenting original data on the extensional tectonics in the Scandinavian Caledonides have focused mostly on characterising structural geometries in restricted areas and/or structural levels, or they have attempted to present large-scale conceptual tectonic models. Comprehensive documentation of the post-orogenic extension in southern Norway has so far only been published from the Bergen–Hardanger (Fossen, 1992) and the Sogn–Nordfjord regions (Chauvet and Séranne, 1989; Dewey et al., 1993; Andersen et al., 1994; Osmundsen, 1996). The extensional structures in the eastern part of the section (Fig. 3) are less well studied. The interpretation from eastern Norway relies on reconnaissance observations by the present author, but mostly on published maps (Sigmond et al., 1984; Nilsen and Wolf, 1989), short papers and abstracts

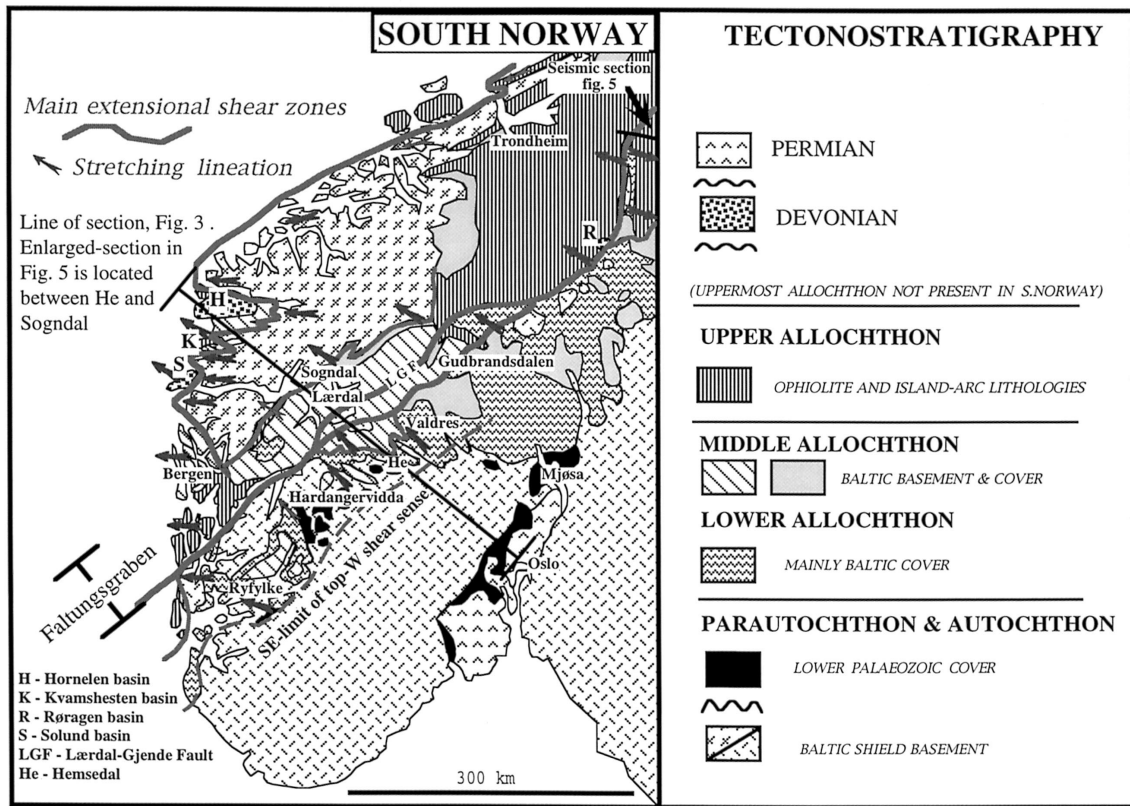


Fig. 2. Simplified map of the Caledonian tectono-stratigraphy in southern Norway. The main extensional shear zones, extension direction (lineation) and faults are shown schematically. Notice locations of profiles, Figs. 3–5.

from the Trondheim–Östersund transect (Sjöström and Bergman, 1989, 1994; Sjöström et al., 1991) and observations adjacent to the Røragen Devonian basin (Norton, 1987; Gee et al., 1994).

The first identification of large-scale late/post-Caledonian structures affecting the nappe stack of southern Norway was by Goldschmidt (1912) who identified a major NE–SW-trending synformal depression in central south Norway (Figs. 2 and 3) which he called the ‘Faltungsg Graben’. This structure has later been referred to as the Lærdal–Gjende/Hardangerfjord Fault Zone (Andersen et al., 1991) or the Hardangerfjord Shear Zone (Fossen, 1992). In the following Goldschmidt’s original term, Faltungsg Graben, is retained because the lineament is characterised by both folding and faulting. As will become apparent from the descriptions below, the Faltungsg Graben is a relatively late structure in the post-Caledonian structural modification. East of the Faltungsg Graben, the Caledonian structure is characterised by relatively thin, dominantly sub-horizontal basement/cover nappes. On the eastern flank of the Faltungsg Graben, Fennoscandian basement and cover as well as the nappes bend down into the NW-facing synformal depression along which structurally higher nappe units can be traced from the Hardanger–Ryfylke area in the south to the Trondheim area in the north (Fig. 2). The western flank of the Faltungsg Graben is defined by the east-dipping contact zone between the Caledonian nappes and the structurally underlying Western Gneiss Region (Fig. 3).

### 2.1. Extensional structures east of the Faltungsg Graben

The easternmost parts of the Caledonides in southern Norway are the foreland fold and thrust belt preserved within the upper Palaeozoic Oslo Graben (Bockelie and Nystuen, 1985; Morley, 1986a) and in the lower allochthon of the Valdres–Gudbrandsdalen (Hossack et al., 1985) and Hardangervidda areas (Andresen, 1982). The foreland is structurally characterised by imbricate fans (Oslo area) and duplexes (Valdres) developed above a sole thrust in the Cambrian to Ordovician alum–shales. The sole thrust probably terminates as a blind thrust, largely masked by the Permian batholiths, in the southern parts of

the Oslo Graben (Bockelie and Nystuen, 1985; Morley, 1986a). Morley (1986b) calculated some 135 km of accumulated shortening from the thrust front to the Mjøsa area. The youngest rocks affected by the Caledonian SE-directed thrusting in the foreland are Late Silurian (Pridoli) fluvial sandstones. According to a recent calibration of the time scale by Tucker and McKerrow (1995) the base of the Devonian is at 417 Ma. Hence the post-depositional thrusting of Late Silurian sediments in the foreland was most likely contemporaneous with the initial extension-related decompression of high-pressure rocks in the hinterland and therefore relevant for the late orogenic extension of the orogen (Andersen et al., 1991; Andersen, 1993). With the exception of minor pop-up structures and associated SE-dipping reverse faults there is, however, no published evidence of major top-west shearing or extensional reactivation along the decollement surface in the alum–shale sequence in the Oslo region. If present at all, obvious Basin and Range type ‘breakaway zones’ (Wernicke, 1992) for top-to-the-west extension has not been identified in the Scandinavian Caledonides (Figs. 2 and 3).

In the northern part of SE Norway, the Trondheim region and along the Swedish–Norwegian border, several authors have shown that the thrust-related basal decollement ramps up from deeper structures involving the Fennoscandian basement (e.g., Gee et al., 1985). An interpretation, based on semi-quantitative cross-sectional balancing (Morley, 1986b) and on seismic reflection profiles (Hurich and Kristoffersen, 1988; Hurich et al., 1989; Palm et al., 1991), indicate that the basement windows and culminations east of Faltungsg Graben (Fig. 2) are allochthonous and entirely related to thrusting.

Work by Sjöström and Bergman (1989, 1994), however, demonstrates that the basement windows are exposed not merely as a result of contractional antiformal stacking (Hurich and Kristoffersen, 1988; Gee et al., 1994), but also as a result of inhomogeneous vertical shortening and horizontal extension of the nappe stack. The earliest structures thinning the nappe complexes in the structural level along the lower and middle allochthon boundary are described by Sjöström and Bergman (1994) from the Trondheim–Östersund transect. These authors state that the nappes were thinned initially by non-coaxial flow, related to east-dipping, top-to-the-southeast

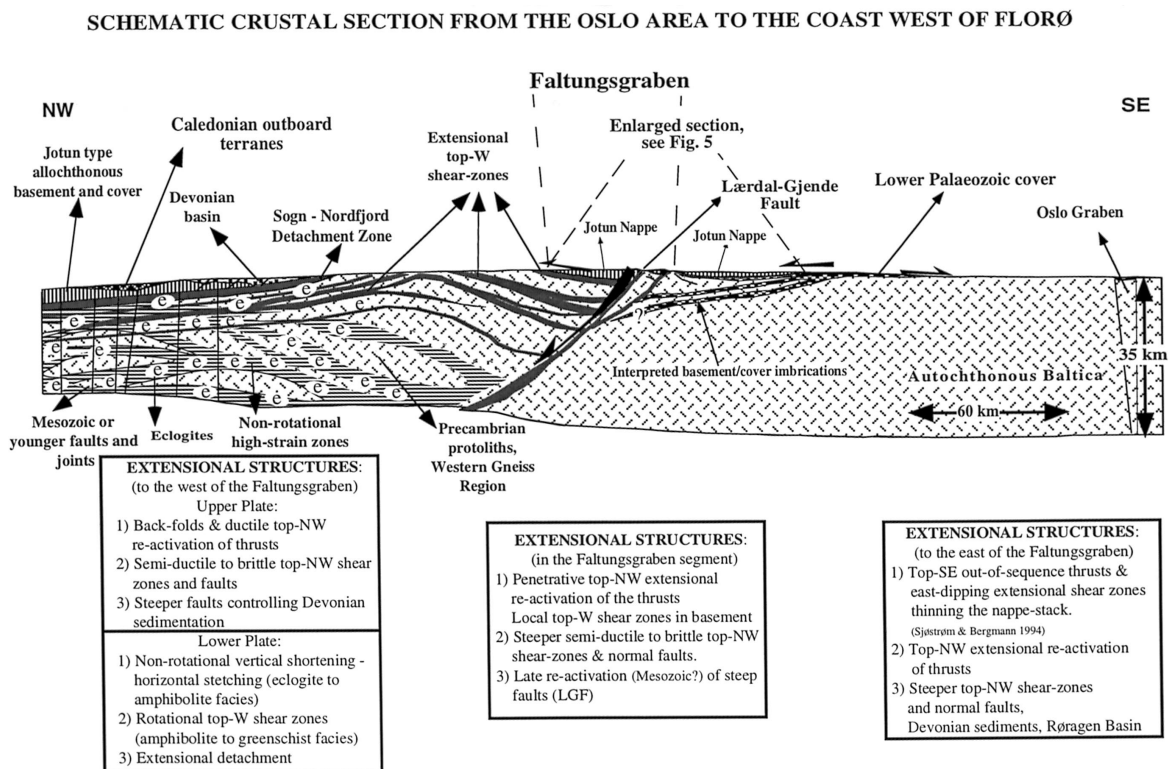


Fig. 3. Southeast–northwest profile across south Norway. The profile has been constructed from available geological maps, geophysical profiles and recent field observations. The text boxes give summaries of the extensional structures to the east, west and within the Faltungsgaben segment. Notice horizontal/vertical scale  $\sim 1/2$ . See text for discussion.

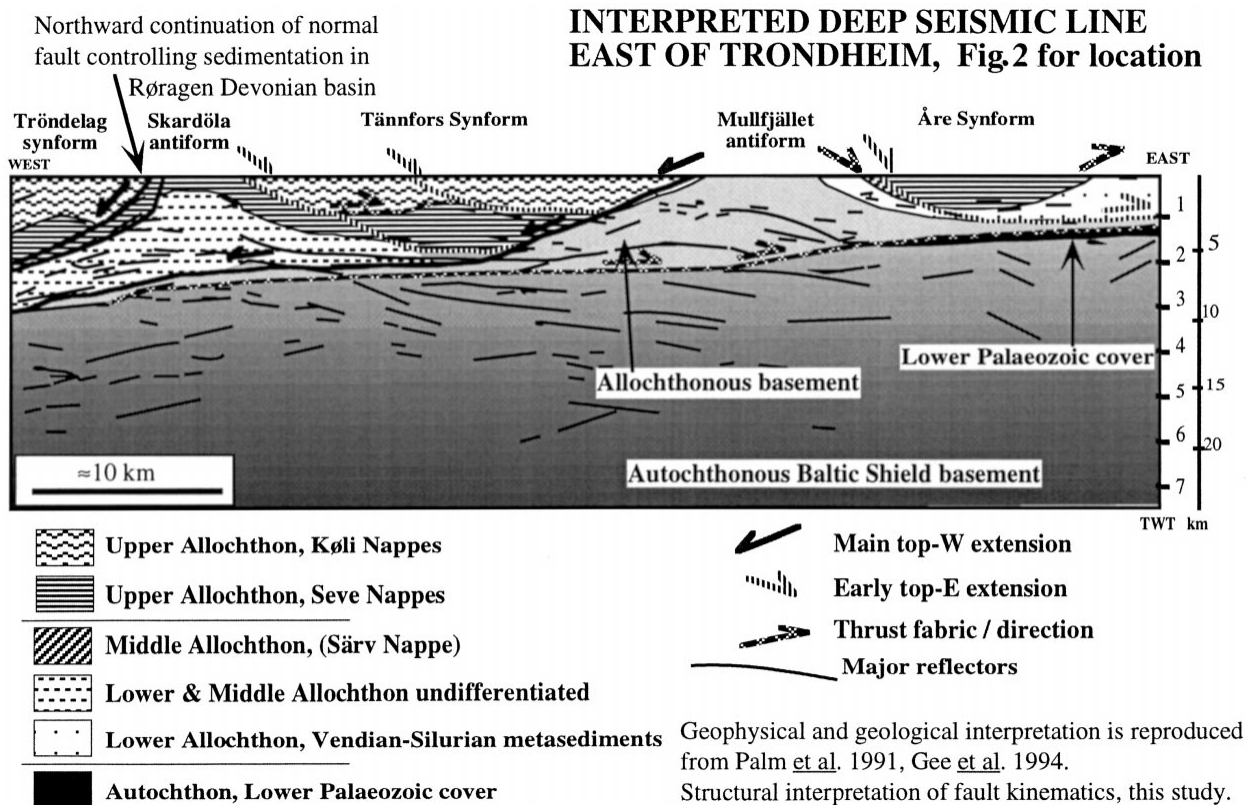


Fig. 4. Line drawing interpretation of deep-seismic reflection profile in the Swedish–Norwegian border zone east of Trondheim (see Fig. 2). The profile is reproduced from Hurich *et al.* (1989) and Palm *et al.* (1991). Interpretation of the tectono-stratigraphic units is after Palm *et al.* (1991) and Gee *et al.* (1994). The kinematic interpretation of the faults (shown by arrows) is drawn by the present author and is based on interpretations by Sjöström *et al.* (1991) and the structural geometry.

extensional shear zones on the southeast flanks of the basement culminations (Fig. 4). Displacement on these shear zones produced large-scale, extension-related synforms with higher tectonic units (Middle and Upper Allochthon) preserved in their hanging walls (Fig. 4). The east-dipping shear zones affected composite nappe units, thus demonstrating their younger relative age with respect to the true contractional structures (Sjöström and Bergman, 1994). Sjöström and Bergman (1994) concluded that ductile, out of sequence top-east shear zones near and east of the Swedish–Norwegian border in Trøndelag (see Fig. 4) were related to gravitational thinning of the nappe pile, and hence substantiate earlier suggestions (Andersen *et al.*, 1991; Andersen, 1993; Dewey *et al.*, 1993) that thrusting of the Lower Allochthon and development of the foreland fold and thrust belt may have been related to gravitational spreading of the orogenic belt.

Sjöström and Bergman (1989, 1994) have further shown that the top-east-directed extension was succeeded by large-scale, top-to-the-west, west-dipping normal faults and shear zones comparable to the Røragen Detachment (Norton, 1987). The kinematics of these faults and shear zones are documented by fabric studies (Norton, 1987; Sjöström and Bergman, 1989, 1994; Sjöström *et al.*, 1991), and the extensional geometries are obvious on the seismic profile (Fig. 4).

Fig. 4 reproduced here is based on the published seismic reflection profile (Hurich *et al.*, 1989; Palm *et al.*, 1991), with geological interpretation from the same authors, and clearly indicates the extensional geometries. If the interpretation is correct, it is difficult to envisage how the sole thrust may have been active as a top-to-the-east contractional structure along its entire E–W length at the same time as the upper units were thinned by top-to-the-west extensional shear zones and faults as suggested by

Gee (1988) and Gee et al. (1994). The surface expression of the normal faults eventually controlled formation and sedimentation in the Devonian Røragen basin (Fig. 2). Several NE–SW-trending shear and fault zones previously interpreted as thrusts have been mapped northeast of the Jotun Nappe (Sigmond et al., 1984; Nilsen and Wolf, 1989). These faults have not, to the present author's knowledge, been studied recently and no fabric analyses are presently available. The map pattern (Nilsen and Wolf, 1989) showing juxtaposition of lower structural units with higher structural units in foot and hanging walls, respectively, indicate that these structures are normal faults. It is suggested that they form part of a system co-genetic with the Lærdal–Gjende Fault (see below), and hence represent a late expression of the extensional collapse east of the Faltungsgaben in southern Norway.

Structures related to crustal extension east of the Faltungsgaben lineament include the following.

(1) Foreland-dipping shear zones recording top-to-the-SE-directed displacement (Fig. 4). These structures thinned the nappe stack at greenschist-facies conditions, and are probably contemporaneous with decollement thrusting in the foreland.

(2) Reversal in polarity of deformation, with major top-to-the-NW movement along most of the previous thrust contacts (Figs. 3 and 5). A well defined breakaway zone for the top-W deformation has not been identified, but if present it is located southeast of the leading edge of the major crystalline nappes of the Hardanger–Ryfylke and Jotun Nappe Complexes (Fig. 2).

(3) Hinterland-dipping, semi-ductile to brittle shear and fault zones with large (several km) displacements. Some of these structures are responsible for the exposed basement windows/culminations by footwall uplift. The surface expression of these faults controlled formation and deposition in Devonian Røragen basin (Fig. 2).

As mentioned above, the Caledonian structure to the east of the Faltungsgaben in south-central Norway (Hardangervidda to Valdres) is characterised by relatively thin nappes belonging to the Lower and Middle Allochthon, overlying a thin autochthonous to para-autochthonous sedimentary cover and the Fennoscandian basement (Andresen and Færseth, 1982; Bryhni and Sturt, 1985; Milnes and Koestler,

1985). Kinematic indicators indicative of back-thrusting on the main tectonic contacts of the basement and cover nappes show that top-west reactivation occurred at greenschist-facies conditions (Milnes and Koestler, 1985). Recent observations by the present author and co-workers (Gathe and Andersen, 1996) show that the fabrics related to inferred (Milnes and Koestler, 1985) SE-directed thrusting is obliterated along the base of the Jotun Nappe in the Hemsedal area (Figs. 2 and 5). The structure and texture of the rocks in the basal shear zone of the Jotun Nappe are characterised by kinematic indicators and stretching lineations indicative of intense WNW-directed non-coaxial flow at greenschist-facies conditions. The entire structural thickness of the micaceous metagreywackes and phyllites of the cover on Hardangervidda as far east as exposures are available on the Haukelisetter transect, is dominated by NW-vergent folds and associated foreland-dipping crenulation cleavage around NE–SW-trending fold and crenulation axes (Andresen, 1982; Haremo, 1987). Similar observations have been made in the Valdres area, although the contractional duplexes are preserved in the SE part of the Valdres section (Milnes and Koestler, 1985).

A model for the back folds and the associated crenulation cleavage was suggested by Osmundsen (1990) based on studies of the upper plate in Sunnfjord. Top-to-the-west reactivation of the main thrust contacts resulted in an inverted strain field from bulk vertical stretching/horizontal shortening to vertical shortening/horizontal stretching. The extensional deformation was partitioned along the plastic instabilities defined by major thrust zones and low shear strength tectono-stratigraphic units. In these shear zones previous hinterland-dipping planes of flattening (main foliation) related to thrusting were positioned in the field of shortening and hence folded during initial top-west rotational deformation (Osmundsen and Andersen, 1994). Fossen (1992) used a similar model to explain the west- and northwest-vergent folds and referred to the initial ductile top-W reactivation as Mode I extension.

## 2.2. Extensional structures in, and along the Faltungsgaben lineament

The Faltungsgaben is a complex large-scale synformal structure formed by NW-vergent folding as

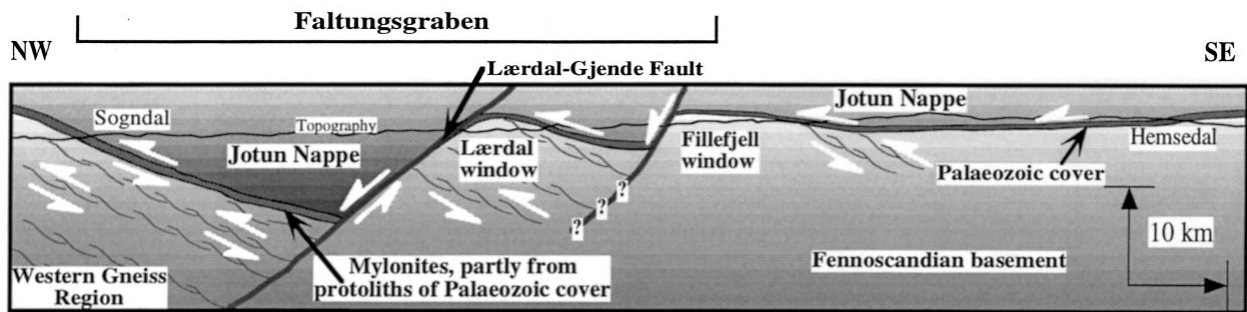


Fig. 5. Geological profile across the Faltungsgruben lineament in south-central Norway (for location see Figs. 2 and 3). The top-west, reactivation of the thrusts obliterated most of the thrust fabrics and the thickness of the Jotun Nappe was strongly modified by the extension. Notice the footwall uplift which exposes the Fillefjell and Lærdal basement windows. Notice also that ductile, top-west shear zones are present and become increasingly common towards the west in the basement and basement windows. Basement shear zones that can be related to Caledonian shortening have not been observed in this section.

well as later semi-ductile to brittle top-W shear zones and normal faults. Some of the faults along the Faltungsgruben lineament have probably been reactivated at a very late stage as indicated by the presence of unconsolidated fault rocks and half-graben geometries imaged on coast-parallel deep-seismic, offshore profiles (Hurich and Kristoffersen, 1988; Færseth et al., 1995). As described above the initial vertical shortening of the nappe stack recognised in the Swedish–Norwegian border area occurred by a top-to-the-SE, out of sequence (with respect to thrust stacking) shear zones, thinning the nappes by gravitational movements in a direction synthetic with the thrusting. Similar top-to-the-SE foreland-dipping shear zones have, however, not been identified in central SE Norway.

The SE-directed movements were succeeded by the reversal in polarity of deformation, and the main tectonic contacts were reactivated as extensional top-west shear zones (Fig. 5). As pointed out above, the fabrics related to the reversal in polarity of deformation are very common. These structures have been described in detail by Fossen (1992) across the Faltungsgruben lineament from its eastern and western limb in the Hardanger–Bergen area. Recent observations along the transect across from Hemsedal to Sogndal in central-south Norway by the present author confirms Fossen's structural observations (Fossen, 1992) of NW-directed movements on all the major tectonic contacts. The SE-dipping, western flank of the Faltungsgruben, where the nappes make contact with the rocks of the Western Gneiss Region, has been studied in two sections near Sogndal

(Fig. 2). Both sections are characterised by several hundred metres thick packages of mylonites in which top-NW to WNW kinematic indicators dominate the fabric. Near Sogndal (Fig. 2), the quality of the exposures along the new road sections on the Sogndal–Fjærland highway, allows good relative dating of the various structural elements and kinematic indicators. Systematic observations show that the structural history is complicated; locally remnants of top-to-the-SE probably related to the thrusting of the Jotun Nappe have been preserved. The mylonites are, however, dominated by fabrics formed by top-to-the-NW non-coaxial deformation. In addition, a set of late top-to-the-SE kinematic indicators, post-dating the dominant top-NW shear fabric, has been observed. The late top-to-the-E structures are mostly represented by spaced SE-directed normal-slip crenulations and shear bands, and occur in narrow zones (<10 m), confined to phyllonites and talc-schists. It is suggested that the late top-E fabric records gravitational sliding down-dip into the central trough of the Faltungsgruben on horizons of low shear strength.

Within the core of the Faltungsgruben, the dominant late extensional structures are NE–SW-trending semi-ductile to brittle normal faults (Mode II extension by Fossen, 1992). These post-date the extensional top-W reactivation of the thrusts, and are clearly younger than some newly discovered ductile top-NW shear zones that occur within the basement culmination in the footwall of these faults (Gathe and Andersen, 1996). The best example of the faults is the Lærdal–Gjende Fault, which is represented by a thick zone (up to 200 m Milnes

and Koestler, 1985) of cataclastic deformation affecting earlier extensional mylonites in its footwall and Jotun Nappe orthogneisses in its hanging wall (Fig. 5). At Lærdal, the footwall comprises an approximately 200-m-thick zone of top-NW mylonites, phyllonites and ultramylonites, parts of which have protoliths in the Caledonian cover beneath the Jotun Nappe. Late movements on the Lærdal–Gjende Fault are indicated by unconsolidated breccias and gauges along its fault plane. The breccias and fault gauge are presently undated. Attempts to date the breccias by palaeomagnetic method and by low-temperature thermo-chronological methods are in progress.

The Lærdal–Gjende Fault is clearly an important structure in controlling the change in the interpreted thickness of the Jotun Nappe from a few hundred metres in its footwall to several kilometres in its hanging wall (Fig. 5) also indicated by gravity modelling by Smithson et al. (1974). The southwestward continuation of the Faltungsgaben has been described in detail by Fossen (1992). Its offshore continuation has been imaged on the coast-parallel ‘Mobil Search’ deep-seismic profiles, where the late normal movements are demonstrated by the occurrences of late Palaeozoic/early Mesozoic (?) half-grabens in its hanging wall (Hurich and Kristoffersen, 1988; Færseth et al., 1995).

### 2.3. Extensional structures in western Norway

The late- to post-orogenic extension in western Norway has been studied and described in a number of theses and publications since the late 1980s. Traditionally, the exhumation of high-pressure rocks in western Norway was attributed to erosional processes combined with thrust tectonics (Cuthbert et al., 1983). One of the most remarkable features of the geology in western Norway is the juxtaposition of late Caledonian eclogites in the footwall (age ~400–420 Ma, pressure 15 to >30 kbar), with Lower and Middle Devonian sedimentary rocks (~390 Ma) in the hanging wall across the Nordfjord–Sogn Detachment. A major difference in the extensional fabrics between western, central and eastern S Norway is the degree with which the Fennoscandian basement is involved in the extensional deformation. To the east of the Faltungsgaben the basement has, as far as one knows, not been significantly affected by ex-

tensional deformation. On the eastern flank of the Faltungsgaben the basement has been locally affected, mostly adjacent to the basal thrust zone of the nappes (Fossen, 1992). Along the core of the Faltungsgaben, basement rocks from deeper levels exposed in the footwall of late normal faults are mylonitised in top-W shear zones of up to 150–200 m structural thickness (see also Fig. 5). The rocks of the Western Gneiss Region along the western flank of the Faltungsgaben are strongly affected by the late Caledonian extensional deformation in a zone down to a few hundred metres below the basement–cover contact. At deeper structural levels the extensional fabrics become increasingly abundant and intense as one approaches the detachments (Milnes et al., 1988). In western Norway, however, deformation related to the extensional decompression of the Fennoscandian basement lithologies within the Western Gneiss Region is pervasive (e.g., Andersen and Jamtveit, 1990; Dewey et al., 1993; Andersen et al., 1994).

The significance of the Nordfjord–Sogn Detachment was initially recognised by Norton (1986, 1987). The contrast in late Caledonian regional metamorphism between the upper (low grade) and lower plate (eclogite facies) of the detachment requires omission of a minimum of 35 to 40 km crustal section in the Sunnfjord area (Andersen and Jamtveit, 1990) and more than 50 km in the Nordfjord area from the Late Silurian (~420 to 425 Ma) to the Lower Devonian (~390 to 400 Ma). The period of time (20 to 35 Ma) during which this dramatic reduction in crustal thickness took place is estimated on the basis of previously published geochronological data from the Western Gneiss Region (see compilation by Kullerud et al., 1986; Wilks and Cuthbert, 1994) and by  $^{40}\text{Ar}/^{39}\text{Ar}$  mineral cooling ages (Berry et al., 1993, 1995) from the lower and upper plate of the detachment (Fig. 6).

Below, a summary of the structures related to the decompression and sub-horizontal extension of the lower as well as the upper plate lithologies is described. For details and documentation refer to the original papers (cf. Norton, 1986; Séranne and Séguret, 1987; Chauvet and Séranne, 1989), and papers by the present author and co-workers (see references).

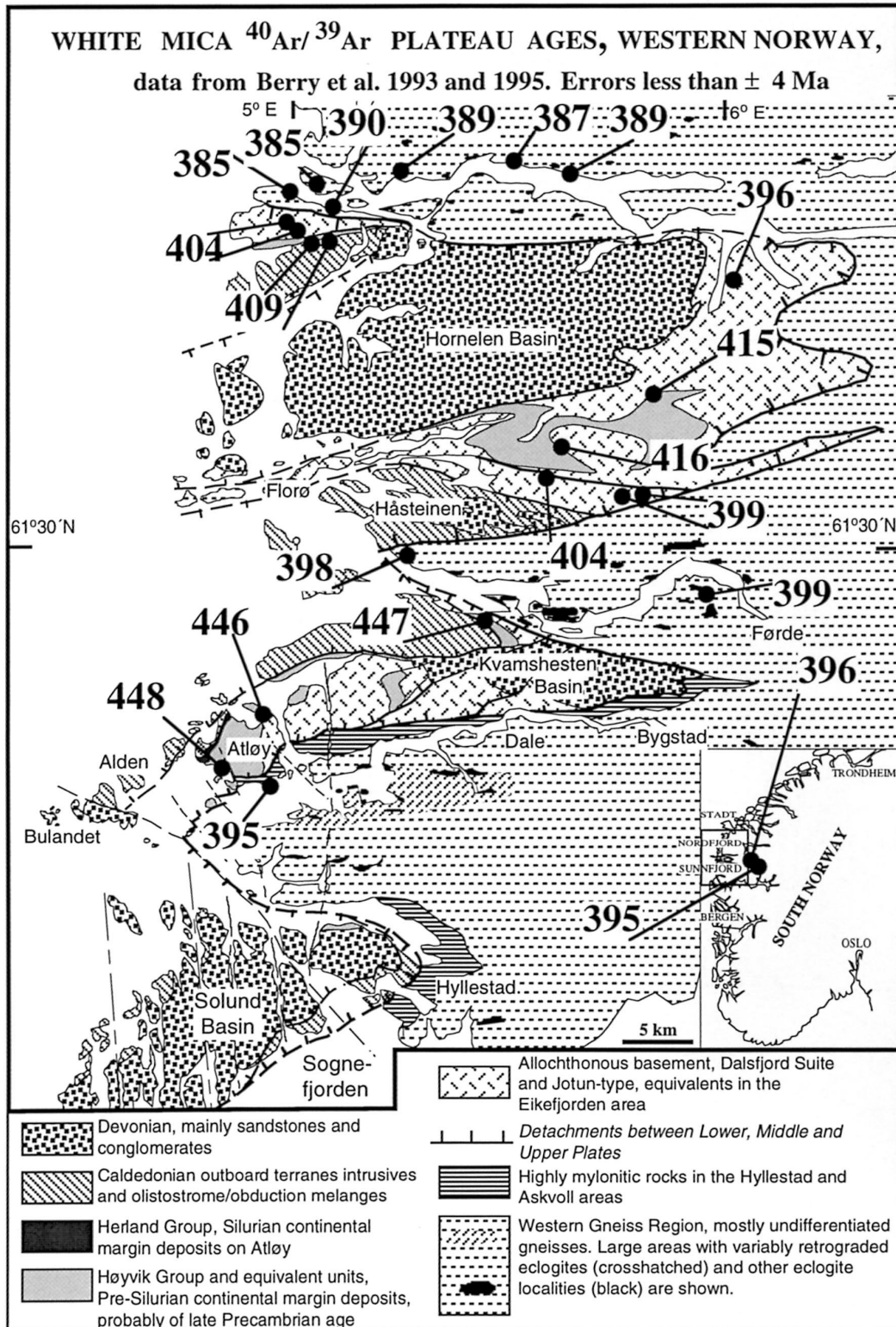


Fig. 6. Geological map of western Norway (after Andersen et al., 1994). The white mica, conventional  $^{40}\text{Ar}/^{39}\text{Ar}$  cooling ages are from Berry et al. (1993, 1995). All ages presented are well defined plateau ages. Comprehensive descriptions and interpretations of the Ar-geochronology will be presented elsewhere (Andersen et al., 1998) and work in progress).

### 2.3.1. Extensional decompression of the lower plate

A model suggesting that the initial extensional decompression of the hinterland eclogites in the Western Gneiss Region occurred contemporaneously with contractional tectonics in the foreland was put forward by Andersen et al. (1991). The principal structures and fabrics in the exhumed deep-crustal rocks that have been related to the decompression of the lower plate rocks are: (1) by coaxial vertical shortening/horizontal stretching at eclogite- to amphibolite-facies conditions; and (2) by non-coaxial deformation related to extensional detachments and shear zones at amphibolite- to greenschist-facies conditions.

*Coaxial decompression fabrics in the exhumed deep-crust of the lower plate.* Because of the complete sections from the lower to the upper part of the syn-orogenic crust that are available in western Norway, it has been possible to suggest models, based on field observations, of how the extensional collapse in the hinterland of the orogen may have been accommodated at various structural levels of the syn-orogenic crust. During the initial stages of the decompression (Stage 1) the lower crust was apparently shortened vertically and stretched horizontally (Andersen et al., 1994). The structures related to this event are represented by eclogite- to amphibolite-facies coaxial fabrics (Andersen et al., 1994; Engvik, 1994; Dransfield, 1994). These fabrics are present in the interior and around well preserved to variously retrograded eclogites. The coaxial fabrics apparently dominate the structure of the gneisses structurally below the detachment mylonites in the Sunnfjord and Nordfjord areas (Andersen et al., 1994; Dransfield, 1994). Detailed studies of the structures associated with the initial decompression of the eclogites suggest an overall coaxial strain regime. Associated hydro-fracturing and segregation of fluid-rich granitic leucosomes by partial melting locally altered the rheology and enhanced the deformation in the zones where they were formed/introduced. Abundant extensional quartz veins emplaced normal to the stretching and parallel to shortening directions at various stages of the deformation, indicate that the orientation of the principal strain axes remained constant during Stage 1 decompression (Andersen et al., 1994). Temperature–pressure estimates

from the Sunnfjord area (Krogh, 1980; Andersen and Jamtveit, 1990; Engvik, 1994) from eclogite-facies ( $T \approx 550\text{--}600^\circ\text{C}$ ,  $P_{\min} \approx 16$  kbar, age  $\sim 415$  Ma) to amphibolite-facies conditions ( $T \approx 600^\circ\text{C}$ ,  $P \approx 10$  kbar, age  $\sim 400\text{--}405$  Ma) during Stage 1 corresponds to a near-isothermal removal of overburden of at least 20 km, corresponding to a denudation rate of 1.5 mm/year or more.

### *Rotational deformation related to the detachments.*

The second major event (Stage 2) related to the decompression of the high-pressure rocks in the lower plate rocks in the Western Gneiss Region is represented by formation of amphibolite- to greenschist-facies non-coaxial mylonites of the extensional detachments. The fabrics of the detachment mylonites formed by rotational deformation with consistent top-to-the-west displacement will not be described in detail here. The top-W sense of shear is documented by a variety of kinematic indicators which have been described in several theses and papers previously (cf. Norton, 1986, 1987; Chauvet and Séranne, 1989; Swensson and Andersen, 1991; Hveding, 1992; Wilks and Cuthbert, 1994).

Although impossible to measure accurately, Hveding (1992) estimated shear strains of more than 20 (detailed fabric analyses) in the Nordfjord–Sogn Detachment mylonites in Sunnfjord. The semi-ductile late shear bands which are ubiquitously present in the detachment zone where not included in Hveding's strain analyses (Hveding, 1992). This implies that the normal displacement related to the mylonitisation on the 2.5-km-thick detachment zone probably was greatly in excess of 40 km. Furthermore, the brittle movements represented by cataclastites and breccias, and more than 10 km of normal displacement after deposition of the Kvamshesten Devonian basin must be added to the total displacement (Osmundsen, 1996; Osmundsen et al., 1998). Hence, the minimum normal displacement of the Nordfjord–Sogn Detachment in the Sunnfjord area is considerably more than 50 km. Together with the coaxial vertical shortening of more than 50% (Dewey et al., 1993) related to the fabrics of Stage 1, more than 50 km of normal displacement on the Nordfjord–Sogn Detachment zone dipping at a moderate 20–30° during the initial movements, is sufficient to explain exhumation of the high-pressure lower crustal rocks

by extensional tectonics and footwall uplift even without major erosional denudation. The present dip of the detachment is approximately  $12^{\circ}$  to  $15^{\circ}$  (Osmundsen, 1996) measured along the axis of the late E–W-trending folds that post-date the Devonian basins and their substrate (see below).

A regional study of  $^{40}\text{Ar}/^{39}\text{Ar}$  mineral cooling ages from muscovite in the Western Gneiss Region of the Sunnfjord and Nordfjord areas apparently gives consistent results on the local and regional scale and demonstrates significant diachronous cooling in the lower plate (Fig. 6). The lower-temperature ( $\sim 600^{\circ}\text{C}$ ) eclogite-bearing rocks in the Sogn–Sunnfjord region cooled below Ar-retention in muscovite at  $\sim 398 \pm 3$  Ma, whereas the high-temperature ( $\sim 700^{\circ}\text{C}$ ) eclogite terrain in Nordfjord cooled at  $\sim 389 \pm 3$  Ma (Berry et al., 1993, 1995). It is suggested that the diachronous cooling with younger muscovite ages in Nordfjord compared to those in Sunnfjord, is a function of the higher pressures and consequently original deeper burial, of the rocks in Nordfjord.

### 2.3.2. Extensional structures in the upper plate

The most important result of the extensional deformation in the upper plate of the Nordfjord–Sogn Detachment is the formation of the Devonian supra-detachment sedimentary basins (see below). In addition a number of post-Caledonian extensional and contractional structures have been identified and systematically studied. These include: (1) top-west-directed major and small-scale ductile shear zones; (2) west-vergent folds; (3) semi-ductile to brittle normal and transtensional faults; (4) large-scale upright to weakly overturned east–west-trending folds affecting the entire tectono-stratigraphy in the Sogn–Sunnfjord region; and finally (5) high-angle faults and fractures that off-set all previous structures, including the Nordfjord–Sogn Detachment. The geology of the hanging wall of the Nordfjord–Sogn Detachment has been described in detail by Osmundsen (1996) and Osmundsen and Andersen (1994).

$^{40}\text{Ar}/^{39}\text{Ar}$  mineral ages of muscovite from rocks in the upper plate of the Nordfjord–Sogn Detachment (Fig. 6) demonstrate polyphase cooling and crystallisation events. The pre-Silurian rocks were affected by an early Caledonian, pre-Scandian event (muscovite ages 445–450 Ma in the Atløy area;

Fig. 6) as well as Scandian and post-Scandian recrystallisation/cooling of 410 Ma to 420 Ma (Fig. 6).

The lack of equilibration and resetting of the Ar-system in muscovite is a result of variable but generally low-grade regional metamorphism in the upper plate during the Scandian event (Andersen et al., 1998). Consequently, rocks that were little affected by Scandian deformation have retained the pre-Scandian cooling ages, whereas deformation and new growth of muscovite in zones affected by Scandian and post-Scandian give younger ages. The  $^{40}\text{Ar}/^{39}\text{Ar}$  muscovite ages from Berry et al. (1993, 1995) are in accordance with previously interpretations (Andersen et al., 1990; Osmundsen and Andersen, 1994) that demonstrated the polyphase nature of both contractional and extensional deformation in the upper plate and suggested that a middle plate was present between the Hornelen and Nordfjord–Sogn Detachments (Andersen and Jamtveit, 1990).

*Ductile to brittle extensional structure in the substrate of the Devonian basins.* The shear zones (1), west-vergent folds (2) and faults (3) apparently represent a continuous ductile to semi-brittle mode of deformation related to a bulk vertical shortening and E–W extension of the thickened crust. The origin of the top-W reactivated shear zones and the mechanisms for the formation of the west-vergent folds have been discussed above. These correspond to the Mode I extension of Fossen (1992). The later brittle normal and transtensional faults (3) transect composite tectonic units and record progressive extensional deformation during exhumation of the Caledonian nappes of the upper plate, prior to and during deposition of the Lower (Solund) to Middle Devonian (Kvamshesten and Hornelen) basins (Osmundsen, 1996).

### 2.3.3. Devonian supra-detachment basins

The Devonian basins exposed in western Norway (Fig. 6) are supra-detachment basins situated in the hanging wall of the regional Nordfjord–Sogn Detachment. The basins display extraordinary stratigraphic thicknesses of mainly alluvial and fluvial sediments. Early models on basin formation (cf. Bryhni, 1964; Nilsen, 1968; Steel and Gloppen, 1980) were focused on the basin fill. After the recognition of the large-scale extensional detachment, models

for formation of the basins have principally emphasised the importance of the detachment as the major control on Devonian sedimentation (Hossack, 1984; Norton, 1986; Séranne and Séguret, 1987; Séguret et al., 1989). Clasts from the lower plate of the detachment have, however, not been identified within any of the basins (Cuthbert, 1991; Osmundsen, 1996; Osmundsen et al., 1998). Thus, the rocks of the lower plate of the detachment were probably not exhumed at the time of basin formation.

The Kvamshesten basin and its depositional substrate (Osmundsen and Andersen, 1994; Osmundsen et al., 1998) highlight the importance of intra-upper plate extensional and transcurrent faults prior to, as well as synchronous with Devonian sedimentation. The facies distribution within the basin is highly asymmetric, the locus of maximum subsidence has shifted with time from the northern to the southeastern margin, and syn-sedimentary faults controlled the migration of facies belts with time. The present detachment fault constituting the boundary between the upper and lower plate did not control sedimentation in the basin and represents post-depositional reactivation of the main detachment (Torsvik et al., 1992; Osmundsen, 1996). Detailed studies in the Kvamshesten basin (Osmundsen et al., 1998) show that the sedimentation was controlled by upper plate normal faults which were rooted in or cut by the detachment. Similar faults have been mapped along the basal unconformity of the Hornelen basin (Hartz, 1998). Andersen and Jamtveit (1990) suggested the presence of a detachment above the main Nordfjord–Sogn Detachment, separating the middle and upper crustal rocks, and controlling formation of the Hornelen basin. This interpretation has been substantiated by Wilks and Cuthbert (1994), and is also supported by older muscovite cooling ages in the middle plate between the Hornelen and Håsteinen basin, which previously has been considered to form part of the lower plate. The geometry and kinematics of normal and transtensional faults above the Nordfjord–Sogn Detachment are highly complex as described in some detail by Osmundsen (1996) and, consequently, the details of the fault-controlled sedimentation in the Devonian basins is similarly complex.

*East–west-trending folds.* The east–west-oriented dominantly upright folds in western Norway affect the entire crustal section including the decompressed high-pressure rocks of the Western Gneiss Region and the youngest Devonian sediments in the basins. It is, however, important to note that folds in both the upper and lower plates are truncated by the brittle reactivated detachment faults along the Kvamshesten and Hornelen basins. The folds record a phase of N–S-directed shortening. Various models have been suggested to explain the folding, but the exact cause of this folding is still uncertain. Hossack (1984) and Norton (1987) indicated that the syn- and antiforms defined by the detachment were related to primary corrugations of the detachment surface commonly observed in the Basin and Range Province. The folds in the upper plate were accommodation structures and thus syn-depositional with respect to the sedimentation in the Devonian basins. Chauvet and Séranne (1994) considered the folding to be syn-depositional and a result of external forces related to a re-arrangement of the relative plate movements after the Caledonian Orogeny and Hercynian tectonics to the south. The arguments for syn-depositional folding with respect to the Devonian basins were partly based on aerial photograph interpretations (Séranne, 1988) suggesting the presence of intra-basinal unconformities in the Hornelen and Kvamshesten basins. The unconformities have not been confirmed by later detailed ground mapping (Wilks and Cuthbert, 1994; Osmundsen, 1996). Based on comprehensive mapping of the Kvamshesten basin and its depositional and tectonic substrate, Osmundsen et al. (1998) interpreted the E–W-trending folds to record a stage of essentially post-depositional N–S shortening associated with constrictional deformation during E–W extension. The N–S shortening of the Devonian basins is apparently younger than the basin fill, and may be of Late Devonian age as suggested previously by the palaeomagnetic data (Torsvik et al., 1987). It is possible that this deformation may be related to a large-scale re-arrangement of the plate-motion configuration and external forces as suggested by Chauvet and Séranne (1994).

#### 2.3.4. Continued late Palaeozoic–early Mesozoic extension

Dating of fault rocks along the Nordfjord–Sogn Detachment (Torsvik et al., 1992) records Permian as well as Late Jurassic brittle movements on the detachment. In addition, two sets, NW–SE (older) and N–S (younger), of high-angle normal faults and extensional fractures are present (Osmundsen, 1996). Both off-set the Nordfjord–Sogn Detachment demonstrating that the rocks on-shore western Norway experienced late, sub-horizontal east–west-directed crustal stretching. Dolerites and rare lamprophyres (middle Permian) are locally present in the Sunnfjord area (Furnes et al., 1982; Torsvik et al., 1997) and one of these cross-cut the detachment. South of Bergen, Triassic (?) to Jurassic dolerites (K/Ar dating; Færseth et al., 1976) have been emplaced along the N–S-trending fractures system, hence a Mesozoic age is suggested for this system north of Bergen (Osmundsen and Andersen, 1994). Although the precise age of fault rocks along the Lærdal–Gjende and other normal faults along the Faltingsgraben lineament is presently unknown, it is tentatively suggested that their brittle reactivation represents the easternmost expression of the late Palaeozoic to Mesozoic extension on the S Norwegian mainland.

Work in progress on the adjacent offshore areas suggests that late Palaeozoic rifting constitutes an important event in the Horda Platform area, and that it was associated with development of half-grabens with shifting polarities (Christiansson et al., 1995). Furthermore, the magnitude of extension accommodated in the upper Palaeozoic–earliest Mesozoic far exceeds extension associated with the Late Jurassic rift phase. With exception of the Viking Graben area, the most significant phase of extension in the North Sea region is probably Devonian to late Palaeozoic in age. The magnitude of displacement accommodated by the detachment exposed onshore western Norway, strongly suggests that the offshore continuation of the detachment must have been a significant structural dislocation during Permian to early Mesozoic rifting in the northern North Sea area. Thus, the Devonian extensional fabrics were likely to form a structural template that was also important during subsequent extension.

### 3. Summary and conclusions

Because of extreme denudation, good accessibility and the quality of exposure of rocks from different crustal levels of the syn-orogenic crust, the Scandinavian Caledonides represents a unique natural laboratory to study the products of the tectonic processes associated with orogenic collision and extensional collapse of continental collision zones. The relationships between contractional and extensional deformation developed (e.g., Hodges et al., 1993) during the collision between India and Eurasia probably represents the best Cenozoic analogue to the Silurian continental collision between Baltica and Laurentia and its extensional modification.

The extensional structures in the south Norwegian Caledonides record the tectonic denudation of the Caledonian nappe pile which were assembled by polyphase lower Palaeozoic plate convergence. Because exhumed rocks in the metamorphic core complex of the Western Gneiss Region, record high- and ultra-high-pressure metamorphism (cf. Smith, 1984; Griffin, 1987; Jamtveit, 1987), it is suggested that the Caledonian Orogen developed extremely thick continental crust capable of stabilising coesite (Smith, 1984) and micro-diamonds (Dobrzynetskaia et al., 1995). Subduction of continental crust, however, requires pervasive eclogitization in order to maintain a reasonable topography above the thickened crust (Richardson and England, 1979; Dewey et al., 1993).

The earliest structures recording tectonic denudation of the nappe stack in southern Scandinavia may be assigned to internal forces within the over-thickened lithosphere of the orogen. The pressure–temperature estimates combined with geochronological data (Kullerud et al., 1986; Chauvet and Dallmeyer, 1992; Berry et al., 1993, 1995; Wilks and Cuthbert, 1994) indicate that decompression of the high- and ultra-high-pressure rocks in the Western Gneiss Region commenced in the Late Silurian (420 Ma) and that the lower plate rocks had cooled from their maximum temperatures of  $\sim 600^\circ$  to  $750^\circ\text{C}$  below the Ar-blocking temperature of muscovite ( $350 \pm 50^\circ\text{C}$ ) at  $390 \pm 10$  Ma. Structural observations (Andersen and Jamtveit, 1990; Andersen et al., 1994; Osmundsen and Andersen, 1994; Dransfield, 1994) suggest that the decompression of the deep-seated rocks initially was related to non-rotational verti-

cal shortening and horizontal stretching at depth and non-coaxial extensional shearing and normal faulting in the middle and upper parts of the thickened crust. These observations support an early model of lower crustal pure shear and upper crustal simple shear suggested by McClay et al. (1986) based on very limited field observations from western Norway and a comparison with the Basin and Range Province of the western USA. Traditional interpretations, that the eclogite-bearing rocks approached the surface by thrusting and erosion, are not supported by structural observations/fabric analyses in the Western Gneiss Region.

In the tectonically telescoped rocks of the miogeocline (Lower and Middle Allochthon) of the eastern part of the orogen, initial vertical thinning and unroofing apparently occurred by top-to-the-E, out-of-sequence extensional shear zones (Sjöström et al., 1991; Sjöström and Bergman, 1994). The eastward transport on foreland-dipping shear zones were rooted on the sole thrust, suggesting that final stages of decollement thrusting in the foreland may have been related to gravitational spreading of the orogen (Andersen et al., 1991; Andersen, 1993).

The mechanism which triggered the extensional deformation in the Caledonides can only be inferred by comparison with theoretical models and comparable regions with active tectonics. By analogy with models for orogenic extensional collapse (Dewey, 1988; England and Houseman, 1988; Platt and England, 1994), it is conceivable that hinterland uplift and decompression by top-east extensional shear zones in the telescoped miogeocline, may have been a consequence of thinning of the mantle lithosphere as previously suggested (Andersen and Jamtveit, 1990; Andersen et al., 1991). This process would have increased the syn-orogenic surface slope, and it could also have reduced the dip of the sole thrust in the eastern parts of the orogen. Both geometrical adjustments, combined with reduced rate of convergence, would favour gravitational spreading of the mountain belt (England and Houseman, 1988; Platt, 1993). After initial extension possibly related to gravitational spreading, belt-wide reversal in the polarity of deformation, from top-east to top-west, occurred in the Scandinavian Caledonides with exception of the thin-skinned foreland fold and thrust belt. Contemporaneous top-to-the-east exten-

sion characterised the East Greenland Caledonides (Hartz and Andresen, 1995; Andresen and Hartz, 1998). In the hinterland of the Caledonides in southern Norway, major top-to-the-west extension on the extensional detachments with heaves in the order of 50 to 100 km, in the Lower to Middle Devonian.

The surface expression of the extensional shearing was normal and transtensional faulting (Osmundsen, 1996), controlling formation of the Devonian supra-detachment basins. Previous models appealing to direct control of the sedimentation in the Old Red basins in western Norway by the main Nordfjord–Sogn Detachment (Séguret et al., 1989) do not explain the highly asymmetric facies distribution in the basins (Osmundsen et al., 1998) and the lack of eclogites or other high-pressure rocks with provenance in the lower plate within the basins (Cuthbert, 1991; Osmundsen, 1996).

Continued Devonian and later upper Palaeozoic extension of the Caledonian Orogen in the North Atlantic region may to a large extent have been controlled by a reorganisation of the plate-motion configuration in the area, from general plate convergence to divergence or transtension. Fossen (1992) argued that a wholesale reorganisation of plate motions was necessary to explain the belt-wide reversal in deformation polarity. Chauvet and Séranne (1994) related the change in tectonic regime in western Norway to external forces related to the Hercynian plate convergence to the south. Divergent plate motions separating Baltica and Laurentia during the late Palaeozoic are, however, too small to be detected within the uncertainties of palaeomagnetic analyses (Torsvik et al., 1996). Some plate divergence seems, however, highly probably in view of the very large extension that can be inferred from the hinterland in Scandinavia, Greenland and the respective continental shelves. Late, large-scale motions sub-parallel to the strike of the orogen, such as the presently active wrench faults in the Himalaya–Tibetan region (Brunel et al., 1995; Tapponnier et al., 1995; Searle, 1995) may have been important in accommodating divergence during the later stages of the deformation in the Scandinavian Caledonides (Séranne, 1992).

The hinterland regions of the Scandinavian and Greenland Caledonides have, since the main lithospheric thickening occurred in the Late Silurian, been a region characterised by extensional tectonics.

The extension of the Caledonides of the North Atlantic region and adjacent offshore areas may very well illustrate the long-term effect of orogenic extensional collapse as modelled by Platt and England (1994). Externally driven plate divergence and/or transtension was probably an important element in driving the extension after the Middle Devonian.

### Acknowledgements

This research has been financed by grants from the Norwegian Research Council. The author would like to thank Dr. Per-Terje Osmundsen and Prof. Arild Andresen for the many stimulating discussions and corrections. I am grateful for suggestions for improvement by Dr. Laurent Jolivet and Dr. Alan Chauvet whose very thorough review improved this paper.

### References

- Andersen, T.B., 1993. The role of extensional tectonics in the Caledonides of south Norway: Discussion. *J. Struct. Geol.* 15, 1379–1380.
- Andersen, T.B., Berry, H.N., Lux, D.R., Andresen, A., 1998. The tectonic significance of pre-Scandian  $^{40}\text{Ar}/^{39}\text{Ar}$  phengite cooling ages the Caledonides of western Norway. *J. Geol. Soc. London*, in press.
- Andersen, T.B., Jamtveit, B., 1990. Uplift of deep crust during orogenic extensional collapse: A model based on field studies in the Sogn–Sunnfjord region, W Norway. *Tectonics* 9, 1097–1111.
- Andersen, T.B., Jamtveit, B., Dewey, J.F., Swensson, E., 1991. Subduction and exhumation of continental crust; major mechanisms during continent–continent collision and orogenic extensional collapse. *Terra Nova* 3, 303–310.
- Andersen, T.B., Osmundsen, P.-T., Jolivet, L., 1994. Deep crustal fabrics and a model for the extensional collapse of the southwest Norwegian Caledonides. *J. Struct. Geol.* 16, 1191–1203.
- Andersen, T.B., Skjerve, K.P., Furnes, H., 1990. The Sunnfjord Melange, evidence of Silurian ophiolite accretion in the West Norwegian Caledonides. *J. Geol. Soc. London* 147, 59–68.
- Andresen, A., 1982. Stratigraphy and Structural History of the Lower Paleozoic Metasediments on Hardangervidda, South Norway. Ph.D. thesis. Univ. of California, 260 pp.
- Andresen, A., Førseth, R., 1982. An evolutionary model for the southwest Norwegian Caledonides. *Am. J. Sci.* 282, 756–782.
- Andresen, A., Hartz, E., 1998. A late orogenic extensional origin for the infracrustal gneiss domes of the East Greenland Caledonides (72°–74°N). *Tectonophysics*, this volume.
- Berry, H.N., Lux, D.R., Andresen, A., Andersen, T.B., 1993. Argon 40–39 dating of rapidly uplifted high-pressure rocks during late-orogenic extension in southwest Norway. (Abstr.) *Geol. Soc. Am., Annual Meeting, Boston*.
- Berry, H.N., Lux, D.R., Andresen, A., Andersen, T.B., 1995. Progressive exhumation during orogenic collapse as indicated by  $^{40}\text{Ar}/^{39}\text{Ar}$  cooling ages from different structural levels, southwest Norway. *Geologynytt* 1, 20–21.
- Bjørlykke, K., 1983. Subsidence and tectonics in late Precambrian and Palaeozoic sedimentary basins of southern Norway. *Nor. Geol. Unders. Bull.* 380, 159–172.
- Bockelie, J.F., Nystuen, J.P., 1985. The southeastern part of the Scandinavian Caledonides. In: Gee, D.G., Sturt, B.A. (Eds.), *The Caledonide Orogen: Scandinavia and Related Areas*. J. Wiley, Chichester, pp. 69–88.
- Brunel, M., Arnaud, N., Tapponnier, P., 1995. Kongur Shan normal fault: Type example of mountain building assisted by extension (Karakoram Fault, eastern Pamir). *Terra Nova*, Abstr. Vol. 7, 43.
- Bryhni, I., 1964. Migrating basins on the Old-Red continent. *Nature* 202, 284–285.
- Bryhni, I., Sturt, B.A., 1985. Caledonides of southwestern Norway. In: Gee, D.G., Sturt, B.A. (Eds.), *The Caledonide Orogen: Scandinavia and Related Areas*. J. Wiley, Chichester, pp. 89–107.
- Chauvet, A., Dallmeyer, R.D., 1992.  $^{40}\text{Ar}/^{39}\text{Ar}$  mineral dates related to Devonian extension in southeastern Scandinavian Caledonides. *Tectonophysics*, 210, 155–177.
- Chauvet, A., Séranne, M., 1989. Microtectonic evidence of Devonian extensional westward shearing in southwest Norway. In: Gayer, R.A. (Ed.), *The Caledonide Geology of Scandinavia*. Graham and Trotman, London, pp. 245–254.
- Chauvet, A., Séranne, M., 1994. Extension-parallel folding in the Scandinavian Caledonides: implications for late-orogenic processes. *Tectonophysics* 238, 31–54.
- Christiansson, P., Odinsen, T., Berge, A.M., Faleide, J.I., Gabrielsen, R.H., 1995. Crustal structure from deep seismic data in the northern North Sea. *Terra Nova*, Abstr. Vol. 7, 55.
- Cuthbert, S.J., 1991. Evolution of the Hornelen Basin, west Norway: new constraints from petrological studies of metamorphic clasts. In: Moton, A.C. Todd, S.P., Haughton, P.D.W. (Eds.), *Developments in Sedimentary Provenance Studies*. Geol. Soc. London, Spec. Publ. 57, 343–360.
- Cuthbert, S.J., Harvey, M.A., Carswell, D.A., 1983. A tectonic model for the metamorphic evolution of the Basal Gneiss Complex, Western South Norway. *J. Metamorph. Geol.* 1, 63–90.
- Dewey, J.F., 1988. Extensional collapse of orogens. *Tectonics* 7, 1123–1139.
- Dewey, J.F., Ryan, P.D., Andersen, T.B., 1993. Orogenic uplift and collapse, crustal thickness, fabrics and metamorphic changes: The role of eclogites. *Geol. Soc. London, Spec. Publ.* 76, 325–343.
- Dobrzhinetskaya, L.F., Eide, E.A., Larsen, R.B., Sturt, B.A., Trønnes, R.G., Smith, D.C., Taylor, W.R., Posukova, T.V., 1995. Microdiamond in high-grade metamorphic rocks of the Western Gneiss region, Norway. *Geology* 23, 597–600.
- Dransfield, M., 1994. Extensional Exhumation of High-Grade Rocks in Western Norway and the Zaskar Himalaya. Dr. Ph. Thesis, Univ. of Oxford.

- England, P.C., Houseman, G.A., 1988. The mechanics of the Tibetan Plateau. *Philos. Trans. R. Soc. London, Ser. A* 326, 301–320.
- Engvik, A.K., 1994. Tektonometamorf utvikling av Vårdalsnes-eklogitten og omgivende bergarter, Sunnfjord, Vest-Norge. *Cand. Sci. Thesis, Univ. of Oslo.*
- Fossen, H., 1992. The role of extensional tectonics in the Caledonides of south Norway. *J. Struct. Geol.* 14, 1033–1046.
- Furnes, H., Mitchell, J.G., Robins, B., Ryan, P.D., Skjerlie, F.J., 1982. Petrography and geochemistry of peralkaline, ultrapotassic syenite dykes of Middle Permian age, Sunnfjord, West Norway. *Nor. Geol. Tidsskr.* 62, 147–159.
- Færseth, R.B., Gabrielsen, R.H., Hurich, C.A., 1995. Influence of basement in structuring of the North Sea basin, offshore southwest Norway. *Nor. Geol. Tidsskr.* 75, 105–119.
- Færseth, R.B., Macintyre, R.M., Naterstad, J., 1976. Mesozoic alkaline dykes in the Sunnhordland Region, western Norway: ages, geochemistry and regional significance. *Lithos* 9, 331–335.
- Gathe, R., Andersen, T.B., 1996. Extensional structures below the Jotun Nappe in Central south Norway; an example from the Lærdal area. *Abstract Volume, Nordisk Geologisk Vintermøte, Åbo.*
- Gee, D.G., 1988. Thrust tectonics in the Scandes — upper crustal extension during Scandean compression. *Geol. Foren. Stockholm Forh.* 110, 390–392.
- Gee, D.G., Guezou, J.-C., Roberts, D., Wolff, F.C., 1985. The central-southern part of the Scandinavian Caledonides. In: Gee, D.G., Sturt, B.A. (Eds.), *The Caledonide Orogen: Scandinavia and Related Areas*. J. Wiley, Chichester, pp. 109–133.
- Gee, D.G., Lobkowicz, M., Singh, S., 1994. Late Caledonian extension in the Scandinavian Caledonides — the Røragen Detachment revisited. *Tectonophysics* 231, 139–155.
- Gilotti, J.A., 1994. Eclogites and related high-pressure rocks from North-East Greenland. *Rapp. Grønl. Geol. Unders.* 162, 77–90.
- Goldschmidt, V.M., 1912. Die kaledonische Deformation der süd-norwegischen Urgebirgstafel. *Skr. Vidensk. Selsk., Christiania* 19, 11 pp.
- Griffin, W.L., 1987. 'On the eclogites of Norway' — 65 years later. *Mineral. Mag.* 51, 333–343.
- Haremo, P., 1987. Stratigrafi og deformasjon i en Kambro-Ordovisisk lagrekke i Kaledonidefronten på Hardangervidda. *Cand. Sci. Thesis, Univ. of Oslo.*
- Hartz, E., 1998. Late orogenic evolution of the East Greenland and Scandinavian Caledonides. *Dr. Sci. Thesis, Univ. of Oslo.*
- Hartz, E., Andresen, A., 1995. Caledonian sole thrust of central East Greenland: A crustal-scale Devonian extensional detachment?. *Geology* 23, 637–640.
- Hodges, K.V., Burchfield, B.C., Royden, L.H., Chen, Z., Liu, Y., 1993. The metamorphic signature of contemporaneous extension and shortening in the central Himalayan orogen: Data from the Nyalam transect, southern Tibet. *J. Metamorph. Geol.* 11, 721–737.
- Hossack, J.R., 1984. The geometry of listric faults in the Devonian basins of Sunnfjord W Norway. *J. Geol. Soc. London* 141, 629–637.
- Hossack, J.R., Garton, M.R., Nickelsen, R.P., 1985. The geological section from the foreland up to the Jotun thrust in the Valdres area, south Norway. In: Gee, D.G., Sturt, B.A. (Eds.), *The Caledonide Orogen: Scandinavia and Related Areas*. J. Wiley, Chichester, pp. 443–456.
- Hveding, B.S., 1992. En strukturgeologisk undersøkelse av mylonittsonen under Dalsfjordforkastningen i Atløy-Askvoll området Sunnfjord. *Unpubl. Cand. Sci. Thesis, Univ. of Oslo.*
- Hurich, C.A., Kristoffersen, Y., 1988. Deep structure of the Caledonide orogen in southern Norway: new evidence from marine seismic reflection profiling. *Nor. Geol. Unders. Spec. Publ.* 3, 96–101.
- Hurich, C.A., Palm, H., Dyrelius, D., Kristoffersen, Y., 1989. Deformation of the Baltic continental crust: views from seismic reflection data. *Geology* 17, 423–425.
- Jamtveit, B., 1987. Metamorphic evolution of the Eiksundal eclogite complex, Western Norway, and some tectonic implications. *Contrib. Mineral. Petrol.* 95, 82–99.
- Kullerud, L., Tørudbakken, B.O., Ilebekk, S., 1986. A compilation of radiometric age determinations from Western Gneiss Region, South Norway. *Nor. Geol. Unders. Bull.* 406, 277–286.
- Krogh, E.J., 1980. Geochemistry and petrology of glaucophane bearing eclogites and associated rocks from Sunnfjord, western Norway. *Lithos* 13, 355–380.
- McClay, K.R., Norton, M.G., Coney, P., Davis, G.H., 1986. Collapse of the Caledonian Orogen and the Old Red Sandstone. *Nature* 323, 147–149.
- Milnes, A.G., Koestler, A.G., 1985. Geological structure of Jotunheimen, southern Norway. (Sognefjell-Valdres section). In: Gee, D.G., Sturt, B.A. (Eds.), *The Caledonide Orogen: Scandinavia and Related Areas*. J. Wiley, Chichester, pp. 457–474.
- Milnes, A.G., Dietler, T.N., Koestler, A.G., 1988. The Sognefjorden north shore log — a 25 km depth section through Caledonized basement in western Norway. *Nor. Geol. Unders. Spec. Publ.* 3, 114–121.
- Morley, C.K., 1986a. Vertical variations in the Osen-Røa thrust sheet, North-western Oslo fjord, Norway. *J. Struct. Geol.* 8, 621–632.
- Morley, C.K., 1986b. The Caledonian thrust front and palinspastic restorations in southern Norwegian Caledonides. *J. Struct. Geol.* 8, 753–765.
- Nilsen, T.H., 1968. The relationship of sedimentation to tectonics in the Solund district of southwestern Norway. *Nor. Geol. Unders. Bull.* 292, 1–20.
- Nilsen, O., Wolf, F.C., 1989. Berggrunnskart Røros og Sveg — 1 : 250,000. *Norges Geologiske Undersøkelse.*
- Norton, M.G., 1986. Late Caledonian extension in western Norway: A response to extreme crustal thickening. *Tectonics* 5, 195–204.
- Norton, M.G., 1987. The Nordfjord–Sogn Detachment, W Norway. *Nor. Geol. Tidsskr.* 67, 93–106.
- Osmundsen, P.T., 1990. Tektonostratigrafi of strukturell utvikling, Staveneset, Sunnfjord. *Cand. Sci. Thesis, Univ. of Oslo.*
- Osmundsen, P.T., 1996. Late-orogenic structural geology and Devonian basin formation in western Norway: A study from

- the hanging wall of the Nordfjord–Sogn Detachment in the Sunnfjord Region. Dr. Sci. Thesis, Univ. of Oslo.
- Osmundsen, P.T., Andersen, T.B., 1994. Caledonian compressional and late orogenic extensional deformation in the Staveneset area Sunnfjord, Western Norway. *J. Struct. Geol.* 16, 1385–1401.
- Osmundsen, P.T., Andersen, T.B., Markussen, S., Svendby, A.K., 1998. Tectonics and sedimentation in the hanging wall of a major extensional detachment: the Kvamshesten Devonian Basin, Western Norway. *Basin Res.*, submitted.
- Palm, H., Gee, D.G., Dyrelus, D., Björklund, L., 1991. A reflection seismic image of Caledonian structure in central Sweden. *Sver. Geol. Unders. Ser. Ca* 75, 1–36.
- Platt, J.P., 1993. Exhumation of high-pressure rocks: a review of concepts and processes. *Terra Nova* 5, 119–133.
- Platt, J.P., England, P., 1994. Convective removal of lithosphere beneath mountain belts: Thermal and mechanical consequences. *Am. J. Sci.* 293, 307–336.
- Richardson, S.W., England, P.C., 1979. Metamorphic consequences of crustal eclogite production in overthrust orogenic zones. *Earth Planet. Sci. Lett.* 42, 183–190.
- Roberts, D., Gee, D.G., 1985. An introduction to the structure of the Scandinavian Caledonides. In: Gee, D.G., Sturt, B.A. (Eds.), *The Caledonide Orogen: Scandinavia and Related Areas*. J. Wiley, Chichester, pp. 55–68.
- Rykkelid, E., Andresen, A., 1994. Late Caledonian extension in the Ofoten area, northern Norway. *Tectonophysics* 231, 157–169.
- Searle, M.P., 1995. Timing and rates of motion on thrusts, normal faults and strike-slip faults in Himalaya, Karakoram and Tibet. *Terra Nova*, Abstr. Vol. 7, 43.
- Séguret, M., Séranne, M., Chauvet, A., Brunel, M., 1989. Collapse basin: A new type of extensional sedimentary basin from the Devonian of Norway. *Geology* 17, 127–130.
- Séranne, M., 1988. *Tectonique des bassins Dévoniens de Norvège: Mise en évidence de bassins sédimentaires en extension formés par amincissement d'une croûte orogénique épaisse*. Thèse de doctorat, Academie de Montpellier.
- Séranne, M., 1992. Late Palaeozoic kinematics of the Møre–Trøndelag Fault Zone and adjacent areas, central Norway. *Nor. Geol. Tidsskr.* 72, 141–158.
- Séranne, M., Séguret, M., 1987. The Devonian basins of western Norway: tectonics and kinematics of an extending crust. In: Coward, M.P., Dewey J.F., Hancock, P.L. (Eds.), *Continental Extensional Tectonics*. Geol. Soc. London, Spec. Publ. 28, 537–548.
- Sigmond, E.M.O., Gustavson, M., Roberts, D., 1984. Berggrunnskart over Norge, M 1:1 million. Norges Geologiske Undersøkelse.
- Sjöström, H., Bergman, S., 1989. Asymmetric extension and Devonian (?) normal faulting; examples from the Caledonides of eastern Trøndelag and western Jämtland. *Geol. Foren. Stockholm Forh.* 111, 407–410.
- Sjöström, H., Bergman, S., Sokoutis, D., 1991. Nappe geometry, basement structure and normal faulting in the central Scandinavian Caledonides: kinematic implications. *Geol. Foren. Stockholm Forh.* 113, 265–269.
- Sjöström, H., Bergman, S., 1994. Contraction and lateral extension in the Caledonian orogenic wedge of central Scandinavia: Evidence from a segment of the Seve-Köli terrane boundary. *Abstr. Vol.*, Nordisk Geologisk Vintermöte, Luleå, 186.
- Skogseid, J., 1994. Dimensions of the Late Cretaceous–Paleocene Northeast Atlantic rift derived from Cenozoic subsidence. *Tectonophysics* 240, 225–247.
- Smith, D.C., 1984. Coesite in clinopyroxene in the Caledonides and its implications for geodynamics. *Nature* 310, 641–644.
- Smithson, S.B., Ramberg, I.B., Grønlie, G., 1974. Gravity interpretation of the Jotun Nappe of the Norwegian Caledonides. *Tectonophysics* 22, 205–222.
- Steel, R.J., Gloppen, T.G., 1980. Late Caledonian (Devonian) basin formation, western Norway: signs of strike-slip tectonics during infilling. *Spec. Publ. Int. Assoc. Sedimentol.* 4, 79–103.
- Strachan, R.A., 1994. Evidence in North-East Greenland for Late Silurian–Early Devonian regional extension during the Caledonian orogeny. *Geology* 22, 913–916.
- Swensson, E., Andersen, T.B., 1991. Contact relationships between the 'Askvoll group' and basement gneisses of the Western Gneiss Region (WGR), Sunnfjord, Western Norway. *Nor. Geol. Tidsskr.* 71, 15–27.
- Tapponnier, P., Leloup, P.H., Lacassin, R., Harrison, T.M., Wenji, C., Ryerson, F., 1995. Diachronic uplift, transtension and sinistral shear rate along the Red River zone. *Terra Nova*, Abstr. Vol. 7, 43.
- Torsvik, T.H., Sturt, B.A., Ramsay, D.M., Vetti, V.V., 1987. The tectono-magnetic signature of the Old Red Sandstone and Pre-Devonian strata in the Håsteinen area, western Norway, and the implications for the later stages of the Caledonian Orogeny. *Tectonics* 6, 305–332.
- Torsvik, T.H., Sturt, B.A., Swensson, E., Andersen, T.B., Dewey, J.F., 1992. Palaeomagnetic dating of fault rocks: Evidence for Permian and Mesozoic movements along the Dalsfjord Fault, Western Norway. *Geophys. J. Int.* 109, 565–580.
- Torsvik, T.H., Smethurst, M.A., Meert, J.G., Van der Voo, R., McKerrow, W.S., Brasier, M.D., Sturt, B.A., Walderhaug, H.J., 1996. Continental break-up and collision in the Neoproterozoic and Palaeozoic — A tale of Baltica and Laurentia. *Earth Sci. Rev.* 40, 229–258.
- Torsvik, T.H., Andersen, T.B., Eide, E.A., Walderhaug, H.J., 1997. The age and tectonic significance of dolerite dykes in western Norway. *J. Geol. Soc. London* 154, 961–973.
- Tucker, R.D., McKerrow, W.S., 1995. Early Palaeozoic chronology: a review in light of new U-Pb zircon ages from Newfoundland and Britain. *Can. J. Earth Sci.* 32, 368–379.
- Wernicke, B., 1992. Cenozoic extensional tectonics of the U.S. Cordillera. In: Burchfield, B.C., Lipman, P.W., Zorback, M.L. (Eds.), *Geology of North America*, Vol. G-3, The Cordilleran Orogen: Conterminous U.S. The Geological Society of America, Boulder, CO, pp. 553–581.
- Wilks, W.J., Cuthbert, S.J., 1994. The evolution of the Hornelen Basin detachment system, western Norway: implications for the style of late orogenic extension in the southern Scandinavian Caledonides. *Tectonophysics* 238, 1–30.
- Ziegler, P.A., 1988. Evolution of the Arctic–North Atlantic and the Western Tethys. *Am. Assoc. Pet. Geol. Mem.* 43, 198 pp.

Available online at [www.sciencedirect.com](http://www.sciencedirect.com)

SCIENCE @ DIRECT®

EPSL

Earth and Planetary Science Letters 242 (2006) 58–72

[www.elsevier.com/locate/epsl](http://www.elsevier.com/locate/epsl)

# Fossil earthquakes recorded by pseudotachylytes in mantle peridotite from the Alpine subduction complex of Corsica

Torgeir B. Andersen\*, Håkon Austrheim

*Physics of Geological Processes and Department of Geosciences, University of Oslo, P.O.Box 1047, Blindern, 0316 Oslo, Norway*

Received 17 March 2005; received in revised form 28 October 2005; accepted 28 November 2005

Available online 10 January 2006

Editor: E. Boyle

## Abstract

Paleo-earthquakes recorded by pseudotachylytes have recently been discovered in the blueschist facies subduction complex of Alpine Corsica. Pseudotachylytes occur in ophiolite gabbro and mantle peridotite belonging to the Schistes Lustrés of Cape Corse. Ultramafic pseudotachylyte fault- and injection veins are found within well-preserved peridotite lenses and are progressively hydrated together with the host rock along the margins of the lenses. Numerous pseudotachylytes ranging in thickness from less than 1 to 380 mm have been identified. Veins thicker than 3 mm may show flow banded chilled glassy margins and cores with dendritic to spherulitic quench textures. The newly formed minerals are zoned olivine (Fo<sub>93–89</sub>), clino- and ortho-pyroxene with compositions indicative of high crystallization temperatures (1300–1400 °C), zoned Cr-spinel, and a glassy to micro-vesicular hydrous matrix showing that frictional melts contained up to 4% water. Frictional heating on co-seismic faults raised the temperature from ambient blueschist facies conditions (450 °C and 1–1.5 GPa) to more than 1700 °C, which is required for ~75% disequilibrium melting of spinel peridotite at 1.5 GPa. The characteristic fault-vein thicknesses observed are 1 to 3 cm, but several fault-veins are thicker than 10 cm. Co-seismic displacement of 1 m, a stress of 300 MPa, and seismic efficiency of 5%, may melt ca 60 kg peridotite pr. m<sup>2</sup> fault surface corresponding to 20 mm thick layer of ultramafic pseudotachylyte. The ultramafic pseudotachylytes described here formed by disequilibrium melting of peridotite in the upper part of the Alpine subduction zone. If the interpretations of typical displacements of approximately 1 m are correct, the most common pseudotachylyte fault-veins are related to magnitude ca. 7 or larger subduction earthquakes.

© 2005 Elsevier B.V. All rights reserved.

*Keywords:* subduction; earthquake; mantle; pseudotachylyte; peridotite; Corsica

## 1. Introduction

Subduction zones are the most seismically active tectonic regime on Earth. A wealth of information regarding the depth distribution of earthquakes has

shown that segments of a subduction zone may change from seismically active to aseismic and that the depth distribution of seismicity may vary between subduction zones and along strike within the same zone. This variation may in some cases relate to age [1] and can be correlated to temperature differences. However, the existing complexity such as double seismic zones [2] makes it obvious that temperature cannot be the only parameter that controls depth distribution. Rocks cycled through subduction zones not only vary in temperature

\* Corresponding author. Tel.: +47 22856415; fax: +47 22855101.

E-mail addresses: [t.b.andersen@geo.uio.no](mailto:t.b.andersen@geo.uio.no) (T.B. Andersen), [hakon.austrheim@geo.uio.no](mailto:hakon.austrheim@geo.uio.no) (H. Austrheim).

but also in composition including water content and metamorphic status. This variation may also influence the mechanism and the depth distribution of the seismic activity [3]. Peridotites and their hydrated equivalent serpentinites are dominant rocks in subduction zones as witnessed by their abundance in exposed subduction complexes. These rocks have widely different petro-physical properties and their distribution may influence the location of epicentres. To better understand the mechanism behind subduction earthquakes and their distribution it is required that we understand the physics on the fault planes transecting ultramafic rocks during seismic events. A central question relates to the behaviour of dry peridotite. Is it possible that the high strength and high melting temperature will prevent faulting or is the strength a prerequisite for the build up of stresses to be released as earthquakes?

In this study we describe ultramafic pseudotachylytes recently discovered in mantle peridotites from the Eocene Alpine subduction complex of Corsica [4]. The pseudotachylytes and frictional heating associated with ultra-fine-grained cataclastic rocks suggests that deformation as well as metamorphic transformations at such depths may be associated with short-lived brittle events. Descriptions of ultramafic pseudotachylytes are rare in the literature. We are aware of 3 previously described examples of pseudotachylyte or pseudotachylyte-like veins from peridotites. Obata and Karato [5], followed by Jin et al. [6] documented frictional faulting at high differential stresses (300–600 MPa) resulting in disequilibrium melting of spinel peridotite from the Ivrea–Verbano zone of the Italian Alps. Morishita, [7] and Lund, [8] have provided detailed description and fabric analyses of ultra-fine-grained, fault-related, veins in spinel and garnet peridotite from Hokkaido, Japan and from Holsnøy, western Norway, respectively. The pseudotachylytes described in the present study from Corsica are important because:

- (1) They record paleo-earthquakes in oceanic mantle lithosphere deformed at high-pressure and low-temperature (HP-LT) conditions in a tectonic setting similar to the subduction environment where most of the energy generated by present-day seismic faulting is released [9]. The blueschist facies pseudotachylytes may therefore provide insight into fault-plane processes on subduction earthquakes in the upper parts of Wadati–Benioff zones.
- (2) Disequilibrium melting as shown by a large number of mafic and ultramafic pseudotachylyte veins in rocks with very high melting temperatures

documents that friction on faults is an extremely effective way to transfer elastic energy into heat. These rocks provide an avenue to understand stress-release and the energy budget on deep seismic faults.

- (3) The ultramafic pseudotachylytes are preserved in the least altered and hydrated peridotites and have not been observed in the metamorphically equilibrated serpentinites. Nevertheless the pseudotachylytes preserve evidence that some fluid was available during their formation. Pseudotachylytes and ultra-cataclastites provide an opportunity to study feedback mechanisms between co-seismic slip events and metamorphism, in particular the relationships between frictional heating and dehydration/hydration reactions.

Pseudotachylytes are products of extreme brittle deformation, resulting in comminution and frictional melting at high ( $>10^{-2}\text{s}^{-1}$ ) strain rates [10]. Pseudotachylytes generated by frictional melting in faults commonly occur in crystalline rocks of intermediate and granitoid composition, but may also be derived from gabbroic, and ultramafic protoliths [5,7,11]. Friction on faults may be an efficient heat generating process capable of transferring kinematic energy into frictional heat and give disequilibrium melting of most rock-compositions. On strong faults, by far most of the kinematic energy is transferred to heat. The dynamic coefficient of friction may, however, be greatly reduced when seismic slip velocities are approached [12]. The most effective transfer of kinematic energy to heat, frictional fusion and generation of pseudotachylyte may therefore be most common along fault tips and fracture propagation fronts, and are not necessarily associated with the maximum fault displacements (c.f. [13]). The energy released during faulting ( $W_f$ ) is mostly dissipated as heat ( $Q$ ) and depending on the seismic efficiency ( $\eta$ ) a very minor component is radiated as seismic energy ( $E_\eta$ ):

$$W_f = Q + E_\eta. \quad (1)$$

Although difficult to quantify in general, estimates of (1) suggest that most of the energy ( $\approx 95\text{--}99\%$ ) is transferred to heat [14]. The energy generated by friction in a single seismic event is essentially adiabatic since the heat-transfer-distance ( $D$ ) into the fracture wall is very small during the seismic event:

$$D = (\kappa t)^{0.5} \quad (\text{thermal diffusivity } \kappa \sim 1.5 \text{ mm}^2\text{s}^{-1}, \\ t = \text{time in sec}). \quad (2)$$

Since the thermal transport in crystalline rocks is extremely inefficient (2) most of the heat will be concentrated in the immediate vicinity (mm to cm) of the fractures. It is therefore to be expected that all fault zones record frictional heating [15]. Some faults, however, do apparently not record detectable frictional heating, and carefully designed studies have failed to document significant increased temperature, and heat-flow measurements in drill-cores from the San Andreas and associated faults in California have also had similar

paradoxical results regarding increased temperatures [16]. Explanations of such observations may include problems with accurate measurements of the temperature, very weak faults with corresponding low normal stresses, dissipation of the heat across wider damage zones, slow deformation and perhaps most importantly advective heat transport by groundwater [17,18]. Many fault zones, however, display dramatic illustrations of how mechanical work has been converted to heat. The most convincing products of frictional heating are pseu-

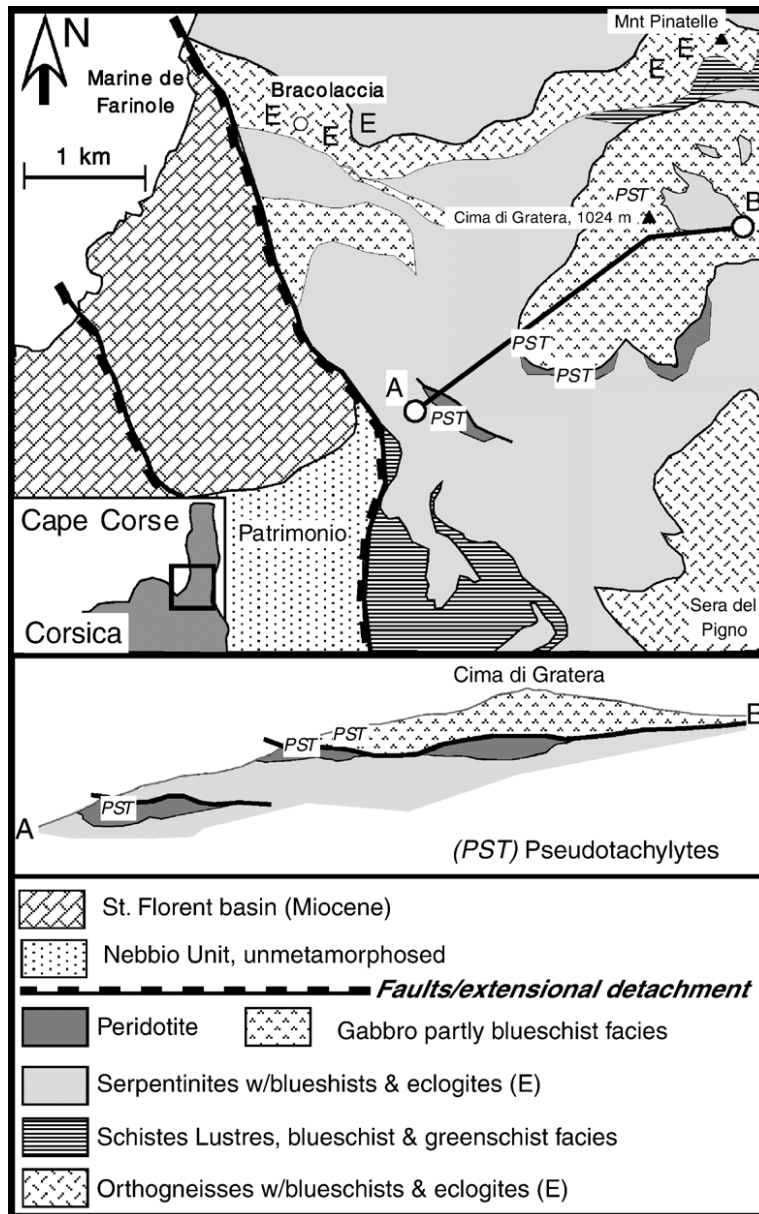


Fig. 1. Simplified geological map and cross-section of the Patrimonio–Cima di Gratera area of the Cape Corse Region, Corsica. Notice that pseudotachylytes are common along the contact between the gabbro and the structurally underlying ultramafic rocks, but also within preserved peridotite lenses preserved within the serpentinite. Most of the detailed observations are from within the lower peridotite body close to A.

dotachylytes such as described in a mostly ignored short paper by Goldschmidt [19], where he interpreted vesicular glass ('frikjonsglass') along faults in the central Norwegian Caledonides as generated by frictional fusion. Theoretical considerations [20,21] as well as experiments [22], see also review [23] and a large number of studies of natural examples show that frictional heating may result in disequilibrium fusion of the fault wall rocks. Frictional heating associated with large mantle earthquakes will potentially melt any silicate-rock composition from highly silicic to ultramafic [24].

We have recently discovered and described a large number of pseudotachylytes in blueschist to eclogite facies ophiolite gabbro and peridotite of Corsica [25]. The pseudotachylytes in the gabbro and the peridotite are closely associated in space at-or in the vicinity of the gabbro–peridotite contact. Both the mafic and the ultra-mafic pseudotachylytes are precursors of the blueschist facies ductile fabrics in the area, implying

that they are associated in both space and time and therefore related to the same seismic events. These pseudotachylytes are particularly interesting since they provide an opportunity to study the relationships between extreme brittle deformation and the regional HP-LT metamorphism and ductile deformation during burial in a subduction complex [4]. In our pilot study of the pseudotachylytes we documented crystallization and quenching of frictional melts from the Cima di Gratera gabbro (Fig. 1) [25]. The vein/quench mineralogy included minerals such as highly aluminous fassaitic clino-pyroxene, epidote, and edenite-to glaucophane amphiboles suggesting that the seismic faulting and crystallization occurred at a pressure compatible with the regional blueschist facies conditions at ~1 to 1.5 GPa and ca 450 °C. Several previous workers have described and calibrated the blueschist-to eclogite facies metamorphism of the Cape Corse region [26–29], and we take these estimates to represent the ambient



Fig. 2. A) Ultramafic pseudotachylyte fault and injection veins in spinel peridotite. Notice that the veins form positive features on the surface, and that the joints with serpentinisation weather out. Scale: 2-Euro coin. B) Thick segment of pseudotachylyte fault vein with maximum thickness of 38 cm. This fault can be traced almost continuously across the peridotite body (see Fig. 3). The stippled lines show the margins of the fault vein. C) Highly fractured and net-veined fault-core in peridotite along a ca 4.5 m wide fault zone with pseudotachylytes. Framed detail shows well-preserved glassy and unaltered pseudotachylyte vein that may constitute 30% to 40% of the several m-wide damage zone. Locality is near the faulted and sheared contact between upper peridotite (see Fig. 1) and the Cima di Gratera gabbro. D) Fault zone with numerous anastomosing pseudotachylyte veins. Notice the asymmetrical damage zone and that the fault veins are more frequent in the left (lower) part of the fault.

pressure–temperature conditions during the seismic faulting.

## 2. Geological setting

The studied pseudotachylytes in Corsica occur across a several hundred meter thick section of gabbro and ultramafic rocks within the Schistes Lustres nappes on the SSW slope of Cima di Gratera at Cape Corse (Fig. 1). The HP-LT complex consists of thrust-stacked units of the Ligurian oceanic lithosphere including plagioclase- and spinel-peridotites imbricated with slices of European continental crystalline rocks with cover [4]. Both the continental and oceanic rocks contain evidence for the late Cretaceous–Oligocene HP-LT metamorphism in the form of blueschists, eclogites and the jadeite-bearing granitoids [28,30,31]. The HP-LT metamorphic rocks include a dismembered ophiolite dominated by variably hydrated and metamorphosed ultramafic rocks, gabbros, pillow lavas and metasedimentary schists (the Schistes Lustrés units). HP-LT metamorphism is also found in allochthonous blueschist (Sera di Pigno and Tenda Units) and eclogite facies (Monte Pinatelle- Farinole Unit) rocks developed from the Hercynian continental basement [4,26,29,32,33]. The eclogites of the Cape Corse Region record peak Alpine metamorphic conditions at pressures of 1.5 to 2 GPa and temperatures of  $550 \pm 50$  °C. They were ex-

humed on a cold geotherm through the blueschist facies at ca 1 GPa and temperatures of 450 to 500 °C and eventually to greenschist facies [26]. Other units, without eclogites reached  $P_{\max}$  at lawsonite–blueschist facies ( $P$  – 1.3 to 1.5 GPa at  $T$  – 350 to 400 °C) and decompressed on a cold geotherm through the blueschist ( $P$  – 1 GPa,  $T$  – 350 °C) to greenschist facies conditions [26]. The pressure–temperature conditions of blueschist facies rocks of the more external Tenda massif have recently been calculated to  $T$  – 300 to 500 °C at  $P$  – 0.8 to 1.1 GPa [29]. Previous work in the Cape Corse area suggest that the blueschist to eclogite facies metamorphism was associated with top-to-the-west and southwest Alpine subduction and thrusting, succeeded by the top-to-the-east extension at blueschist to greenschist facies conditions, which eventually juxtaposed the HP-LT rocks with the low-grade to unmetamorphosed Balange and Nebbio units (tectonic summary in [4]).

## 3. Field description

In outcrop, the ultra-mafic pseudotachylytes form orange to dark brown and occasionally grey to black veins on weathered surfaces and may easily be mistaken for commonly present serpentinite veins. On weathered surfaces they are, however, more resistant and normally define positive features, contrary to most

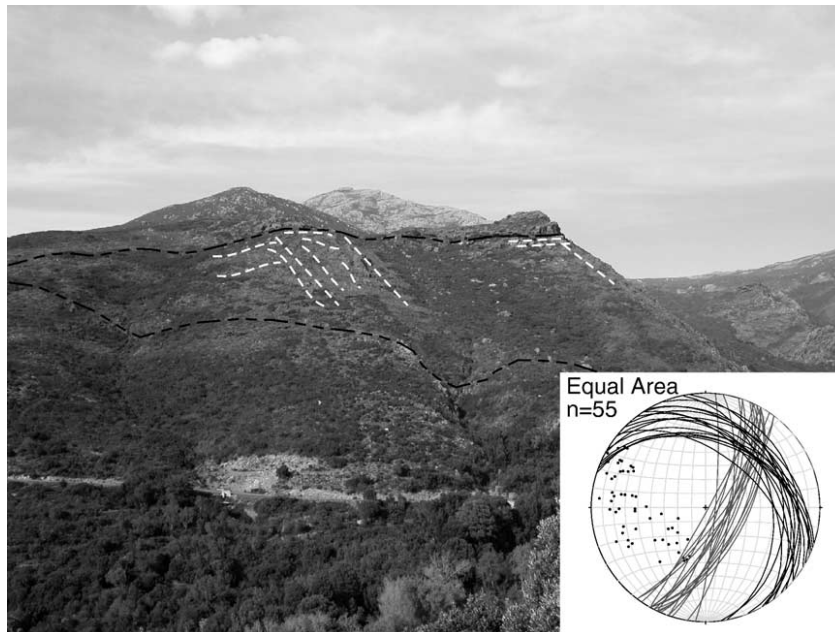


Fig. 3. View showing outline of the lower peridotite body (Fig. 1), between the top and bottom black-dotted lines. Stippled white lines inside the peridotite body show common occurrences and the principal orientations of the pseudotachylytes. The orientation of veins ( $n=55$ ) is shown in the stereogram as poles and great circles. They define a system of mutually crosscutting veins considered to represent a conjugate system.

serpentinite veins, which are softer and weather to form depressions (Fig. 2a). On fresh surfaces they are very dark greenish grey to black aphanitic veins with variable, but usually low content of wall-rock fragments. Flow banding is occasionally visible in hand specimen and commonly observed in thin sections. Most veins are less than 2 cm thick, but occasionally they are much thicker with an observed maximum thickness of 38 cm (Fig. 2b). Hairline-thin veins and fractures are commonly associated with thicker veins (Fig. 2a and c). The weathered surfaces of the wall rocks may be massive and smooth, but more commonly the wall rock surfaces are rough with a fractured appearance formed by better-preserved peridotite cut by abundant small fractures and veins. The pseudotachylytes occasionally occur as single or a few discrete injection veins but more commonly they form networks along faults (Fig. 2). Reconnaissance mapping of pseudotachylytes within two of the peridotite lenses at Cima de Gratera reveal that the veins from which orientations have been measured ( $n=55$ ) can be grouped in two systems. A prominent system comprises laterally consistent and commonly 1–3 cm-thick veins with an average orientation of 025/74 (Fig. 3). A second vein-system dips more gently, is less well oriented but contains some very thick (5–20 cm) fault veins. Near the upper contacts of both peridotite lenses there are continuous and thicker fault-veins that are sub-parallel with the contacts to the serpentinite (lower peridotite) and the blueschist facies foliation in the Cima di Gratera gabbro (upper peridotite, see Fig. 1). Some fault veins are part of systems that can be traced laterally for several meters to several tens of meters, and in one case across most of the lower peridotite body (Fig. 3). A characteristic feature of individual faults with pseudotachylyte veins is that they form an anastomosing network where individual veins may vary in thickness from mm up to a maximum observed width of 38 cm (Fig. 2). The observation of thickness variations by as much as 2-orders of magnitude along the same fault zone suggest that the fault vein thicknesses are commonly secondary, reduced by drainage and thickened by injection into releasing-bend pull-apart segments. These observations indicate that relating fault-vein thicknesses directly to fault displacement [13,21] should be used with considerable caution, since the width of individual pseudotachylyte veins on faults in many cases probably are secondary. In spite of the uncertainty of relating fault vein-thicknesses to displacement we have used the observed characteristic fault vein thickness of ca 2 cm because we lack other accurate displacement indicators for the principal faults (see discussion below). The

peridotite wall rocks are mostly without obvious stratification or banding. Attempts to determine throw or in some cases even relative movement along the continuous faults are therefore difficult. In some cases veins occur within damage-zones that are several meters (max 5 m) wide. The geometry and distribution of fault- and injection veins suggest that the faults constitute a conjugate system accompanied by mode-1 fractures.

Both field- and thin section observations show that the brittle faulting generating pseudotachylytes in general was a precursor of the ductile deformation (Fig. 4b). The pseudotachylyte veins are deformed into the ductile fabric engulfing the lenses. Crosscutting pseu-

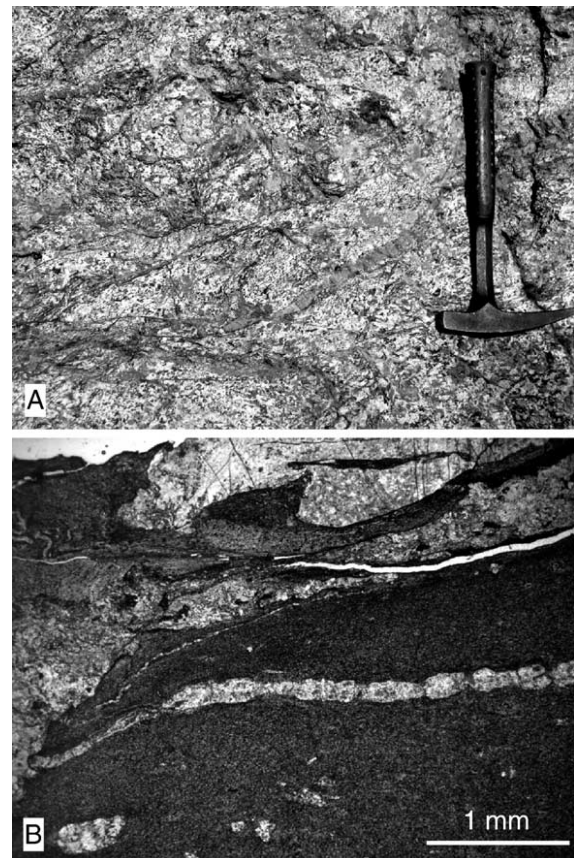


Fig. 4. A) Pseudotachylyte veins in gabbro near the sheared contact to the upper peridotite and serpentinite at Cima di Gratera (see Fig. 1). Notice the well-preserved igneous texture between the fractures and fault/injection veins within the gabbro. B) Optical micrograph (parallel light) of fine-grained blueschist facies deformation zone developed in gabbro near at the contact between mafic and ultramafic rocks at Cima di Gratera. Small glaucophane crystals, (10–30  $\mu\text{m}$ , not visible at this magnification), define a foliation of the fine-grained fault rock. Notice the intrusive features (veins and horn) of the ultrafine-grained margin of the fault rock, suggesting that the fault-rock intruded the wall rock. Notice also pinch and swell of the light-coloured vein (see text for discussion of brittle–ductile relationships).

dotachylytes indicating multiple seismic events along the same faults are commonly observed (see also [25]). Alteration of extreme brittle deformation and creep is witnessed by pseudotachylytes overprinted by ductile fabrics, which in turn are truncated by new fault and/or injections veins (Fig. 5f). Pseudotachylytes truncated by fractures associated with serpentinisation are common on all scales. Pseudotachylytes are, however, only preserved within the least altered peridotite lenses,

which are engulfed within foliated serpentinites and metamorphically more equilibrated rocks. The large seismic events can thus be related to the earlier and driest parts of the structural and metamorphic history. This pattern is akin to brittle–ductile relationships in other HP-LT metamorphic terrains such as the relative timing of eclogite facies pseudotachylytes and shear zones in western Norway [8,34–36]. Once the strength of the peridotites and gabbros become sufficiently re-

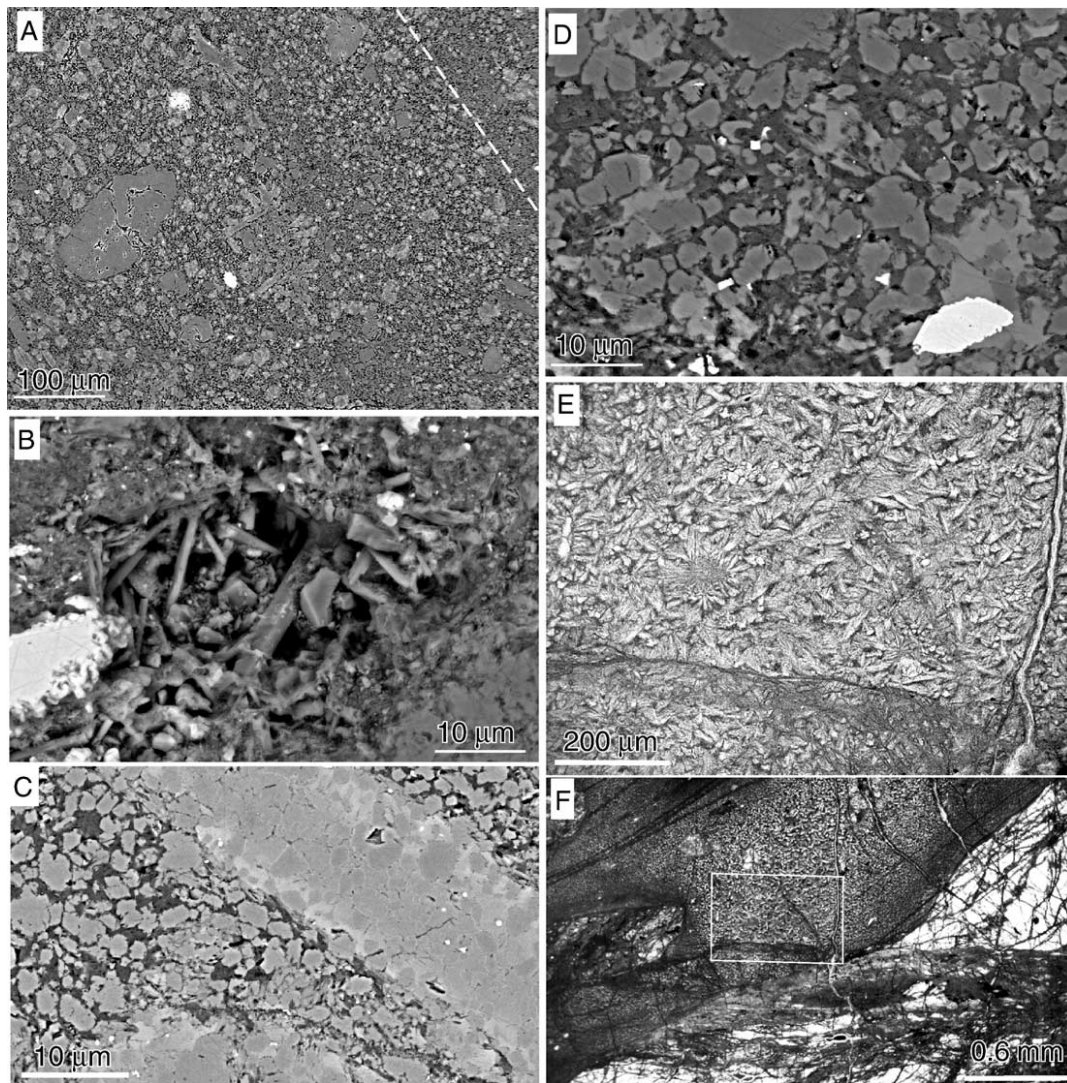


Fig. 5. A) Backscatter-electron (BSE) image of ultramafic pseudotachylyte with flow-banding (parallel dotted line), thermally rounded ol clasts and newly formed ol, opx and cpx (light grey) crystals in darker glassy to fibrous hydrous matrix. The cpx crystals form dendritic to acicular poikilitic crystals. Ol and opx are undistinguishable on the BSE images. Mineral abbreviations after [47] B) BSE image showing vesicle with idiomorphic cpx crystals in ultramafic pseudotachylyte. Light mineral (left) is Cr-spl. C) BSE image showing detail of acicular cpx micro-phenocrysts (light) with abundant (<5-micron) ol inclusions. Notice also chemical zoning, Fe-rim to Mg-core (darker) in the small ol crystals. D) BSE detail showing zoned ol, opx, poikilitic cpx, zoned spl and the micro-vesicular and fibrous hydrous matrix. E) Optical micrograph (parallel light) showing quench texture with spherulitic (sunflower-like) and acicular/dendritic cpx phenocrysts in ultramafic pseudotachylyte. F) Optical micrograph showing quenched pseudotachylyte with micro-phenocrystic core and chilled margin. The vein cuts an older pseudotachylyte with ductile overprint (lower part of photo). The framed area is shown in detail in Fig. 5E.

duced, primarily controlled by hydration of olivine and pyroxenes, crystal–plastic deformation mechanisms and ductile flow dominate and in turn enhance recrystallization and equilibration of tectonites.

The relationships between the pseudotachylyte in peridotite lenses and the foliated serpentinites can be studied along the margins of the lenses. The best-studied peridotite body has a width–thickness ratio of ca 1 to 6 and a maximum thickness ca 100 m. The upper contact is marked by a sharp front of alteration and intense foliation forming a break in the topography (Fig. 3). The lower boundary is less pronounced and less well exposed, with a transition from peridotite to completely hydrated serpentinite over a distance of a few meters. The pseudotachylytes near the contacts are overprinted to obliterated by ductile deformation associated with serpentinisation. Very fine-grained fault-rocks, ultra-cataclastites or former pseudotachylytes, are also overprinted by ductile deformation along the tectonic contact between the Cima di Gratera gabbro and the underlying ultramafic rocks (Fig. 1). Locally the gabbro contains spectacularly preserved pseudotachylytes along this contact ([25] and Fig. 4a). Ductile fabric overprinting former pseudotachylyte or ultra-cataclastite characterizes fine-grained blue mylonites from the contact zone. Well-oriented, small crystals (~0.1 mm) of glaucophane define a CPO fabric in the mylonite (Fig. 4b).

#### 4. Solidification, mineralogy and texture

The ultramafic pseudotachylytes are dark glassy veins, which sharply crosscut individual mineral grains, older veins or deformation zones in the peridotite wall rock. Thin sections reveal that many veins are hairline-thin and difficult to see in the field. Very thin injection veins and grain-boundary wetting-like features require extremely low viscosity for the melt. High-pressure experiments show that ultramafic melts (komatiites and pyroxenites) have very low viscosities of  $10^{-1}$  Pa s or less [37]. Such low viscosity is consistent with the intrusive features associated with the mm-thin ultramafic pseudotachylytes. The mm- to cm-thin veins must have been emplaced and solidified in seconds and ca 10–15 min respectively according to Eq. (3).

$$t_s = b^2 / 4\kappa\lambda^2, \quad (3)$$

where  $t_s$  — time for solidification,  $b$  — vein thickness in mm,  $\kappa$  — thermal diffusivity ( $\sim 1.5 \text{ mm}^2\text{s}^{-1}$ ),  $\lambda \sim 0.45$ , a dimensionless variable depending on the latent heat

of fusion ( $8.6 \times 10^5 \text{ J kg}^{-1}$ ), heat capacity ( $1150 \text{ J kg}^{-1} \text{ }^\circ\text{C}^{-1}$ ) and temperature difference ( $>1200 \text{ }^\circ\text{C}$ ) between melt and wall rock (see [38] for derivation of Eq. (3)).

Most of the sampled veins are texturally zoned, commonly with ultra-fine grained, colour banded glassy margins and a banding defined by variable content of porphyroclasts. In the best-developed pseudotachylytes, the porphyroclasts are dominated by thermally rounded olivine and minor ortho-pyroxene (Fig. 5a). Veins thicker than 2–3 mm may contain micro-porphyrific domains, mainly in the cores. The micro-phenocrysts are clino-pyroxene crystallized directly from the frictional melt. Other minerals crystallized from the melt include olivine, ortho-pyroxene, chrome-spinel, and nickel-sulphide. Combined optical microscopy, back-scatter electron images (BSE) and X-ray element mapping on scanning electron microscope (SEM) and electron microprobe (EMP) analyses show that the minerals which crystallized are small, commonly less than 10  $\mu\text{m}$ , zoned crystals of olivine ( $\text{Fo}_{89.0-93.9}$ ), ortho-pyroxene ( $\text{Wo}_{11.7-3.0}$ ,  $\text{En}_{87.3-77.4}$ ,  $\text{Fs}_{14.2-9.6}$ ) and up to 300  $\mu\text{m}$  long dendritic, spherulitic to acicular clino-pyroxene ( $\text{Wo}_{38.9-24.3}$ ,  $\text{En}_{65.4-53.0}$ ,  $\text{Fs}_{10.3-7.1}$ ) microliths (Table 1 and Fig. 5c and d). The olivine crystals are consistently zoned with Mg-rich cores ( $\text{Fo}_{93}$ ) and more Fe-rich margins ( $\text{Fo}_{89}$ ). The clino-pyroxene crystals are strongly poikilitic to dendritic and may contain more than 80% olivine inclusions in their cores (Fig. 5c, d and e). Pyroxene compositions from crystallites that crystallized from the pseudotachylyte melt, as well as the average wall-rock pyroxene compositions are shown in Fig. 6a. The extreme composition of both ortho- and clino-pyroxene require crystallization temperatures in the range of 1300 to 1400  $^\circ\text{C}$  at a pressure of 1 to 1.5 GPa, in accordance with the ambient blueschist-to eclogite facies pressure conditions [39]. Olivine crystallites in pseudotachylyte also have unusual composition, particularly a high content of CaO compared to the wall rock mineral composition (Fig. 6b).

The interstitial matrix contains small idiomorphic to sub-idiomorphic chromite, chrome spinel and occasional Ni-sulphide crystals ( $\sim 1-2 \mu\text{m}$ ), and larger chrome-spinel crystals, which may be chemically zoned. The zoned spinel crystals have slightly higher average atomic number along the rims (Fig. 5b). These crystals may be up to 10  $\mu\text{m}$  across and may represent spinel porphyroclasts with a Fe-rich rim overgrowth. Veins thinner than  $\sim 2 \text{ mm}$  are generally without the micro-porphyrific texture, but commonly have flow foliation and folding.

Table 1  
Mineral composition from Ultramafic pseudotachyites and wall-rock peridotite, Corsica

PST ol		Zoned of crystallite												Wall rock olivine													
Sample	Cor9-3	Cor9-3	Cor9-3	Cor9-3	Cor9-3	Cor9-3	Cor9-3	Cor9-3	Cor9-3	Cor9-3	Cor9-3	Cor9-3	Average	of core	of inter	of margin	Cor10-03	Cor10-03	Cor10-03	Cor10-03	Cor10-03	Average	Cor11-03	Cor11-03	Cor11-03	Average	
SiO <sub>2</sub>	40.66	41.33	41.55	42.49	41.85	40.77	40.53	40.18	40.82	40.55	40.18	39.93	40.90	42.34	41.58	41.71	40.53	40.82	40.63	40.98	40.86	40.76	41.53	40.91	40.95	41.13	
Na <sub>2</sub> O	0.00	0.00	0.00	0.00	0.00	0.00	0.00	0.00	0.00	0.00	0.00	0.00	0.00	0.00	0.00	0.00	0.00	0.00	0.04	0.00	0.00	0.01	0.00	0.03	0.00	0.01	
NiO	nd	nd	nd	nd	nd	nd	nd	nd	nd	nd	nd	nd	nd	0.40	0.34	0.33	nd	nd	nd	nd	nd	nd	0.39	0.03	0.32	0.25	
MgO	49.10	50.60	49.62	47.27	47.11	48.85	48.96	49.16	48.06	48.48	48.88	49.02	48.76	51.95	48.98	48.02	49.09	49.06	48.98	48.93	48.74	48.96	49.42	45.68	48.40	47.83	
Al <sub>2</sub> O <sub>3</sub>	0.09	0.08	0.09	0.29	0.64	0.31	0.00	0.00	0.02	0.01	0.00	0.01	0.13	0.00	0.03	0.12	0.02	0.01	0.03	0.00	0.00	0.01	0.00	0.01	0.00	0.00	
K <sub>2</sub> O	0.00	0.00	0.00	0.00	0.01	0.01	0.02	0.00	0.00	0.03	0.00	0.00	0.01	0.00	0.00	0.00	0.00	0.00	0.00	0.00	0.00	0.00	0.00	0.00	0.02	0.01	
CaO	0.22	0.15	0.20	0.99	0.95	0.66	0.01	0.00	0.04	0.41	0.03	0.00	0.30	0.13	0.05	0.10	0.04	0.04	0.11	0.01	0.06	0.05	0.03	0.14	0.03	0.07	
TiO <sub>2</sub>	0.05	0.04	0.00	0.03	0.04	0.01	0.00	0.01	0.01	0.01	0.03	0.01	0.02	0.02	0.00	0.00	0.00	0.00	0.01	0.02	0.01	0.01	0.01	0.01	0.01	0.01	
Cr <sub>2</sub> O <sub>3</sub>	0.20	0.23	0.29	0.20	0.26	0.26	0.00	0.02	0.00	0.06	0.00	0.03	0.13	0.18	0.07	0.17	0.02	0.01	0.05	0.00	0.00	0.02	0.00	0.00	0.00	0.00	
MnO	0.14	0.11	0.10	0.15	0.12	0.11	0.13	0.11	0.18	0.16	0.12	0.13	0.13	0.07	0.20	0.14	0.12	0.15	0.14	0.20	0.13	0.15	0.13	0.35	0.14	0.21	
FeO	9.56	7.79	7.98	9.33	9.28	8.19	9.97	10.32	10.55	10.48	10.62	10.87	9.58	5.93	10.51	10.36	9.91	9.84	9.57	10.05	10.01	9.88	10.39	14.06	11.17	11.87	
Total	100.02	100.33	99.83	100.75	100.26	99.18	99.62	99.80	99.68	100.17	99.86	100.00	99.96	101.02	101.76	100.95	99.73	99.93	99.56	100.19	99.81	99.84	101.90	101.22	101.04	101.39	
Fo	90.02	91.95	91.63	89.89	89.93	91.30	89.63	89.36	88.87	89.04	89.03	88.82	89.96	93.92	89.07	89.07		89.72					89.55	89.33	84.96	88.41	87.57
Fa	9.83	7.94	8.27	9.95	9.94	8.59	10.24	10.52	10.94	10.80	10.85	11.05	9.91	6.01	10.72	10.78		10.16					10.32	10.53	14.67	11.44	12.21

PST opx		PST opx												Wall rock opx											
Sample	cor11	cor11#6	cor11#7	Cor6#19	Cor6#26	#29	#34	Average	Cor11#9	#21	#24	Cor6#22	Cor6#24	Cor6#25	Average	Cor10#6	Cor10#7	Cor10#5	Cor10#4	Average	Cor10#8	Cor10#10	Cor10#9	Cor10#17	Average
SiO <sub>2</sub>	52.11	54.91	52.38	53.68	52.47	52.01	51.69	52.75	56.52	54.94	54.15	54.80	56.93	56.20	55.20	51.17	50.86	51.38	51.08	51.12	54.27	54.81	54.72	53.16	54.24
Na <sub>2</sub> O	0.00	0.02	0.05	0.01	0.06	0.00	0.00	0.02	0.00	0.00	0.00	0.00	0.01	0.04	0.00	0.16	0.09	0.12	0.24	0.15	0.01	0.02	0.00	0.00	0.01
NiO	nd	0.10	0.11	0.09	0.11	nd	nd	0.10	0.06	nd	nd	0.16	0.17	0.11	0.06	0.12	0.05	0.01	0.00	0.05	nd	nd	nd	nd	nd
MgO	20.60	23.29	20.40	20.71	18.94	22.53	24.14	21.52	31.88	34.36	29.44	35.09	32.92	32.63	31.89	17.46	17.36	17.36	17.00	17.30	32.59	32.47	32.40	32.05	32.38
Al <sub>2</sub> O <sub>3</sub>	3.22	2.32	3.64	3.12	4.02	3.07	3.84	3.32	1.46	1.41	1.81	0.70	2.05	1.95	1.56	3.41	3.41	3.51	3.23	3.39	2.56	2.64	2.57	4.87	3.16
K <sub>2</sub> O	0.02	0.00	0.01	0.00	0.00	0.02	0.00	0.01	0.00	0.00	0.00	0.00	0.00	0.01	0.00	0.01	0.01	0.02	0.00	0.01	0.01	0.00	0.01	0.00	0.01
CaO	17.55	13.94	16.61	18.11	19.35	15.03	12.48	16.15	3.13	1.66	6.17	2.83	1.84	2.35	3.65	22.62	22.61	22.43	22.87	22.63	1.36	1.47	1.35	1.03	1.30
TiO <sub>2</sub>	0.12	0.11	0.24	0.13	0.18	0.18	0.20	0.17	0.02	0.02	0.04	0.00	0.03	0.02	0.03	0.36	0.35	0.34	0.32	0.34	0.19	0.18	0.16	0.11	0.16

Cr <sub>2</sub> O <sub>3</sub>	1.03	0.63	0.53	0.71	0.97	0.66	0.39	0.70	1.19	1.12	0.92	0.72	1.57	1.43	1.08	1.20	1.14	1.19	1.05	1.15	0.77	0.74	0.69	1.01	0.80
MnO	0.14	0.16	0.14	0.16	0.12	0.13	0.15	0.14	0.15	0.13	0.18	0.17	0.11	0.17	0.15	0.09	0.16	0.12	0.10	0.12	0.14	0.16	0.13	0.15	0.15
FeO	5.70	5.96	6.05	4.43	4.94	5.72	6.66	5.64	6.68	6.70	7.27	6.73	6.04	6.42	6.88	3.28	3.18	3.17	3.21	3.21	6.70	6.83	6.94	6.94	6.85
Total	100.49	101.44	100.16	101.15	101.16	99.35	99.54	100.47	101.09	100.32	99.99	101.20	101.67	101.33	100.47	99.88	99.22	99.65	99.10	99.46	98.60	99.32	98.97	99.32	99.05
Wo	34.58	27.24	33.28	35.84	38.89	29.52	24.31	31.95	5.93	3.03	11.66		5.14	4.44	6.87					45.66					2.51
En	56.58	63.34	56.88	57.04	52.97	61.58	65.43	59.12	83.98	87.33	77.43		80.55	85.73	82.91					48.58					86.95
Fs	8.93	9.34	9.65	7.09	7.92	8.90	10.26	8.87	10.09	9.64	10.91		14.26	9.71	10.92					5.22					10.51

Low total glassy/fibrous PST matrix

Sample	Low total glassy/fibrous PST matrix														Srp vein			Cr spl		Wall rock pl						
	cor11#10	cor11#11	#23	#7	#9	#18	#8	#7	#8	#9	cor11#10	cor11#11	cor11#12	cor11#13	cor11#14	Average	Cor10	Cor11	Cor10	Average	Cor10	Cor10	Cor10	Cor10	Cor10	
SiO <sub>2</sub>	42.35	40.42	42.29	42.35	40.17	37.16	40.43	42.96	41.24	41.53	50.57	53.39	46.52	41.31	38.72	42.76	40.89	40.16	40.96	40.67	0.01	0.00	44.40	44.51	44.78	
SiO	nd	nd	nd	nd	nd	nd	nd	nd	nd	nd	nd	nd	nd	nd	nd	nd	nd	nd	nd	nd	nd	nd	nd	nd	nd	
B <sub>2</sub> O	nd	nd	nd	nd	nd	nd	nd	nd	nd	nd	nd	nd	nd	nd	nd	nd	nd	nd	nd	nd	nd	nd	nd	nd	nd	
Na <sub>2</sub> O	0.36	0.18	0.09	0.37	0.02	0.02	0.19	0.00	0.00	0.00	0.43	0.76	0.26	0.00	0.00	0.18	0.00	0.01	0.00	0.00	0.00	0.00	0.00	0.00	0.00	
NiO	0.12	0.05	0.34	0.12	0.09	0.10	0.06	nd	nd	nd	nd	nd	nd	nd	nd	0.13	nd	0.09	nd	nd	nd	nd	nd	nd	nd	
MgO	35.71	36.51	42.55	35.72	38.66	35.28	36.51	40.98	38.20	38.08	28.17	25.00	31.81	36.41	38.21	35.85	37.99	38.65	37.68	38.11	11.34	10.83	0.05	0.07	0.09	
Al <sub>2</sub> O <sub>3</sub>	8.89	8.99	1.19	8.90	1.05	11.92	8.99	1.06	3.46	2.80	3.04	2.98	4.49	6.99	7.23	5.46	2.30	1.04	2.65	2.00	25.41	24.59	34.91	35.19	34.93	
K <sub>2</sub> O	0.08	0.04	0.04	0.08	0.00	0.02	0.04	0.02	0.02	0.01	0.01	0.03	0.03	0.02	0.00	0.03	0.02	0.00	0.00	0.01	0.00	0.00	0.00	0.00	0.00	
CaO	0.03	0.08	0.64	0.04	0.19	0.10	0.08	1.44	0.18	0.88	7.91	10.27	4.57	1.60	0.06	1.87	0.05	0.19	0.02	0.09	0.02	0.01	19.41	19.66	19.52	
TiO <sub>2</sub>	0.04	0.00	0.02	0.04	0.01	0.00	0.00	0.03	0.02	0.03	0.12	0.12	0.08	0.02	0.01	0.03	0.01	0.00	0.00	0.00	0.35	0.38	0.04	0.02	0.00	
Cr <sub>2</sub> O <sub>3</sub>	0.05	0.08	0.92	0.06	0.06	1.64	0.09	0.25	0.47	0.30	0.19	0.10	0.12	0.20	0.24	0.32	0.14	0.06	0.00	0.03	37.11	37.99	nd	nd	nd	
MnO	0.03	0.01	0.12	0.03	0.09	0.01	0.02	0.09	0.04	0.02	0.09	0.08	0.06	0.03	0.02	0.05	0.15	0.09	0.09	0.11	0.20	0.24	0.24	0.01	0.00	0.00
FeO	2.77	3.22	8.11	2.77	10.05	3.49	3.23	6.83	3.63	3.14	3.37	3.43	3.30	3.08	2.97	4.23	3.90	10.05	3.81	5.92	23.51	24.15	0.24	0.25	0.21	
Total	90.43	89.58	96.32	90.48	90.38	89.74	89.63	93.65	87.26	86.80	93.90	96.15	91.23	89.67	87.46	90.84	85.35	90.34	85.21	86.97	97.95	98.19	99.96	100.61	100.23	
																						An	94.00	94.00	94.00	

Representative electron microprobe analyses (UCSB and UiO) of glassy to fibrous matrix (low-totals) and micro-phenocrysts (ol, opx, cpx, Cr-spl) from the ultramafic pseudotachylytes (PST), srp from serpentine vein, and magmatic minerals (ol, opx, cpx, pl) from wall-rock peridotite. Solid-solution end-member contents are shown for minerals with significant compositional variation. Mineral abbreviations are after [47].

T.B. Andersen, H. Austrheim / Earth and Planetary Science Letters 242 (2006) 58–72

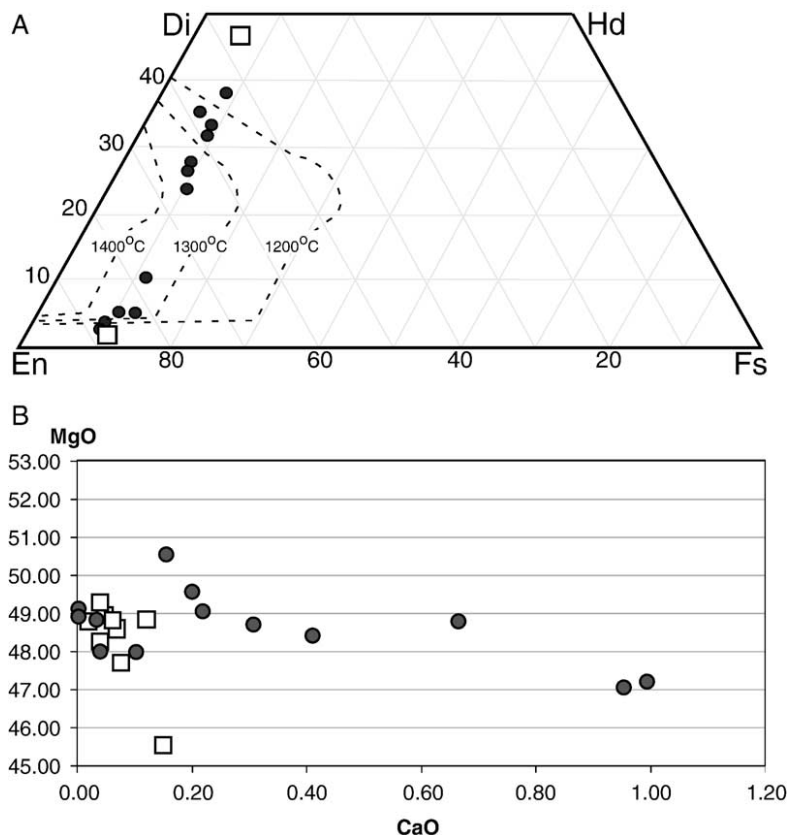


Fig. 6. A) Pyroxene compositions from peridotite wall rock (squares) and from ultramafic pseudotachylyte micro-crystals (circles). Isotherms are from [37]. See text for discussion. B) MgO–CaO composition of ol from pseudotachylyte micro-crystals (circles) and from the wall-rock peridotite (squares) showing high content of CaO in ol from the pseudotachylyte.

BSE images show that the interstitial matrix between porphyroclasts and new-formed crystallites has a low average atomic weight. EMP analyses give a range of ultramafic compositions with SiO<sub>2</sub> and MgO contents from 37.2% to 53.4% and 25% to 42.5%, respectively. The analyses give low totals ranging from 86.8% to 96.5% (see Table 1). Variations between individual nearby analyses points are, however, difficult to reconcile with real mineral compositional variations. We therefore interpret the analyses to represent mixed, non-stoichiometric data and not to represent well-defined individual serpentine crystals. This is supported by the BSE images, which show that the matrix may be glassy homogeneous- to micro-fibrous and micro-porous. Cavities are normally smaller than 1 μm across. In one sample (Cor7b-03), however, a few larger cavities up to 20 μm across have been observed. These probably represent vesicles present at the melt stage since idiomorphic clino-pyroxene crystals have crystallized into the cavity (Fig. 5b). The presence of a micro-vesicular interstitial matrix suggests that the frictional melting was accompanied by high fluid-pressures, which at

least locally was sufficient to release a free gas phase from the melt. The fibrous domains of the matrix probably formed by devitrification of original glass to serpentine, whereas the homogenous domains may be sub-micron scale mineral intergrowths or possibly still glass.

### 5. Conditions for formation of ultramafic pseudotachylyte

The texture and mineralogy described above show that the pseudotachylyte veins formed by near complete melting of the wall rock composed of olivine (Fo<sub>87–90</sub>), *ortho*-pyroxene (En<sub>87</sub>), diopside-rich clino-pyroxene (Wo<sub>46</sub>, En<sub>49</sub>, Fs<sub>5</sub>) and Cr-rich spinel. Some studied samples also contain minor plagioclase (An<sub>94</sub>), and all samples have alteration represented by grain-boundary fringes, veins and fracture networks of serpentine. The pseudotachylytes contain small, variably idiomorphic to sub-idiomorphic zoned olivine grains (~10–15 μm) with Mg-rich cores and higher Fe-content along the margins (see above). The compositional range of ana-

lyzed wall rock olivine crystals is more restricted (Fo<sub>87–90</sub>). The small olivine crystals in the pseudotachylyte also have higher Cr<sub>2</sub>O<sub>3</sub>, Al<sub>2</sub>O<sub>3</sub> and considerably higher CaO contents than the wall rock olivine (Fig. 6b). We interpret them to be micro-phenocrysts crystallized directly from the friction melt. The zoning patterns as well as the compositional variations between the wall rock and the pseudotachylyte minerals are very similar to the pseudotachylyte described from the Balmuccia peridotite [5]. The pseudotachylyte pyroxenes have extreme compositional variation and reduced opx–cpx immiscibility indicative of high-temperature crystallization (Fig. 6, Table 1, and [39]).

The micro-vesicles observed with SEM (see above) and the low-total-oxide analyses (~90%) of the interstitial matrix suggest that the melt had a high fluid-content and that the melt became fluid-saturated as the water-free micro-phenocrysts formed. Image analyses (Matlab script, written com., Dani Schmid, 2004) from two high-magnification SEM micrographs show that typical pseudotachylyte is composed of 56.4% to 59.2% crystals (ol, cpx, opx, opaques), 39.4% to 41.6% matrix and 1.4% to 2.0% micro-porosity interpreted to represent vesicles (Fig. 5b). The preservation of the primary texture and mineralogy of the micro-phenocrysts suggest that the fluid was originally dissolved in the melt and that the matrix was not hydrated by introduced water at a later stage. The original peridotite must therefore have had an appreciable content of water before it melted by frictional heating. Based on the fluid content of the matrix (low total analyses and micro-porosity) the friction melt contained approximately 12% by volume of a hydrous fluid, or close to 4% by weight assuming an ultramafic melt with density of 2.85 [40]. Experiments and theoretical estimates of water-saturation in a melt at 1 GPa give 13% water by weight [41,42].

The fluid-composition in the studied rocks was most likely dominated by water since carbonates have not been identified in our thin sections. Idiomorphic diopside crystals in vesicles suggest that clino-pyroxene crystals grew after vesiculation (Fig. 5b). Assuming a H<sub>2</sub>O fluid content of 4 wt.%, a pressure of 1 to 1.5 GPa as suggested by the ambient blueschist facies regional metamorphic conditions, solidification of the pseudotachylyte melts may have occurred at ca 1200 °C [42]. Based on these observations and the published experimental and theoretical parameterization of peridotite melting by Katz et al. [42], we estimate that friction on the co-seismic faults producing pseudotachylytes in the peridotite must have raised the temperature from the ambient metamorphic conditions of 400 to 450 °C by at

least 1250 °C ( $\delta T$  in Eq. (4)) to a melting temperature of 1650–1700 °C or more.

Paleopiezometry from studies of grain-size and dislocation density ( $4$  to  $5 \times 10^{13} \text{m}^{-2}$ ) in olivine associated with pseudotachylyte in peridotite, compared with experimental results, indicate that peridotites may sustain extreme differential stresses of ca 3–600 MPa [5,6]. We have not been able to measure exact displacement on the studied main faults in the field because well-defined, offset markers have not been identified. However, if we assume that there is a characteristic relationships between energy per m<sup>2</sup> fault surface and the volume of melted peridotite, and that fault veins with consistent pseudotachylyte thicknesses represent faults with a minimal leakage of melt into the wall-rocks or releasing bends, we can use the volume of melt to estimate displacement [13]. A magnitude ~7 earthquake with displacement  $d \sim 1$  m [43] and a differential stress of 300 MPa in mantle peridotite [5] will release energy according to Eq. (1):  $W_f = Q + E_\eta$ ; which is equal to:  $W_f = d \times \sigma_n = d \times (\sigma_1 - \sigma_3) / 2 = 1 \text{ m} \times (300 \text{ MPa}) / 2 \approx 1.5 \times 10^8 \text{ Jm}^{-2}$ . If the seismic efficiency ( $\eta$ ) is ~5%, the radiated seismic energy  $E_\eta$  is  $7.5 \times 10^6 \text{ Jm}^{-2}$ , the remaining energy ( $Q = 1.425 \times 10^8 \text{ Jm}^{-2}$ ) turns to heat and surface energy along the fault. The process is adiabatic since the fault movement occurs in seconds and no heat is lost by conduction (thermal diffusivity  $\kappa \sim 1.5 \text{ mm}^2 \text{ s}^{-1}$ ).

Taking heat capacity of peridotite:

$$C_p = 1150 \text{ J kg}^{-1} \text{ }^\circ\text{C}^{-1};$$

Heat of fusion of peridotite:

$$H = 8.6 \times 10^5 \text{ Jkg}^{-1}$$

Temperature increase:

$$\delta T = 1200 \text{ }^\circ\text{C}$$

The thermal energy ( $Q$ ) required to melt 1 kg of peridotite according to Eq. (4) is:

$$\begin{aligned} Q &= C_p(\delta T) + HQ = 1150 \text{ Jkg}^{-1} \text{ }^\circ\text{C}^{-1}(1200^\circ\text{C}) \\ &\quad + 8.6 \times 10^5 \text{ Jkg}^{-1} \\ &= 2.24 \times 10^6 \text{ Jkg}^{-1}. \end{aligned} \quad (4)$$

A magnitude-7 mantle earthquake at these conditions may therefore melt ca 63.6 kg peridotite per m<sup>2</sup> of the fault plane, corresponding to ca 2 cm thick layer of ultramafic pseudotachylyte. This estimate is considered to be a reasonable based on the field observations where 1–3 cm-thick pseudotachylyte fault veins are common. The heat of fusion ( $H$ ) for peridotite is not well determined. Here we use a value of  $H$  for olivine given by [44] and a stress of 300 MPa in the calcu-

lation. This is close to an order of magnitude higher than stress-drops commonly measured by seismology [9]. The high stress value was chosen from a minimum estimate based on paleopiezometric measurements in the seismically faulted Balmuccia peridotite, where a stress of 3–600 MPa was obtained from detailed micro-textural studies of olivine dislocation-densities and olivine re-crystallized grain size distribution [5,6]. Extremely high stresses are also implied by the system of apparently conjugate fault veins (Fig. 3) and the high-pressure mineralogy of the pseudotachylytes [25]. We therefore prefer the high stress values derived from the combined geological/mineralogical criterion rather than those suggested by seismology. Alternatively, if the stresses were closer to those suggested from seismology, the near complete melting of peridotite would require larger displacement (closer to 10 m rather than 1 m suggested here) at lower stresses, implying much larger magnitude-9 earthquakes. It is suggested that several magnitude 7 or larger paleo-earthquakes generated the common 1–3 cm-thick pseudotachylyte fault veins in a close to conjugate fault system preserved in the mantle peridotite at Cima di Gratera.

## 6. Relationships between co-seismic slip, ductile fabric and metamorphism

It follows from the descriptions and interpretations above that co-seismic faulting at blueschist facies produced pseudotachylytes in the studied mantle rocks. The brittle faulting was in general a precursor to ductile deformation, although pseudotachylytes cutting small-scale shear zones and foliations can be observed (Fig. 5f). Pseudotachylytes were only generated in rocks retaining their mechanical framework supported by pyroxene and olivine (+plagioclase in gabbro). The ductile ultramafic rocks are dominated by serpentine, requiring introduction of vast quantities of water to form ( $\sim 100 \text{ g H}_2\text{O kg}^{-1}$ ). Similarly, hydrous minerals including amphibole, epidote and sheet-silicates characterize the foliated mafic rocks. In detail, the better-preserved rocks with pseudotachylytes also display evidence of minor hydration predating generation of pseudotachylyte and ultra-cataclastite (Fig. 5f) [25]. Serpentine micro-veins and/or grain-boundary alteration textures have been observed in the wall rocks of pseudotachylyte. Previously described textures within pseudotachylyte veins from the gabbro also show replacement of *ortho*-pyroxene by talc prior to pseudotachylyte formation, and frictional heating in ultra-cataclastite associated with pseudotachylyte veins has

dehydrated serpentine to olivine (see Fig. 3 in [25]). If co-seismic faults truncated zones of serpentinisation, significant volumes of water may have been released by the dehydration reaction of serpentine to olivine [25,45]. Release of water may in turn have caused new seismic events by reducing the effective stress and may potentially have created swarms of earthquakes similar to those related to the release of  $\text{CO}_2$  [46]. Indeed multiple events generating pseudotachylyte are common in all fault vein complexes observed in the present study.

The relationship and interdependence between frictional heating releasing water by dehydration reactions, frictional melting and hydration reactions related to ductile deformation may be more complicated. Evidence for dehydration reactions has so far only been observed at a small-scale in our previous study [25]. If seismic faults produce frictional melts, the water released may have been dissolved in the melt since silicate melts may contain very large amounts of water at high pressure [41]. It is therefore possible that significant frictional melting may reduce rather than increase local fluid pressure, whereas frictional faulting without melting may release water and increase the local fluid pressure. In spite of the limited observation of frictional-heat driven dehydration textures we suggest that local frictional heating may be a potentially important water-release mechanism in serpentine bearing rocks for reducing the strength and to trigger earthquakes.

## 7. Conclusions

The field, micro-textural and mineralogical data presented here documents that large paleo-earthquakes (magnitude-7 or larger?), from the Alpine HP-LT complex in Corsica resulted in common frictional fusion in both gabbro and mantle peridotite. The frictional heating on co-seismic faults in peridotite resulted in near complete disequilibrium melting, and raised the temperature by more than 1200 °C to over 1650 °C. Microphenocrysts of olivine, *ortho*-, and clino-pyroxene and spinel crystallized directly from the friction melts, and veins thicker than  $\sim 5 \text{ mm}$  commonly have acicular clinopyroxene forming radiating single crystals or disorder dendrites, which may have idiomorphic crystal habit adjacent to vesicles. This demonstrates that microphenocrysts crystallized directly from the melt and were not formed by later devitrification of a solidified glass. Solutions of Eq. (3) show that mm-thin veins solidified in seconds, whereas thicker melt pockets and veins ( $> 2 \text{ cm}$ ) may have preserved liquid cores for minutes, hours

and in some cases days (38 cm thick vein solidified in ca 33 h). The characteristic fault-vein thicknesses, the mineralogy and micro-textures of the pseudotachylyte veins developed in a conjugate fault system within peridotites at blueschist facies pressure conditions suggest that the stress associated with the faulting was extremely high; alternatively the displacement and the paleo-earthquakes must have been much larger than magnitude-7.

Even though the co-seismic fault products are only preserved in the least hydrated rocks of the subduction complex, it is important to note that all the studied rocks preserve evidence of some earlier serpentinisation. Micro-porosity and chemical analyses of the mostly devitrified (?) interstitial matrix show that the fluid content of the ultramafic melt was up to 4%. The generation of pseudotachylyte may dehydrate wall rocks, whereas shear heating on seismic slip-zones without melting may release fluids by localized shear-heat-driven prograde reactions [25,45]. This may in turn locally lower effective stresses and trigger swarms of new co-seismic slip-events [46]. Frictional heating on shear zones and faults may therefore be important for seismic stress-release in adjacent drier rocks. Carefully designed studies are necessary to further assess and quantify the feedback mechanism between ductile deformation and earthquakes at HP-LT metamorphic conditions such as those prevailing in subduction zones.

### Acknowledgements

A centre of excellence grant (SFF) to PGP from the Norwegian Research Council supported this study. Analyses were carried out at UiO and UCSB during a sabbatical of one of us (TBA). B. Hacker and M. Erambert are thanked for assistance with the analyses. D. Schmid wrote a matlab-script used in image analyses. We thank L. Jolivet and anonymous reviewer for their improvements and C. Marfisi and the staff at Kalliste for support in Corsica.

### References

- [1] S.H. Kirby, Intermediate-depth intraslab earthquakes and arc volcanism as physical expressions of crustal and uppermost mantle metamorphism in subducting slabs, *Geophys. Monogr.* 96 (1996) 195–213.
- [2] A. Rietbrock, F. Waldhauser, A narrowly spaced double-seismic zone in the subducting Nazca plate, *Geophys. Res. Lett.* 31 (2004) L10608, doi:10.1029/2004 GL019610.
- [3] B.R. Hacker, S.M. Peacock, G.A. Abers, S. Holloway, Subduction factory 2. Are intermediate-depth earthquakes in subduction slabs linked to metamorphic dehydration reactions? *J. Geophys. Res.* 108 (2003), doi:10.1029/2001JB001129.
- [4] L. Jolivet, C. Faccenna, B. Goffé, E. Burov, P. Agard, Subduction tectonics and exhumation of high-pressure metamorphic rocks in the Mediterranean orogens, *Am. J. Sci.* 303 (2003) 353–409.
- [5] M. Obata, S.I. Karato, Ultramafic pseudotachylyte from the Balmuccia peridotite, Ivrea–Verbano zone, northern Italy, *Tectonophysics* 242 (1995) 313–328.
- [6] D. Jin, S.I. Karato, M. Obata, Mechanism of shear localization in continental lithosphere: inferences from the deformation microstructures of peridotites from the Ivrea zone, northwestern Italy, *J. Struct. Geol.* 20 (1998) 195–209.
- [7] T. Morishita, Possible pseudotachylyte from the Horoman peridotite complex of the Hidaka belt, Hokkaido, northern Japan, *J. Geol. Soc. Jpn.* 104 (1998) 18–23.
- [8] M.G. Lund, Metamorphism, earthquakes and fracturing of the deep continental crust, Unpubl. PhD, Univ. Oslo (2002) 169 pp.
- [9] S.C. Scholz, *The Mechanism of Earthquakes and Faulting*, Cambridge University Press, 1990, 439 pp.
- [10] J.G. Spray, Pseudotachylyte controversy: fact of friction?, *Geology* 12 (1995) 1119–1122.
- [11] H.R. Wenk, L.E. Weiss, Al-rich calcic pyroxene in pseudotachylyte: an indicator of high pressure and high temperature? *Tectonophysics* 84 (1982) 329–341.
- [12] G. Di Toro, D.L. Goldsby, T.E. Tullis, Friction falls to zero in quartz rock as slip velocity approaches seismic rates, *Nature* 427 (2004) 436–439.
- [13] H.R. Wenk, L.R. Johnson, L. Ratschbacher, Pseudotachylytes in the Eastern peninsular ranges of California, *Tectonophysics* 321 (2000) 253–277.
- [14] A. McGarr, On relating apparent stress to the stress causing earthquake fault slip, *J. Geophys. Res.* 104 (B2) (1999) 3003–3011.
- [15] K. Mair, C. Marone, Shear heating in granular layers, *Pure Appl. Geophys.* 157 (2000) 1847–1866.
- [16] M.A. d'Alessio, A.E. Blythe, R. Bürgmann, No frictional heat along the San Gabriel fault, California: evidence from fission-track thermochronology, *Geology* 31 (2003) 541–544.
- [17] C.H. Scholz, A fault in the weak San Andreas' theory, *Nature* 406 (2000) 234.
- [18] D.M. Saffer, B.A. Bekins, S. Hickman, Topographically driven groundwater flow and the San Andreas heat flow paradox revisited, *J. Geophys. Res.* 108 (B5) (2003) 2274, doi:10.1029/2002JB001849.
- [19] V.M. Goldschmidt, Om friksjonsglass (pseudo-tachylitt) i fjellkjeden, *GFF* 65 (1943) 83–84.
- [20] D.P. McKenzie, J.N. Brune, Melting of fault planes during large earthquakes, *Geophys. J. R. Astron. Soc.* 29 (1972) 8053–8068.
- [21] R.H. Sibson, Generation of pseudotachylyte by ancient seismic faulting, *Geophys. J. R. Astron. Soc.* 43 (1975) 775–794.
- [22] J.G. Spray, Artificial generation of pseudotachylyte using friction welding apparatus: simulation of melting on a fault plane, *J. Struct. Geol.* 9 (1987) 49–60.
- [23] J.F. MacLoughlin, J.G. Spray, Frictional melting processes and products in geological materials: introduction and discussion, *Tectonophysics* 204 (1992) 197–206.
- [24] H. Kanamori, D.L. Anderson, T.H. Heaton, Frictional melting during the rupture of the 1994 Bolivian earthquake, *Science* 279 (1998) 839–842.
- [25] H. Austrheim, T.B. Andersen, Pseudotachylytes from Corsica, fossil earthquakes from a subduction complex, *Terra Nova* 16 (2004) 193–197.

- [26] M. Fournier, L. Jolivet, B. Goffé, R. Dubois, Alpine Corsica Metamorphic core complex, *Tectonics* 10 (1991) 1173–1186.
- [27] D. Lahondère, Les schistes bleus et les eclogites a lawsonites des unites continentales et oceanques de la Corse alpine, Orleans, France, Bureau de Recherches Geol. et Minieres, Doc., vol. 240, 1996, 285 pp.
- [28] D. Lahondère, D. Guerrot, Datation Sm–Nd du metamorphisme eclogitique en Corse alpine: un argument pour l'existence au Cretace superieur d'une zone de subduction active localisee sous le bloc Corso–Sarde, *Geol. Fr.* 3 (1997) 3–11.
- [29] R. Tribuzio, F. Giacomini, Blueschist facies metamorphism of peralkaline rhyolites from the Tenda crystalline massif (northern Corsica): evidence for involvement in the Alpine subduction event?, *J. Metamorph. Geol.* 20 (2002) 513–526.
- [30] E.J. Essene, Relatively pure jadeite from a siliceous Corsican gneiss, *Earth Planet. Sci. Lett.* 5 (1969) 270–272.
- [31] C. Brunet, P. Monié, L. Jolivet, J.P. Cadet, Migration of compression and extension in the Tyrrhenian Sea, insights from  $^{40}\text{Ar}/^{39}\text{Ar}$  ages on micas along a transect from Corsica to Tuscany, *Tectonophysics* 321 (2000) 127–155.
- [32] J. Warburton, The ophiolite-bearing Schistes lustrés nappe in the Alpine Corsica: a model for the emplacement of ophiolites that have suffered HP/LT metamorphism, *Geol. Soc. Am. Mem.* 164 (1986) 313–331.
- [33] D. Lahondère, Eclogitic metamorphism in Farinoles orthogneisses and ophiolitic metabasites (Northern Corsica, France), *Bull. Soc. Geol. Fr.* 4 (1988) 579–585.
- [34] H. Austrheim, T.M. Boundy, Pseudotachylytes generated during seismic faulting and eclogitization of deep crust, *Science* 265 (1994) 82–83.
- [35] M.G. Lund, H. Austrheim, High-pressure metamorphism and deep-crustal seismicity: evidence from contemporaneous formation of pseudotachylytes and eclogite facies coronas, *Tectonophysics* 372 (2003) 59–83.
- [36] M.G. Bjornerud, H. Austrheim, M.G. Lund, Processes leading to eclogitization (densification) of subducted and tectonically buried crust, *J. Geophys. Res.* 107 (2002), doi:10.1029/2001JB000527.
- [37] A. Suzuki, and collaborators, Viscosity of komatiite magma at high pressure, Bayerisches Geoinstitut Annual Report, 2001 [http://www.bgi.uni-bayreuth.de/annual\\_report/navigat.php3?year=2001](http://www.bgi.uni-bayreuth.de/annual_report/navigat.php3?year=2001).
- [38] D.L. Turcotte, G. Schubert, *Geodynamics*, Cambridge University Press, 2002, 472 pp.
- [39] D.H. Lindsley, Pyroxene thermometry, *Am. Mineral.* 68 (1983) 477–493.
- [40] E. Stolper, D. Walker, Melt density and the average composition of basalt, *Contrib. Mineral. Petrol.* 74 (1980) 7–12.
- [41] B.O. Mysen, K. Wheeler, Solubility behavior of water in haploandesitic melts at high pressure and high temperature, *Am. Mineral.* 85 (2000) 1128–1142.
- [42] R.F. Katz, M. Spiegelman, C.H. Langmuir, New parameterization of hydrous mantle melting, *Geochem. Geophys. Geosyst.* 4 (2003) 1073, doi:10.1029/2002GC000433.
- [43] M.G. Bonilla, R.K. Mark, J.L. Lienkaemper, Statistical relations among earthquake magnitude, surface rupture length and surface fault displacement, USGS Open File Report 84–256, 1984 <http://geopubs.wr.usgs.gov/open-file/of84-256/>.
- [44] R.S. Bradley, Thermodynamic calculations on phase equilibria involving fused salts: Part II. Solid solutions and the application to the olivines, *Am. J. Sci.* 260 (1962) 550–554.
- [45] B. Wunder, W. Schreyer, Antigorite: high-pressure stability in the system MgO–SiO<sub>2</sub>–H<sub>2</sub>O (MSH), *Lithos* 41 (1997) 213–227.
- [46] S.A. Miller, C. Collettini, L. Chiaraluce, M. Cocco, M. Barchi, B.J.P. Kaus, Aftershocks driven by a high-pressure CO<sub>2</sub> source at depth, *Nature* 427 (2004) 724–727.
- [47] R. Kretz, Symbols for rock-forming minerals, *Am. Mineral.* 68 (1983) 277–279.

## Evidence for hyperextension along the pre-Caledonian margin of Baltica

TORGEIR B. ANDERSEN<sup>1\*</sup>, FERNANDO CORFU<sup>2</sup>, LOIC LABROUSSE<sup>3</sup> & PER-TERJE OSMUNDSEN<sup>4</sup>

<sup>1</sup>University of Oslo, Physics of Geological Processes, PO Box 1048, Blindern, 0316 Oslo, Norway

<sup>2</sup>Department of Geosciences, University of Oslo, PO Box 1047, Blindern, 0316 Oslo, Norway

<sup>3</sup>Institut des Sciences de la Terre Paris, Université Pierre et Marie Curie—Paris 6, UMR 7193, Paris, France

<sup>4</sup>Geological Survey of Norway, 7491 Trondheim, Norway

\*Corresponding author (e-mail: [t.b.andersen@geo.uio.no](mailto:t.b.andersen@geo.uio.no))

**Abstract:** We propose that a mantle-peridotite-bearing mélange unit, which has been mapped for more than 400 km in southern Norway, represents vestiges of deep basin(s) formed by hyperextension of the Baltic margin during the inception of the Caledonian Wilson cycle. In the mélange, which occurs below the crystalline nappes of the Middle Allochthon in southern Norway, solitary mantle peridotites, detrital serpentinites, metabasalts, gabbros and deep basin sediments are interlayered and imbricated with allochthonous, coarse-grained siliciclastic sediments and slivers of Proterozoic basement rocks. The siliciclastic sediments have detritus derived from Proterozoic rocks, similar to those of the large crystalline nappes and the autochthonous basement of Baltica. The mélange unit shares many similarities with the hyperextended Tethyan margin complexes that have been described from the Alps, the Pyrenees and several segments of the present-day passive ocean margins, and we interpret it to represent an ancient late Proterozoic to Palaeozoic analogue to present-day hyperextended passive margins. Regional maps show that the mélange continues into the central Scandinavian Caledonides and that this basin assemblage may have had a much wider geographical distribution. The new model suggests that a major reinterpretation of the Lower and Middle Allochthons of the Scandinavian Caledonides is required.

Hyperextended ocean–continent transition (OCT) zones at passive margins are extremely complex geological provinces. Our conception of such provinces has recently changed, based on combinations of modern high-quality geophysical data, drill-core information and comparative studies of analogue areas onshore (e.g. Boillot *et al.* 1987; Manatschal 2004; Péron-Pinvidic & Manatschal 2009). One of the most novel results of these studies is that large areas of subcontinental mantle may be exhumed to the sea floor in mantle windows controlled by large-scale extensional detachments rather than by breakup-related magmatic processes. For example, one of the largest exhumed mantle peridotites in the world exposed to the sea floor or covered by thin post-rift sediments occurs along the continent–ocean boundary (COB) in the Brazilian passive margin of the South Atlantic (Zalan *et al.* 2011). Recently, it has been recognized that processes of hyperextension are not exclusive to magma-poor margins such as Iberia. The magma-rich NE Atlantic margin was affected by hyperextension in the Late Jurassic–Early Cretaceous (Osmundsen & Ebbing 2008; Lundin & Doré 2011). Conversely, it has been argued that so-called magma-poor margins may host significantly higher magmatic volumes than previously recognized (Müntener & Manatschal 2006). The studies on passive margins have also stimulated academic research in mountain belts and inspired new concepts for the initiation of subduction and mountain building. These exposures of mantle material are related to extension rather than to magmatic emplacement and magmatic sea-floor spreading processes. The best-developed models for hyperextended passive margins have developed from offshore studies combined with onshore analogues (e.g. Manatschal 2004; Lagabrielle *et al.* 2010). New models have been presented for many Alpine ophiolites and associated sedimentary and tectonic units and have revolutionized palaeogeographical reconstructions even for the most mature study areas such as the western and central Alps, Alpine Corsica or

the lherzolite-bearing assemblages of the Pyrenees (Lagabrielle & Bodinier 2008; Lagabrielle *et al.* 2010; Mohn *et al.* 2010; Vitale Brovarone *et al.* 2011). The main revision within the European Alps is that ‘Alpine’ peridotites associated with deep-marine basin deposits, which previously were viewed as Tethyan oceanic mantle sequences in dismembered ophiolite complexes, are now interpreted to represent subcontinental mantle rocks, exhumed in the footwalls of major low-angle detachments that formed by hyperextension of the European continental margin. Similar models have, however, not yet been tested for enigmatic peridotite-bearing mélanges within older Phanerozoic orogens, such as the Caledonides.

Contrary to sea-floor spreading ophiolites these Alpine peridotites are characterized by the ‘Steinmann trinity’ association (serpentinite, greenstone and chert) and a paucity of gabbros and basaltic lavas (e.g. Bernoulli & Jenkyns 2009). They mostly lack the sheeted-dyke complexes that commonly are taken to be the signature of an oceanic spreading-ridge. Unlike sea-floor spreading ophiolites, these peridotites are intimately associated with slivers of highly deformed older crystalline continental crust, and continentally derived siliciclastic sediments, as well as deep-water deposits and in some cases passive-margin carbonates (e.g. Manatschal *et al.* 2006; Lagabrielle *et al.* 2010). Intensely deformed contacts reflect several stages of deformation, superimposed on the original extensional fabrics, leading to juxtaposition on the mantle of rocks that originally had formed at different crustal levels. The reinterpretations of these mélange associations have resulted in revised models for the pre-Alpine Tethyan margins and basins: (1) they are hyperextended continental crust rather than ocean basins formed by sea-floor spreading and (2) their imbrication into the nappe complexes is part of the sequential slicing and stacking of the continental margin involved in the collision rather than the result of an obduction stage.

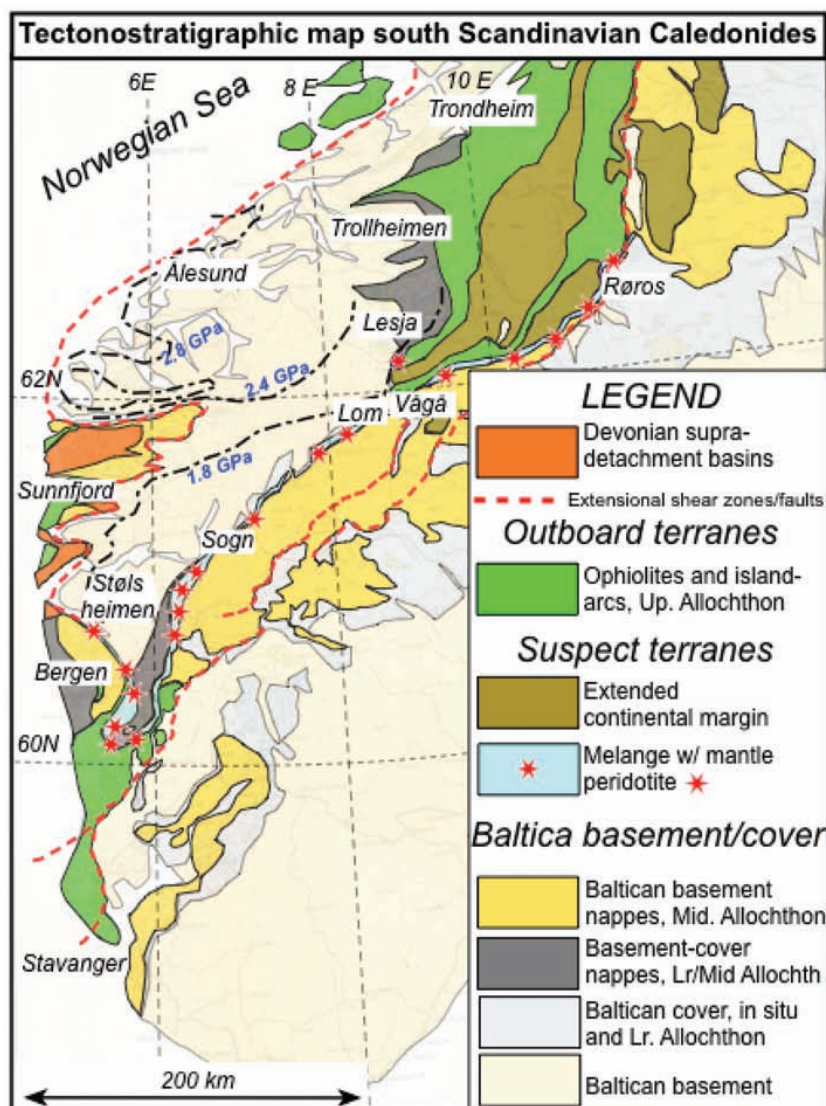


Fig. 1. Tectonostratigraphic map of the South Norwegian Caledonides, highlighting the regional distribution of the highly deformed transitional crust mélangé assemblages structurally positioned below the large crystalline nappes (Lindås, Upper Bergsdalen, Jotun Nappes) of the Middle Allochthon. It should be noted that this level with solitary mantle peridotites can be traced continuously to the Røros area, and along the eastern side of the Western Gneiss Region past Lesja towards Trollheimen. Major units such as nappes assigned to the Gula and the Seve nappes are here labelled suspect, but they most probably belong to the hyperextended distal margin of Baltica. Major post-Caledonian extensional structures are shown in red. The Scandian collision pressure isobars in the Western Gneiss Region are also shown.

The mantle-peridotite-bearing mélangé unit discussed here is structurally positioned below major nappes of crystalline continental crust of Proterozoic age including the Upper Bergsdalen, Jotun and Lindås nappes in the SW Norwegian Caledonides (Fig. 1). In previous tectonic models for the Scandinavian Caledonides the significance of the large number of mantle peridotites occurring below these crystalline nappe complexes has been mostly ignored. In this paper we present a new interpretation based on detailed field studies of selected areas combined with a regional study between Bergen and Vågå (Fig. 1).

### Regional geology

The Caledonian mountain belt of Scandinavia and east Greenland was assembled by a major, continent–continent collision comparable in dimensions, dynamics and relative chronology of events with the Himalayan collision (Labrousse *et al.* 2010). The collision

commenced as the Iapetus Ocean closed by subduction in the Middle Silurian (*c.* 430 Ma) and the incipient collision is dated by the cessation of subduction-related island-arc magmatism (Torsvik & Cocks 2005; Corfu *et al.* 2006) and obduction of marginal basin ophiolites in the Middle Silurian (Andersen *et al.* 1990; Furnes *et al.* 1990). The convergence and continental collision continued for *c.* 30 Ma into the early Devonian when the high- and ultrahigh-pressure rocks of the Western Gneiss Region reached their maximum burial depth at *c.* 410–400 Ma (e.g. Hacker *et al.* 2010). The collision is commonly referred to as the Scandian Orogeny, but it also affected vast areas in East Greenland and caused shortening far into the overriding Laurentian plate.

The present models for the Scandinavian Caledonides were mostly developed during the IGCP project 27 summarized by Gee & Sturt (1985). An important result of this project was the compilation of a tectonostratigraphic map described by Roberts & Gee (1985). This map has since been a template for most regional studies

and its four-fold division of allochthonous units (Lower, Middle, Upper and Uppermost Allochthons) has been extended to represent terranes of sequential origins (Stephens & Gee 1989). The Uppermost and Upper Allochthons (except the Seve Units) are considered outboard and believed to represent the overriding Laurentian plate (Uppermost Allochthon) and outboard oceanic terranes (Upper Allochthon), respectively (e.g. Roberts *et al.* 2002). Palaeomagnetic, palaeontological and geological studies show that major plate rotation and convergence accompanied by magmatic and collision events took place within wide (several thousand kilometre) oceanic domains (Ægir Sea and Iapetus Ocean) throughout the Ordovician and early Silurian, prior to the Scandian orogeny (Torsvik & Cocks 2005). The Upper and Uppermost Allochthons are of undisputed non-Baltican origin, whereas the regionally extensive Middle and Lower Allochthons originally were assigned to Baltica. This latter interpretation has recently been challenged by several detailed studies from northernmost Norway (Corfu *et al.* 2007, 2011; Kirkland *et al.* 2008a,b). These studies suggest that an exotic, non-Baltican origin of the continental basement–cover nappes of the Kalak Nappe complex cannot be excluded. Further to the south in the central Caledonides (between *c.* 64 and 69°N), large dyke-swarms, intrusions and associated volcanic rocks in the continental Seve Nappes lithologies have been interpreted to represent a volcanic passive margin formed in the latest Proterozoic and dated at 608 Ma (Andreasson 1994; Andreasson *et al.* 1998; Svenningsen 2001). In some of these units there are also minor volcanic rocks and gabbro, local occurrences of serpentinite conglomerates and peridotites with black-rock alteration zones at the border between the continental and oceanic terranes of the Seve–Køli units. Studies of these rocks demonstrate that the ultramafic mantle rocks and siliciclastic sediments were intimately associated throughout the Caledonian orogenic cycle (Qvale & Stigh 1985; van Roermund 1985; Bucher *et al.* 2005).

The complex tectonic evolution and assembly of the Middle to Upper Allochthon continental margin rocks is witnessed by at least two stages of eclogite-facies metamorphism, at  $482 \pm 1$  and  $446 \pm 1$  Ma respectively (e.g. Root & Corfu 2011). These parts of the mountain belt, which host the evidence of pre-Scandian, Early to Middle Ordovician deformation and metamorphic events, are normally considered endemic Baltican terranes (Andreasson *et al.* 1998). Given the new interpretations introduced for equivalent units of Finnmark and Troms (see above), their origin should be viewed with considerable caution, as it follows from the recent studies that major revisions in interpretations of the Seve–Kalak terranes in northernmost Scandinavia and their continuation toward southern Scandinavia are required (Corfu *et al.* 2011).

In southern Scandinavia the Middle Allochthon is dominated by very large crystalline nappe complexes of Proterozoic age. These include the Dalsfjord, Lindås, Jotun, Bergsdalen and Hardanger–Ryfylke nappe complexes (Fig. 1). Most of these have a cover of metasedimentary rocks dominated by quartzite, arkosic sandstone and schists. Geochronological studies of both the crystalline allochthonous basement units and their cover sequences suggest an affinity to the autochthonous basement of southern Baltica and hence an origin on its Caledonian margin before collision (Corfu & Andersen 2002; Lundmark *et al.* 2007; Glodny *et al.* 2008; Bingen *et al.* 2011). This simple relationship is, however, challenged by the regional occurrence of a relatively thin, but continuous mélange zone containing numerous lenses of peridotite and minor mafic meta-igneous rocks, which is located structurally below these crystalline nappe complexes along their western boundary adjacent to the Bergen Arcs and the Western Gneiss Region (Fig. 1). The mélange has largely been ignored in the compilation of the tectonostratigraphic map (see above) or believed to represent ophiolitic

rocks belonging to the Upper Allochthon. This enigmatic mélange unit occurs structurally above the Western Gneiss Region and the discontinuous thin black schist–phyllite, micaschist and quartzite with local pockets of preserved basal conglomerates, which represent the original cover to the autochthonous gneisses below the Caledonian floor thrust. The mélange with solitary mantle peridotites can be identified almost continuously along a distance of more than *c.* 400 km from the Bergen Arcs northeastwards across South Norway. In the present study, this unit has been traced as far as Lom (Fig. 1), but a simple map correlation suggests that it continues further towards the Røros area as well as the western side of the Trondheim region north of Lesja (Fig. 1). These rocks have received very little attention in tectonic reconstructions of the Caledonides, in spite of their long economic history with talc and soapstone quarries.

## The mélange

### Ultramafic rocks

The most conspicuous rocks within the regionally extensive mélange are the metaperidotites, now mostly present as serpentinite, soapstone and talc-schist, which occur in very large numbers between the Bergen Arcs and the northeastern part of the study area in central South Norway and beyond (Fig. 1). In this study we have examined the structural setting and association of the solitary ultramafic rocks in the Samnanger–Osterøy area of the Major Bergen Arc (Fig. 2), in Stølsheimen (Fig. 3) and along the eastern border between the Jotun Nappe and the Western Gneiss Region between Sogn and Lom (Fig. 1).

The majority of the ultramafic bodies are low-Al, high-Mg mantle peridotites, but more evolved varieties are also locally present (Qvale & Stigh 1985). Some of the best-preserved larger lenses still contain primary minerals and may attain dimensions of up to 2 km, but more commonly they occur as serpentinite lenses less than 100 m in size (Figs 3 and 4a, b). Hydration and metasomatic alteration zones are ubiquitous and many are completely serpentinized or talcified. Serpentine and soapstone veins are very common (Fig. 4f) and locally quartz–carbonate rocks (listwanite) and ophiolite alterations are present. Some bodies have been mined to exhaustion for talc and soapstone such as the talc mines at Framfjord (Fig. 3) and the soapstone quarries in the Bergen Arcs (Fig. 2). Alteration to serpentinite and talc–carbonate–spinel rocks is very common; such rock types contain breunnerite, magnesite, chlorite, chromite and magnetite (see NGU mineral database, occurrence 1417-301, Rauberget). Black-wall alteration zones are common (Fig. 4e), but detailed descriptions of these are mostly lacking except from one that was described in detail from the Seve complex north of our study area, the ultramafic rocks at Baldersheim (Fig. 2) and the rodingite alteration present in the Major Bergen Arc (Bøe 1985; Qvale & Stigh 1985; Bucher *et al.* 2005).

Isolated detrital serpentinites (Fig. 4c) occur in several localities as both conglomerate and sandstone (Heldal & Jansen 2000; see also descriptions by Qvale & Stigh 1985). More common are lenses containing blocky to rounded serpentinite breccias that partly also may have a sedimentary origin (Fig. 4d). The intense Caledonian deformation and later syn- to post-orogenic extension have, however, largely obliterated primary structures. The most spectacular occurrence of detrital serpentinite, described by Sturt & Ramsay (1999), occurs near Otta (Fig. 1), where a Middle Ordovician fauna (Llanvirn) occurs in serpentinite conglomerates overlying ultramafic rocks assigned to the Vågåmo ophiolite. Those workers suggested that the serpentinite conglomerate represents a major unconformable sequence deposited on

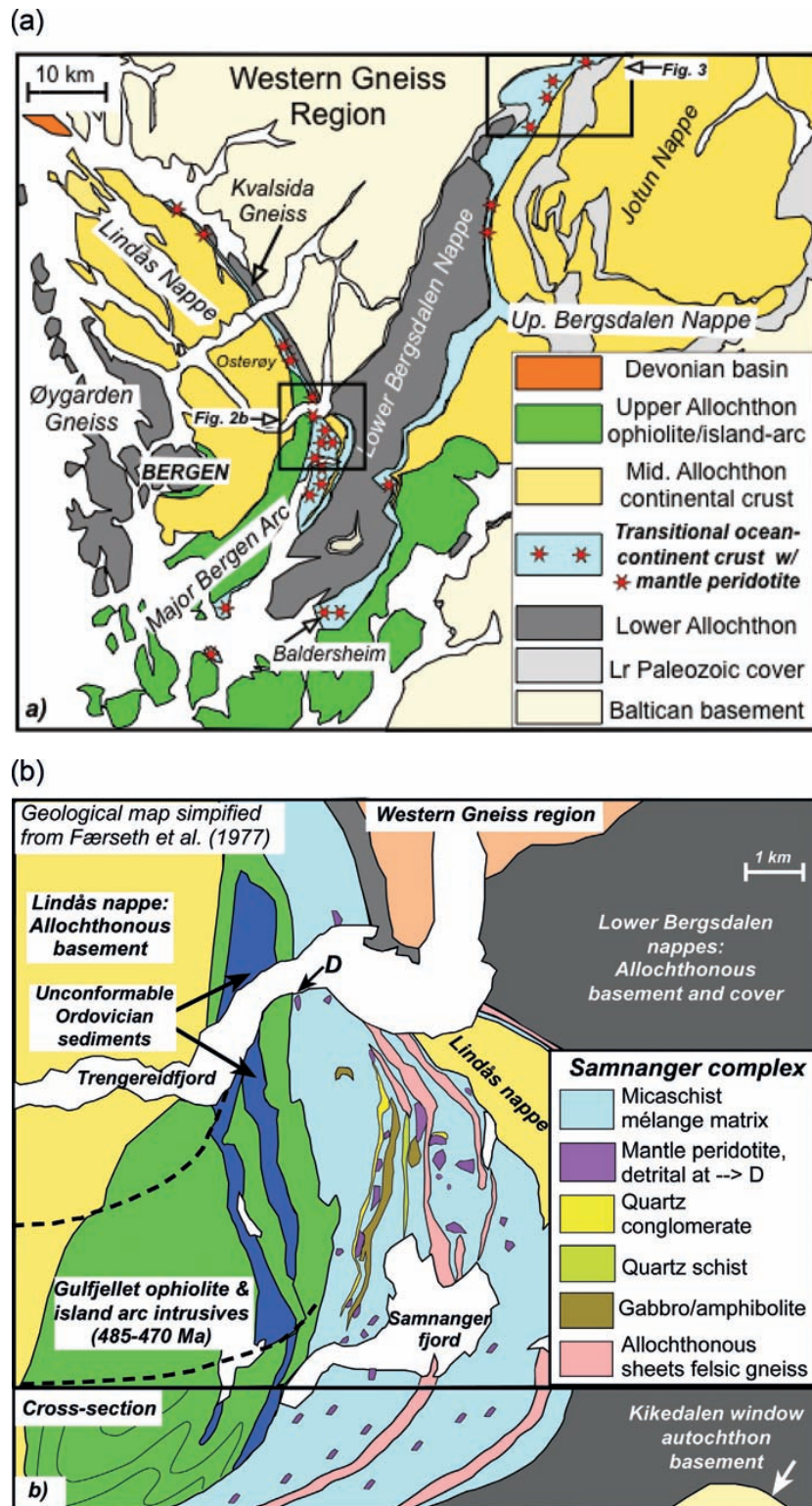


**Fig. 2.** (a) Geological map of the Bergen–Hardanger region and (b) map with cross-section of the Samnanger–Osterøy area simplified from Faerseth *et al.* (1977). It should be noted that the mélange unit is situated structurally above the Lower Bergsdalen and Kvalsida Gneiss Nappes, but below the Upper Bergsdalen and Lindås nappes as well as the ophiolite–island-arc units of the Upper Allochthon. Also noteworthy are the numerous solitary mantle peridotite bodies in the Samnanger area, and their intimate association with sheets of gneisses and quartz-rich sediments. Detrital serpentinites are found at Baldersheim, shown in (a), and on the south shore of Trengereidfjorden at locality D, shown in (b).

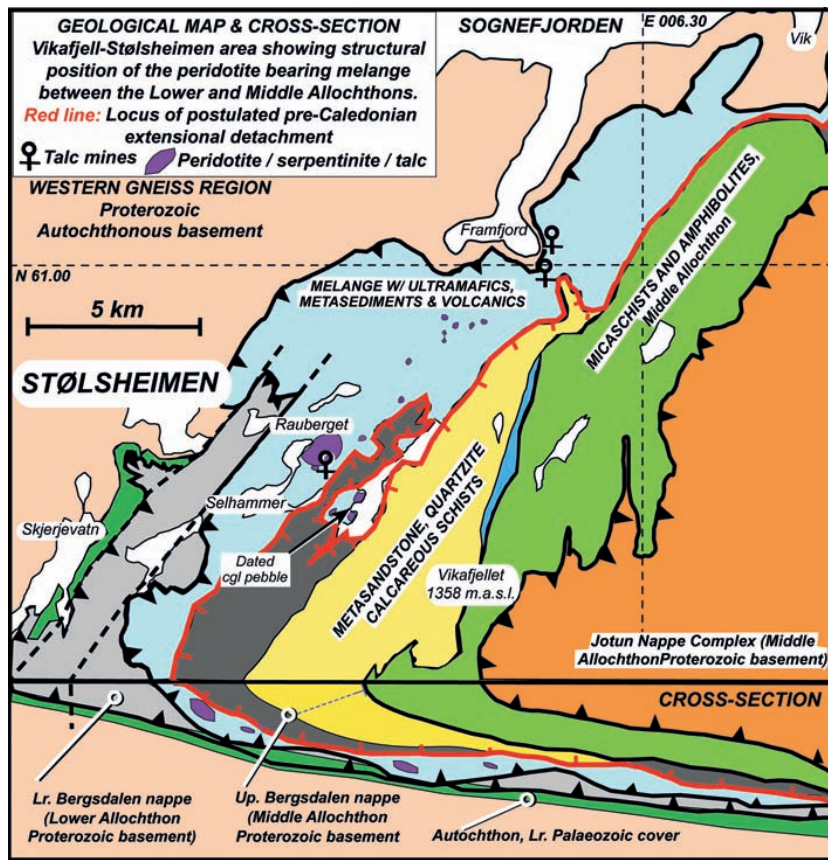


Fig. 3. Geological map with cross-section of the Stølsheimen region. Noteworthy features are the abundance of solitary mantle peridotites in this area and that the mélangé is sandwiched between the Lower and Upper Bergsdalen nappes. We suggest that the pre-Caledonian extensional exhumation of the mantle peridotites must have taken place along major extensional shear zone(s) positioned below the base of the Upper Bergsdalen and Jotun Nappe Complexes, here shown as the red line.

the Vågåmo ophiolite after obduction onto Baltica. In view of the tectonostratigraphic position of these rocks, which is comparable with that of other ultramafic rocks discussed here, previous interpretations should probably be reconsidered. As pointed out by Qvale & Stigh (1985) and their obvious map signature, many of the peridotites including the detrital serpentinites are 'solitary ultramafites, where an ophiolite association is not easily recognized'. Lenses of metagabbro and metavolcanic rocks can be observed in many of the localities, but the traditional ophiolite pseudostratigraphy and in particular sheeted-dyke complexes are not present in these units.

#### Metasedimentary matrix

The metaperidotites are set in a matrix dominated by metasedimentary rocks, now graphitic schists, phyllites and garnet micaschists recrystallized during the Caledonian greenschist- to lower amphibolite-facies metamorphism. Metasomatic alteration is common and tremolite- to actinolite-bearing schists are intercalated with quartzschists and originally pebbly sandstones in some localities. Similar intimate associations of metaperidotites engulfed in metasediments have been described from widely separated localities such as the Major Bergen Arc (Faereth *et al.* 1977; Ingdahl 1985), in Stølsheimen and Sogn, as well as near Lom (Fig. 1). Metamorphism related to the Scandian orogeny attained low amphibolite-facies conditions at the level of the floor thrust along the eastern margin of the Western Gneiss Region in central South Norway (500 °C,

0.6–0.8 GPa; work in progress). Although now dominated by micaschist and phyllite, the original sediments of the matrix had a composition and grain-size variation from originally very fine-grained graphitic shale and cherty horizons to calcareous sandstone and marls with local limestone, to coarse sandstone and quartzite horizons with local conglomerates (see also [www.ngu.no](http://www.ngu.no), geological map database). Matrix-supported, debris-flow-like conglomerate horizons are also locally present. In Stølsheimen (Figs 3 and 5), a conglomerate contains a variety of pebbles including fine-grained basement-derived granite, quartzite and vein quartz suggesting a dominantly continental provenance (see below). The transition zone from a peridotite into the sedimentary matrix is shown in Figure 4e. The ultramafic green-coloured schists occur in close proximity with conglomerate containing quartzite and granite pebbles (Fig. 5a), and grade into micaschists with scattered mafic lenses across few metres.

#### Continental basement and sediments in the mélangé

In the western part of the study area, the ultramafic mélangé is stacked together with sheets of felsic crystalline gneisses commonly referred to as the Bergsdalen nappes (e.g. Fossen 1993). In the Stølsheimen area and southwards towards the Bergen Arcs (Figs 2a and 3), basement of granitic gneiss, metasandstones and schists constitute the Upper Bergsdalen nappe (Fossen 1993). In the Rauberget area, this highly attenuated basement-cover pair

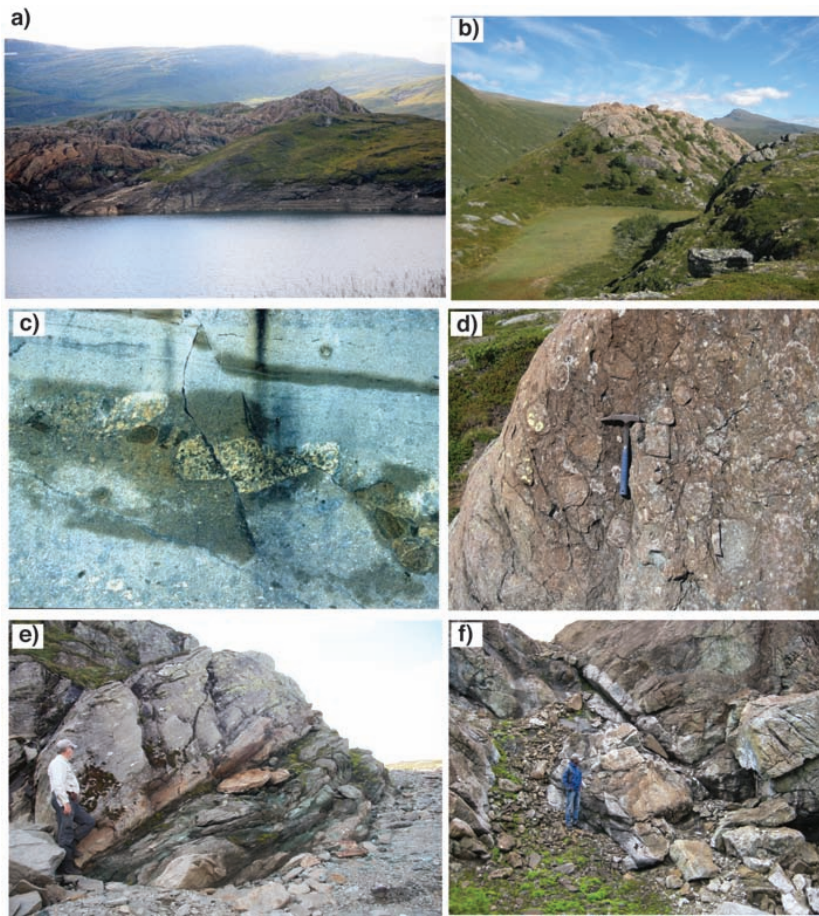


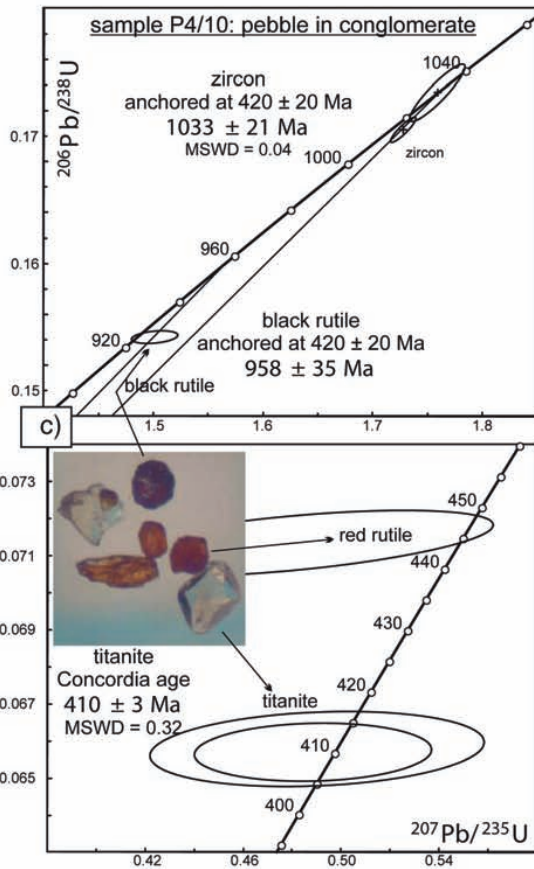
**Fig. 4.** (a) View towards the SE of a major solitary mantle peridotite near Rauberget (Fig. 3) in Stølsheimen. The regional SE-dipping foliation, placing the peridotite below the Upper Bergsdalen nappe seen in the hillside behind the peridotite, should be noted. (b) View towards the NE of a c. 100 m thick solitary mantle peridotite at Bøverdalen near Lom (see Fig. 1 for location). The steep SE-dipping regional foliation, clearly showing that the mélange unit occurs structurally above the Western Gneiss Region (left) and below the Jotun Nappe (right), should be noted. (c) Example of a little deformed fluviatile serpentinite conglomerate and sandstone from a quarry at Trengereidfjord marked D in Figure 2b. The detrital serpentinites with pebbles up to 15 cm long quarried from the now exhausted locality were used as decorative stone and building material in Bergen and elsewhere. Photograph provided by Ø. J. Jansen (see also Heldal & Jansen 2000, pp. 80 and 168). (d) Serpentinite breccia at Bøverdalen near Lom (Fig. 1) showing the highly brecciated nature, and possibly detrital structure(?), typically displayed by many serpentinite bodies. (e) Black-wall alteration zone (base of outcrop) along the top of the serpentinite shown in (a), where the hydrated peridotite makes contact with schists and conglomerates (top of outcrop; see also Fig. 5). (f) Serpentinite with soapstone (talc, magnesite) alteration (white) along veins and adjacent to the wall-rock schists. Locality near the dated conglomerate pebble (Figs 3 and 5).

immediately overlies the best-developed ultramafic mélange, which in turn is overlain by the Jotun and Lindås nappes (see Figs 2 and 3, and for further details, Fossen (1993)). The contact of the mélange with mantle peridotite and the overlying continental rocks is a tectonic contact, which preserves evidence of Scandian thrusting and the secondary post-collisional extension. Internally, however, some sheets of the Proterozoic ortho- and paragneisses are less deformed with granitic dykes cutting Proterozoic metasediments (Fossen 1993). This allochthonous basement contains Neoproterozoic granites (the youngest Rb/Sr whole-rock age of granite is  $953 \pm 16$  Ma (Grey 1978)) cutting both the metavolcanic and sedimentary units as described by Fossen (1993). The structure is dominated by the Scandian thrust-fabric (top-to-the-SE) overprinted by a co-metamorphic to retrograde top-to-the-NW shear fabric formed during the regional orogenic extensional collapse of the Caledonides (Andersen 1998; Fossen 2010).

The mélange unit and the continental crust rocks were most likely juxtaposed prior to thrusting because both generations of thrust and extensional Caledonian fabrics are developed in the mantle-derived peridotites, their sedimentary matrix as well as in the continental basement-cover rocks. In spite of careful examination near the best-preserved peridotites at Rauberget in Stølsheimen (Figs 3 and 4), pre-thrusting structural relationships have not yet been observed and their exact stratigraphic

and structural relationships prior to the Caledonian thrusting have not been determined. It is, however, obvious that the mélange with mantle peridotites constitute the substrate to both the highly attenuated Upper Bergsdalen nappe and the Jotun nappe (Fig. 3).

The most systematic mapping of the mélange has been carried out in the Major Bergen Arc (Faereth *et al.* 1977; Qvale 1978; Henriksen 1981; Bøe 1985; Ingdahl 1985). This mapping demonstrates the intimate association of a large number of serpentinite and peridotite lenses with amphibolite, graphitic schists, hornblende-garben-schist, garnet-micaschists, quartz-rich metasandstone, quartzite conglomerates and several sheets of felsic gneisses. The researchers listed above regarded the Samnanger complex of the Major Bergen Arc to represent a tectonic mélange structurally positioned below the Gulfjellet ophiolite complex (Fig. 2b). The mélange was primarily considered to represent a tectonic mélange deformed, imbricated and assembled during several stages of Caledonian deformation (Faereth *et al.* 1977; Thon 1985). The intimate mixing of mantle-derived rocks with continental gneisses and sediments is, however, not easily explained by deformation during the Scandian continental collision, and we suggest that juxtaposition of these rocks, particularly the Proterozoic basement and the solitary mantle peridotites, is inherited from pre-Caledonian extension.



*U–Pb geochronology from the mélangé conglomerate*

Near Rauberget in Stølsheimen (Fig. 3) the contact relationships between ‘talcified’ ultramafic rocks (Fig. 4a and f) and the black-wall alteration zone in the sedimentary matrix is well exposed (Fig. 4e). Foliated black-wall alteration schists with abundant quartz veins are interlayered with pebbly quartzite and a matrix-supported conglomerate dominated by quartz and quartzite pebbles (Fig. 5a). The conglomerate also contains pebbles of a leucogranite, which may be up to 15 cm in size (Fig. 5b). One part of a pebble was crushed, pulverized and subjected to mineral separation following standard methods. The handpicked minerals were processed by isotope dilution thermal ionization mass spectrometry (Krogh 1973) as described in more detail by Corfu (2004). Besides rounded zircons, probably from the rind of the pebble and of detrital origin, there is a subpopulation of sharp euhedral short prisms (inset in Fig. 5c). A selection of these crystals was abraded and two of them were analysed. The data (Table 1, Fig. 5c) plot on or close to the concordia curve, and a line anchored at  $420 \pm 20$  Ma, the approximate time of metamorphism, has an intercept age of  $1033 \pm 21$  Ma, which dates the original crystallization of the rock. Dark rutile is nearly concordant and can be projected (anchoring the lower intercept at  $420 \pm 20$  Ma) to an upper intercept age of  $958 \pm 35$  Ma. In contrast, the red rutile is much younger, and is presumably on its way to full resetting owing to its reaction to titanite. It is also observed as inclusions in the latter (inset in Fig. 5c). The titanite analyses yield concordant data and give an age of  $410 \pm 3$  Ma for the Scandian metamorphic event. The Proterozoic ages agree well with previously published Rb/Sr whole-rock ages from the Upper Bergsdalen nappe in the same area (Grey 1978). U/Pb dating of titanite from the same pebble is concordant and documents the Caledonian regional metamorphic overprint at  $410.4 \pm 3.1$  Ma, which is similar to other Scandian metamorphic ages from the nappes in western Norway (e.g. Fossen & Dunlap 1998; Glodny *et al.* 2008).

**Discussion**

Previous descriptions of Neoproterozoic basins in the Scandinavian Caledonides have documented that the Caledonian margin of Baltica constituted a wide (up to 600 km) extended margin facing the outboard oceanic domains (e.g. Nystuen *et al.* 2008). The mélangé discussed here has, however, not been included in the previous models. The mélangé with its numerous lenses of variably altered mantle peridotite constitutes an enigmatic unit that can be identified at the same structural level continuously through most of southern Norway and beyond into the central Scandinavian Caledonides. The mélangé is allochthonous, situated structurally above the Caledonian floor thrust and above basement–cover units assigned to the Lower Allochthon, but below major nappe complexes such as the Jotun, Upper Bergsdalen and Lindås nappes (e.g. Roberts & Gee 1985; Wennberg *et al.* 1998). The mélangé thus

**Fig. 5.** (a) Pebbly quartz-rich sandstone and quartz-rich conglomerate interlayered with the conglomerate immediately above one of the peridotites in Stølsheimen (Fig. 4a and e). (b) The conglomerate at Stølsheimen, with well-rounded pebbles of fine-grained granite. The dated pebble is shown above the car key, together with another white granitoid pebble to the right of the key. (c) Concordia U/Pb plots of zircon, rutile and titanite from the conglomerate pebble shown in (b). The image insets show dated zircons, titanite and rutile. Details of the U–Pb data are given in Table 1.

Table 1. U–Pb data for conglomerate pebble P4/10, Stolsheimen

Mineral characteristics <sup>1</sup>	Weight <sup>2</sup> (µg)	U <sup>2</sup> (ppm)	Th/U <sup>3</sup>	Pbc <sup>4</sup> (pg)	<sup>206</sup> Pb/ <sup>206</sup> Pb <sup>5</sup>	<sup>207</sup> Pb/ <sup>235</sup> U <sup>6</sup>	±2σ (abs.)	<sup>206</sup> Pb/ <sup>238</sup> U <sup>6</sup>	±2σ (abs.)	ρ	<sup>207</sup> Pb/ <sup>206</sup> Pb <sup>6</sup>	±2σ (abs.)	<sup>206</sup> Pb/ <sup>238</sup> U <sup>6</sup> (Ma)	±2σ	<sup>207</sup> Pb/ <sup>235</sup> U <sup>6</sup>	±2σ	<sup>207</sup> Pb/ <sup>206</sup> Pb <sup>6</sup>	±2σ	Disc. (%)
Z eu.A [1]	1	282	0.82	1.3	2284	1.7276	0.0093	0.17049	0.00080	0.90	0.07349	0.00017	1014.8	4.4	1018.9	3.5	1028	5	1.4
Z eu.A [1]	1	129	0.43	0.8	1788	1.739	0.021	0.1734	0.0018	0.91	0.07356	0.00036	1030.9	10.0	1030.4	7.6	1030	10	-0.1
R black [1]	7	28	0.03	8.8	228	1.501	0.017	0.15424	0.00042	0.32	0.07059	0.00077	924.7	2.4	930.9	7.0	946	22	2.4
R red [1]	1	30	0.09	4.3	50	0.479	0.068	0.07134	0.00073	0.56	0.0487	0.00067	444.2	4.4	397	46	—	—	—
T pale [4]	71	70	0.12	675	48	0.490	0.056	0.06578	0.00083	0.18	0.0540	0.0061	410.7	5.1	405	37	—	—	—
T pale [15]	48	119	0.08	603	57	0.489	0.040	0.06570	0.00064	0.09	0.0539	0.0044	410.2	3.9	404	27	—	—	—

<sup>1</sup>Z, zircon; R, rutile; T, titanite; eu, euhedral; A, treated with air abrasion; [1], number of grains.

<sup>2</sup>Weight and concentrations are known to better than 10%, except for those near and below the c. 1 µg limit of resolution of the balance.

<sup>3</sup>Th/U model ratio inferred from 208/206 ratio and age of sample.

<sup>4</sup>Pbc, total common Pb in sample (initial + blank).

<sup>5</sup>Raw data corrected for fractionation.

<sup>6</sup>Corrected for fractionation, spike, blank and initial common Pb; error calculated by propagating the main sources of uncertainty.

occupies a position between the Middle and Lower Allochthons: it is sandwiched between major continental nappe complexes and their associated cover sequences (Figs 1 and 3). This enigmatic structural position was pointed out by Andersen *et al.* (1991, fig. 2), who suggested that the mélange represented a ‘suture-1’ structurally below the main ‘suture-2’ represented by the ophiolite and island-arc complexes of the Upper Allochthon. The basement–cover nappes of the Lower and Middle Allochthons are commonly interpreted to have originated from the Caledonian margin of Baltica because their Proterozoic history is similar to that of the autochthonous basement of southern Scandinavia (Lundmark *et al.* 2007; see also Corfu & Andersen 2002; Glodny *et al.* 2002). A simple map examination reveals that the mélange with its abundant mantle peridotite lenses continues across southern Norway directly into the Gula, Seve and equivalent ‘suspect’ nappe complexes in the Røros area (Fig. 1). It is obvious that the Seve, Gula and lower parts of the Køli nappes containing abundant mantle peridotites, which commonly are of detrital origin (Stigh 1979), need a new interpretation. A revised interpretation of these units will also have major influence on our understanding of the continental crystalline rocks of the Lower, Middle and Upper Allochthons and therefore also of the original architecture of the pre-Caledonian margin of Baltica (Corfu *et al.* 2007, 2011; Kirkland *et al.* 2008b). Even if no specific structures can be assigned with confidence to the original pre-Caledonian formation of the basin in which the continental mantle peridotites were exhumed and the sediments of the mélange accumulated, the hypothesis of a hyperextended margin origin is supported by direct and indirect evidence.

First, sedimentary structures are preserved in some detrital serpentinites associated with larger lenses of altered peridotites (see also Qvale & Stigh 1985). Mantle peridotites must have been exhumed to the surface to provide clastic material to the basin. Their unroofing and erosion is therefore pre-tectonic with respect to Caledonian deformation and metamorphism. The best analogues for this type of deposits are probably the detrital and auto-brecciated serpentinites (S-type lherzolites) around major lherzolites, which were described in some detail from the partly well-preserved basins in the north Pyrenean zone by Lagabrielle *et al.* (2010). Those workers interpreted the mixed deposits to have formed by major synextensional olistostromes in the Middle Cretaceous prior to the early Eocene Pyrenean orogeny. Detrital serpentinites may also have formed around protrusions, giving rise to erosion and sedimentation of fluvial to marine clastic serpentinites such as those forming at present in the extended margin of the Red Sea (e.g. Bonatti *et al.* 1981; Marshak *et al.* 1992). The solitary peridotites discussed here underwent serpentinization before they were eroded, and the detrital serpentinites formed as part of the pre-Caledonian basin-forming (rifting) processes.

Second, the widespread alteration, which includes serpentinization, talcification and formation of ophicalcite, is a hallmark of the peridotites that were originally exhumed by hyperextension in passive continental margins (Bernoulli & Jenkyns 2009). Even if all the contacts between the various lithologies in the example discussed here were overprinted by deformation during the Scandian collision, here dated at 410±3 Ma, as well as the late to post-orogenic extension, the lithological association and transitions from serpentinites to mafic micaschists are difficult to explain by a late-stage tectonic mixing of originally distinct peridotites separated from the sedimentary rocks. This was also pointed out by Qvale and Stigh (1985), who noted that the solitary Alpine-type peridotites had a more complex structure and geochemistry and were more ‘polymetamorphic’ than those associated with the typical ophiolites of the Upper Allochthon. The formation of the lithological association of the mélange is clearly pre-metamorphic with

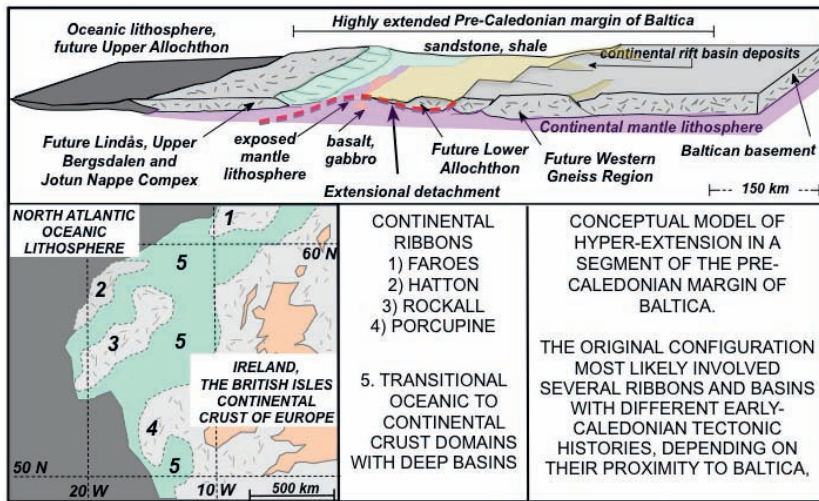


**Fig. 6.** A conceptual drawing showing a possible geometry of a segment of the hyperextended, pre-Caledonian margin of Baltica. The most important implication of this study is that large crystalline nappes must have been positioned outboard of the deep basins as continental ribbons and/or microcontinents separated by transitional ocean–continent domain with exposed subcontinental mantle lithosphere. Large mantle culminations must have been exposed before plate convergence and collision commenced, as shown by the presence of detrital serpentinites. The new interpretation implies that distal units on the hyperextended margin may have experienced early Caledonian deformation and metamorphism not recorded in the margin of Baltica. The sketch of the present-day North Atlantic margin west of the British Isles and Ireland is shown for comparison and to indicate a possible present-day analogue (redrawn from Péron-Pinvidic & Manatschal 2010).

respect to the Caledonian orogeny and must therefore relate to an early stage in the evolution of the Caledonian Wilson cycle.

Third, it is not possible to explain the emplacement of the *mélange* peridotites by magmatic intrusion and crystallization, because there is no evidence to suggest intrusive relationships between high-*T* ultramafic magmas and the sediments. There is no contact metamorphism and common black-wall alteration zones are related to metasomatism, not contact metamorphism by heat diffusion from a crystallizing ultramafic magma (e.g. Bucher *et al.* 2005). Minor gabbros and metabasalts mapped in several areas of the *mélange* may, however, be related to magmatism and extension similar to those documented from other ocean–continent transition zones (Müntener *et al.* 2010). The emplacement of mantle peridotites within the *mélange* must therefore be caused by other mechanisms than magma emplacement, the only likely alternative being structural emplacement. We suggest that this most probably was related to large-scale unroofing of extensional detachment footwall(s), perhaps in combination with serpentinite protrusion where widespread hydration of an exhuming mantle lithosphere took place. Zones of exhumed mantle documented from present-day OCT zones, such as that offshore Iberia, are complex assemblages of faulted serpentinized mantle, rafted extensional allochthons of continental crust and sedimentary rocks derived from both crustal protoliths and from exhumed mantle rocks (e.g. Manatschal 2004; Péron-Pinvidic & Manatschal 2009). We propose that the *mélange* unit described in this paper represents an obducted part of a pre-Caledonian OCT with exhumed mantle.

The sedimentary matrix of the *mélange* has no preserved fossils except those found in the monomict serpentinite conglomerate east of Vågå (Fig. 1). The unusual ‘Celtic fauna’ with mixed provinciality of island origin was described by Bruton & Harper (1981), who suggested that the ‘serpentinite island’ was separated by a considerable distance from Baltica and other continents in the early Middle Ordovician (Llanvirn, 470–464 Ma). Other clastic serpentinites such as those in the Bergen–Hardanger area (Qvale 1978; Heldal & Jansen 2000) were probably also formed by erosion and sedimentation in and near island environments (serpentinite protrusions?), but are devoid of fossils.

Within the major Bergen Arc, fossiliferous rocks of late Ordovician age (448–443 Ma, Ashgill) unconformably overlie the *mélange* (Sturt & Thon 1976; Faerseth *et al.* 1977). It is obvious that the *mélange* as well as the associated basement lenses have

evidence of a pre-Scandian tectonic history, which at present is poorly understood (see below).

The dominant graphitic micaschists and phyllites are commonly interlayered or foliated with coarser-grained (synrift?) conglomerates and sandstones. These clearly have provenance from continental crust, and the dated pebble from the conglomerate at Stølsheimen is one example. It suggests that the provenance of the *mélange* matrix was in a Proterozoic basement of similar age to the Lower and Middle Allochthons as well as the autochthonous basement of Baltica (see above). As shown above, the *mélange* occupies a position between the Lower and Middle Allochthons as originally defined by Roberts & Gee (1985). By comparison with equivalent Alpine complexes and present-day hyperextended margins, juxtaposition of thin slices of continental basement, synrift to post-rift sediment infill and hydrated mantle lithosphere commonly takes place in passive margins (Manatschal 2004; Péron-Pinvidic & Manatschal 2010; Unternehr *et al.* 2010).

#### *Polyphase deformation and metamorphism in the *mélange**

Internally the *mélange* was intensely deformed during the Scandian orogeny, which at the present erosion level typically is characterized by upper greenschist- to amphibolite-facies metamorphism, here dated at  $410 \pm 3$  Ma. The main fabric development in these rocks took place during the Scandian collision, accompanied by large-scale thrusting of nappes and deep burial of Baltica as witnessed by the high- to ultra-high pressure metamorphism (Fig. 1) developed in the basement of Baltica (e.g. Andersen *et al.* 1991; Fossen 1993). There are, however, also records of pre-Scandian deformation and metamorphism affecting the *mélange* in the study area and locally fabrics related to pre-Scandian events are preserved in the Major Bergen Arc (Sturt & Thon 1976; Faerseth *et al.* 1977; Henriksen 1981). This is also the case with the continental basement of the Dalsfjord Suite (*c.* 1640 Ma) covered by the sandstone-dominated Høyvik Group in Sunnfjord (Fig. 1), which experienced a pre-Scandian event at *c.* 450 Ma (Andersen *et al.* 1998; Corfu & Andersen 2002). Similar rocks in the Seve nappe *c.* 1000–1500 km to the NE also have evidence of early and middle Ordovician metamorphic events, which in parts reached eclogite-facies conditions (e.g. Root & Corfu 2011). Recently, eclogites most probably associated with the allochthonous Hardanger–Ryfylke Nappe Complex

near Stavanger (Fig. 1) have been dated at *c.* 470 Ma (Smit *et al.* 2011). It is clear that these Middle Allochthon rocks, traditionally interpreted to have originated along the Caledonian margin of Baltica, experienced variably intense deformation and metamorphism prior to their emplacement onto Baltica during the Scandian collision. The early and middle Ordovician events post-date the formation of a hyperextended margin, and took place when these rocks had achieved their maximum separation by hyperextension and were partly outboard of Baltica. The exact nature of the pre-Scandian deformation and metamorphism is at present not understood, and the interpretation of the *mélange* unit has been significantly complicated as a result of these early Caledonian events.

Post-collision fabrics are also common, and in some areas constitute the dominant structure, particularly adjacent to major nappe boundaries (Andersen 1998; Fossen 2010). Both the Scandian collision and later extensional events were accompanied by regional amphibolite- to greenschist-facies metamorphism (Fossen 1993; Osmundsen & Andersen 1994). Therefore, there is no preserved record of pre-Caledonian extensional structures that can be assigned to the original rifting and formation of the deep basin(s) in which the *mélange* sediments accumulated and where the mantle peridotites were emplaced. Exceptions to this are the very local but well-preserved sedimentary structures observed within some detrital serpentinites. Otherwise, all main contacts are overprinted by the strong Scandian thrust fabrics and by the co-facial to retrograde post-orogenic deformation.

The rock association including mantle peridotites, which in parts were exposed to erosion, and the fine-grained graphitic schists and micaschists interlayered with coarser-grained metasediments and conglomerates point to a very complex depositional environment in a basin, which at times was subjected to catastrophic deposition of coarser-grained material either from adjacent continental areas, from a severely faulted 'necking zone' or from extensional allochthons in the distal margin. Formation of the basin(s) was probably also accompanied by minor magmatic activity as evidenced by minor gabbros and metabasalt horizons. It is, however, not possible to explain the solitary peridotites by magmatic intrusion and crystallization, because there is no evidence to suggest intrusive relationships between ultramafic magmas and the sediments. There is no contact metamorphism other than the hydrothermal black-wall alteration related to fluid–rock interaction. Minor gabbros and metabasalts may, however, be related to magmatism and extension similar to those described from highly extended ocean–continent transition zones (Müntener *et al.* 2010).

The internal architecture of the Lower and Middle Allochthons, as well as the Seve nappes, changes considerably along strike in the Scandinavian Caledonides. In particular, the Lower Allochthon is a much larger tectonic unit in the central parts of the orogen than in the SW, whereas the crystalline nappes in the Middle Allochthon (Hardanger–Ryfylke, Bergsdalen and Lindås–Jotun nappe complexes) are reduced to mostly thin slivers of basement in the NE. Similarly, equivalents of the Seve nappes are less important in the SW than in the NE (see the tectonostratigraphic map of Roberts & Gee 1985). Already from these lateral variations it is clear that the Caledonian margin of Baltica originally must have had a very complex structure prior to the Scandian collision. By comparison with present-day passive margins (Fig. 6), such as the North Atlantic including the Norwegian Sea, this is not at all a surprising observation.

## Conclusion

The regionally distributed *mélange* unit discussed in this paper has not been adequately incorporated in geotectonic reconstructions

that are based on the traditional interpretation of tectonostratigraphic units in the Scandinavian Caledonides. Because of the polyphase deformation and metamorphic overprint in the *mélange*, attempts to explain its geodynamic significance will probably always be controversial. The association of solitary mantle peridotite with continentally derived deep-basin sediments and slivers of Proterozoic basement is, however, a characteristic feature that can be easily explained by comparison with Cenozoic mountain belts such as the Alps and the Pyrenees, and with the geometry and lithological association of present-day hyperextended continental margins.

The rock association of solitary mantle peridotites and detrital ultramafic rocks mostly without or with very limited volumes of associated gabbros and basalts and all intimately associated with a variety of siliciclastic- and carbonate-rich sediments points to formation in deep basin(s) formed by large-magnitude extension rather than in a magma-dominated spreading-ridge environment. Thin sheets of highly attenuated continental crystalline basement and associated metasediments structurally overlie the mantle-peridotite-bearing *mélange*. These may represent original extensional allochthons juxtaposed on continental mantle lithosphere by large-magnitude extensional detachments similar to those interpreted from the seismic structure in present-day continental margins (e.g. Unternehr *et al.* 2010) and partly preserved in exposed sections in the Alps (e.g. Manatschal 2004). We therefore suggest that the regional *mélange* unit found between the Lower and Middle Allochthons in the SW Scandinavian Caledonides is best explained as representing the vestiges of a hyperextended pre-Caledonian continental margin of Baltica (Fig. 6). Primary extensional fabrics between the mantle rocks, the continental crust and the deep basin sediments were destroyed by subsequent Caledonian events. The association of rocks in the *mélange* is very similar to those described from the Alps in a series of papers by Manatschal and co-workers (e.g. Manatschal 2004; Manatschal *et al.* 2006) and from the Pyrenees (Lagabrielle *et al.* 2010). The presence of such a highly extended continental margin below large crystalline nappes of southern Norway, including the Lindås and Jotun nappes, implies that these were separated from Baltica by wide and deep rift basins that included zones of exhumed continental mantle, and possibly also true oceanic basins, at the early stages of the Caledonian Wilson cycle. If this interpretation is correct the Lindås, Upper Bergsdalen and Jotun Nappe complexes can therefore be considered as ancient 'continental ribbons' or outboard 'microcontinents' (Fig. 6) with equivalent status to the Briançonnais zone of the Alps or even the Jan Mayen microcontinent of the Norwegian–Greenland sea. The pre-Caledonian margin of Baltica must therefore have had a much more complicated structure than the traditional simple passive margin as envisaged from previous reconstructions based on the interpretation of basement–cover systems of the Lower and Middle Allochthons. The shortening of the Caledonian margin of Baltica during the Scandian collision has consequently also been grossly underestimated, as the transitional ocean–continent domain now represented by the *mélange* below the major crystalline continental nappes has been largely ignored in previous reconstructions.

A detailed reconstruction that precisely explains the formation of the *mélange* by primary stratigraphic or structural relationships is not yet possible. Any advance in our understanding of the ocean–continent transition of the pre-Caledonian margin of Baltica, however, requires an adequate explanation of this hitherto unexplained association of rocks, which constitutes a continuous unit extending for several hundred kilometres in southern Norway and probably beyond in the Scandinavian Caledonides.

We conclude that the *mélange* unit described here, which contains abundant lenses of mantle peridotite and is associated with the

Lower and Middle Allochthons of the Scandinavian Caledonides, represents the vestiges of a hyperextended pre-Caledonian passive continental margin. The key to understanding its complexity is to be found by new detailed studies and by comparisons with similar complexes from other orogenic belts, most notably the European Alpine systems, and from present-day continental margins.

We acknowledge Ø. J. Jansen for providing information about soapstone quarries in the Bergen area and the picture here shown as Figure 4c. G. Manatschal and O. Nilsen are thanked for discussion at several stages before and during the course of this work, which was financed by the Norwegian Research Council Centre of Excellence grant to Physics of Geological Processes (PGP).

## References

- ANDERSEN, T.B. 1998. Extensional tectonics in the Caledonides of southern Norway, an overview. *Tectonophysics*, **285**, 333–351.
- ANDERSEN, T.B., FURNES, H. & SKJERLIE, K.P. 1990. The Sunnfjord Mélange, evidence of Silurian ophiolite accretion in the West Norwegian Caledonides. *Journal of the Geological Society, London*, **147**, 59–69.
- ANDERSEN, T.B., JAMTVEIT, B., DEWEY, J.F. & SWENSSON, E. 1991. Subduction and eduction of continental crust—major mechanisms during continent–continent collision and orogenic extensional collapse, a model based on the South Norwegian Caledonides. *Terra Nova*, **3**, 303–310.
- ANDERSEN, T.B., BERRY, H.N., LUX, D.R. & ANDRESEN, A. 1998. The tectonic significance of pre-Scandian <sup>40</sup>Ar/<sup>39</sup>Ar phengite cooling ages in the Caledonides of western Norway. *Journal of the Geological Society, London*, **155**, 297–309.
- ANDREASSON, P.G. 1994. The Baltoscandian margin in the Neoproterozoic–early Paleozoic times—some constraints on the terrane derivation and accretion in the Arctic Scandinavian Caledonides. *Tectonophysics*, **231**, 1–32.
- ANDREASSON, P.G., SVENNINGSEN, O.M. & ALBRECHT, L. 1998. Dawn of Phanerozoic orogeny in the North Atlantic tract; evidence from the Seve–Kalak Superterrane, Scandinavian Caledonides. *GFF*, **120**, 159–172.
- BERNOULLI, D. & JENKYN, H.C. 2009. Ancient oceans and continental margins of the Alpine–Mediterranean Tethys: deciphering clues from Mesozoic pelagic sediments and ophiolites. *Sedimentology*, **56**, 149–190.
- BINGEN, B., BELOUSOVA, E.A. & GRIFFIN, W.L. 2011. Neoproterozoic recycling of the Sveconorwegian orogenic belt: Detrital–zircon data from the Sparagmite basins in the Scandinavian Caledonides. *Precambrian Research*, **189**, 347–367.
- BOE, R. 1985. Rodingite from Lindås, western Norway. *Norwegian Journal of Geology*, **65**, 301–320.
- BOILLOT, G., RECO, M., ET AL. 1987. Tectonic denudation of the upper mantle along passive margins: a model based on drilling results (ODP Leg 103, western Galicia margin, Spain). *Tectonophysics*, **132**, 335–342.
- BONATTI, E., HAMLIN, P.R. & OTTONELLO, G. 1981. Upper mantle beneath a young oceanic rift: peridotites from the island of Zabargad (Red Sea). *Geology*, **9**, 474–479.
- BRUTON, D.L. & HARPER, D.A.T. 1981. Brachiopods and trilobites of the early Ordovician serpentinite Otta Conglomerate, south central Norway. *Norwegian Journal of Geology*, **61**, 3–18.
- BUCHER, K., DE CAPITANI, C. & GRAPES, R. 2005. The development of a margarite–corundum blackwall by metasomatic alteration of a slice of mica schist in ultramafic rock, Kvesjøen, Norwegian Caledonides. *Canadian Mineralogist*, **43**, 129–156.
- CORFU, F. 2004. U–Pb age, setting, and tectonic significance of the anorthosite–mangerite–charnockite–granite suite, Lofoten–Vesterålen, Norway. *Journal of Petrology*, **45**, 1799–1819.
- CORFU, F. & ANDERSEN, T.B. 2002. U–Pb ages of the Dalsfjord Complex, SW Norway, and their bearing on the correlation of allochthonous crystalline segments of the Scandinavian Caledonides. *International Journal of Earth Sciences*, **91**, 955–963.
- CORFU, F., TORSVIK, T.H., ANDERSEN, T.B., ASHWAL, L.D., RAMSAY, D.M. & ROBERTS, R.J. 2006. Early Silurian mafic–ultramafic and granitic plutonism in contemporaneous flysch, Magerøy, northern Norway: U–Pb ages and regional significance. *Journal of the Geological Society, London*, **163**, 291–301.
- CORFU, F., ROBERTS, R.J., TORSVIK, T.H., ASHWAL, L.D. & RAMSAY, D.M. 2007. Peri-Gondwanan elements in the Caledonian Nappes of Finnmark, Northern Norway: implications for the paleogeographic framework of the Scandinavian Caledonides. *American Journal of Science*, **307**, 434–458.
- CORFU, F., GERBER, M., ANDERSEN, T.B., TORSVIK, T.H. & ASHWAL, L.D. 2011. Age and significance of Grenvillian and Silurian orogenic events in the Finnmark Caledonides, northern Norway. *Canadian Journal of Earth Sciences*, **48**, 419–440.
- FAERSETH, R.B., THON, A., LARSEN, S.G., SIVERTSEN, A. & ELVESTAD, L. 1977. Geology of the lower Palaeozoic rocks in the Samnanger–Osterøy, area, major Bergen Arc, western Norway. *Bulletin Norges Geologiske Undersøkelse*, **334**, 19–58.
- FOSSEN, H. 1993. Linear fabrics in the Bergsdalen Nappes, southwest Norway—implications for deformation history and fold development. *Norwegian Journal of Geology*, **73**, 95–108.
- FOSSEN, H. 2010. Extensional tectonics in the North Atlantic Caledonides: a regional view. In: LAW, R.D., BUTLER, R.W.H., HOLDSWORTH, R.E., KRABBENDAM, M. & STRACHAN, R.A. (eds) *Continental Tectonics and Mountain Building: The Legacy of Peach and Horne*. Geological Society, London, Special Publications, **335**, 767–793.
- FOSSEN, H. & DUNLAP, W.J. 1998. Timing and kinematics of Caledonian thrusting and extension collapse, southern Norway; evidence from 40Ar/39Ar thermochronology. *Journal of Structural Geology*, **20**, 765–781.
- FURNES, H., SKJERLIE, K.P., ET AL. 1990. The Solund–Stavfjord Ophiolite complex and associated rocks, West Norwegian Caledonides—geology, geochemistry and tectonic environment. *Geological Magazine*, **127**, 209–224.
- GEE, D.G. & STURT, B.A. 1985. *The Caledonide Orogeny—Scandinavia and Related Areas*. Wiley, Chichester.
- GLODNY, J., KUHN, A. & AUSTRHEIM, H. 2002. Rb/Sr record of fluid–rock interaction in eclogites, Bergen Arcs, Norway. *Geochimica et Cosmochimica Acta*, **66**, A280–A280.
- GLODNY, J., KUHN, A. & AUSTRHEIM, H. 2008. Geochronology of fluid-induced eclogite and amphibolite facies metamorphic reactions in a subduction–collision system, Bergen Arcs, Norway. *Contributions to Mineralogy and Petrology*, **156**, 27–48.
- GREY, J.W. 1978. *Structural history and Rb–Sr geochronology of Eksingedalen, West Norway*. PhD thesis, University of Aberdeen.
- HACKER, B.R., ANDERSEN, T.B., JOHNSTON, S., KYLANDER-CLARK, A., PETERMAN, E., WALSH, E. & YOUNG, D. 2010. Deformation during continental margin subduction and exhumation: the ultrahigh-pressure Western Gneiss Region of Norway. *Tectonophysics*, **480**, 149–171.
- HELDAL, T. & JANSEN, O.J. 2000. *Steinbyen Bergen: Fortellingen om Brostein, Bygg og Brudd*. NGU, Trondheim.
- HENRIKSEN, H. 1981. A major unconformity within the metamorphic Lower Palaeozoic sequence of the Major Bergen Arc, Osterøy, western Norway. *Bulletin Norges Geologiske Undersøkelse*, **367**, 65–75.
- INGDAHL, S.E. 1985. *Stratigraphy, structural geology and metamorphism in the Os area, Major Bergen Arc*. Cand. scient. (Master) thesis, University of Bergen.
- KIRKLAND, C.L., DALY, J.S., CHEW, D.M. & PAGE, L.M. 2008a. The Finnmarkian Orogeny revisited: an isotopic investigation in eastern Finnmark, Arctic Norway. *Tectonophysics*, **460**, 158–177.
- KIRKLAND, C.L., DALY, J.S. & WHITEHOUSE, M.J. 2008b. Basement–cover relationships of the Kalak Nappe Complex, Arctic Norwegian Caledonides and constraints on Neoproterozoic terrane assembly in the North Atlantic region. *Precambrian Research*, **160**, 245–276.
- KROGH, T.E. 1973. A low contamination method for hydrothermal decomposition of zircon and extraction of U and Pb for isotopic age determinations. *Geochimica et Cosmochimica Acta*, **37**, 485–494, doi:10.1016/0016-7037(73)90213-5.
- LABROUSSE, L., HETÉNYI, G., RAIMBOURG, H., JOLIVET, L. & ANDERSEN, T.B. 2010. Initiation of crustal-scale thrusts triggered by metamorphic reactions at depth: insights from a comparison between the Himalayas and the Scandinavian Caledonides. *Tectonics*, **29**, TC5002, doi:10.1029/2009TC002602, 2010.
- LAGABRIELLE, Y. & BODINIER, J.L. 2008. Submarine reworking of exhumed sub-continental mantle rocks: field evidence from the Lherz peridotites, French Pyrenees. *Terra Nova*, **20**, 11–21.
- LAGABRIELLE, Y., LABAUME, P. & DE SAINT BLANQUAT, M. 2010. Mantle exhumation, crustal denudation, and gravity tectonics during Cretaceous rifting in the Pyrenean realm (SW Europe): insights from the geological setting of the Lherz peridotite bodies. *Tectonics*, **29**, TC4012.
- LUNDIN, E.R. & DORÉ, A.G. 2011. Hyperextension, serpentinisation and weakening: a new paradigm for rifted margin compressional deformation. *Geology*, **39**, 347–350.
- LUNDMARK, A.M., CORFU, F., SPÜRGIN, S. & SELBEKK, R.S. 2007. Proterozoic evolution and provenance of the high-grade Jotun Nappe complex, SW Norway: U–Pb geochronology. *Precambrian Research*, doi:10.1016/j.precamres.2006.12.015.
- MANATSCHAL, G. 2004. New models for evolution of magma-poor rifted margins based on a review of data and concepts from West Iberia and the Alps. *International Journal of Earth Sciences*, **93**, 432–466.
- MANATSCHAL, G., ENGSTRÖM, A., DESMURS, L., SCHALTEGGER, U., COSCA, M., MÜNTNER, O. & BERNOULLI, D. 2006. What is the tectono-metamorphic evolution of continental break-up: the example of the Tasna ocean–continent transition. *Journal of Structural Geology*, **28**, 1849–1869.
- MARSHAK, S., BONATTI, E., BRUECKNER, H.K. & PAULSEN, T. 1992. Fracture-zone tectonics at Zabargad Island, Red Sea (Egypt). *Tectonophysics*, **216**, 379–385.

- MOHN, G., MANATSCHAL, G., MÜNTENER, O., BELTRANO, M. & MASINI, E. 2010. Unravelling the interaction between tectonic and sedimentary processes during lithospheric thinning in the Alpine Tethys margins. *International Journal of Earth Sciences*, **99**, S75–S101.
- MÜNTENER, O. & MANATSCHAL, G. 2006. High degrees of melt extraction recorded by spinel harzburgite of the Newfoundland margin: the role of inheritance and consequences for the evolution of the southern North Atlantic. *Earth and Planetary Science Letters*, **252**, 437–452.
- MÜNTENER, O., MANATSCHAL, G., DESMURS, L. & PETTKE, T. 2010. Plagioclase peridotites in ocean–continent transitions: refertilized mantle domains generated by melt stagnation in the shallow mantle lithosphere. *Journal of Petrology*, **51**, 255–294.
- NYSTUEN, J.P., ANDRESEN, A., KUMPULAINEN, R.A. & SIEDLECKA, A. 2008. Neoproterozoic basin evolution in Fennoscandia, East Greenland and Svalbard. *Episodes*, **31**, 35–43.
- OSMUNDSEN, P.T. & ANDERSEN, T.B. 1994. Caledonian compressional and late-orogenic extensional deformation in the Stavaneset area, Sunnfjord, Western Norway. *Journal of Structural Geology*, **16**, 1385–1401.
- OSMUNDSEN, P.T. & EBBING, J. 2008. Styles of extension offshore mid-Norway and implications for mechanisms of crustal thinning at passive margins. *Tectonics*, **27**, TC6016, doi:10.1029/2007TC002242.
- PÉRON-PINVIDIC, G. & MANATSCHAL, G. 2009. The final rifting evolution at deep magma-poor passive margins: a new point of view based on observations from Iberia–Newfoundland. *International Journal of Earth Sciences*, **98**, 1581–1597, doi:10.1007/s00531-009008-00337-00539.
- PÉRON-PINVIDIC, G. & MANATSCHAL, G. 2010. From microcontinents to extensional allochthons: witnesses of how continents rift and break apart? *Petroleum Geoscience*, **16**, 189–197.
- QVALE, H. 1978. *Geologisk undersøkelse av et kaledonsk serpentinitfelt ved Balderheim, Hordaland*. Cand. Real (Master) thesis, University of Oslo.
- QVALE, H. & STIGH, J. 1985. Ultramafic rocks in the Scandinavian Caledonides. In: GEE, D.G. & STURT, B.A. (eds) *The Caledonide Orogen—Scandinavia and Related Areas*. Wiley, Chichester, 693–715.
- ROBERTS, D. & GEE, D.G. 1985. An introduction to the structure of the Scandinavian Caledonides. In: GEE, D.G. & STURT, B.A. (eds) *The Caledonide Orogen—Scandinavia and Related Areas*. Wiley, Chichester, 55–68.
- ROBERTS, D., MELEZHUK, V.A. & HELDAL, T. 2002. Carbonate formations and early NW-directed thrusting in the highest allochthons of the Norwegian Caledonides: evidence of a Laurentian ancestry. *Journal of the Geological Society, London*, **159**, 117–120.
- ROOT, D.B. & CORFU, F. 2011. U–Pb geochronology of two discrete Ordovician high-pressure metamorphic events in the Seve Nappe complex, Scandinavian Caledonides. *Contributions to Mineralogy and Petrology*, **163**, 769–788.
- SMIT, M.A., BRÖCKER, M., KOOLJMAN, E. & SCHERER, E.E. 2011. The provenance and exhumation of exotic eclogite-facies rocks in SW Norway: a Rb–Sr and U–Pb study. *Journal of the Geological Society, London*, **168**, 423–439.
- STEPHENS, M.B. & GEE, D.G. 1989. Terranes and polyphase accretionary history in the Scandinavian Caledonides. In: DALLMEYER, R.D. (ed.) *Terranes in the Circum-Atlantic Paleozoic Orogens*. Geological Society of America, Special Papers, **230**, 17–30.
- STIGH, J. 1979. *Ultramafites and detrital serpentinites in the central and southern parts of the Caledonian Allochthon in Scandinavia*. PhD thesis, Chalmers University of Technology Gothenburg.
- STURT, B.A. & RAMSAY, D.M. 1999. Early Ordovician terrane-linkages between oceanic and continental terranes in the central Scandinavian Caledonides. *Terra Nova*, **11**, 79–85.
- STURT, B.A. & THON, A. 1976. The age of the orogenic deformation in the Swedish Caledonides. *American Journal of Science*, **276**, 385–390.
- SVENNINGSEN, O. 2001. Onset of seafloor spreading in the Iapetus Ocean at 608 Ma: precise age of the Sarek Dyke Swarm, northern Swedish Caledonides. *Precambrian Research*, **110**, 241–254.
- THON, A. 1985. The Gullfjellet ophiolite complex and the structural evolution of the major Bergen Arc, West Norwegian Caledonides. In: GEE, D.G. & STURT, B.A. (eds) *The Caledonide Orogen—Scandinavia and Related Areas*. Wiley, Chichester, 671–677.
- TORSVIK, T.H. & COCKS, L.R.M. 2005. Norway in space and time: a centennial cavalcade. *Norwegian Journal of Geology*, **85**, 73–86.
- UNTERNEHR, P., PERON-PINVIDIC, G., MANATSCHAL, G. & SUTRA, E. 2010. Hyperextended crust in the South Atlantic: in search of a model. *Petroleum Geoscience*, **16**, 207–215.
- VAN ROERMUND, H.L.M. 1985. Eclogites of the Seve Nappe, central Scandinavian Caledonides. In: GEE, D.G. & STURT, B.A. (eds) *The Caledonide Orogen—Scandinavia and Related Areas*. Wiley, Chichester, 873–886.
- VITALE BROVARONE, A., BELTRANDO, M., *ET AL.* 2011. Inherited ocean–continent transition zones in deeply subducted terranes: insights from Alpine Corsica. *Lithos*, doi:10.1016/j.lithos.2011.02.013.
- WENNERBERG, O.P., MILNES, A.G. & WINSVOLD, I. 1998. The northern Bergen Arc shear zone—an oblique-lateral ramp in the Devonian extensional detachment system of western Norway. *Norwegian Journal of Geology*, **78**, 169–184.
- ZALAN, P.V., SERVINO, M.C.G., RIGOTI, C.A., MAGNAVITA, L.P., OLIVEIRA, J.A.B. & VIANNA, A.R. 2011. Continuous mantle exhumation at the outer continental margin of the Santos, Campos and Espírito Santo Basins, Brazil. AGU-2011 Annual Meeting, Session T31D, Abstract T31D-02. World Wide Web address: <http://www.agu.org/meetings/fm11/waisfm11.html>

Received 24 January 2012; revised typescript accepted 12 April 2012.  
Scientific editing by Erdin Bozkurt.

TECTONICS, VOL. 9, NO. 5, PAGES 1097-1111, OCTOBER 1990

UPLIFT OF DEEP CRUST DURING  
OROGENIC EXTENSIONAL COLLAPSE: A  
MODEL BASED ON FIELD STUDIES IN  
THE SOGN-SUNNFJORD REGION OF  
WESTERN NORWAY

Torgeir B. Andersen and Bjørn Jamtveit

Department of Geology, University of Oslo,  
Oslo, Norway

**Abstract.** The Western Gneiss Region (WGR) in Norway experienced high-pressure metamorphism during Silurian-Devonian continent-continent collision. The eclogite-bearing lower crust is separated from the middle and upper crust by major detachment zones formed during extensional collapse of the orogen; formation of the Devonian basins is related to the extension. The footwall of the detachment zones comprises three structural and metamorphic zones. The upper zone, zone 1, is characterized by penetrative homogeneous down-to-the-west simple shear developed under retrograde greenschist-facies metamorphism. Zone 2 suffered inhomogeneous simple shear of the same polarity. Petrography and mineral chemistry data from the lower zone, zone 3, show a record of initial eclogite facies metamorphism at 600°C and >16 kbar, which was decompressed almost isothermally to amphibolite-facies conditions at 550°C and 10-12 kbar. Both the eclogite- and amphibolite-facies metamorphism developed in a regime of pure shear with vertical shortening. The rapid decompression records an approach of approximately 20 km to the surface, related to

uplift that was probably the result of the removal of a thickened thermal boundary layer in the mantle lithosphere. The pure shear regime, which developed initially in the lower crust, was truncated by zones of simple shear as the lower crust was uplifted to middle and upper crustal levels. Extension by simple shear in the upper crust was rooted in the lower crust where extension occurred by pure shear. The shear zones in zones 1 and 2 did not penetrate the pure shear regime of the lower crust. A considerable amount of tectonic stripping of the orogenic welt predates deposition of the Devonian sedimentary basins.

## INTRODUCTION

Most tectonic models for the uplift of deeply buried metamorphic terrains during extensional collapse of orogens are based on field studies in the middle and upper crust and interpretation of geophysical data from the deep roots of the orogen [Dewey et al., 1988; England and Houseman, 1988]. Few models based on direct observations of the deep crust are available. The Western Gneiss Region (WGR) of southwest Norway experienced eclogite-facies metamorphism during Caledonian continent-continent collision in Late Silurian-Early Devonian times [Griffin and Brueckner, 1980; Griffin et al., 1985]. The northwestern parts of

Copyright 1990  
by the American Geophysical Union.

Paper number 90TC00731.  
0278-7407/90/90TC-00731\$10.00

the WGR bear evidence of extreme crustal thicknesses. Jamtveit [1987] reported pressures of around 25 kbar from the Eiksundal eclogite, and coesite-bearing eclogites indicating pressures as high as 30 kbar have been reported from the area north of the Hornelen Basin (Figure 1) [Smith, 1988; Smith and Lappin, 1989]. The pressure (P) and temperature (T) increase progressively in a north westerly direction through the gneiss region [Krogh, 1977]. Eclogites ( $P > 18$  kbar) also occur in the Bergen arcs, but their structural relationship to those of the WGR is yet unknown [Austrheim and Griffin, 1985; Austrheim, 1987, 1990]. The WGR is structurally overlain by Caledonian thrust nappes, parts of which have experienced only low greenschist-facies metamorphism, and the low-grade sedimentary basins of Middle Devonian age [Kildal, 1970]. With the exception of the Håsteinen Basin, the northern, eastern, and southern margins of the basins are fault bounded, and their western contacts are unconformities [Bryhni, 1964]. Several authors have discussed recently the contact relationships among the Devonian basins, the Caledonian nappes, and the WGR [Hossack, 1984; Norton, 1986; 1987; Séranne and Séguret, 1987]. The hanging wall characteristically contains semiductile to brittle fault rocks, although restricted zones of ductile deformation of the Devonian conglomerates have been described [Norton, 1987; Séranne and Séguret, 1987]. In the footwall, mylonite zones, several kilometers thick, are present (Figure 2a). Kinematic indicators in the mylonites show that they, and presumably therefore the Devonian basins, formed as a result of extension [Norton, 1986, 1987; Séranne and Séguret, 1987]. This interpretation has been disputed by some authors arguing mainly from studies of magnetic fabric [Torsvik et al., 1987, 1988]; however, the widespread presence and variety of kinematic indicators described by previous workers and in the present study show that the basins formed above major extensional detachments. As such, the WGR is similar to a metamorphic core complex [Davis, 1983]. The uniqueness of the area is that it exposes very deep sections of the continental crust, the former root of a continent-continent collision zone. Almost all prior detailed studies in the WGR have focused on eclogite petrology; very few combined structural and metamorphic studies have been carried out that may clarify the mechanism of uplift.

This paper summarizes evidence for exten-

sion in the detachment zones and discusses their geometry. The main object, however, is to present a tectonic model for the structural pattern developed between the deep, eclogite-bearing crust and the middle to upper crustal rocks that are juxtaposed across the detachment zones.

## KINEMATIC INDICATORS

Thick mylonite zones characterize the detachment zones between the lower, middle, and upper crust along the western margin of the WGR from Sognefjorden to Bremangerlandet (Figure 1). The uplifted deep crust comprises the Fjordane and Jostedal complexes of the WGR and, probably, also the kyanite-bearing schists in Hyllestad and parts of the Askvoll Group near Atløy (Figure 1). Middle crustal rocks occur mainly in the units belonging to the Middle Allochthon, whereas the upper crust is represented by the Caledonian outboard terrains and the Devonian basins. In order to illustrate the evidence for noncoaxial strain and sense of shear in the mylonite zones of the detachments adjacent to the lower crust, a summary of the kinematic indicators commonly observed at the scale of outcrop will be presented. Detailed descriptions of these features are discussed elsewhere [Swensson and Andersen, 1989, also manuscript in preparation, 1990]. A penetrative stretching lineation is developed in the mylonites in the area, with an azimuth generally between E-W and WNW-ESE with shallow plunges, dominantly to the west. In the upper parts of the mylonite zones, late extensional crenulation cleavages are common in mica-rich mylonites and phyllonites, also indicating a down-to-the-west movement of the hanging wall (Figure 2b). Shear bands are ubiquitous in the mylonites and the asymmetry between S and C planes shows consistent westward movement of the hanging wall relative to the footwall (Figure 2c). Spectacular examples of asymmetrical boudinage indicating the same sense of movement are common (Figure 2c). Asymmetrical, west vergent folds are common, in many places associated with compressional structures such as foliation duplexes, indicating a consistent rotation sense. Fold axes are parallel or subparallel with the stretching lineation, and sheath folds are common. In the structurally lower part of the mylonite zones, extensional veins showing

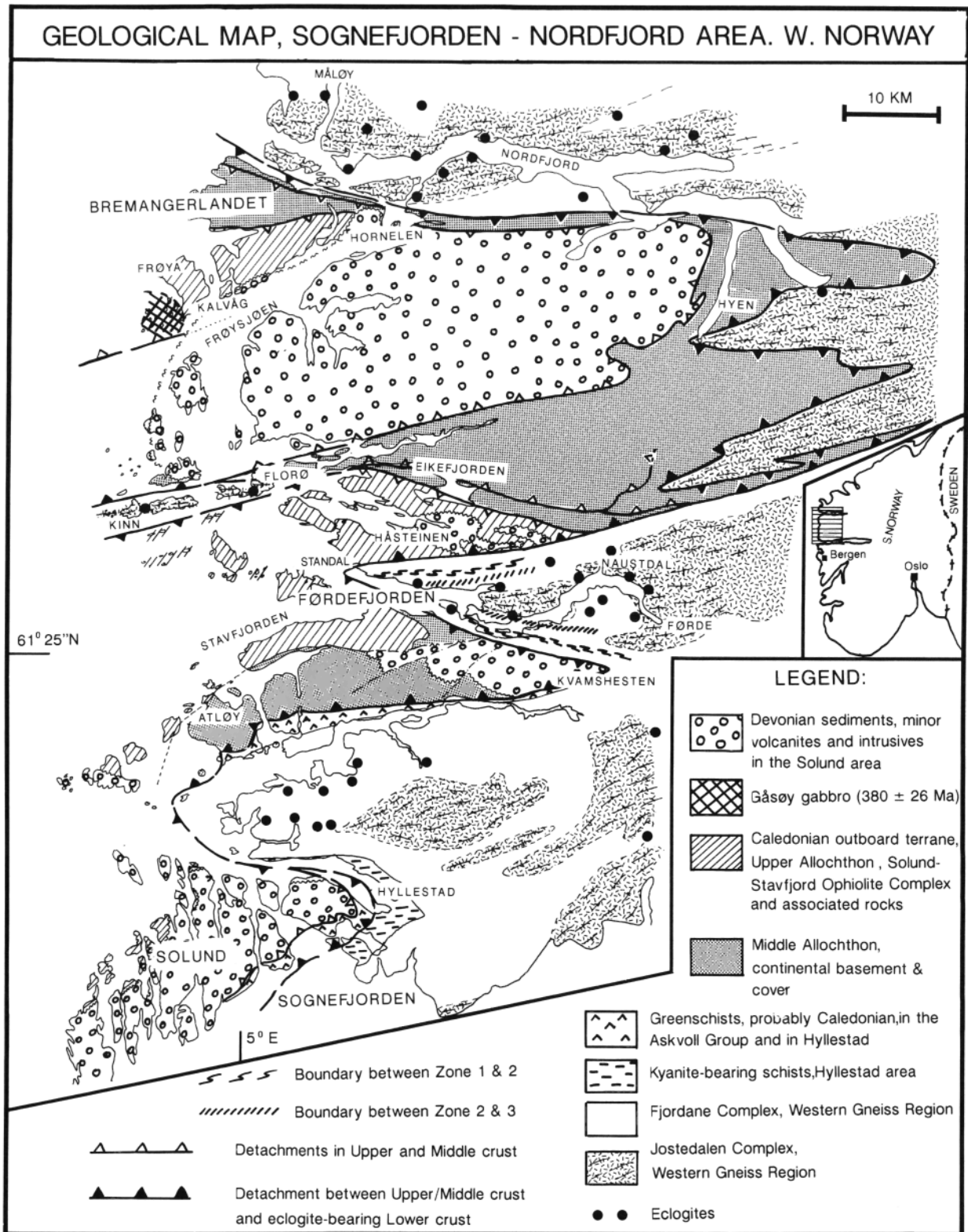
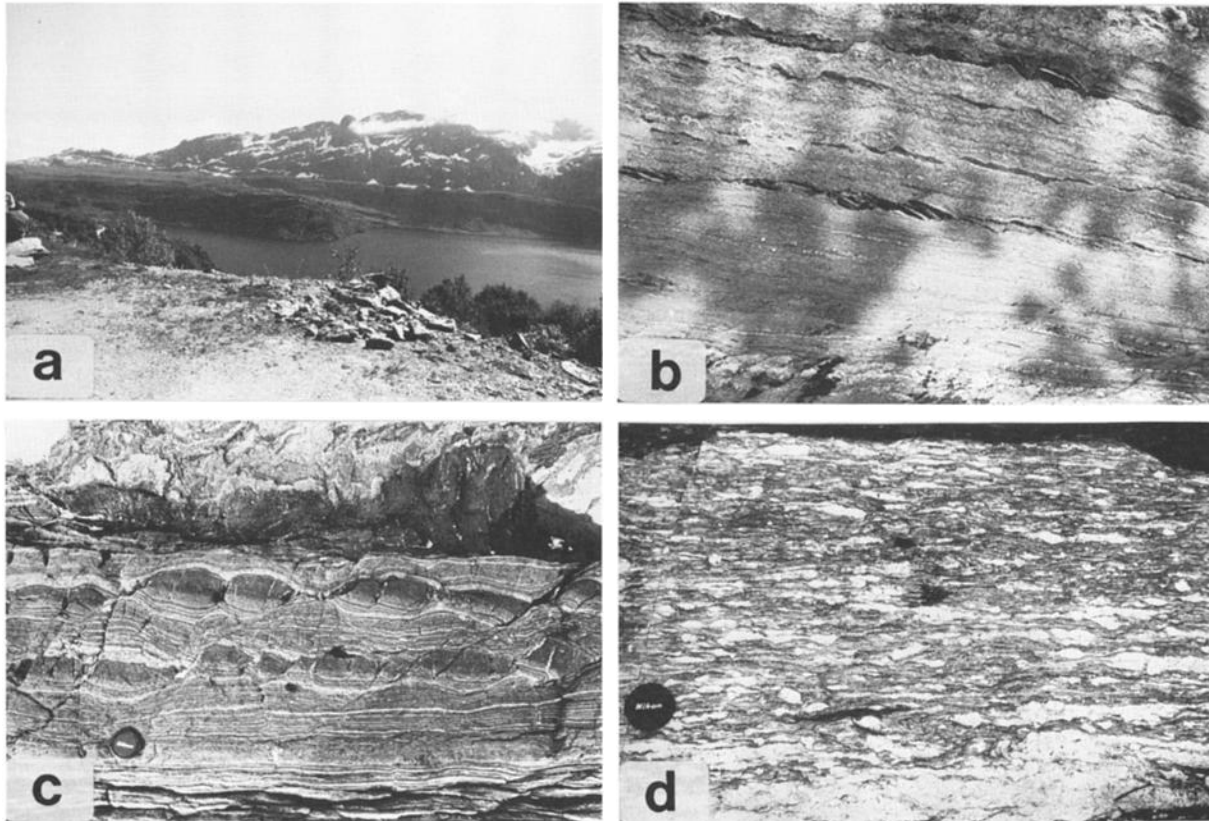


Fig. 1. Simplified geological map of western Norway between Sognefjorden and Nordfjord. The reinterpretation of the geology in the northeast corner of the map is based on published maps by Bryhni and coworkers.



**Fig. 2. (a) View from the north, across Førdefjorden of the Kvamshesten Devonian Basin and the underlying detachment zone. Line, dipping to the right (west), marked by patches of snow, is the brittle fault which truncate the detachment fabric. Mylonites of zones 1 and 2 form the hills between the fjord and the late fault. (b) Extensional crenulation cleavage and shear bands developed in mylonitic greenschists of the Askvoll Group in the detachment zone south of the Kvamshesten Basin. Displacement is to the left (west). Width of section is  $\approx 1.20$  m. (c) Asymmetrical boudins from detachment south of the Kvamshesten Basin. Boudin necks and extensional veins are filled with quartzfeldspatic material. Displacement is to the left (west). (d) Mylonitic augen gneiss from zone 1 in the Standalen detachment. Shear bands and asymmetry of augen shows down-to-the-west (left) displacement.**

progressive rotation from the compressional to the extensional field of the strain ellipsoid occur. The sense of shear derived from the orientation and deformation of the veins is consistent with the other kinematic indicators.

The evidence for rotational strains in the penetratively mylonitized detachment zones is ubiquitous and consistent with a westward translation of the hanging wall. The zones have structural thicknesses across the mylonite foliation of 2-3 km and have evidence of very high shear strains. Although the strains are difficult to estimate precisely, shear strain  $>20$  represents a minimum estimate as the angle

between the S and C planes commonly is very small and difficult to measure. Thus a conservative estimate of displacement based on uncertain determination of shear strain suggests minimum displacements of the order of 50-60 km in the detachment mylonites.

#### GEOMETRY OF THE DETACHMENT ZONES

In discussions of metamorphic core complexes a terminology including an upper

and a lower plate separated by a detachment is commonly used [e.g. Davis, 1983; Wernicke, 1985; Hamilton, 1987]; This has been adopted in models where the Devonian basins in western Norway have been described as a result of extensional tectonics. The detachment faults have been described as parts of one continuous structure variably termed the Måløy fault [Hossack, 1984], the Nordfjord-Sogn Detachment [Norton, 1986, 1987] or the Basal Contact [Séranne and Séguret, 1987]. The most important criterion for identifying lower plate rocks in western Norway is the presence of eclogites. These rocks are separated from areas without eclogites by shear zones, as shown in Figure 1; the boundary of the lower crustal rocks does not always coincide with the faults along the margins of the Devonian basins. These relationships are particularly well displayed between the Standalen fault and the south margin fault of the Hornelen Basin (Figure 1). This area, described by Bryhni [1989, and references therein], comprises rocks of the Eikefjord and Lykkjebø groups, correlated with the Middle Allochthon in the Caledonian tectonostratigraphy and parts of the Fjordane Complex within the WGR. To the west, rocks of the Upper Allochthon belong to the cover sequence of the Solund-Stavfjord Ophiolite Complex [Furnes et al., 1990] and are unconformably overlain by the Håsteinen Devonian basin (Bryhni et al., The southern

Norwegian Caledonides-Oslo-Sognefjord-Ålesund, excursion guide, Uppsala Caledonide Symposium A1, pp. 1-151, herein after referred to as Bryhni et al., 1981). The Caledonian metamorphic grade of the Middle and Upper Allochthon in this area is greenschist/lower amphibolite-facies. Relics of Precambrian granulites have been described from mangerite and anorthosite in this area (Bryhni et al., 1981) and from similar rocks in the Dalsfjord Suite below the Kvamshesten Basin (Figures 1 and 3). Hence a major part of the middle crust that preserves Caledonian tectonostratigraphy has been preserved structurally below the marginal fault of the Hornelen Basin and along the Standalen detachment where the eclogite-bearing lower crust appears to the south. The middle crustal rocks in this area thus constitute a middle plate. The rocks in this structural position are highly deformed, and several shear zones branching from major shear zones like the Eikefjorden fault (Bryhni et al., 1981) and the Standalen detachment have been mapped [Kildal, 1970]. Shear sense indicators from such zones clearly indicate down-to-the-west movement, partly by reactivation of earlier east directed compressional structures.

Mapping by Bryhni and coworkers [Bryhni and Grimstad, 1970] (Bryhni et al., 1981) shows that the middle plate rocks continue east and north of the Hornelen Basin (Figure 1). In this area, however, the shear zones between the

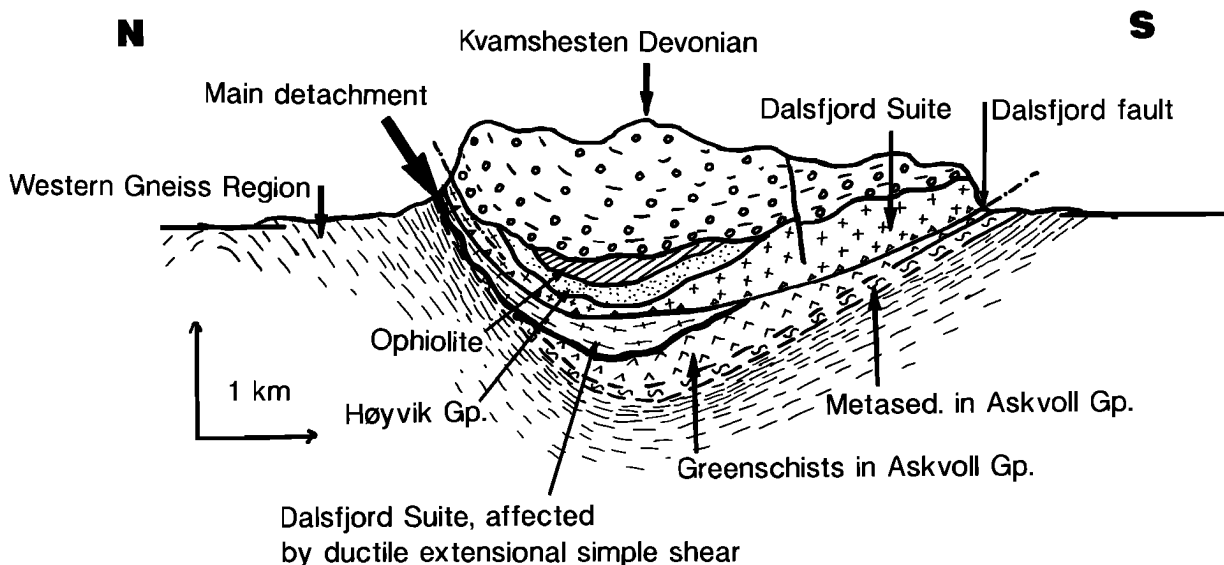


Fig. 3. N-S section of the Kvamshesten Basin and substrate. Note that the the late Dalsfjord fault truncates the detachment fabric which is subparallel to the lithological contacts in the substrate.

upper, middle and lower crustal rocks gradually merge and apparently branch from one major detachment north of Bremangerlandet (Figure 1). Rocks similar to those of the Eikefjord and Lykkjebø groups also occur in rocks of the lower crust where they form a heterogeneous superstructure, the Fjordane Complex, on the migmatitic gneisses of the Jostedal Complex [Bryhni, 1989].

The configuration of extensional faults around the Hornelen Basin shows that the detachment geometry was complex and probably consisted of anastomosing high-strain zones with variable orientation, cutting up and down through the Caledonian nappe pile. A similar geometry can be demonstrated from the Kvamshesten detachment. On the south side of the basin (Figure 3), the Dalsfjord Suite, correlated with the Jotun nappe of the Middle Allochthon [Brekke and Solberg, 1987], occurs in the hanging wall. In this area, the Dalsfjord Suite is unaffected by ductile strains related to the detachment. On the north side, however, penetrative mylonitization of meta-anorthosite and mangerite syenite (Figure 3) is related to shearing along the detachment. These relationships suggest that the detachments did not form low-angle structures everywhere as suggested by Séguret et al. [1989]. A consequence of this is that the Devonian basins were deposited at variable distances from the eclogite-bearing lower crust.

The basal unconformity of the Hornelen Basin is exposed along the west and northwest parts of the basin (Figure 1). In this area, the unconformity oversteps from little-deformed low-grade regional metamorphic rocks of the Upper Allochthon in the Kalvåg Melange [Bryhni and Lyse, 1985; Furnes et al., 1990] near Smørhavn, onto highly deformed gneisses and garnet amphibolites of unknown tectonostratigraphic positions on the islands northwest of Florø. On Bremangerlandet, the basal unconformity of the Hornelen Basin oversteps amphibolite-facies rocks of the Middle Allochthon and greenschist-facies rocks of the Upper Allochthon. Between these tectonostratigraphic units, steeply dipping semiductile to ductile extensional fabrics indicating down-to-the-west movement are superimposed on east directed shortening structures. These relationships suggest that the Devonian sediments were deposited on a basement of Caledonian rocks which already had undergone considerable extensional tectonic stripping and uplift.

#### RELATIONSHIPS BETWEEN THE DETACHMENT ZONES AND ROCKS OF THE LOWER CRUST

As shown above, the detachment zones comprise 2 to 3 km thick mylonite zones characterized by very high rotational strains. In the present study, tectonometamorphic relationships from the Kvamshesten and Standalen detachment zones are described. Adjacent to the Kvamshesten Basin [Bryhni and Skjerlie, 1975], the detachment is truncated [Torsvik et al., 1987] by semiductile to brittle faults of the Dalsfjord fault which mark the present margin of the basin (Figure 3). To both the north and the south of the basin, continuous sections from the faulted top of the detachment to the eclogite-bearing lower crust are exposed as the entire region is folded in large-scale E-W trending folds. The detachment mylonites are more tightly folded than the brittle faults along the basins (Figure 3). Torsvik et al. [1987, 1988] proposed that the folding was a result of late Paleozoic N-S compression. The mechanism and timing for this folding will not be discussed here. Its presence, however, provides a deep structural section through the moderately to steeply dipping detachment zones into rocks of the lower crust.

A cross section from the Kvamshesten detachment into the deepest parts of the lower crust that are exposed along Førdefjorden is described as a basis for the discussion of deformation mechanism during the extension (Figure 4). The section has a structural thickness of approximately 4-5 km across the foliation which dips about 45° north and south away from the axial trace of the Førdefjorden antiform. The detachment mylonites are truncated by semibrittle to brittle fault rocks at the contact with the hanging wall, and these rocks will not be discussed further here.

Within the mylonites of the detachment, three structural zones with transitional contacts can be identified on the basis of variation in deformation intensity, strain pattern and degree of metamorphic retrogression.

Zone 1 on the north side of the Kvamshesten basin has a structural thickness of approximately 1.5 km (Figure 4). The entire zone is characterized by very high strains developed during rotational deformation. The rocks comprise green and grey phyllonites, ultramylonites, mylonites, and mylonitic gneisses. The phyllonites commonly have large

## E - W section along the Kvamshesten detachment zone

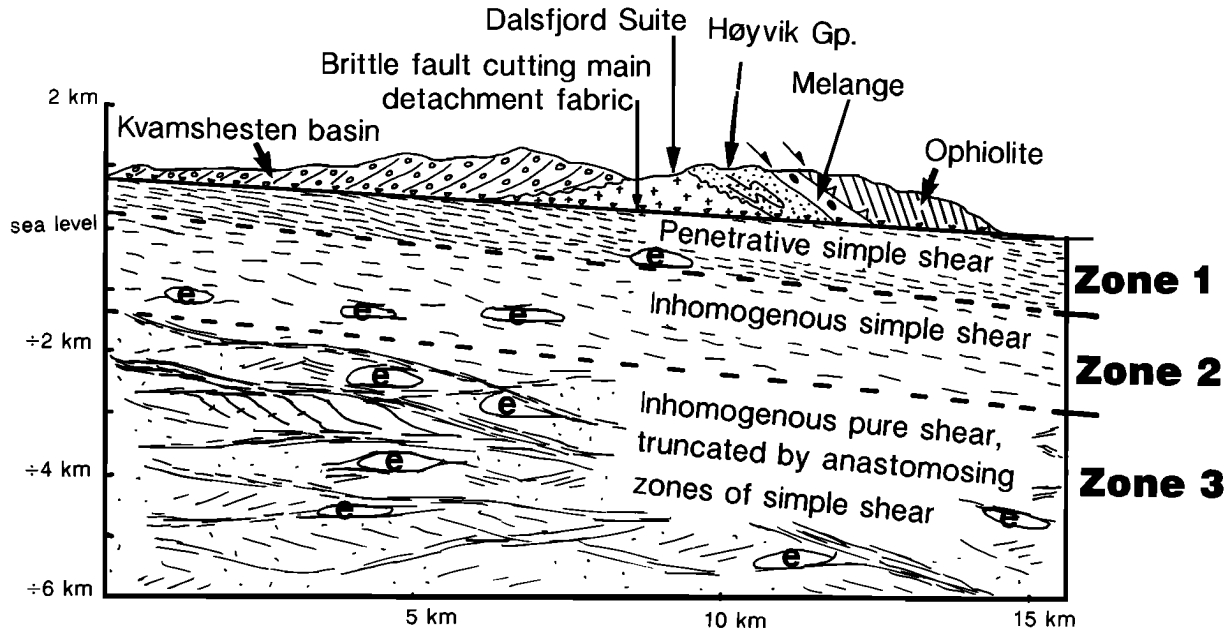


Fig. 4. E-W section of the Kvamshesten basin and substrate. In the hanging wall, the Caledonian compressional tectonostratigraphy has been preserved, although previous thrusts have been re-activated as normal faults. In the footwall, the zonal subdivision of the detachment is shown. Contacts between the zones are transitional. In zone 3, the rocks are characterized by early inhomogeneous irrotational strain fabrics developed at eclogite and amphibolite-facies metamorphism. This is cut by lower-grade zones of simple shear, which displaces down-to-the-west. The 4- to 6-km structural thickness can be studied because of the folding around E-W fold axes, see Fig 6.

diaphoretic white micas and have been mapped previously as mica schists [Kildal, 1970]. Locally, characteristic lithologies, such as white weathering meta-anorthosites and gabbros with relict igneous textures may be recognized as protoliths in the mylonites. Narrow zones of grey quartz-feldspar-muscovite schists have been interpreted as original psammities [Kildal, 1970]. Kinematic indicators (see previous discussion and Figure 2) occur throughout this zone and show consistent simple shear-type deformation with down-to-the-west movement of the hanging wall. Quartz-poor lithologies with grain-size reduction and retrograde syntectonic crystallization of epidote, biotite, chlorite, muscovite, and albite are characteristic of the mylonites in this zone. Quartz veins and segregations with dynamically recrystallized quartz are common. The chlorite-rich phyllonites, particularly abundant in the structurally higher parts of zone 1, develop spectacular extensional crenulation

cleavage. Garnetiferous rocks have not been observed in zone 1 of the Kvamshesten detachment, and the syntectonic mineral assemblages indicate that the deformation occurred during progressive retrogression at greenschist-facies conditions.

Zone 1 of the Standalen detachment has been studied in sections at Steindalen (UTM 125 266) near the Håsteinen Basin and at Standal (Figure 1). The zone is approximately 1 km wide in these areas, and the mylonites generally have steep dips between 40° and 70° to the north. At Standal, a dark ultramylonite with an indistinguishable protolith occurs along the contact to the brittily deformed hanging wall. Structurally below the ultramylonite, protoliths of meta-anorthosite, mica schist, quartzite, and a megacrystic augengneiss with large porphyroclasts of K-feldspar can be identified in the mylonite sequence. The mica schist in the lower part of the zone contains

partly to completely retrograded garnets up to a centimeter in diameter, which in outcrop can be seen to contain inclusion fabrics indicating syntectonic growth prior to the retrogression.

Zone 2 in the Kvamshesten detachment has a structural thickness of approximately 1.5 km. Because of variable dips of the foliation, which are a result of the E-W folding, and its transitional contacts, it is difficult to give a precise estimate of the structural thickness. The dominant lithologies within zone 2 comprise banded grey-green quartz-poor, biotite-plagioclase gneisses possibly of a supracrustal origin, amphibolitic rocks, and granodioritic augen gneisses. The structural style of zone 2 is characterized by anastomosing mylonitic and phyllonitic fabrics of variable intensity. Shear sense indicators characteristic of rotational strains are developed in these zones and show consistent down-to-the-west movement of the structurally higher parts of the zone. Banded garnet amphibolites, locally, have a bright green color, characteristic of retrograded eclogites. Relict eclogites are found mainly in the lower part of zone 2 in both the Standalen and Kvamshesten sections. Near the Kvamshesten Basin, however, an eclogite body, not yet studied by us, occurs as close as 1.5 km from the upper plate, possibly within zone 1 (Figure 4), of the Kvamshesten detachment (W.L. Griffin and M.B.E. Mørk, *Eclogites and basal gneisses in western Norway*, excursion guide, Uppsala Caledonide Symposium B1, pp. 1-88, 1981).

The heterogeneity of the mylonitic lithologies in zone 2 suggests that it is best correlated with similar rocks assigned to the Fjordane Complex elsewhere in the WGR. The deformation pattern is characterized by variable strains, developed in an anastomosing pattern. Within the high-strain zones, however, unambiguous shear sense indicators show a consistent, simple shear-type deformation, which is synthetic with the sense of shear found within zone 1. Hence a structural continuity, regarding deformation in both a simple shear regime and shear sense, between zones 1 and 2, can be suggested.

Zone 3 constitutes the deepest part of the WGR that is exposed in the area. It comprises rocks assigned to the Fjordane Complex and the dominantly quartz-feldspathic gneisses of the Jostedal Complex [Bryhni, 1989]. Both complexes are eclogite bearing but in the

studied area around Førdefjorden (Figure 1), the eclogites are mainly confined to rocks of the Fjordane Complex. Because the eclogite-facies metamorphism is Caledonian [Griffin and Brueckner, 1980], the structural and metamorphic modifications of these rocks are taken to be of Late Silurian-Early Devonian age. A comprehensive study of zone 3 has not yet been carried out. However, a number of observations from the coast and road section along Førdefjorden clearly distinguish the structural pattern in this zone from that of zones 1 and 2.

The granitic and migmatitic banded gneisses of the Jostedal Complex, comprising major parts of zone 3 in the studied area, are heterogeneously deformed. Protomylonitic granitoid gneisses grade into fine-grained mylonites. The high-strain zones anastomose between areas in which older structures and textures, presumably of Precambrian age, are preserved. The structural intensity within the complex apparently increases toward the ill-defined contact with the Fjordane Complex in which eclogites are common. A number of the high-strain zones have been examined to determine their shear sense; no consistent indicators of noncoaxial deformation have been found in the zones (Figure 4). Within a single high-strain zone, kinematic indicators, which are ubiquitous and consistent within zones 1 and 2, may be absent or show inconsistent sense of shear (Figure 5c). Later shear zones, which usually are narrow and have a more phyllonitic character, may show a down-to-the-west sense of shear developed in a simple shear regime. Both generations of high-strain zones generally strike E-W.

Structural and metamorphic aspects of high-strain zones in and adjacent to the eclogites south of Naustdal (UTM 236 232), near the previously mapped contact between the Fjordane and Jostedal complexes (Figure 1), have been studied in some detail. The mineralogical and petrological characteristics of these eclogites are consistent with Krogh's [1980] description of the Sunnfjord eclogites. Electron microprobe analyses in the present study show that the preserved eclogite-facies mineral assemblage (Figure 5a and 5b) consists of prograde zoned (increasing Mg/Fe ratio rimward) garnets, omphacite (Jd 50), phengite (X celadonite = 0.30-0.35), barroisitic amphibole, clinozoisite, quartz, and rutile.

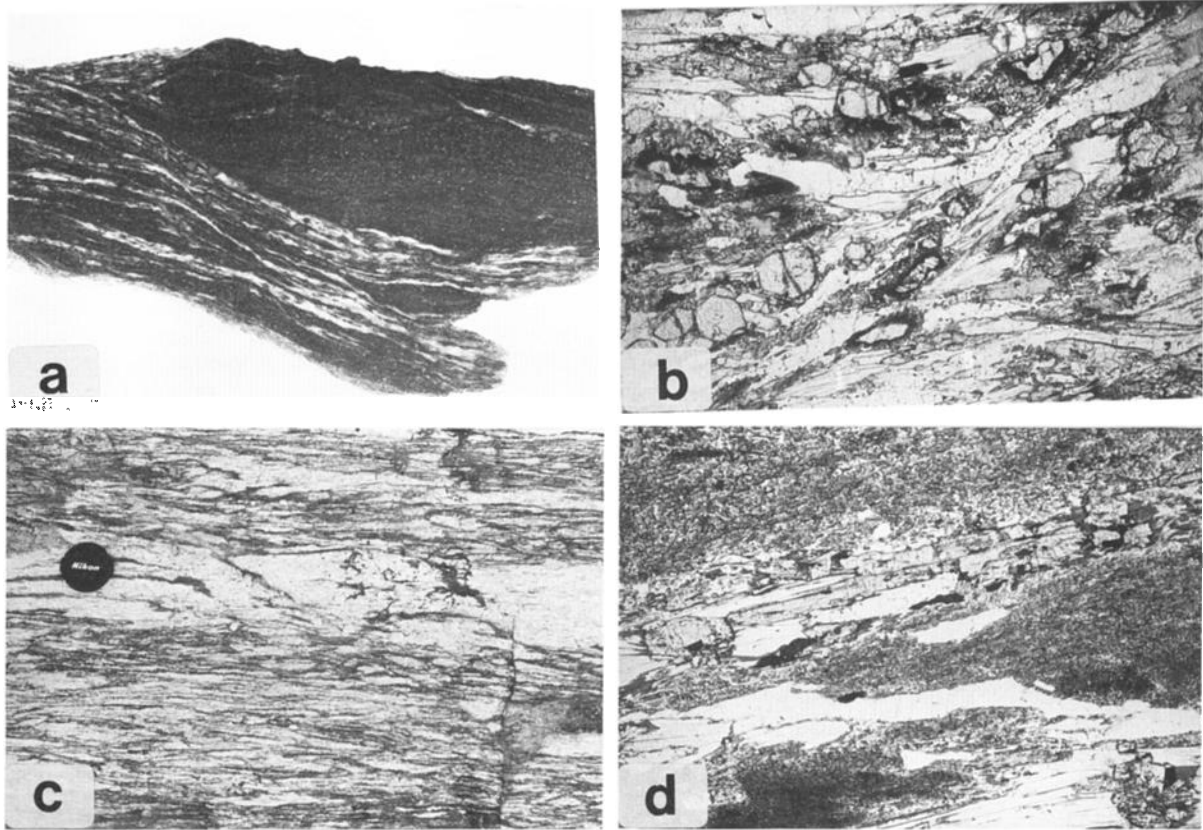


Fig. 5. (a) Cut and polished specimen of eclogite boudin in amphibolite-facies matrix from zone 3 on the north side of Førdefjorden. Width of photograph is 15 cm. Note that conjugate shear bands in both the eclogite and the matrix displaces both to the left (west) and right (east), indicating an overall irrotational deformation. (b) Micrograph of eclogite facies shear band defined by omphacite (with rim of dark symplectite), clinozoisite, phengite, and lenticular quartz. Shear bands, displacing in both directions (east and west), anastomose in the thin section. Width of the micrograph is approximately 3 mm. (c) Amphibolite facies, high-strain zone in quartz-feldspar augen gneiss of the Jostedal Complex within zone 3 in the Førdefjorden area. Note that no systematic sense of shear can be determined in this lithology. (d) Micrograph showing the amphibolite facies foliation defined by quartz, plagioclase, epidote, muscovite, and hornblende in a retrograded eclogite from zone 3. Dark mineral aggregates are symplectites with quartz, plagioclase, and hornblende formed by retrograde metamorphism of the eclogite. Width of micrograph is approximately 3 mm.

Additional phases present as inclusions in the garnets are Al- and Fe-rich sodic-calcic amphibole, paragonite, and hematite. These phases, however, are not observed among the matrix minerals. The eclogite-facies mineralogy is partly to completely replaced by an amphibolite-facies mineralogy characterized by the assemblage plagioclase, calcic amphibole, epidote, phlogopite, and sphene.

The metamorphic conditions during eclogite formation, based on the Fe-Mg exchange reaction between coexisting garnet and omphacite, calibrated by Ellis and Green [1979], and on the jadeite-content of omphacite coexisting with quartz [Holland, 1980], are  $T = 600 \pm 25^\circ\text{C}$ ,  $P_{\text{min}} = 16$  kbar. The estimated pressure for the eclogites in Sunnfjord corresponds to a crustal depth of approximately

50 km. North of the Hornelen Basin, however, the pressure estimates indicate a crustal depth of near 100 km [Smith and Lappin, 1989] and this suggests that areas that have experienced major differential uplifts exist within the WGR.

The tectonometamorphic relationships of the Liabø eclogites show that the high-P assemblage crystallized syntectonically (Figures 5a and 5b). A  $L > S$  fabric defined by omphacite, clinozoisite, phengite, barroisite, and lenticular quartz-segregations was developed. Textural analysis shows that the high-P fabric comprises shear bands (C planes) as well as a foliation defined by crystal shape and crystal lattice fabrics (S planes) (Figure 5b). At the scale of a thin section, the composite foliation shows an inconsistent relationship of the acute angle between the S and C planes. Similarly, shear bands observed at outcrop and in hand specimen (Figure 5a) show shear sense in opposite directions. This implies that the deformation associated with the high-P metamorphism was characterized by inhomogeneous coaxial strains in a pure shear regime.

The superimposed amphibolite-facies metamorphism characterized above apparently crystallized as a result of nearly isothermal uplift of the eclogites. Krogh [1980] suggested  $T = 550^{\circ}\text{C}$  and  $P = 10$  to  $12$  kbar for the amphibolite-facies assemblages superimposed on the eclogite-facies parageneses in the area.

The amphibolite-facies foliation, in which preserved relics of eclogites are found as boudins, has a pure shear deformation pattern similar to the pattern described above for the eclogite facies deformation (Figure 5d). This suggests that the lower crust in this area underwent coaxial deformation during uplift from  $P > 16$  kbar to  $P \approx 10$  kbar, corresponding to a crustal thinning of at least 15-20 km.

$L > S$  fabrics with E-W lineation suggest that the strains were constrictional with a subvertical principal axis of shortening and an intermediate strain axis producing N-S compression. In some localities, however, no obvious stretching lineation has been observed, and this suggests pure shear flattening strains; presently we have inadequate data to evaluate the role of flattening versus constrictional strains.

A general observation, however, is that the eclogite-facies and the early amphibolite-facies anastomosing high-strain zones within zone 3 (Figure 4) developed, apparently, during

nonrotational deformation in a pure shear regime because shear bands in these rocks define a conjugate pattern. The strains are particularly high in quartz-rich segregations where the rheology of quartz has controlled the deformation (Figure 5a). Later greenschist facies shear zones in zone 3 have evidence of rotational deformation similar to that developed in zones 1 and 2 of the detachments.

## DISCUSSION AND CONCLUSIONS

Modeling of the strength of continental crust suggests that extensional collapse of overthickened continental crust in orogens occurs by lateral spreading as a result of body forces in the thickened orogenic welt [England and Houseman, 1988; Dewey, 1988]. The array of extensional mylonite zones in west Norway, which partly truncate earlier compressional structures and underlie the Devonian basins, represents evidence of tectonic thinning of the Caledonian nappe pile. The very deep sections of the continental crust exposed in the WGR in the footwall of the detachments provide a unique opportunity to study the geological processes that have occurred during crustal extension and uplift. The configuration of Devonian basins, detachment zones, strain pattern, and E-W folding is shown in Figure 6.

A popular model for post compressional extension of orogens implies uniform simple shear of the continental lithosphere following Wernicke's [1985] model from the Basin and Range Province in the western United States. This model has been adopted with few modifications to explain the extension and Old Red basin formation in western Norway [Norton, 1986, 1987; McClay et al., 1986; Séranne and Séguret, 1987; Séguret et al., 1989]. From our work, mainly adjacent to the Kvamshesten and Standalen detachments it is clear that they preserve evidence of a simple shear regime during their evolution and that displacements in excess of 50 km were accommodated in these zones. In the Sunnfjord area of western Norway, the Middle Devonian basins are juxtaposed across the detachments with deep crust containing eclogites that crystallized at pressures corresponding to depths of  $>50$  km. The present distance between the Devonian supracrustal rocks and the eclogite-bearing complexes is less than 3 km in the area north

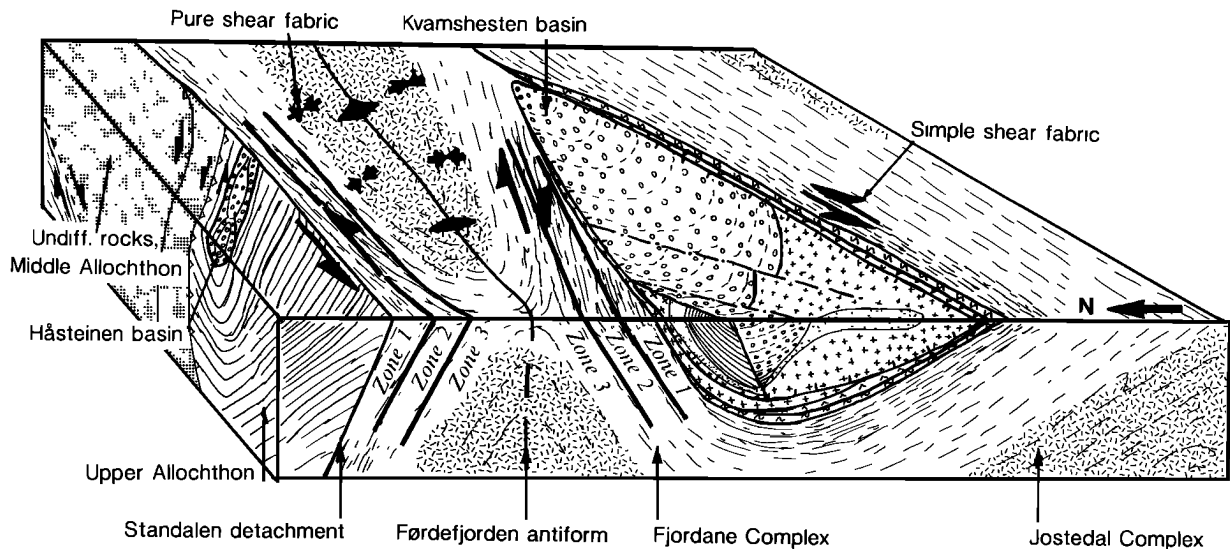


Fig. 6. Block diagram with N-S and E-W sections of the central Sunnfjord area showing the relationships between the lower, middle, and upper crustal plates of the area. Note that the simple shear domain is developed in the upper part of the lower crust and that pure shear regime occurs in the deepest parts of the area. The E-W, nearly vertical folds provide the deep section into the lower crustal plate of the WGR.

of the Kvamshesten Basin. This shows that a minimum of 40-50 km of crustal thickness has been excised along the detachments. If this occurred on a uniformly inclined ( $30^\circ$ ) extensional shear zone penetrating the entire continental lithosphere, it would imply a displacement of the order of 105 km on the detachment. However, if the extension were accompanied by uplift, which is suggested by the progressive retrograde metamorphism and which is inherent in the Wernicke model, the detachment surface would gradually attain very low dips and become subhorizontal. In this case, the crustal thinning by uniform simple shear would be inefficient. Consequently, the displacement would have to be increased by a factor of 10, depending on the orientation of the shear zone in the framework of time and amount of extension. This is incompatible with the regional geology in southern Norway and unacceptable in the present case. It seems clear that the uplift of the WGR cannot be explained fully by Wernicke's [1985] model. However, the presence of the major detachments characterized by a simple shear regime in zones 1 and 2 of the detachment clearly shows that uniform simple shear deformation was important. A common feature of the rotational

deformation fabric is that it records deformation mainly at greenschist-facies metamorphic conditions. Hence the simple shear model appears to explain the structural and metamorphic relationships recorded in zones 1 and 2 in the upper and middle crust.

As suggested above, the eclogite-bearing rocks in zone 3 underwent inhomogeneous deformation in a pure shear regime during eclogite-facies conditions ( $P > 16$  kbar) and in the time interval during which they were isothermally uplifted to amphibolite-facies conditions ( $P = 10-12$  kbar). Radiometric age determinations from WGR are numerous and have been summarized by Kullerud et al. [1986]. These data indicate that rocks in the WGR experienced eclogite-facies metamorphism at around 420 Ma, although other workers have suggested that the maximum crustal thickness was reached at around 450 Ma [Cuthbert et al., 1983]. From studies in the hanging wall of the detachment, it is clear that crustal thickening went on in Middle Silurian times ( $\approx 425$  Ma), as the Solund-Stavfjord Ophiolite Complex of Middle-Late Ordovician age [Dunning and Pedersen, 1988] was obducted at this time [Andersen et al., 1990]. The widespread amphibolite-facies metamorphism in the WGR

occurred at around 400 Ma [Brueckner, 1972; Kullerud et al., 1986]. This suggests that the nearly isothermal decompression occurred over a period of approximately 20 m.y. Based on P-T estimates from the WGR of the Sunnfjord area, this suggests a denudation rate of approximately  $1 \text{ mm yr}^{-1}$ . This estimate is very close to the highest rates suggested from the Himalayas within the period of the last 5 m.y. [Zeitler, 1985]. Carefully designed combined structural, metamorphic, and geochronological studies are necessary to refine estimates of uplift in WGR.

England and Houseman [1988] suggest that catastrophic removal of a major part of a thickened thermal boundary layer (TBC) in the lithospheric mantle will cause rapid uplift of the orogenic welt [Dewey, 1988; Platt and Vissers, 1989]. The increased potential energy of the welt during uplift provides body forces resulting in deviatoric extensional stresses which result in spreading of the welt [Dewey, 1988; Dewey et al., 1988]. This model is very appealing in the present case as it explains satisfactorily decompression from eclogite-facies to amphibolite-facies, which occurred isothermally and rapidly. Dewey [1988] argues that the replacement of the TBL by hot mantle material will cause a higher geothermal gradient accompanied by late to posttectonic magmatism in the extending lithosphere. In western Norway, the presence of late Caledonian magmatic rocks has been documented. They have, however, not yet been systematically studied and have received little attention in geotectonic modeling. Devonian intermediate to acid alkaline lavas [Furnes and Lippard, 1983] occur in the Solund area and a suite of gabbros and granitic rocks from the same area is probably also of Devonian age. Late dolerites of continental tholeiitic affinity occur at several localities, particularly in the Florø area (Figure 1) [Skjerlie and Tysseland, 1981]. A major calc-alkaline gabbro dated at  $380 \pm 26 \text{ Ma}$  by the Sm-Nd method occurs near Frøya. [Furnes et al., 1989]. Also a number of late Caledonian granodioritic dykes and bodies occur in the area between Hyllestad and Florø. Most of the intrusives occur in rocks in middle and upper crustal position. Some of the continental tholeiite dykes, however, intrude rocks of both the upper middle and lower crust in the Florø area (Figure 1). Farther to the north in the WGR, a number of minor granitic rocks of Devonian age have been recognized [Kullerud

et al., 1986, and references therein]. It is suggested that the formation of the Devonian magmatic rocks may be related to introduction of hot mantle material to the lower part of the lithosphere, as proposed by Dewey [1988]. Their very heterogeneous geochemical signatures may be related to partial melting of a highly variable source, including crust and mantle lithosphere and possibly also sub-lithospheric mantle. The apparent scarcity of Devonian magmatic rocks in the lower crustal rocks of the WGR is enigmatic with respect to this model.

A schematic model for crustal uplift and extension is shown in Figure 7. In stage 1, the compressional construction of the orogenic welt is completed, and the orogen contains a structural anisotropy defined by the compressional thrust. Stage 2 of the model (Figure 7) represents the main uplift stage, caused by TBC removal; this is where vertical

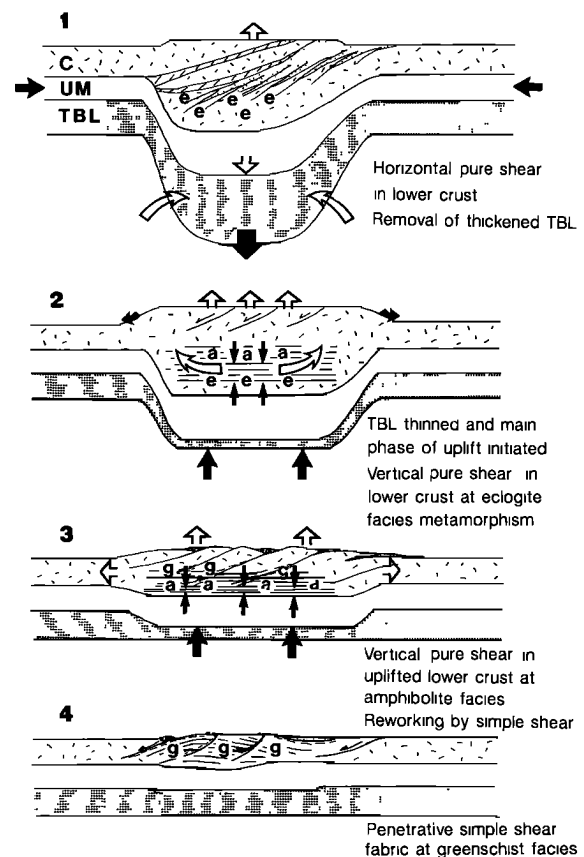


Fig. 7. Model, discussed in the text, for Devonian uplift and extension in the Norwegian Caledonides.

( $\sigma'$ ) compressional stresses cause pure shear eclogite-facies deformation in the lower crust. The isothermal decompression results in amphibolite-facies overprinting of the eclogite-facies fabric. The observed structures described above suggest that a deformation regime of inhomogeneous pure shear characterizes the deepest parts of the crust during the uplift. The northwest part of the WGR, in which the deepest part of the region is exposed, has not yet been studied. Observations from Molde area by Kullerud [1987] show that the gneisses were thoroughly reworked in amphibolite-facies shear zones ( $T = 650^\circ\text{C}$ ,  $P = 10$  kbar) which post dated the eclogite-facies metamorphism. A characteristic feature of these zones, which are steeply dipping and have subhorizontal stretching lineations, is that they lack consistent shear sense indicators [Kullerud, 1987], and this is consistent with our observations. Apparently, they constitute a system of anastomosing high-strain zones up to 1 km wide, which formed under inhomogeneous pure shear constrictional strains. Stage 3 of the model represents the main spreading event and shows reworking of structures formed in the pure shear regime by simple shear, also in accordance with the observations described above.

The model that we suggest for the extensional collapse of the Caledonian orogenic belt in southern Norway is a combined pure and simple shear model. It corresponds closely with the model suggested for the Tibetan plateau which is based on lithospheric modeling [England and Houseman, 1988], observations of seismic activity, and surface geology in upper and middle crustal rocks [Dewey et al., 1988, and references therein]. The simple shear domain in the upper and middle crust was apparently rooted and progressively cut into the pure shear domain of the lower crust as the uplifted deep crust was cooled from an amphibolite-facies to a greenschist-facies metamorphic condition. The rapid uplift recorded by the presence of eclogites formed at extreme depths in the continental lithosphere was probably a result of removal by the TBC layer of the lithospheric mantle. Introduction of juvenile hot mantle material to the base of the lithosphere may explain the Devonian magmatic rocks in the area. Extension continued by deformation in localized extensional shear zones in an already thinned crust and resulted in formation of the Middle Devonian sedimentary basins.

**Acknowledgments.** The manuscript has benefited from discussions with Arild Andresen, Harald Furnes, Eivind Swensson, Håkon Austrheim, Henry Berry, Olav Eldholm, and John Dewey, who also corrected the English. Financial support has been received from NAVF. Norwegian ILP contribution 95.

#### REFERENCES

- Andersen, T.B., K.P. Skjerlie, and H. Furnes, The Sunnfjord Melange, evidence of Silurian ophiolite accretion in the West Norwegian Caledonides, *J. Geol. Soc. London*, **147**, 59-68, 1990.
- Austrheim, H., Eclogitization of lower crustal granulites by fluid migration through shear zones, *Earth Planet. Sci. Lett.*, **81**, 221-232, 1987.
- Austrheim, H., The granulite - eclogite facies transition: A comparison of experimental work and a natural occurrence in the Bergen Arcs, W-Norway, *Lithos*, in press, 1990.
- Austrheim, H., and W.L. Griffin, Shear deformation and eclogite formation within granulite-facies anorthosites of the Bergen arcs, western Norway, *Chem. Geol.*, **50**, 267-281, 1985.
- Brekke, H., and P.O. Solberg, The geology of Atløy, Sunnfjord, western Norway, *Nor. Geol. Unders., Bull.* **410**, 73-94, 1987.
- Bruockner, H.B., Interpretation of Rb-Sr ages from the Precambrian and Palaeozoic rocks of southern Norway, *Am. J. Sci.*, **272**, 334-358, 1972.
- Bryhni, I., Migrating basins on the Old Red Continent, *Nature*, **202**, 384-385, 1964.
- Bryhni, I., Status of the supracrustal rocks in the Western Gneiss Region, S. Norway, in *The Caledonide Geology of Scandinavia*, edited by R. Gayer, pp. 221-228, Graham and Trotman, London, 1989.
- Bryhni, I., and E. Grimstad, Supracrustal and intracrustal rocks in the gneiss region of the Caledonides west of Breimsvatn, *Bull. Nor. Geol. Unders.*, **226**, 105-140, 1970.
- Bryhni, I., and K. Lyse, The Kalvåg melange, Norwegian Caledonides, in *The Caledonide Orogen - Scandinavia and Related Areas*, edited by D.G. Gee and B.A. Sturt, pp. 417-426, John Wiley, New York, 1985.
- Bryhni, I., and F. Skjerlie, Syndepositional tectonism in the Kvamshesten district (Old

- Red Sandstone), western Norway, Geol. Mag., **112**, 593-600, 1975.
- Cuthbert, S.J., M.A. Harvey, and D.A. Carswell, A tectonic model for the metamorphic evolution of the Basal Gneiss Complex, western south Norway, J. Metamorph. Geol., **1**, 63-90, 1983.
- Davis, G.H., Shear-zone model for the origin of metamorphic core complexes, Geology, **11**, 342-347, 1983.
- Dewey, J.F., Extensional collapse of orogens, Tectonics, **7**, 1123-1139, 1988.
- Dewey, J.F., R.M. Shackelton, C. Chengfa, and S. Yiuin, The tectonic evolution of the Tibetan Plateau, Philos. Trans. R. Soc. London, Ser. A, **327**, 379-413, 1988.
- Dunning, G.R., and R.B. Pedersen, U/Pb ages of ophiolites and arc related plutons of the Norwegian Caledonides: Implications for the development of Iapetus, Contrib. Mineral. Petrol., **98**, 13-23, 1988.
- Ellis, D.J., and D.H. Green, An experimental study of the effect of Ca upon garnet-clinopyroxene Fe-Mg exchange equilibria, Contrib. Mineral. Petrol., **4**, 403-416, 1979.
- England, P.C. and G.A. Houseman, The mechanics of the Tibetan Plateau, Philos. Trans. R. Soc. London, Ser. A, **326**, 301-320, 1988.
- Furnes, H. and S.J. Lippard, Devonian lavas from Solund, West Norway – Field relationships and Geochemistry, Bull. Nor. Geol. Unders. **382**, 1-15, 1983.
- Furnes, H., R.B. Pedersen, B. Sundvoll, M. Tysseland, and O. Tumyr, The age, geochemistry, and tectonic setting of the late Caledonian Gåsøy intrusion, west Norway, Nor. Geol. Tidsskr. **69**, 273-289, 1989.
- Furnes, H., K.P. Skjerlie, R.B. Pedersen, T.B. Andersen, C.J. Stillman, R. Suthren, M. Tysseland, and L.B. Garmann, The Solund-Stavfjord Ophiolite Complex and associated rocks, west Norwegian Caledonides: Geology, geochemistry and tectonic environment, Geol. Mag., **27**, 209-224, 1990.
- Griffin, W.L., and H.K. Brueckner, Caledonian Sm-Nd ages and a crustal origin for Norwegian eclogites, Nature, **285**, 319-321, 1980.
- Griffin, W.L., H. Austrheim, K. Brastad, I. Bryhni, A.G. Krill, E.J. Krogh, M.B.E. Mørk, H. Qvale, and B. Tjørndal, High-pressure metamorphism in the Scandinavian Caledonides, in The Caledonide Orogen – Scandinavia and Related Areas, edited by D.G. Gee and B.A. Sturt, pp. 783-801, John Wiley, New York, 1985.
- Hamilton, W., Crustal extension in the Basin and Range Province, southwestern United States, Geol. Soc. Spec. Publ. London, **28**, 517-536, 1987.
- Holland, T.J.B., The reaction albite-jadeite + quartz determined experimentally in the range 600-1200°C, Am. Mineral., **65**, 129-134, 1980.
- Hossack, J.R., The geometry of listric faults in the Devonian basins of Sunnfjord, W. Norway, J. Geol. Soc. London, **141**, 629-637, 1984.
- Jamtveit, B., Metamorphic evolution of the Eiksundal eclogite complex, Western Norway, and some tectonic implications, Contrib. Mineral. Petrol., **95**, 82-99, 1987.
- Kildal, E.S., Geologisk kart over Norge, berggrunnskart: Måløy, scale 1:250,000, Nor. Geol. Unders., Trondheim, 1970.
- Krogh, E.J., Evidence for a Precambrian continent-continent collision in western Norway, Nature, **267**, 17-19, 1977.
- Krogh, E.J., Geochemistry and petrology of glaucophane-bearing eclogites and associated rocks from Sunnfjord, western Norway, Lithos, **13**, 355-380, 1980.
- Kullerød, L., Rb-Sr studie av gneiser i Ytre Romsdal, Vest Norge, Cand. sci. thesis, pp. 1-173, Univ. of Oslo, Oslo, 1987.
- Kullerød, L., B.O. Tjørndal, and S. Ilebekk, A compilation of radiometric age determinations from Western Gneiss Region, South Norway, Bull. Nor. Geol. Unders., **406**, 17-42, 1986.
- McClay, K.R., M.G. Norton, P. Coney, and G.H. Davis, Collapse of the Caledonide orogen and the Old Red Sandstones, Nature, **323**, 147-149, 1986.
- Norton, M.G., Late Caledonian extension in western Norway: A response to extreme crustal thickening, Tectonics, **5**, 195-204, 1986.
- Norton, M.G., The Nordfjord-Sogn Detachment, W. Norway, Nor. Geol. Tidsskr., **67**, 93-106, 1987.
- Platt, J.P. and R.L.M. Vissers, Extensional collapse of thickened continental lithosphere: A working hypothesis for the Alboran Sea and Gibraltar arc, Geology, **17**, 540-543, 1989.
- Séguret, M., M. Séranne, A. Chauvet, and M. Brunel, Collapse basin: A new type of

Andersen and Jamtveit: Orogenic Extensional Collapse, Western Norway

1111

- extensional sedimentary basin from the Devonian of Norway, Geology, **17**, 127-130, 1989.
- Séranne, M. and M. Séguret, The Devonian basins of western Norway: tectonics and kinematics of an extending crust, Geol. Soc. Spec. Publ. London, **28**, 537-548, 1987.
- Skjerlie, F.J. and M. Tysseland, Geochemistry and petrology of dolerite dykes of probable Late Caledonian age from the outer Sunnfjord Region, West Norway, Bull. Nor. Geol. Unders., **363**, 25-44, 1981.
- Smith, D.C., A review of the peculiar mineralogy of the Norwegian coesite-eclogite province, Eclogites and Eclogite-facies rocks, edited by D.C. Smith, pp. 1-206, Elsevier, New York, 1988.
- Smith, D.C. and M.A. Lappin, Coesite in the Straumen kyanite-eclogite pod, Norway, Terra Nova, **1**, 47-56, 1989.
- Swensson, E. and T.B. Andersen, Bevegelsesindikatorer langs Kvamshesten of standalforkastningene-indikasjoner på sen-kaledonsk normal og sidelengs bevegelse og stor-skala skorpe ekstensjon, abstract, Geonytt, **17**, 112-113, Norsk Geologisk Forening, Trondheim, 1990.
- Torsvik, T.H., B.A. Sturt, D.M. Ramsay, and V. Vetti, The tectono-magnetic signature of the Old Red Sandstone and Pre-Devonian strata in the Håsteinen area, western Norway, and implications for the later stages of the Caledonian Orogeny, Tectonics, **6**, 305-322, 1987.
- Torsvik, T.H., B.A. Sturt, D.M. Ramsay, D. Bering, and P.R. Fluge, Palaeomagnetism, magnetic fabrics and the structural style of the Hornelen Old Red Sandstone, Western Norway, J. Geol. Soc. London, **145**, 413-430, 1988.
- Wernicke, B., Uniforme-sense normal simple shear of the continental lithosphere, Can. J. Earth Sci., **22**, 108-125, 1985.
- Zeitler, P.K., Cooling history of the NW Himalaya, Tectonics, **4**, 127-151, 1985.
- T.B. Andersen and B. Jamtveit, Department of Geology, University of Oslo, P.O. Box 1047, Blindern, 0316 Oslo 3, Norway.
- (Received September 9, 1989;  
revised December 14, 1989;  
accepted March 14, 1990.)

# Subduction and eduction of continental crust: major mechanisms during continent–continent collision and orogenic extensional collapse, a model based on the south Norwegian Caledonides

Torgeir B. Andersen<sup>1</sup>, Bjørn Jamtveit<sup>1</sup>, John F. Dewey<sup>2</sup> and Eivind Swenson<sup>1</sup>

<sup>1</sup>Department of Geology, University of Oslo, 0316 Blindern, Oslo 3, Norway; <sup>2</sup>Department of Earth Sciences, University of Oxford, Parks Road, Oxford OX1 3PR, UK

## ABSTRACT

During continental collision in the middle Silurian, the thickness of the lithosphere under the Caledonides of S. Norway was doubled by subduction of the western margin of Baltica, including the Western Gneiss Region, under Laurentia. Crustal rocks of the Baltic plate reached sub-Moho depths of near 100 km or more as inferred from the presence of coesite in eclogites. Isostatic calculations indicate an average elevation of the mountain chain of about 3 km at this stage. The subducted lithosphere experienced vertical constrictional strains as a result of slab-pull by its heavy and cold root. Eduction of the deeply buried crustal material was initiated by decoupling of the Thermal Boundary Layer in the subducted lithosphere. Isostatic rebound resulted in very rapid uplift (1–2 mm yr<sup>-1</sup>), and the deep crust was exhumed, mainly by tectonic extensional stripping over a period of 30–40 Myr. The eduction was probably related to a rolling hinge, footwall uplift mechanism, and the early high-pressure coaxial fabrics were overprinted by extensional simple shear as the deep crust reached middle and upper crustal levels. The model explains the present-day normal crustal thickness under the exhumed deep rocks without necessarily invoking large-scale lateral flow of material in the lower crust or igneous underplating.

*Terra Nova*, 3, 303–310

## INTRODUCTION

Geophysical data from orogenic belts in continental collision zones show that collision results in a greatly thickened crust. In the Alps, a maximum Moho depth of about 55 km is recorded (St. Mueller, 1990), and in the Himalayan–Tibetan system a near doubling of the crust with Moho depths of approximately 70 km has occurred (Dewey *et al.*, 1988; Holt and Wallace, 1990). The Moho is defined by an increase in P-wave velocities to  $\geq 7.8$  km s<sup>-1</sup> in the upper mantle, and the lithostatic pressures (P) at these Moho levels are in the

range of 14 to 20 kbar. Such pressures are in good agreement with the  $P_{\min}$  estimates based on jadeite contents of clinopyroxene in country-rock eclogites from exposed high-P terranes in orogenic belts (Griffin *et al.*, 1985; Carswell, 1990). Recently, however, several occurrences of extremely high-P rocks of crustal origin have been described. Based on mineral equilibria, Jamtveit (1987) estimated  $P \geq 25$  kbar from the Eiksundal eclogite (Fig. 1) in the Western Gneiss Region (WGR) in S. Norway, corresponding to a burial depth of  $\geq 75$  km. Furthermore, the occurrences

of coesite in crustal rocks, outside impact structures, recorded from the Dora Maira massif in the western Alps (Chopin, 1984, 1987), the WGR (Smith, 1984, 1988; Smith and Lappin, 1989) and from the Shandong province in E. China (Enami & Zang, 1990), suggested  $P \geq 28$  kbar. This indicates that rocks of crustal origin may be subducted to depths far below the geophysical Moho recorded under modern collision zones. They also provide unequivocal evidence that such deeply buried rocks may be brought to the surface.

A crustal thickness of 100 km is, however, highly unlikely. Simple isostatic calculations imply that if these rocks retained their crustal petrophysical signature (average density  $\approx 2.8$  g cm<sup>-3</sup>), the mountain range above such an area would rise to unrealistic heights (10–11 km, see below). With reference to lithospheric strength parameters and observation of present-day mountain ranges, Dewey (1988) argued that orogenic belts shortened by thrusting generally will have average topographic reliefs  $\leq 3$  km, and rise higher during the initial stages of orogenic collapse.

Based on recent and previous studies in the WGR and the Bergen Arcs in W. Norway (Fig. 1), we suggest and discuss a model in which the lithosphere was doubled during Caledonian plate convergence through the Middle Silurian. The orogenic extensional collapse initiated by decoupling of the thickened Thermal Boundary Layer (TBL) (England and Houseman, 1988; Dewey *et al.*, 1988; Platt and Vissers, 1989; Andersen and Jamtveit, 1990), resulted in rapid uplift and spreading of the orogenic welt. The deeply buried crust was educted, dominantly by vertical uplift, from its latent position in the mantle by

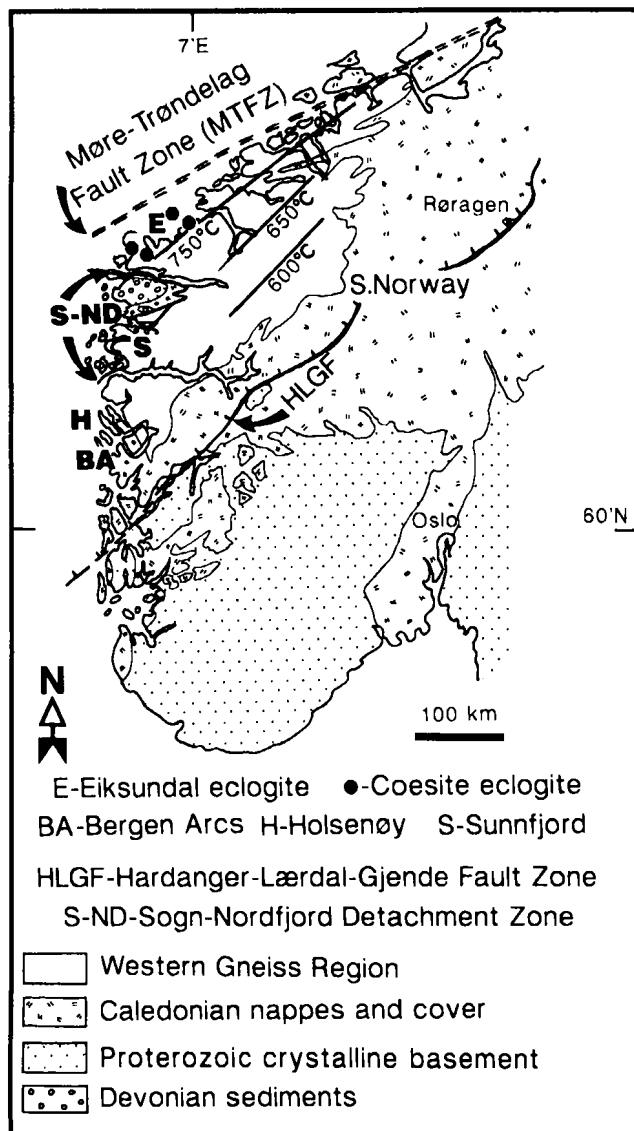


Fig. 1. Simplified geological map of South Norway. Isotherms in the WGR are from Krogh (1977).

the isostatic rebound. The rebound was accompanied by extensional faulting in the hanging wall and uplift of the footwall is related to a rolling hinge mechanism (Buck, 1988; Hamilton, 1988). The exhumed crustal material experienced substantial retrograde metamorphism and extensional deformation during the exhumation.

#### REGIONAL GEOLOGICAL SETTING OF THE WESTERN GNEISS REGION (WGR)

Caledonian eclogites occur in two areas in S. Norway (Fig. 1); in the WGR and in

the Bergen Arcs (Griffin and Brueckner, 1980, 1985; Cohen *et al.*, 1987). The WGR occupies the lowermost tectonostratigraphic level in W. Norway (Andersen and Jamtveit, 1990); the tectonostratigraphic position of the eclogite-bearing rocks in the Bergen Arcs is uncertain.

The WGR consists of ortho- and paragneisses, peridotites, anorthosites and gabbros; eclogites occur in all these lithologies (Bryhni, 1989). Radiometric age determinations by a variety of methods demonstrate that the eclogite facies metamorphism is Caledonian (Griffin and Brueckner, 1980; Gebauer

*et al.*, 1985; Mørk and Mearns, 1986; Jamtveit *et al.*, 1991). Based on geothermometric studies on eclogitic rocks, Krogh (1977) concluded that the P and T conditions for the eclogite facies parageneses increase from SE to NW across the WGR (Fig. 1). The WGR is overlain in the E and SE by a thin autochthonous/parautochthonous Late Precambrian cover and a number of Caledonian allochthonous units including outboard terranes and nappes of Precambrian crystalline rocks. In the Sogn-Nordfjord area (Fig. 1), the WGR constitutes a lower plate, separated from middle and upper crustal rocks by major extensional detachments (Norton, 1986; Séranne and Séguret, 1987; Andersen and Jamtveit, 1990).

Evidence from the Sunnfjord area in W. Norway (Fig. 1) shows that plate convergence and thickening continued until the Middle Silurian (Andersen *et al.*, 1990). In the foreland sediments preserved in the Permian Oslo Graben in SE Norway (Fig. 1), shallow-marine sedimentation dominated by carbonates continued through the Wenlock. The platform sediments are overlain by the Upper Silurian to Early Devonian molasse deposits of the Ringerike Group. Thrusting of the platform sediments occurred after deposition of the Ringerike Group in the Lower Devonian (Bjørlykke, 1983). This coincided with the major phase of uplift in the WGR as the eclogite-bearing rocks in this region underwent nearly adiabatic decompression to amphibolite facies conditions at around 400–410 Ma (Kullerud *et al.*, 1986; Lux, 1985). The uplift is considered to be associated with the extensional collapse (Andersen and Jamtveit, 1990), and the compressional structures in the foreland can therefore most likely be related to spreading of the orogenic welt during the orogenic collapse. As the rocks of the WGR are nowhere seen to be structurally emplaced onto other units, it is highly unlikely that their uplift at this stage was related to thrusting as suggested by Cuthbert *et al.* (1983).

#### STRUCTURAL AND METAMORPHIC CHARACTERISTICS OF THE UPLIFTED DEEP CRUST

The numerous occurrences of high-P and T eclogite facies rocks within the

## CONTINENTAL CRUST

WGR show that it represents a large terrane of uplifted deep crust. Below, we summarize some structural and metamorphic characteristics of the WGR. We refer also to observations from the Bergen Arcs that are necessary in the discussion of the model.

## Structures

As eclogite facies rocks occur abundantly in the WGR, the high-P rocks are useful time-markers in the tectono-metamorphic history of the structurally complex, exhumed deep crust. Detailed studies of the fabrics in the eclogite facies rocks are still in progress. Preliminary results show that the high-P fabrics are characterized by L-tectonites, conjugate shear-planes and constrictional folds, developed by deformation in a dominantly constrictional, irrotational strain regime. In both the Bergen Arcs and the WGR, formation of eclogites from dry granulites was associated with a dramatic reduction of the rock strength, as the stress-bearing strong plagioclase was consumed by the metamorphic reactions that formed the eclogite facies assemblages, including kyanite, phengite and clinozoisite (Austrheim, 1987, 1990; Austrheim and Mørk, 1988). Caledonian deformation was localized in anastomosing high-strain zones. The inconsistent asymmetry of the kinematic indicators and the insignificant translations parallel with these eclogite facies high-strain zones suggest, also, a non-rotational strain regime during the high-P metamorphism.

The high-P rocks were retrograded syn-tectonically during amphibolite to greenschist facies conditions. Andersen and Jamtveit (1990) described three structural zones to characterize progressive formation of fabrics during uplift; the irrotational strains typical of the eclogite and early amphibolite facies fabrics in the lower crust (Zone 3) were progressively reworked by inhomogeneous simple shear (Zone 2) and completely overprinted by extensional mylonites in the detachments (Zone 1) (Swensson and Andersen, 1991).

## Metamorphic characteristics

Our knowledge of the high-P history of the WGR is based largely on studies of

eclogites and various garnet peridotites. Smith (1988) reported coesite from two localities and suggested the former presence of coesite in eclogites from five additional localities (Fig. 1). At  $T = 750^{\circ}\text{C}$ ,  $P \geq 28$  kbar is required to stabilize coesite (Mirwald and Massonne, 1980), which is consistent with the estimated equilibration pressure for Proterozoic, Alpine-type peridotite bodies that occur scattered throughout a large portion of the WGR (Jamtveit *et al.*, 1991). The Proterozoic assemblages in these mantle fragments have experienced extensive deformation and recrystallization during the Caledonian orogeny, leading to the formation of a new garnet-bearing assemblage that equilibrated at significantly lower P-T conditions ( $T \approx 700^{\circ}\text{C}$ ,  $P \approx 20$  kbar, Jamtveit *et al.*, 1991).

The rocks of the WGR, however, are dominated by amphibolite facies assemblages. This metamorphic contrast has resulted in a controversy of exotic versus *in situ* metamorphism of the high-P rocks in the WGR. Griffin (1987) gives numerous examples of relict high-P assemblages in the felsic rocks and concludes that most of the gneiss terrane experienced Caledonian high-P metamorphism. However, it is quite obvious from petrographic observations that major parts of the orthogneisses, gabbros and dolerites within the WGR never recrystallized to assemblages compatible with the P-T conditions inferred from the eclogites; they retained their low-density (-pressure) assemblage during crustal thickening.

The work of Austrheim (1978, 1990) and co-workers from the Bergen Arcs clearly demonstrates the crucial role of fluids for the metamorphic transformations during crustal thickening. Within the Bergen Arcs, dry granulites, outside fluid-channels, survived high-T ( $T \approx 700^{\circ}\text{C}$ ) eclogite facies metamorphism without significant alteration of their metastable, plagioclase-bearing, assemblages (Jamtveit *et al.*, 1990). This also applies to many of the essentially 'dry' orthogneisses, gabbros, dolerites and anorthosites within the WGR (Mørk, 1985). Thus, it is not likely that the mineral assemblages of all subducted crustal rocks were compatible with the high-P conditions reflected by the eclogites. As discussed below, this has important implications for the

isostatic constraints on the crustal thickening process.

## DISCUSSION

A tectonic model consistent with the observations from the WGR must allow for (1) subduction of crustal material to a depth of  $\geq 100$  km; (2) eclogite formation during constructional, irrotational strains; (3) intercalation of mantle fragments formed at depths  $\geq 100$  km into the crust; and (4) uplift of the deeply buried crust during extension to near surface environments during a period of 30 to 40 million years.

Isostatic calculations imply that crustal thicknesses of  $\approx 100$  km cannot be achieved for an average crustal density  $< 3.0 \text{ g cm}^{-3}$ . Provided that the upper 50 km of the crust retained an average density of  $2.8 \text{ g cm}^{-3}$ , the lower 50 km must have had a density  $\geq 3.2 \text{ g cm}^{-3}$  to avoid an average topographic elevation of  $\geq 4$  km during the collision. If the lower part of the crust had an average tonalitic composition, this could hardly have been achieved even if the entire lower 50 km was completely recrystallized to eclogite facies assemblages. Furthermore, studies in the Bergen Arcs and in the WGR (see above) show that complete eclogitization is highly unlikely. An obvious way to avoid the isostatic problem is by subducting crustal rocks beneath heavy mantle as suggested in Fig. 2a. This model implies that a velocity and density inversion was formed in the lower part of the thickened lithosphere prior to the extensional collapse. A possible modern analogy for this transient configuration may exist in the Pamir-Hindu Kush region of the W. Himalayas where Roecker (1982), on the basis of seismic activity, suggested that a low-velocity zone formed by subducted continental crust extends to a depth of  $\approx 150$  km. In our model, subducted crustal material may have experienced  $P \geq 28$  kbar, even if a maximum total crustal thickness never exceeded  $\approx 80$  km ( $2 \times$  normal crustal thickness + thickening due to internal crustal imbrication). In this case, reasonable surface elevations can be obtained for only a moderate density increase in the subducted crust. For a 40 km thick upper crust with a density of  $2.8 \text{ g cm}^{-3}$ , a 40 km thick subducted crustal volume with an average density

of  $2.9 \text{ g cm}^{-3}$  underlain by  $\approx 100 \text{ km}$  of still cold mantle lithosphere would result in a reasonable average elevation of  $\approx 3 \text{ km}$ . A density increase of  $0.1 \text{ g cm}^{-3}$  would, for a tonalitic average crust, be achieved if  $\approx 30\%$  of the rocks equilibrated at eclogite facies conditions, or alternatively if all the Na-feldspar component of the rocks were converted to a NaAl-pyroxene component by the reaction: albite = jadeite + quartz.

Irrational, constrictional strain in the subducted crust is consistent with subduction driven by a slab-pull mechanism (Bott, 1982). Subduction terminated when the relatively cold and dense TBL was decoupled from the lithosphere and removed by gravitational and thermal instability (England and Houseman, 1988; Molnar, 1990). Furthermore, loss of the TBL would cause a rapid isostatic rebound of the orogenic welt.

The actual cooling and uplift rates of the WGR are constrained by geochronological and petrological data. The best Sm-Nd dates obtained for the eclogite facies parageneses in country-rock eclogites cluster around 410–420 Ma (Griffin and Brueckner, 1980, 1985; Mørk and Mearns, 1986; Jamtveit *et al.*, 1991). Available data (see discussion by Jamtveit *et al.*, 1991) suggest that most country-rock eclogites in the WGR never exceeded the blocking temperature for diffusional resetting of the Sm-Nd system in mm-cm sized garnets. Cooling ages and their corresponding temperatures have been reported by several authors;  $500^\circ\text{C}$  at 410 Ma for amphiboles and  $300^\circ\text{C}$  at 375 Ma for biotites, based on the  $^{40}\text{Ar}/^{39}\text{Ar}$  dating of mafic pods near the coesite localities (Lux, 1985);  $500^\circ\text{C}$  at 395 Ma based on U-Pb dating of sphene from the northern parts of the WGR (Tucker *et al.*, 1987);  $500^\circ\text{C}$  at 400 Ma based on Rb-Sr mineral data (Brueckner, 1972). Also, the deposition of Middle Devonian ( $\approx 380 \text{ Ma}$ ) sediments on top of an already extended basement puts constraints on the uplift rate of the eclogite-bearing terrane. Cooling from  $\approx 700^\circ\text{C}$  at 420 Ma to  $\approx 500^\circ\text{C}$  at 400 Ma reflects a cooling rate of  $10^\circ/\text{Myr}$ , twice the cooling rate given by Lux (1985) for the cooling from 500 to  $300^\circ\text{C}$ . Lack of good P-estimates for the low-T assemblages limits the possibility for obtaining precise uplift rates, and the best

estimate that can be suggested at the present time is  $1 \text{ to } 2 \text{ mm yr}^{-1}$  for the early part of the uplift history. In spite of the uncertainties, uplift rates  $> 1 \text{ mm yr}^{-1}$  are much higher than can be obtained from erosion-controlled uplift.

Cuthbert *et al.* (1983) suggested thrusting along a flat-lying fault zone as an alternative uplift mechanism. However, thrust-controlled uplift is not compatible with the extensional deformation seen in the medium to low-grade metamorphic rocks in the WGR, and is also unlikely because it requires unrealistic erosion rates during thrusting. A more plausible model, consistent with the structural observations and the rapid uplift, is provided by recent models describing normal faulting associated with rolling hinge footwall uplifts (Buck, 1988; Hamilton, 1988). This model (Fig. 2b) provides a mechanism by which the deeply buried crustal rocks may be exhumed from the mantle and returned to the surface by footwall uplift associated with extensional stripping of the middle and upper crust in the hanging wall. In the model presented here, large-scale intracrustal lateral flow of material or alternatively igneous underplating as proposed by Asmeron *et al.* (1990) to retain the crustal thickness under the exhumed deep crust, is unnecessary as the mantle reservoir of subducted crust replaces the uplifted material progressively by dominantly vertical movements during the exhumation (Fig. 2b and c).

#### SUBDUCTION AND EXHUMATION OF CONTINENTAL CRUST; MODEL APPLIED TO THE SOUTH NORWEGIAN CALEDONIDES

In Fig. 2, three stages in the evolution of the S. Norwegian Caledonides are shown in SE-NW sections from the Middle Silurian until the lithosphere returned to normal thickness at an unspecified time in the Late Palaeozoic. Because of the complications related to the later opening of the N. Atlantic, Caledonian structures in the overriding plate have been omitted northwest of the inferred suture II (Fig. 2a). Deep seismic reflection data from the area north of the British Isles, however, show major SE-dipping reflectors of

presumed Caledonian age in the crust and at sub-Moho depths (Snyder and Flack, 1990), indicating a symmetrical distribution of collision and collapse related structures along the axis of the orogen. With time, Suture II (Fig. 2a) formed the Møre-Trøndelag Fault Zone (MTFZ) (Grønlie and Roberts, 1989) in the reconstruction (Fig. 2c). In the present model the MTFZ is taken to represent a controlling structure during the extensional collapse. Unpublished deep seismic reflection data by Hurich *et al.* (pers. comm.) show that the MTFZ is a major  $45^\circ$  NW-dipping reflector to the base of the crust off the north-west coast of S. Norway (Fig. 1).

The original lithospheric and crustal thickness in the profiles have been taken to be about 100 and 35 km, respectively. The presence of the inferred Suture I (Fig. 2a) is based on the occurrences of ophiolitic rocks beneath the crystalline nappes in central S. Norway and in Sunnfjord (Fig. 1). The maximum depth to the Moho before the orogenic collapse is approximately 60 km (Fig. 2a), and the dotted area (Fig. 2a) represents subducted crust of the Baltic plate. The partial eclogitization of the subducted continental crust may have given these rocks a geophysical signature transitional between those of crust and mantle (see above and: Roecker, 1982; Austrheim, 1987). The approximate area of the subducted crustal rocks in the profiles is estimated on the basis of the isograds (Fig. 1) in the WGR and the present-day crustal thickness in the area, under the assumption that the uplifted deep rocks presently exposed in the WGR have not been replaced at depth by large-scale flow or underplating.

By the Middle Silurian (420 Ma) the Iapetus Ocean had closed (Andersen *et al.*, 1990). The collision between Baltica and the overriding Laurentian continent was established, and a major part of the Baltic plate was subducted (Fig. 2a). As discussed above, the topographic relief in the orogen above the thickened lithosphere did not exceed 3 km at this stage. The deepest part of the subducted crust may have reached extreme depths, perhaps close to 150 km. The slab-pull on the subducted crustal material exerted by the thickened, heavy lithospheric mantle resulted in an overall vertical constrict-

CONTINENTAL CRUST

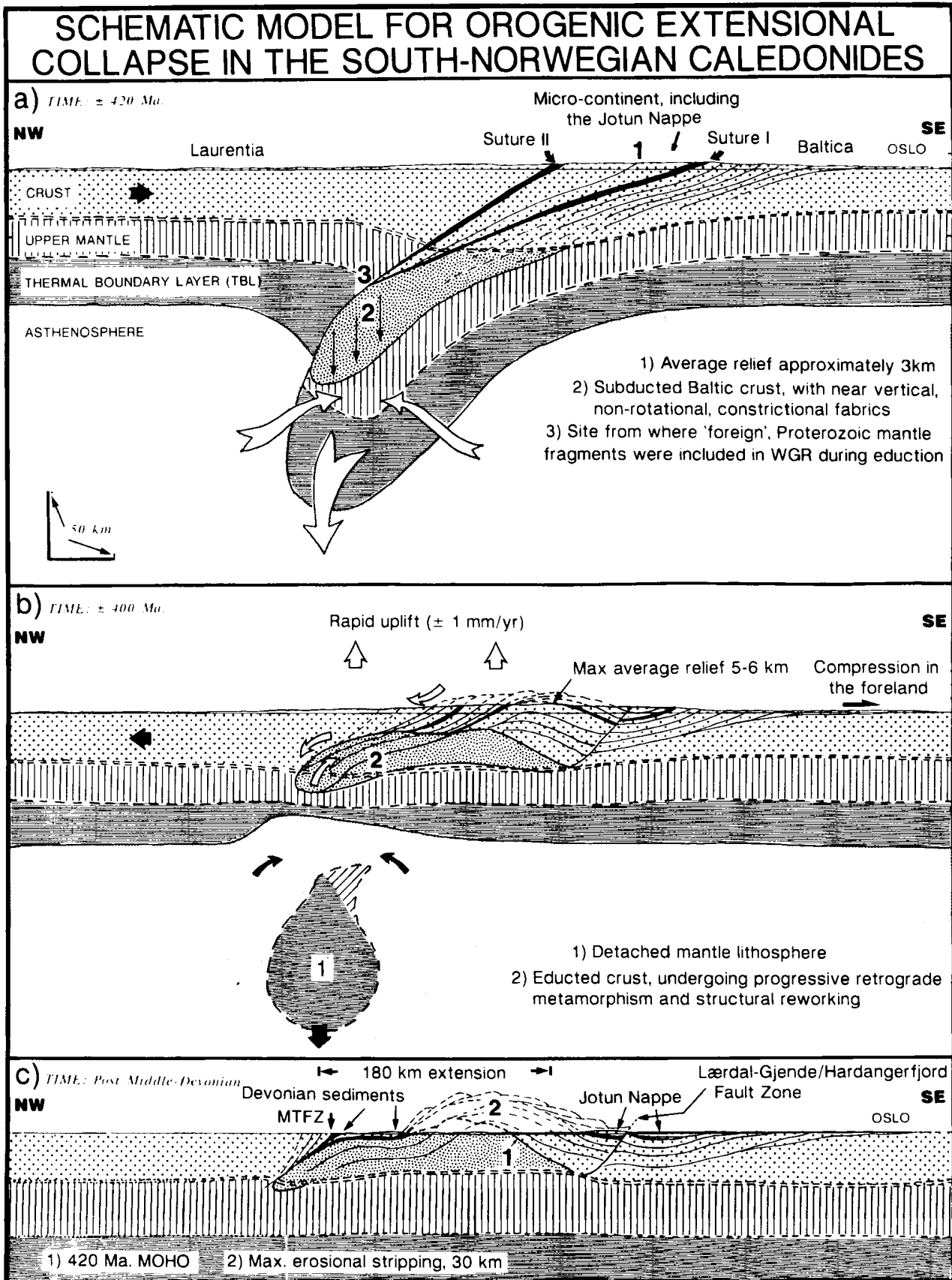


Fig. 2. A tectonic model for continent–continent collision and the subsequent orogenic extensional collapse in the South Norwegian Caledonides. See text for discussion.

## T.B. ANDERSON ET AL.

tional strain-regime in the subducted crust before decoupling of the lower lithosphere.

The collapse was initiated by decoupling of the TBL in the thickened lithosphere and resulted in a very rapid ( $\geq 1 \text{ mm yr}^{-1}$ ) isostatic rebound (Fig. 2b). The subducted crustal rocks were educted from their position in the mantle and the limited residence time (about 20 Myr) of the deeply subducted crust prevented major conductive heating of the rocks (England and Thompson, 1986). Only minor amounts of melt were produced during the decompression (Andersen and Jamtveit, 1990). The mantle peridotites from the overriding plate were structurally intercalated with the deeply subducted crust and educted together with the crustal rocks (Fig. 2a and b). The steep constrictional fabrics, developed at an early stage, underwent progressive rotation (clockwise in the W-E profiles) during the eduction. Non-coaxial fabrics developed in and adjacent to the large-scale extensional shear zones as the educted crust rose to middle and upper crustal levels (Andersen and Jamtveit, 1990).

The topographic relief of the mountain range at this stage may have reached average altitudes comparable with those in the Himalayan-Tibetan system, and internal body-forces in the uplifted welt resulted in vertical compression and spreading of the orogen (Anderson and Jamtveit, 1990). The post-Early Devonian shortening in the foreland (Oslo Region) is considered to be a result of the collapse. Back-folding and extensional reactivation of older thrust planes in central S. Norway was widespread (Andresen, 1982).

To exhume the deepest rocks exposed in the WGR, an extension in the order of 180 km in combination with a maximum erosion of approximately 30 km over the central parts of the WGR (Fig. 2c) is suggested. The extension ( $\approx 180 \text{ km}$ ) is estimated by combining the approximate metamorphic gradient across the S. Norwegian Caledonides and the WGR which is the basis for constructing Fig. 2a, with the crustal profile shown in Fig. 2c.

## CONCLUSIONS

Mineralogical evidence from exhumed deep crustal rocks show that contin-

ental crust may be subducted to depths greatly in excess of the typical Moho levels seen under modern collision zones. Although partial eclogitization of subducted crust, largely controlled by a free fluid phase (Austrheim, 1987, 1990), may give subducted crust petrophysical signatures similar to the upper mantle, a major part of the subducted material may retain metastable mineral assemblages in the mantle. Convergence across a continental collision zone may continue as long as the slab-pull exerted by heavy and cold subducted lithosphere is maintained. This may in part explain large-scale indentation tectonics as seen by the collision between India and Eurasia (1000 km) and in the western Alps. Partially eclogitized crustal lithologies may be depressed below mantle rocks in the overriding plate. Sub-vertical constrictional deformation at eclogite facies metamorphism characterizes the strain regime in the subducted lithosphere. Rapid ( $1\text{--}2 \text{ mm yr}^{-1}$ ) eduction of subducted crustal material is initiated by catastrophic decoupling of the heavy and cold lower lithosphere and its replacement by asthenosphere (England and Houseman, 1988). A short residence time at depth limits conductive heating of the subducted crust and prevents large-scale production of melts. The eduction occurs principally by a footwall rolling hinge mechanism. The early irrotational constrictional strain-pattern is overprinted by simple shear as the educted material approaches middle and upper crustal levels. Mantle inclusions may be structurally emplaced in the crustal material during both subduction and eduction, and the heavy mantle and eclogite lithologies are brought to the surface in a 'life-belt' of crustal material. The subduction-eduction model presented explains preservation of normal crustal thicknesses under exhumed deep crustal provinces without large-scale lateral flow of material or igneous underplating in the lower crust during the orogenic extensional collapse.

## ACKNOWLEDGEMENTS

The authors are grateful to Dr H. Austrheim for providing updated information on the eclogites in the Bergen area, and for his critical reading of

various preliminary drafts of this manuscript. Dr C. Hurich is thanked for useful discussions and for providing access to unpublished data on the deep structure of the S. Scandinavian Caledonides. Discussion and assistance with calculation of isostasy by E. Vågnes is gratefully acknowledged. Dr P. Ryan suggested a number of improvements to the manuscript. A review by Dr D. Roberts improved the manuscript. This work was supported by grants from the Norwegian Research Council of Science and the Humanities (NAVF).

## REFERENCES

- Andersen T.B. and Jamtveit B. (1990) Uplift of deep crust during orogenic extensional collapse: A model based on field studies in the Sogn-Sunnfjord region of Western Norway, *Tectonics*, **9**, 1097–1111.
- Andersen T.B., Skjerlie K.P. and Furnes H. (1990) The Sunnfjord Melange, evidence of Silurian ophiolite accretion in the West Norwegian Caledonides, *J. geol. Soc. London*, **146**, 59–68.
- Andresen A. (1982) *Stratigraphy and structural history of the Lower Paleozoic metasediments on Hardangervidda, South Norway*, PhD thesis, University of California, Davis, USA, 260 pp.
- Asmerom Y., Snow J.K., Holm D.K., Jacobsen S.B., Wernicke B.P. and Lux D.R. (1990) Rapid uplift and crustal growth in extensional environments: An isotopic study from the Death Valley region, California, *Geology*, **18**, 223–226.
- Austrheim H. (1987) Eclogitization of lower crustal granulites by fluid migration through shear zones, *Earth Planet. Sci. Lett.*, **81**, 221–232.
- Austrheim H. (1990) The granulite-eclogite facies transition; A comparison of experimental work and a natural occurrence in the Bergen Arcs, W. Norway, *Lithos*, **25**, 163–169.
- Austrheim H. and Griffin W.L. (1985) Shear deformation and eclogite formation within granulite-facies anorthosites of the Bergen arcs, Western Norway, *Chem. Geol.*, **50**, 267–281.
- Austrheim H. and Mørk M.B.E. (1988) The lower continental crust in continent-continent collision zones; evidence from former deep seated section in Western Norway, *Nor. geol. Unders. Spec. Publ.*, **3**, 102–113.

## CONTINENTAL CRUST

- Bjørlykke K. (1983) Subsidence and tectonics in late Precambrian and Paleozoic sedimentary basins of southern Norway, *Nor. geol. Unders. Bull.*, **380**, 159–172.
- Bott M.H.P. (1982) Origin of lithospheric tension causing basin formation, *Phil. Trans. R. Soc. A*, **305**, 319–324.
- Brueckner H.B. (1972) Interpretation of Rb–Sr ages from the Precambrian and Paleozoic rocks of southern Norway, *Am. J. Sci.*, **272**, 334–358.
- Bryhni I. (1989) Status of the supracrustal rocks in the Western Gneiss Region, S. Norway. In: *The Caledonide Geology of Scandinavia* (ed. by R.A. Gayer), pp. 221–228. Graham & Trotman Ltd, London.
- Buck W.R. (1988) Flexural rotation of normal faults, *Tectonics*, **7**, 959–973.
- Carswell D.A. (1990) Eclogites and eclogite facies: definition and classification. In: *Eclogite Facies Rocks* (ed. by D.A. Carswell), pp. 1–13. Blackie, Glasgow.
- Chopin C. (1984) Coesite and pure pyrope in high-grade blueschists of the Western Alps: A first record and some consequences, *Contrib. Miner. Petrol.*, **86**, 107–118.
- Chopin C. (1987) Very-high-pressure metamorphism in the western Alps: Implications for subduction of continental crust, *Phil. Trans. R. Soc. A*, **321**, 183–197.
- Cohen A.S., O’Nions R.K., Siegentaler R. and Griffin W.L. (1987) Chronology of the pressure-temperature history recorded by a granulite terrain, *Contrib. Miner. Petrol.*, **98**, 303–311.
- Cuthbert S.J., Harvey M.A. and Carswell D.A. (1983) A tectonic model for the metamorphic evolution of the Basal Gneiss Complex, Western South Norway, *J. Metamorph. Geol.*, **1**, 63–90.
- Dewey J.F. (1988) Extensional collapse of orogens, *Tectonics*, **7**, 1123–1139.
- Dewey J.F., Shackelton R.M., Chengfa C. and Yiuin S. (1988) The tectonic evolution of the Tibetan Plateau, *Phil. Trans. R. Soc. A*, **327**, 379–413.
- Enami M. and Zang Q. (1990) Quartz pseudomorphs after coesite in eclogites from Shandong province, east China, *Am. Miner.*, **75**, 381–386.
- England P.C. and Houseman G.A. (1988) The mechanics of the Tibetan Plateau, *Phil. Trans. R. Soc. A*, **326**, 301–320.
- England P.C. and Thompson A. (1986) Some thermal and tectonic models for crustal melting in continental collision zones. In: *Collision Tectonics* (ed. by M.P. Coward and A.C. Ries). *Spec. Pap. geol. Soc. London*, **19**, 83–94.
- Gebauer D., Lappin M.A., Grünenfelder M. and Wytenbach A. (1985) The age and origin of some Norwegian eclogites: A U–Pb zircon and REE study, *Chem. Geol.*, **52**, 227–247.
- Griffin W.L. (1987) ‘On the eclogites of Norway’—65 years later, *Min. Mag.*, **51**, 333–343.
- Griffin W.L., Austrheim H., Brastad K., Bryhni I., Krill A.G., Krogh E.J., Mørk M.B.E., Qvale H. and Tørudbakken B. (1985) High-pressure metamorphism in the Scandinavian Caledonides. In: *The Caledonide Orogen—Scandinavia and related areas* (ed. by D.G. Gee and B.A. Sturt), pp. 783–801. John Wiley & Sons, New York.
- Griffin W.L. and Brueckner H.K. (1980) Caledonian Sm–Nd ages and a crustal origin for Norwegian eclogites, *Nature*, **285**, 319–321.
- Griffin W.L. and Brueckner H.K. (1985) REE, Rb–Sr and Sm–Nd studies of Norwegian eclogites, *Chem. Geol.*, **52**, 249–271.
- Gronlie A. and Roberts D. (1989) Resurgent strike-slip duplex development along the Hitra–Snåsa and Verran Faults, Møre–Trøndelag Fault Zone, Central Norway, *J. Struct. Geol.*, **11**, 295–305.
- Hamilton W.B. (1988) Detachment faulting in the Death Valley region, California and Nevada, *Bull. geol. Soc. Am.*, **1790**, 51–85.
- Holt W.E. and Wallace T.C. (1990) Crustal thickness and upper mantle velocities in the Tibetan plateau region from the inversion of regional Pnl waveforms: Evidence for a thick upper mantle lid beneath southern Tibet, *J. geophys. Res.*, **95**, 12499–12525.
- Jamtveit B. (1987) Metamorphic evolution of the Eiksundal eclogite complex, Western Norway, and some tectonic implications, *Contrib. Miner. Petrol.*, **95**, 82–99.
- Jamtveit B., Bucher-Nurminen K. and Austrheim H. (1989) Fluid controlled eclogitization of granulites in deep crustal shear zones, Bergen arcs, Western Norway, *Contrib. Miner. Petrol.*, **104**, 184–193.
- Jamtveit B., Carswell D.A. and Mearns E.W. (1991) Chronology of Norwegian garnet periodities/pyroxenites, *J. Metamorph. Geol.*, **9**, 125–139.
- Krogh E.J. (1977) Evidence for a Precambrian continent-continent collision in western Norway, *Nature*, **267**, 17–19.
- Kullerud L., Tørudbakken B.O. and Illebekk S. (1986) A compilation of radiometric age determinations from Western Gneiss Region, South Norway, *Nor. geol. Unders. Bull.*, **406**, 17–42.
- Lux D.R. (1985) K/Ar ages from the Basal Gneiss Region, Stadlandet area, Western Norway, *Norsk geol. Tidsskr.*, **65**, 277–286.
- Mirwald P.W. and Massonne H.J. (1980) Quartz-coesite transition and the comparative friction measurements in piston-cylinder apparatus using talc–asimagic–glass (TAG) and NaCl high pressure cells, *Neues Jb. Min. Monatshefte*, **10**, 469–477.
- Molnar P. (1990) S-wave residuals from earthquakes in the Tibetan region and lateral variations in the upper mantle, *Earth Planet. Sci. Lett.*, **101**, 68–77.
- Mueller St. (1989) Deep-reaching geodynamic processes in the Alps. In: *Alpine Tectonics* (ed. by M.P. Coward, M.P.D. Dietrich and R.G. Park). *Spec. Publ. geol. Soc. London*, **45**, 303–328.
- Mørk M.B.E. (1985) A gabbro to eclogite transition of Flemsøy, Sunnmøre, SW-Norway, *Chem. Geol.*, **50**, 283–310.
- Mørk M.B.E. and Mearns E. (1986) Sm–Nd isotope systematics of a gabbro–eclogite transition, *Lithos*, **19**, 255–267.
- Newton R.C. (1986) Metamorphic temperatures and pressures of group B and C eclogites, *Mem. geol. Soc. Am.*, **164**, 17–30.
- Norton M.G. (1986) Late Caledonian extension in western Norway: A response to extreme crustal thickening, *Tectonics*, **5**, 195–204.
- Platt J.P. and Vissers R.L.M. (1989) Extensional collapse of thickened continental lithosphere: A working hypothesis for the Alboran Sea and Gibraltar arc, *Geology*, **17**, 540–543.
- Roecker S.W. (1982) Velocity structure of the Pamir–Hindu Kush region: Possible evidence of subducted crust, *J. geophys. Res.*, **87**, 945–959.
- Séranne M. and Séguert M. (1987) The Devonian basins of western Norway: tectonics and kinematics of an extending crust. In: *Continental Extensional Tectonics* (ed. by M.P. Coward, J.F. Dewey and P.L. Hancock). *Spec. Publ. geol. Soc. London*, **28**, 537–548.
- Smith D.C. (1984) Coesite in clinopyr-

**T.B. ANDERSON ET AL.**

- oxene in the Caledonides and its implications for geodynamics, *Nature*, **310**, 641–644.
- Smith D.C. (1988) A review of the peculiar mineralogy of the Norwegian coesite-eclogite province, with crystal-chemical, petrological, geochemical and geodynamical notes and an extensive bibliography. In: *Eclogites and Eclogite-facies Rocks* (ed. by D.C. Smith), pp. 1–206. Developments in Petrology 12, Elsevier, Amsterdam.
- Smith D.C. and Lappin M.A. (1989) Coesite in the Straumen kyanite-eclogite pod, Norway, *Terra Nova*, **1**, 47–56.
- Snyder D.B. and Flack C.A. (1990) A Caledonian age for reflectors within the mantle lithosphere north and west of Scotland, *Tectonics*, **9**, 903–922.
- Swensson E. and Andersen T.B. (1991) Contact relationships between the Askvoll Group and the basement gneisses of the Western Gneiss Region (WGR), Sunnfjord, W. Norway, *Norsk geol. Tidssk.*, **71**, in press.
- Tucker R.D., Råheim A., Krogh T.E. and Corfu F. (1987) Uranium-lead zircon and titanite ages from the northern portion of the Western Gneiss Region, south-central Norway, *Earth Planet. Sci. Lett.*, **81**, 203–211.

*Manuscript received 23 January 1991; revision accepted 11 April 1991*

# Stress release in exhumed intermediate and deep earthquakes determined from ultramafic pseudotachylyte

Torgeir B. Andersen, Karen Mair, Håkon Austrheim, Yuri Y. Podladchikov, Johannes C. Vrijmoed  
University of Oslo, Physics of Geological Processes, P.O. Box 1048, Blindern, 0316 Oslo, Norway

## ABSTRACT

Stresses released by coseismic faults during subduction toward lawsonite-eclogite facies conditions in the Alpine subduction complex of Corsica can be estimated based on the energy required to form pseudotachylyte fault veins where shear strain can be measured. Congruent peridotite melting at ambient conditions of 1.5 GPa and 470 °C requires a temperature increase of 1280 °C to 1750 °C. We assume that more than 95% of the work is converted to heat during faulting, hence that the stress drop is nearly proportional to the amount of melting and inversely proportional to shear strain. Minimum estimates of released stress are typically greater than 220 MPa and as high as 580 MPa. The abundance of pseudotachylyte on small faults in the studied peridotite suggests that melting is very common on intermediate and deep earthquakes and that shear heating is important for seismic faulting at depth.

## INTRODUCTION

The main strength of the lithosphere is carried by upper mantle peridotite and possibly also by dry granulites in the lowermost continental crust (e.g., Jackson et al., 2004). Rock-mechanical experiments and numerical models based on results from such experiments, extrapolated to subduction zone conditions, suggest that old ( $10^8$  yr) and cold ( $500 \pm 50$  °C) upper mantle rocks with olivine rheology are strong ( $>1.5$  GPa) at geological strain rates ( $10^{-14}$  s $^{-1}$ ). Strength is also grain-size-dependent, and coarse-grained peridotite, as studied here, is particularly strong (e.g., Kelemen and Hirth, 2007; Stüwe, 2007). Byerlee's (1978) friction data also indicate that faults are strong ( $\sim 10^2$  to  $10^3$  MPa at confining pressures discussed here). The strong versus weak fault disparity may be a result of most earthquakes being associated with variably efficient weakening processes (Rice, 2006), such as high pore fluid pressure and/or prefractured, noncohesive, or extremely fine-grained rocks, implying reactivation (e.g., Faulkner et al., 2006). The shortcomings of using seismics and field studies to quantify heating may also be important (e.g., d'Alessio et al., 2003; Scholz, 2006).

The study of pseudotachylyte (PST) where temperature change ( $\Delta T$ ) and shear strain ( $\gamma$ ) can be determined provides an independent avenue to explore the strength of exhumed deep-seated rocks. This method has been used previously for faults at middle and high crustal level (e.g., Di Toro et al., 2005; Sibson, 1977; Wenk et al., 2000). Here, we apply this technique to determine minimum stresses released by coseismic faulting near the crust-mantle boundary in an ophiolite subjected to high-pressure and low-temperature metamorphism in a paleo-subduction environment. Shear-induced melting down to the base of the seismogenic zone ( $\sim 15$  km) is to be expected (e.g., Sibson, 1977). In the subduction environment, both the order(s) of magnitude of stresses and the mechanism of deep earthquakes are the subject of debate mostly based on seismological constraints or numerical models. We present stress estimates from recently discovered PST occurrences within the Alpine blueschist to eclogite facies complex in Corsica (Andersen and Austrheim, 2006; Austrheim and Andersen, 2004). This complex is considered a type example of fossil subduction (e.g., Jolivet et al., 2003). Our stress estimate is based on the energy balance combined with direct field and microstructural observations, and is independent of much-debated mechanisms of strain localization (e.g., Braeck and Podladchikov, 2007; Green and Houston, 1995; Kelemen and Hirth, 2007).

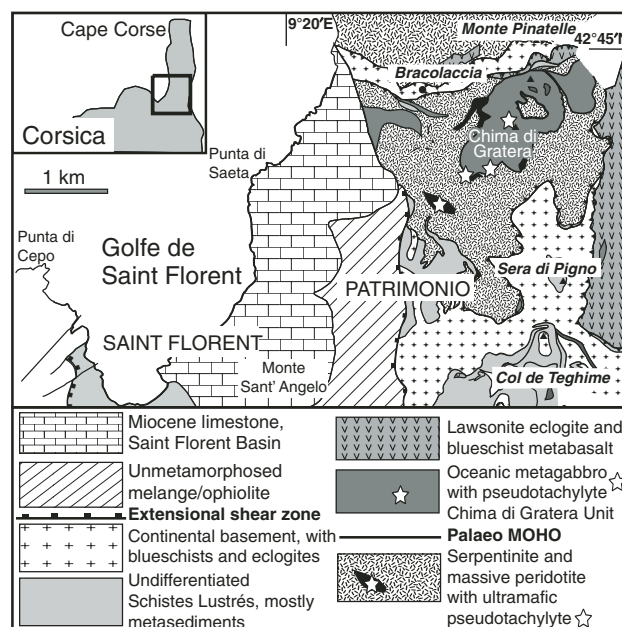


Figure 1. Simplified map of the Chima di Gratera area, Cape Corse, showing main geological units and the locations (stars) of ultramafic and mafic pseudotachylytes (in gabbro). The paleo-Moho is shown as a thick solid line.

## FAULTING IN THE MANTLE PERIDOTITE

The  $P$ - $T$  conditions of subduction-related faulting in Cape Corse (Fig. 1) are given by the regional metamorphism (e.g., Lahondère [1988] and unpublished lawsonite eclogite data giving pressures of 2.4 GPa at 470 °C [E.K. Ravna, 2008, personal commun.]). The eclogites were exhumed at blueschist and greenschist facies conditions (e.g., Fournier et al., 1991). The PSTs are variably pristine to completely overprinted by deformation and metamorphism associated with the exhumation (Andersen and Austrheim, 2006). Faulting took place at earlier stages of subduction, but it is difficult to precisely constrain at which stage in the

prograde loop toward maximum  $P$ - $T$  conditions individual faults were active. We use 470 °C and 1.5 GPa as the  $P$ - $T$  conditions during faulting. Crosscutting PST veins are common in some of the larger fault zones (see Andersen and Austrheim, 2006) and show that faulting occurred repeatedly in this zone as predicted by the Kelemen and Hirth (2007) model. The faults analyzed in the present study, however, formed by single displacement events.

Omphacite, fassaitic (high- $\text{Al}_2\text{O}_3$ ) pyroxene, and glaucophane are present in quenched mafic PST (Austrheim and Andersen, 2004), whereas ultramafic PST has zoned olivine (Fig. 2D), high- $T$  pyroxenes, spinel, and in some cases preserved glassy or hydrated glassy material (Andersen and Austrheim, 2006). Exhumation-related fabrics mostly obliterate evidence for the subduction paleoearthquakes, but quench textures in PST (Fig. 2) are well preserved within peridotite least affected by serpentinization.

The PST occurs near the contact previously interpreted as paleo-Moho within a Ligurian ophiolite of the “Schistes Lustés” nappe complex at Chima di Gratera (Fig. 1). The Jurassic Ligurian ophiolites (155–160 Ma) were cold and strong during the early Alpine subduction event (e.g., Jolivet et al., 2003). Because the well-preserved peridotite lenses (max 0.2 km<sup>2</sup>) are mostly without markers, it is difficult to determine fault displacements. It is therefore difficult to ascertain how vast amounts of energy required for melting large volumes of peridotite along 1–15-cm-thick major fault veins (~30–450 kg m<sup>-2</sup>) partitioned between stress and displacement. To quantify stresses in the fault energy budget we have instead studied a number of small faults (Fig. 2) where apparent displacement  $d_a$  (2–990 mm, no piercing points) and melt thickness  $h$  can be determined (Fig. 3). Melt thickness, taken to represent the width across which the displacement occurred, is measured in the microscope to be from 0.15 to 12.9 mm. Outcrop conditions make

sampling difficult, therefore only 14 of 51 faults were sampled successfully (mostly drill cores). Optical and electron backscatter microscopy and probe analyses document near-complete congruous melting, common injection veins, and quench textures in 5%–25% of the damage zone of the faults measured in the field (Figs. 2C and 2D). Based on the microtextures of the 14 studied fault rocks, we assume that an average of 10% of the field-measured fault rock thicknesses of the 37 faults not studied microscopically are constituted by melted peridotite. Hence, we use  $h$  measured directly from thin sections, or alternatively, 10% of the thicknesses measured in the field as  $h$  in stress calculations.

### STRESS ESTIMATES

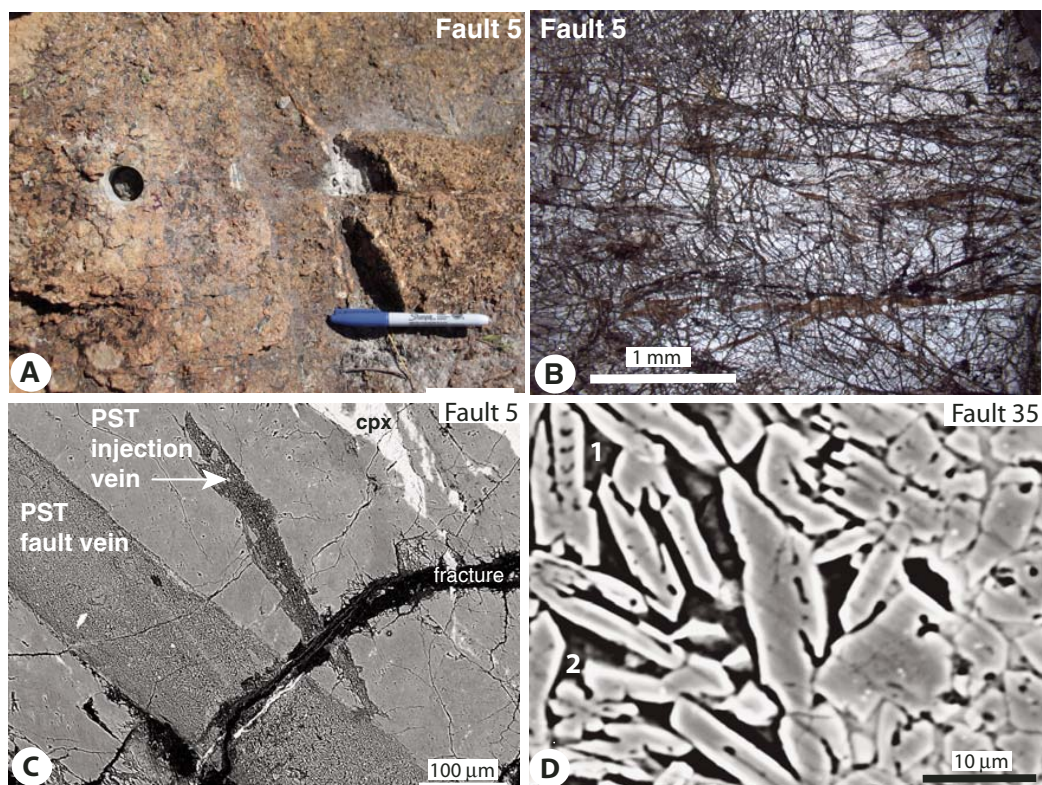
In calculating the stress release by a fault breaking unfractured rock, we assume (Scholz, 2004) that the work ( $W$ ) is partitioned into thermal energy ( $Q$ ), seismic energy ( $S$ ), and surface energy ( $U$ ). Laboratory studies (Lockner and Okubo, 1983) and seismological studies (McGarr, 1999) suggest that both  $S$  and  $U$  are very small (<5%) in unfractured rock compared to the total energy in an earthquake; hence, we consider work per unit area,  $W \approx Q$ , which can be written

$$W = d\sigma; \text{ rearranged as } \sigma = W/d, \quad (1)$$

where  $d$  is true displacement and  $\sigma$  is the shear stress at the time of deformation. Lacking piercing points, the field-measured  $d_a$  given by offset markers is the best estimate of true displacement. Not considering potential superheating, the thermal energy required to heat and melt a unit mass is

$$Q = C_p \Delta T + H, \quad (2)$$

**Figure 2.** A: Small fault (fault 5 in Fig. 3A) offsetting an ~5-cm-thick gabbro vein by 40 mm. Notice that the drill core sample is taken entirely within the peridotite. B: Micrograph (plane-polarized) of fault 5 drill core (Fig. 2A) showing micro fault strands, fractured peridotite, and numerous injection veins in the damage zone of the fault. The pseudotachylyte thickness  $h$  is 0.3 mm. C: Electron backscatter image of fault strand and injection vein from fault 5. Notice near-complete melting and well-preserved quench texture of the pseudotachylyte (PST), which truncates the coarse-grained but fractured peridotite. Ol—olivine; Cpx—clinopyroxene. Pseudotachylyte is truncated by fractures associated with serpentinization. D: Backscatter image of “spinfex-like” olivine crystals from fault vein 35 (Fig. 3A). Notice the compositional zoning ( $\text{Fo}_{93-99}$ ) with forsterite-rich cores and the skeleton and dendritic crystals (near points marked 1 and 2, respectively). The glassy matrix is partly hydrated (dark) and partly nonhydrated (lighter-colored along right-hand side of the image) where it has a cpx-like, but nonstoichiometric, composition.



where  $C_p$  is specific heat,  $\Delta T$  is the temperature difference between ambient and melting temperature, and  $H$  is the latent heat of fusion. Because nearly all the energy is preserved as heating and melting, Equation 1 can be written

$$\sigma = \rho(C_p \Delta T + H) \gamma^{-1}, \quad (3)$$

where  $\rho$  is density and  $\gamma$  is shear strain. In our case,  $\gamma = d_a/h$ , recorded by field and/or microstructural analysis. Estimates of  $Q$  for a given  $\gamma$  therefore give quantitative information regarding the dynamic conditions that existed during earthquake rupture. A more precise definition of the shear stress estimate from Equation 3 is the *strain-averaged stress*. The energy balance across the shear zone integrated over time of deformation yields

$$C_p \int_{-h/2}^{h/2} \Delta T dx + hH = \int_{-h/2}^{h/2} \left( \int_0^{t_d} \sigma(t) \frac{\partial}{\partial t} \left( \frac{\partial u}{\partial x} \right) dt \right) dx = \int_0^d \sigma(u) du, \quad (4)$$

where  $t$  is time,  $x$  is the spatial coordinate across the shear zone,  $t_d$  is the time to achieve maximum displacement  $d$ , and  $u$  is the shear zone displacement field. Rearranging this equation we obtain the definition of the strain-averaged stress:

$$\sigma = \frac{1}{d} \int_0^d \sigma(u) du = \frac{h}{d} \left( C_p \frac{\int_{-h/2}^{h/2} \Delta T dx}{h} + H \right). \quad (5)$$

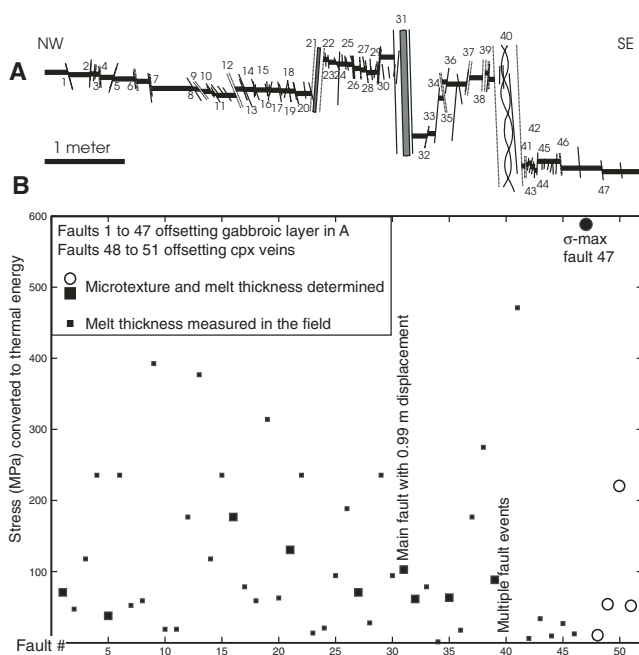


**Figure 3. A:** Field record of 47 faults offsetting a 5 cm gabbroic vein (see also Fig. 2A) cutting spinel peridotite. The main single-event fault is 31 with  $d_a = 0.99$  m. Fault 40 records multiple events. Fault 47 gives the maximum strain-averaged stress of  $\sim 580$  MPa. All samples studied by microtexture analyses were collected within the peridotite. **B:** Diagram showing strain-averaged stress from all measured faults (see text). Large circles and squares denote faults with microtexture information, i.e., melt volumes were measured in thin sections; small symbols denote faults where melt volumes are estimated as described in the text. Faults 1–47 (solid symbols) are shown in Figure 3A; faults 48–51 (open symbols) are small faults offsetting thin pyroxene veins.

Stresses obtained from Equation 3 are presented in Figure 3B. We assume that displacement took place across the melted zone  $h$ , which gives an overestimate of  $\gamma$  and an underestimate of  $\sigma$ . We have not corrected for injection (Figs. 2B and 2C), commonly assumed to be 50% or more in large fault veins (e.g., Di Toro et al., 2005; Wenk et al., 2000), since we have no good control on the scaling relations between the melt loss on the very small faults used here and more commonly studied larger faults. The field-measured  $d_a$  is always a minimum estimate due to lack of piercing points. Approximations of  $h$  and  $d_a$  therefore both have the effect of reducing estimates of  $\sigma$ . Improvement to these estimates relies on better determination of the melt volumes in a larger number of faults and wall rocks.

## RESULTS AND DISCUSSION

Commonly accepted mechanisms for subduction earthquakes are embrittlement by devolatilization of minerals at progressive metamorphism during subduction (recent overview, Hacker et al., 2003; and case study, Rietbrock and Waldhauser, 2004). Shear heating may also lead to extreme localization of deformation at seismic strain rates in viscoelastic materials (e.g., Braeck and Podladchikov, 2007; T. John, 2007, personal commun.; Kelemen and Hirth, 2007). These models demonstrate that extreme temperatures similar to those suggested by Kanamori et al. (1998) may be viable for high- $P$  faults in subduction and collision zones. Here we interpret  $\sigma$  as the strain-averaged stress associated with a single rupture event (Equation 5). We make no assumptions about the manner in which the stress drops during slip, but infer that both higher and lower stresses were available during the rupture process. We suggest that the rocks that hosted these events must have experienced stresses that were at least as high as the characteristic stress estimates from these small-scale faults, and most likely considerably higher. Stress estimates from large faults in the area cannot be carried out with this method because displacements are indeterminable (Andersen and Austrheim, 2006).

The temperature rise required for near-complete melting of mostly dry spinel peridotite at 1.5 GPa and 470 °C is  $\Delta T \approx 1280$  °C (Katz et al., 2003). Because it is difficult to accurately determine pressures for individual events, we used 1.5 GPa, intermediate between 1 and 2.4 GPa in agreement with commonly referenced metamorphic conditions in the area (see summary by Jolivet et al., 2003). In Equation 3 we use  $\Delta T = 1280$  °C,  $C_p = 1150$  J kg<sup>-1</sup> °C<sup>-1</sup>,  $H = 8.6 \times 10^5$  J kg<sup>-1</sup>, and  $\rho = 3200$  kg m<sup>-3</sup>. The highest  $\sigma$  calculated from a fault where  $h$  is determined directly by microscopy is 220 MPa (fault 50), whereas the maximum  $\sigma$  is 580 MPa (fault 47) where  $h$  was estimated without microstructural inspection (Fig. 3B). The reactivated fault 40 is not used. The main fault 31 ( $d_a = 0.99$  m) gives  $\sigma \approx 110$  MPa. We suggest this is underestimated, as the fault rock thickness varies considerably in the field. The fault 31 sample was from a 43-mm-thick fault rock with only  $h = 2.9$  mm measured in thin section. Field measurement of  $h$  varies from 35 to 57 mm along the studied 1.42 m segment of fault 31. The uncertainty in  $\gamma$  (based on  $h$ ) is therefore close to a factor of 3, and the stress may be underestimated accordingly.

The conservative melt estimates, notwithstanding the problems of quantifying loss to injection veins, grain boundaries, and dilation bends, give a clear indication that the stresses released to thermal energy in most of the faults observed were commonly higher than 200 MPa, and higher than 580 MPa on fault 47 (Fig. 3B). It is interesting to observe that this is very similar to the estimates of 300–600, MPa by Obata and Karato (1995) based on dislocation density and grain size from olivine in PST from the Balmuccia peridotite. Kelemen and Hirth (2007) modeled coseismic failure at high stress ( $10^2$  to  $10^3$  MPa) in subducting mantle peridotite and demonstrated that repeated seismic events could be related to shear heating and grain-size-sensitive creep laws. The modeling also indicates stress fluctuations, and it may be that our stress variations, approaching an order of magnitude, may be an effect of grain size (smaller grain size lowers

strength and volume of melting). Melting along faults, however, may destroy evidence for preexisting grain size variation and render precise observational interpretation uncertain.

Byerlee's (1978) classic study suggested that frictional faulting is independent of composition. With shear heating as a possible failure mechanism, however, rheology and grain size also become important elements (Braeck and Podladchikov, 2007; John et al., 2007; Kelemen and Hirth, 2007). The absence of a fault-zone weakening mechanism such as pressurization of pore fluids (Rice, 2006; Sibson, 1977) has commonly been taken as a prerequisite for generation of PST and used to explain their relative scarcity compared to other exposed fault rocks (Sibson and Troy, 2006). Coseismic faulting occurs because faults weaken with increasing slip, observed in our data and by Di Toro et al. (2005). In cases where PST is produced, shear heating may in fact be the dominant weakening mechanism, since melting both lubricates and dries wall rocks, particularly at elevated pressures (e.g., Di Toro et al., 2004; Mysen and Wheeler, 2000). Subduction earthquakes are obvious candidates for high-stress failure. Fault rocks produced from subduction are, however, very rarely exposed, because they generally are lost by subduction, destroyed during exhumation, or not recognized in the field. These unique Corsican occurrences are therefore generally important for understanding failure mechanisms and for estimating the strength of rocks in subduction complexes. We document that peridotite can sustain stresses of several hundred MPa over geologic time, and that even very small faults at such high stress generate melt in refractory mantle. It is suggested that most intermediate and deeper earthquakes produce PST and that the apparent relative scarcity of PST is simply a function of the global sampling depth.

#### ACKNOWLEDGMENTS

We thank Q. Gautier and University of Oslo Physics of Geological Processes (PGP) colleagues for discussions and support in the field, and M. Erambert for help with the microprobe. Reviews by Peter Kelemen, Kurt Stüwe, and Chris Scholz improved the manuscript. A Centre of Excellence grant from the Norwegian Research Council to the PGP department financed the study.

#### REFERENCES CITED

- Andersen, T.B., and Austrheim, H., 2006, Fossil earthquakes recorded by pseudotachylytes in mantle peridotite from the Alpine subduction complex of Corsica: *Earth and Planetary Science Letters*, v. 242, p. 58–72, doi: 10.1016/j.epsl.2005.11.058.
- Austrheim, H., and Andersen, T.B., 2004, Pseudotachylytes from Corsica: Fossil earthquakes from a subduction complex: *Terra Nova*, v. 16, p. 193–197, doi: 10.1111/j.1365-3121.2004.00551.x.
- Braeck, S., and Podladchikov, Y.Y., 2007, Spontaneous thermal runaway as an ultimate failure mechanism of materials: *Physical Review Letters*, v. 98, 095504, doi: 10.1103/PhysRevLett.98.095504.
- Byerlee, J.D., 1978, Friction of rocks: *Pure and Applied Geophysics*, v. 116, p. 615–629, doi: 10.1007/BF00876528.
- d'Alessio, M.A., Blythe, A.E., and Bürgmann, R., 2003, No frictional heat along the San Gabriel fault, California: Evidence from fission-track thermochronology: *Geology*, v. 31, p. 541–544, doi: 10.1130/0091-7613(2003)031<0541:NFHATS>2.0.CO;2.
- Di Toro, G., Goldsby, D.L., and Tullis, T.E., 2004, Friction falls towards zero in quartz rock as slip velocity approaches seismic rates: *Nature*, v. 427, p. 436–439, doi: 10.1038/nature02249.
- Di Toro, G., Pennacchioni, G., and Teza, G., 2005, Can pseudotachylytes be used to infer earthquake source parameters? An example of limitations on the study of exhumed faults: *Tectonophysics*, v. 402, p. 3–20, doi: 10.1016/j.tecto.2004.10.014.
- Faulkner, D.R., Mitchell, T.M., Healy, D., and Heap, M.J., 2006, Slip on “weak” faults by the rotation of regional stress in the fracture damage zone: *Nature*, v. 444, p. 922–925, doi: 10.1038/nature05353.
- Fournier, M., Jolivet, L., Goffé, B., and Dubois, R., 1991, Alpine Corsica metamorphic core complex: *Tectonics*, v. 10, p. 1173–1186, doi: 10.1029/91TC00894.
- Green, H.W., and Houston, H., 1995, The mechanics of deep earthquakes: *Annual Review of Earth and Planetary Sciences*, v. 23, p. 169–213, doi: 10.1146/annurev.ea.23.050195.001125.
- Hacker, B.R., Peacock, S.M., Abers, G.A., and Holloway, S.D., 2003, Subduction factory. 2: Are intermediate-depth earthquakes in subducting slabs linked to metamorphic dehydration reactions? *Journal of Geophysical Research*, v. 108, 2030, doi: 10.1029/2001JB001129.
- Jackson, J.A., Austrheim, H., McKenzie, D., and Priestley, K., 2004, Metastability, mechanical strength, and the support of mountain belts: *Geology*, v. 32, p. 625–628, doi: 10.1130/G20397.1.
- John, T., Rüpkke, L.H., Medvedev, S., Podladchikov, Y.Y., and Andersen, T.B., 2007, Spontaneous thermal run-away as an earthquake mechanism at elevated pressure: Insights from petrology and numerical analysis [abs]: *Eos (Transactions, American Geophysical Union)*, Fall Meeting, Abstract D151A-0282.
- Jolivet, L., Faccenna, C., Goffé, B., Burov, E., and Agard, P., 2003, Subduction tectonics and exhumation of high-pressure metamorphic rocks in the Mediterranean orogens: *American Journal of Science*, v. 303, p. 353–409, doi: 10.2475/ajs.303.5.353.
- Kanamori, H., Anderson, D.L., and Heaton, T.H., 1998, Frictional melting during the rupture of the 1994 Bolivian earthquake: *Science*, v. 279, p. 839–842, doi: 10.1126/science.279.5352.839.
- Katz, R.F., Spiegelman, M., and Langmuir, C.H., 2003, A new parameterization of hydrous mantle melting: *Geochemistry, Geophysics, Geosystems*, v. 4, 1073, doi: 10.1029/2002GC000433.
- Kelemen, P.B., and Hirth, G., 2007, A periodic shear-heating mechanism for intermediate-depth earthquakes in the mantle: *Nature*, v. 446, p. 787–790, doi: 10.1038/nature05717.
- Lahondère, D., 1988, Eclogitic metamorphism in Farinole orthogneisses and ophiolitic metabasites (northern Corsica, France): *Bulletin de la Société Géologique de France*, v. 4, p. 579–585.
- Lockner, D.A., and Okubo, P.G., 1983, Measurements of frictional heating in granite: *Journal of Geophysical Research*, v. 88, p. 4313–4320, doi: 10.1029/JB088iB05p04313.
- McGarr, A., 1999, On relating apparent stress to the stress causing earthquake fault slip: *Journal of Geophysical Research*, v. 104, p. 3003–3012, doi: 10.1029/1998JB900083.
- Mysen, B.O., and Wheeler, K., 2000, Solubility behaviour of water in haplo-andesitic melts at high pressure and high temperature: *American Mineralogist*, v. 85, p. 1128–1142.
- Obata, M., and Karato, S.I., 1995, Ultramafic pseudotachylyte from the Balmuccia peridotite, Ivrea-Verbano zone, northern Italy: *Tectonophysics*, v. 242, p. 313–328, doi: 10.1016/0040-1951(94)00228-2.
- Rice, J.R., 2006, Heating and weakening of faults during earthquake slip: *Journal of Geophysical Research*, v. 111, B05311, doi: 10.1029/2005JB004006.
- Rietbrock, A., and Waldhauser, F., 2004, A narrowly spaced double-seismic zone in the subducting Nazca plate: *Geophysical Research Letters*, v. 31, no. 10, L10608.
- Scholz, C.H., 2004, *The mechanics of earthquakes and faulting* (2nd edition): Cambridge, UK, Cambridge University Press, 471 p.
- Scholz, C.H., 2006, The strength of the San Andreas fault: A critical analysis: *American Geophysical Union Geophysical Monograph* 170, p. 301–311.
- Sibson, R.H., 1977, Fault rocks and fault mechanisms: *The Geological Society of London Journal*, v. 133, p. 191–214, doi: 10.1144/gsjgs.133.3.0191.
- Sibson, R.H., and Troy, V.G., 2006, The habitat of fault-generated pseudotachylyte: Presence vs. absence of friction-melts: *American Geophysical Union Geophysical Monograph* 170, p. 153–166.
- Stüwe, K., 2007, *Dynamics of the lithosphere*: Berlin, Heidelberg, New York, Springer Verlag, 449 p.
- Wenk, H.R., Johnson, L.R., and Ratschbacher, L., 2000, Pseudotachylytes in the Eastern Peninsular Ranges of California: *Tectonophysics*, v. 321, p. 253–277, doi: 10.1016/S0040-1951(00)00064-0.

Manuscript received 5 June 2008

Revised manuscript received 1 September 2008

Manuscript accepted 3 September 2008

Printed in USA

# Pseudotachylytes from Corsica: fossil earthquakes from a subduction complex

Håkon Austrheim and Torgeir B. Andersen

Department of Geosciences – PGP, University of Oslo, PO Box 1047 Blindern, 0316 Oslo, Norway

## ABSTRACT

Subduction zones are the most seismically active tectonic environment on Earth. Here we report fault-rock evidence of palaeoearthquakes from a subduction complex. Pseudotachylyte veins formed by shear heating on faults at seismic strain rates contain dendrites, spherulites and acicular minerals characteristic of blueschist facies conditions. The veins have

been found in both mantle peridotite and gabbro. Our discovery from Corsica opens a new avenue of research towards understanding mechanisms related to subduction zone earthquakes and the conditions at which these are released.

Terra Nova, 16, 193–197, 2004

## Introduction

Tectonic processes along convergent plate margins, particularly in subduction zones, generate most of the global energy radiated by earthquakes. Although the mechanism behind interplate earthquakes is generally related to stick-slip during underthrusting on shallowly dipping fault planes, there are a number of phenomena regarding intra- and interplate earthquakes that await explanation. A major unresolved question concerns the interaction of earthquakes with fluids and metamorphic processes (Hacker *et al.*, 2003; Lund and Austrheim, 2003). Subduction zones are typified by low geothermal gradients, where high differential stresses may result in fracturing rather than creep. Although most models view the properties of subducted crust as a function of temperature, it is increasingly recognized that the rheological properties of rocks depend on their metamorphic status and importantly on the fluid content. Release of fluids from dehydration reactions in subduction complexes will reduce the effective stress and allow brittle failure (Hacker *et al.*, 2003), but fluids may also reduce the likelihood for frictional melting in shear zones (Sibson, 1975). Blueschist terrains are characterized by low-temperature and high-pressure (LT–HP) metamorphism and are often regarded

as having formed in the upper 15–50 km of subduction zones. Such rock complexes are potential sources for direct observational information regarding the physical properties of subducted rocks.

## Geological setting

The Alpine HP–LT complex of Corsica (Fig. 1) contains carpholite schists, blueschist and eclogite facies rocks formed by late Cretaceous (?) – early Tertiary subduction, involving thrust stacking and accretion of European continental crust and Ligurian oceanic units on to the margin of Europe (cf. Figure 4 in Jolivet *et al.*, 2003). The HP–LT rocks include a dismembered ophiolite dominated by variably metamorphosed ultramafics, gabbros, pillow lavas and metasedimentary schists (the Schistes Lustrés units), as well as allochthonous blueschist (Sera di Pigno Unit) and eclogite facies (Monte Pinatelle – Farinole Unit) rocks developed from the Hercynian basement (Warburton, 1986; Fournier *et al.*, 1991). The eclogites of the Cap Corse Region record peak Alpine metamorphic conditions of  $P \approx 15\text{--}20$  kbar and  $T \approx 550 \pm 50$  °C. They were exhumed on a cold geotherm through the blueschist facies at  $P \approx 7\text{--}9$  kbar and  $T \approx 450\text{--}500$  °C and eventually to greenschist facies (Fournier *et al.*, 1991; Lahondre, 1988). Other units without eclogites reached  $P_{\max}$  at lawsonite-blueschist facies ( $P \approx 13\text{--}15$  kbar at  $T \approx 350\text{--}400$  °C) and decompressed on a cold geotherm through blueschist ( $P \approx 10$  kbar,  $T \approx 350$  °C) to greenschist facies conditions (Fournier *et al.*, 1991).

## The fault rocks

Pseudotachylyte veins occur in gabbros and mantle peridotites exposed around the peak of Cima di Gratera (Fig. 1). The Cima di Gratera gabbro is a cumulate-layered to varied-textured gabbro. The gabbro is partly transformed to blueschist facies, except in shear zones (Fournier *et al.*, 1991) where the transformation has run to completion. Our field observations suggest that parts of the gabbros that were incorporated into the subduction complex remained undeformed and partly unreacted during both subduction and the subsequent exhumation, and that the pseudotachylytes are located in the least reacted parts. The pseudotachylytes can also be studied in boulders on the beach at Sole du Marine (Fig. 1) and along the river Fium Albino, draining the Cima di Gratera area (dotted line in Fig. 1). A large number of gabbro and some peridotite boulders with partly preserved primary structures, textures and mineralogy display fine-grained, brittle-deformation zones and pseudotachylyte zones (Figs 2 and 3).

The pseudotachylytes are dark, grey, occasionally greenish to bluish, aphanitic veins, < 3 cm thick. They are clearly related to faults and form single discrete veins, injection-vein complexes and ladder-network breccias (Fig. 2a,b). Several examples of cross-cutting veins of different generations (Fig. 2a) indicate a polyphase slip history on the faults. Locally, small pull-apart mesoscopic structures have been opened and filled with pseudotachylyte (Fig. 2a). Some samples preserve evidence of interaction between brittle and ductile deforma-

Correspondence: Håkon Austrheim, Department of Geology – PGP, University of Oslo, PO Box 1047 Blindern, 0316 Oslo, Norway. Tel.: +47 22854316; e-mail: hakon.austrheim@geo.uio.no

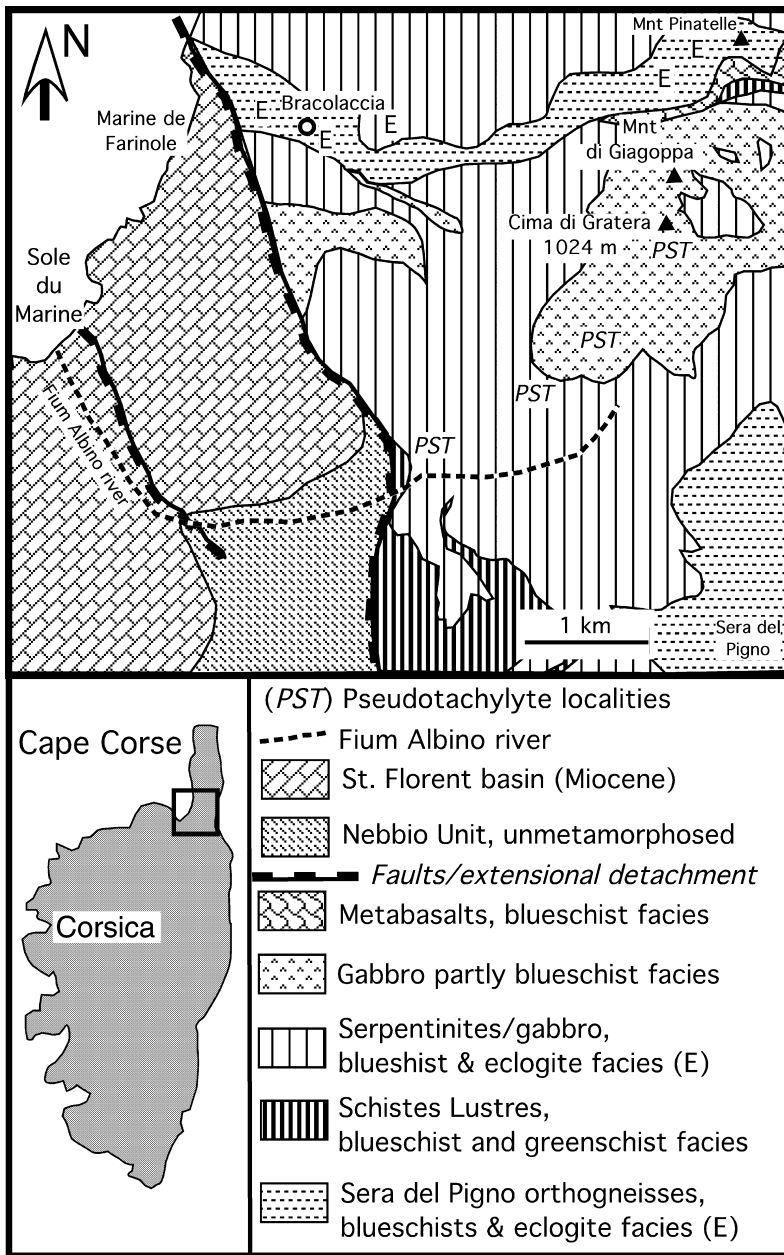


Fig. 1 Simplified geological map of the St. Florent area with an inset map of Corsica. Modified from Fournier *et al.* (1991).

tion as shear strain gradients locally can be observed along fault-vein margins, and some veins are partly overprinted by ductile fabrics (Fig. 2b). A colour banding defined by variable size and/or content of porphyroclasts and commonly convoluted by folds is present in many veins. Textural and mineralogical characteristics of the veins and their wall-rocks are given in Table 1. The gabbro-hosted veins locally display intricate dendrites

(Figs 2c and 3b,c) of fassaitic pyroxene (Table 2). Veins 0.2–1 cm across have a central part with 10 µm euhedral pyroxene crystals, some of which have cores of diopside (Fig. 3c). The vein margins are characterized by dendrites and spherulites (Fig. 3c,d). The dendrites branch outward from orthopyroxene clasts that are partly replaced by talc (Fig. 3d). The hydration of orthopyroxene to talc cannot have occurred after the growth of the

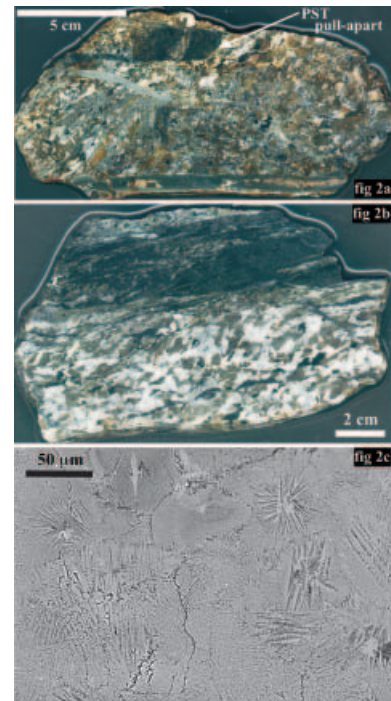
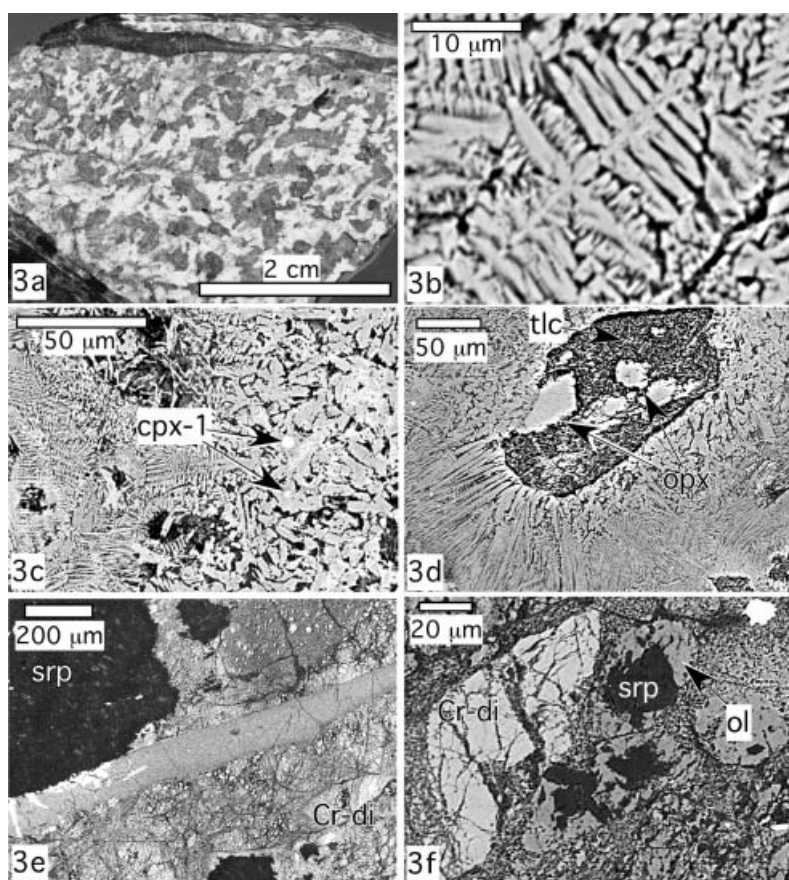


Fig. 2 (a) Multiple-generation fault-breccia of gabbro with network of pseudotachylyte veins. Notice pull-apart with fragments of wall-rock (top and bottom) filled with pseudotachylyte. (b) Pseudotachylyte vein along right-lateral fault, showing a shear-strain gradient defined by the foliation in the gabbro wall-rock highlighted by dotted white lines in the figure. (c) BSE image (Cor30) of spherulitic texture in pseudotachylyte, with epidote, dendritic fassaite and plagioclase.

dendrite as this would have destroyed the delicate texture. Acicular epidote grains locally form spherulites. The clasts and wall-rock minerals are similar in composition, suggesting that they are locally derived. The fassaitic pyroxene contains up to 18 wt%  $Al_2O_3$  as jadeite, Ca-tschermak and in the most Al-rich pyroxenes up to 15 mol.% Ca-Eskola component. Fassaitic pyroxenes with similar composition have been reported from pseudotachylytes in the Musgrave range, Central Australia (Wenk and Weiss, 1982). Wenk and Weiss (1982) pointed out that the high Al-pyroxene was similar to pyroxenes from eclogites and kimberlites that formed at 30 kbar and argued that the high pressure represented dynamic stresses released during catastrophic brittle failure. Fassaitic pyroxenes have also



**Fig. 3** (a) Pseudotachylyte vein containing fassaitic cpx, boulder (sample Cor30) from the beach at Sole du Marine (all mineral abbreviations after Kretz, 1983). (b) Back-scattered electron (BSE) image from pseudotachylyte, showing dendrite of fassaitic cpx. (c) BSE image showing centre (right) to rim (left) of pseudotachylyte vein (Cor30). The centre contains euhedral crystals of fassaitic cpx locally surrounding clasts of cpx (cpx-1). The rim of the vein is characterized by dendrites of fassaitic cpx. (d) BSE image from pseudotachylyte vein (Cor30), showing dendrite of fassaitic cpx that has grown out from clasts consisting of relict opx partly replaced by talc. Talc must have formed before the faulting. (e) BSE image of pseudotachylyte vein transecting peridotite. Note that serpentinization stops at the margin of the vein. (f) BSE image of pseudotachylyte vein showing serpentine with overgrowth of younger olivine. Note also clast of Cr-diopside.

been produced during frictional melting experiments at 10 kbar conducted to simulate earthquakes at amphibolite facies conditions (Spray, 1988). Some of the gabbro-hosted veins contain blueschist facies parageneses including 10–20  $\mu\text{m}$  sodic amphibole grains that are typically zoned from edenitic cores to glaucophane rims (Table 2) or from actinolite to edenite. Pumpellyite, albite, epidote and titanite typically coexist with amphibole (Table 2).

The peridotite contains remnants of primary olivine ( $\text{Fo}_{91}$ ), chromediopside ( $\text{Wo}_{46}\text{En}_{51}\text{Fs}_4$ ), orthopyroxene ( $\text{En}_{88}$ ) and a Cr-rich spinel. Such minerals are typical for spinel lherzolites of mantle origin. Ultrafine-grained, millimetre- to centimetre-thick injection and fault veins of pseudotachylyte containing clasts of Cr-diopside and olivine transect the peridotite (Fig. 3e). Olivine close to the vein is granulated and locally contains injection veins. A characteristic and intriguing feature observed in pseudotachylyte-like veins are serpentine inclusions partly surrounded by neoblastic olivine ( $\text{Fo}_{90}$ ) (Fig. 3f). The interpretation of these textures is not clear, but the dehydration reaction  $\text{serpentine} = \text{olivine} + \text{H}_2\text{O}$  may have occurred. The replacement of serpentine by olivine requires a minimum temperature of *c.* 450  $^{\circ}\text{C}$  at a pressure of 10 kbar (Bucher and Frey, 1994). Because the dehydration textures have not been observed outside the vein it is suggested that the dehydration occurred as a response to shear heating and not to a regional temperature increase. The serpentine

**Table 1** Petrography of pseudotachylyte veins and their wall rocks

Sample	Vein			Wallrock				Rock type
	Clast	Neolith	Texture	Primary minerals	Secondary minerals	Textures		
Cor29a	di, ol, srp	ol	ol growth on srp clasts	ol, cpx, opx, spl	srp, chl, mt	chl rims on mt	peridotite	
Cor30	di, pl, srp, tc + opx	fst, zo, pl, tre	dend, sphe, opx growth on tc	di, pl, hbl, ol/opx	tlc, ep, pl	ol/opx replaced by tc, plag	gb	
Cor32	di, pl	act, ep, ab, chl		di, pl, ol/opx	tlc, ep, pl	strong alteration	gb	
Cor36	pl + ep, chl	pmp, amph, ep	zoned amph(ed-act)	pl, cpx/ol/opx	chl, epid, alb, amph	strong hydration	gb	
Cor48c	ep	gln, Pmp, pl, spn	zoned amph(gln-act)	cpx, pl	ep, ab	plag altered to alb + ep	gb	
Cor47	di	amph		cpx, pl		kb and db in cpx, pl altered to zo + alb	gb	
Cor62	di, aug, pl	fst, pl, amph	fst growth on di clasts	cpx, pl	ep, ab	kb and db in cpx	gb/do	

Mineral abbreviations after Kretz (1983).

Additional abbreviations: gabbro, gb; dolerite, do; dendrite, dend; spherulite, sphe; kink bands, Kb; deformation bands, db.

**Table 2** Compositions of pyroxenes and amphiboles from pseudotachylyte veins and their wallrock

Sample Texture Mineral	Cor30 dend. fst	Cor30 clast di	Cor30 dend. fst	Cor30 neolith fst	Cor30 dend. fst	Cor62 neolith fst	Cor29 pri. min. cr-di	Cor29 pri. min. opx	Cor30 clast opx	Cor36 core ktp	Cor36 rim tr	Cor48C core bar	Cor48C rim bar	Cor48C core gln	
SiO <sub>2</sub>	50.7	50.71	50.6	48.39	50.84	49.72	50.88	53.88	54.33	45.26	57.81	44.64	57.37	57.58	
TiO <sub>2</sub>	0.49	1.19	0.39	0.32	0.32	0.34	0.28	0.14	0.29	1.19	0.04	0.28	0	0	
Al <sub>2</sub> O <sub>3</sub>	16.21	3.7	12.93	14.05	18.54	10.94	5.5	5.89	1.38	10.63	1.22	13.86	11.39	11.37	
FeO	5.28	8.03	5.65	5.17	4.93	4.92	2.15	6.67	13.64	16.57	5.42	10.01	8.46	8.16	
MnO	0.19	0.14	0.19	0.14	0.16	0.11	0.03	0.14	0.32	0.44	0.15	0.04	0.07	0.04	
MgO	11.04	14.24	15.32	15.99	9.88	16.86	17.42	32.35	28.35	10.96	19.84	15.12	11.78	11.46	
CaO	13.93	20.77	13.26	14.63	13.85	16.48	21.89	0.71	1.22	8.05	12.84	8.91	2.72	2.28	
Na <sub>2</sub> O	2.37	0.52	1.63	0.97	2.69	0.8	0.76	0.06	0.05	4.2	0.38	4.02	6.18	6.41	
K <sub>2</sub> O	0	0	0	0	0	0	0	0	0	0.03	0	0	0	0.12	
Cr <sub>2</sub> O <sub>3</sub>	0	0.35	0.14	0.16	0.09	0.12	1.22	0.63	0.13	0	0.04	0.01	0.01	0.01	
Total	100.21	99.65	100.11	99.82	101.3	100.29	100.13	100.47	99.71	97.33	97.74	96.89	97.98	97.43	
Structural formula based on 6(O) and 23(O) for pyroxene and amphiboles, respectively															
Si	1.799	1.89	1.804	1.737	1.779	1.785	1.852	1.862	1.953	Si	6.743	7.998	6.474	7.655	7.886
Al <sup>IV</sup>	0.201	0.11	0.196	0.263	0.221	0.215	0.148	0.138	0.047						
Al <sup>VI</sup>	0.477	0.053	0.347	0.331	0.544	0.248	0.88	0.102	0.005	Al	1.866	0.199	2.369	1.791	1.835
Ti	0.013	0.033	0.01	0.009	0.008	0.009	0.008	0.004	0.008	Ti	0.133	0.004	0.031	0	0
Cr <sup>3+</sup>	0	0.012	0.005	0.006	0.002	0.003	0.029	0.016	0.003	Cr	0	0.001	0	0	0
Fe	0.157	0.25	0.168	0.155	0.144	0.148	0.065	0.193	0.41	Fe	2.064	0.627	1.214	0.944	0.934
Mn	0.006	0.004	0.006	0.004	0.005	0.003	0.001	0.004	0.01	Mn	0.056	0.018	0.005	0.008	0.005
Mg	0.584	0.791	0.814	0.856	0.515	0.902	0.945	1.667	1.519	Mg	2.434	4.092	3.269	2.861	2.34
Ca	0.53	0.829	0.506	0.563	0.519	0.634	0.854	0.026	0.047	Ca	1.285	1.903	1.384	0.389	0.335
Na	0.163	0.038	0.113	0.067	0.183	0.056	0.054	0.004	0.003	Na	1.213	0.102	1.13	1.599	1.702
										K	0.006	0	0	0	0.021
Sum cations	3.93	4.011	3.97	3.99	3.921	4.002	4.044	4.015	4.011		15.794	14.944	15.875	15.247	15.036
Na(Mg,Ti)0.5Si <sub>2</sub> O <sub>6</sub>	0.03		0.02	0.02	0.02										
Jd	0.14		0.09	0.05	0.17										
CaEs	0.14		0.06	0.02	0.16										
CaTs	0.2		0.2	0.26	0.22										
Aug	0.06		0.08	0.03	0										
Opx	0.34		0.45	0.49	0.33										

End-members calculated for pyroxene with sum cations < 4 according to Katayama *et al.* (2000).  
Cor30, 36, 48 and 62: gabbro. Cor29: peridotite. Abbreviations as in footnotes to Table 1.

indicates that some hydrous minerals were present prior to faulting.

The gabbro wall-rock is variably hydrated. Plagioclase is typically altered to epidote and albite. Clinopyroxene is locally replaced by actinolite and chlorite. Orthopyroxene is altered to aggregates of quartz, chlorite and actinolite or replaced by talc. Olivine in the peridotite is locally replaced by serpentine and magnetite, the latter often along fractures. Cr-spinel is rimmed by chlorite. Although some hydration must have taken place prior to faulting, as demonstrated by clasts of serpentine and talc, the hydration also continued after faulting as veins in the peridotite are replaced by serpentine and magnetite along fractures and locally are totally overprinted by serpentine.

The contacts with wall-rocks in both gabbro- and peridotite-hosted veins are sharp, and the wall-rock is

transected by microfractures. Although clinopyroxenes locally have well-developed kink bands and deformation lamellae, the gabbro preserves the subophitic texture. An origin of frictional melts as a plastic instability (Hobbs and Ord, 1988) in a deforming shear zone seems to be incompatible with our observations. The textures found in the pseudotachylyte are typical of frictional melts formed during seismic faulting (Magloughlin, 1992). The change from euhedral crystals in the vein centre to dendrite at the vein rims suggests that the fassaitic pyroxene crystallized directly from the melt. Thus the dendritic texture supports the structural observations, which demonstrate that the veins are the result of faulting and represent true frictional melts. The spherulitic/dendritic textures shown in Figs 2(c) and 3(b–d) are similar to those produced during quenching of melt in experiments.

## Discussion

The pseudotachylytes described occur in a blueschist facies terrain that experienced maximum metamorphic conditions of  $550 \pm 50$  °C and 15–20 kbar, corresponding to subduction at a depth of 45 km or more. Although we cannot provide quantitative depth estimates for the faulting, the veins contain neoblasts and parageneses characteristic of blueschist facies metamorphism (glaucofane and other high-pressure amphiboles such as barroisite). The composition of the dendritic pyroxene with a high CaEs component is in accordance with pyroxene formed at 10 kbar (Spray, 1988) and further supports the idea that the seismic faulting occurred at considerable depth. Occurrence of pseudotachylyte at HP–LT conditions in the eclogite facies has previously been documented

from the orogenic root zone of the Caledonides in Western Norway (Austrheim and Boundy, 1994; Lund and Austrheim, 2003). These pseudotachylytes occur in dry Precambrian granulites and gabbros and it was argued that seismicity was an integral part of the fluid-driven Caledonian (420 Ma) eclogitization of the root zone by assisting fluid transport (Bjornerud *et al.*, 2002). These observations have recently been taken to support models of a dry, strong and seismically active lower crust beneath the Himalayas (Jackson, 2002). The Alpine example reported here has several analogies with the Caledonian HP–LT pseudotachylytes. The complex is partly metamorphosed to HP–LT assemblages and pseudotachylytes have been identified in rocks that partly preserve their previous mineralogy and textures. This suggests that dry strong rocks are a prerequisite for the faulting that produces pseudotachylyte. However, clasts of talc and inclusions of globular serpentine may give support for some hydration prior to faulting. A detailed search for dehydration textures on a regional scale is required to test whether the dehydration reaction represented by serpentine to olivine is related to a regional heating event and therefore supports existing models for subduction zone earthquakes (Hacker *et al.*, 2003) or if the dehydration took place during shear heating as suggested here. Pseudotachylytes have recently also been described from the Shiman-to accretionary complex in Japan by Ikesawa *et al.* (2003). The finding of palaeo-seismic fault zones in subduction complexes is exciting and represents a new source of information on subduction earthquakes. We anticipate that similar relationships will be found in other subduction complexes and blueshist terrains, which will open a new avenue for research towards a

better understanding of subduction zone processes.

### Acknowledgements

Professor Bradley R. Hacker and Dr Muriel Erambert are thanked for comments and improvements to an early version of the text. We thank Joseph Allen and Hideo Takagi for constructive reviews. We thank Laurent Jolivet for introducing us to the geology of Alpine Corsica. Financial support was received from PGP (H.A. and T.B.A.) and NGU (T.B.A.).

### References

- Austrheim, H. and Boundy, T.M., 1994. Pseudotachylytes generated during seismic faulting and eclogitization of deep crust. *Science*, **265**, 82–83.
- Bjornerud, M.G., Austrheim, H. and Lund, M.G., 2002. Processes leading to eclogitization (densification) of subducted and tectonically buried crust. *J. Geophys. Res.*, **107**, DOI 10.1029/2001JB000527.
- Bucher, K. and Frey, M., 1994. *Petrogenesis of Metamorphic Rocks*. Springer Berlin.
- Fournier, M., Jolivet, L., Goffe, B. and Dubois, R., 1991. Alpine Corsica Metamorphic core complex. *Tectonics*, **10**, 1173–1186.
- Hacker, B.R., Peacock, S.M., Abers, G.A. and Holloway, S., 2003. Subduction factory 2. Are intermediate-depth earthquakes in subduction slabs linked to metamorphic dehydration reactions? *J. Geophys. Res.*, **108**, DOI 10.1029/2001JB001129.
- Hobbs, B.E. and Ord, A., 1988. Plastic instabilities: implications for the origin of intermediate and deep focus earthquakes. *J. Geophys. Res.*, **93**, 10521–10540.
- Ikesawa, E., Sakaguchi, A. and Kimura, G., 2003. Pseudotachylyte from an ancient accretionary complex: evidence for melt generation during seismic slip along a master décollement? *Geology*, **31**, 637–640.
- Jackson, J., 2002. Strength of the continental lithosphere: time to abandon the jelly sandwich? *GSA Today*, **12**, 4–10.
- Jolivet, L., Faccenna, C., Goffe, B., Burov, E. and Agard, P., 2003. Subduction tectonics and exhumation of high-pressure metamorphic rocks in the Mediterranean orogens. *Am. J. Sci.*, **303**, 353–409.
- Katayama, I., Parkinson, C.D., Okamoto, D., Nakajima, Y. and Maruyama, S., 2000. Supersilicic clinopyroxene and silica exsolution in UHPM eclogite and pelitic gneiss from the Kokchetav massif, Kazakhstan. *Am. Miner.*, **85**, 1368–1374.
- Kretz, R., 1983. Symbols for rock-forming minerals. *Am. Miner.*, **68**, 277–279.
- Lahondre, D., 1988. Eclogitic metamorphism in Farinoles orthogneisses and ophiolitic metabasites (Northern Corsica, France). *Bull. Soc. Geol. France*, **4**, 579–585.
- Lund, M.G. and Austrheim, H., 2003. High-pressure metamorphism and deep-crustal seismicity: evidence from contemporaneous formation of pseudotachylytes and eclogite facies coronas. *Tectonophysics*, **372**, 59–83.
- Magloughlin, J.F., 1992. Microstructural and chemical changes associated with cataclasis and frictional melting at shallow crustal levels: the cataclasis–pseudotachylyte connection. *Tectonophysics*, **204**, 243–260.
- Sibson, R.H., 1975. Generation of pseudotachylyte by ancient seismic faulting. *Geophys. J. Astr. Soc.*, **43**, 775–794.
- Spray, J.G., 1988. Generation and crystallization of an amphibolite shear melt: an investigation using radial friction welding. *Contrib. Miner. Petrol.*, **99**, 464–475.
- Warburton, J., 1986. The ophiolite-bearing Schistes lustrés nappe in the Alpine Corsica: a model for the emplacement of ophiolites that have suffered HP/LT metamorphism. *Geol. Soc. Am. Mem.*, **164**, 313–331.
- Wenk, H.R. and Weiss, L.E., 1982. Al-rich calcic pyroxene in pseudotachylyte: an indicator of high pressure and high temperature? *Tectonophysics*, **84**, 329–341.

Received 24 October 2003; revised version accepted 19 March 2004



Contents lists available at ScienceDirect

## Tectonophysics

journal homepage: [www.elsevier.com/locate/tecto](http://www.elsevier.com/locate/tecto)

# A weakening mechanism for intermediate-depth seismicity? Detailed petrographic and microtextural observations from blueschist facies pseudotachylytes, Cape Corse, Corsica

N. Deseta <sup>a,\*</sup>, T.B. Andersen <sup>b</sup>, L.D. Ashwal <sup>a</sup><sup>a</sup> Department of Geosciences, University of the Witwatersrand, Private Bag 3, 2050 Johannesburg, South Africa<sup>b</sup> Department of Geosciences, CEED, University of Oslo, PO Box 1047, Blindern, 0316 Oslo, Norway

## ARTICLE INFO

## Article history:

Received 9 July 2013

Received in revised form 16 October 2013

Accepted 3 November 2013

Available online 12 November 2013

## Keywords:

Shear localisation

Intermediate-depth earthquakes

Pseudotachylyte

blueschist

## ABSTRACT

Gabbro- and peridotite-hosted pseudotachylytes from the Alpine Schistes Lustres Unit in Corsica, previously determined to have formed at blueschist to lawsonite-eclogite facies conditions, have been causally linked to the generation of intermediate-depth earthquakes, which occur at depths of 50–300 km. Detailed petrographic and microtextural analyses of these pseudotachylytes suggest that their initiation may be controlled by a thermally-activated shear runaway process that is controlled by rheology rather than mineralogy. This is documented by sheared out, prolate, kinked and twinned wallrock clasts that have been peeled off and entrained into the pseudotachylyte vein as sigmoid survivor clasts. The presence of metastable high temperature crystallisation products in the pseudotachylyte, such as hoppers and dendrites of olivine, enstatite and diopside (peridotite) and Al-rich omphacite and Fe-rich anorthite in metagabbro, are suggestive of a short-lived high-temperature event resulting from thermal instability. These high temperature mineral assemblages are overprinted by ones indicating a return to ambient conditions of lower temperatures, but still high pressures: glaucophane, albite and epidote in metagabbro and clinocllore; and fine-grained granoblastic olivine, enstatite and diopside in peridotite. The observations from this detailed study of natural samples suggest that intermediate-depth seismicity may be generated by a thermal runaway process.

© 2014 Elsevier B.V. All rights reserved.

## 1. Introduction

The initiation of intermediate-depth earthquakes has long been a subject of debate. These phenomena occur at depths from 50 km to 350 km, which, due to high confining pressures, preclude traditional brittle failure (Green and Houston, 1995; Hacker, 2003; Jung et al., 2004; Ogawa, 1987). In order to address this problem researchers have put forth several hypotheses, which include dehydration embrittlement, transformational faulting and thermal runaway processes. These hypotheses can be divided into brittle – (solid-state dehydration embrittlement and transformational faulting) and crystal-plastic – (shear-heating and thermal runaway) controlled processes. These models are based on experimental, numerical and geophysical modeling, with no field observations and little work on natural samples (Green and Houston, 1995; Hacker, 2003; John et al., 2009; Kelemen and Hirth, 2007; Ogawa, 1987). In the past two decades however, several discoveries of high pressure pseudotachylytes associated with intermediate-depth earthquakes have been made (Austrheim and Boundy, 1994; Jin et al., 1998; John and Schenk, 2006; Kanamori et al., 1998), providing researchers with natural material with which to evaluate previous models. This paper presents detailed petrographic

and microstructural observations of peridotite- and metagabbro-hosted pseudotachylytes associated with subduction zone seismicity, in the Cima di Gratera area of Cap Corse, Corsica. Previous work suggests that faulting and pseudotachylyte generation took place during subduction at blueschist to lawsonite-eclogite facies conditions under pressures of 1.8–2.6 GPa (Austrheim and Andersen, 2004; Andersen and Austrheim, 2006; Ravna et al., 2010; Vitale Brovarone et al., 2011). A detailed discussion on the geochemistry of these rocks and the role that water plays in earthquake generation will be addressed in a separate paper.

## 2. Geological setting

The study area is located on the SSW side of Cima di Gratera, Cape Corse, northern Corsica (Fig. 1). The pseudotachylytes, first described by Austrheim and Andersen (2004), occur within lenses of gabbro and mantle peridotite enclosed by serpentinite (Fig. 2). These rocks form part of the Schistes Lustres Complex (part of the Alpine age high pressure–low temperature subduction complex), and which has been interpreted as either nappes of exhumed Ligurian oceanic lithosphere, which have slivers of crystalline continental material, or hyperstretched continental lithosphere interleaved with mantle imbricates (Agard et al., 2002; Beccaluva et al., 1977; Jolivet, 1993; Mohn et al., 2009; Vitale Brovarone et al., 2011). This rock package was thrust onto

\* Corresponding author.

E-mail address: [suridae@gmail.com](mailto:suridae@gmail.com) (N. Deseta).

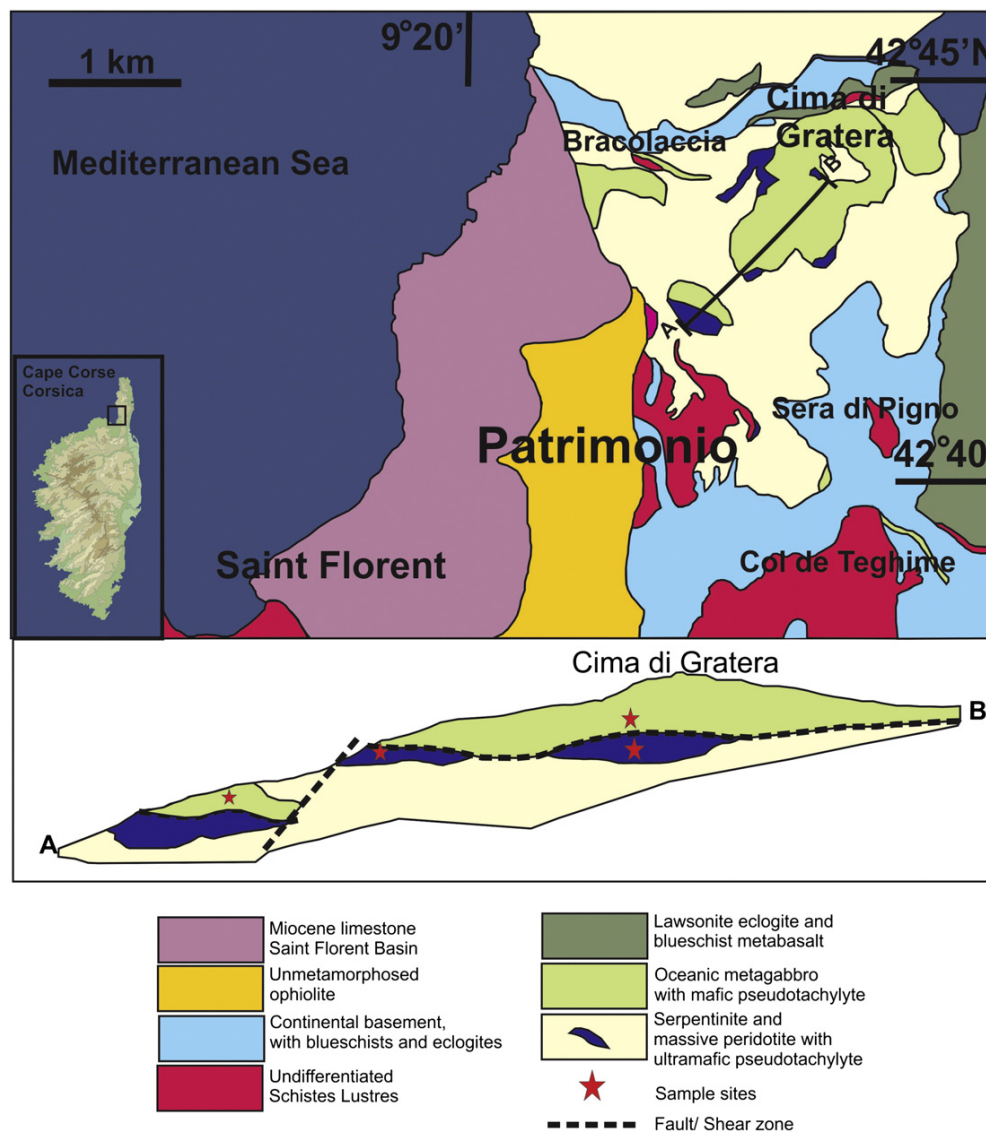


Fig. 1. Simplified geological map of the study area in Cima di Gratera. Modified after Andersen and Austrheim (2006).

the continental margin of Europe during the Late Cretaceous to Tertiary Periods (Fig. 1) (Jolivet, 1993).

The metagabbros are compositionally uniform and encompass a range of igneous textures marked by differences in grain size. Common textures are cumulate layering and the interfingering of irregularly shaped domains of fine- and coarse-grained gabbro. Conversely, the peridotites are relatively uniform in terms of composition, texture and grain size. The pseudotachylyte-bearing fault rocks have been partially metamorphosed to blueschist and greenschist facies only in patches, except within the shear zones where the metamorphic reactions are fully equilibrated. The pseudotachylytes occur within the pristine lenses of gabbro and peridotite that are relatively undeformed and least affected by the regional HP–LT metamorphism (Andersen and Austrheim, 2006).

### 2.1. Field observations

In outcrop the pseudotachylytes typically have a positive relief with respect to the host rocks. The pseudotachylyte veins weather to a rust-red colour but on fresh surfaces are black-grey and aphanitic (Fig. 2). Comminuted wallrock clasts and flow banding are commonly observed.

In the peridotite, the pseudotachylytes occur in two sets that extend for up to 1 km: a sub-vertical set and a sub-horizontal set. Within the vein sets the pseudotachylytes form complex vein networks that over-print and re-inject one another, indicating multiple generations of pseudotachylyte (Fig. 2). In the peridotite, the pseudotachylyte veins occasionally form radial 'explosive' networks. These veins are thicker than other injection or fault veins and contain more re-injections and comminuted wallrock material (Fig. 2b). In contrast with the peridotite-hosted veins, those in the gabbro are thinner and more discrete, commonly (but not always) occurring along the boundary between the very coarse-grained (<15 mm) metagabbro and fine-grained (<2 mm) metagabbro (Fig. 2). The peridotite pseudotachylytes show cross-cutting relationships with serpentinised host rocks, which have been entrained into the veins as sigmoidal lozenges, indicating a brittle-ductile overprint relationship. In the metagabbro fault rock, the pseudotachylytic crystallisation products (glaucofanite) have formed CPO (crystallographic preferred orientation) fabrics and contain boudinaged wallrock clasts, indicating a ductile overprint post-dating pseudotachylyte generation (Fig. 12) (Andersen and Austrheim, 2006). Many of the pseudotachylytes are cut by later serpentine veins and show a hydration

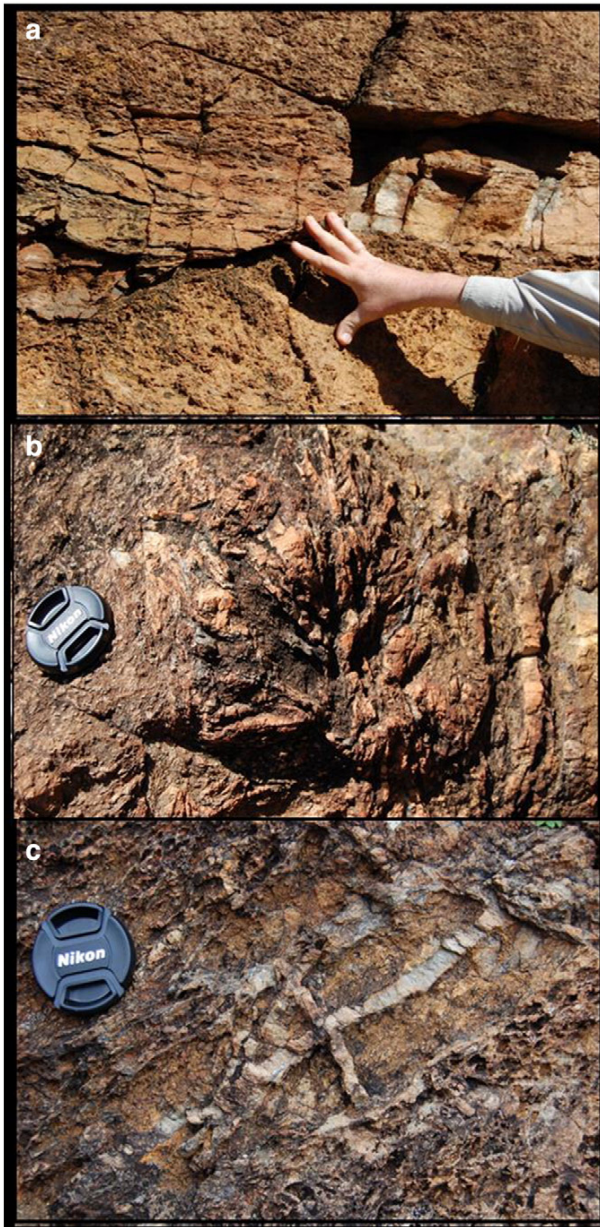


**Fig. 2.** Photographs of pseudotachylyte hosted by peridotite. Panel a shows one of the thickest (up to 25 cm) pseudotachylyte fault veins observed in the field. The thickness of this vein is principally due to multiple generations of pseudotachylyte that have nucleated along the same plane. (b) Explosive network veining of pseudotachylytes that radiate in all directions away from the centre of the fault plane. (c) Cross-cutting relationships of pseudotachylyte self-injecting.

overprint. Care was taken to analyse only pristine, unaltered pseudotachylytes.

### 3. Materials and methods

Detailed thin section petrography and back-scatter electron (BSE) imaging for mineral identification and microtextural analysis were done on both gabbro- and peridotite-hosted pseudotachylyte. Electron microprobe analyses were conducted using a Cameca SX-100 instrument at Spectra Laboratory, University of Johannesburg, South Africa. Analyses of the bulk matrix (wide beam (10  $\mu\text{m}$ ) and narrow (1  $\mu\text{m}$ ),

wallrock, entrained minerals as well as crystallisation products (glass and crystallites) were done. The beam current was reduced to minimise sodium loss on glass, but tests on higher currents showed loss to be negligible. Analyses were run at 20 kV, 10 nA. The reference standard used was a Ni-bearing glass. Refer to Merlet (1994) for more detailed operating parameters.

### 4. Petrographic and microtextural observations

Detailed petrographic microtextural analyses were carried out on the pseudotachylyte and the adjacent wallrock in both the metagabbro and peridotite in order to ascertain the rheological behaviour of the rock at the time of fusion. Features of the host rocks and microtextures common to both rock types will be discussed in the first section, followed by those characteristic to only the metagabbro or the peridotite.

#### 4.1. Metagabbro host rock

The metagabbro host rock is heterogeneous in grain size with large, irregular domains (up to approximately a metre in outcrop) of very coarse-grained (up to 15 mm) gabbro occurring in contact and inter-fingering with a much more fine-grained (~1 mm) gabbro. The margin between the coarse- and fine-grained domains is consistently sharp, less than 5 mm thick. Despite the large grain-size variability in the metagabbro, the constituent mineral assemblage is not significantly variable.

The primary gabbro mineralogy is largely preserved and comprises plagioclase, diopside, olivine and minor ilmenite. In thin section the gabbro adjacent to pseudotachylyte faults retains little of its original igneous texture, most of which has been transformed into an annealed granoblastic texture with poikiloblasts of olivine and diopside. Grain boundary migration and dynamic recrystallisation are common, particularly in diopside. Early greenschist facies metamorphism of the host rock has led to variable replacement and recrystallisation of diopside by actinolite, bastite and Mg-hornblende. Plagioclase alteration to sericite has also taken place, causing the grains to become cloudy and grey. Alteration of the olivine to serpentine, magnetite or iddingsite has also been observed. Post-dating the early greenschist alteration is the development of blueschist facies assemblages, which manifest in the replacement of diopside, actinolite, Mg-hornblende and plagioclase by glaucophane, barroisite, albite and epidote. Late blueschist facies metamorphism that post-dates pseudotachylyte generation at these conditions is associated with ductile deformation and pseudotachylyte recrystallisation (Fig. 12). Late retrograde metamorphism, particularly marked by serpentine veins and the presence of epidote, clinocllore and pumpellyite overprints the blueschist assemblage phase and patches of the pristine material (Fig. 13).

The early greenschist metamorphism of the host rock may be associated with seafloor hydration and/or hydration-associated fracturing in the slab bend, as well as earlier hydration associated with extensional tectonics (Mohn et al., 2009; Vitale Brovarone et al., 2011). The late greenschist metamorphic overprint has been observed in thin section and BSE images and is interpreted to be associated with hydration and faulting upon slab exhumation. This late retrograde metamorphism overprints some of the pseudotachylyte veins and is not cut by later pseudotachylyte generations (Fig. 13).

#### 4.2. Peridotite host rock

The peridotite host rocks show gradational transitions from fine- to coarse-grained (<1 mm–7 mm) textures. The mineralogy corresponds to that of a plagioclase lherzolite with olivine > diopside > enstatite, as well as minor plagioclase and magnetite. The rocks exhibit a granoblastic texture with annealed poikiloblasts and some grain boundary migration. The diopside and enstatite commonly show exsolution lamellae of each other and twinning of the diopside and olivine has been observed.

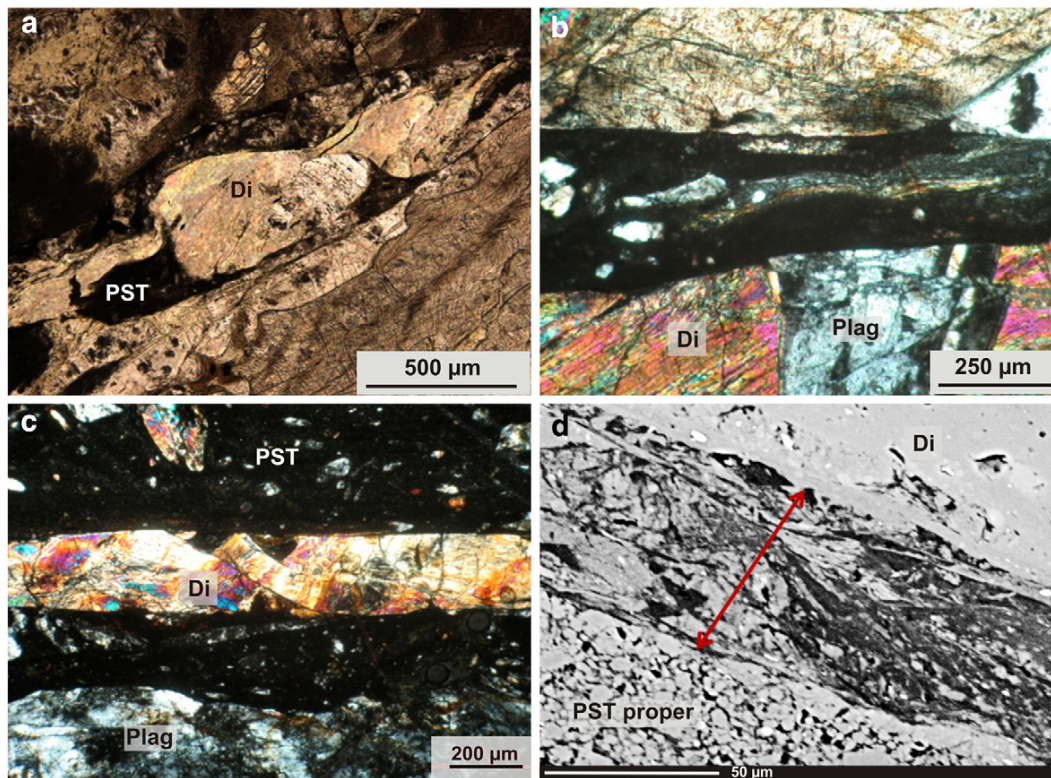


**Fig. 3.** Images of microstructures at fault vein boundaries in metagabbro. All these images clearly show that wallrock material at these boundaries has been subjected to crystal plastic deformation. Panel a shows a boudinaged, kink-banded diopside enclosed in a dark brown, glassy pseudotachylyte matrix. (b) Pseudotachylyte vein with entrained, boudinaged, wallrock aggregate of plagioclase and diopside. The wallrock diopside and plagioclase clearly show kinking and deformation twinning, respectively.

There is some early greenschist facies metamorphism of diopside and enstatite to fine-grained clinocllore and tremolite by dynamic recrystallisation. The clinocllore has a plumose and feathery texture. Various generations of serpentinisation (including magnetite and Cr-spinel) overprint all pre-existing features and are variably distributed throughout the rock; occasionally associated with late reactivation of pseudotachylyte veins (Fig. 12c). The peridotite shows no blueschist facies mineral assemblages; only multiple stages of early and late greenschist metamorphism are observed prior to and after the period(s) of pseudotachylyte generation. The early greenschist metamorphism has been attributed to events occurring prior to pseudotachylyte generation

associated with ocean–continent hyperextension and hydrothermal alteration due to prograde subduction (Vitale Brovarone et al., 2011). The late greenschist facies metamorphism is likely associated with slab exhumation processes.

#### 4.3. Fault vein characteristics

Fault veins form parallel to displacement surfaces in the host rock. Wallrock clasts locally underwent crystal plastic deformation in proximity to vein boundaries or melted along/with the fault plane (Fig. 3). Microscope- and BSE-based observations of the pseudotachylyte vein

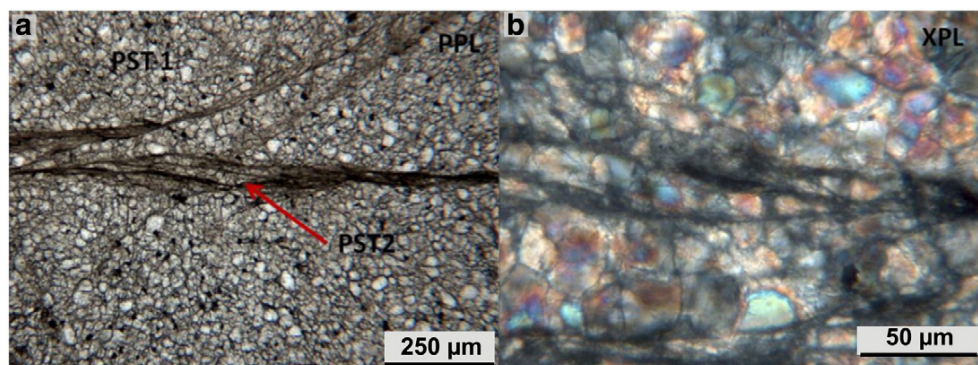


**Fig. 4.** Micrographs of fine-grained, recrystallized peridotite-hosted pseudotachylyte (PST 1) cut by later pseudotachylyte (PST 2). Panel b is a high magnification view with crossed nicols of where the red arrow is pointing to in panel a. In panel b the grains enclosed by the glassy black melt veins are prolate and lozenge-shaped compared to those grains not in contact with PST 2. Grain boundary migration is suggested by the grain boundary alignment of grains enclosed by fault veins. In contrast to the previous figure (Fig. 5), where coarser-grained wallrock was deformed, these photomicrographs show fine-grained recrystallised peridotite-hosted pseudotachylyte cut by a later generation of pseudotachylyte.

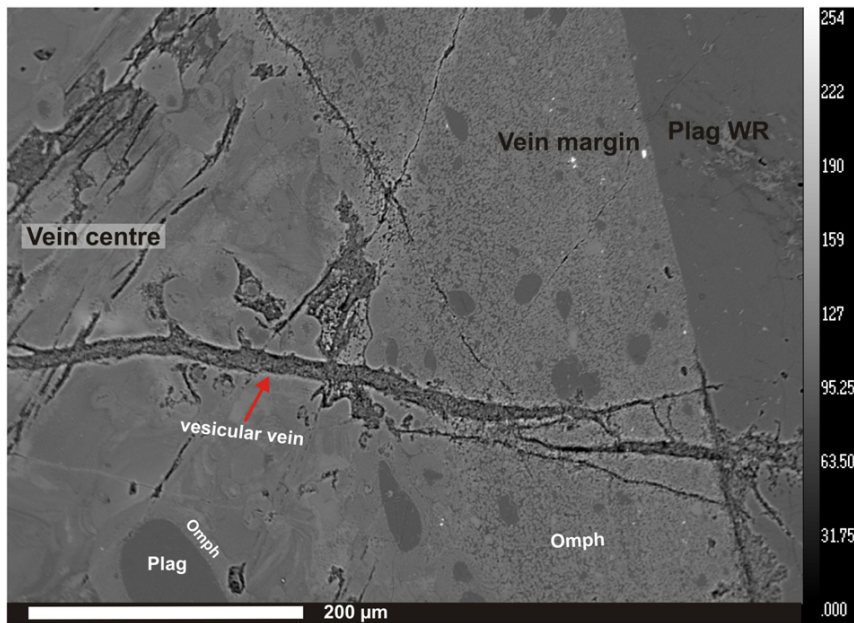


**Fig. 5.** BSE image of a pseudotachylyte fault vein hosted by metagabbro. The dark grey thermally rounded clasts are plagioclase upon which dendrites of omphacite have crystallised with interstitial glass. The smaller veins cross-cutting the main pseudotachylyte vein in this image, are contemporaneous with the molten pseudotachylyte, as can be seen by the lobate–cusped boundaries enclosing the dendrites. These cross-cutting veins appear, by their low atomic numbers and low totals (on EPMA analysis) to have contained dissolved hydrous fluids that later vesiculated. Plag: plagioclase, Plag WR: Wallrock plagioclase, Omph: omphacite.

boundaries reveal a syndeformational zone in the associated wallrock that begins several grain widths from the vein ‘proper’. This region is dominated by highly strained, sheared, kinked, elongate wallrock grains (Figs. 3, 6). The vein boundary is sharply cut by the pseudotachylyte and has commonly been observed to be dragged or peeled off into the vein and is surrounded by injecting melt (Fig. 3b).

Creep textures associated with the formation of the pseudotachylytes were observed in the full range of grain sizes observed in the wallrock; from 20 mm to 30 μm (Figs. 3 and 4), from shearing and kinking as seen in the coarser-grained material (Fig. 4) to what appears to be grain boundary creep in fine-grained re-crystallised pseudotachylytes that were subsequently reactivated to generate a melt (Fig. 4).

The thickness of fault veins ranges from less than 1 mm to more than 30 cm. Fault veins were typically formed by a single event. However, reactivation and multiple fusion events are exemplified by older pseudotachylyte survivor clasts entrained into younger veins (Fig. 4) and by cross-cutting relations. The lack of offset markers as well as the injection of melt into dilational fractures precludes the determination of the true dimensions of the fault zone during a single pseudotachylyte-forming event. However, due to the pristine nature of the pseudotachylyte matrices studied, we have concluded that no significant post-pseudotachylyte vein deformation occurred.

#### 4.4. Injection vein characteristics

The injection veins are secondary pseudotachylyte veins that emanate from parent fault veins into the adjacent wallrock. Injection veins cannot in all instances be traced to their sourcing fault vein. This is due to chaotic networks of nearby multiple injection veins in proximity and arching self-injections that cross-cut one another. The veins vary widely in thickness, ranging from 200 μm, thinner than the average fault vein, to >20 cm, thicker than the average fault vein. They inject at all angles from their parent veins, from near-parallel to perpendicular. They cut between and through wallrock grains and are not associated with or dependent on precursory wallrock deformation or foliations.

#### 4.5. Microtextures of ultracataclasite

Syndeformational ultracataclasite at the margins of coarse-grained pseudotachylyte fault veins is a common feature in both the metagabbro and peridotite host rocks. The ultracataclasite comprises a mixture of comminuted clasts, melt and plastic ribbons (Fig. 6). The size range in comminuted wallrock material is from 30 μm < 1 μm. The mineral assemblage in the ultracataclasite matches that of the adjacent wallrock. The deformation of different mineral species in the ultracataclasite appears to be determined by fracture toughness, as predicted by Spray (1992). Minerals with greater relative fracture toughness such as diopside, plagioclase, Mg-hornblende and olivine typically form the portion of comminuted grains and mineral ribbons. Softer minerals such as clinocllore, tremolite, serpentine and actinolite comprise the melt and the rest of the ribbon portion in the ultracataclasite (Fig. 6). It is possible that some of the displacement in the fault veins is accommodated by preferential crystal plastic deformation and fusion within the ultracataclasite, explaining the lack of kinematic markers between the fault vein pseudotachylyte and wallrock (Kim et al., 2010; Sibson, 1980; Spray, 1992). The microtextures of this unusual crystal-plastic ultracataclasite may hold information regarding the earliest stages of pseudotachylyte generation. It is important to take note that no ultracataclasite appears to form in pseudotachylyte fault veins hosted by equigranular, fine-grained rock (~20 μm) in both the peridotite and metagabbro.

#### 4.6. Microtextures of the pseudotachylyte matrix

The matrices of the metagabbro and peridotite pseudotachylytes are typically dominated by crystallisation products of the melt, with interstitial crypto-crystalline material or glass and entrained wallrock clasts that vary greatly in size and can constitute up to 20% of the vein, but are normally much less. The presence of interstitial glass was confirmed with XRD synchrotron analysis (Fig. 8). The veins are commonly marked by streaks or colour bands that indicate compositional variation, predominantly due to clusters of spinel, and inefficient mixing of the melt

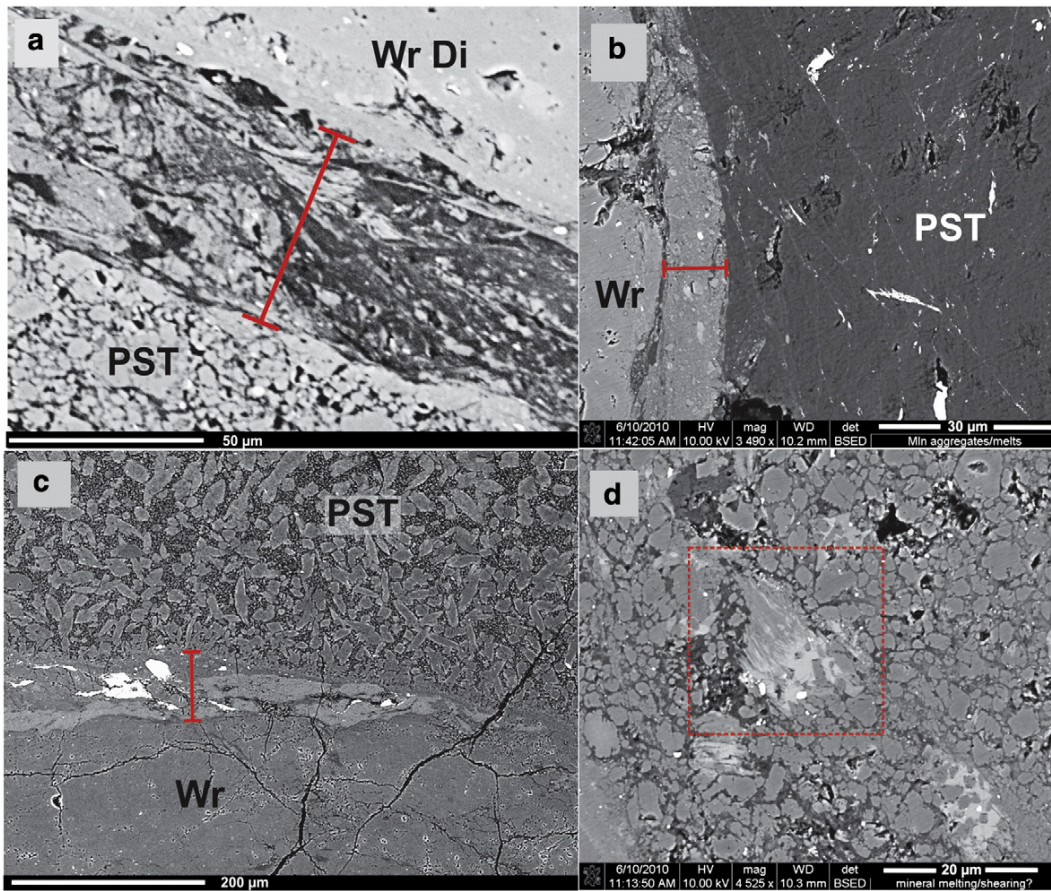


**Fig. 6.** BSE images a–c of ultracataclasites at fault vein boundaries in peridotite. A range of brittle–ductile textures are present in the ultracataclasite, the width of which is shown by the capped red line. (a) Close-up of the ultracataclasite; the black areas are a hydrous Al-rich melt, the dark grey areas are a sheared out pseudotachylyte matrix, and the lighter grey is a combination of sheared out survivor clasts of wallrock diopside and pseudotachylyte matrix. Image d shows a pseudotachylyte matrix crystallising olivine (grey) and diopside (light grey) in a hydrous matrix (dark grey). The red box encloses an olivine–diopside crystal complex being sheared out prior to total solidification indicating continued displacement along fault veins post melt production and failure. Panel c shows a similar feature; brittle-looking ultracataclasites with a matrix hosting ribbons of stretched out diopside microlites (in white). Wr: Wallrock, Wr Di: Wallrock diopside grain.

(Fig. 7). The crystallisation products have various habits: hopper crystals, simple acicular laths, and feathery plumes, which nucleate on clastic material in the vein forming dendrites or along vein boundaries. A principal control on microlite size is the presence or absence of a

nucleation surface and the size of this surface. When the nucleating surface is particularly small it generally forms the core of a larger than average complex dendrite composed of several mineral species. Space may also exert a control on crystallisation; areas that appear to be

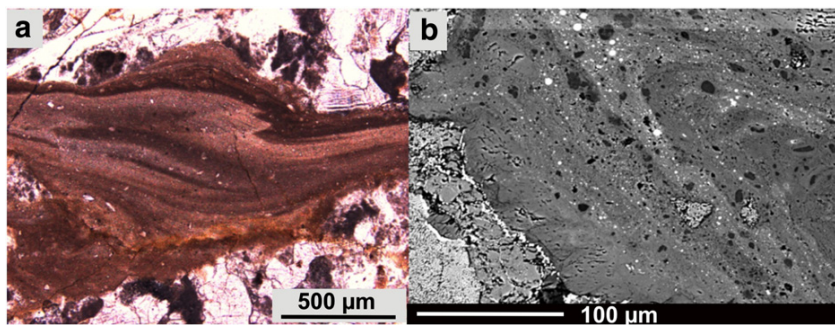


**Fig. 7.** Micrograph (a) and BSE image (b) of pseudotachylyte matrix in a metagabbro. Colour bands in these veins are evident in both images and are attributed to zones where individual minerals or aggregates have fused and become decrepitated and sheared out. Clusters of microlites and glassy material are also observed to form bands. However, the crystallisation products of the melt are strongly controlled by its composition, and hence the pre-existing minerals that fused will be the dominant control over the formation of these colour bands. Minimal physical sorting or fractionation has been observed in these veins, so this is not considered to be a significant factor.

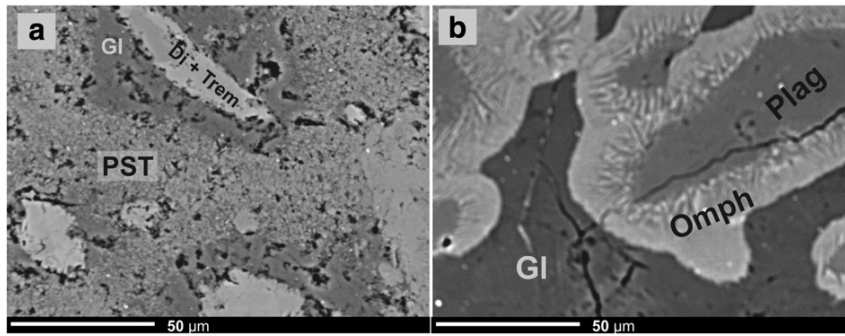


**Fig. 8.** BSE images of individually fusing clasts enclosed in a pseudotachylyte matrix. (a) The matrix is dominated by microlites and minute relict clasts. However, at the boundary of melting clasts there is a zone of Al-rich, hydrous glass (Gl). Conversely, in panel b the matrix is glass dominated (anhydrous) and the fusing grains are bounded by a crystallisation front of Al-rich omphacite (Omph) nucleating on plagioclase (Plag) derived from wallrock. Di + Trem: aggregate clast of wallrock diopside and tremolite.

absent of any nucleating surface are typically host to some of the largest crystals.

#### 4.7. Microtextures of survivor clasts

Survivor clasts comprise wallrock material that has been dragged into the pseudotachylyte during its formation. These can be monomineralic or composed of aggregates of minerals. They are typically angular or tabular in shape, with thermally rounded margins. The larger tabular forms are aggregates from the deformed wallrock that have been scoured away from the vein boundary by injecting melt (Fig. 3). The composition of the clasts is the same as that of the adjacent wallrock mineralogy, but not in the same proportions. Hydrous minerals such as Mg-hornblende, clinocllore and serpentine occur only in rare aggregates with anhydrous minerals and are thus inferred to have melted preferentially. Monomineralic olivine, diopside, magnetite, ilmenite and plagioclase have all been observed in the matrix of both types of host rock. Diopside and plagioclase are the most common clasts derived from the metagabbro host rock, whilst olivine and diopside are those abundantly found in the peridotite. Survivor clasts commonly exhibit undulose extinction and kink-banding similar to that observed just beyond fault vein boundaries in the wallrock, suggesting that they may be derived from the wallrock and underwent similar crystal plastic deformation. Sieve textures in sheared out wallrock and partially resorbed survivor clasts of older pseudotachylyte have also been observed (Fig. 9).

Further detailed petrographic data have been divided according to the metagabbro and peridotite host rocks. Within those groups the

most pristine samples were selected for microtextural and geochemical analysis. The pseudotachylytes are highly heterogeneous in composition down to the micron scale, so this separation is the best way to gain information from these veins and interpret their mechanism of formation meaningfully.

##### 4.7.1. Metagabbro: pseudotachylyte

Compositionally the pseudotachylytes hosted by metagabbro are highly heterogeneous, strongly reflecting local mineral compositions of the adjacent wallrock and survivor clasts. However, despite the compositional variability of the melt, the mineralogy of the crystallisation products in the pseudotachylytes is simple albeit showing great chemical variability. The pseudotachylyte matrix is defined as a combination of glass, crystallisation products and comminuted material that are too small to be resolved by electron microprobe analysis (EPMA) beam (<1 µm). The crystallisation products are divided into two groups: a high temperature quench assemblage with pockets of interstitial glass, and a lower temperature assemblage in which devitrification of the glass and recrystallisation of the pseudotachylyte matrix have taken place.

**4.7.1.1. Microlite assemblage in the metagabbro pseudotachylytes.** This microlite assemblage is dominated by omphacite and plagioclase, with minor ilmenite (Fig. 10). This is the first reported evidence of natural crystallisation of omphacite directly from a melt. Omphacite has been reclassified from fassaite, as it was termed by Andersen and Austrheim (2006). The composition of the minerals is highly variable and is strongly controlled by melt composition in the matrix or by fusing

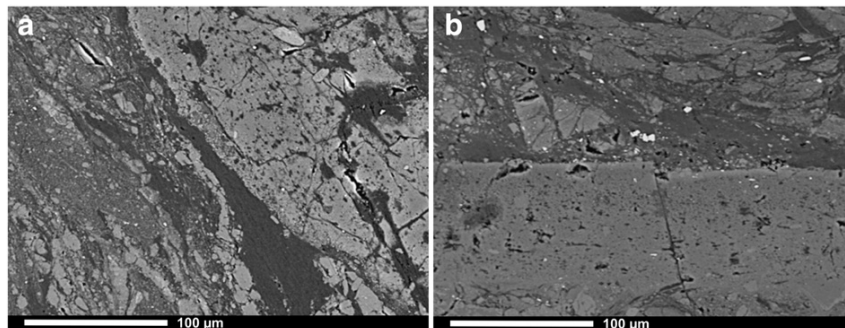


**Fig. 9.** BSE images of sieve textures in a peridotite-hosted pseudotachylyte matrix. Both panels a and b show at least two generations of pseudotachylyte. The sieve textured material in both images is the oldest generation that has been deformed and partially digested by a younger pseudotachylyte generation into which sheared out clasts of the older pseudotachylyte have been entrained. The oldest generation of pseudotachylyte contains inclusions of relative low atomic number (and low totals when analysed with EPMA; ~86%), suggesting that these are quenched melt inclusions with fluids dissolved in them to varying degrees. Preliminary Raman spectroscopy shows these vesicles to contain glassy material and empty cavities, presumably once filled with fluid.

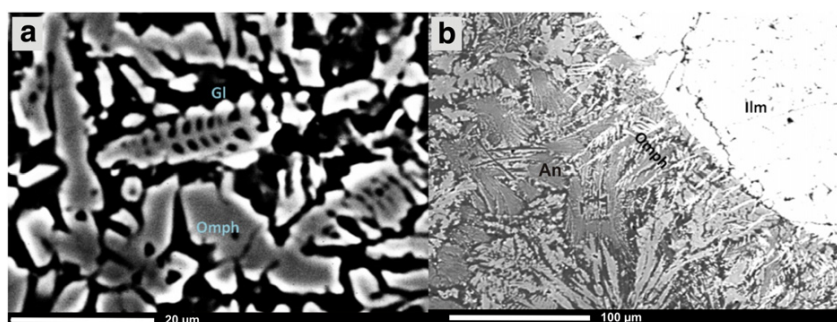


**Fig. 10.** Omphacite is the principal high temperature mineral crystallising from gabbroic pseudotachylyte, with anorthite and ilmenite to lesser degrees. Panel a shows delicate, zoned hopper crystals of omphacite enclosed by glass; this crystal habit is an indicator of rapid, high temperature quenching. Panel b shows omphacite in white and light grey with feathered and dendritic textures. The dark grey dendrites are anorthite. The variation in the composition of omphacite is controlled by the mineral that it nucleates on, as shown by the change in greyscale; its local melt composition and zoning in the crystals. Omph: omphacite, Ilm: Ilmenite.

clasts on which the microlites have nucleated. The omphacite is characterised by significant Al-enrichment relative to typical omphacite, which could be due to the high temperature and pressure of crystallisation (average  $\text{Al}_2\text{O}_3$ : 17.3 wt.%). The plagioclase is characterised by high  $\text{FeO}_{\text{total}}$  and MgO contents (average  $\text{FeO}_{\text{total}} = 1.3$  wt.%,  $\text{MgO} = 1.1$  wt.%), possibly due to the rapidity or high temperature of crystallisation, or inclusions of unresolvable omphacite or ilmenite. These microlites take the form of laths, dendrites and skeletal hoppers crystallising freely in the pseudotachylyte matrix or nucleating on vein boundaries or on survivor clasts. The omphacite is clearly zoned with Mg-rich cores and Fe-rich rims (Fig. 10).

**4.7.1.2. Metagabbro: devitrification and recrystallisation of pseudotachylytes.** Devitrification of glass and recrystallisation of the higher temperature minerals that quenched directly from the pseudotachylyte melt produce its own assemblage of blueschist facies minerals: glaucophane, Fe-rich albite, epidote and minor sphene (Fig. 11a, b). The crystals in this assemblage are commonly coarser than those in the higher temperature assemblage (up to 2 mm). They are also more irregular and blocky in form, no longer exhibiting the dendritic habits of the replaced minerals. They occasionally show a deformation fabric expressed as folds and boudins of pseudotachylyte at the thin section scale, indicating a ductile blueschist facies overprint (Fig. 12a).

#### 4.7.2. Peridotite: pseudotachylyte

At the millimetre to micron scale the peridotite pseudotachylytes show great variability in composition and abundance of bulk matrix, glass and crystallisation products. Despite this variability, the microlites consistently comprise diopside, olivine and enstatite. As with the metagabbro, the peridotite fusion products can be divided into a high temperature quench assemblage and a lower temperature devitrification assemblage.

##### 4.7.2.1. Microlite assemblage in peridotite-hosted pseudotachylytes.

Olivine, diopside and enstatite occur as clusters of monomineralic blocky microlites (particularly olivine) or as dendritic complexes. Also common are larger, polymineralic laths and dendrites (Fig. 11). The interstitial material of the bulk matrix ranges is a variable mixture of olivine and enstatite and has an  $\text{H}_2\text{O}$  content ranging from 0 to 14.2 wt.%  $\text{H}_2\text{O}$ .

##### 4.7.2.2. Peridotite: devitrification and recrystallisation of pseudotachylytes.

Devitrification of glass and recrystallisation of the higher temperature minerals that quenched directly from the pseudotachylyte melt produce distinct assemblages. Typically the devitrified melt is characterised by the formation of microfibrillar clinocllore, serpentine and tremolite (Fig. 9). In contrast, pseudotachylyte that has completely recrystallised

comprises fine-grained ( $<50 \mu\text{m}$ ) granoblastic diopside, olivine and enstatite (Fig. 4).

## 5. Discussion

The microtextures analysed in this study are spatially and temporally associated with pseudotachylyte generation. The observed crystal-plastic phenomena that are considered to be causally linked to fusion and seismic failure include: dislocation creep/glide, deformation twinning, kinking, bending and ultracataclasis/melt formation (Figs. 6 and 13). The ultracataclasis observed in these rocks is unusual in that it contains angular comminuted wallrock minerals as well as ribbons and strings of minerals exhibiting syndeformational ductile features (Fig. 6). The interstitial areas of the ultracataclasis contain glassy pockets of preferentially melted hydrous minerals, e.g. tremolite and clinocllore. Together, these textures suggest that the wallrock minerals may have undergone power law creep-dominated deformation that reached seismic strain rates, to induce the heating and fusion of the wallrock that is characterised by the presence of pseudotachylyte in these rocks (John et al., 2009; Kameyama et al., 1999).

The quench products of the pseudotachylytes indicate initially very high temperatures ( $\sim 1600^\circ\text{C}$ ), followed by a return to blueschist to lawsonite-eclogite conditions ( $\sim 430^\circ\text{C}$ – $550^\circ\text{C}$ , 1.8–2.6 GPa) (Andersen and Austrheim, 2006; Ravna et al., 2010). When the pseudotachylytes devitrify or recrystallise, the resulting mineral assemblages (glaucophane, albite and epidote in the metagabbro and diopside, olivine, enstatite and clinocllore in the peridotite) indicate a high pressure, low temperature environment (Ravna et al., 2010).

### 5.1. Precursors to pseudotachylyte formation

To date, several mechanisms have been put forward to explain the initiation of intermediate-depth seismicity. They all share the commonality of being fundamentally dependent on precursory conditions (Green and Houston, 1995; John et al., 2009; Kelemen and Hirth, 2007). Therefore, we need to investigate in detail the evidence of any preserved pre-existing elements that may elucidate the sequence of events that culminate in the production of these high pressure pseudotachylytes. A close spatial relationship between pseudotachylyte formation and fabric development is observed in the host rocks. This is not a unique occurrence and has been noted by previous workers in other pseudotachylyte studies (Bestmann et al., 2011; Hobbs et al., 1986; Jin et al., 1998; Kim et al., 2010; Lin, 1994; Lund and Austrheim, 2003). Hobbs et al. (1986) were amongst the first to propose the possibility that in high pressure cases, pseudotachylyte and mylonite formation may be inter-related processes; suggesting that at the highest deformation rates pseudotachylyte would form, followed by cataclasis

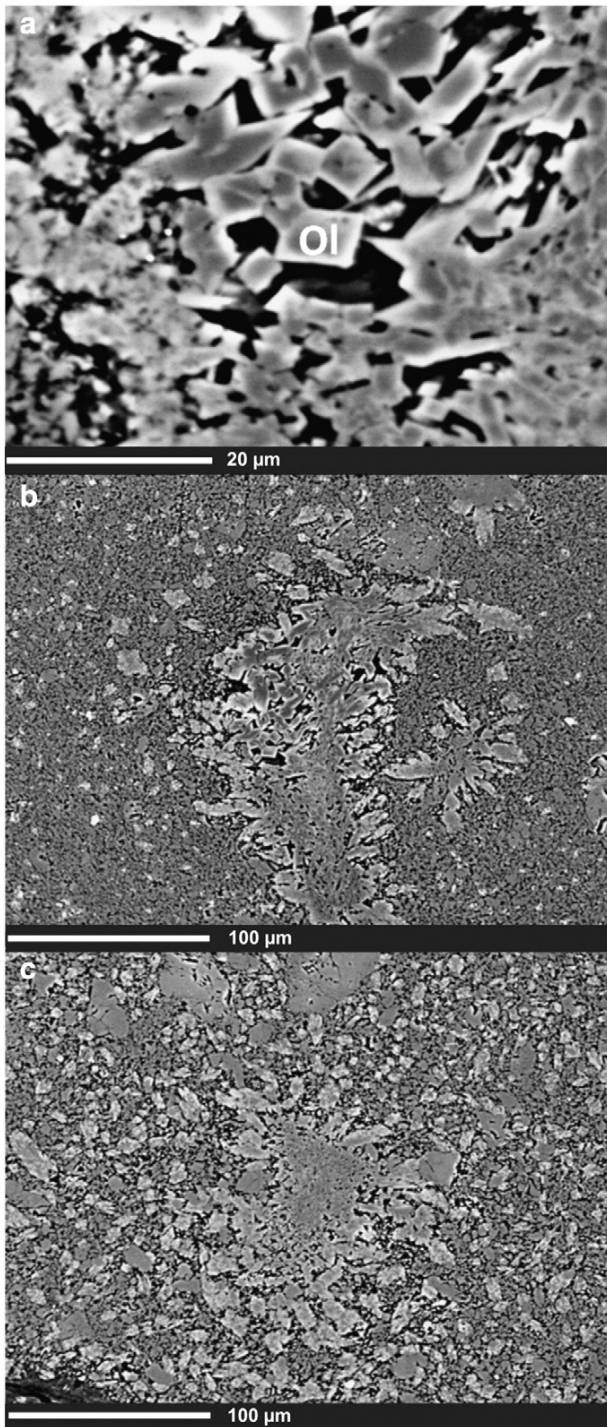


**Fig. 11.** BSE images showing the three principal types of crystallisation styles in peridotite hosted pseudotachylyte. Panel a shows blocky microlites of olivine surrounded by glass (black in images). The olivine crystals show strong Mg–Fe zoning from core to rim. Panel b shows pure olivine dendrites clustered in an aggregate with interstitial glass in a matrix of blocky olivine crystals and complex laths of diopside (light grey) and olivine (darker grey). (c) This image shows an aggregate of crystallised material in the centre. Close inspection shows that the aggregate is composed of three minerals; enstatite (darkest grey), olivine (mid-grey) and diopside (light grey). The aggregate is dominated by these complex, tri-mineralic dendrites. The black interstitial matrix in all three images was analysed to be a variably Al-, H<sub>2</sub>O-enriched glassy material.

and then fabric development, potentially culminating in mylonite at the lowest deformation rates.

Incipient fabric development prior to and after pseudotachylyte formation has been observed (Figs. 6d, 12a, 14). Detailed EBSD analysis of a peridotite fault section from the same field area shows that the wallrock minerals are exposed to increasing strain towards pseudotachylyte fault veins. The wallrock has undergone recrystallisation to form an incipient lattice preferred orientation (LPO) prior to and/or during fault vein development (Silkose, 2013). Crystal plastic deformation such as folding, boudinaging, annealing and foliation development occurring after fault vein formation has been observed within veins and the associated wallrock (Figs. 6d, 12, 14). The time lapse between pseudotachylyte generation and fabric development (before and after) is unknown. However, the simplest explanation of the observations involves: recrystallisation in the wallrock with increasing strain towards vein boundaries as well as rotation of elongate wallrock clasts into parallelism with developing fault vein boundaries. Continued shearing (Fig. 6) occurs after displacement and fusion have taken place, at which point the fault zone had cooled enough to crystallise glaucophane (in the metagabbro) and clinocllore (in the peridotite). We suggest the following sequence of events to explain our observations:

The majority of wallrock material for both metagabbro and peridotite is coarse-grained and partially deformed due to previous events. As a result the wallrock grains will likely contain numerous crystallographic imperfections that can be exploited when in the right orientation in the stress field to form the loci of fault nucleation and initial fusion due to low temperature creep, followed by power law creep.

1. The fault wallrocks developed a damage zone with synchronous recrystallisation and an increasing strain-gradient towards the future fault plane as also observed by Silkose (2013).
2. Anisotropic wallrock fragments have rotated so that long axes become parallel with the developing slip surface.
3. Deformed wall-rock fragments become entrained, as survivor clasts in the pseudotachylyte melt and their deformation is associated with the shearing event that produced the melt. Some undergo near complete to complete fusion.
4. In some veins, shearing and displacement continued after fusion, locally attested to by deformed and recrystallised pseudotachylyte.
5. Pseudotachylyte and fault damage zones cooled down sufficiently to devitrify or recrystallise to glaucophane (in metagabbro) and clinocllore (in peridotite).

It is possible that at lower deformation rates foliations may develop in the pseudotachylyte and wallrock between major faulting events.

Based on the observations and sequence of events presented above, we suggest the following model for pseudotachylyte generation:

The metagabbro and peridotite were mostly coarse-grained rocks, but both host rocks had structural and mineralogical heterogeneities inherited from earlier events. During subduction-related deformation, pre-existing zones with numerous crystallographic imperfections at favourable orientation relative to the new stress field become the loci of enhanced deformation (Jessell and Lister, 1991; Kameyama et al., 1999; Sibson, 1980). Low temperature and subsequent power law creep, induced by seismic strain rates eventually gave rise to fusion. It is possible that several loci in the same orientation underwent contemporaneous strain-induced fusion. These individual melt spots may in turn have linked up to form primitive fault planes. Stick-slip action along such plane will be preferentially activated for further slip and facilitate comminution and fusion. As the stress is released by comminution, displacement and fusion, the temperature of the fault and damage zone will remain elevated until the stress has dropped below the strength of the transient melted material of the fault. Thereafter, heat is dissipated by diffusion beyond the cooling vein and damage zone to facilitate crystallisation of the wallrocks. The delicate preservation of quench textures in pseudotachylytes suggests negligible post-quenching

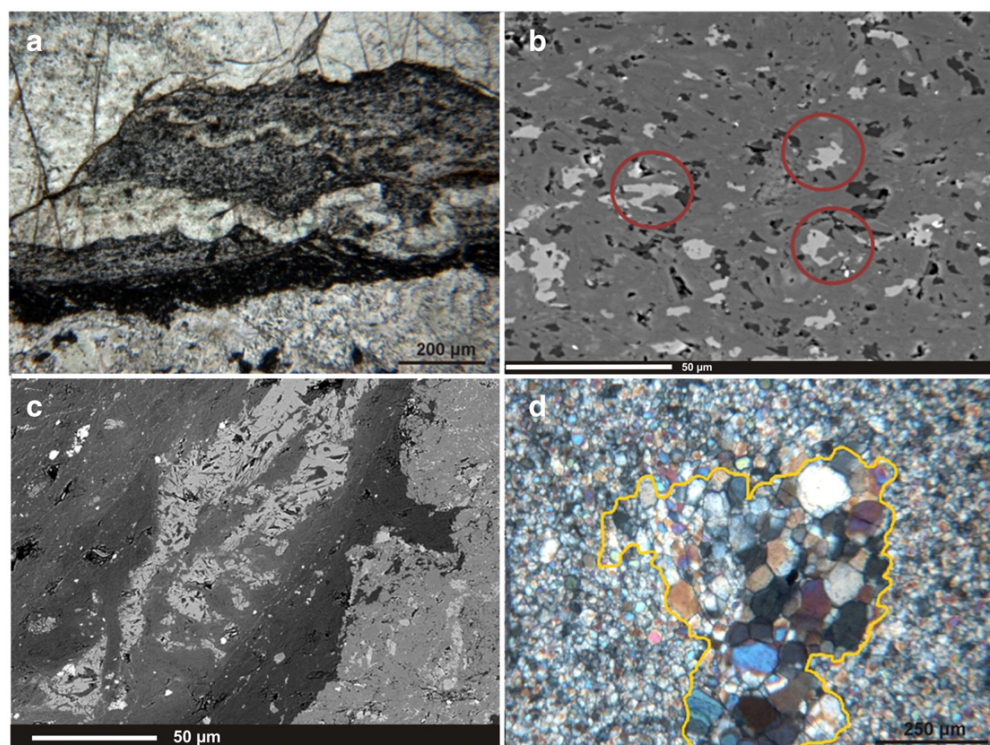


**Fig. 12.** Micrographs and BSE images showing the various recrystallisation textures in pseudotachylytes from both host rocks. Panels a and b metagabbro pseudotachylyte (a) from the same thin section sample as panel b, only at a lower magnification. (a) Folding of the recrystallised pseudotachylyte. The microlites in panel b are blocky, no longer the dendritic forms shown in previous examples. EPMA analyses show the mineral assemblage to be glaucophane, sphene (light grey crystals), albite (dark grey crystals) and epidote (darkest grey). The crystals are subhedral and deformed and aligned in a subtle fabric due to folding, as shown in panel a. Images c and d: peridotite–pseudotachylyte. (c) A devitrified pseudotachylyte matrix that has an ultrafine (<1 µm) of clinocllore composition. The matrix is not recrystallised as pristine quenched dendrites of diopside are observed (light grey dendrites (c) and stretched out, deformed clasts are evident along with zoning/colour banding in the vein that are preserved. Panel d shows a recrystallised matrix; the yellow line indicates the form of a recrystallised wallrock aggregate that was entrained into the pseudotachylyte. The surrounding fine-grained material comprises olivine and enstatite clasts which have replaced earlier dendrites and upon stage rotation under the microscope, shadows of now replaced dendrites can be observed. The clasts in this photomicrographs are annealed, forming a granoblastic texture and show no evidence of deformation. It is important to note that peridotite pseudotachylyte recrystallises to a harzburgitic composition.

deformation in most of the pseudotachylyte veins except in those areas where later regional deformation and metamorphism are penetrative.

### 5.1. Possible influence of grain size on pseudotachylyte formation

The grain size of both the metagabbro and the peridotite ranges from approximately 20 µm–260 µm. The principal deformation mechanism of the wallrock material and entrained survivor clasts that have been sheared and kinked but show no evidence of crystallographic recovery prior to pseudotachylytic fusion is interpreted to be dislocation creep/glide. EBSD analysis in a recent study indicates that the wallrock encountered rapidly increasing strain towards the pseudotachylyte boundaries, with weakly developed LPOs (Silkose, 2013). The incipient LPO development could be due to localised stresses in the rock being accommodated by high dislocation densities in different grains (Branlund et al., 2000; Kameyama et al., 1999; Newman et al., 1999). EBSD analysis by Silkose (2013) and intracrystalline microtextural observations (Figs. 3) in this study suggest dislocation creep as a possible dominant deformation mechanism associated with pseudotachylyte formation. If this is the case then there would be little grain size reduction through dynamic recrystallisation associated with the instability as diffusion creep would be a secondary deformation mechanism (Kameyama et al., 1999; Kelemen and Hirth, 2007). In finer-grained material (grain-size approximately 20 µm) strain has been accommodated by grain boundary sliding as opposed to intra-grain deformation; grain boundaries

associated with the pseudotachylyte are aligned and grains appear squamous in shape as opposed to equant (Fig. 4).

It appears that higher volumes of melt are formed in the coarser-grained host rock. Of course, the current fault and injection vein thicknesses are not expected to be an exact indication of melt volume. However, taking vein dilation, draining and deformation into account the melt volume produced by coarse-grained rock relative to fine-grained rock is orders of magnitude greater; refer to Fig. 2a vs Fig. 4 where an outcrop scale image of an average fault vein is compared to the largest fault vein observed in the finest grained host rock, seen in thin section as it is so small. This may correspond with power law creep as a principal deformation mechanism as coarser-grained material would be easier to deform than finer-grained material. Coarser grains can accumulate more dislocations and higher dislocation densities in local areas of slip than can finer grains suggesting a greater potential for localised heating (Kameyama et al., 1999). Images of pseudotachylyte in the finer-grained host rock (Fig. 4) suggest that grain boundary sliding occurs preferentially over intra-grain deformation to resolve the applied stress.

Furthermore, our geochemical results show that grain size influences melt composition such that the bulk composition of a pseudotachylyte derived from a fine-grained host rock will better approximate fusion akin to that of an equilibrium melt (this is due to melt formation occurring primarily along grain boundaries), whereas in pseudotachylyte derived from a coarser-grained host, the bulk melt composition tends to reflect wholesale fusion of individual minerals such as olivine or diopside.

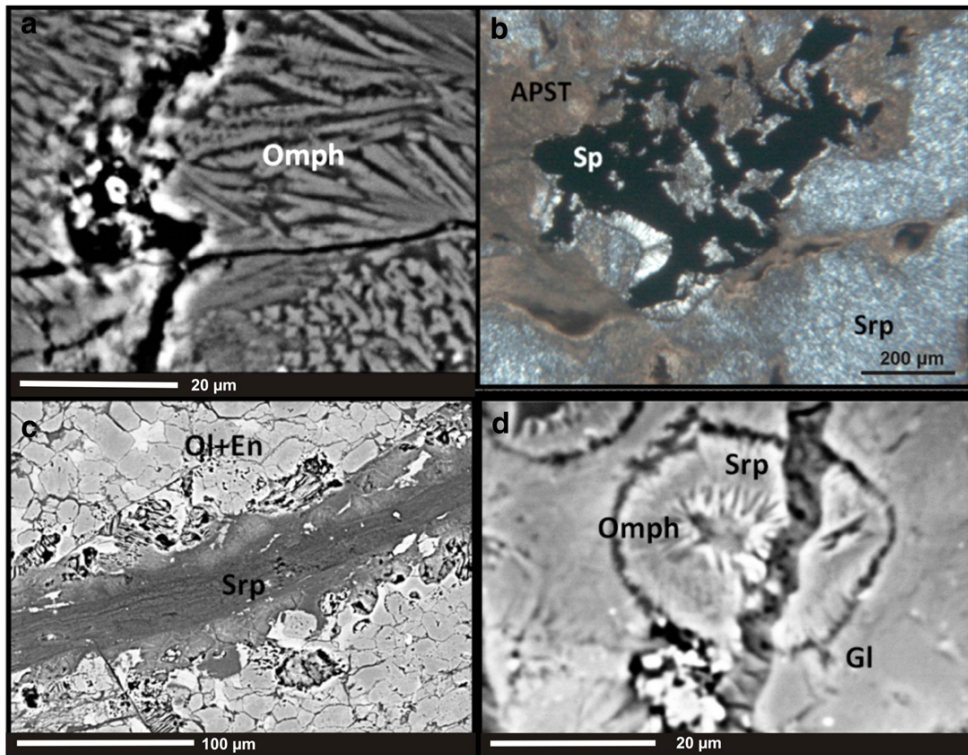


**Fig. 13.** BSE images and a photomicrograph (b) of hydrated/alternated pseudotachylyte. In all images serpentine and associated spinel is the principal late alteration mineral (as is the case in both host rocks), but late epidote and actinolite are also present in the metagabbro. These images show how serpentinisation destroys the delicate textures associated with the pseudotachylyte forming event (dendrites and vein boundaries) and bleaches the pseudotachylyte, removing magnesium. (a) A black vein crosscuts a pristine pseudotachylyte matrix of omphacite in a metagabbro. The boundaries of the vein can be seen on BSE to have bleached the matrix enriching it in Fe. (b) Serpentinised peridotite pseudotachylyte where all microscopic crystallisation textures have been obliterated. (c) A late serpentine vein cuts through a recrystallised peridotite pseudotachylyte. Microfibres of serpentine can be seen eroding the fine-grained granoblastic texture. (d) Serpentine vein crosscutting spherulitic omphacite in an otherwise glassy pseudotachylyte matrix. Ol: olivine, En: enstatite, Srp: serpentine, Omph: omphacite, Gl: glass, Sp: spinel APST: altered pseudotachylyte.

Grain size reduction adjacent to vein boundaries was observed from the outcrop scale to the micron scale. Microtextural relationships suggest that this change in grain size is a feature contemporaneous with pseudotachylyte generation and is due to intense shearing along the fault surface, whereby the heat released by shearing facilitates recrystallisation and the shearing itself induces the re-orientation of wallrock clasts and/or their comminution. This is in contrast with the results of Kelemen and Hirth (2007) and John et al. (2009) where a pre-existing fine-grained zone in the host rock was proposed in order to provide a nucleation site for shear instabilities to take place.

## 5.2. Present model compared to previous mechanisms

The Corsican pseudotachylytes contain up to 15 wt.% H<sub>2</sub>O. This coupled with the large melt volumes produced by these events, apparently precludes dehydration embrittlement as a mechanism for the observed paleofaults. There is no evidence that free water or other fluids were available before faulting. Previous work by Green (1973), Jung et al. (2004) and Kirby et al. (1991), indicates that dehydration embrittlement is related to a solid-state monomineralic reaction. Its occurrence in polymineralic materials such as those studied here has to our knowledge not been tested experimentally. Instead we suggest that the high

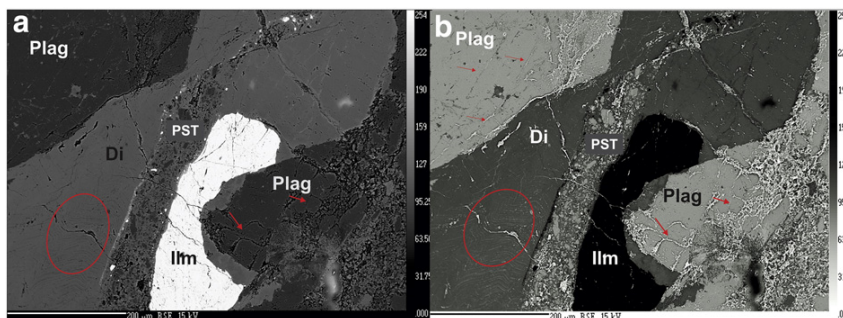


**Fig. 14.** BSE image of metagabbro with several generations of pseudotachylyte. The image on the left is the original BSE image and the image on the right has been inverted to highlight some features. The red circle highlights kinkbanding in wallrock diopside (Di). A minute fault vein has formed within a kink plane. The arrows indicate preferential fusion in the plagioclase (Plag) along certain planes. The white clast in the centre is ilmenite (Ilm).

temperature deformation related to local shear-heating was more significant for failure than a solid-state dehydration reaction weakening. Previously published shear heating models (John et al., 2009; Kelemen and Hirth, 2007) are not perfect fits either. Both these models prescribe precursory mylonites or fine-grained zones that act as strain concentrators in order to initiate self-localisation. Our observations from the rocks in Corsica however, indicate that, despite various differences in the host rocks, seismic faulting and fusion took place regardless of grain size, rock fabric or composition. The only discernible restriction on mineralogy is fracture toughness; minerals must have a shear yield strength great enough to allow for a sufficiently large stress build-up (Spray, 1992), which explains why no pseudotachylytes occur in the serpentinites surrounding the peridotite and metagabbro blocks. A non-quantified and speculative option may be that the rheological behaviour of rocks traditionally predicted at high pressure may not be simply constrained by visco-elasticity or Von Mises Criterion as suggested by (Mancktelow, 2006).

## 6. Conclusions

Both shear instabilities and dehydration reactions are thermally activated processes. However, the activation of thermal instability is derived from local rheological heterogeneities that provide a viscosity contrast in the host rock material at sufficiently high stresses that it behaves as a non-linear viscoelastic material (Braeck and Podladchikov, 2007; John et al., 2009; Kameyama et al., 1999; Ogawa, 1987). Conversely, dehydration embrittlement is induced by warming of the previously hydrated slab making it dependent on the presence of pre-existing hydrous mineralogy and an efficiently warmed slab. In addition, there is no evidence in the petrographic data to support the hypothesis of a dehydrated precursor to pseudotachylyte nucleation. This is not to say that dehydration embrittlement does not occur; it may well occur in the serpentinite enclosing the blocks of peridotite and metagabbro. The results from this study suggest that these pseudotachylytes produced at high pressure and seismic strain rates, in different host rocks, with different degrees of hydration, may have been generated by a high temperature crystal-plastic shear process. Detailed petrographic analysis suggests that low temperature and power law creep may play dominant roles in producing thermal instabilities and high pressure pseudotachylytes. Deformation of wallrock grains at the boundary of fault veins results in the formation of subtle LPOs in olivine grains and grain size reduction due to comminution (Silkose, 2013). These features form at the onset of and during pseudotachylyte generation, not before, and they are not the precursory elements that form the nucleation sites of pseudotachylyte generation in previous models (John et al., 2009; Kelemen and Hirth, 2007). Future work to test this interpretation might involve high pressure fusion experiments, numerical modelling, detailed EBSD on more complex fault veins and geochemical analysis.

## Acknowledgements

This work is supported Wits University, the National Research Foundation and the Mellon Foundation as well as the Research Council of Norway through its Centres of Excellence funding scheme, project number 223272 (CEED). Thanks to Prof. M. Zolensky of NASA for assisting with EBSD and XRD synchrotron analysis of some samples.

## References

Agard, P., Monié, P., Jolivet, L., Goffé, B., 2002. Exhumation of the Schistes Lustrés complex: in situ laser probe  $^{40}\text{Ar}/^{39}\text{Ar}$  constraints and implications for the Western Alps. *J. Metamorph. Geol.* 20, 599–618.

- Andersen, T., Austrheim, H., 2006. Fossil earthquakes recorded by pseudotachylytes in mantle peridotite from the Alpine subduction complex of Corsica. *Earth Planet. Sci. Lett.* 242, 58–72.
- Austrheim, H., Andersen, T.B., 2004. Pseudotachylytes from Corsica: fossil earthquakes from a subduction complex. *Terra Nova* 16, 193–197.
- Austrheim, H., Boundy, T., 1994. Pseudotachylytes generated by seismic faulting and eclogitization of the deep crust. *Science* 265, 82–83.
- Beccaluva, L., Ohnenstetter, D., Ohnenstetter, M., Venturelli, G., 1977. The trace element geochemistry of Corsican ophiolites. *Contrib. Miner. Pet.* 64, 11–31.
- Bestmann, M., Pennacchioni, G., Frank, G., Göken, M., de Wall, H., 2011. Pseudotachylyte in muscovite-bearing quartzite: coseismic friction-induced melting and plastic deformation of quartz. *J. Struct. Geol.* 33, 169–186.
- Braeck, S., Podladchikov, Y., 2007. Spontaneous thermal runaway as an ultimate failure mechanism of materials. *Phys. Rev. Lett.* 98.
- Branlund, J.M., Kameyama, M.C., Yuen, D.A., Kaneda, Y., 2000. Effects of temperature-dependent thermal diffusivity on shear instability in a viscoelastic zone: implications for faster ductile faulting and earthquakes in the spinel stability field. *Earth Planet. Sci. Lett.* 182, 171–185.
- Green, D.H., 1973. Experimental melting studies on a model upper mantle composition at high pressure under water-saturated and water-undersaturated conditions. *Earth Planet. Sci. Lett.* 19, 37–53.
- Green, H.W., Houston, H., 1995. The mechanics of deep earthquakes. *Annu. Rev. Earth Planet. Sci.* 23, 169–213.
- Hacker, B.R., 2003. Subduction factory 2. Are intermediate-depth earthquakes in subducting slabs linked to metamorphic dehydration reactions? *J. Geophys. Res.* 108.
- Hobbs, B.E., Ord, A., Teyssier, C., 1986. Earthquakes in the ductile regime? *Pure Appl. Geophys. J. R. Astron. Soc.* 124, 309–336.
- Jessell, M.W., Lister, G.S., 1991. Strain localization behaviour in experimental shear zones. *Pure Appl. Geophys.* 137, 421–438.
- Jin, D., Karato, S., Obata, M., 1998. Mechanisms of shear localization in the continental lithosphere: inference from the deformation microstructures of peridotites from the Ivrea zone, northwestern Italy. *J. Struct. Geol.* 20, 195–209.
- John, T., Medvedev, S., Rüpke, L.H., Andersen, T.B., Podladchikov, Y.Y., Austrheim, H., 2009. Generation of intermediate-depth earthquakes by self-localizing thermal runaway. *Nat. Geosci.* 2, 137–140.
- John, T., Schenk, V., 2006. Interrelations between intermediate-depth earthquakes and fluid flow within subducting oceanic plates: constraints from eclogite facies pseudotachylytes. *Geology* 34, 557.
- Jolivet, L., 1993. Extension of thickened continental crust, from brittle to ductile deformation: examples from Alpine Corsica and Aegean Sea. *Ann. Geophys.* 36, 139–153.
- Jung, H., Green, H.W., Dobrzhinetskaya, L., 2004. Intermediate-depth earthquake faulting by dehydration embrittlement with negative volume change. *Nature* 428, 545–549.
- Kameyama, M., Yuen, D.A., Karato, S.-I., 1999. Thermal-mechanical effects of low-temperature plasticity (the Peierls mechanism) on the deformation of a viscoelastic shear zone. *Earth Planet. Sci. Lett.* 168, 159–172.
- Kanamori, H., Anderson, D., Heaton, T., 1998. Frictional melting during the rupture of the 1994 Bolivian earthquake. *Science* 279, 839–842.
- Kelemen, P.B., Hirth, G., 2007. A periodic shear-heating mechanism for intermediate-depth earthquakes in the mantle. *Nature* 446, 787–790.
- Kim, J.-W., Ree, J.-H., Han, R., Shimamoto, T., 2010. Experimental evidence for the simultaneous formation of pseudotachylyte and mylonite in the brittle regime. *Geology* 38, 1143–1146.
- Kirby, S., Durham, W., Stern, L., 1991. Mantle phase changes and deep earthquake faulting in subducting lithosphere. *Science* 252, 216–225.
- Lin, A., 1994. Glassy pseudotachylyte veins from Fuyun fault zone, northwest China. *J. Struct. Geol.* 16, 71–83.
- Lund, M., Austrheim, H., 2003. High-pressure metamorphism and deep-crustal seismicity: evidence from contemporaneous formation of pseudotachylytes and eclogite facies coronas. *Tectonophysics* 372, 59–83.
- Mancktelow, N.S., 2006. How ductile are ductile shear zones? *Geology* 34, 345.
- Merlet, C., 1994. An accurate computer correction program for quantitative electron microprobe analysis. *Mikrochim. Acta* 114/115, 363–376.
- Mohn, G., Manatschal, G., Muntener, O., Beltrando, M., Masini, E., 2009. Unravelling the interaction between tectonic and sedimentary processes during lithospheric thinning in the Alpine Tethys margins. *Int. J. Earth Sci.* 99, S75–S101.
- Newman, J., Lamb, W., Drury, M.R., Vissers, R.L., 1999. Deformation processes in a peridotite shear zone: reaction-softening by an  $\text{H}_2\text{O}$ -deficient, continuous net transfer reaction. *Tectonophysics* 303, 193–222.
- Ogawa, M., 1987. Shear instability in a viscoelastic material as the cause of deep focus earthquakes. *J. Geophys. Res.* 92, 13801–13810.
- Ravna, E.J.K., Andersen, T.B., Jolivet, L., De Capitani, C., 2010. Cold subduction and the formation of lawsonite eclogite – constraints from prograde evolution of eclogitized pillow lava from Corsica. *J. Metamorph. Geol.* 28, 381–395.
- Sibson, R.H., 1980. Transient discontinuities in ductile shear zones. *J. Struct. Geol.* 2, 165–171.
- Silkose, P., 2013. Microstructure of Ultramafic Pseudotachylyte From Alpine Corsica – Insights Into Earthquakes in Mantle Lithosphere. Unpublished Master thesis: University of Oslo, Norway.
- Spray, J., 1992. A physical basis for the frictional melting of some rock-forming minerals. *Tectonophysics* 204, 201–221.
- Vitale Brovarone, Groppo, Hetenyi, Compagnoni, R., Malavieille, 2011. Coexistence of lawsonite-bearing eclogite and blueschist: phase equilibria modelling of Alpine Corsica metabasalts and petrological evolution of subducting slabs. *J. Metamorph. Geol.* 29, 583–600.

## Exhumation of high-pressure rocks beneath the Solund Basin, Western Gneiss Region of Norway

B. R. HACKER,<sup>1</sup> T. B. ANDERSEN,<sup>2</sup> D. B. ROOT,<sup>1</sup> L. MEHL,<sup>1</sup> J. M. MATTINSON<sup>1</sup>  
AND J. L. WOODEN<sup>3</sup>

<sup>1</sup>Department of Geological Sciences, University of California, Santa Barbara, CA 93106–9630, USA  
(hacker@geology.ucsb.edu)

<sup>2</sup>Department of Geology, University of Oslo, PO Box 1047 Blindern 0316, Oslo, Norway

<sup>3</sup>U.S. Geological Survey, Menlo Park, CA 94025, USA

**ABSTRACT** The Solund–Hyllestad–Lavik area affords an excellent opportunity to understand the ultrahigh-pressure Scandian orogeny because it contains a near-complete record of ophiolite emplacement, high-pressure metamorphism and large-scale extension. In this area, the Upper Allochthon was intruded by the *c.* 434 Ma Sogneskollen granodiorite and thrust eastward over the Middle/Lower Allochthon, probably in the Wenlockian. The Middle/Lower Allochthon was subducted to *c.* 50 km depth and the structurally lower Western Gneiss Complex was subducted to eclogite facies conditions at *c.* 80 km depth by *c.* 410–400 Ma. Within < 5–10 Myr, all these units were exhumed by the Nordfjord–Sogn detachment zone, producing shear strains > 100. Exhumation to upper crustal levels was complete by *c.* 403 Ma. The Solund fault produced the last few km of tectonic exhumation, bringing the near-ultrahigh-pressure rocks to within *c.* 3 km vertical distance from the low-grade Solund Conglomerate.

**Key words:** eclogite; exhumation; Norway; Solund; ultrahigh pressure.

### INTRODUCTION

The Norwegian Caledonides are one of the best places to study the exhumation of high-pressure (HP) and ultrahigh-pressure (UHP) rocks because of excellent exposure across the vast Western Gneiss Region (WGR), which contains spectacular coesite-bearing eclogites, garnet peridotites, and coesite- and diamond-bearing gneisses (Cuthbert *et al.*, 2000; Wain *et al.*, 2000) (Fig. 1). Salient incompletely answered questions about the Norwegian Caledonian UHP rocks include the following.

(1) How and when did the HP–UHP metamorphism occur? Was there more than one HP or UHP event? Was it the result of an arc–continent or continent–continent collision? For many years, the palaeomagnetic record of collision at *c.* 425 Ma (Torsvik, 1998), the pioneering Sm/Nd geochronology that dated HP metamorphism at 425 Ma (Griffin & Brueckner, 1980), and the stratigraphic record on the island of Atløy implying ophiolite emplacement in the Wenlockian (Andersen *et al.*, 1990), were interpreted as indicating that the UHP metamorphism occurred during a continental collision. The subsequent realization that the age of the UHP event is 410–400 Ma (Tucker, in Lutro *et al.*, 1997; Mearns, 1986; Mørk & Mearns, 1986; Terry *et al.*, 2000) indicates that the orogeny spanning collision and HP–UHP metamorphism may have lasted for 25 Myr. Moreover, the material emplaced onto the Caledonian margin of Baltica includes not only

telescoped continental margin rocks, but also ophiolites, outboard Baltica crystalline and sedimentary rocks, and Laurentian continental rocks. Constraining the time that these various units were emplaced relative to the time of UHP metamorphism is still an important issue.

(2) How did the exhumation occur? Was it syn-collisional or post-collisional? Did the subducted plate simply roll back as a semirigid sheet, did it rise buoyantly through the upper plate, or was it thrust onto the Baltica margin accompanied by higher-level extension? A significant part of the exhumation of the HP–UHP rocks can be attributed to an array of regionally extensive normal faults and extensional detachments, of which the Nordfjord–Sogn detachment zone (NSDZ) is the most important (Andersen & Jamtveit, 1990). The NSDZ is a Caledonian amphibolite- to greenschist facies shear zone commonly capped by younger brittle faults that were reactivated in the Permian and Late Jurassic (Eide *et al.*, 1997; Norton, 1986). The age of the ductile shearing is not well known because, despite concerted <sup>40</sup>Ar/<sup>39</sup>Ar dating (e.g. Andersen, 1998), most of the movement on the ductile zone occurred at temperatures in excess of hornblende closure to Ar diffusion. Thus, constraining the time of motion along the ductile NSDZ is important to constraining the exhumation history.

Both of these two general problems can be addressed in the Solund–Hyllestad–Lavik area of the WGR. The Solund–Hyllestad–Lavik area is noteworthy because it

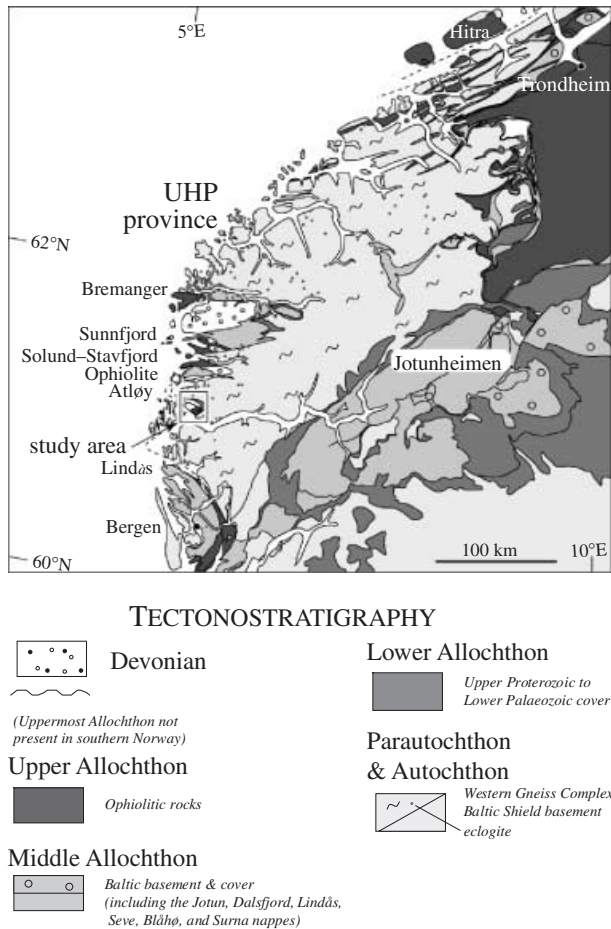


**Fig. 1.** Geology of southern Norway. Heavy dark lines show major extensional structures and UHP area is ruled.

contains a record of ophiolite emplacement, near-UHP metamorphism, and large-scale displacement on the NSDZ and the overlying Solund fault. The purpose of this paper is to document the emplacement and exhumation histories of high-pressure rocks in this key area.

**SCANDINAVIAN CALEDONIDES**

The Scandinavian Caledonides are 1700 km long, comparable to the length of the Himalaya. They are a type example of an orogen composed of thin (= 10 km), far-traveled (= 300 km), and areally extensive (= 50 000 km<sup>2</sup>) thrust sheets (Andersen, 1998). The SE-directed emplacement of these thrust sheets is conventionally explained as the result of continent–continent collision between Baltica (including Norway) and Laurentia (including Greenland). The nappes and thrust sheets are conventionally lumped into structurally distinct entities separated by regionally extensive faults: autochthon/parautochthon, Lower Allochthon, Middle Allochthon, Upper Allochthon and Uppermost Allochthon (Roberts & Gee, 1985).

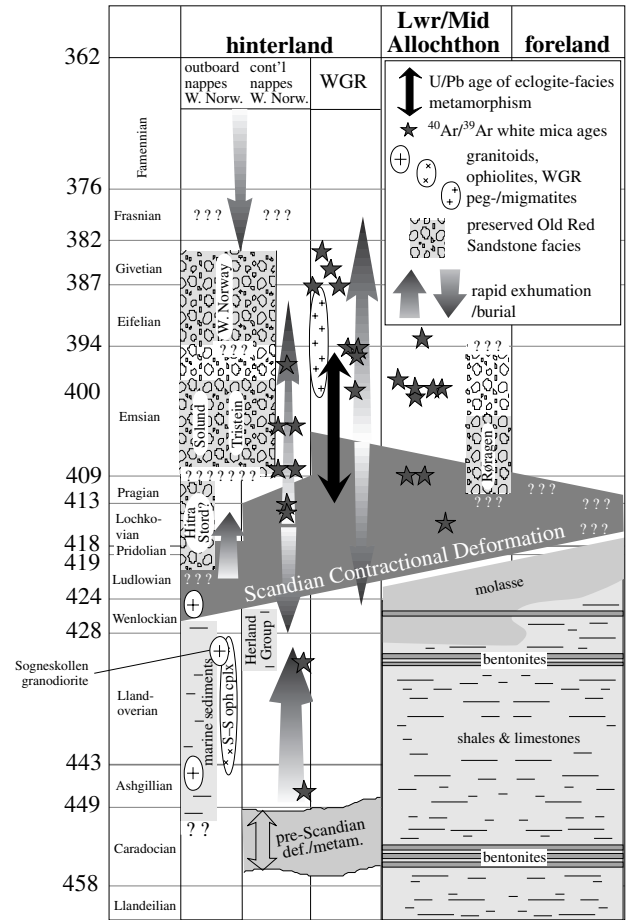


**Fig. 2.** Timeline of tectonic events in southern Norway. Time-scale based on (Tucker *et al.*, 1998; Tucker & McKerrow, 1995). Beginning of Scandian deformation signaled by emplacement of Solund–Stavfjord ophiolite complex (S–S oph cplx), deposition of Herland Group, and molasse sedimentation in foreland. Switch from contraction to extension at deep levels heralded by white-mica ages in the Western Gneiss Region (WGR).

**Geological Units**

The autochthon/parautochthon is the west-facing passive margin of Baltica, which consists of Archean to Proterozoic crystalline basement overlain by Upper Proterozoic rift sediments, Cambrian to Wenlockian shelf sediments, and Ludlovian–Pridolian molasse (Fig. 2) (Bockelie & Nystuen, 1985). West of the autochthon, and separated from it horizontally by as little as 20 km of overlying allochthonous units, is the Western Gneiss Complex (WGC) (Milnes *et al.*, 1997), which contains HP and UHP eclogites; the UHP eclogites are found along the coast north of 62°N, whereas HP eclogites crop out NE, E, SE and S. The S and SE part of the WGC is correlated with the Baltic shield because both have basement and sedimentary cover of similar rock types and ages (Gee *et al.*, 1994; Milnes *et al.*, 1997; Skår, 1998), but whether the WGC is nearly autochthonous or has been displaced horizontally a significant distance is unknown.

The Lower Allochthon is composed chiefly of sedimentary rocks correlated with the sedimentary cover of the autochthon that was thrust eastward over the autochthon (Hossack *et al.*, 1985). Orthogneisses overlain by unfossiliferous feldspathic sandstones are characteristic of the Middle Allochthon (including the Jotun, Dalsfjord, Särvi and Sætra nappes) and the Seve/Blåhø/Surma

nappes of the Upper Allochthon. Strong similarities between these sialic nappes and the Lower Allochthon and autochthon imply original contiguity (Gee & Zachrisson, 1979), hence the sialic nappes are generally interpreted as Baltica crust or transitional continental/oceanic crust (Seve/Blåhø/Surna) that lay outboard of the WGC (Milnes *et al.*, 1997) or as a microcontinent (Andersen & Andresen, 1994).

The Upper Allochthon includes predominantly intraoceanic arc and marginal basin assemblages (Stephens & Gee, 1985). Its oldest plutonic and volcanic rocks have zircon ages in the range of 497–472 Ma. Intercalated and overlying sediments have late Arenigian–early Llanvirnian (*c.* 470 Ma) fossils of Baltica, Laurentian, or mixed Laurentian–Baltica affinity, implying local geographic separation from Baltica (Pedersen *et al.*, 1992; Sturt *et al.*, 1991). Sr isotopes in stitching plutons reveal that the Karmøy and Lykling ophiolites were emplaced onto continental crust by 474 Ma, and the Vågåmo Ophiolite was faulted onto the arenaceous Heidal Series before deposition of the overlapping late Arenigian–early Llanvirnian Otta Conglomerate (Sturt *et al.*, 1991). The Heidal Series rests depositionally on crystalline Baltica basement, mandating ophiolite emplacement onto the Baltica margin (Sturt *et al.*, 1991).

These Late Cambrian–Early Ordovician ophiolites are intruded/overlain by Ordovician to Silurian arc plutonic and volcanic rocks, Ashgillian (449–443 Ma) limestones, Llandoveryan (443–428 Ma) black shales and turbidites and volcanic rocks of unknown age (cf. Andersen & Andresen, 1994). The Ashgillian–Llandoveryan sedimentary rocks are similar to the Lower Allochthon, implying proximity to Baltica (Stephens & Gee, 1985). The Sulitjelma (437 ± 2 Ma) and Solund–Stavfjord (443 ± 3 Ma) ophiolites may have formed exclusively at this time. Many of these oceanic rocks, plus the Uppermost Allochthon (ascribed to Laurentia) and the westernmost edge of the WGC, are intruded by a suite of gabbroic through granitic plutons and dykes ranging in age from 443 to 432 Ma. Two features suggest that this intrusive event predated emplacement of the oceanic nappes onto the Baltica margin: (i) intrusions of this age are absent within all units structurally below the oceanic nappes and above the parautochthon; and (ii) plutons piercing the Uppermost Allochthon have Sr initial ratios = 0.706, implying crustal contamination, whereas plutons piercing the oceanic nappes have Sr initial ratios < 0.706, implying that they did not interact with the continental rocks that currently underlie the oceanic nappes (references listed below).

### Allochthon emplacement and extension history

Initial emplacement of the allochthons onto the Baltica craton can be constrained as Wenlockian (428–423 Ma) by several criteria (Fig. 2) (Greiling *et al.*, 1998). (i) On the island of Atøy, the Wenlockian Herland Group was deposited during emplacement of the Solund–Stavfjord ophiolite on Middle Allochthon basement and cover (Dalsfjord Suite and Høyvik Group) (Andersen *et al.*, 1998; Andersen & Jamtveit, 1990; Andersen *et al.*, 1990). (ii) As noted above, 443–432 Ma plutons have Sr isotopic ratios and a spatial distribution that suggest that their intrusion predates allochthon emplacement. (iii) The youngest sedimentary rocks in the Lower Allochthon are Wenlockian (Bassett, 1985), requiring that the faults bounding the Lower Allochthon be no older than Wenlockian. (iv) The youngest sedimentary rocks in the Upper Allochthon are upper Llandoveryan (*c.* 430 Ma), and these are overlain by a thick turbiditic succession that may stretch into the Wenlockian (Bassett, 1985), requiring that the faults bounding the Upper Allochthon be no older than upper Llandoveryan. (v) The absence of post-Wenlockian strata throughout the allochthons, with the exception of the extension-related Late Silurian (?) to Middle Devonian continental basins, implies ongoing tectonism. (vi) The transition from marine carbonate platform to continental fluvial molasse sedimentation in the foreland took place in the latest Wenlockian (Fig. 2). (vii) Similarities in the 420–430 Ma palaeomagnetic poles for Baltica, Scotland and North America imply that Baltica collided, probably obliquely, with Laurentia at this time (Torsvik, 1998). (viii) The southward

transgression of flysch from Laurentia (Scotland) onto Avalonia (S Ireland) also indicates a late Llandoveryan–early Wenlockian continental collision (Soper *et al.*, 1992).

Toward the end of the Scandian orogeny (Fig. 2), Devonian sedimentary rocks were deposited unconformably on the Lower, Middle and Upper Allochthons (Norton *et al.*, 1987; Séguret *et al.*, 1989; Séranne & Séguret, 1987). Fossils within these basins are Ludlovian(?)–Pridolian through Emsian–Eifelian (Siedlecka, 1975) or possibly upper Llandoveryan–lower Wenlockian on Hitra, Lower Devonian in the Røragen basin, and Ludlovian through Pridolian(?) in the Oslo graben (see summaries in Bockelie & Nystuen, 1985; Steel *et al.*, 1985). The sedimentation in and structure of the western Norway basins were controlled by an early system of normal and strike-slip faults (Andersen, 1998; Cuthbert, 1991; Osmundsen & Andersen, 2001; Osmundsen *et al.*, 1998).

Following their emplacement onto the Baltica continental margin, the Caledonide thrust sheets were reworked by a major extensional event that resulted most significantly in collapse of the thrust sheets and exhumation of eclogites in the WGC. The best-known extensional structure is the Nordfjord–Sogn detachment zone (NSDZ). The NSDZ carried the Middle and Upper Allochthons and overlying Devonian sedimentary rocks in the hanging wall down to the west over eclogite-bearing gneisses of the WGC in the footwall (Norton, 1987). The horizontal displacement on the NSDZ is at least 70 km, but even allowing for a considerable vertical shortening component in the footwall (Andersen *et al.*, 1994; Dewey *et al.*, 1993), this is probably insufficient to account for the juxtaposition of *c.* 3 GPa eclogites with Devonian sedimentary rocks in the hanging wall, indicating earlier or coeval contributions from another exhumation process.

### SOLUND–HYLLESTAD–LAVIK AREA GEOLOGY

The significance of the Solund–Hyllestad–Lavik area (Fig. 3) stems from its exposure of (i) one of the rare syn-kinematic plutons in the Norwegian Caledonides, the Sogneskollen granodiorite (Skjerlie *et al.*, 2000); (ii) a nearly complete stack of the Caledonian nappes and overlying sediments; and (iii) an excellent structural section from the WGC up through the Upper Allochthon, the Solund fault, and into the Solund Devonian Basin.

The Western Gneiss Complex (WGC) is the structurally lowest unit in the area. It is chiefly a granitic to gabbroic orthogneiss with sparse lenses of eclogite. Except for the eclogite blocks, the WGC in the Solund–Hyllestad–Lavik area is dominantly amphibolite facies and has a weak retrograde greenschist facies overprint. Structurally above the WGC is the Hyllestad Complex, named and subdivided by Tillung (1999) into the Aksevatn psammite, Kleive mafic schist, Gåsetjørn pelite, Sæsol semipelite and Nygård amphibolite. The lowest of these units, the Aksevatn psammite, is a quartzose meta-sandstone. The WGC contains structurally interleaved layers of similar rocks with local pebbly layers, suggesting that this unit *may* have been deposited on the WGC, analogous to basal conglomerates elsewhere in the WGR (Tillung, 1999). The Kleive mafic schist is characterized by hornblende + biotite + garnet + plagioclase assemblages, the Gåsetjørn pelite contains local highly aluminous horizons with kyanite + staurolite + garnet + chloritoid, and the Sæsol semipelite includes marble to calc-silicate layers. The Nygård unit comprises epidote + biotite amphibolites and minor felsic gneisses and may represent a highly attenuated sheet of allochthonous basement (Tillung, 1999).

The overlying Hyllestad Complex is *c.* 1 km thick and has been correlated with the Lower Allochthon (Chauvet & Dallmeyer, 1992; Swenson & Anderson, 1991) or the Høyvik Group of the Middle Allochthon on Atøy (Tillung, 1999); all three units contain similar highly aluminous pelites. If correlative with the Lower Allochthon, which elsewhere contains sedimentary rocks as young as Wenlockian, this places an older limit on the metamorphic age of the Hyllestad Complex. If correlative with the Høyvik Group, which (i) lies depositionally on top of the Jotun-like Dalsfjord Suite (Brekke & Solberg, 1987) (ii) is depositionally overlain by the Wenlockian Herland Group (Andersen *et al.*, 1990; Brekke &

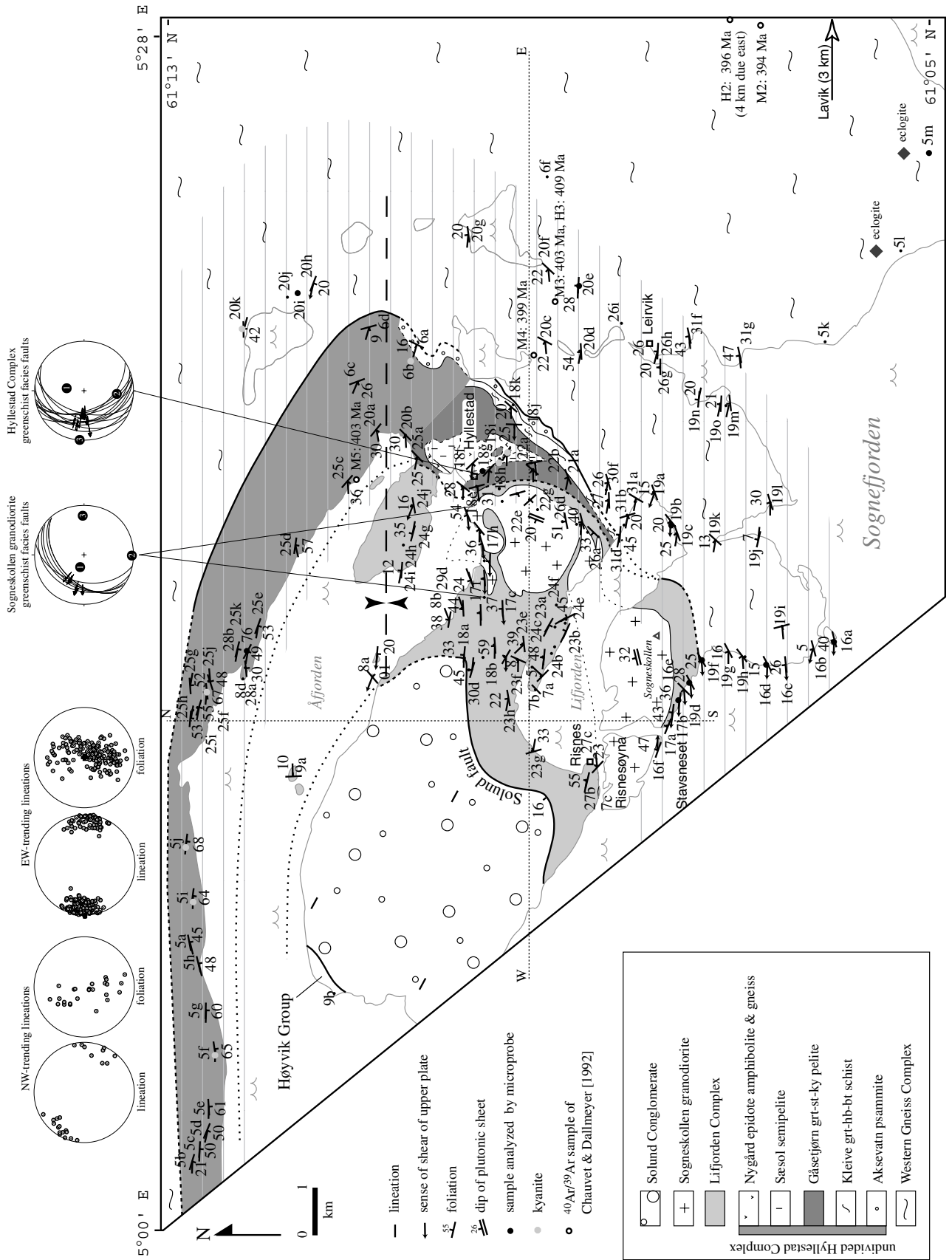
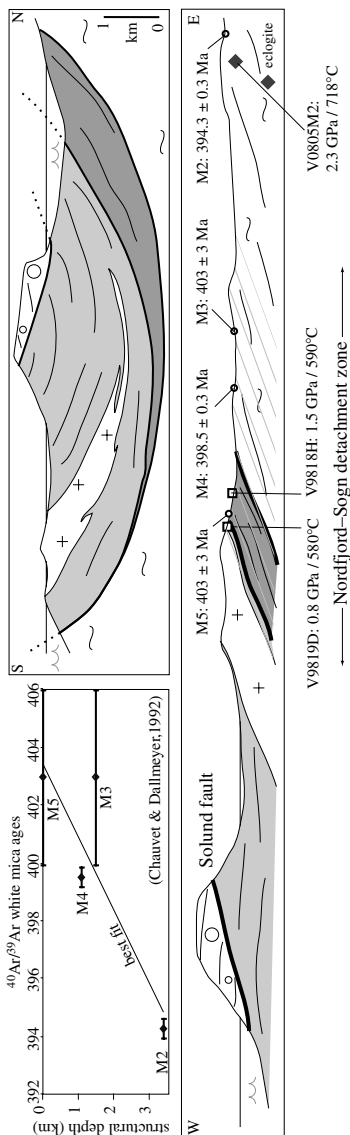


**Fig. 3.** Geology of the Solund–Hyllestad–Lavik area, from our own mapping and Tillung (1999). Low-grade Solund Conglomerate and high-grade WGR eclogite are separated by only a few km of the medium-pressure ophiolitic Lifjorden Complex and high-pressure passive margin(?) Hyllestad Complex. 'M', 'H' refer to muscovite and hornblende  $^{40}\text{Ar}/^{39}\text{Ar}$  ages of Chauvet & Dallmeyer (1992); some ages have been interpreted slightly differently than in the original paper. The three lineations from the Solund Conglomerate are from Chauvet & Serranne (1989). Horizontal ruling shows extent of NSDZ.



Solberg, 1987), and (iii) contains muscovite with *c.* 447 Ma  $^{40}\text{Ar}/^{39}\text{Ar}$  ages (Andersen *et al.*, 1998), the Hyllestad Complex is older than 447 Ma.

Structurally overlying the Hyllestad Complex is the Lifjorden Complex (Tillung, 1999), which consists of *c.* 3 km structural thickness (Fig. 3) of mostly metagraywacke, greenschist and greenstone, with minor serpentinite, metagabbro, chert, quartzose sandstones, marble and volcanogenic conglomerates. The greenstones, serpentinites and metagabbros occur chiefly toward the bottom of the section, whereas the top of the section is dominantly clastic (Tillung, 1999). The volcanogenic conglomerates, which appear in the middle of the section, include pebbles to cobbles of chiefly greenstone, plus sandstone, metagabbro, granodiorite and quartzose rock in a volcanogenic matrix (Tillung, 1999). The rock types and deformation of the Lifjorden Complex are similar to, and probably correlative with, the Staveneset Group (Furnes *et al.*, 1990) metagraywacke and metavolcanic rocks that overlie the 443-Ma Solund–Stavfjord Ophiolite just west of the study area (Fig. 1, Skjerlie *et al.*, 2000).

The youngest unit in the area is the Devonian conglomerates and minor sandstones of the Solund Basin (Nilsen, 1968), which crops out in the Solund, Bulandet and Værlandet areas (Steel *et al.*, 1985). The unit is > 6 km thick and contains probable Early Devonian fossils (Steel *et al.*, 1985), a broad spectrum of proximally derived graywacke, quartzite, greenstone and gabbro cobbles, and giant landslide deposits. The landslides contain an Early Silurian rhyolite with a U/Pb zircon age of  $439 \pm 1$  Ma (Hartz *et al.*, in press). Sedimentary structures indicate north-westward flow of braided streams on alluvial fans built against a NW-dipping fault scarp (Nilsen, 1968). While most of the Devonian basin in the study area are underlain by the Solund fault, it rests positionally on the Solund–Stavfjord Ophiolite, and on the Høyvik Group at the west end of the study area (Fig. 3).

### SOGNESKOLLEN GRANODIORITE

The Sogneskollen granodiorite is a medium- to fine-grained leucocratic granodiorite to quartz monzonite with < 5 vol% biotite and epidote (Skjerlie *et al.*, 2000; Tillung, 1999). The epidote occurs in clusters of crystals commonly associated with biotite and is interpreted as magmatic (Tillung, 1999).

The granodiorite forms a sheetlike body intruding the Lifjorden Complex that is > 300 m thick and dips *c.* 20° west. Skjerlie *et al.* (2000) interpreted the high Ba, Sr, and Na/K, and low Y,  $\epsilon_{\text{Nd}}$ ,  $^{87}\text{Sr}/^{86}\text{Sr}$  and HREE concentrations to indicate formation of the Sogneskollen granodiorite by melting of hydrous sediments outside the stability field of calcic plagioclase and within the stability field of garnet. They specifically proposed that the Sogneskollen granodiorite formed from melting of graywackes like the Lifjorden Complex during thrusting beneath the Solund–Stavfjord Ophiolite. Granite veins and dykes with similar compositions are common in the upper parts of the obduction melange thrust on top of the Herland Group in the Sunnfjord area (Osmundsen & Andersen, 1994; Skjerlie *et al.*, 2000). Similar high-Sr and Ba, biotite–epidote granites with Rb/Sr whole-rock ages of  $430 \pm 10$  and  $430 \pm 6$  Ma and Sr initial ratios of 0.7056–0.7066 intrude ophiolites and metagreywackes of the Upper Allochthon south of Bergen (Andersen & Jansen, 1987; Fossen & Austrheim, 1988).

In general the pluton is strongly affected by the extensional fabrics described below, but locally, the base of the pluton has been sheltered from the deformation and details of its original intrusive relationships may be discerned. The basal contact is a *c.* 10 m thick swarm of aplite and plagioclase–porphyry dykes ('grey dykes' of Skjerlie *et al.*, 2000) (Fig. 4). Both types of dyke are mutually intrusive, although the aplites appear to record a slightly more complex deformation history, implying that they began intruding first. The aplite dykes are < 1 m in width and have a mutually intrusive relationship with the pluton. The plagioclase–porphyry dykes cut the pluton; they consist of plagioclase in a fine-grained matrix of quartz, epidote, feldspar and biotite, and are slightly elevated in Fe + Ti relative to the pluton (Tillung, 1999).

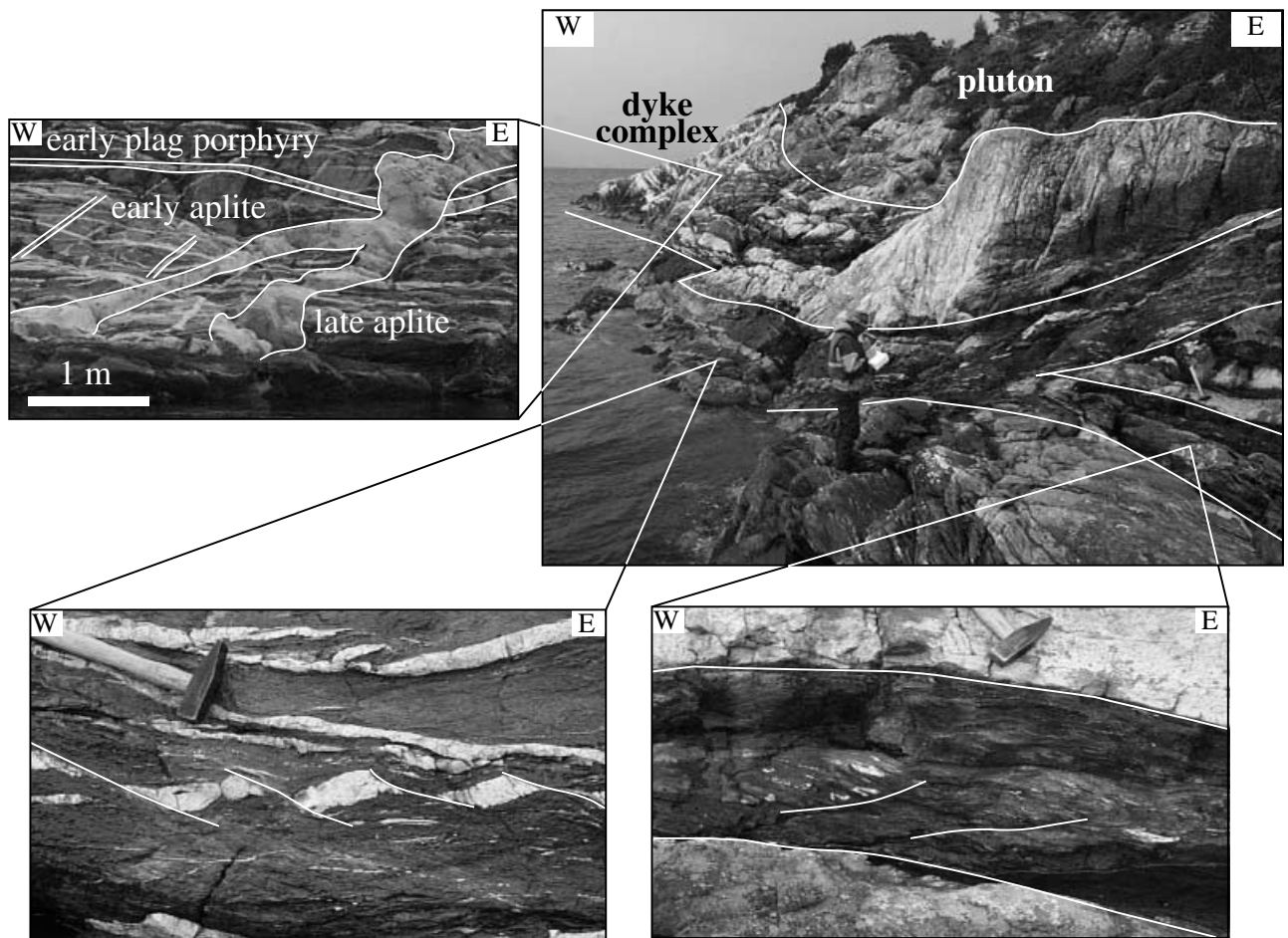


**Fig. 4.** Ductile shear zone at the base of the Sogneskollen granodiorite shows coaxial to weak top-E fabrics in wallrock graywacke and early aplite dykes (lower left), and top-W simple shear in younger plagioclase porphyries (lower right).

### METAMORPHIC PETROLOGY

Metamorphic grade increases downsection in the Solund–Hyllestad–Lavik area. The Solund Conglomerate reached prehnite–pumpellyite facies (Norton, 1987) during a metamorphic episode that must post-date the Early Devonian depositional age of the sediments. The Lifjorden Complex above the Sogneskollen granodiorite is generally of greenschist facies, with quartz + plagioclase + muscovite + biotite stable in metasedimentary rocks and the same minerals plus epidote and chlorite in volcanogenic rocks. Garnet was found at two localities above the Sogneskollen granodiorite, in metasedimentary rock at V0807a and in metamafic rock at V0807c.

The portion of the Lifjorden Complex beneath the Sogneskollen granodiorite, the bulk of the Hyllestad Complex and the non-eclogitic rocks of the WGC, contain amphibolite facies assemblages of biotite + muscovite + plagioclase + quartz ± garnet in felsic rocks and biotite + hornblende + plagioclase + quartz ± garnet in mafic varieties (mineral

compositions in Table S1). Most of the garnet-bearing rocks are in the Hyllestad Complex. All the garnet show bell-shaped Mn profiles, implying that temperatures remained too low for volume diffusion (< 600 °C, Florence & Spear, 1991). All the aluminous samples contain garnet with core-to-rim increases in Mg# and decreases in Ca. The increase in Mg# implies growth during increasing temperature for these mineral assemblages, but the decrease in Ca is more difficult to assess because of the consumption of plagioclase and the growth of paragonite. Using THERMOCALC, we assessed pressures and temperatures for garnet-bearing samples, and recalculated pressures and temperatures for the ‘micaschist’ and ‘gneiss’ samples of Chauvet *et al.* (1992) (Table 1). Metamorphic conditions for the felsic rocks, assessed chiefly with garnet–biotite Fe–Mg thermometry and garnet–biotite–muscovite–plagioclase barometry, fall mostly in the range 500–600 °C, 0.7–0.9 GPa, implying metamorphism at depths of *c.* 30 km. The two mafic rocks, evaluated with garnet–hornblende Fe–Mg thermometry and garnet–hornblende–plagioclase–quartz barometry, fall in the same range.

Higher peak pressures, indicating metamorphism at depths of *c.* 50 km, are recorded by highly aluminous and ferric rocks in the Gåsetjørn unit that contain subassemblages of garnet + staurolite + kyanite + chloritoid + paragonite + muscovite + quartz without biotite or talc (Chauvet *et al.*, 1992). Textural relationships indicate that garnet, staurolite, chloritoid and kyanite constitute the highest-pressure equilibrium assemblage. This aluminous paragenesis defines a reaction (575–600 °C and 1.4–1.6 GPa) in the KFMASH system where staurolite + chloritoid change to kyanite + garnet with increasing pressure or temperature (program GIBBS v. 2/01, Spear & Menard, 1989) (Fig. 4; Table 1). Two Hyllestad Complex samples (V9818I & V9825f) contain kyanite + staurolite + garnet, which defines a narrow *P–T* region from 575 °C, 1.6 GPa to 670 °C, 0.7 GPa; with THERMOCALC, *P–T* conditions were calculated near the high-*P* end of this divariant field for sample V9818I.

Textures and mineral zoning reveal that the *P–T* path leading to the peak recorded conditions involved

heating. (i) Aluminous sample V9819H2 contains chloritoid inclusions in garnet, indicating that chloritoid-consuming reactions were active during the prograde path. (ii) Sample V9820I has the Fe-rich assemblage garnet + staurolite + biotite; the staurolite is small and rare, and garnet contains chloritoid and chlorite inclusions, suggesting progression from the garnet–chloritoid–chlorite field to higher temperatures, across the chloritoid = garnet + biotite + chlorite and garnet + chlorite = staurolite + biotite reactions. Using the program GIBBS (Spear & Menard, 1989), inverse modelling of zoning in Fe–Mg phases, and forward *P–T* path modelling to replicate the zoning observed in garnet, we calculate that the prograde path for sample V9820I involved a pressure increase of 450 MPa and a temperature increase of 80 °C. (iii) All nonclogite garnet exhibit core-to-rim increases in Mg#, and plagioclase in garnet–epidote bearing rocks shows core-to-rim increases in Ca.

Retrograde metamorphism of the aluminous rocks involved nearly isothermal decompression. Two distinctive mineral assemblages developed in the

**Table 1.** Thermobarometry results.

Sample	Minerals	Thermometer	Barometer	T (°C)	P (kbar)	cor
V9816A1	Gr <sub>t</sub> Ms Bt Pl Qtz Chl Rt	KFMASH grid	Gr <sub>t</sub> Bt Ms Pl	540–610	9.4 ± 1.0	n/a
V9816D2	Gr <sub>t</sub> Hbl Bt Ms Pl Qtz Rt Ep	Gr <sub>t</sub> –Bt	Gr <sub>t</sub> Bt Ms Pl	560 ± 50	7.5 ± 0.8	0.917
V9818G	Gr <sub>t</sub> Hbl Ms Pl Qtz Chl Rt Ep	Gr <sub>t</sub> –Hbl	Gr <sub>t</sub> Hbl Pl Qtz	523 ± 39	7.4 ± 0.9	0.651
V9818H	Ky St Cld Gr <sub>t</sub> Ms Qtz Rt Sil	KFMASH grid		575–600	14–16	n/a
V9818I1	Ky St Gr <sub>t</sub> Ms Pg Qtz Chl Rt Sil	Ky Gr <sub>t</sub> St Ms Qtz intersection KFMASH grid KFMASH grid	Ky Gr <sub>t</sub> St Ms Qtz reaction	616 ± 201 575–670 570–585	18.4 ± 6.6 7.4–16 15–16	0.959 n/a n/a
V9818I9B	Ky St Cld Gr <sub>t</sub> Ms Pg Rt Sil	Ky St Gr <sub>t</sub> Ms Qtz intersection KFMASH grid		595 ± 175 575–600	14.5 ± 5.0 14–16	0.930
V9819D	Gr <sub>t</sub> Hbl Ms Bt Pl Qtz Chl Rt Ep Ilm	Gr <sub>t</sub> –Bt Gr <sub>t</sub> –Hbl	Gr <sub>t</sub> Bt Ms Pl Gr <sub>t</sub> Hbl Pl Qtz	580 ± 48 577 ± 38	8.3 ± 0.8 5.0 ± 1.2	0.845 0.405
V9819E	Gr <sub>t</sub> Hbl Ms Gr <sub>t</sub> Pl Qtz Chl Rt Ep	Gr <sub>t</sub> –Bt Gr <sub>t</sub> –Hbl	Gr <sub>t</sub> Bt Ms Pl Gr <sub>t</sub> Hbl Pl Qtz	520 ± 72 521 ± 36	7.2 ± 0.8 5.4 ± 0.8	0.875 0.583
V9819F	Gr <sub>t</sub> Hbl Ms Bt Pl Qtz Chl Rt Ep Ilm	Gr <sub>t</sub> –Bt Gr <sub>t</sub> –Hbl	Gr <sub>t</sub> Bt Ms Pl Gr <sub>t</sub> Hbl Pl Qtz	543 ± 46 513 ± 34	7.4 ± 0.7 4.6 ± 0.9	0.850 0.430
V9820E	Gr <sub>t</sub> Hbl Bt Pl Qtz Rt Ep	Gr <sub>t</sub> –Hbl	Gr <sub>t</sub> Hbl Pl Qtz	552 ± 38	8.7 ± 0.8	0.755
V9820I	Gr <sub>t</sub> St Ms Bt Pl Qtz Ep	KFMASH grid	Gr <sub>t</sub> Bt Ms Pl	600–630	10.3 ± 1.1	n/a
V9820K	Gr <sub>t</sub> Hbl Bt Pl Qtz Chl Rt Ilm	Gr <sub>t</sub> –Hbl	Gr <sub>t</sub> Hbl Pl Qtz	585 ± 39	7.7 ± 0.7	0.651
V9825F	Ky St Gr <sub>t</sub> Ms Bt Pl Qtz Chl Rt	Ky St Gr <sub>t</sub> Bt Ms KFMASH grid	Qtz intersection Gr <sub>t</sub> ASt Pl	614 ± 56 620 ± 10	11.4 ± 2.2 11.8 ± 1.1	–0.41 n/a
V0805M 1	Gr <sub>t</sub> Om Pg Ms	Gr <sub>t</sub> Om Pg	Gr <sub>t</sub> Om Pg Ms	687 ± 77	22.1 ± 2.2	0.515
V0805M 2	Gr <sub>t</sub> Om Pg Ms	Gr <sub>t</sub> Om Pg	Gr <sub>t</sub> Om Pg Ms	718 ± 83	24.7 ± 2.4	0.670
EC§	Gr <sub>t</sub> Om Pg	Gr <sub>t</sub> Om Pg Ms		654 ± 72	23.0 ± 1.8	0.475
MS§		Gr <sub>t</sub> –Bt	Gr <sub>t</sub> Bt Ms Pl	516 ± 44	6.9 ± 0.7	0.881
GN§		Gr <sub>t</sub> –Bt	Gr <sub>t</sub> Bt Ms Pl	607 ± 59	9.1 ± 1.0	0.953

Note: 'KFMASH grid' refers to pelite phase diagram produced with Gibbs (Spear & Menard, 1989) from Powell & Holland 1998 database; 'reaction' and 'intersection' refer to THERMOCALC v3.1 with May, 2001 database (Powell & Holland, 1988). Mineral formulae and activities were calculated with the program 'A-X', by T.J.B. Holland and R. Powell; A-X calculates Fe<sup>3+</sup> in clinopyroxene using charge balance considerations, which Carswell *et al.* (2000) demonstrated is a good approximation to Fe<sup>3+</sup> measured by Mössbauer spectrometry. Uncertainties are ± 1 σ; 'cor' is correlation coefficient from THERMOCALC. §: calculations based on mineral compositions reported by Chauvet *et al.* (1992).

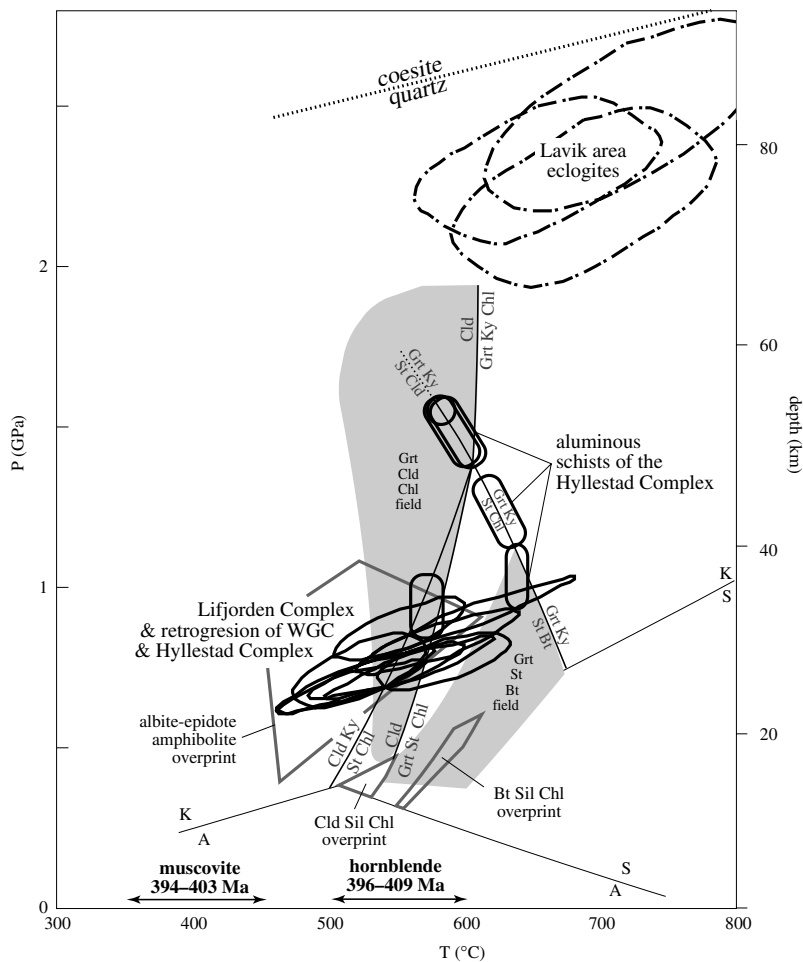


**Fig. 5.** Calculated pressures and temperatures for the Solund–Hyllestad–Lavik area. Eclogites in the Lavik area record peak near-UHP conditions and albite-epidote amphibolite facies overprint. Aluminous schists of the Hyllestad Complex decompressed nearly isothermally from *c.* 1.5 GPa to 0.4 GPa at *c.* 600 °C. Lifjorden complex was buried to depths of *c.* 30 km.

aluminous rocks: (i) Fe-rich chloritoid between boudinaged staurolite grains and on kyanite rims, and late-stage top-W shear bands with sillimanite and chlorite (*c.* 500 °C and 400 MPa); and (ii) biotite + sillimanite + chlorite (550–600 °C and 300–600 MPa).

The Sogneskollen granodiorite predates the amphibolite facies metamorphism and associated top-W extension. Garnet atolls developed around plagioclase grains in the aplite dykes (Tillung, 1999) might have grown during at this time.

Eclogites crop out at a few localities in the Lavik area (Fig. 3). Chauvet *et al.* (1992) described phengite + epidote + rutile bearing eclogite variably retrogressed to amphibolite and then albite-epidote-amphibolite facies. The garnet in the examined samples are homogeneous  $\text{alm}_{58}\text{grs}_{21}\text{prp}_{19}\text{sps}_{01}$  and contain inclusions of  $(\text{K}_{0.1}\text{Na}_{0.5})(\text{Na}_{1.1}\text{Ca}_{0.9})(\text{Mg}_{2.1}\text{Fe}_{1.3})(\text{Fe}_{0.4}\text{Al}_{1.2})(\text{Al}_{1.5}\text{Si}_{6.5})\text{O}_{22}(\text{OH})_2$  hornblende, epidote and plagioclase, indicating prograde amphibolite facies metamorphism. Clinopyroxene is also nearly homogeneous, lacks the exsolved  $\text{SiO}_2$  rods common in eclogites farther north in the WGC and has core compositions of  $\text{jd}_{50-54}\text{di}_{31-33}\text{hed}_{11-12}\text{acm}_{07-11}$ ;

Chauvet *et al.* (1992) reported much lower jadeite contents of 25–30 mol% from their sample. The highest phengite content found in K-white mica was 3.32 Si atoms pfu, slightly less than the 3.36 reported by Chauvet *et al.* (1992). Following the logic outlined by Carswell *et al.* (2000), we used THERMOCALC to calculate  $P$ ,  $T_{\text{max}}$  using the lowest Fe/Mg garnet, highest Fe/Mg omphacite and highest Fe/Mg phengite compositions, and  $P_{\text{max}}$ ,  $T$  using the most jadeite-rich omphacite, most siliceous phengite, and the garnet with the highest  $a_{\text{prp}}a_{\text{grs}}^2$ .  $P$ – $T$  were calculated based on Fe–Mg exchange between garnet and clinopyroxene and the inverse Tschermak substitution in coexisting phengite, finding conditions of *c.* 700 °C, 2.3 GPa for our two eclogite samples and Chauvet *et al.*'s sample, regardless of whether the  $T_{\text{max}}$  or  $P_{\text{max}}$  criteria of Carswell *et al.* (2000) were used.

In summary, the metamorphic petrology places the following significant constraints on the evolution of the area. (1) The WGC experienced definitively higher pressures and temperatures than all overlying units, reaching *c.* 700 °C at *c.* 80 km depth. (2) The Hyllestad Complex experienced definitively higher pressures

and temperatures (*c.* 600 °C at *c.* 50 km depth) than the Lifjorden Complex (*c.* 550 °C at *c.* 30 km depth). (3) The similarity of the prograde amphibolite facies pressures and temperatures of the Lifjorden Complex with the retrograde amphibolite facies pressures and temperatures of the Hyllestad Complex and the WGC imply that all three units shared a common late-stage history. (4) All three units reached peak conditions via a heating path, which was then followed by decompression to *c.* 15 km depth and only minor cooling of *c.* 50 °C. (5) This metamorphism post-dates intrusion of the Sogneskollen granodiorite. (6) The pressure differences between the three major units implies considerable excision or thinning of the section. The 2.3 GPa eclogites and the 1.5 GPa rocks in the Hyllestad Complex are separated by only *c.* 2.7 km of structural section, implying thinning by a factor of *c.* 11. If this exhumation occurred along a normal-sense shear zone with a dip of 40–25°, this corresponds to a shear strain of 17–27. The 1.5 GPa rocks in the Hyllestad Complex and the 0.8 GPa rocks in the Lifjorden Complex are separated by only *c.* 0.3 km of structural section, implying thinning by a factor of *c.* 66. If this exhumation occurred along a normal-sense shear zone with a dip of 40–25°, this corresponds to a shear strain of 100–150.

## STRUCTURE

The large-scale structure of the study area is a > 20-km wavelength, W-plunging synform whose axis is parallel to the regional stretching lineation. The WGC, Hyllestad Complex and Lifjorden Complex contain a gently plunging E–W stretching lineation in most localities (Fig. 3). In the WGC and Hyllestad Complex, this lineation formed at amphibolite facies conditions, whereas the lineation in the part of the Lifjorden Complex above the Sogneskollen granodiorite formed at greenschist facies conditions. The E–W lineation is contemporaneous with the noncoaxial top-W extension (Chauvet & Séranne, 1989). The extensional fabric is fairly homogeneous throughout the WGC and Hyllestad Complex between Lavik and Hyllestad, but higher in the section, it is less penetrative and mafic orthogneisses along the shore south of Sogneskollen are highly phyllonitic. The portion of the Lifjorden Complex structurally beneath the Sogneskollen pluton is also strongly deformed and partly phyllonitic, except in a local strain shadow adjacent to the pluton at Risnesøyna (see above and Fig. 4). Structurally above the pluton, however, the extensional deformation is less penetrative. We interpret domains in the upper part of the Lifjorden Complex where the lineation plunges NW (Fig. 3), rather than E–W, as a younger fabric.

The most significant structural feature in the area is the ductile shear zone at the base of the Lifjorden Complex (Fig. 4). The first 10 m of the dyke swarm beneath the Sogneskollen granodiorite at Risnesøyna are weakly deformed, and contain important struc-

tural and intrusive relationships obliterated elsewhere. Here, the intrusive relationships between aplite dykes and their envelope show that the aplites post-date early contractional folds, cleavage formation and thrust-related top-east fabrics. The country-rock greywackes between the dykes contain an S1 cleavage parallel to compositional layering, S0, that is folded into isoclinal m-scale folds. An axial-planar cleavage, S2, is developed in the hinges of these folds. These folds and S1 and S2 cleavages are truncated by both the aplite and plagioclase-phyric dykes. The greywacke and aplite dykes in the low-strain zone have dominantly symmetrical structures implying dominantly coaxial deformation at the scale of the preserved low-strain zone, but locally the dykes have asymmetric boudins indicating thrust-related top-E shear. The pre to syn-granite emplacement contractional fabrics yield no evidence for HP metamorphism, supporting our interpretation of a major metamorphic pressure break below the Lifjorden complex. The plagioclase-phyric dykes truncate these fabrics and themselves locally exhibit top-W shear. At Stavneset (Fig. 3, headland east of Risnesøyna) deformation intensifies about 50 m below the base of the pluton: the host greywacke develops strong top-W asymmetric fabrics, and the dykes become disrupted, asymmetrically boudinaged and transposed parallel to an intensified foliation. This zone is succeeded downward by a few metres of strongly deformed greywacke with rare boudins of the aplite and plagioclase-phyric dykes. Below this, the asymmetric top-W fabric becomes phyllonitic, strengthens abruptly and no further dykes are seen, suggesting very large shear strains and correspondingly large-scale displacement.

In aggregate, the structural and intrusive relationships reveal that the aplite dykes intruded at a late stage of the top-E thrusting, and that the top-W shear began after dyke intrusion. The plagioclase-phyric dykes exhibit variable degrees of deformation in the extensional shear bands; but we ascribe this variation to the inhomogeneous bulk strain preserved in the local strain shadow at Risnesøyna. Textbook-quality shear bands, asymmetric boudinage,  $\sigma$  and  $\delta$  clasts indicate pervasive top-W extension in all rocks exposed structurally beneath the Sogneskollen granodiorite (Fig. 4).

We measured quartz lattice preferred orientations in eight samples (Fig. 6). V9816A shows the strongest fabric, with a *c*-axis maximum parallel to Y and the prism planes aligned parallel to the foliation, implying prism- $\langle a \rangle$  slip, characteristic of amphibolite facies deformation, during coaxial deformation (Schmid & Casey, 1986). Two other samples in the deeper part of the section are similar, whereas the remaining samples have rather weak fabrics. Only the uppermost sample, V9823F exhibits any evidence of low-temperature  $\langle a \rangle$  slip in the basal plane.

Deformation in the Solund Basin sedimentary rocks is different than that in lower units. Pebbles

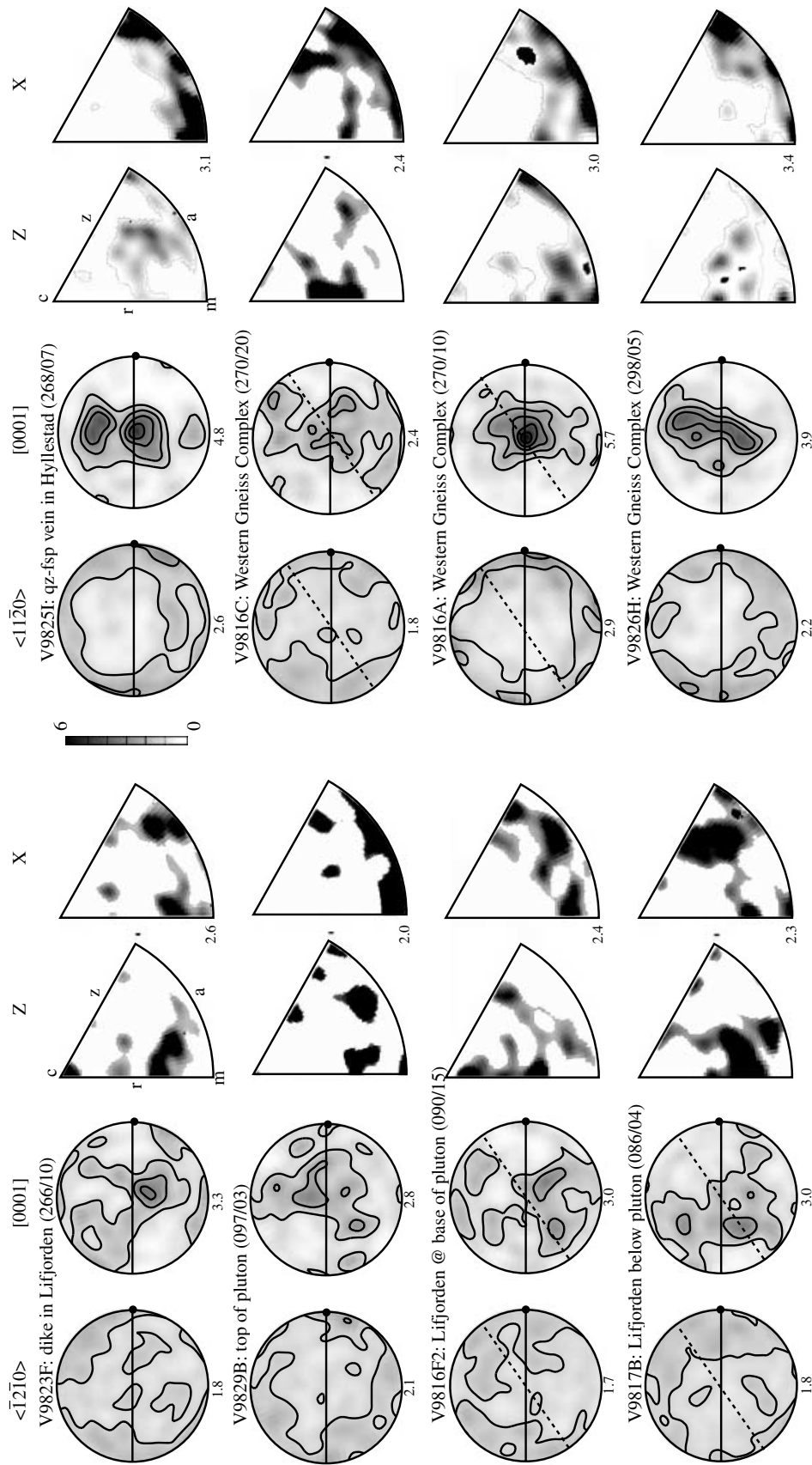


**Fig. 6.** Quartz lattice preferred orientations (= 200 grains per sample), arranged from structurally highest (V9823F) to structurally lowest (V9826H) sample. Structurally lower samples show evidence for prism- $\langle a \rangle$  slip during coaxial deformation, whereas shallower samples have weak fabrics. Circles are equal-area, lower hemisphere, stereographic projections of  $\langle a \rangle$  and  $\langle c \rangle$  axes (foliation shown by horizontal line, down-plunge direction of lineation shown by filled dot, and shear bands shown with dashed lines). Wedges are inverse pole Figs for foliation (Z) and lineation (X) (c, m, r and z refer to basal, prism, positive rhomb and negative rhomb planes). Contour intervals are multiples of mean uniform distribution (Kamb, 1959); number beneath each Figure is maximum density. Trend and plunge of lineation given in parentheses.

throughout the basin are oriented NW–SE (Séranne & Séguret, 1987), and have NW–SE trending strain shadows and NE-striking tension gashes developed during metamorphism (Chauvet & Séranne, 1989). The Solund fault, where it bounds the Solund Conglomerate, is a few-metre thick zone with pseudotachylite, ultracataclasite and ultramylonite derived mainly from the Solund Conglomerate. Outcrop/topography relations indicate a dip of *c.* 16° toward 320, implying that the Solund fault truncates structures within the underlying Lifjorden Complex; this is also evident in the discordant relationship between the NE-trending folds in the Solund–Bulandet–Værlandet Basin (Norton, 1987; Osmundsen & Andersen, 2001) and the E–W folds developed in all deeper units. The upper 7 m of the underlying Lifjorden Complex are mylonitized with a 302/18 stretching lineation and shear bands indicating extensional movement along the Solund fault (Norton, 1987). Less than 100 m beneath the Solund fault, the greenschist facies Lifjorden Complex is less deformed. It bears the folds and S<sub>1</sub> and S<sub>2</sub> foliations similar to those beneath the Sogneskollen granodiorite.

Chauvet & Séranne's (1989) reconnaissance investigation of brittle faults within the Solund Basin also showed NW–SE extension. We measured brittle-ductile faults with quartz + chlorite + epidote mineralization at two well-exposed localities within the Sogneskollen granodiorite and Hyllestad Complex (Fig. 3). At both localities, fault-striae analysis (Ratschbacher *et al.*, 1994), indicates roughly E–W extension after the local foliation is restored to pre-folding horizontal.

Thus, the section in the Hyllestad area is marked from top to bottom by (i) NW-directed extension within the weak prehnite-pumpellyite facies Solund Conglomerate; (ii) NW-directed normal slip along the discrete Solund fault; (iii) NW-directed extension within the weakly deformed greenschist facies section of the Lifjorden Complex; (iv) W-directed extension within the Sogneskollen granodiorite; (v) the profound top-W extensional shear zone, which began at amphibolite facies conditions (sillimanite stable) and which contains the HP rocks in its footwall; and (vi) penetrative top-W extensional fabric throughout the Hyllestad Complex and extending down into the WGC at least as far as Leirvik. Features iv, v and vi comprise the NSDZ, quite different from suggestions that the NSDZ is a homogeneous 2-km thick shear zone restricted to the Lifjorden Complex (e.g. Chauvet & Brunel, 1988).

## GEOCHRONOLOGY

Previous attempts to date zircon and titanite from the Sogneskollen granodiorite have been unsuccessful, although Skjerlie *et al.* (2000) reported zircon rim ion-probe spot ages of *c.* 450–400 Ma. Skjerlie *et al.* (2000) argued that the Sogneskollen granodiorite is

*c.* 420 Ma, based on compositional similarity to a 419 ± 9 Ma granitic dyke from the Lindås nappe (U/Pb zircon age, Austrheim, 1990) and the assumption that contractional structures within the Sogneskollen granodiorite developed during the Wenlockian emplacement of the Solund–Stavfjord Ophiolite.

We separated zircon from three samples for U/Pb dating: the Sogneskollen granodiorite (V9817A3), an aplite dyke (V9817A1) and a plagioclase–phyric dyke (V9817A2). All three samples were taken from the base of the pluton and its associated dyke swarm. The zircon exhibit obvious cathodoluminescent cores and rims (Fig. 7) that proved to have high and low Th/U, respectively. As a preliminary investigation, we analyzed one fraction of zircon from each of the three samples by single-step digestion and thermal-ionization mass spectrometry (TIMS) (Fig. 8; Table S2). All three fractions are discordant. Sample V9817A3 contains both clear and strongly cloudy zircon. A small population of clear grains was used for Sensitive High Resolution Ion Microprobe (SHRIMP) work, and a fraction of the cloudy grains analysed by TIMS. This zircon has a high U content (*c.* 1100 p.p.m.), and yields <sup>206</sup>Pb\*/<sup>238</sup>U and <sup>207</sup>Pb\*/<sup>206</sup>Pb\* ages of *c.* 373 and *c.* 610 ± 50 Ma, respectively (the large error on the <sup>207</sup>Pb\*/<sup>206</sup>Pb\* age stems from a high common Pb content). By comparison with the other TIMS data and the SHRIMP data (discussed below), these ages suggest significant Pb loss plus inheritance. The Pb loss is unsurprising in light of the high U content and cloudy appearance of the zircon. TIMS fractions V9817A1 and A2 consist of clear zircon, and are relatively low in U (*c.* 125 and 34 p.p.m., respectively). These fractions are strongly discordant, with <sup>206</sup>Pb\*/<sup>238</sup>U and <sup>207</sup>Pb\*/<sup>206</sup>Pb\* ages of 932 and 1208 ± 1.7 Ma, respectively, for V9817A1, and 662 and 972 ± 9 Ma, respectively, for V9817V2. For reference, these data define a lower intercept age of 437.4 ± 9.3 Ma, but we place little confidence in this two-point intercept. For the lower intercept to have rigorous age significance, the zircon would need to have differing proportions of an inherited component of identical age (or at least identical mean age), and no post-crystallization Pb loss (a distinct possibility given the moderate to low U concentrations). In any case, the lower intercept age is in agreement with the SHRIMP results reported below and thus tends to reinforce those results.

The Sensitive High Resolution Ion Microprobe (SHRIMP) at the Stanford/USGS Microanalytical Facility was used to obtain 37 spot ages from grain cores and rims (Fig. 8). Seven spot analyses of grain cores from the aplite dyke have ages that lie along a rough mixing line from *c.* 0.95 to *c.* 1.6 Ga, and Th/U ratios of 0.2–1.3, indicating an igneous provenance. Textural relations visible in cathodoluminescence images reveal that this range of ages is not the result of mixing of different age domains during ion-probe

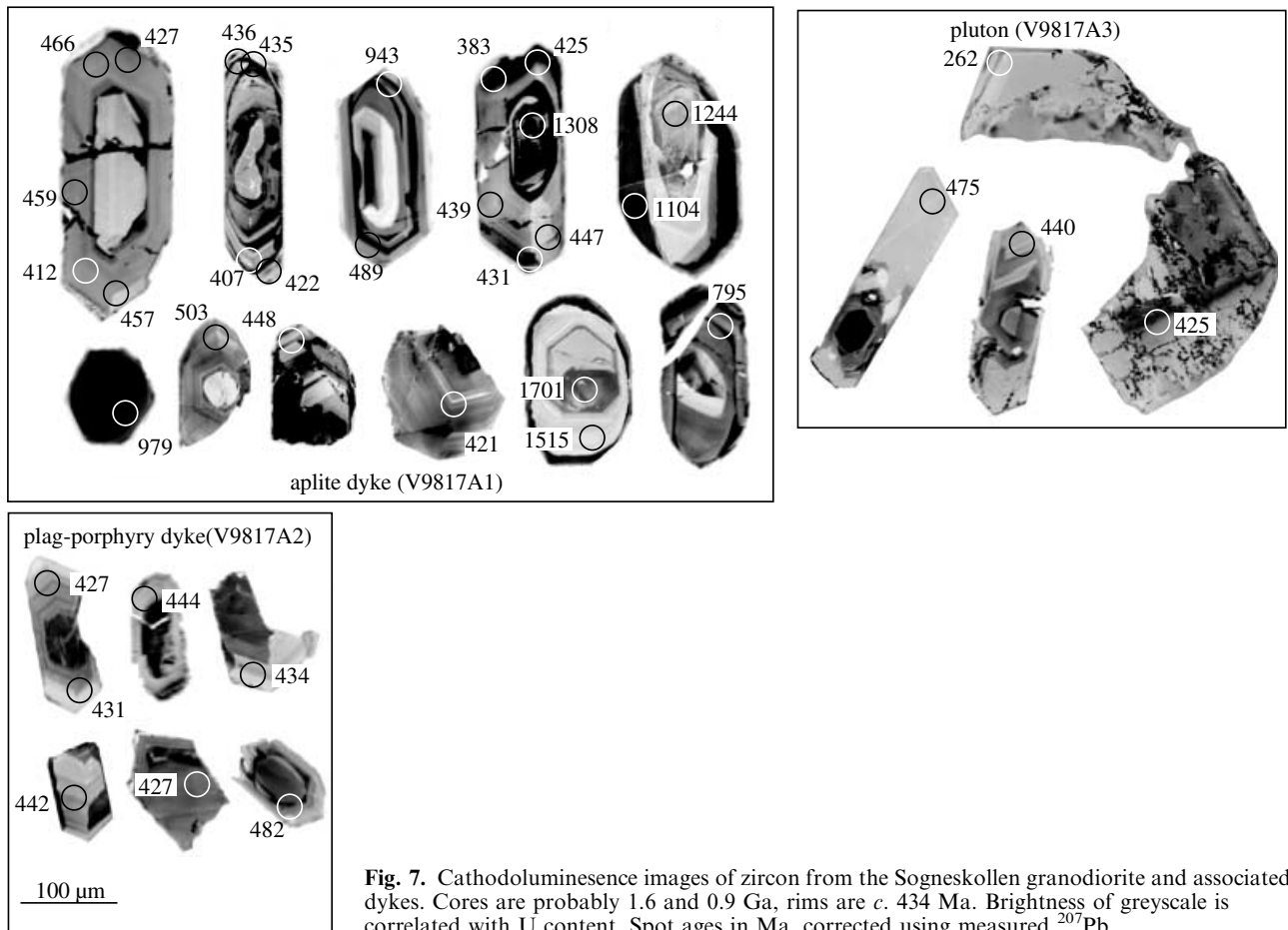


**Fig. 7.** Cathodoluminescence images of zircon from the Sogneskollen granodiorite and associated dykes. Cores are probably 1.6 and 0.9 Ga, rims are *c.* 434 Ma. Brightness of greyscale is correlated with U content. Spot ages in Ma, corrected using measured  $^{207}\text{Pb}$ .

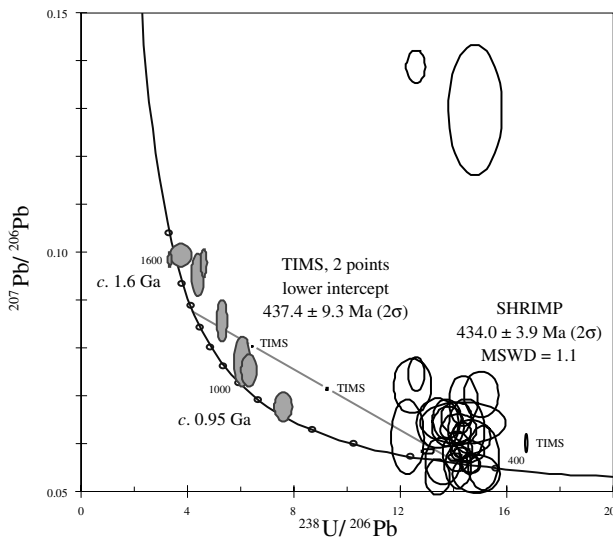


**Fig. 8.** Tera-Wasserburg diagram of U/Pb zircon analyses of the Sogneskollen granodiorite and associated dykes. SHRIMP ratios are uncorrected and shown as  $\pm 1\sigma$ . Core analyses shown with filled grey ellipses.

analysis; the range therefore most likely reflects Early Proterozoic grains that underwent Late Proterozoic Pb loss. Tectonics events of 1.75–1.45 Ga and 1.25–0.95 Ga are known in Scandinavia as the Gothian and Sveconorwegian, respectively, and have both been identified in the southern part of the WGC immediately east of the study area (Skår, 1998). Except for one spot age of 795 Ma, which cathodoluminescence imaging suggests is the result of simultaneous analysis of two age domains, the remainder of the spot ages from the zircon rims are Palaeozoic—503–262 Ma. The three oldest Palaeozoic spot ages, 503, 489 and 482 Ma also appear to be the result of mixing of two age domains. Twenty-one of the remaining spot ages can be pooled to form a  $^{207}\text{Pb}$ -corrected, weighted mean  $^{238}\text{U}/^{206}\text{Pb}$  age of  $434.0 \pm 3.9$  Ma ( $2\sigma$  internal error) with a good fit ( $\text{MSWD} = 1.1$ ). The three separate samples have weighted mean  $^{238}\text{U}/^{206}\text{Pb}$  SHRIMP ages that are equivalent at the 95% confidence interval, and are therefore coeval at the current level of precision. Four younger Palaeozoic spot ages, 412, 407, 383 and 262 Ma, lie significantly (95% confidence interval) outside the  $434.0 \pm 3.9$  Ma population. The low 262 Ma result is from a spot with extremely high (*c.* 3300 ppm) U concentration and clearly reflects significant Pb loss. The 412, 407 and 383 Ma results

are from spots with low U concentrations: *c.* 78, 61 and 42 p.p.m., respectively. Pb loss associated with radiation-induced lattice damage is a less attractive option to explain these results and perhaps they reflect very thin overgrown rims at *c.* 400 Ma. Considering all the results, *c.* 434 Ma is interpreted as the crystallization age of the magma and the younger Palaeozoic spot ages as the result of Pb loss and/or later overgrowths. It is possible, however, that the 434 Ma age includes inherited grains.

The age of metamorphism in the Solund–Hyllestad–Lavik area has been partly constrained by Chauvet & Dallmeyer (1992), who dated four muscovite and two hornblende (Fig. 3a). Two of the four muscovite yielded well-behaved spectra with ages of  $398.5 \pm 0.3$  and  $394.3 \pm 0.3$  Ma (our recalculations); the other two spectra show serially increasing or decreasing step ages for which we take weighted mean ages of  $c. 403 \pm 3$  Ma. The muscovite ages may decrease with structural depth (Fig. 3b)—a progression typical of muscovite  $^{40}\text{Ar}/^{39}\text{Ar}$  ages within the NSDZ (Andersen, 1998; Boundy *et al.*, 1996; Chauvet & Dallmeyer, 1992; Eide *et al.*, 1997); they indicate that the amphibolite facies extension along the NSDZ was over by 403 Ma. The two hornblende ages of Chauvet & Dallmeyer (1992), *c.*  $395.9 \pm 1.1$  Ma and *c.*  $409 \pm 3$  Ma, are systematically older than muscovite from the same localities by 2–4 Ma.

There are presently no radiometric ages on the eclogites in the Lavik area, so, we provisionally assume that the Lavik eclogites formed during the *c.* 410–400 (?) Ma HP event in the WGC (Lutro *et al.*, 1997; Mearns, 1986; Mørk & Mearns, 1986; Root *et al.*, 2000; Terry *et al.*, 2000) because the Lavik eclogites are part of this complex.

## DISCUSSION

An important finding from our study is that E-directed thrusting recorded in the dyke swarm at the base of the Sogneskollen granodiorite finished after  $434 \pm 4$  Ma, and that major top-W extension at amphibolite facies conditions developed subsequently. As implied above, igneous rocks similar in age to the Sogneskollen granodiorite are widespread in the Uppermost and Upper Allochthons. These bodies include, for example, the Bindal Batholith ( $430 \pm 7$ – $447 \pm 7$  Ma U/Pb zircon ages, Nordgulen *et al.*, 1993) and the Smøla–Hitra Batholith (*c.* 435 Ma U/Pb zircon, Nordgulen *et al.*, 1995). In western Norway, the Sunnhordland Batholith (Rb/Sr *c.* 430 Ma, Andersen & Jansen, 1987; Fossen & Austrheim, 1988), the Bremanger Granodiorite and the Gåsøy diorite (U/Pb zircon  $440 \pm 5$  Ma, Hansen *et al.*, 2001) are arc plutons intruding ophiolites, arc volcanic rocks and olistostromes. Thus, the relationships observed in the Hyllestad area—a granodiorite intruding oceanic rocks and their sedimentary cover, but not the structurally lower continental rocks—are

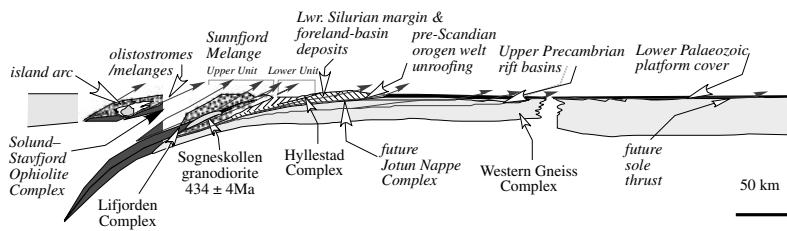
typical of this suite of broadly Llandoveryan to Wenlockian igneous rocks, and support a correlation of the Lifjorden Complex with the oceanic nappes of the Upper Allochthon. The nearest oceanic rocks of the Upper Allochthon are the Solund–Stavfjord ophiolite, which has a U/Pb zircon age of  $443 \pm 3$  Ma (Dunning & Pedersen, 1988) and is overlain by the Staveneset Group metagraywacke and arc-related metavolcanics (Furnes *et al.*, 1990). The ophiolite probably formed near a continent, because some of the MORB sills intruded greywackes containing metamorphic rock fragments, abundant clastic quartz grains and clastic zircon of Early Proterozoic to Middle Ordovician age (Pedersen & Dunning, 1993; Skjerlie *et al.*, 1989). Recently, an arc rhyolite landslide block in the Devonian Solund Basin has been dated at  $439 \pm 1$  Ma (Hartz *et al.*, in press), and unpublished U/Pb data from a quartz-diorite dyke in the ophiolite suggest that the terminal magmatic stage of the ophiolite is late Llandoveryan (Y. Dilek & H. Furnes pers. com. 2001). The final stages of the ophiolite emplacement onto the continental Middle Allochthon Høyvik Group took place during deposition of the Sunnfjord obduction melange and the Herland Group, a Wenlockian passive-margin sequence (Andersen *et al.*, 1990).

The presence of the  $434 \pm 4$  Ma Sogneskollen granodiorite within oceanic rocks correlated with the Solund–Stavfjord ophiolite does not conflict with the Wenlockian emplacement age of that ophiolite (Fig. 2). Whether the top-E deformation recorded in the Sogneskollen granodiorite can be correlated with the Wenlockian emplacement age of the Solund–Stavfjord ophiolite is, however, an open question. There are at least two possible scenarios that can explain the geological observations: (1) While the base of the Wenlockian is quoted as 428 Ma, the actual radiochronologic constraint is  $= 430.1 \pm 2.4$  Ma (Tucker & McKerrow, 1995). This age is indistinguishable from  $434 \pm 4$  Ma at the 95% confidence interval, and thus, the top-E displacement in the Solund–Hyllestad–Lavik area could be temporally and kinematically equivalent to emplacement of the Solund–Stavfjord ophiolite, but it must have taken place in the earliest Wenlockian. (2) The crystallization age we report for the Sogneskollen granodiorite may be wrong. As discussed above, at the current level of precision, nearly all of the SHRIMP rim ages form a single population but the spread of rim ages is large enough that higher precision analyses might reveal more than one population within the cluster.

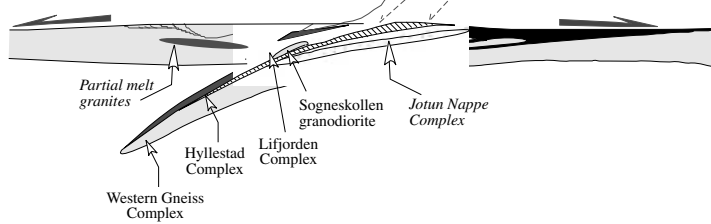
## BURIAL AND EXHUMATION OF THE HP ROCKS

We infer the following tectonic history for the study area (Fig. 9). (1) The Hyllestad Complex was deposited on the WGC; it could possibly be as young as Wenlockian if it is part of the Lower Allochthon,

428 Ma (base of the Wenlockian): convergence rate 8–12 cm/a



410 Ma Early Devonian: subduction of WGC & onset of extension at high structural levels



400 Ma Middle Devonian: major extension across the belt

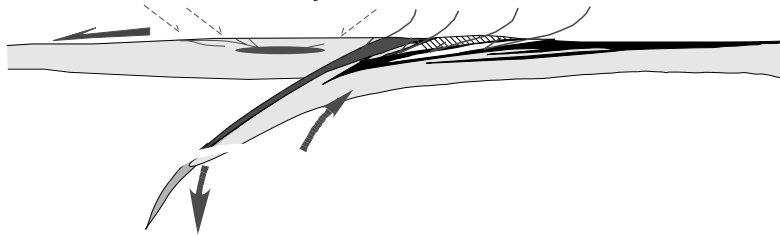


**Fig. 9.** Tectonic evolution of western Norway. Following crystallization of Sogneskollen granodiorite at *c.* 434 Ma, Upper Allochthon emplaced onto lower units around *c.* 428 Ma. Lower Allochthon and WGC subducted to high pressures at *c.* 410 Ma. Major exhumation finished by *c.* 400 Ma.

and likely experienced a *c.* 447 Ma metamorphism if it is part of the Middle Allochthon Høyvik Group. (2) The Lifjorden Complex formed as part of the Upper Allochthon (chiefly as sediments deposited on mafic crust) and then was intruded by the 434 Ma Sogneskollen granodiorite. (3) The Lifjorden Complex was thrust eastward over the Hyllestad Complex soon thereafter—likely extending into the Wenlockian—and imprinting minor top-E structures in both units. (4) At *c.* 410–400 (?) Ma, the WGC was subducted to 80 km depth, forming the Lavik eclogites; the Hyllestad Complex was buried/subducted to 50 km depth, metamorphosing the highly aluminous schists; and the Lifjorden Complex was buried to 30 km depth. (5) By 403 Ma, when muscovite within the WGC closed to Ar loss (Chauvet & Dallmeyer, 1992), the 0.7–0.9 GPa metamorphism common to all the units in the Solund–Hyllestad–Lavik area occurred. This implies that, by that time, the WGC and Hyllestad Complex were exhumed *c.* 50 km and *c.* 20 km vertically by the NSDZ, respectively. This exhumation corresponds to a normal displacement of 70–110 km depending on the synkinematic dip (40–25°) of the NSDZ (present dip *c.* 25°). While 70 km of normal displacement is compatible with the

integrated shear strain calculated from strain measurements in the *c.* 2–3 km thick NSDZ in the Sunnfjord area (Hveding, 1992), the 110 km estimate based on the present orientation of the shear zone may be too high, because of the asymmetrical uplift that accompanied the denudation of the mountain belt in western Norway. (6) At an unknown later time, the Solund fault juxtaposed the *c.* 0.4 GPa sillimanite-stable overprint of the Hyllestad Complex against the prehnite–pumpellyite facies Solund Conglomerate (= 0.3 GPa)—only a few km of exhumation.

## CONCLUSIONS

Geological field relations, combined with thermobarometry, structural petrology and geochronology, document that the geological history of the Solund–Hyllestad–Lavik area involved (i) intrusion of 434 Ma granodiorite into oceanic rocks; (ii) emplacement of those rocks over continental margin sediments; (iii) subduction of the continental margin sediments to 50 km and the underlying continental crystalline rocks to 80 km; and (iv) exhumation and attenuation of the entire sequence by normal-sense motion along the

Nordfjord–Sogn detachment zone by 403 Ma. These observations solidify our understanding of the timing and nature of the cycle of ophiolite emplacement, continental subduction and large-scale exhumation that appears to typify the Caledonian history of western Norway.

#### ACKNOWLEDGEMENTS

Physics of Geological Processes publication no. 13. Supported by NSF grant EAR-9814889 and the Physics of Geological Processes Center, University of Oslo. Helpful reviews were given by H. Brueckner and S. Cuthbert. Some of the samples and data were collected by A. Vasquez.

#### SUPPLEMENTARY MATERIAL

Tables S1 and S2 are available for downloading from <http://www.blackwellpublishing.com/products/journals/suppmat/JMG/JMG468/JMG468sm.htm>.

#### REFERENCES

- Andersen, T. B., 1998. Extensional tectonics in the Caledonides of southern Norway, an overview. *Tectonophysics*, **285**, 333–351.
- Andersen, T. B. & Andresen, A., 1994. Stratigraphy, tectono-stratigraphy and the accretion of outboard terranes in the Caledonides of Sunnhordland, W. Norway. *Tectonophysics*, **231**, 71–84.
- Andersen, T. B., Berry, H. N., Lux, D. R. & Andresen, A., 1998. The tectonic significance of pre-Scandian  $^{40}\text{Ar}/^{39}\text{Ar}$  phengite cooling ages from the Caledonides of western Norway. *Journal of the Geological Society of London*, **155**, 297–309.
- Andersen, T. B. & Jamtveit, B., 1990. Uplift of deep crust during orogenic extensional collapse: a model based on field studies in the Sogn–Sunnfjord region of western Norway. *Tectonics*, **9**, 1097–1111.
- Andersen, T. B. & Jansen, Ø. J., 1987. The Sunnhordland Batholith, W. Norway; regional setting and internal structures, with emphasis on the granitoid plutons. *Norsk Geologisk Tidsskrift*, **67**, 159–183.
- Andersen, T. B., Osmundsen, P. T. & Jolivet, L., 1994. Deep crustal fabrics and a model for the extensional collapse of the southwest Norwegian Caledonides. *Journal of Structural Geology*, **16**, 1191–1203.
- Andersen, T. B., Skjerlie, K. P. & Furnes, H., 1990. The Sunnfjord Melange, evidence of Silurian ophiolite accretion in the West Norwegian Caledonides. *Journal of the Geological Society of London*, **147**, 59–68.
- Austrheim, H., 1990. Fluid-induced processes in the lower crust as evidenced by Caledonian eclogitization of Precambrian granulites, Bergen Arcs, Western Norway. *PhD Thesis, University of Oslo, Oslo*.
- Bassett, M. G., 1985. Silurian stratigraphy and facies development in Scandinavia. In: *The Caledonide Orogen–Scandinavia and Related Areas* (eds Gee, D. G. & Sturt, B. A.), pp. 283–292. John Wiley and Sons, Chichester.
- Bockelie, J. F. & Nystuen, J. P., 1985. The southeastern part of the Scandinavian Caledonides. In: *The Caledonide Orogen–Scandinavia and Related Areas* (eds Gee, D. G. & Sturt, B. A.), pp. 69–88. John Wiley and Sons, Chichester.
- Boundy, T. M., Essene, E. J., Hall, C. M., Austrheim, H. & Halliday, A. N., 1996. Rapid exhumation of the lower crust during continent-continent collision and late extension: Evidence from  $^{40}\text{Ar}/^{39}\text{Ar}$  incremental heating of hornblendes and muscovites, Caledonian orogen, western Norway. *Geological Society of America Bulletin*, **108**, 1425–1437.
- Brekke, H. & Solberg, P. O., 1987. The geology of Atløy, Sunnfjord western Norway. *Norges Geologiske Undersøkelse Bulletin*, **410**, 73–94.
- Carswell, D. A., Wilson, R. N. & Zhai, M., 2000. Metamorphic evolution, mineral chemistry and thermobarometry of schists and orthogneisses hosting ultra-high pressure eclogites in the Dabieshan of central China. *Lithos*, **52**, 121–155.
- Chauvet, A. & Brunel, M., 1988. La grande faille normale ductile du Sunnfjord; Une extension NW–SE dans la chaîne caledonienne de l'Ouest Norvege. *Comptes Rendus de L'Academie des Sciences, Serie 2, Mecanique, Physique, Chimie, Sciences de L'universite, Sciences de la Terre*, **307**, 415–422.
- Chauvet, A. & Dallmeyer, R. D., 1992.  $^{40}\text{Ar}/^{39}\text{Ar}$  mineral dates related to Devonian extension in the southwestern Scandinavian Caledonides. *Tectonophysics*, **210**, 155–177.
- Chauvet, A., Kienast, J. R., Pinardon, J. L. & Brunel, M., 1992. Petrological constraints and PT path of Devonian collapse tectonics within the Scandian mountain belt (Western Gneiss Region, Norway). *Journal of the Geological Society of London*, **149**, 383–400.
- Chauvet, A. & Séranne, M., 1989. Microtectonic evidence of Devonian extensional westward shearing in southern Norway. In: *The Caledonide Geology of Scandinavia* (ed. Gayer, R. A.), pp. 245–254. Graham and Trotman, London.
- Cuthbert, S. J., 1991. Evolution of the Devonian Hornelen Basin, west Norway: new constraints from petrological studies of metamorphic clasts. In: *Developments in Sedimentary Provenance Studies, Special Publication 57* (eds Morton, A. C., Todd, S. P. & Haughton, P. D. W.), pp. 343–360. Geological Society, London.
- Cuthbert, S. J., Carswell, D. A., Krogh-Ravna, E. J. & Wain, A., 2000. Eclogites and eclogites in the Western Gneiss Region, Norwegian Caledonides. *Lithos*, **52**, 165–195.
- Dewey, J. F., Ryan, P. D. & Andersen, T. B., 1993. Orogenic uplift and collapse, crustal thickness, fabrics and metamorphic phase changes. In: *Magmatic Processes and Plate Tectonics, Special Publication 76* (eds Prichard, H. M., Alabaster, T., Harris, N. B. W. & Neary, C. R.), pp. 325–343. Geological Society, London.
- Dunning, G. R. & Pedersen, R. B., 1988. U/Pb ages of ophiolites and arc-related plutons of the Norwegian Caledonides: implications for the development of Iapetus. *Contributions to Mineralogy and Petrology*, **98**, 13–23.
- Florence, F. P. & Spear, F. S., 1991. Effects of diffusional modification of garnet growth zoning on P-T path calculations. *Contributions to Mineralogy and Petrology*, **107**, 487–500.
- Fossen, H. & Austrheim, H., 1988. Age of the Krossnes Granite, west Norway. *Norges Geologiske Undersøkelse Bulletin*, **413**, 61–65.
- Furnes, H., Skjerlie, K. P., Pedersen, R. B., Andersen, T. B., Stillman, C. J., Suthren, R., Tysseland, M. & Garman, L. B., 1990. The Solund–Stavfjord ophiolite complex and associated rocks, west Norwegian Caledonides: Geology, geochemistry and tectonics environment. *Geological Magazine*, **127**, 209–224.
- Gee, D. G., Lobkowicz, M. & Singh, S., 1994. Late Caledonian extension in the Scandinavian Caledonides—the Røragen detachment revisited. *Tectonophysics*, **231**, 139–155.
- Gee, D. G. & Zachrisson, E., 1979. The Caledonides in Sweden. *Sveriges Geologiska Undersökning*, **C769**, 48.
- Greiling, R. O., Garfunkel, Z. & Zachrisson, E., 1998. The orogenic wedge in the central Scandinavian Caledonides: Scandian structural evolution and possible influence on the foreland basin. *Geologiska Föreningens I Stockholm Förhandlingar*, **120**, 181–190.
- Griffin, W. L. & Brueckner, H. K., 1980. Caledonian Sm–Nd ages and a crustal origin for Norwegian eclogites. *Nature*, **285**, 319–321.

- Hansen, J., Skjerlie, K. P., Pedersen, R. B. & Rosa, J., 2001. Age and petrogenesis of the Bremanger granitoid complex, west Norwegian Caledonides. *Geonytt* (Abstract), **28**, 57.
- Hartz, H. H., Martin, M. W., Andresen, A. & Andersen, T. B., in press. Volcanic rocks in the Devonian Solund Basin, Western Norway: large landslides of Silurian (439 Ma) rhyolites. *Journal of the Geological Society of London*, in press.
- Hossack, J. R., Garton, M. R. & Nickelsen, R. P., 1985. The geological section from the foreland up to the Jotun thrust sheet in the Valdres area, south Norway. In: *The Caledonide Orogen – Scandinavia and Related Areas* (eds Gee, D. G. & Sturt, B. A.), pp. 443–456. John Wiley & Sons, Chichester.
- Hveding, B., 1992. Structural geology of the mylonites below the Dalsfjord Fault, Atløy-Askvoll area, Sunnfjord, Western Norway. *Cand. Scient. Thesis (in Norwegian)*, University of Oslo, Oslo.
- Kamb, W. B., 1959. Ice petrofabric observations from Blue Glacier, Washington, in relation to theory and experiment. *Journal of Geophysical Research*, **66**, 259–271.
- Lutro, O., Robinson, P., Solli, A., Tucker, R. D., Wain, A., Terry, M. P. & Krabbendam, M., 1997. Proterozoic geology and Scandian high-pressure overprinting in the Western Gneiss Region. *Norges Geologiske Undersøkelse Report*, **132**, 1–86.
- Mearns, E. W., 1986. Sm-Nd ages for Norwegian garnet peridotite. *Lithos*, **19**, 269–278.
- Milnes, A. G., Wennberg, O. P., Skår, Ø. & Koestler, A. G., 1997. Contraction, extension, and timing in the South Norwegian Caledonides: the Sognefjord transect. In: *Orogeny Through Time, Special Publication, 121*, (eds Burg, J.-P. & Ford, M.), pp. 123–148. Geological Society, London.
- Mørk, M. B. E. & Mearns, E. W., 1986. Sm-Nd isotopic systematics of a gabbro-eclogite transition. *Lithos*, **19**, 255–267.
- Nilsen, T. H., 1968. The relationship of sedimentation to tectonics in the Solund Devonian District of southwestern Norway. *Norges Geologiske Undersøkelse Bulletin*, **259**, 1–108.
- Nordgulen, Ø., Bickford, M. E., Nissen, A. L. & Wortman, G. L., 1993. U-Pb zircon ages from the Bindal Batholith, and the tectonic history of the Helgeland Nappe Complex, Scandinavian Caledonides. *Journal of the Geological Society of London*, **150**, 771–783.
- Nordgulen, Ø., Solli, A. & Sundvoll, B., 1995. Caledonian granitoids in the Frøya-Froan area. *Norges Geologiske Undersøkelse Bulletin*, **427**, 48–51.
- Norton, M. G., 1986. Late Caledonide extension in western Norway: a response to extreme crustal thickening. *Tectonics*, **5**, 195–204.
- Norton, M. G., 1987. The Nordfjord-Sogn detachment, W. Norway. *Norsk Geologisk Tidsskrift*, **67**, 93–106.
- Norton, M. G., McClay, K. R. & Way, N. A., 1987. Tectonic evolution of Devonian basins in northern Scotland and southern Norway. *Norsk Geologisk Tidsskrift*, **67**, 323–338.
- Osmundsen, P. T. & Andersen, T. B., 1994. Caledonian compressional and late-orogenic extensional deformation in the Staveneset area, Sunnfjord, Western Norway. *Journal of Structural Geology*, **16**, 1385–1401.
- Osmundsen, P. T. & Andersen, T. B., 2001. The middle Devonian basins of western Norway: sedimentary response to large-scale transtensional tectonics? *Tectonophysics*, **332**, 51–68.
- Osmundsen, P. T., Andersen, T. B., Markussen, S. & Svendby, A. K., 1998. Tectonics and sedimentation in the hanging wall of a major extensional detachment: the Devonian Kvamshesten Basin, western Norway. *Basin Research*, **10**, 213–234.
- Pedersen, R. B., Bruton, D. L. & Furnes, H., 1992. Ordovician faunas, island-arcs and ophiolites in the Scandinavian Caledonides. *Terra Nova*, **4**, 217–222.
- Pedersen, R. B. & Dunning, G. R., 1993. Provenance of turbiditic cover to the Caledonian Solund Stavfjord Ophiolite from U-Pb single zircon dating. *Journal of the Geological Society of London*, **150**, 673–676.
- Powell, R. & Holland, T. J. B., 1988. An internally consistent dataset with uncertainties and correlations: 3. Applications to geobarometry, worked examples and a computer program. *Journal of Metamorphic Geology*, **6**, 173–204.
- Ratschbacher, L., Sperner, B., Meschede, M. & Frisch, W., 1994. Computer techniques and applications: a program library for quantitative structural analysis. *Tübinger Geowissenschaftliche Arbeiten*, **21**, 1–73.
- Roberts, D. & Gee, D. G., 1985. An introduction to the structure of the Scandinavian Caledonides. In: *The Caledonide Orogen – Scandinavia and Related Areas* (eds Gee, D. G. & Sturt, B. A.), pp. 55–68. John Wiley and Sons, Chichester.
- Root, D. B., Hacker, B. R. & Mattinson, J. M., 2000. Exhumation of Norwegian UHP eclogites. III. Expansion of the UHP terrane and U/Pb zircon ages of synorogenic plutonic rocks. *Geological Society of America Abstracts with Programs*, **32**, A236.
- Schmid, S. M. & Casey, M., 1986. Complete fabric analysis of some commonly observed quartz c-axis patterns. *Geophysical Monograph*, **36**, 263–286.
- Séguret, M., Séranne, M., Chauvet, A. & Brunel, M., 1989. Collapse basin: a new type of extensional sedimentary basin from the Devonian of Norway. *Geology*, **17**, 127–130.
- Séranne, M. & Séguret, M., 1987. The Devonian basins of western Norway: Tectonics and kinematics of extending crust. *Geological Society of London Special Publication*, **28**, 537–548.
- Siedlecka, A., 1975. Old Red Sandstone lithostratigraphy and sedimentation of the Outer Fosen area, Trondheim region. *Norges Geologiske Undersøkelse*, **321**, 1–35.
- Skår, Ø., 1998. The Proterozoic and Early Palaeozoic evolution of the southern part of the Western Gneiss Complex, Norway. *Dr. scient. Thesis, University of Bergen, Norway*.
- Skjerlie, K. P., Furnes, H. & Johansen, R., 1989. Magmatic development and tectono-magmatic models for the Solund-Stavfjorden Ophiolite Complex, W. Norwegian Caledonides. *Lithos*, **23**, 137–151.
- Skjerlie, K. P., Pedersen, R. B., Wennberg, O. P. & de la Rosa, J., 2000. Volatile-phase fluxed anatexis of metasediments during late Caledonian ophiolite obduction: evidence from the Sogneskollen Granitic Complex, west Norway. *Journal of the Geological Society of London*, **157**, 1199–1213.
- Soper, N. J., Strachan, R. A., Holdsworth, R. W., Gayer, R. A. & Greiling, R. O., 1992. Sinistral transpression and the Silurian closure of Iapetus. *Journal of the Geological Society of London*, **149**, 871–880.
- Spear, F. & Menard, T., 1989. Program GIBBS: a generalized Gibbs method algorithm. *American Mineralogist*, **74**, 942–943.
- Steel, R. J., Siedlicka, A. & Roberts, D., 1985. The Old Red Sandstone basins of Norway and their deformation: a review. In: *The Caledonide Orogen – Scandinavia and Related Areas* (eds Gee, D. G. & Sturt, B. A.), pp. 293–316. John Wiley and Sons, Chichester.
- Stephens, M. B. & Gee, D. G., 1985. A tectonic model for the evolution of the eugeoclinal terranes in the central Scandinavian Caledonides. In: *The Caledonide Orogen – Scandinavia and Related Areas* (eds Gee, D. G. & Sturt, B. A.), pp. 953–978. John Wiley and Sons, Chichester.
- Sturt, B. A., Ramsay, D. M. & Neuman, R. B., 1991. The Otta Conglomerate, the Vågåmo Ophiolite—further indications of early Ordovician orogenesis in the Scandinavian Caledonides. *Norsk Geologisk Tidsskrift*, **71**, 107–115.
- Swenson, E. & Anderson, T. B., 1991. Contact relationships between the Askvoll group and the basement gneisses of the Western Gneiss Region (WGR), Sunnfjord, Western Norway. *Norsk Geologisk Tidsskrift*, **71**, 15–27.
- Terry, M. P., Robinson, P., Hamilton, M. A. & Jercinovic, M. J., 2000. Monazite geochronology of UHP and HP metamorphism, deformation, and exhumation, Nordøyane, Western

- Gneiss Region, Norway. *American Mineralogist*, **85**, 1651–1664.
- Tillung, M., 1999. Structural and Metamorphic Development of the Hyllestad–Lifjorden Area, Western Norway. *Cand. Scient. Thesis, University of Bergen, Bergen*.
- Torsvik, T. H., 1998. Palaeozoic palaeogeography: a North Atlantic viewpoint. *Geologiska Föreningens I Stockholm Förhandlingar*, **120**, 109–118.
- Tucker, R. D., Bradley, D. C., Straeten, C. A. V., Harris, A. G., Ebert, J. R. & McCutcheon, S. R., 1998. New U-Pb zircon ages and the duration and division of Devonian time. *Earth and Planetary Science Letters*, **158**, 175–186.
- Tucker, R. D. & McKerrow, W. S., 1995. Early Paleozoic chronology: a review in light of new U-Pb zircon ages from Newfoundland and Britain. *Canadian Journal of Earth Sciences*, **32**, 368–379.
- Wain, A., Waters, D., Jephcoat, A. & Olijnyk, H., 2000. The high-pressure to ultrahigh-pressure transition in the Western Gneiss Region, Norway. *European Journal of Mineralogy*, **12**, 667–687.

*Received 14 February 2002; revision accepted 21 August 2002.*

# Generation of intermediate-depth earthquakes by self-localizing thermal runaway

Timm John<sup>1\*</sup>†, Sergei Medvedev<sup>1</sup>, Lars H. Rüpke<sup>1,2</sup>, Torgeir B. Andersen<sup>1</sup>, Yuri Y. Podladchikov<sup>1</sup> and Håkon Austrheim<sup>1</sup>

**Intermediate-depth (50–300 km) earthquakes commonly occur along convergent plate margins but their causes remain unclear. In the absence of pore-fluid pressures that are sufficiently high to counter the confining pressure in such settings, brittle failure is unlikely. In such conditions, the rocks could fail by the mechanism of progressively self-localizing thermal runaway<sup>1</sup>, whereby ductile deformation in shear zones leads to heating, thermal softening and weakening of rock<sup>1–3</sup>. Here we test this hypothesis by focusing on fault veins of glassy rock (pseudotachylyte) formed by fast melting during a seismic event, as well as associated ductile shear zones that occur in a Precambrian terrane in Norway. Our field observations suggest that the pseudotachylytes as well as shear zones have a single-event deformation history, and we also document mineralogical evidence for interaction of the rocks with external fluids. Using fully coupled thermal and viscoelastic models, we demonstrate that the simultaneous occurrence of brittle and ductile deformation patterns observed in the field can be explained by self-localizing thermal runaway at differential stresses lower than those required for brittle failure. Our results suggest that by perturbing rock properties, weakening by hydration also plays a key role in shear zone formation and seismic failure; however, thermal runaway enables the rocks to fail in the absence of a free fluid phase.**

The intense seismicity in subduction zones at depths greater than 50 km has puzzled geoscientists for decades because high ambient pressures should inhibit brittle failure at such depths. Two main failure mechanisms for intermediate-depth earthquakes have been hypothesized: (1) dehydration embrittlement and (2) shear instabilities. Metamorphic dehydration reactions have the potential to raise the pore fluid pressure and thereby lower the effective pressure to values that permit brittle failure<sup>4–6</sup>. Elastic energy stored in a viscoelastic material may be spontaneously released at seismic strain rates by the formation of very high-temperature self-localizing shear instabilities<sup>1,3,7</sup>, and the most unknown critical factor for this failure mode is the conditions under which an initial perturbation of the system either decays or self-amplifies, leading to extreme localization of deformation and shear heating. Both mechanisms are theoretically viable but it is difficult to discriminate between them.

Pseudotachylyte fault veins (quenched melts) provide evidence for paleo-earthquakes<sup>8</sup>, and they can be used to study the details of seismic failure. It has been suggested that pseudotachylytes associated with shallow earthquakes (10–15 km depth) are usually formed by brittle failure followed by frictional melting<sup>9</sup>, but at low background temperatures and high stresses ductile deformation

facilitated by thermal feedback and rock weakening due to dynamic recrystallization may also lead to seismic slip<sup>10,11</sup>. High-pressure pseudotachylytes are found in exhumed deep continental rocks<sup>12–14</sup> and in exhumed fragments of subducted oceanic slabs<sup>15–17</sup>. These observations show that extreme shear heating may play an active role in earthquakes at high confining pressures. However, under these conditions it is questionable whether brittle failure precedes deformational melting. We present results of detailed studies of eclogite-facies pseudotachylytes and a theory for intermediate-depth earthquakes that is consistent with the geological evidence. We propose that self-localizing thermal runaway (SLTR) is the failure mechanism.

Whereas ref. 1 quantified the conditions under which viscoelastic materials fail by SLTR, we focus on the applicability of this theory to intermediate-depth earthquakes. In this setting, brittle deformation is prohibited by the high confining pressures. Nevertheless, the high shear stress will be relaxed, and parts of the initial elastic energy will be converted into heat, even without macroscopic deformation. Because of rock heterogeneity, preferential heating will occur in domains of lower effective viscosity, and this will amplify the initial effective viscosity variation. Mechanical energy dissipation due to ductile shearing will cause additional temperature increase and further localization of the initial spatial heterogeneity. This positive feedback eventually leads to SLTR relaxation of differential stresses by intensely localized shear and possibly coseismic deformation. This mechanism, based on ductile shear zone formation before the seismic rupture, requires no brittle failure.

The Precambrian Kråkenes gabbro, located within the Caledonian (410 ± 10 Myr) high- to ultrahigh-pressure metamorphic Western Gneiss Complex (WGC) in Norway, provides a spectacular example of intensely localized shear failure of rocks at high confining pressures<sup>13</sup>. The almost pristine gabbro is transected by a swarm of alternating shear zones and pseudotachylyte fault veins that share the same structural orientation and can be traced over several tens of metres<sup>13</sup>. The WGC formed the root zone of the Caledonides and experienced a regional southeast–northwest temperature–pressure gradient with temperatures  $T$  ranging from 600 to 850 °C and pressures  $P$  ranging from 1.6 to more than 3 GPa (ref. 18). The gabbro was deformed and metamorphosed ( $T \approx 650$ – $700$  °C;  $P \approx 2$  GPa) during the Caledonian orogeny<sup>13,18</sup>. Deformation and metamorphism are always associated with infiltration of external fluids and the fluids caused the infiltrated parts of the gabbro to become more reactive and thereby weaker relative to their dry precursors<sup>19–21</sup>. However, some internal parts of the body in which fluid infiltration was inhibited show no overprint,

<sup>1</sup>Physics of Geological Processes (PGP), University of Oslo, PO Box 1048, Blindern, N-0316, Oslo, Norway, <sup>2</sup>The Future Ocean, IFM-GEOMAR, Wischhofstr. 1-3, 24148 Kiel, Germany. \*Present address: Institut für Mineralogie, Universität Münster, Corrensstr. 24, 48149 Münster, Germany. †e-mail: timm.john@uni-muenster.de.

and hence the protolith and evidence of the incipient local shear failure<sup>13</sup> was preserved. This gabbro is also linked with subduction zone earthquakes, because (1) relatively dry gabbro constitutes most of the lower oceanic crust, (2) the kinetically delayed conversion of oceanic gabbro to eclogite during subduction is often associated with intermediate-depth seismicity and (3) the  $P$ - $T$  conditions of the WGC are representative of intermediate-depth earthquakes in subducting slabs<sup>5,6,15,16,22–25</sup>.

The shear zones have maximum widths of 5 cm, with cores of intensely deformed material surrounded by reaction haloes in which deformation is less obvious (Fig. 1a). Water-bearing minerals are concentrated in shear zones and their abundance decreases towards the deformation front. The metamorphic minerals form strongly deformed symplectites, with grain sizes that are approximately a thousand times smaller than those of the magmatic precursor minerals (Figs 1a and 2a). The symplectites surround only vaguely deformed magmatic clinopyroxene relicts (Fig. 2a). Even very limited subsequent reactivation of deformation would have erased the delicate symplectite textures, indicating that the shear zone was formed during a single event, and that the adjacent wall rocks did not experience polyphase deformation.

Pseudotachylyte fault veins are less than 1 cm thick with sharp contacts to the wall rocks, which are only locally fractured and injected by veins (Fig. 1b). Pseudotachylytes contain  $\mu\text{m}$ - to mm-scale amoeboid and dendrite-like textures of garnet and plagioclase intergrown with eclogite-facies minerals including orthopyroxene, omphacite and amphibole (Fig. 2b), which evince rapid disequilibrium crystallization under high-pressure conditions. These quench textures are formed by rapid solid-state ripening of a microcrystalline matrix<sup>13</sup>. Like the shear zones, the pseudotachylytes record single, rapid events, as the delicate internal textures otherwise would have been erased by even minor reactivated deformation and/or recrystallization. Neither shear zones nor coexisting pseudotachylytes show evidence of a multiphase history, and it is therefore likely that they are manifestations of the same deformation event.

The key observations are that (1) cofacial, eclogite-facies shear zones and pseudotachylytes coexist, (2) both have higher degrees of hydration, caused by infiltration of external fluids, and up to three-orders-of-magnitude-smaller grain sizes than the almost dry wall rock, and (3) both types formed in a single, continuous and fast event. A quantitative model of intermediate-depth seismicity should account for the geological observations outlined above. In particular, the model should explain fault veins with quenched cores and undeformed margins coexisting with un-molten shear zones ( $\gamma \approx 3$ ; 300% shear strain) and causal links between the two. The model of ref. 1 was modified to account for latent heat of melting and the drop in effective viscosity of molten material. The presence of hydrous mineral assemblages in the shear zone and pseudotachylyte led us to consider local perturbations of material properties. The intensity of the perturbation is given by  $\delta$ , the ratio of initial effective viscosities of the background and hydrated rocks. In our numerical simulations, we use  $\delta \approx 100$  estimated from the reduced activation energy for creep due to hydrous minerals and a reduced viscosity coefficient due to grain-size reduction associated with initial hydration reactions (see Supplementary Information, Table S1).

Two numerical simulations were designed to analyse how gabbro reacts to imposed stress and to demonstrate that a one-dimensional model of thermal runaway is consistent with the field observations. Both simulations used an ambient temperature of 680 °C, an initial differential stress of 1.5 GPa and the rheology of diabase<sup>26</sup>. Diabase was chosen because it is a fine-grained equivalent to a gabbro and a grain-size-independent flow law (dislocation creep) was used. The models share the same geometry with a perturbed zone 600 times smaller than the model domain, in accordance with the field observations. The only difference between the models is in

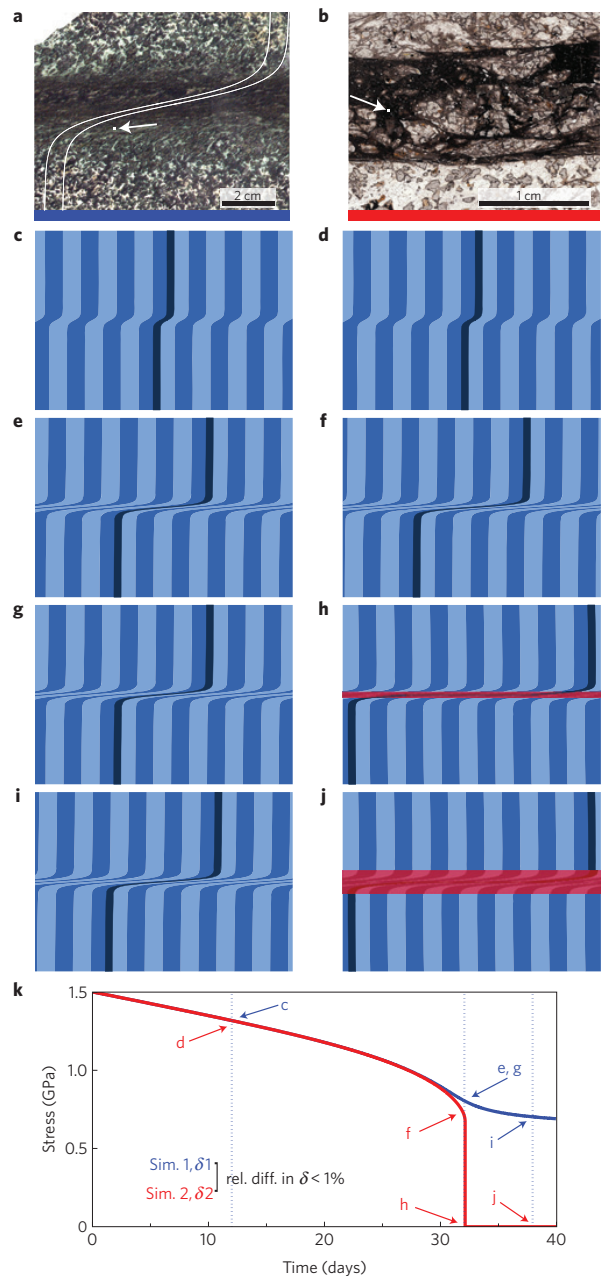


**Figure 1 | Comparison of field observations with the numerical simulations.**

**a, b**, Photomicrographs of a typical shear zone (**a**) and a pseudotachylyte (**b**) from the Kråkenes gabbro. The shear zone shows no signs of melting, whereas the pseudotachylyte has a molten core and limited deformation at the margins. **c–j**, The results of two numerical simulations that reproduce the observed structures. The left-hand column (**c, e, g, i**) illustrates a shear-zone-forming simulation (1) and the right-hand column (**d, f, h, j**) a pseudotachylyte-forming simulation (2). Both columns show the evolution of passive markers together with regions of complete melting (red) for model times shown in the lower plot (**k**). **k**, The time dependence of the stress. The predicted unloading of Simulation 1 (**g**) and the thermal relaxation in Simulation 2 (**j**) are fully consistent with the strain marker patterns recorded in the field. The white curves in **a** are initially vertical lines with the deformation field from **g**. The images in Fig. 2 show the microstructure at the white arrows in **a, b**.

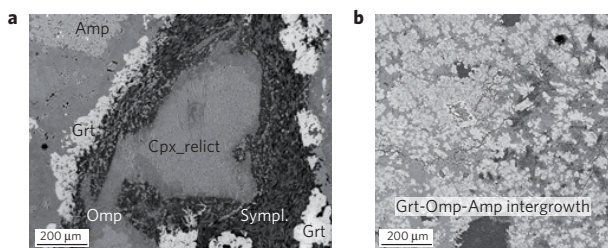


**Figure 2 | Microstructures of a hydrous shear zone and a hydrous pseudotachylyte.** **a**, Hydrous shear zone; **b**, hydrous pseudotachylyte. The delicate fine-grained eclogite-facies textures visible in both images indicate that no reactivation or recrystallization occurred after the primary deformation event. Even minor secondary deformation, reactivation and/or recrystallization would have erased the observed textures (Amp—amphibole; Omp—omphacite; Grt—garnet; Symp.—symplectite consisting mainly of albite + clinzoisite + amphibole; Cpx\_relict—magmatic clinopyroxene relict).

the slightly lower (<1%) initial effective viscosity of the perturbed zone in simulation (2). Figure 1 shows the simulated deformation pattern at four different times. During the first phase (up to the time corresponding to Fig. 1e,f) the two simulations develop similarly and create similar shear zones.

Although the difference between the initial conditions is minor (<1% in  $\delta$ ), the final results are dramatically different, and this sharp transition is consistent with the theory of ref. 1. Although the deformation in simulation (1) becomes localized and the stress drop during the evolution from the time corresponding to Fig. 1e to that corresponding to Fig. 1g is significant (200–300 MPa), the temperatures never exceed 780 °C and no melts are formed. The shear zone predicted by the model is strikingly similar to shear zones in the field (see Fig. 1a,g). In contrast, the transition from the time corresponding to Fig. 1f to the time corresponding to Fig. 1h in simulation (2) results in catastrophic thermal runaway with localization ( $\gamma > 10^3$  in the central part of the zone, which is less than 1 mm wide), a stress drop of ~750 MPa in milliseconds, extensive shear heating that melts the deformation zone (Fig. 1h), and no subsequent deformation. The thermal field in simulation (2) continues to evolve after the initial melting (Fig. 1h–j), and this is consistent with the observed microstructures that indicate stress-free crystallization (Fig. 2b). The final product is a quenched fault-vein with undeformed margins, analogous to field observations (Fig. 1j,b). The second phase of simulation (2) (Fig. 1h) unloads the system owing to the rupture (earthquake) and the stress drop would terminate further evolution of the shear zone in simulation (1). This illustrates that the two modes of deformation may coexist with the same structural orientation and may occur during a single, non-reactivated event.

The numerical simulations provide strong support for the idea that SLTR is a viable mechanism for intermediate-depth earthquakes, under conditions corresponding to those of the metamorphic assemblages in the studied gabbro. An initial stress of 1.5 GPa is chosen in our simulations. We do not address the stress build-up process, but find that the initial conditions used are consistent with laboratory deformation experiments<sup>27–29</sup> so that in the context of strain localization and potential local stress amplification (for example asperity stresses) use of a 1.5 GPa initial stress for modelling is reasonable. More elaborate simulations that include continuous stress loading and weakening due to fluid infiltration or low-temperature plasticity at high confining pressures<sup>29</sup> could significantly lower the stress required to initiate SLTR (see Supplementary Information, Figs S3,S4). The calculated stress drops of about 750 MPa are similar to the conservative

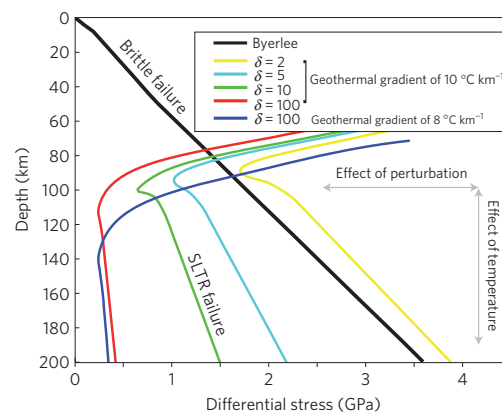


**Figure 3 | Comparison of failure envelopes of SLTR (coloured lines) and Byerlee brittle failure (black line).** The different colours indicate different SLTR parameters. For a wide parameter range, SLTR occurs at lower differential stresses than brittle failure at depths greater than 70 km. Lower geothermal gradients result in a deeper crossover point whereas bigger perturbations (induced by fluid infiltration) result in lower yield stresses. For typical subduction zone geothermal gradients, SLTR is the preferred failure mechanism because it occurs at lower differential stresses. Byerlee brittle failure stress was calculated for a compressional regime assuming zero fluid pressure.

estimates in ref. 17, which showed that paleo-earthquakes in a subduction setting have stress drops of at least 580 MPa. It is also in agreement with seismological evidence that points to stress drops up to 250 MPa (see ref. 30).

Figure 3 shows that the critical stress required to initiate SLTR depends on the average geothermal gradient and initial viscosity perturbation. Comparison of critical stresses with the Byerlee-law brittle yield stress shows that the crossover between failure modes occurs at 60–80 km, comparable to the characteristic pressures of blueschist-to-eclogite-facies metamorphic terrains. At hotter geotherms, the crossover usually occurs at shallower depths, but requires more intense perturbations (see Supplementary Information, Fig. S5). Our findings imply that at greater depths failure by SLTR is more likely than brittle failure, and that SLTR is a viable mechanism for intermediate-depth earthquakes in subducting slabs and continental root zones. SLTR, tested by the combined petrological and numerical study, is an alternative to dehydration embrittlement. Fluids play a major role in both mechanisms, but, in contrast to dehydration embrittlement, the fluid weakening in SLTR is accomplished without a free fluid phase because it is based mainly on an existing perturbation.

Received 25 June 2008; accepted 19 December 2008;  
published online 25 January 2009

## References

- Braeck, S. & Podladchikov, Y. Y. Spontaneous thermal runaway as an ultimate failure mechanism of materials. *Phys. Rev. Lett.* **98**, 095504 (2007).
- Wright, T. W. *Cambridge Monographs on Mechanics* 241 (Cambridge Univ. Press, 2002).
- Kelemen, P. & Hirth, G. A periodic shear-heating mechanism for intermediate-depth earthquake in the mantle. *Nature* **446**, 787–790 (2007).
- Green, H. W. & Houston, H. The mechanics of deep earthquakes. *Annu. Rev. Earth Planet. Sci.* **23**, 169–213 (1995).
- Kirby, S. H., Engdahl, E. R. & Denlinger, R. P. in *Subduction Top to Bottom* (eds Bebout, G. E., Scholl, D. W., Kirby, S. H. & Platt, J. P.) 195–214 (Geophysical Monograph 96, American Geophysical Union, 1996).
- Hacker, B. R., Peacock, S. M., Abers, G. A. & Holloway, S. D. Subduction factory 2. Are intermediate-depth earthquakes in subducting slabs linked to metamorphic dehydration reactions? *J. Geophys. Res.* **108**, 1–16 (2003).

7. Ogawa, M. Shear instability in a viscoelastic material as the cause of deep focus earthquakes. *J. Geophys. Res.* **92**, 13801–13810 (1987).
8. Sibson, R. H. & Troy, V. G. The habitat of fault-generated pseudotachylite: Presence versus absence of friction-melts. *Geophys. Monogr. Ser.* **170**, 153–166 (2006).
9. Di Toro, G., Hirose, T., Nielsen, S., Pennacchioni, G. & Shimamoto, T. Natural and experimental evidence of melt lubrication of faults during earthquakes. *Science* **311**, 647–649 (2006).
10. Hobbs, B. E., Ord, A. & Teyssier, C. Earthquakes in the ductile regime? *Pure Appl. Geophys.* **124**, 309–336 (1986).
11. Obata, M. & Karato, S.-I. Ultramafic pseudotachylite from the Balmuccia peridotite, Ivrea-Verbano zone, northern Italy. *Tectonophysics* **242**, 313–328 (1995).
12. Austrheim, H. & Boundy, T. M. Pseudotachylites generated during seismic faulting and eclogitization of the deep crust. *Science* **265**, 82–83 (1994).
13. Lund, M. G. & Austrheim, H. High-pressure metamorphism and deep-crustal seismicity: Evidence from contemporaneous formation of pseudotachylites and eclogite-facies coronas. *Tectonophysics* **372**, 59–83 (2003).
14. Steltenpohl, M. G., Kassos, G. & Andresen, A. Retrograded eclogite-facies pseudotachylites as deep-crustal paleoseismic faults within continental basement of Lofoten, north Norway. *Geosphere* **2**, 61–72 (2006).
15. Austrheim, H. & Andersen, T. B. Pseudotachylites from Corsica: Fossil earthquakes from a subduction complex. *Terra Nova* **16**, 193–197 (2004).
16. John, T. & Schenk, V. Interrelations between intermediate-depth earthquakes and fluid flow within subducting oceanic plates: Constraints from eclogite-facies pseudotachylites. *Geology* **34**, 557–560 (2006).
17. Andersen, T. B., Mair, K., Austrheim, H., Podladchikov, Y. Y. & Vrijmoed, J. C. Stress-release in exhumed intermediate-deep earthquakes determined from ultramafic pseudotachylite. *Geology* **36**, 995–998 (2008).
18. Labrousse, L. *et al.* Pressure–temperature–time–deformation history of the exhumation of ultra-high-pressure rocks in the Western Gneiss Region, Norway. *Geol. Soc. Am. Spec. Paper* **380**, 155–183 (2004).
19. Austrheim, H. Eclogitization of lower crustal granulites by fluid migration through shear zones. *Earth Planet. Sci. Lett.* **81**, 221–232 (1987).
20. Karato, S.-I. & Jung, H. Effects of pressure on high-temperature dislocation creep in olivine. *Phil. Mag.* **83**, 401–414 (2003).
21. Kohlstedt, D. L. in *Water in Nominally Anhydrous Minerals* (eds Keppler, H. & Smyth, J. R.) 377–396 (Reviews in Mineralogy and Geochemistry, Vol. 62, 2006).
22. Hacker, B. R. in *Subduction Top to Bottom* (eds Bebout, G. E., Scholl, D. W., Kirby, S. H. & Platt, J. P.) 337–346 (Geophysical Monograph 96, American Geophysical Union, 1996).
23. Yuan, X. *et al.* Subduction and collision processes in the central Andes constrained by converted seismic phases. *Nature* **408**, 958–961 (2000).
24. Wayte, G. J., Worden, R. H., Rubie, D. C. & Droop, G. T. R. A TEM study of disequilibrium plagioclase breakdown at high pressure; the role of infiltrating fluid. *Contrib. Mineral. Petrol.* **101**, 426–437 (1989).
25. Rondenay, S., Abers, G. A. & van Keken, P. E. Seismic imaging of subduction zone metamorphism. *Geology* **36**, 275–278 (2008).
26. Mackwell, S. J., Zimmerman, M. E. & Kohlstedt, D. L. High-temperature deformation of dry diabase with application to tectonics on Venus. *J. Geophys. Res.* **103**, 975–984 (1998).
27. Li, L., Weidner, D., Raterron, P., Chen, J. & Vaughan, M. Stress measurements of deforming olivine at high pressure. *Phys. Earth Planet. Inter.* **143**, 357–367 (2004).
28. Boettcher, M. S., Hirth, G. & Evans, B. Olivine friction at the base of oceanic seismogenic zones. *J. Geophys. Res.* **112**, B01205 (2007).
29. Renshaw, C. E. & Schulson, E. M. Limits on rock strength under high confinement. *Earth Planet. Sci. Lett.* **258**, 307–314 (2007).
30. Kanamori, H. Mechanics of earthquakes. *Annu. Rev. Earth Planet. Sci.* **22**, 207–237 (1994).

### Acknowledgements

We acknowledge discussions at PGP, particularly with S. Braeck, and proof reading by P. Meakin, G. Hirth and C. Marone provided constructive and helpful reviews. This study was supported by a Center of Excellence grant to PGP from the Norwegian Research Council.

### Author contributions

All authors participated in collecting the data, interpretation of results and developing the model. T.J., T.B.A. and H.A. focused on the fieldwork, sampling and petrology, and T.J., S.M., L.H.R. and Y.Y.P. focused on the numerical simulations.

### Additional information

Supplementary Information accompanies this paper on [www.nature.com/naturegeoscience](http://www.nature.com/naturegeoscience). Reprints and permissions information is available online at <http://npg.nature.com/reprintsandpermissions>. Correspondence and requests for materials should be addressed to T.J.

## Clinopyroxene–rutile phyllonites from the East Tenda Shear Zone (Alpine Corsica, France): pressure–temperature–time constraints to the Alpine reworking of Variscan Corsica

MATTEO MAGGI<sup>1</sup>, FEDERICO ROSSETTI<sup>1\*</sup>, FERNANDO CORFU<sup>2</sup>, THOMAS THEYE<sup>3</sup>,  
TORGEIR B. ANDERSEN<sup>2</sup> & CLAUDIO FACCHENNA<sup>1</sup>

<sup>1</sup>*Dipartimento di Scienze Geologiche, Università Roma Tre, Roma, Italy*

<sup>2</sup>*Department of Geosciences, Oslo University, Oslo, Norway*

<sup>3</sup>*Institut für Mineralogie und Kristallchemie, Universität Stuttgart, Stuttgart, Germany*

\*Corresponding author (e-mail: [rossetti@uniroma3.it](mailto:rossetti@uniroma3.it))

**Abstract:** The East Tenda Shear Zone is the regional structure that marks the Alpine overthrusting of the Ligurian–Piedmontese ocean onto the Variscan Corsica. We present the first report of a Na-pyroxene (acmite)–rutile-bearing assemblage from a phyllonitic shear zone that occurs within the gneissic lithologies of the East Tenda Shear Zone. Acmite hosts inclusions of Na-amphibole and titanite, and is rimmed by retrogressive biotite. Forward modelling of the shear zone assemblages in the NCKFMASHO chemical system indicates a cold burial–exhumation path (palaeogeothermal gradient <10 °C km<sup>-1</sup>) and a metamorphic climax with minimum pressure of 1.2 GPa and temperatures of 350–400 °C. U–Pb thermal ionization mass spectrometry analyses on synkinematic rutile yield a 3D array with an age of 48 ± 18 Ma (MSWD 7.3), whereas coexisting acmite–phengite and coatings of oxides or sulphides provide an intercept at 54 ± 8 Ma (MSWD = 48). The scatter of the arrays is considered to reflect secondary disturbances of the system and the age provided by acmite–phengite and the coatings at 54 ± 8 Ma is considered the most reliable estimate for shear zone formation. Implications of these new metamorphic and geochronological data are discussed in the regional framework of the Alpine geology and integrated in the plate-tectonic scenario of the central Mediterranean.

Shear zones in the middle and lower crust exert an important control on the metamorphic processes and tectonic reworking in orogenic belts (e.g. Austrheim 1987; Selverstone *et al.* 1991; Imber *et al.* 1997; Jolivet *et al.* 2005). The systematic spatial association between zones of ductile deformation and zones of fluid infiltration has led many researchers to suggest that deformation, fluid flow, metamorphic reactions and changes in the bulk rheology are mutually reinforcing processes (e.g. Austrheim 1987; Dipple & Ferry 1992; Jolivet *et al.* 2005; John *et al.* 2009). Furthermore, enhanced fluid–rock interaction in shear zones may cause major changes in mineralogy and bulk-rock chemistry via metasomatism, including the resetting of radiogenic as well as stable isotopes (e.g. Selverstone *et al.* 1991; Clark *et al.* 2005). Such pervasive changes are useful for determining the conditions and timing of deformation, which otherwise may be subtle and barely detectable in the unreacted rock mass. This is particularly relevant at depth within continental basement complexes reactivated during orogenic events, as granitoids and high-grade metamorphic or other mostly ‘dry’ rocks are the dominant lithology (e.g. Labrousse *et al.* 2010).

In this paper we present new petrological and geochronological data from the East Tenda Shear Zone of Alpine Corsica (Fig. 1). This shear zone is the deformation zone that marks the Alpine overthrusting of the Ligurian–Piedmontese oceanic domain (Schistes Lustrés unit) onto the basement rocks of the Variscan Corsica (see Gueydan *et al.* 2003; Molli & Malavieille 2010; Fig. 1b). Despite the regional significance, the pressure–temperature–time (*P–T–t*) evolution of this shear zone is still poorly constrained, particularly concerning the timing of the Alpine metamorphic climax. We report the first occurrence of clinopyroxene (acmite)–rutile assemblages from the East Tenda Shear Zone and fix the time of the Alpine high-pressure stage in the Early Eocene (54 ± 8 Ma) by

U–Pb isotope dilution thermal ionization mass spectrometry (ID-TIMS) dating of the synkinematic assemblage. The implications of these new metamorphic and geochronological data, which are coupled to fabric development within the East Tenda Shear Zone, are discussed in the regional framework of the Alpine geology of the central Mediterranean.

### Regional geological setting

The island of Corsica is located in the centre of the western Mediterranean, between the Liguro-Provençal and Tyrrhenian back-arc basins (Fig. 1a). The island consists mostly of a variably deformed Variscan crystalline basement with a Permian–Eocene sedimentary cover, which constituted part of the European foreland domain of the Alpine orogeny (e.g. Rossi *et al.* 2003; Malasoma & Marroni 2007). Alpine Corsica forms the northeastern parts of the island, and is made up of a nappe stack largely composed of ophiolitic rocks with associated (meta)-sedimentary cover and slivers of continental basement, composed of rocks originally formed within the Neotethyan Ligurian–Piedmontese oceanic basin and along the Tethyan ocean–continent transition (see Vitale Bravarone *et al.* 2011a; Fig. 1b). The structural architecture of Alpine Corsica consists of a lower nappe system (the Schistes Lustrés nappe) affected by subduction zone metamorphism and an upper, low-grade metamorphosed nappe complex comprising the Balagne, Nebbio and Macinaggio units (e.g. Mattauer *et al.* 1981; Dallon & Nardi 1984; Durand-Delga 1984; Waters 1990; Fournier *et al.* 1991; Dallon & Pulcinelli 1995; Daniel *et al.* 1996; Malavieille *et al.* 1998; Rossi *et al.* 2003; Molli & Malavieille 2010). During the Alpine orogeny the continental European basement, the ophiolitic rocks of the Ligurian–Piedmontese basin and their deep-marine sedimentary

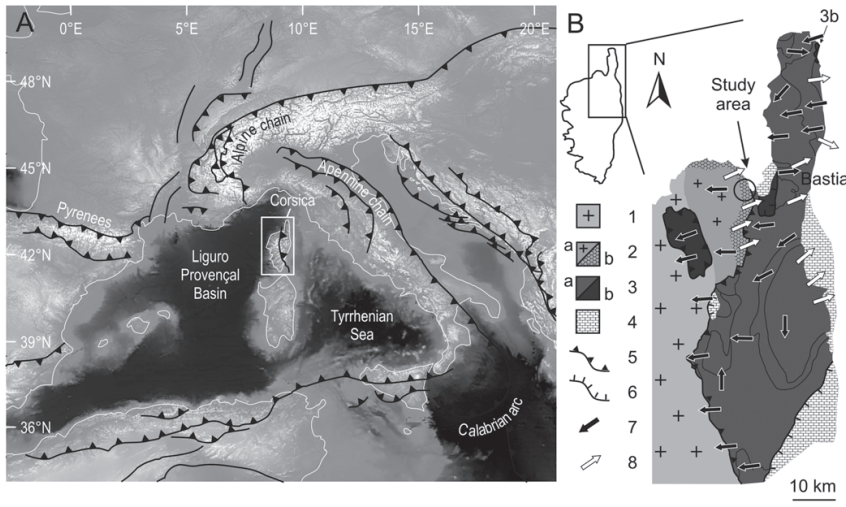


**Fig. 1.** (a) Digital elevation model of the western Mediterranean region with the main tectonic boundaries indicated (modified after Jolivet *et al.* 1998). The white rectangle indicates the position of Corsica. (b) Synthetic structural–geological map of Alpine Corsica (modified after Daniel *et al.* 1996; Molli & Malavieille 2010, and reference therein). 1, Hercynian basement; 2a, Tenda unit; 2b, East Tenda Shear Zone (ETSZ); 3, Ocean-derived units (a, Schistes Lustrés units; b, Balagne, Nebbio and Macinaggio units); 4, Miocene and Quaternary deposits; 5, main thrusts; 6, main extensional faults and detachments; 7, D<sub>1</sub> sense of shear; 8, D<sub>2</sub> sense of shear.

cover were affected by the subduction-related blueschist- to eclogite- and lawsonite-eclogite-facies metamorphism (e.g. Essene 1968; Caron *et al.* 1981; Lahondère & Guerrot 1997; Tribuzio & Giacomini 2002; Chopin *et al.* 2008; Ravna *et al.* 2010; Vitale Bravarone *et al.* 2011a, b).

The transition between the Variscan and the Alpine domains occurs along the Tenda Massif, in a deformation zone that formerly constituted the extended continental margin of the European basement (see Molli & Malavieille 2010), known as the East Tenda Shear Zone. This portion of the Variscan crust was strongly reworked during the Alpine orogeny, synkinematically with epidote- to blueschist-facies metamorphism (Gibbons & Horak 1984; Daniel *et al.* 1996; Tribuzio & Giacomini 2002; Gueydan *et al.* 2003; Molli *et al.* 2006). The fabrics of the East Tenda Shear Zone are composite, recording both the overthrusting and the subsequent exhumation of the Schistes Lustrés nappe. Contrasting kinematic and tectonic interpretations have previously been proposed to explain these fabrics. Molli *et al.* (2006) emphasized the top-to-the-west compressional shearing as the dominant structural grain in the East Tenda Shear Zone, whereas others considered top-to-the-east ductile-to-brittle extensional reactivation along the contact with the Schistes Lustrés to be the dominant fabric (Jolivet *et al.* 1990; Gueydan *et al.* 2003; Daniel *et al.* 1996).

The age of the HP–LT Alpine deformation and metamorphism in Corsica is still poorly constrained (see recent summary by Martin *et al.* 2011). The earliest and coldest metamorphic stage, which produced lawsonite-bearing eclogites near the ‘forbidden zone’ in parts of the Schistes Lustrés units (Ravna *et al.* 2010; Vitale Bravarone *et al.* 2011b) is believed to be late Cretaceous (e.g. Molli & Malavieille 2010, and references therein), based on the available Sm–Nd whole-rock (garnet–glaucophane–clinopyroxene) isochron age of  $84 \pm 5$  Ma (Lahondère & Guerrot 1997) and the *c.* 90 Ma  $^{40}\text{Ar}/^{39}\text{Ar}$  glaucophane ages (Maluski 1977) from eclogite lenses within the Schistes Lustrés. Lawsonite eclogites were synkinematically decompressed at both blueschist and later greenschist facies, and have therefore experienced a protracted structural and metamorphic history. Recent U–Pb zircon ages from continental-derived granulite slivers found within the Schistes Lustrés gave an age of  $34.4 \pm 0.8$  Ma that is considered to date the Alpine pressure peak during reactive fluid infiltration in Alpine Corsica (Martin *et al.* 2011). This Tertiary age is in line with the biostratigraphic constraints provided by the nummulite-bearing sedimentary

sequences of the Alpine foreland involved in the Alpine nappe construction, which suggests a post Middle Eocene orogenic construction and metamorphism at the expense of the Corsica–Europe continental margin (Bezert & Caby 1988; Egal 1992; Brunet *et al.* 2000; Malasoma & Marroni 2007). In the Schistes Lustrés, Tertiary metamorphic ages are provided by  $^{40}\text{Ar}/^{39}\text{Ar}$  geochronology (Maluski 1977; Amaudric Du Chaffaut & Saliot 1979; Brunet *et al.* 2000). In particular, discordant  $^{40}\text{Ar}/^{39}\text{Ar}$  phengite ages ranging from 65 to 55 Ma and from 55 to 37 Ma are derived from eclogite and blueschist units, respectively (Brunet *et al.* 2000). In the East Tenda Shear Zone,  $^{40}\text{Ar}/^{39}\text{Ar}$  phengite dating provided ages between 45 and 30 Ma (Brunet *et al.* 2000), whereas earlier Rb–Sr whole-rock data point to a Middle Cretaceous ( $108 \pm 5$  Ma) age (Cohen *et al.* 1981).

### Structures and petrography

Deformation is heterogeneously distributed within the East Tenda Shear Zone, with zones of localized ductile-to-brittle shearing (SZ) that wrap around lens-shaped massive lenses (ML) with a prominent gneissic texture (Figs 2 and 3a). The main foliations in the East Tenda Shear Zone and the overlying Schistes Lustrés are nearly concordant and strike NW–SE and dominantly dip shallowly towards the NE (Fig. 2). In the following, mineral abbreviations follow Whitney & Evans (2010).

The mineralogy of the ML consists of a high-variance assemblage of Qz, Ph and relic igneous Fsp with Ep, Fe-oxides, relic Zrn and Aln as accessory phases. The SZ mineralogy is invariably dominated (40–60 vol%) by highly substituted Ph ( $\text{Si}^{4+} = 3.5\text{--}3.7$  a.p.f.u.), modally abundant Qz (30–50 vol%), Ab (10–20 vol%), Ep (5–10 vol%) and Mc (5–10 vol%). Locally, Na–Amp (10–20 vol%) also occurs in the SZ assemblage to form mostly thin (up to 0.5 m thick) dark bluish mylonitic layers (Fig. 3a and b). Stretching lineations trend WSW–ENE to east–west (Fig. 2) and are provided by aggregates of Qz–Ph–Ab in the ML and of Qz–Ph–Ab ± Na–Amp in the SZ. Kinematic indicators, at outcrop and thin-section scale, systematically indicate top-to-the-west ductile shear sense in both ML and SZ (Fig. 3b and c). Semi-brittle to brittle top-to-the-east shear bands locally reactivate the main top-to-the-west ductile shear fabrics. This late deformation is mostly localized within the phyllonitic shear zones (Fig. 3d).

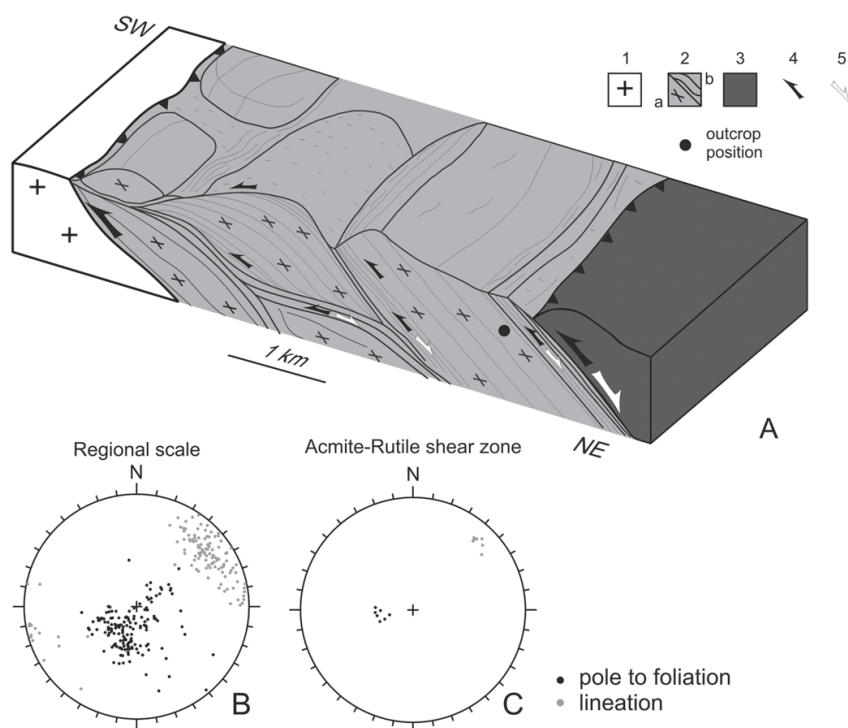


**Fig. 2.** (a) Schematic 3D interpretative block diagram to illustrate the structural architecture and shear fabric within the East Tenda Shear Zone. Shear strain partitioning occurs within this shear zone, with low-strain domains corresponding to the gneissic (massive) lenses wrapped by high-strain domains consisting of mylonitic to phyllonitic shear zones. The kinematics relative to the main compressional fabric development ( $D_1$ ) and the later extensional reactivation ( $D_2$ ) are also indicated. 1, protolith rocks; 2, East Tenda Shear Zone units (2a, massive lenses; 2b, shear zones); 3, Schistes Lustrés units; 4, compressional shear senses; 5, extensional shear reactivation. (b, c) Representative stereoplots (Schmidt net, lower hemisphere projection) showing the plano-linear shear fabrics at regional (b) and outcrop (c) scale.

Approximately 200 m structurally below the main contact with the Schistes Lustrés (i.e. normal to the main foliation), a 10 cm thick, discontinuous clinopyroxene (acmite)–rutile (Cpx–Rt) phyllonitic shear zone was found, in sharp contact with the host ML (Fig. 3g and f; geographical coordinates  $42^{\circ}39'23.34''N$ ,  $9^{\circ}16'20.74''E$ ). Stretching lineations are provided by Ph–Qz–Cpx–Rt aggregates  $\pm$  Fsp (Fig. 3g). The modal composition of the phyllonite consists of Ph (>60 vol%), Cpx (20–25 vol%), Qz (2–5 vol%), Rt (2–5 vol%) and alkaline Fsp (Ab and Mc) + Ep + relic Zrc (<5 vol%) as minor phases (Fig. 4a). The Cpx crystals host inclusions of Na–Amp and Ttn and are rimmed by retrogressive Bt; Rt forms porphyroblasts along the main phyllonitic foliation (Fig. 4b and c). Microprobe data and back-scattered electron (BSE) images indicate a rather homogeneous composition both for the Ph (3.6–3.7  $Si^{4+}$  a.p.f.u.) and Cpx (average composition  $Acm_{72}Jd_{17}Di_9Hed_1Opx_{0.05}$ ) (Table 1; Fig. 5). In contrast, Ph in the host rocks shows a strong core-to-rim zonation ( $Si^{4+}$  content ranging from 3.3 a.p.f.u. in the core to 3.6 a.p.f.u. in the rim) (Table 1; Figs 4d and 5a). The phengite compositions of rims and in the Cpx–Rt shear zone significantly deviate from the ideal Tschermak's substitution line, suggesting that some of the iron is ferric (Fig. 5a).

### Thermobarometry of the Cpx–Rt shear zone

Because of the high-variance shear zone assemblage (Ph–Cpx–Rt–Qz  $\pm$  Fsp (Ab and Mc)  $\pm$  Ep), the inverse (conventional and multi-equilibrium) thermobarometry is not applicable. Accordingly, we adopted a forward modelling technique to infer the pressure–temperature ( $P$ – $T$ ) conditions of formation of the Cpx–Rt shear zone. The  $P$ – $T$ – $X$  modelling was computed using the Perple\_X\_07 software (Connolly 2005; <http://www.perplex.ethz.ch/>) in the NKFMASTO ( $Na_2O$ – $K_2O$ – $FeO$ – $MgO$ – $Al_2O_3$ – $SiO_2$ – $H_2O$ – $TiO_2$ – $O_2$ ) chemical system, for bulk-rock compositions as calculated

from mineral modal compositions and electron microprobe data. We used the thermodynamics dataset of Holland & Powell (1998; updated in 2002) for minerals and aqueous fluids, integrated with those of Massonne & Willner (2008) for low-grade metamorphic  $Fe^{3+}$ -bearing phases (Cpx and Na–Amp). In particular, the following solution models offered by Perple\_X\_07 were chosen: Bio(HP) for Bt, Chl(HP) for Chl, Ep(HP) for Ep, GlTrTsMr for Na–Amp, Acm(M) for Cpx, Gt(HP) for Grt, and fsp11 for Fsp. Water content was considered to be always in excess.

A representative pseudosection is shown in Figure 6. The synkinematic Rt–Cpx–Ph–Qz  $\pm$  Na–Amp assemblage occurs in a narrow divariant field with minimum pressure of 1.1–1.2 GPa and temperature between 350 and 400 °C. The  $Si^{4+}$  isopleths for Ph were calculated to derive a possible  $P$ – $T$  path. Metamorphic climax is not well constrained. Nevertheless, the presence of Cpx and Rt (and not Ab or Ttn; for pressure) and the absence either of Lws or Bt (for temperature) indicate minimum peak  $P$ – $T$  conditions for the shear zone development at 1.1–1.2 GPa and *c.* 400 °C.

To constrain the  $P$ – $T$  path of the East Tenda Shear Zone, the following points should be taken into account: (1) the systematic rimward increase of  $Si^{4+}$  in Ph (from 3.3 to 3.6 a.p.f.u.) from the gneissic host rocks; (2) the Na–amph inclusion in Cpx; (3) the only minor core-to-rim variation of  $Si^{4+}$  a.p.f.u. in Ph from the Cpx–Rt shear zone. Points (1) and (2) indicate a prograde increase in pressure, whereas point (3) suggests maintenance of highly substituted phengite compositions during exhumation of the East Tenda Shear Zone (Fig. 6). We then propose that the Alpine reworking of the Variscan basement along the East Tenda Shear Zone occurred under a cold (<10 °C km<sup>−1</sup>) geothermal gradient during a clockwise burial–exhumation path, nearly parallel to the phengite isopleths after achievement of the metamorphic peak (Fig. 6).

The results described above are affected by some degree of uncertainty, mainly owing to the following: (1) representativeness

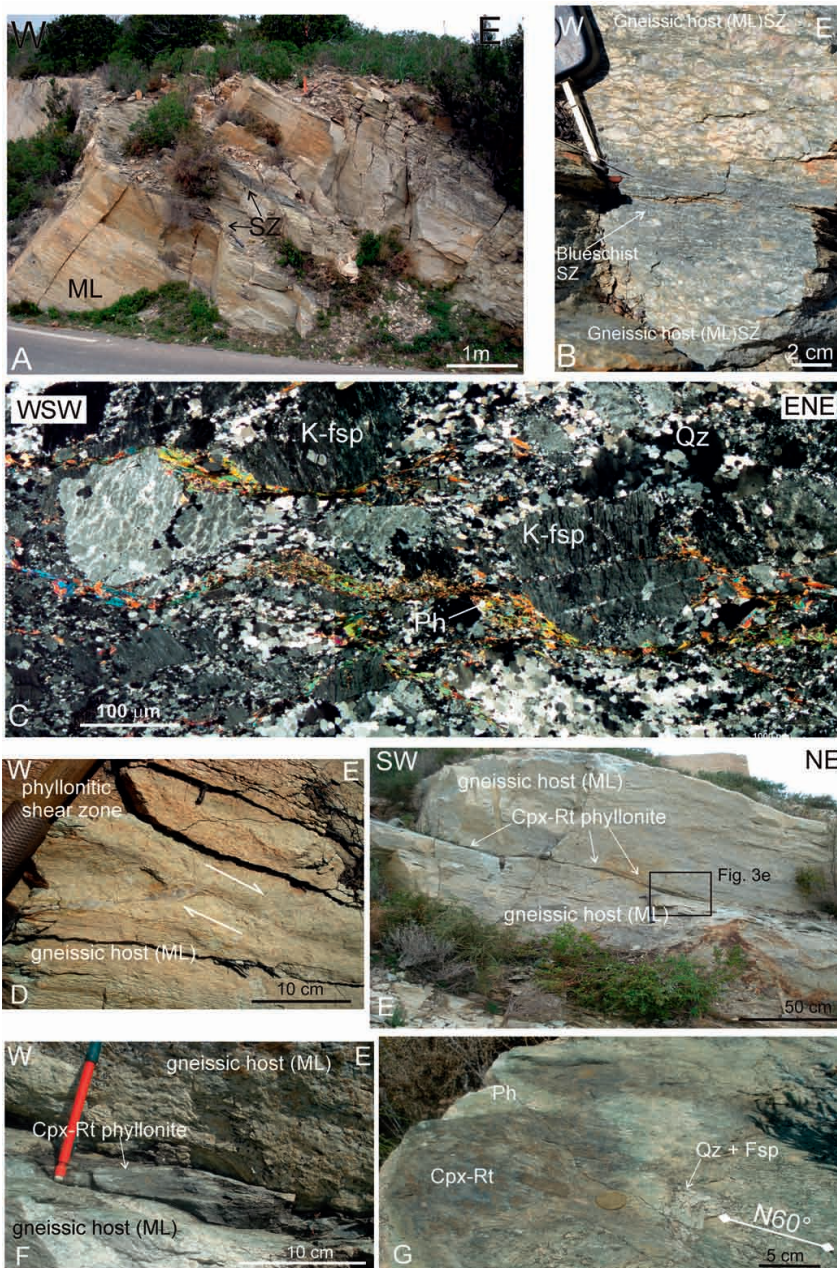


**Fig. 3.** (a) Discrete, blueschist-facies mylonites (phylonites) cutting across gneissic bodies along the East Tenda Shear Zone. (b) A detail of the gneiss–blueschist mylonite transition at the outcrop scale. The pronounced grain-size reduction on entering the shear zone should be noted. Shear sense sinistral (top-to-the-west) as primarily provided by the overall S-C fabric and  $\sigma$ -type quartz and feldspar porphyroclasts in the gneissic host rocks (exposure normal to foliation and parallel to stretching direction). (c) Thin section of the gneissic host rocks (section normal to foliation and parallel to stretching lineation; crossed polars). Relic  $\sigma$ -shaped K-feldspar porphyroclasts are embedded in a fine-grained recrystallized quartz–phengite shear matrix. Shear sense sinistral (top-to-the-WNW) as indicated by oblique foliation, mica fish and  $\sigma$ -type feldspar porphyroclasts. (d) Semi-brittle, top-to-the-east shearing that reworks the early top-to-the-west mylonitic shear fabrics of the East Tenda Shear Zone. (e) The acmite–rutile (Cpx–Rt) phyllonite in the field. The sharp boundaries of the shear zone with the massive gneissic host rocks should be noted. (f) Detail of (e), showing the shear zone–host rock transition marked by the progressive grain-size reduction and increase of the phengite content. (g) Plane view of the acmite–rutile shear zone showing well-developed stretching lineations as provided by the Cpx–Rt–Qz–Fsp assemblage. Mineral abbreviations follow Whitney & Evans (2010).

of the used bulk composition, particularly of the  $O_2$  content; (2) variation of the bulk-rock composition induced by fluid–rock interaction during progressive shearing; (3) significant uncertainty of the thermodynamic dataset in the low  $T$  range. Accordingly, forward modelling of the Cpx–Rt shear zone can be considered as tentative only and  $P$ – $T$  estimates as semi-quantitative. Nevertheless, trial calculations with variations of  $O_2$  content, as well as using different bulk compositions, did not result in significant modification of the general aspects of the derived  $P$ – $T$  path, which was dominantly constrained by the positive slope of the Ph isopleths in the  $P$ – $T$  interval of interest. In addition, the obtained results are compatible with the previous  $P$ – $T$  estimates on the Alpine metamorphic

climax along the East Tenda Shear Zone, which collectively document epidote- to blueschist-facies peak metamorphism (Tribuzio & Giacomini 2002; Molli *et al.* 2006)

### TIMS U–Pb geochronology

To establish the age of shearing along the East Tenda Shear Zone, we analysed Rt and coexisting Cpx, Ph, and oxide or sulphide coatings on Qz. The minerals used for analysis were extracted from the schist by crushing, pulverizing and enrichment on a Wilfley table, and by using magnetic separators and heavy liquid. The selected minerals were dissolved in concentrated HF (+  $HNO_3$ ); the Rt in

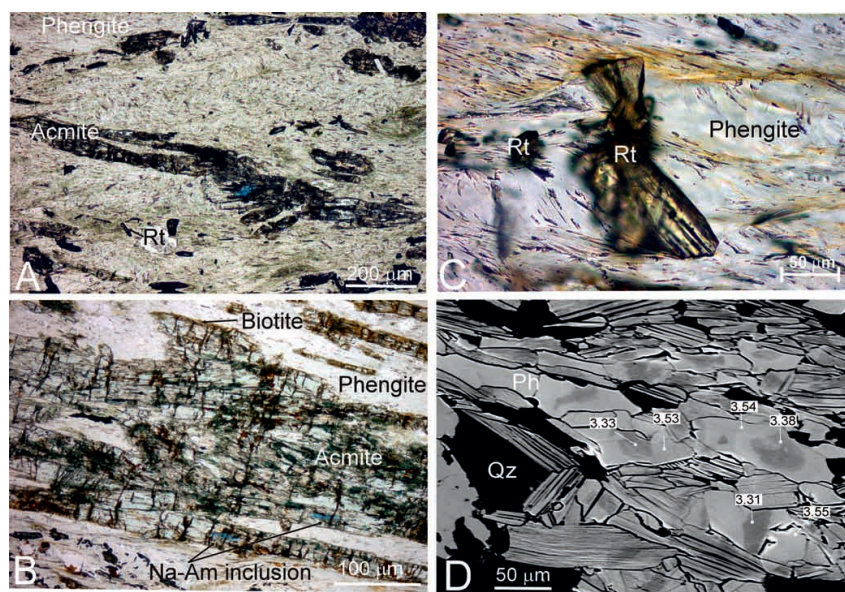


**Fig. 4.** (a) Thin section of the acmite-rutile (Cpx-Rt) shear zone showing Cpx and Rt neoblasts embedded in a microcrystalline phengite (Ph) matrix (plane-polarized light). (b) Thin section showing porphyroblastic Cpx hosting inclusions of Na-Amph, rimmed by retrogressive biotite (plane-polarized light). (c) Porphyroblastic Rt in the rock matrix (plane-polarized light). (d) BSE image of the gneissic host rock showing Ph zoning as documented by the Si<sup>4+</sup> a.p.f.u. content.

**Table 1.** Representative mineral compositions of the Cpx-Rt shear zone samples

Mineral: Sample:	Phengite						Clinopyroxene			Biotite			Na-amphibole (inclusion in Cpx)					
	Host rock		Cpx-Rt shear zone				Cpx-Rt shear zone			Cpx-Rt shear zone			Cpx-Rt shear zone					
	core	rim	core	rim	15	19	1	4	10	6	13	17	20	14	19			
Analysis:	1	3	5	7	15	19	1	4	10	6	13	17	20	14	19			
SiO <sub>2</sub>	49.48	50.20	49.85	50.72	51.88	55.13	SiO <sub>2</sub>	54.29	54.04	52.91	SiO <sub>2</sub>	37.18	37.02	37.77	SiO <sub>2</sub>	55.11	55.63	55.34
TiO <sub>2</sub>	0.09	0.53	0.03	0.62	0.53	0.22	TiO <sub>2</sub>	0.77	0.30	0.10	TiO <sub>2</sub>	1.70	0.80	0.57	TiO <sub>2</sub>	0.06	0.06	0.15
Al <sub>2</sub> O <sub>3</sub>	27.83	23.51	27.99	22.19	19.00	18.43	Al <sub>2</sub> O <sub>3</sub>	5.07	5.64	2.64	Al <sub>2</sub> O <sub>3</sub>	12.50	11.86	10.94	Al <sub>2</sub> O <sub>3</sub>	2.27	2.31	2.28
FeO <sub>tot</sub>	3.87	6.33	3.48	6.02	6.28	4.57	FeO <sub>tot</sub>	22.18	20.51	27.34	FeO <sub>tot</sub>	31.58	33.00	34.37	FeO <sub>tot</sub>	22.47	21.03	22.28
MnO	0.24	0.12	0.23	0.17	bdl	0.04	MnO	0.01	0.05	0.02	MnO	0.15	0.12	0.08	MnO	0.12	0.12	0.15
MgO	1.85	2.49	1.96	2.42	5.18	6.62	MgO	1.70	2.22	0.43	MgO	2.72	3.40	1.56	MgO	8.63	9.40	8.60
CaO	bdl	bdl	bdl	0.01	0.03	0.00	CaO	2.54	3.12	0.56	CaO	0.02	bdl	Bdl	CaO	0.36	0.28	0.39
Na <sub>2</sub> O	0.01	0.06	0.01	0.26	0.25	0.03	Na <sub>2</sub> O	12.53	12.29	13.28	Na <sub>2</sub> O	0.07	0.05	1.00	Na <sub>2</sub> O	6.97	7.33	7.09
K <sub>2</sub> O	11.71	11.42	11.65	10.41	10.00	11.04	K <sub>2</sub> O	bdl	bdl	bdl	K <sub>2</sub> O	9.55	9.66	8.47	K <sub>2</sub> O	0.28	0.47	0.31
BaO	0.04	0.04	0.01	0.24	0.05	0.04	BaO	bdl	0.02	bdl	BaO	0.03	0.05	0.18	BaO	bdl	bdl	bdl
Total	95.12	94.70	95.21	93.06	93.20	96.11	Total	99.09	98.19	97.28	Total	95.50	95.96	94.94	Total	96.27	96.63	96.59
Si	3.363	3.471	3.372	3.541	3.589	3.698	Si	1.993	1.990	1.997	Si	3.011	3.011	3.114	Si	7.988	7.977	7.991
Ti	0.004	0.027	0.001	0.033	0.028	0.011	Al <sub>T</sub>	0.007	0.010	0.003	Al <sub>T</sub>	0.989	0.989	0.886	Ti	0.006	0.007	0.017
Al	2.229	1.916	2.231	1.826	3.098	2.914	Al <sub>O</sub>	0.213	0.235	0.115	Al <sub>O</sub>	0.204	0.148	0.176	Al	0.388	0.390	0.389
Fe <sup>2+</sup>	0.220	0.366	0.197	0.352	0.237	0.196	Ti	0.021	0.008	0.003	Ti	0.104	0.049	0.035	Fe <sup>3+</sup>	1.531	1.595	1.526
Mn	0.014	0.007	0.013	0.010	0.000	0.000	Fe <sup>3+</sup>	0.643	0.632	0.855	Fe <sup>2+</sup>	2.139	2.245	2.370	Fe <sup>2+</sup>	1.193	0.927	1.164
Mg	0.188	0.257	0.198	0.252	0.534	0.662	Fe <sup>2+</sup>	0.038	0.000	0.008	Mn	0.011	0.008	0.006	Mn	0.015	0.015	0.018
Ca	0.000	0.000	0.000	0.001	0.000	0.000	Mn	0.000	0.001	0.001	Mg	0.328	0.413	0.191	Mg	1.865	2.009	1.851
Ba	0.001	0.001	0.000	0.007	0.000	0.000	Mg	0.093	0.122	0.024	Ba	0.001	0.000	0.000	Ca	0.056	0.043	0.060
Na	0.001	0.008	0.001	0.035	0.034	0.004	Ca	0.100	0.123	0.022	Ca	0.003	0.004	0.016	Na	1.959	2.038	1.985
K	1.015	1.007	1.005	0.927	0.882	0.944	Na	0.892	0.877	0.972	Na	0.011	0.008	0.160	K	0.052	0.086	0.057
							K				K	0.986	1.003	0.891				
							Jd	0.227	0.245	0.118					Gln	0.118	0.128	0.121
							Acm	0.665	0.632	0.855	X <sub>Mg</sub>	0.133	0.155	0.075	Fe-Gln	0.075	0.059	0.076
							Di	0.071	0.123	0.017					Mg-Rbk	0.480	0.556	0.488
							Hd	0.029	0.000	0.006					Rbk	0.3069	0.2566	0.3070
							Opx	0.008	0.000	0.005					Act	0.0206	0.0000	0.0076

The analyses are normalized to fixed oxygen: phengite, O=11; biotite, O=11; amphibole, O=23; total cations without K=15; pyroxene, O=6, total cations=4. bdl, below detection limit. Mineral abbreviations follow Whitney & Evans (2010).

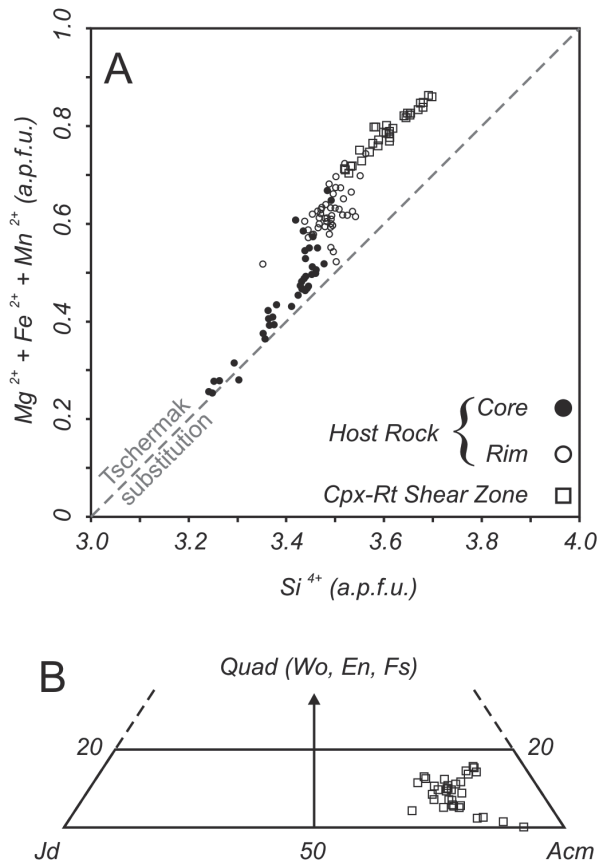


**Fig. 5.** (a) Si vs (Mg + Fe + Mn) diagram showing the phengite compositions both in the host rock and in the Cpx-Rt shear zone. Host rock analyses (rim + core) scatter along the muscovite-celadonite substitution line (slope = 1) and range between 3.3 and 3.6  $Si^{4+}$  a.p.f.u. whereas the Cpx-Rt shear zone analyses are clustered in the 3.6–3.7 range. (b) Quad-Jd-Acm diagram showing the Cpx chemical composition. Quad represents the Ca-Fe-Mg pyroxene vertex.

bombs at *c.* 190 °C, and the other minerals in Savillex vials on a hotplate at around 100 °C. Chemical separation was performed with a two-stage anion exchange procedure using HBr for Pb and  $HNO_3 + HCl$  for U on AG 1-X8, 200–400 mesh resin. The samples were spiked with a  $^{202}Pb$ - $^{205}Pb$ - $^{235}U$  spike. Other details of the procedure and measurement have been given by Corfu (2004). The decay constants are those of Jaffey *et al.* (1971). Plotting and regressions employed the program Isoplot of Ludwig (2003). Results are listed in Table 2 and shown in Figure 7.

Rt consists largely of tabular twinned prisms containing 5–15 ppm U and 0.3–4 ppm initial Pb. Cpx has mostly about 0.5 ppm U and half as much initial Pb. One fraction of Cpx was selected among grains full of Rt inclusions, the Cpx was dissolved at low temperature, and the residual Rt was recovered and dissolved separately. In this case the Cpx analysis yielded much higher U (11 ppm) and initial common Pb (5 ppm) contents; the liberated Rt consisted of very small and fragile pieces that could not be weighed. The data for all these minerals are all relatively unradiogenic, hence the age calculation is strongly dependent on the common Pb correction. The least radiogenic composition was found in the coatings of oxide or sulphide on Qz, although these values are clearly more radiogenic than

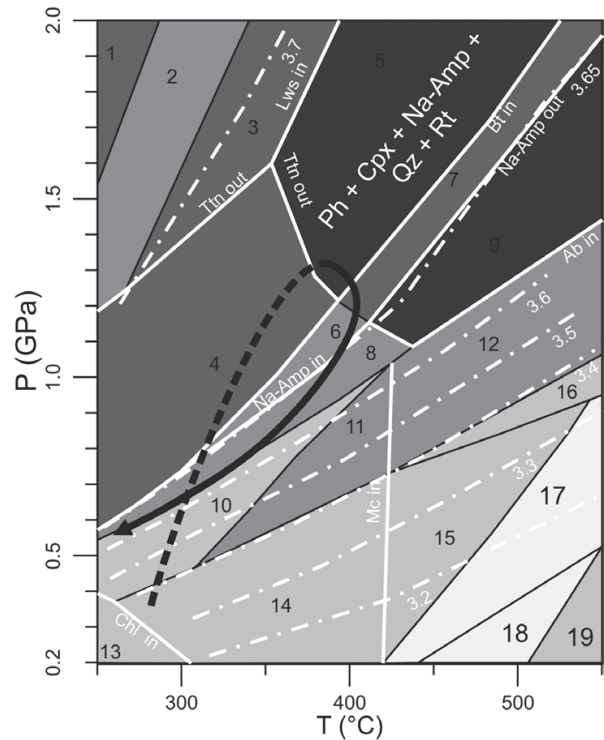


**Fig. 6.** *P*-*T* pseudosection in the NCKFMASHTO system as obtained with the *Perple\_X\_07* software using a bulk composition of (wt %)  $Na_2O$  0.82,  $CaO$  0.53,  $K_2O$  9.50,  $FeO_{tot}$  7.54,  $MgO$  4.40,  $Al_2O_3$  16.35,  $SiO_2$  53.60,  $TiO_2$  1.76 and  $O_2$  0.30, with  $H_2O$  as saturated phase (mineral abbreviations after Whitney & Evans 2010). The continuous white lines indicate stability fields of the main phases; the white dot-dash lines are isopleths of the  $Si^{4+}$  a.p.f.u. content in Ph. It should be noted that highly substituted phengite compositions (i.e. 3.5–3.6  $Si^{4+}$  a.p.f.u.) are maintained to low-pressure conditions when rocks are exhumed along a cold path nearly parallel to the phengite isopleths. The inferred *P*-*T* path followed by the Variscan basement rocks during the Alpine reworking is also indicated (dashed and continuous bold black arrow). Field assemblages: 1, Chl Ph Cpx Lws Qz Rt; 2, Chl Ph Cpx Na-Amp Lws Qz Rt; 3, Ph Cpx Na-Amp Lws Qz Rt; 4, Ph Cpx Na-Amp Ttn Qz Rt; 5, Ph Cpx Na-Amp Qz Rt; 6, Bt Ph Cpx Na-Amp Ttn Qz Rt; 7, Bt Ph Cpx Na-Amp Qz Rt; 8, Bt Ph Cpx Ttn Ab Qz Rt; 9, Bt Ph Cpx Qz Rt; 10, Bt Ph Cpx Ttn Ab Mc Qz Rt; 11, Bt Ph Cpx Ab Mc Qz Rt; 12, Kfs Bt Ph Cpx Ab Qz Rt; 13, Bt Chl Ttn Ab Mc Qz Rt Hem; 14, Bt Ph Ttn Ab Mc Qz Rt Hem; 15, Kfs Bt Ph Ttn Ab Qz Rt Hem; 16, Kfs Bt Ph Cpx Ab Qz Rt Hem; 17, Kfs Bt Ep Ph Ab Qz Rt Hem Mag; 18, Kfs Bt Ph Ab Qz Rt Hem Mag; 19, Kfs Bt Ph Ab Qz Rt Mag.

normal crustal values ( $^{206}Pb/^{204}Pb$  of 20.5). Such elevated initial values, however, are provided independently by regression lines through the various datasets. Use of the 3D concordia plot provides the means to deal with these types of data without exerting over-strong external controls by choosing specific compositions to correct the initial Pb (Fig. 7). The data define separate arrays for Rt (the low precision of this array reflecting the very small amount of Pb available for analysis) and the other minerals, although both lines are variously scattered. The intercepts with concordia, however, are similar, giving  $53.7 \pm 7.7$  Ma for the Cpx-Ph-oxide regression and  $48 \pm 18$  Ma for Rt (except for one of the Rt analyses, which plots very far from the line, but the significantly higher U content

**Table 2.** U–Pb data for the acmite–rutile-bearing shear zone, sample T5A

Properties	Weight (µg)	U (ppm)	Pbc (ppm)	Pbcom (pg)	238/204*	2σ%	206/204*	2σ%	235/204*	2σ%	207/204*	2σ%	238/206*	2σ%	207/206*	2σ%	204/206*	2σ%
R	5	15.19	0.31	3.5	3141	198	29	74	23	198	16.3	9.8	107	10	0.55773	0.30	0.03417	0.60
R	11	5.68	0.84	11	446	13	23.56	3.0	3.23	13	16.08	0.84	18.9	10	0.68267	0.15	0.04245	0.50
R	15	5.28	0.95	16	364.0	8.1	22.66	1.7	2.64	8.1	15.84	0.68	16.1	8	0.69928	0.30	0.04414	0.50
R	8	9.28	3.96	32	153.8	3.5	21.29	0.59	1.12	3.5	15.82	0.39	7.2	10	0.74277	0.15	0.04697	0.50
R	10	6.31	1.21	14	342.4	9.6	22.68	1.9	2.48	9.6	15.69	0.66	15.1	10	0.69204	0.17	0.04410	0.50
R incl in A				8	250	22	21.76	3.7	1.81	22	15.86	1.1	11.5	10	0.72866	0.15	0.04596	0.50
A with R incl	360	11.49	4.83	1663	156.06	0.48	21.578	0.31	1.132	0.48	15.79	0.38	7.2	1.0	0.73176	0.10	0.04634	0.40
A	2423	0.60	0.22	515	177.39	0.53	22.13	0.29	1.287	0.53	15.86	0.33	8.0	1.0	0.71675	0.11	0.04520	0.30
A fibrous	437	0.41	0.23	98	116.36	1.2	21.71	0.37	0.844	1.2	15.85	0.37	5.4	1.5	0.73018	0.20	0.04607	0.50
A blocky	2823	0.55	0.30	814	120	9	21.46	0.79	0.87	9.2	15.69	0.76	5.6	10	0.73118	0.30	0.04660	1.00
P				87	68.58	1.3	20.98	0.43	0.497	1.3	15.77	0.44	3.3	1.5	0.75147	0.15	0.04766	0.50
C				598905	0.078	0.61	20.518	0.20	0.001	0.61	15.774	0.30	0.00	1.0	0.76879	0.10	0.04874	0.10

R, rutile; A, acmite; P, phengite; C, oxide or sulphide coatings on quartz; incl, inclusions. Pbc, initial amount of common Pb. Pbcom, total amount of common Pb (initial + blank).  
\*Corrected for fractionation, spike and blank; error calculated by propagating the main sources of uncertainty.

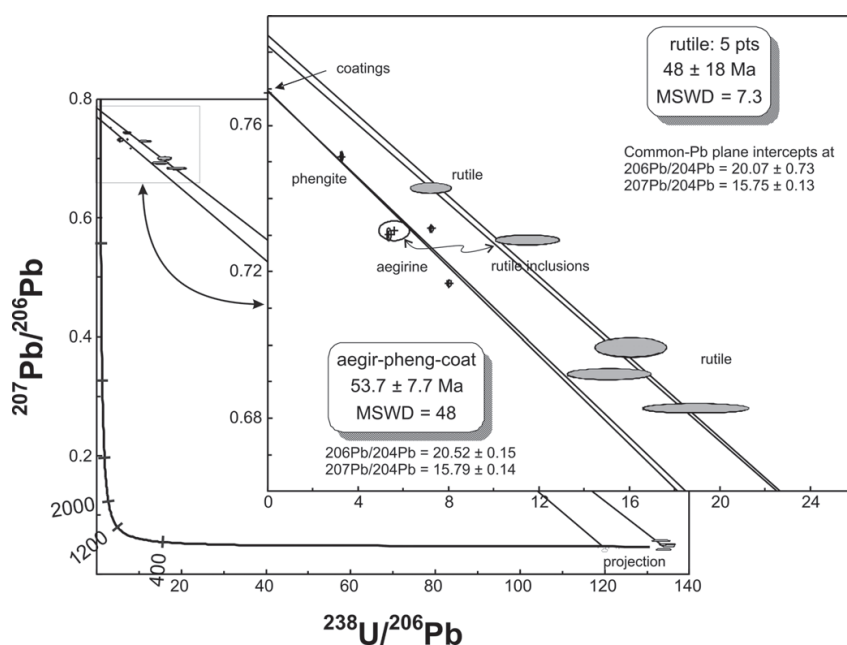


**Fig. 7.** TIMS U–Pb data showing a 3D concordia plot for the entire dataset. The data define separate arrays for Rt (its low precision reflecting the very small amount of Pb available for analysis) and the other minerals, although both lines are variously scattered. The intercepts with concordia, however, are similar. The age provided by Cpx–Ph and the coatings at  $53.7 \pm 7.7$  Ma is considered the most reliable estimate for the age of shearing. The ellipses on the concordia curve (bottom right) are the calculated projections of the data points.

suggests that the fraction may have had inclusions of Zrn, which in this sample is very U-rich and discordant). The difference between the two arrays could be interpreted in two ways. One is that Rt formed after the Cpx, but that seems unlikely given their close paragenetic association. The alternative is that Rt remained open for the diffusion of Pb, or was affected by younger Pb loss that shifted the data towards younger ages. Interestingly, the very same age relationship is observed for the rutile inclusions liberated from the Cpx. In conclusion, the age provided by Cpx–Ph and the coatings at  $53.7 \pm 7.7$  Ma is considered the most reliable estimate for development of these minerals.

## Discussion

The new data integrating information on the fabrics and kinematics with geochronology and metamorphic petrology show that the Variscan basement along the East Tenda Shear Zone of Corsica

underwent prograde high-pressure blueschist metamorphism in the Early Eocene (*c.* 50 Ma) during top-to-the-west-directed shearing. This shear sense is consistent with the kinematics of the Schistes Lustrés units overthrusting onto the European foreland (see Daniel *et al.* 1996; Molli & Malavieille 2010). Late reworking of the early-formed top-to-the-west ductile shear fabric by east-directed shear senses is also documented.

The Early Eocene timing of the Alpine peak metamorphism and the fabric-forming events reconstructed from the East Tenda Shear Zone confirms a Tertiary age for the Alpine metamorphism in Corsica. In particular, the U–Pb Rt ages presented herein are compatible with the maximum, discordant  $^{40}\text{Ar}/^{39}\text{Ar}$  ages ( $46.6 \pm 1.2$  Ma) obtained from the East Tenda Shear Zone (Brunet *et al.* 2000), but older than the Late Eocene–Early Oligocene ages reported both from the East Tenda Shear Zone (Brunet *et al.* 2000) and the Schistes Lustrés nappe (Brunet *et al.* 2000; Martin *et al.* 2011). We emphasize here that the shape of the *P–T* path reconstructed for the

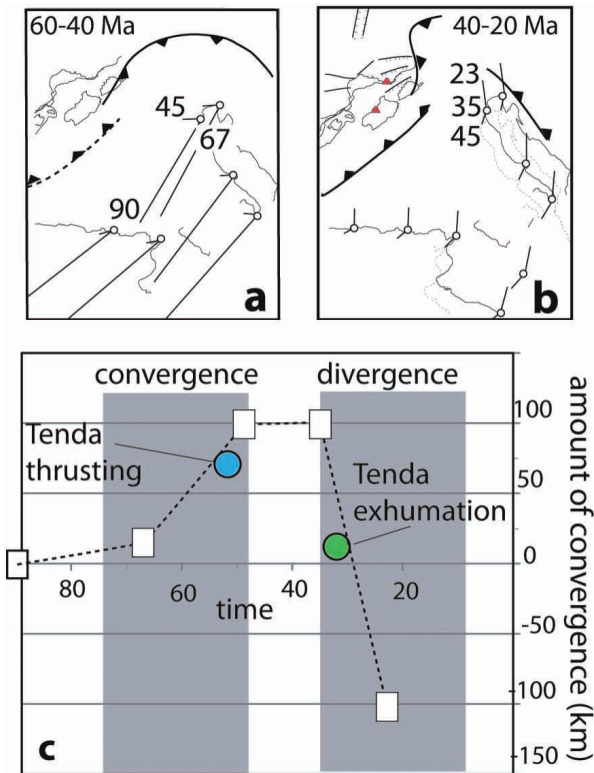


**Fig. 8.** Simplified palaeotectonic map of the central Mediterranean at (a) 60–40 Ma and (b) 40–20 Ma. The relative motion between Africa–Adria and Eurasia, from Dewey *et al.* (1989) rotation poles, is shown for reference points (white circle) with numbers referring to the age (Ma). Red triangles (dark grey in printed version) show calc-alkaline volcanoes, and the line indicates the main thrust fault (dashed if incipient). (c) Amount of net convergence or divergence (dashed line) expected along the East Tenda Shear Zone from the Dewey *et al.* (1989) rotation poles. The amount of trench rollback from 35 to 23 Ma is from Faccenna *et al.* (2001). Circles show the position of the Variscan basement rocks within the East Tenda Shear Zone considering that the Ligurian–Piedmontese overthrusting and subsequent extensional reactivation was accommodated along a 30°-dipping shear zone.

Cpx–Rt shear zone suggests that the  $^{40}\text{Ar}$ – $^{39}\text{Ar}$  phengite ages from the East Tenda Shear Zone probably record the continuous exhumation of this shear zone, as highly substituted phengite compositions persisted down to lower  $P$ – $T$  conditions along a cooling–exhumation path (Fig. 6). This cooling–exhumation path can then provide a reason for the staircase geometry of the phengite argon release spectra obtained from the East Tenda Shear Zone samples (Brunet *et al.* 2000). A protracted history of deformation along this shear zone is also derived from stratigraphic data from the Alpine foreland (Egal 1992; Malasoma & Marroni 2007) and from the  $^{40}\text{Ar}$ – $^{39}\text{Ar}$  phengite ages (Brunet *et al.* 2000), which collectively document a Middle Eocene–Early Miocene timespan (see Molli *et al.* 2006). Consequently, a revised tectonic scenario is required to describe the polyphase deformation history along the East Tenda Shear Zone.

Assuming the East Tenda Shear Zone marks the major Alpine convergence boundary between the Ligurian–Piedmontese ocean and the Variscan Corsica, the activity of this shear zone can be framed within the Tertiary plate-tectonic framework of the central

Mediterranean, estimating the expected convergence from plate kinematics reconstruction. To evaluate the relative motion between Adria and Eurasia, we adopt the Dewey *et al.* (1989) rotation pole for the Africa–Eurasia convergence and assume that the Adria motion was coherent with that of Africa (Van Der Voo 1993). The coherent motion of Adria with Africa during most of the Cenozoic is well established by palaeomagnetic data and palaeogeographical evidence (Channell *et al.* 1979; Muttoni *et al.* 2001). From this reconstruction it is possible to derive the direction and the amount of plate convergence expected along the main plate boundary in Corsica; that is, along the future East Tenda Shear Zone (Jolivet & Faccenna 2000; Piromallo & Faccenna 2004). We note that, for the time frame crucial for this tectonic reconstruction (Eocene), different velocity models converge towards the same solution (Savostin *et al.* 1986; Jolivet & Faccenna 2000; Rosenbaum *et al.* 2002; Capitanio & Goes 2006), which has been recently confirmed by new kinematic reconstructions (Cande & Stegman 2011).

The results are shown in Figure 8. Prior to 67 Ma, the convergence between Africa and Eurasia had a NE–SW trend, parallel to the East Tenda Shear Zone (Fig. 8a). In this scenario, the net convergence along the East Tenda Shear Zone was probably very minor, being dominated by a sinistral strike-slip component (Fig. 8c). Between *c.* 67 and *c.* 45 Ma, the motion changed sharply towards an east–west-striking convergence direction (Dewey *et al.* 1989; Jolivet & Faccenna 2000; Piromallo & Faccenna 2004). This significant kinematic change, well documented also in the recent kinematic model of Cande & Stegman (2011), probably had a profound influence on the tectonic evolution of the central Mediterranean and western Alps (Malusà *et al.* 2011). Decomposing the convergence vector into components parallel and perpendicular to the East Tenda Shear Zone, we expect a net convergence perpendicular to the East Tenda Shear Zone of about 80–90 km and a right lateral strike-slip component of the order of *c.* 40–50 km (Fig. 8c). From *c.* 45 to *c.* 30–35 Ma, the plate convergence was NNE–SSW directed, and hence parallel to the East Tenda Shear Zone, probably producing significant left-lateral deformation (Fig. 8b). At *c.* 30–35 Ma, the dynamics of the system again changed and the roll-back of the Apennines subduction system commenced. Rifting in the Provençal–Ligurian basin started during the latest Eocene–Early Oligocene (34–28 Ma) and ended in Aquitanian (21 Ma) (Séranne 1999). Subsequently, the central oceanic portion of the basin was generated between the late Aquitanian and late Burdigalian (21–16 Ma), associated with the counterclockwise rotation of the Corsica–Sardinia Block (Speranza *et al.* 2002) and the onset of the Tyrrhenian back-arc extension (Jolivet *et al.* 1998). The East Tenda Shear Zone therefore may have been active as a major thrust in the period from *c.* 67 to 40–45 Ma. It is expected to have been subsequently reactivated as an extensional shear zone at *c.* 30–20 Ma when the high-pressure core of the Alpine orogen in Corsica was finally exhumed during post-orogenic extension (Jolivet *et al.* 1990).

The Early Eocene timing of the Alpine peak metamorphism and the fabric-forming events in the East Tenda Shear Zone reconstructed in this study imply that net convergence in Corsica may have lasted slightly more than 20 Ma (between *ca.* 67 and 45–40 Ma; Early–Middle Eocene), and that a large part of the expected 80–90 km of shortening was mostly accommodated along the East Tenda Shear Zone to produce underthrusting of the Variscan basement to a minimum depth of *c.* 40 km (assuming an average density for the basement rocks of  $2800 \text{ kg m}^{-3}$ ) along a 30°-dipping thrust zone (Fig. 8c). This pulse of convergence was probably mostly accommodated along the former continent–ocean transition zone (Vitale Brovarone *et al.* 2011b) with final shear strain localization along the East Tenda Shear Zone. This process caused the compressional reactivation of the former continental passive margin, which resulted in overthrusting of the

subducted tracts of the Ligurian–Piedmontese Ocean onto the Variscan Corsica. The recent zircon U–Pb dating of eclogitic metamorphism in continental-derived slivers embedded within the Schistes Lustrés nappe (Martin *et al.* 2011) suggests that convergence and related subduction metamorphism affected the Ligurian–Piedmontese oceanic up to Late Eocene time. This long-lasting compressional tectonism is also recorded by post-37 Ma thrusting in the Alpine foreland of Corsica (Egal 1992; Brunet *et al.* 2000; Malasoma & Marroni 2007), which also suggests that East Tenda Shear Zone rocks were exhumed and entered brittle deformation environments at that time.

In the timespan relevant for this study (Eocene), correlation with the tectono-metamorphic evolution of the Western Alps may contribute to elucidate the sequence of deformation events along the Corsica–Europe active margin of the Alpine chain. In particular, two points deserve consideration. First, the main phase of exhumation of the Schistes Lustrés accretionary complex in the Western Alps (Agard *et al.* 2002) occurred concurrently with the Early Eocene climax of Alpine metamorphism in the Variscan basement of Corsica documented in this study. Second, as for Alpine Corsica (see Martin *et al.* 2011), the climax of subduction-zone metamorphism in the Western Alps occurred later, during the Middle–Late Eocene (from *c.* 45 to 35 Ma; e.g. Rubatto & Hermann 2003; Meffan-Main *et al.* 2004; Di Vincenzo *et al.* 2006; Malusà *et al.* 2011), in a scenario there dominated by the continuous subduction of the European margin and collision with the Adria plate (see Schmid *et al.* 1996). A polyphase evolution can be thus envisaged: (1) the Alpine activation of the East Tenda Shear Zone within the Variscan basement of Corsica occurred synchronously with exhumation of the oceanic-derived Schistes Lustrés accretionary complex, and the East Tenda Shear Zone may be thus interpreted as the basal thrust of the early structured Schistes Lustrés accretionary complex; (2) shortly after achievement of the Alpine metamorphic climax (Middle–Late Eocene), exhumation of the high-pressure core of the orogen occurred; Corsica was disconnected from the Alpine system and incorporated in the back-arc domain of the Apennine subduction system, which accommodated the overall plate convergence at least from the Late Eocene onward (e.g. Faccenna *et al.* 2001; Lustrino *et al.* 2009). This evolutionary scenario requires an along-strike space–time transition in the mode and regimes of oceanic subduction along the Alpine–Apennine junction (see, e.g. Vignaroli *et al.* 2008; Argnani 2010).

## Conclusion

The finding of a clinopyroxene–rutile-bearing shear zone within the East Tenda Shear Zone and definition of its *P–T–t* evolution provide new constraints on the metamorphic regimes and timing of the Alpine reworking of the Variscan crust in Corsica. We document an Early Eocene phase of orogenic construction that can be linked to the general scenario of plate convergence in the central Mediterranean during the Palaeogene. Evidence is provided for a polyphase evolution of the East Tenda Shear Zone, which was first activated as a major thrust to exhume the fossil Schistes Lustrés accretionary complex of the Western Alps during the Eocene and then reactivated as an extensional shear zone in Oligocene–Miocene times at the back of the eastward retreating Apennine subduction system.

We are indebted to L. Jolivet for having introduced us to the geology of the Alpine Corsica. This paper benefited from discussions on themes dealing with the Alpine geology of Corsica held with J. Malavieille, G. Molli and A. Vitale Bravarone, and during the CorseAlp2011 meeting. We also acknowledge advice from and discussion with H. J. Massone. This paper benefited from constructive criticism and advice from three anonymous

reviewers. Part of the research was funded by grants provided by the GeoQuTe Lab coordinated by F. Salvini.

## References

- AGARD, P., MONIÉ, P., JOLIVET, L. & GOFFÉ, B. 2002. Exhumation of the Schistes Lustrés complex: in situ laser probe  $^{40}\text{Ar}/^{39}\text{Ar}$  constraints and implications for the Western Alps. *Journal of Metamorphic Geology*, **20**, 599–618, doi:10.1046/j.1525-1314.2002.00391.x.
- AMAUDRIC DU CHAFFAUT, S. & SALIOT, P. 1979. La région de Corte: secteur-clé pour la compréhension du métamorphisme alpin en Corse. *Bulletin de la Société Géologique de France*, **21**, 149–154.
- ARGNANI, A. 2010. Plate tectonics and the boundary between Alps and Apennines. *Bollettino della Società Geologica Italiana*, **128**, 317–330.
- AUSTRHEIM, H. 1987. Eclogitization of lower crustal granulites by fluid migration through shear zones. *Earth and Planetary Science Letters*, **81**, 221–232.
- BEZERT, P. & CABY, R. 1988. Sur l'âge post-bartonien des événements tectono-métamorphiques alpins en bordure orientale de la Corse cristalline. *Bulletin de la Société Géologique de France*, **8**, 965–971.
- BRUNET, C., MONIÉ, P., JOLIVET, L. & CADET, J.P. 2000. Migration of compression to extension in the Tyrrhenian Sea, insight from  $^{40}\text{Ar}/^{39}\text{Ar}$  ages on micas along a transect from Corsica to Tuscany. *Tectonophysics*, **321**, 127–155.
- CANDE, S.C. & STEGMAN, D.R. 2011. Indian and African plate motions driven by the push force of the Réunion plume head. *Nature*, **475**, 47–51.
- CAPITANO, F.A. & GOES, S. 2006. Mesozoic spreading kinematics: consequences for Cenozoic Central and Western Mediterranean subduction. *Geophysical Journal International*, **165**, 804–816, doi:10.1111/j.1365-246X.2006.02892.x.
- CARON, J.M., KIENAST, J.R. & TRIBOULET, C. 1981. High-pressure–low-temperature metamorphism and polyphase Alpine deformation at Sant'Andrea di Cotone (Eastern Corsica, France). *Tectonophysics*, **78**, 419–451.
- CHANNELL, J.E.T., D'ARGENIO, B. & HORVATH, F. 1979. Adria, the African promontory, in Mesozoic Mediterranean palaeogeography. *Earth-Science Reviews*, **15**, 213–292.
- CHOPIN, C., BEYSSAC, O., BERNARD, S. & MALAVIEILLE, J. 2008. Aragonite–grossular intergrowths in eclogite-facies marble, Alpine Corsica. *European Journal of Mineralogy*, **20**, 857–865.
- CLARK, C., MUMM, A.S. & FAURE, K. 2005. Timing and nature of fluid flow and alteration during Mesoproterozoic shear zone formation, Olary Domain, South Australia. *Journal of Metamorphic Geology*, **23**, 147–164, doi:10.1111/j.1525-1314.2005.00568.
- COHEN, C.R., SCHWEICKERT, R.A. & ODOM, A.L. 1981. Age of emplacement of the Schistes Lustrés nappe, Alpine Corsica. *Tectonophysics*, **73**, 267–283.
- CONNOLLY, J.A.D. 2005. Computation of phase equilibria by linear programming: a tool for geodynamic modelling and its application to subduction zone decarbonation. *Earth and Planetary Science Letters*, **236**, 524–541.
- CORFU, F. 2004. U–Pb age, setting, and tectonic significance of the anorthosite–mangerite–charnockite–granite suite, Lofoten–Vesterålen, Norway. *Journal of Petrology*, **45**, 1799–1819.
- DALLAN, L. & NARDI, R. 1984. Ipotesi sulla evoluzione dei domini 'Liguri' della Corsica nel quadro della paleogeografia e della paleotettonica delle unità alpine. *Bollettino della Società Geologica Italiana*, **103**, 517–527.
- DALLAN, L. & PUCCINELLI, A. 1995. Geologia della regione tra Bastia e St-Florent (Corsica Settentrionale). *Bollettino della Società Geologica Italiana*, **114**, 23–66.
- DANIEL, J.M., JOLIVET, L., GOFFÉ, B. & POINSSOT, C. 1996. Crustal-scale strain partitioning: footwall deformation below the Alpine Oligo-Miocene detachment of Corsica. *Journal of Structural Geology*, **18**, 41–59.
- DEWEY, J.F., HELMAN, M.L., TURCO, E., HUTTON, D.H.W. & KNOTT, S.D. 1989. Kinematics of the western Mediterranean. In: COWARD, M.P., DIETRICH, D. & PARK, R.G. (eds) *Alpine Tectonics*. Geological Society, London, Special Publications, **45**, 265–283.
- DIPPLE, G.M. & FERRY, J.M. 1992. Metasomatism and fluid flow in ductile fault zones. *Contributions to Mineralogy and Petrology*, **112**, 149–164.
- DI VINCENZO, G., TONARINI, S., LOMBARDO, B., CASTELLI, D. & OTTOLINI, L. 2006. Comparison of  $^{40}\text{Ar}$ – $^{39}\text{Ar}$  and Rb–Sr data on phengites from the UHP Brossasco–Isasca Unit (Dora Maira Massif, Italy): implications for dating white mica. *Journal of Petrology*, **47**, 1439–1465, doi:10.1093/petrology/egl018.
- DURAND-DELGA, M. 1984. Principaux traits de la Corse Alpine et correlations avec les Alpes Ligures. *Memorie della Società Geologica Italiana*, **28**, 285–329.
- EGAL, E. 1992. Structures and tectonic evolution of the external zone of Alpine Corsica. *Journal of Structural Geology*, **14**, 1215–1228.
- ESSENE, E. 1968. Relatively pure jadeite from a siliceous Corsican gneiss. *Earth and Planetary Science Letters*, **5**, 270–272.

- FACCENNA, C., BECKER, T.W., LUCENTE, F.P., JOLIVET, L. & ROSSETTI, F. 2001. History of subduction and back-arc extension in the Central Mediterranean. *Geophysical Journal International*, **145**, 809–820.
- FOURNIER, M., JOLIVET, L., GOFFÉ, B. & DUBOIS, R. 1991. The Alpine Corsica metamorphic core complex. *Tectonics*, **10**, 1173–1186.
- GIBBONS, W. & HORAK, J. 1984. Alpine metamorphism of Hercynian hornblende granodiorite beneath the blueschist facies Schistes Lustrés nappe of NE Corsica. *Journal of Metamorphic Geology*, **2**, 95–113.
- GUEYDAN, F., LEROY, Y.M., JOLIVET, L. & AGARD, P. 2003. Analysis of continental midcrustal strain localization induced by microfracturing and reaction-softening. *Journal of Geophysical Research*, **108**, doi:10.1029/JB000611.
- HOLLAND, T.J.B. & POWELL, R. 1998. An internally consistent thermodynamic data set for phases of petrological interest. *Journal of Metamorphic Geology*, **16**, 309–343.
- IMBER, J., HOLDSWORTH, R.E., BUTLER, C.A. & LLOYD, G.E. 1997. Fault-zone weakening processes along the reactivated Outer Hebrides Fault zone, Scotland. *Journal of the Geological Society, London*, **154**, 105–109.
- JAFFEY, A.H., FLYNN, K.F., GLENDENIN, L.E., BENTLEY, W.C. & ESSLING, A.M. 1971. Precision measurement of half-lives and specific activities of  $^{235}\text{U}$  and  $^{238}\text{U}$ . *Physical Review, Section C, Nuclear Physics*, **4**, 1889–1906.
- JOHN, T., MEDVEDEV, S., RÜPKE, L.H., ANDERSEN, T.B., PODLADCHIKOV, Y.Y. & AUSTRHEIM, H.O. 2009. Generation of intermediate-depth earthquakes by self-localizing thermal runaway. *Nature Geoscience*, **2**, 137–140.
- JOLIVET, L. & FACCENNA, C. 2000. Mediterranean extension and the Africa–Eurasia collision. *Tectonics*, **19**, 1095–1106.
- JOLIVET, L., DUBOIS, R., FOURNIER, M., GOFFÉ, B., MICHARD, A. & JOURDAN, C. 1990. Ductile extension in Alpine Corsica. *Geology*, **18**, 1007–1010.
- JOLIVET, L., FACCENNA, C., ET AL. 1998. Midcrustal shear zones in postorogenic extension: example from the Northern Tyrrhenian Sea. *Journal of Geophysical Research*, **103**, 12123–12160.
- JOLIVET, L., RAIMBOURG, H., LABROUSSE, L., AVIGAD, D., LEROY, Y., AUSTRHEIM, H. & ANDERSEN, T.B. 2005. Softening triggered by eclogitization, the first step toward exhumation during continental subduction. *Earth and Planetary Science Letters*, **237**, 532–547.
- LABROUSSE, L., HETÉNY, G., RAIMBOURG, H., JOLIVET, L. & ANDERSEN, T.B. 2010. Initiation of crustal-scale thrusts triggered by metamorphic reactions at depth: insights from a comparison between the Himalayas and the Scandinavian Caledonides. *Tectonics*, **29**, doi:10.1029/2009TC002602.
- LAHONDÈRE, D. & GUERROT, C. 1997. Sm–Nd dating of Alpine eclogitic metamorphism in Corsica: evidence for Late Cretaceous subduction beneath the Corsican–Sardinian block. *Géologie de la France*, **3**, 3–11.
- LUDWIG, K.R. 2003. *Isoplot 3.0. A Geochronological Toolkit for Microsoft Excel*. Berkeley Geochronology Center, Special Publications, **4**.
- LUSTRINO, M., MORRA, V., FEDELE, L. & FRANCIOSI, L. 2009. Beginning of the Apennine subduction system in central western Mediterranean: constraints from Cenozoic ‘orogenic’ magmatic activity of Sardinia (Italy). *Tectonics*, **28**, doi:10.1029/2008TC002419.
- MALASOMA, A. & MARRONI, M. 2007. HP/LT metamorphism in the Volparone Breccia (Northern Corsica, France): evidence for involvement of the Europe/Corsica continental margin in the Alpine subduction zone. *Journal of Metamorphic Geology*, **25**, 529–545.
- MALAVIEILLE, J., CHEMENDA, A. & LARROQUE, C. 1998. Evolutionary model for Alpine Corsica: mechanism for ophiolite emplacement and exhumation of high-pressure rocks. *Terra Nova*, **10**, 317–322.
- MALUSÀ, M., FACCENNA, C., GARZANTI, E. & POLINO, R. 2011. Divergence in subduction zones and exhumation of high pressure rocks (Eocene Western Alps). *Earth and Planetary Science Letters*, **310**, 21–32.
- MALUSKI, H. 1977. Application de la méthode  $^{40}\text{Ar}/^{39}\text{Ar}$  aux minéraux des roches cristallines perturbées par les événements thermiques et tectoniques en Corse. *Bulletin de la Société Géologique de France*, **19**, 849–850.
- MARTIN, L.A.J., RUBATTO, D., VITALE BROVARONE, A. & HERMANN, J. 2011. Late Eocene lawsonite-eclogite facies metasomatism of a granulite sliver associated to ophiolites in Alpine Corsica. *Lithos*, **125**, 620–640, doi:10.1016/j.lithos.2011.03.015.
- MASSONNE, H.J. & WILLNER, A.P. 2008. Phase relations and dehydration behaviour of psammopelinite and mid-ocean ridge basalt at very-low-grade to low-grade metamorphic conditions. *European Journal of Mineralogy*, **20**, 867–879.
- MATTAUER, M., FAURE, M. & MALAVIEILLE, J. 1981. Transverse lineation and large scale structures related to Alpine obduction in Corsica. *Journal of Structural Geology*, **3**, 401–409.
- MEFFAN-MAIN, F., CLIFF, R.A., BARNICOAT, A.C., LOMBARDO, B. & COMPAGNONI, R. 2004. A Tertiary age for Alpine metamorphism in the Gran Paradiso massif, western Alps: a Rb–Sr microsampling study. *Journal of Metamorphic Geology*, **22**, 267–281.
- MOLLI, G. & MALAVIEILLE, J. 2010. Orogenic processes and the Corsica/Apennines geodynamic evolution: insights from Taiwan. *International Journal of Earth Sciences*, **100**, 1207–1224, doi:10.1007/s00531-010-0598-y.
- MOLLI, G., TRIBUZIO, R. & MARQUER, D. 2006. Deformation and metamorphism at the eastern border of the Tenda Massif (NE Corsica): a record of subduction and exhumation of continental crust. *Journal of Structural Geology*, **28**, 1748–1766.
- MUTTONI, G., GARZANTI, E., ALFONSI, L., CIRILLI, S., GERMANI, D. & LOWRIE, W. 2001. Motion of Africa and Adria since the Permian: paleomagnetic and paleoclimatic constraints from northern Libya. *Earth and Planetary Science Letters*, **192**, 159–174.
- PIROMALLO, C. & FACCENNA, C. 2004. How deep can we find the traces of Alpine subduction? *Geophysical Research Letters*, **31**, doi:10.1029/2003GL019288.
- RAVNA, E.J.K., ANDERSEN, T.B., JOLIVET, L. & DE CAPITANI, C. 2010. Cold subduction and the formation of lawsonite eclogite—constraints from prograde evolution of eclogitized pillow lava from Corsica. *Journal of Metamorphic Geology*, **28**, 381–395, doi:10.1111/j.1525-1314.2010.00870.x.
- ROSENBAUM, G., LISTER, G.S. & DUBOZ, C. 2002. Relative motions of Africa, Iberia and Europe during Alpine orogeny. *Tectonophysics*, **359**, 117–129.
- ROSSI, P.H., DURAND-DELGA, M., LAHONDÈRE, J.C. & LAHONDÈRE, D. 2003. *Carte géologique de la France à 1/50.000, feuille Santo Pietro di Tenda*. BRGM, Orleans.
- RUBATTO, D. & HERMANN, J. 2003. Zircon formation during fluid circulation in eclogites (Monviso, Western Alps): implications for Zr and Hf budget in subduction zones. *Geochimica et Cosmochimica Acta*, **67**, 2173–2187.
- SAVOSTIN, L.A., SIBUET, J.-C., ZONENSHAIN, L.P., LE PICHON, X. & ROULET, M.-J. 1986. Kinematic evolution of the Tethys Belt from the Atlantic Ocean to the Pamirs since the Triassic. *Tectonophysics*, **123**, 1–35.
- SCHMID, S.M., PFIFFNER, O.A., FROITZHEIM, N., SCHÖNBORN, G. & KISSLING, E. 1996. Geophysical–geological transect and tectonic evolution of the Swiss–Italian Alps. *Tectonics*, **15**, 1036–1064.
- SILVERSTONE, J., MORTEANI, G. & STAUBE, J.-M. 1991. Fluid channeling during ductile shearing: transformation of granodiorite into aluminous schist in the Tauern Window, Eastern Alps. *Journal of Metamorphic Geology*, **9**, 419–431.
- SÉRANNE, M. 1999. The Gulf of Lion continental margin (NW Mediterranean) revisited by IBS: an overview. In: DURAND, B., JOLIVET, L., HORVÁTH, F. & SÉRANNE, M. (eds) *The Mediterranean Basins: Tertiary Extension within the Alpine Orogen*. Geological Society, London, Special Publications, **156**, 15–36.
- SPERANZA, F., VILLA, I.M., SAGNOTTI, L., FLORINDO, F., COSENTINO, D., CIPOLLATI, P. & MATTEI, M. 2002. Age of the Corsica–Sardinia rotation and Ligure–Provençal Basin spreading: new paleomagnetic and Ar/Ar evidence. *Tectonophysics*, **347**, 231–251.
- TRIBUZIO, R. & GIACOMINI, F. 2002. Blueschist facies metamorphism of peralkaline rhyolites from the Tenda crystalline massif (northern Corsica): evidence for involvement in the Alpine subduction event? *Journal of Metamorphic Geology*, **20**, 513–526.
- VAN DER VOO, R. 1993. *Paleomagnetism of the Atlantic, Tethys and Iapetus Oceans*. Cambridge University Press, Cambridge.
- VIGNAROLI, G., FACCENNA, C., JOLIVET, L., PIROMALLO, C. & ROSSETTI, F. 2008. Subduction polarity reversal at the junction between the Western Alps and the Northern Apennines, Italy. *Tectonophysics*, **450**, 34–50.
- VITALE BROVARONE, A., BELTRANDO, M., ET AL. 2011a. Inherited ocean–continent transition zones in deeply subducted terranes: insights from Alpine Corsica. *Lithos*, **124**, 273–290, doi:10.1016/j.lithos.2011.02.013.
- VITALE BROVARONE, A., GROppo, C., HETÉNY, G., COMPAGNONI, R. & MALAVIEILLE, J. 2011b. Coexistence of lawsonite-bearing eclogite and blueschist: phase equilibria modelling of Alpine Corsica metabasalts and petrological evolution of subducting slabs. *Journal of Metamorphic Geology*, **29**, 583–600, doi:10.1111/j.1525-1314.2011.00931.x.
- WATERS, C.N. 1990. The Cenozoic tectonic evolution of Alpine Corsica. *Journal of the Geological Society, London*, **147**, 811–824.
- WHITNEY, D.L. & EVANS, B. 2010. Abbreviations for names of rock-forming minerals. *American Mineralogist*, **95**, 185–187.

## Tectonics and sedimentation in the hangingwall of a major extensional detachment: the Devonian Kvamshesten Basin, western Norway

P. T. Osmundsen,\* T. B. Andersen,\* S. Markussen† and A. K. Svendby\*

\*Department of Geology, University of Oslo, PO Box 1047, Blindern, 0316 Oslo, Norway

†Esso Norge a.s., Stavanger, Norway

### ABSTRACT

The Middle Devonian Kvamshesten Basin in western Norway is a late-orogenic basin situated in the hangingwall of the regional extensional Nordfjord–Sogn Detachment Zone. The basin is folded into a syncline with the axis subparallel to the ductile lineations in the detachment zone. The structural and stratigraphic development of the Kvamshesten Basin indicates that the basin history is more complex than hitherto recognized. The parallelism stated by previous workers between mylonitic lineation below the basin and intrabasinal fold axes is only partly reflected in the configuration of sedimentary units and in the time–relations between deposits on opposing basin margins. The basin shows a pronounced asymmetry in the organization and timing of sedimentary facies units. The present northern basin margin was characterized by bypass or erosion at the earliest stage of basin formation, but was subsequently onlapped and eventually overlain by fanglomerates and sandstones organized in well-defined coarsening-upwards successions. The oldest and thickest depositional units are situated along the present southern basin margin. This as well as onlap relations towards basement at low stratigraphic level indicates a significant component of southwards tilt of the basin floor during the earliest stages of deposition. The inferred south–eastwards tilt was most likely produced by north–westwards extension during early stages of basin formation. Synsedimentary intrabasinal faults show that at high stratigraphic levels, the basin was extending in an E–W as well as a N–S direction. Thus, the basin records an anticlockwise rotation of the syndepositional strain field. In addition, our observations indicate that shortening normal to the extension direction cannot have been both syndepositional and continuous, as suggested by previous authors. Through most of its history, the basin was controlled by a listric, ramp–flat low-angle fault that developed into a scoop shape or was flanked by transfer faults. The basin-controlling fault was rooted in the extensional mylonite zone. Sedimentation was accompanied by formation of a NE- to N-trending extensional rollover fold pair, evidenced by thickness variations in the marginal fan complexes, onlap relations towards basement and the fanning wedge geometry displayed by the Devonian strata. Further E–W extension was accompanied by N–S shortening, resulting in extension-parallel folds and thrusts that mainly post-date the preserved basin stratigraphy. During shortening, conjugate extensional faults were rotated to steeper dips on the flanks of a basin-wide syncline and re-activated as strike-slip faults. The present scoop-shaped, low-angle Dalsfjord fault cross-cut the folded basin and juxtaposed it against the extensional mylonites in the footwall of the Nordfjord–Sogn detachment. Much of this juxtaposition may post-date sedimentation in the preserved parts of the basin.

Basinal asymmetry as well as variations in this asymmetry on a regional scale may be explained by the Kvamshesten and other Devonian basins in western Norway developing in a strain regime affected by large-scale sinistral strike-slip subparallel to the Caledonian orogen.

P. T. Osmundsen *et al.*

## INTRODUCTION

Late-orogenic extension of overthickened crust has been described from ancient as well as modern orogens (e.g. Burchfiel & Royden, 1985; Séranne & Séguret, 1987; Dewey, 1988; Platt & Vissers, 1989; Jolivet *et al.*, 1994; Hartz & Andresen, 1995; Andersen & Jamtveit, 1990; Dewey *et al.*, 1993). While considerable advance has been made on the processes of detachment faulting and on the exhumation of deep crustal rocks, comparably few studies have focused directly on the late-orogenic extensional basins. The Devonian Kvamshesten Basin in western Norway is a late-orogenic supradetachment basin situated on the remains of the Caledonian mountain belt. We have mapped the Kvamshesten Basin in terms of contact relationships, sedimentology and structure to test recent conceptual models of late-orogenic extension and basin formation. The structural and sedimentological observations described below may serve as an example of the complexity encountered in late-orogenic basins. We think that in the present case, this complexity cannot be explained by continuous dip-slip extension on one low-angle normal fault.

### The Devonian basins of western Norway

The Devonian basins of western Norway (Fig. 1) are regarded as classic study areas for tectonically controlled sedimentation (e.g. Bryhni, 1964a,b; Steel *et al.*, 1977; Steel & Gloppen, 1980; Byörlykke, 1983; Roberts, 1983). The documentation of low-angle extensional detachment faults and shear zones in the Sogn–Nordfjord area (Hossack, 1984; Norton, 1986, 1987; Séranne & Séguret, 1987) provided a new tectonic framework for western Norway. The Devonian basins are currently interpreted as products of the late-orogenic extension of the Caledonian mountain belt (Séguret *et al.*, 1989; Andersen & Jamtveit, 1990; Chauvet & Séranne, 1994). The basins are situated in the hangingwall of a regional extensional detachment zone (Andersen & Jamtveit, 1990) (Fig. 1). The detachment zone comprises up to 2 km of extensional mylonites that separate the eclogite-bearing Western Gneiss Region (WGR) in the footwall from Caledonian allochthon and Devonian basins in the hangingwall. The extensional mylonites carry a W- to WNW-plunging lineation and record a minimum of 40 km of ductile, top-to-the-W displacement that partly controlled exhumation of the Caledonian (Kullerud *et al.*, 1986) eclogites of the WGR (Andersen & Jamtveit, 1990; Hveding, 1992; Andersen *et al.*, 1994).  $^{40}\text{Ar}/^{39}\text{Ar}$  cooling ages from amphibole and white mica in the footwall of the detachment zone cluster in the Early to Middle Devonian (Chauvet *et al.*, 1992; Berry *et al.*, 1995). Based on plant and fish fossils, the Devonian basins have been assigned Middle Devonian ages (Kolderup, 1916, 1921; Jarvik,

1949). Thus, ductile extensional shearing is usually taken to be roughly contemporaneous with Devonian sedimentation. Along their western margins, the Devonian basins are unconformable upon their depositional substrate of Precambrian and Caledonian rocks (Bryhni & Skjerlie, 1975). The eastern margins of the Devonian basins comprise brittle, undulating low-angle normal faults (Hossack, 1984; Norton, 1986, 1987; Séranne & Séguret, 1987). In the case of the Hornelen Basin, the southern and northern basin margins comprise steep, brittle strike-slip faults that cross-cut the detachment at the eastern basin margin (Norton, 1986; Torsvik *et al.*, 1988; Andersen *et al.*, 1997). The tectonostratigraphy described above is folded in large-scale, E–W-trending folds with axes roughly parallel with the ductile lineation in the detachment mylonites below. The Devonian basins and their depositional substrate crop out in the synforms, while the high-pressure rocks of the WGR crop out in the antiforms between the basins. Chauvet & Séranne (1994) described the folds as extension-parallel and argued that they were synsedimentary with respect to the Middle Devonian basins. Palaeomagnetic data, however, indicate that the folds are Late Devonian or Early Carboniferous in age (Torsvik *et al.*, 1986). An increasing amount of evidence from palaeomagnetic studies as well as from  $^{40}\text{Ar}/^{39}\text{Ar}$  dating (Torsvik *et al.*, 1986, 1992; Eide *et al.*, 1997) indicate that the crustal section exposed in western Norway experienced deformation that is young with respect to the Devonian basins. Thus, some of the structures that bound the Devonian basins may entirely post-date basin formation and be Late Devonian, Permian or even Mesozoic in age (Torsvik *et al.*, 1988, 1992). In our view, these observations highlight the importance of a thorough re-investigation of the Devonian basins.

### The Kvamshesten Basin – scope of the present study

The Kvamshesten Basin (Fig. 2) sits in the hangingwall of the Dalsfjord fault, a W-plunging, scoop-shaped detachment fault that separates the Devonian basin and its depositional substrate from extensional mylonites and the WGR (Fig. 3). The Dalsfjord fault constitutes the basin's present eastern, northern and southern margins, and experienced slip in Permian as well as Mesozoic times (Torsvik *et al.*, 1992). The Middle Devonian unconformity beneath the Kvamshesten Basin is exposed for more than 15 km. The well-exposed basin fill comprises roughly equal amounts of conglomerates and sandstones. The Kvamshesten Basin is thus well-suited for investigations of the basin floor topography, as well as of the relations between coarse- and fine-grained sedimentary units. In this paper the following points are highlighted.

Tectonics and sedimentation, Devonian, western Norway

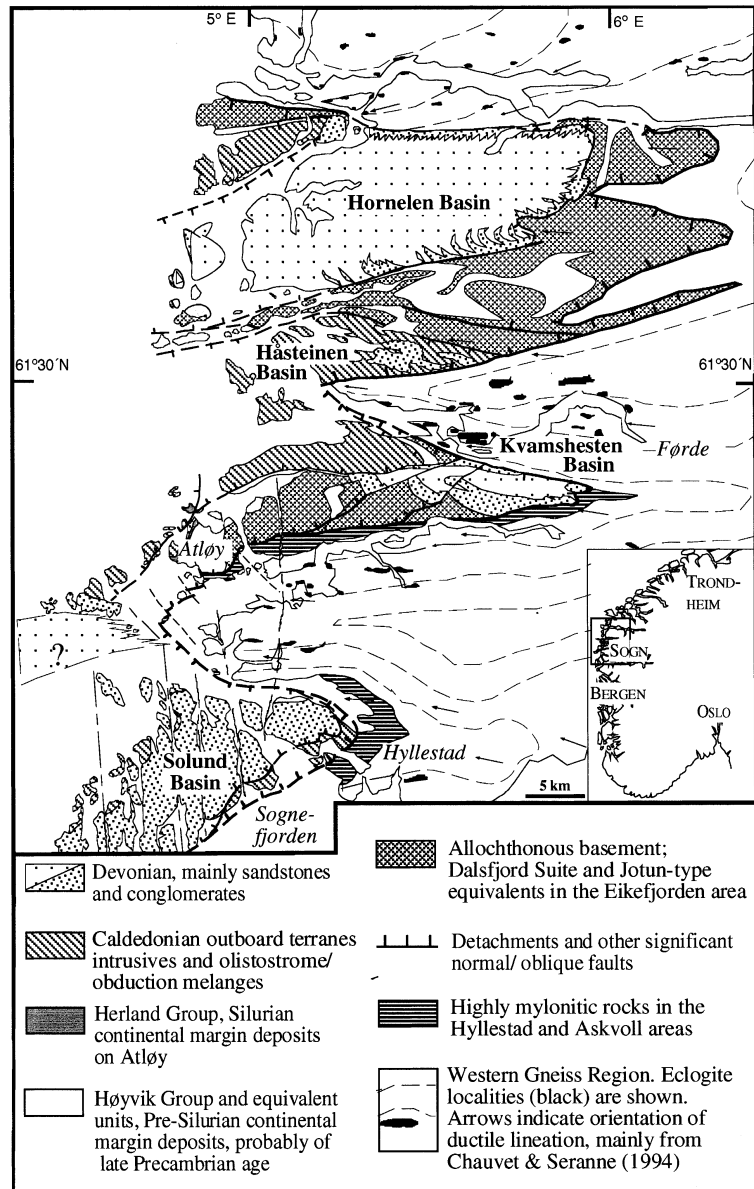


Fig. 1. Simplified overview map of the Sogn–Nordfjord area showing tectonostratigraphic units, main structural architecture and Devonian basins.

- 1 The geometry and distribution of individual sedimentary units and the geometrical relations between sedimentary units and depositional basement.
- 2 Relations between the basin fill and the Dalsfjord fault. The question whether the present basin margins were the original ones is highlighted by the documentation of young slip events along the basin boundaries.
- 3 The geometry and timing of intrabasinal faults with respect to sedimentation, the strain fields that can be inferred from them and their relations to the strain field encountered in the detachment zone. Significant syn-sedimentary intrabasinal faults have been suggested not to exist in the Devonian basins of western Norway (Seranne *et al.*, 1989). We dispute this interpretation.

- 4 Constraints on the syndepositional geometry of the original basin-bounding fault and on the mylonitic detachment zone. A principal discussion with respect to detachments is related to whether they are active at low dips, or if detachments initiate with a high dip (45° or more) and rotate towards a subhorizontal position (Jackson, 1987; Buck, 1988).
- 5 The geometry and timing of extension-parallel folds and thrusts. Extension-parallel folds have been described also in other areas that have undergone large-magnitude extension (Manktelow & Pavlis, 1994; Fletcher & Bartley, 1994).
- 6 The regional tectonic control on Devonian basin formation in Western Norway.

P. T. Osmundsen et al.

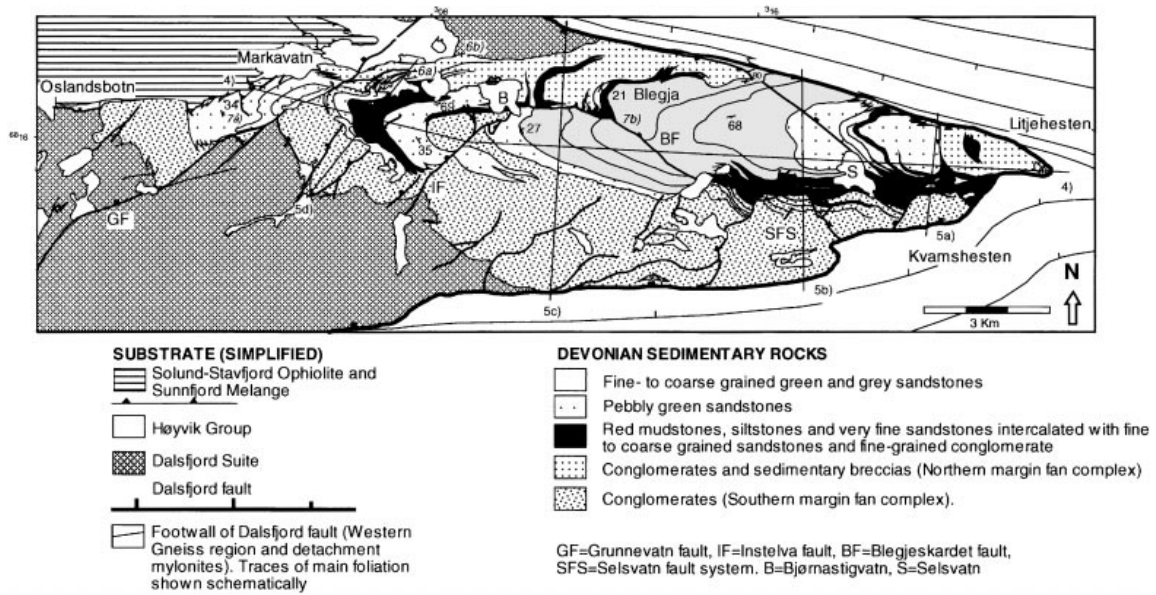


Fig. 2. Geological map of the Kvamshesten Basin showing distribution of main sedimentary units, as well as extensional and contractional intrabasinal structures. Map and profile figures to appear later in this paper follow legend outlined here. Note positions of sections in Figs 4 and 5. Letters in italics refer to logs in Figs 6 and 7.



Fig. 3. Eastern parts of the Kvamshesten Basin viewed from the north. The Dalsfjord fault is outlined by the lowermost snow-covered area. Bedding dips towards the east, in a topographic section that is approximately east-west.

### THE KVAMSHESTEN BASIN: BASIN FILL ARCHITECTURE - FACIES DISTRIBUTION AND RELATIONSHIPS

Four main lithological associations have been mapped in the Kvamshesten Basin. These are (1) conglomerates, (2) heterolithic units with abundant red, very fine-grained sandstone and siltstone, (3) green pebbly sandstones and (4) green fine- to coarse-grained sandstones. Each sedimentary unit contains vertical and lateral variations

and display various relationships of interfingering and intergradation.

#### 1. Conglomerates

The conglomerates along the southern and northern margins show distinct differences regarding internal organization, relationships to surrounding facies units and timing of initial deposition. Although the conglomerates partly intercalate beneath the central parts of the

## Tectonics and sedimentation, Devonian, western Norway

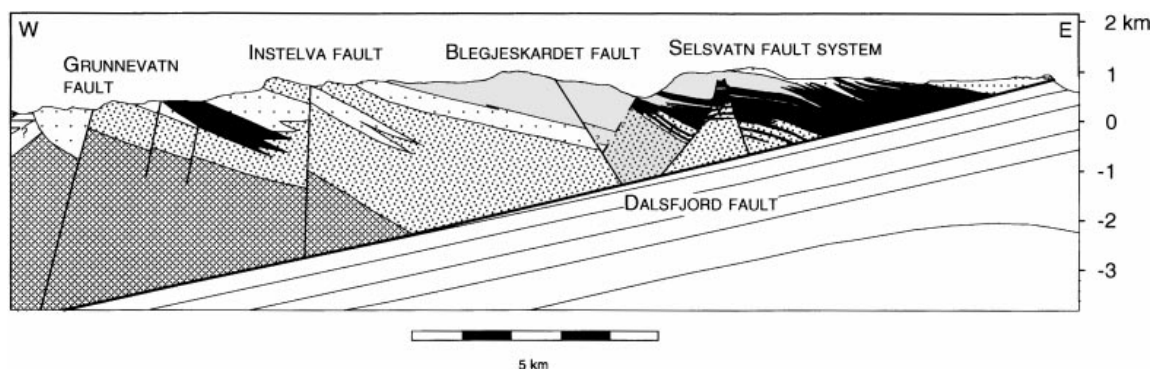


Fig. 4. East-west section through the Kvamshesten Basin. The profile is constructed parallel to the axis of the basinal syncline. Note break in slope of the basal unconformity across the Instelva fault, as well as the onlap relations towards basement as well as between sedimentary units. Note anticlinal geometry and fanning wedge geometry displayed by the Devonian strata in the eastern parts of the basin.

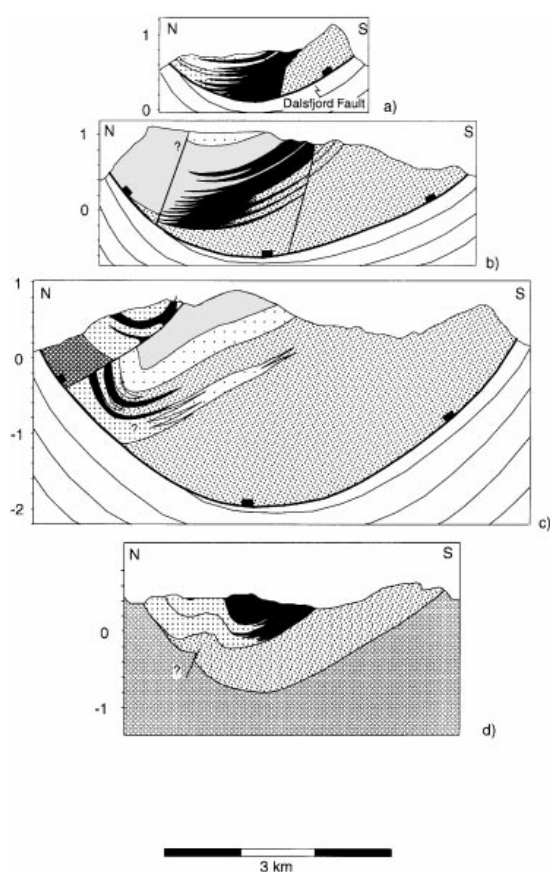


Fig. 5. North-south profiles through the Kvamshesten Basin. The profiles are constructed normal to the axis of the basinal syncline. Geometries of individual facies units at depth are schematic and variably speculative. Note that in (a), the southern margin fan complex is faulted out of the section. In (c), displacement on the Kringlefjellet reverse fault is dependent on the correlation of units in the map plane. The gradual widening of the preserved basin in (a-c) is due to the westerly plunge of the scoop-shaped Dalsfjord Fault. Correspondingly, the width of the preserved basin decreases in (d), due to the eastwards plunge of the basinal syncline.

basin, we find it convenient to describe the southern and northern margin units separately.

#### *The southern margin fan complex*

The wedge-shaped southern margin fan complex is exposed for more than 20 km, and is segmented into a series of NW-tapering fan bodies. Fan segmentation is mostly observed at medium to high stratigraphic levels. The fan complex reaches a present thickness of  $\approx 2$  km above the basement hangingwall cutoff, but thins dramatically in the area between the Instelva and Grunnevatn faults. In the hangingwall of the Grunnevatn fault, the fan complex thickens again to more than 1 km. Minor fans prograde into the hangingwalls of both the Instelva and Grunnevatn faults, to interfinger with sandstones that overlie the main fanglomerate body. Clast sizes are variable, but reach more than 2 m locally. With the exception of a number of outsized basement blocks interpreted as landslides (below), these are the coarsest deposits encountered in the basin. Clasts are generally subrounded, but subangular and well-rounded clasts are common. The clast population is dominated by syenitic gneisses, granites, gabbro, anorthosite and diorite, derived from the underlying Dalsfjord Suite (Skjerlie, 1971; Osmundsen, 1996). Sedimentary structures are generally scarce, but close to the top of the fan complex, trough cross-bedding and lenticular sandstone intercalations have been observed.

#### *The northern margin fan complex*

At low stratigraphic levels, the northern margin fan complex is segmented into a large number of fans. Close to the basin margin, individual fan segments constitute  $\approx 100$ -m-thick coarsening upwards successions (Fig. 6a). Along west-central parts of the northern basin margin, fans onlap the depositional substrate. Above the hangingwall cutoff of basement, individual fan segments are rooted in a  $\approx 1$ -km-thick, wedge-shaped fanglomerate body. The rock types that constitute the northern margin

P. T. Osmundsen et al.

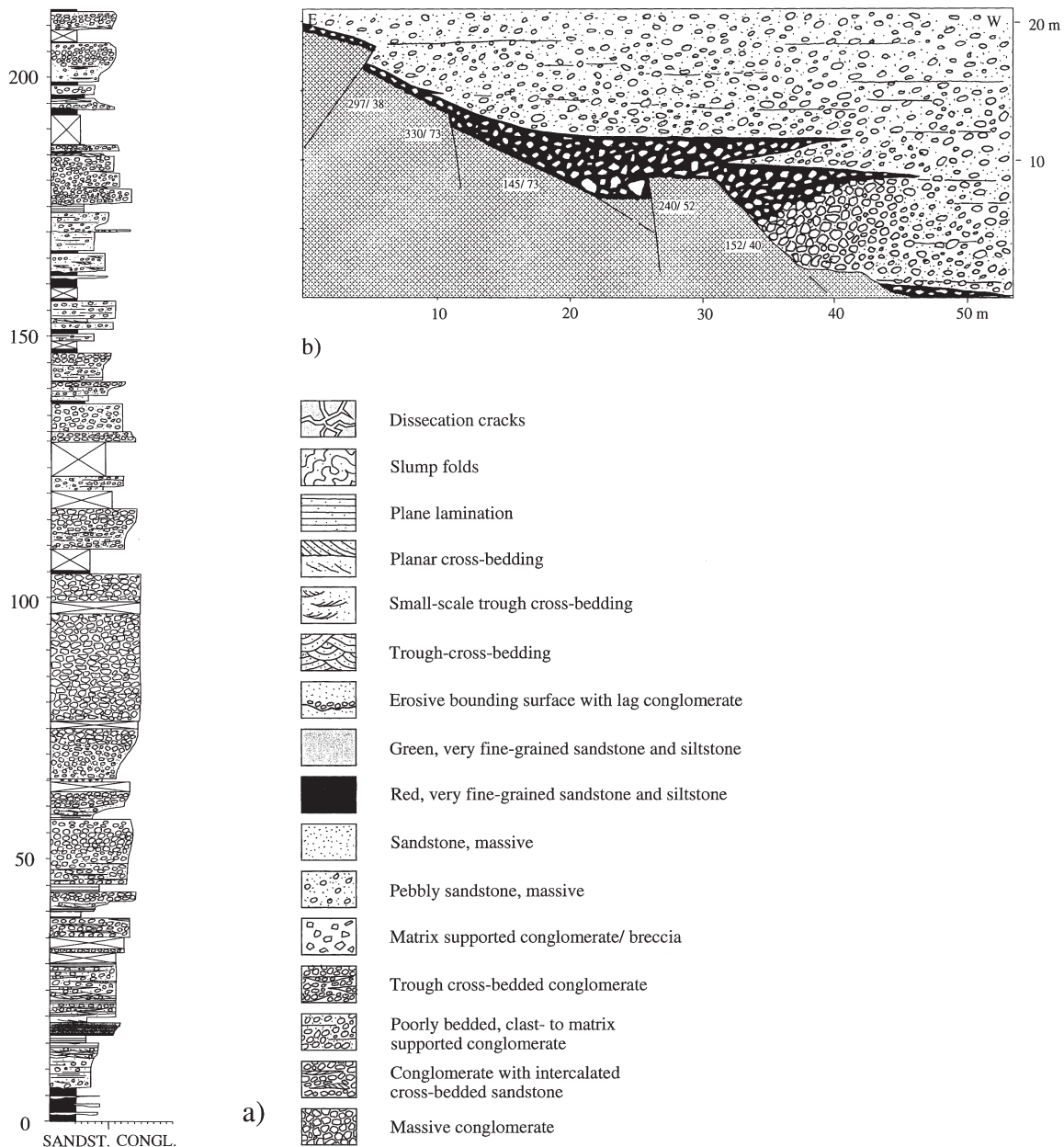


**Fig. 6.** Vertical scales are in metres for these and following logs. The grain-size scale of this and other logs follows the modified Wentworth scale of Lane *et al.* (1947), reproduced by the American Geological Institute. Vertical scales are in metres for this and logs in Fig. 7. Legend applies also to Fig. 7. (a) Log through some 200 m of the northern margin fan complex. Note organization in coarsening-upwards successions at various scales. Also, note variations in lithofacies in the coarse-grained units.

(b) Lateral log of outcrop at northern basin margin. Small fans of sedimentary breccia with abundant red matrix intercalate with clast- to matrix-supported cobble and boulder conglomerates with green sandstone and fine gravel matrix. The sediments drape a palaeotopography that displays small, synsedimentary fault scarps. Clasts are generally of cobble size in the green conglomerates, while the angular blocks of the fans reach metre size.

fan complex can be described as (1) sedimentary breccias, (2) massive to crudely bedded conglomerates and (3) cross-bedded conglomerates with sandy interlayers.

1 The clast- to matrix-supported breccias commonly occur as thin (<5 m) sheet-like drapes on the basal unconformity, as infill in palaeotopographical lows and

as lenticular and fan-shaped bodies that intercalate with conglomerates or sandstones (Fig. 6b). Eastwards along the northern basin margin, breccias intercalate with progressively higher stratigraphic levels of the basin fill (Bryhni & Skjerlie, 1975). In the north-central basin area, two comparably large fan segments have been classified

## Tectonics and sedimentation, Devonian, western Norway

as sedimentary breccias (Osmundsen, 1996). Based on clast populations derived mainly from the local depositional substrate to the north and west of the basin, we infer that a number of small, fan-like bodies of sedimentary breccia along the basal unconformity prograded south or south-east into the basin. The breccias in the central basin area have provenance in the Dalsfjord Suite and probably had a westwards component of progradation (Osmundsen, 1996).

2 Massive and crudely bedded conglomerates comprise a volumetrically significant part of the northern margin fan complex (e.g. Fig. 6). The coarsest and thickest deposits of this type are found above the hangingwall cutoff of the basement, where clasts reach boulder size (up to 1 m).

From the massive conglomerate complex in the NE, smaller fans splay off to intercalate with the heterolithic units of the central basin area. Basinwards progradation is usually associated with grain size reduction and increased abundance of structures that indicate fluvial transport.

3 Cross-bedded conglomerates occur at several stratigraphic levels and often constitute the lower parts of large-scale, conglomeratic coarsening-upwards successions (Fig. 6a). Clasts are subrounded to rounded and generally of pebble to cobble size. Elongate cluster bedforms with imbricate clasts, wedge-shaped lenses of cross-bedded sandstone and sheet-like bodies of massive conglomerate are common in the cross-bedded conglomerates. Towards the NE, the cross-bedded conglomerates grade laterally into the more proximal massive and crudely bedded conglomerates. Towards the central basin area, the cross-bedded conglomerates grade laterally into sandstone.

## 2. Heterolithics with abundant red very fine-grained sandstone and siltstone

Generally, the rock units mapped as heterolithic units contain more than 30% of red, very fine- to fine-grained sandstone and siltstone that intercalate with green sandstones or conglomerates. Red fines occur also in surrounding rock units, but in significantly lower proportions. Red fines are particularly common within three areas of the Kvamshesten Basin, notably in the west-central parts, along the central part of the northern basin margin and along the south-eastern basin margin. Within the red, fine-grained sandstones, sedimentary structures are common and dominated by plane and climbing ripple lamination.

## 3. Green pebbly sandstones

The pebbly sandstones typically occur in cycles of varying thickness, separated by red, fine-grained beds (Fig. 7a). Sedimentary structures are dominated by trough cross-bedding, planar cross-bedding and plane lamination, out of which the two former dominate. Pebbles drape

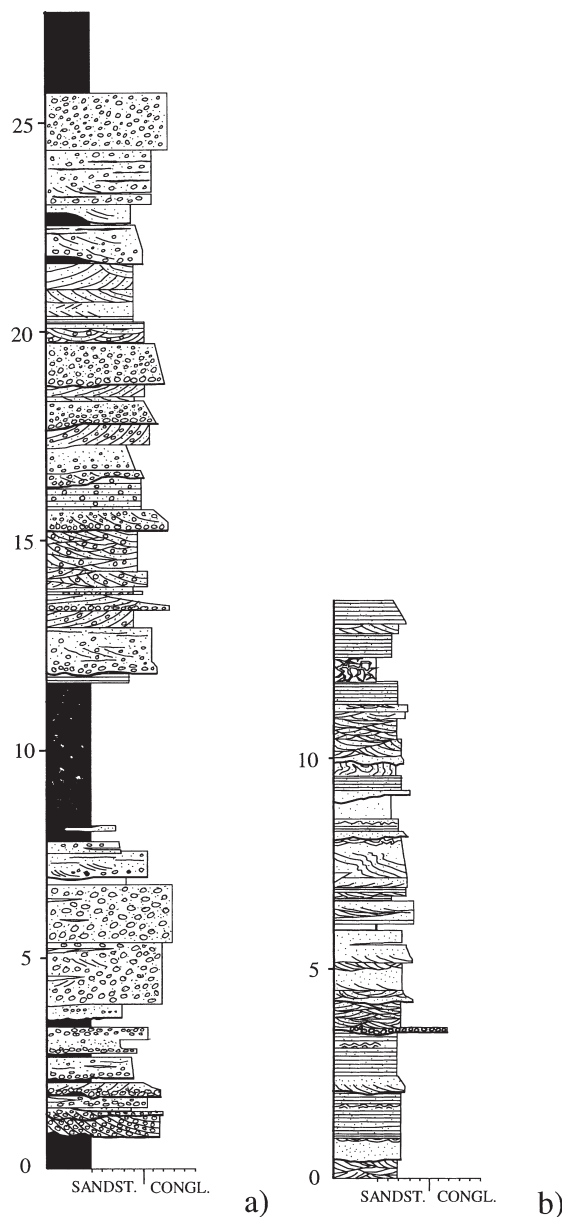


Fig. 7. Logs from two stratigraphic levels in the sandstones of the central basin area. (a) Trough cross-bedded, pebbly sandstones intercalated with red fines. From area west of the Gunnevatn fault. (b) Plane laminated and trough cross-bedded, medium-grained sandstones, south of Blegja. The subdivision of the sandstones is mainly based on the overall reduction in grain size, and on the increased abundance of plane lamination that characterizes the fine- to medium-grained units.

through-shaped erosive boundary surfaces or are dispersed in the sandy matrix. At low to medium stratigraphic levels, the amount of intercalated, red fine-grained deposits increases upwards, and the pebbly sandstones merge laterally as well as vertically into the heterolithic units described above.

P. T. Osmundsen et al.

#### 4. Fine- to coarse-grained green and grey sandstones

The sandstones that crop out in the east-central part of the basin are fine to coarse grained, less pebbly and commonly display trough and planar cross-bedding (Fig. 7b). Plane laminated sets constitute a larger proportion of the stratigraphic column than in the pebbly sandstones. Red very fine-grained sandstones and siltstones are rare through much of the green sandstones, but reappear at high stratigraphic levels where the green sandstones interfinger with heterolithic units. Intercalations of green siltstone and very fine-grained sandstone are, however, common. Pebbles recur in the sandstones along the north-eastern basin margin in a position proximal to the conglomerates in the easternmost basin area.

#### Landslides

Several large (tens to hundreds of metres) blocks of metamorphosed igneous and sedimentary rocks crop out at low, medium and high stratigraphic levels in the Kvamshesten Basin (Fig. 2), including the highest stratigraphic level exposed in the basin at Litjehesten. Block lithology seems to reflect closely lithological units found in the depositional substrate, notably rocks of the Sunnfjord Melange, Høyvik Group and Dalsfjord Suite (Markussen, 1994; Osmundsen, 1996). The basement blocks are variably brecciated, but apparently not faulted against their substrate of Devonian sedimentary rocks. Clastic dikes are found locally, and where the Devonian strata below the blocks can be studied in detail, small-scale normal faults and slump folds are present (Markussen, 1994). Based on the above observations, we interpret the basement blocks to represent landslides similar to the ones described by Bryhni (1975) from the Solund Basin.

#### General facies interpretation

The clast-supported *conglomerates* of the southern margin fan complex were probably deposited by stream-related processes. The large clast sizes and the general lack of well-defined sedimentary structures at low stratigraphic levels indicate that the conglomerates were deposited on the proximal parts of an alluvial fan, characterized by fairly steep topographic gradients and high-energy stream-flow conditions (see also Steel *et al.*, 1985). In their interpretation the conglomerates along the northern basin margin were deposited on small, debris-flow-dominated fans. We agree that the sedimentary breccias along the northern basin margin were probably deposited by massflow type processes and in the central basin area, angular clasts chaotically orientated in a red fine-grained matrix suggests a debris-flow origin for some of the conglomerates (Osmundsen, 1996). The cross-bedded conglomerates are, however, clearly fluvial in origin; this

is probably also the case with some of the crudely bedded conglomerates. Thus, in our interpretation, fluvial deposits were more important in the northern margin fan complex than indicated previously. Also, our map of the northern basin margin differs from that of Steel *et al.* (1985), as individual fan segments are rooted in a kilometre-thick, wedge-shaped complex above the basement cutoff. In the interpretation of Steel *et al.* (1985), palaeo-current directions along the basin margins were towards the central basin area, that is towards the south and SW in the conglomerates of the northern basin margin, and towards the north and NW along the southern basin margin.

The *sandstones* of the central basin area are undoubtedly fluvial in origin, and record lateral and vertical variations in fluvial style. Based on the abundance of plane and ripple laminated, red very fine-grained sandstone and siltstone, the heterolithic units are interpreted to represent floodplain/floodbasin deposits. The distribution of the heterolithic units through the basin stratigraphy indicates that the locus of the floodplain shifted several times during deposition. The green, pebbly sandstones are interpreted as channel and bar deposits. Based on the predominance of relatively coarse-grained pebbly sandstones over red fines through much of the section, we interpret the pebbly sandstone units to represent a braided fluvial environment. The existence and lateral persistence of red, fine-grained sandstone and siltstone beds within the pebbly sandstones indicate that flooding was occasionally widespread, and point towards a system of some sinuosity. Asphaug (1975) reported palaeocurrent directions that were towards the east in the sandstones of the central basin area. The fine- to coarse-grained green sandstones exposed in the east-central parts of the basin contain a higher percentage of plane lamination, and may represent a more ephemeral fluvial system. Most likely, the green, fine- to coarse-grained sandstones were deposited on a sandy fluvial plain, in a position more distal with respect to the source area than the pebbly sandstones. The sandy fluvial plain was associated with a floodplain located along the present SE basin margin. In the SE, the floodplain received coarse debris from the southern margin fan complex.

The organization of the northern margin fan complex into upwards-coarsening units at a variety of scales (Fig. 6) differs from the less well organized, massive conglomerates encountered at low stratigraphic levels in the southern margin fan complex. The coarsening-upwards motif recognized in the conglomerates of the northern margin can be traced into the sandstones of the central basin area, as documented earlier from the Hornelen Basin (e.g. Steel & Gloppen, 1980). A log through some 200 m of the westernmost parts of the southern margin fan complex (Osmundsen, 1996) revealed, however, that the organization of conglomerates at low stratigraphic levels along the southern margin is less distinct, or occurs at a different scale than on the northern margin. At high stratigraphic levels, the

## Tectonics and sedimentation, Devonian, western Norway

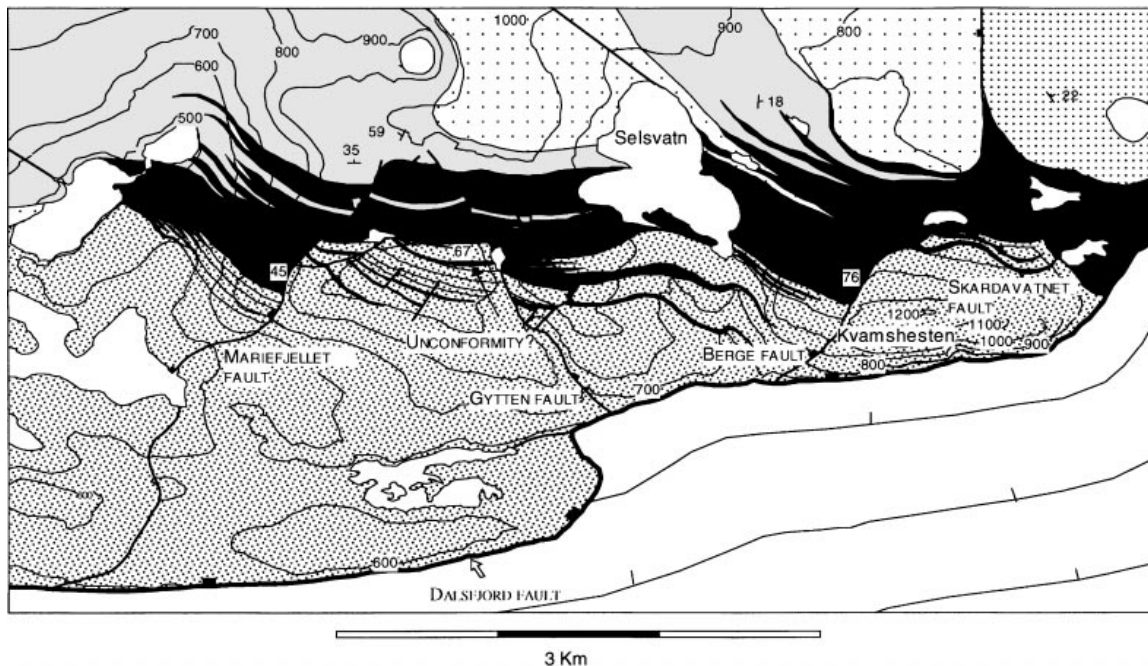


Fig. 8. Detailed geological map showing main facies units and synsedimentary faults in the Selsvatn area. Note that in the hangingwalls of the Mariefjellet and Berge faults, the intercalated contact between grey and green sandstones (dense stipple) and heterolithics (black) migrates stratigraphically upwards towards the faults, indicating synsedimentary activity. The Selsvatn fault system is rotated on the flank of the basinal synform, but constitutes an orthorhombic fault system when restored with bedding. See discussion in text. Note angular dislocation in the footwall of the Gyttén fault.

organization of the southern margin fan complex is similar to low stratigraphic levels of the northern margin fan complex. A very rough fining-upwards motif may be defined on the basin scale, and is related to the eastwards migration of the basin depocentre. The eastwards depocentre migration is also shown by the geometry of the sandy facies units (Fig. 4). The rough fining-upwards motif was apparently interrupted by distinct episodes of fan progradation far into the basin, notably at medium and high stratigraphic levels. Thus, the Kvamshesten Basin apparently contains a cyclicity at a scale of several hundred metres, repeated 3–4 times through the basin stratigraphy.

The importance of the *landslides* described briefly above is related to their provenance in the Caledonian nappe units. During deposition of the entire preserved stratigraphy, the topography that surrounded the Kvamshesten Basin must have been developed in the hangingwall of the detachment zone. Also, the syndepositional topography must have been significant enough for large rock masses to be emplaced into the basin by gravity-driven, probably tectonically triggered processes.

#### Marginal and intrabasinal unconformities

In the Hornelen and Kvamshesten basins, a number of intrabasinal unconformities were proposed by Seranne *et al.* (1989) and by Chauvet & Seranne (1994). Some of

the proposed unconformities have been rejected in the Hornelen (Wilks & Cuthbert, 1994) and Kvamshesten (Osmundsen, 1996) basins. East of the Instelva fault, progressive westward onlap onto depositional basement is evidenced by the wedge-shape of the marginal conglomerate complexes. The exact geometry of this onlap is difficult to quantify due to the general lack of bedding at low stratigraphic levels. Along the NW basin margin, the Devonian strata display a low-angle onlap onto basement (Bryhni & Skjerlie, 1975; Seranne *et al.*, 1989) although, locally, the basement is faulted against the Devonian (Fig. 9). The unconformity, where preserved, generally displays an E–W orientation. At low stratigraphic levels west of Markavatn (Fig. 2) the direction of onlap is mainly towards the north and north-east, as NE-dipping pebbly sandstones are separated from the unconformity only by a thin zone of sedimentary breccia or conglomerate. In the area north of Bjørnastigvatn, onlap is more easterly (Fig. 10). Small-scale, fault-related palaeotopography is present along the contact and makes its orientation somewhat variable (Fig. 6). North of Blegja, an intrabasinal unconformity displays downwards truncation of strata to the west. Inside the basin, a number of discontinuities occur that lack critical exposure. West of the Gyttén fault, beds are apparently truncated stratigraphically downwards towards the west (Fig. 8). An apparent truncation of beds downwards towards the east has been observed in the Litjhesten

P. T. Osmundsen et al.

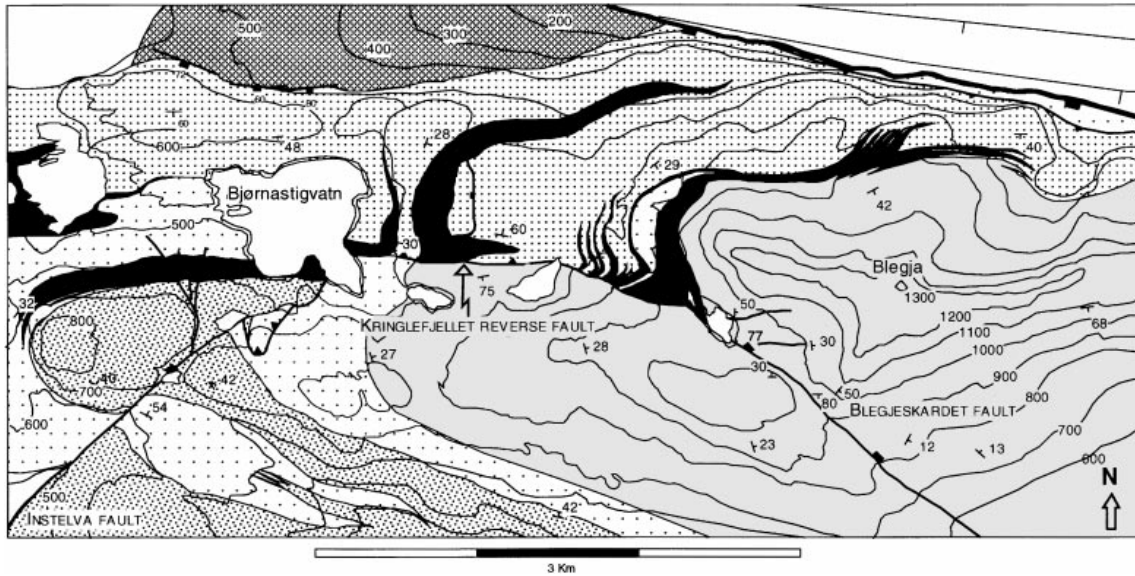


Fig. 9. Detail map of parts of the central basin area. The map shows the distribution of sedimentary units in the area, as well as the relations between the Kringlefjellet reverse fault and the Instelva and Blegjeskardet faults.

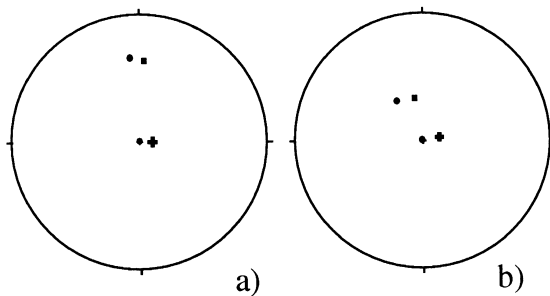


Fig. 10. (a) Stereographic (Schmidt-net) representation of basal unconformity (square) and bedding (cross) north of Bjørnastigvatn. When bedding is rotated to a horizontal position, the unconformity (filled square) displays a westwards dip. This shows that the onlap relationship along this part of the northern margin cannot be related to a southerly dipping fold flank, as indicated by Chauvet & Seranne (1994). See text for discussion and further inferences.  $n = 4$ . (b) Intrabasinal unconformity north of Blegja. If bedding above the unconformity (cross) is rotated to a horizontal position, the beds below the unconformity dip towards the west-southwest (circle unrotated, square rotated position of bedding below unconformity).  $n = 4$ .

area. In the central basin area (Fig. 9), a discontinuity occurs in the northern margin fan complex between the conglomerates that rest directly upon the basal unconformity and the overlying succession of conglomerates and red fines. The discontinuity cuts stratigraphically downwards in a northwards direction. The plane of discontinuity apparently marks the base of a stratigraphic level characterized by increased basinwards fan progradation. An interpretation of this as an internal unconformity is, however, somewhat ambiguous, as it occurs

in an area of transfer and accommodation of compressional strains (Osmundsen, 1996).

## STRUCTURAL GEOLOGY

### Normal and oblique faults

Along the southern basin margin, the Devonian unconformity is cut by an array of NW-dipping, steep faults that terminate stratigraphically upwards in the southern margin fan complex, or near the conglomerate-sandstone interface (Fig. 11a). Some of the faults can be traced towards the detachment zone where they are cut by the Dalsfjord fault. The Grunnevatn fault (Skjerlie, 1971; Fig. 2) apparently accommodates a map-plane displacement of more than 2 km on the southern basin margin, but produces only negligible displacement where it cuts the northern basin margin (Fig. 2). Across the Instelva fault, the thickness of the lower part of the southern margin fan complex is reduced by  $\approx 1$  km. To the east of the Grunnevatn fault, a NE-dipping fault displaces the unconformity by more than 200 m down to the north-east.

East of the hangingwall cutoff of the basement, the Selsvatn fault system (Fig. 8) comprises an array of NW- and NE-dipping faults that cut the boundary between the southern margin fan complex and the floodplain/floodbasin sequence (Figs 11 and 13b). Displacements at this stratigraphic level are of the order of 150–500 m. Stratigraphically upwards, displacement decreases rapidly and the faults pass into monoclinical flexures. For a distance of  $\approx 1.5$  km, bedding in the hangingwalls of the Mariefjellet and Berge faults displays a more northerly strike than the subregional E–W strike encountered in

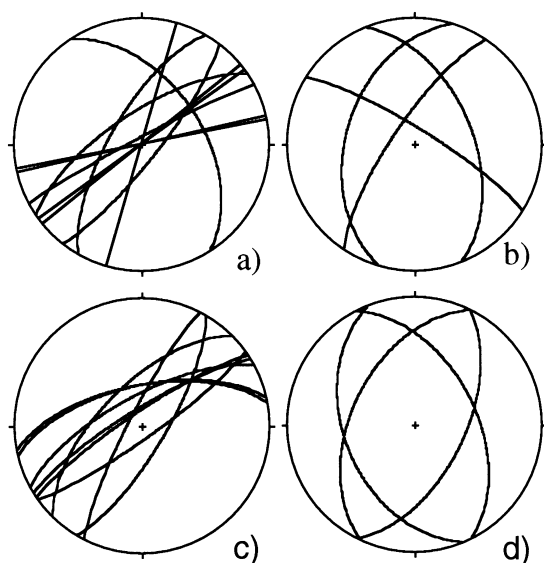


Fig. 11. Stereographic (Schmidt-net) representations of syndimentary intrabasinal faults in the study area. (a) Present orientations of oblique faults that cut the basal unconformity.  $n = 10$ . (b) Present orientation of main faults of the Selsvatn fault system. (c) Faults in (a) unfolded and back-rotated with bedding.  $n = 10$ . (d) Data in (b) unfolded and back-rotated. The syndimentary orientations of the four main faults reveal that the Selsvatn fault system originated as an orthorhombic fault system characterized by positive elongation in east–west and north–south directions. See discussion in text.

the footwalls. Towards the west, the regional E–W strike of bedding is gradually restored. Although the regional E-trending fold pattern could produce deflections of this type, the close association with the faults suggest that the deflections were genetically related to the faults. Adjacent to the fault planes, a low-wavelength, oblique drag of bedding is observed. To the north-west of the Mariefjell and Berge faults, the lower boundary of the green, fluvial sandstones shows a considerable stratigraphic climb without migrating much further (south) eastwards into the basin. Between the faults, the lower green sandstone boundary occupies a fairly constant stratigraphic level (Fig. 9). Some of the larger faults contain excess stratigraphy in their hangingwalls (Fig. 8). Lineations have been recorded from a restricted number of faults along the southern basin margin (Fig. 12). In general, lineations are oblique and indicate relative west to south-west displacement of the hangingwalls (present configuration).

### Contractional structures

Contractional structures encountered within the Kvamshesten Basin comprise folds, reverse faults and fault-propagation folds. Generally, the contractional structures display east and south-east trends.

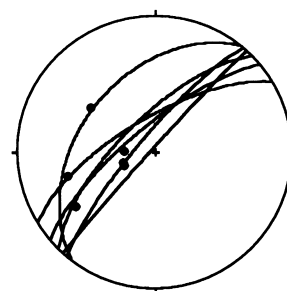


Fig. 12. Stereographic (Schmidt-net) representation of striated fault planes and shear fractures along the southern basin margin. The relative age of fault movement could not be demonstrated for any of the faults represented here and it is uncertain whether the striae record movements that are syn- or post-sedimentary. Within the present configuration of the fault planes, the lineations record displacements that are between normal and sinistral.  $n = 12$ .

### Folds

The Kvamshesten Basin and its depositional substrate is deflected by a large-scale, gently E-plunging syncline (Skjerlie, 1971), and by a number of parasitic folds on a variety of scales. The main syncline is open with an upright to steeply N-dipping axial plane. Trend of the fold axis as calculated from readings of bedding is  $090^\circ \pm 5^\circ$  through most of the basin (Fig. 13). West of the Instelva fault, however, the trend is  $100\text{--}105^\circ$ . The plunge of the fold axis decreases systematically through the basin, from values close to  $30^\circ$  at low stratigraphic levels to  $8\text{--}9^\circ$  in the uppermost parts of the stratigraphy. A closed anticline (Fig. 5) with a steeply N-dipping axial surface and an amplitude of several hundred metres can be traced through large parts of the basin. The steep southern limb of the anticline is cut by the Kringlefjellet reverse fault (see below). Open to closed folds with amplitudes one order of magnitude less than the main syncline are present through most of the basin fill (Fig. 14a). In the heterogeneous sequences rich in red siltstone and sandstone, folds with amplitudes of a few metres are frequently found. The thicker (i.e.  $>10$  m) gravel beds are generally not deflected by folds of this magnitude. Thus, dislocations exist between beds deflected by folds of different wavelength and amplitude. N- to NE-plunging lineations recorded from fine-grained bedding surfaces in the south-central basin area were interpreted as flexural slip lineations by Markussen (1994).

### Reverse faults

Along segments of both the northern and the south-western basin margins, the Devonian basin fill is overthrust by rocks of the local depositional substrate (Fig. 2). Two reverse faults that cut the northern basin margin die out upsection in the Devonian rocks, and give way to E-plunging fault-propagation folds. Displacement on one of these faults is of the order of some tens of metres. For other thrusts (Fig. 14b),

P. T. Osmundsen et al.

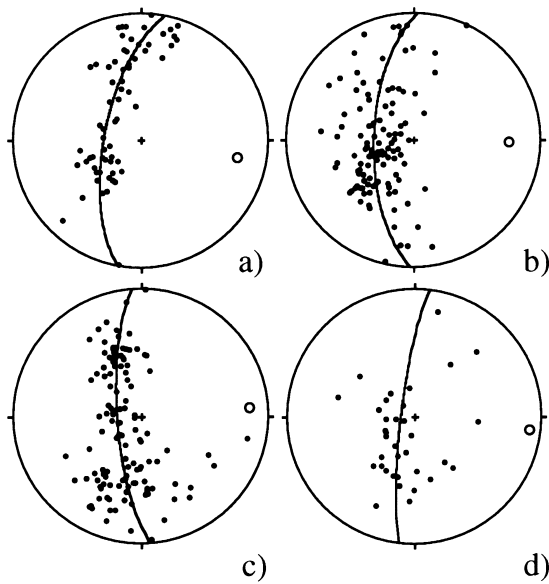


Fig. 13. Stereographic (Schmidt-net) representation of bedding from low to high stratigraphic levels in the Kvamshesten Basin. The basin has been divided into four domains that correspond to progressively higher stratigraphic levels in the basin. Poles to best fit great circles have been calculated for each stratigraphic level, to record any changes in plunge for the basin syncline. A general decrease in plunge is observed from low to high stratigraphic levels. The decrease in plunge is interpreted to represent an original fanning wedge relationship in the Devonian strata. (a) Central basin area between the Grunnevatn and Instelva faults. Pole to best-fit great circle 101/23.  $n=70$ . (b) Bjørnastigvatn–Blegja area. Pole to best-fit great circle 092/26.  $n=121$ . (c) Kvamshesten–Blegja area. Pole to best-fit great circle 086/15.  $n=127$ . (d) Litjehesten area. Pole to best-fit great circle 097/08.  $n=35$ .

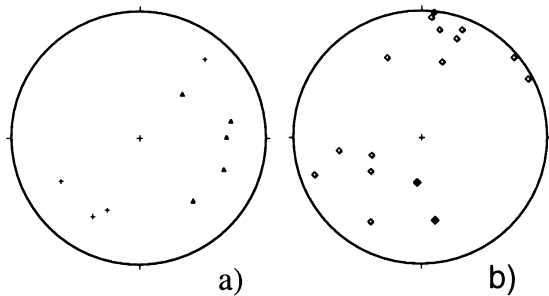


Fig. 14. Stereograms of outcrop-scale structural elements related to north–south shortening of the Kvamshesten Basin. (a) Fold axes (triangles) and axial planes (crosses) of outcrop-scale folds, central basin area.  $n=9$ . (b) Small-scale reverse faults (open diamonds) and Kringlefjellet reverse fault (closed diamonds). The scatter in orientation displayed by the small-scale structures indicate that early contractional structures were rotated prior to formation of the Kringlefjellet fault.  $n=16$ .

displacements are generally unconstrained as the basal unconformity is not preserved in the hangingwalls. In the central basin area, the E–W-striking Kringlefjellet

reverse fault (Fig. 9) cuts the anticline described previously. In our interpretation (Fig. 5c), the reverse fault juxtaposes basement with Devonian at depth. Stratigraphic separation may approach 1 km. The Kringlefjellet reverse fault merges with the Instelva and Blegjeskardet faults, respectively. In the hangingwalls of these faults, the basin fill is deflected by fold trains that are not recognized in the trapezoid-shaped fault block that constitutes the footwall. At the scale of outcrop, many small-scale reverse faults have been observed. These range from apparently ductile structures with no sign of cataclasis or brittle fracture (Fig. 15) to entirely brittle faults marked by discrete fractures. Locally, reverse faults that cut heterolithic rock units display apparently ductile smears of red, fine-grained siltstone along the fault planes. A number of folds and reverse faults (Fig. 14) display orientations that deviate significantly from the E–W trend defined by the Kringlefjellet reverse fault and by the basinal syncline.

## TECTONOSEDIMENTARY RELATIONSHIPS

### The Dalsfjord fault

In E–W section, the Dalsfjord fault cuts down to the west through the basin and its depositional substrate. In N–S section (Figs 5 and 16), it is evident that the fault cuts the large-scale, E–W-trending folds in the basin as well as major lithological units like the southern margin fan complex. The scoop-shaped Dalsfjord fault has a more gentle amplitude than the folds in the basin fill (see also Torsvik *et al.*, 1986). As no clasts from the Western Gneiss Region nor from the extensional mylonite zone have been identified in the basin fill, the juxtaposition of Devonian sediments with extensional mylonites across the Dalsfjord fault cannot have taken place at the surface at the time of deposition. The Permian and Mesozoic resetting of magnetic fabrics in the fault zone (Torsvik *et al.*, 1992) confirms that the Dalsfjord fault accommodated post-Devonian displacement. The Dalsfjord fault apparently also excises part of the detachment mylonites in its footwall (maps and profiles by Kildal, 1970; Hveding, 1992). The above observations demonstrate that the Dalsfjord fault does not represent the Middle Devonian basin margin. More likely, the basin was rotated out of its original position during N–S shortening and later cut by the fault.

### Constraints on syndepositional basin-margin morphology

The fault that controlled sedimentation in the Kvamshesten Basin is nowhere preserved. The apparent lack of rocks from the Western Gneiss Region and the detachment mylonites in the conglomerates as well as lithologies exposed in landslides found at high stratigraphic levels indicate that the basin-bounding fault must

## Tectonics and sedimentation, Devonian, western Norway

**Fig. 15.** Small-scale, soft-sedimentary reverse fault, Leknesvatna. The fault is rooted in planar cross-beds (lower part of photograph). The fault plane can be traced as a localized, but apparently ductile zone of deformation through the coarse-grained layer in the upper half of the photograph.



**Fig. 16.** The Dalsfjord fault viewed from the east along the south-eastern basin margin, towards Kvamshesten mountain. The fault is outlined by the marked break in topography and vegetation, and clearly truncates the steeply dipping beds along the basin's south-eastern margin.



have been developed entirely in the hangingwall of the detachment zone. As the Dalsfjord fault cross-cuts the synsedimentary configuration, the dip of the synsedimentary basin-bounding fault cannot be exactly quantified. Independent evidence is provided, however, from the size and geometry of the marginal deposits. The size of the southern margin fan complex indicates that the basin-bounding fault on the south-east margin had a moderate or shallow north-westwards dip, as fan size is usually taken to be directly proportional to the size of the drainage basin that feeds the fan (Leeder & Gawthorpe, 1987). Drainage basins that develop in the footwalls of steep normal faults are not extensive enough to provide large amounts of sediment. The exposed footwall of a low-angle fault will constitute a much larger drainage area than the footwall of a steep normal fault. Thus, the low-angle normal fault will have the potential of producing a larger alluvial fan (Friedman & Burbank, 1995). The large clast sizes encountered in the marginal fan complexes suggest, however, that significant topography

existed in the feeder drainage basin. Another line of argument based on clast provenance studies was presented for the Hornelen Basin by Cuthbert (1991). No eclogite clasts were identified in the Hornelen Basin, and the metamorphic grade of the clast population was not found to increase upwards through basin stratigraphy. Thus, Cuthbert (1991) concluded that the 50 km of displacement inferred for the syndepositional Hornelen Basin bounding fault must largely have taken place along a low-angle fault. We have found no clasts of eclogite in the Kvamshesten Basin, and a similar argument applies here, strongly supported by the geometrical and tectono-sedimentary relationships referred above. The presence of a large-scale rollover anticline-syncline pair during basin deposition indicates that the basin-bounding fault had a ramp-flat topography at depth. The detachment zone was probably at depth during the formation of the basin. Based on Ar-Ar geochronology (Chauvet *et al.*, 1992) and on *P-T-t* modelling, Wilks & Cuthbert (1994) concluded that the rocks of the Western Gneiss Region

P. T. Osmundsen et al.

in the Hornelen Basin area were at a depth corresponding to 300 °C at the time of basin deposition. We suggest that in the Kvamshesten Basin area, the basin-controlling fault detached along the mylonite zone. Although the cutoff angle between the Devonian unconformity and the top of the extensional mylonites is  $\approx 45^\circ$ , the restoration of the unconformity to shallower dips away from the fault suggests a rollover shape that is most consistent with a ramp-flat normal fault that soles into a basal detachment at depth.

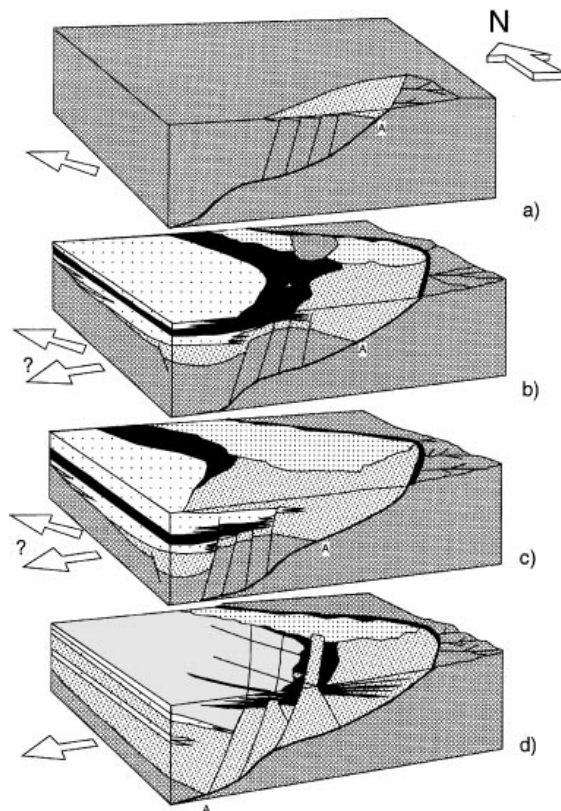


**Fig. 17.** Schematic 3D cartoon for the tectonosedimentary development of the Kvamshesten Basin. (a) A NW-dipping normal fault controlled deposition of the lower part of the southern margin fan complex (see text). The present northern basin margin was an area of nondeposition or erosion at this stage. The basal deposits onlap basement towards the north-west, north and north-east in the preserved basin area. Probably, a SW-dipping transfer fault developed along the northern basin margin towards the end of this stage. Also, an extensional rollover was developing. The basin was extending in a north-west direction. Evidence for this stage is mainly the onlap and time-relations observed at low stratigraphic levels in the westernmost basin area. (b) Tectonosedimentary framework during deposition of lower middle (preserved) stratigraphic levels. At this time, the depositional systems corresponding to the northern margin fan complex and the sandstones of the central basin area were established. The basin was bounded by faults in the south-east and north, and coarse debris was

### Geometry and age relationships of facies units

From our map (Fig. 2) it is evident that the southern margin fan complex contains stratigraphy that cannot be recognized in the north. West of Markavatn, the unconformity is onlapped by sandstones that are stratigraphically higher than the southern margin fan complex. Several hundred metres of stratigraphy must have been deposited in the southern margin fan complex prior to the onset of sedimentation on the northern basin margin. Thus, the oldest sediments in the Kvamshesten Basin are encountered along the present southern basin margin, on the present north-east flank of the basinal synform.

transported basinwards from the margins. While fluvial processes dominated in the south, the northern margin was characterized by both fluvial and debris flow processes, probably controlled by a fault with a steeper dip than the one at the south-eastern margin. In the central basin area, a sandy fluvial environment persisted, fining gradually upwards from the pebbly braided channels represented by the pebbly green sandstones to the floodplain represented by the heterolithic units. The heterolithic unit is fairly symmetrically distributed in the (preserved) basin. Palaeocurrents were flowing east-west, at least periodically towards the east. This indicates that some of the sandstones were sourced in the hangingwall of the basin-bounding fault. The sediments onlapped the crest of an evolving rollover anticline from the (south)east and (north)west, respectively, producing thickness variations in the marginal fan complexes. Evidence for this stage is the distribution of sedimentary units mapped by us, the onlap relations onto basement at medium stratigraphic levels (Bjørnastigvatn area), onlap relations onto the top of the southern margin fan complex and synsedimentary activity on NE-striking intrabasinal faults. (c) At middle stratigraphic levels, an episode of marked fan progradation took place from both the northern and the southern basin margins. A fan segment several hundred metres thick prograded from the southern basin margin towards the central basin areas. Correspondingly, a series of thick conglomeratic fans prograded basinwards from the northern margin and intercalated with floodplain deposits. Apparently, the floodplain shifted its position relative to stage (b), where it covered a larger part of the basin floor, to a more restricted area along the northern margin during this stage. Evidence for this stage is mainly the configuration of sedimentary units. (d) At high stratigraphic levels, the main locus of the floodplain had shifted southwards, and was receiving coarse debris from fan segments that prograded basinwards from the southern margin fan complex. The floodplain was interacting with the fluvial channel belt. The fluvial channel belt was migrating (south)eastwards together with the floodplain, as a response to progressive eastwards tilting of the basin. The eastwards migration of the fine-grained fluvial units was apparently hindered temporarily by subsidence on the intrabasinal faults in the Selsvatn fault system. The basin was extending in east-west and north-south directions. Evidence for this stage comprises the distribution of sedimentary units mapped by us and the strain field deduced from the orthorhombic Selsvatn fault system.

*Tectonics and sedimentation, Devonian, western Norway*

The onlap observed in the westernmost parts of the basin together with the overall geometry of the southern margin fan complex is consistent with a southwards component of tilt of the basin floor during early stages of deposition. The change in facies from sandstones to conglomerates along the basal unconformity is associated with an abrupt reduction of contact topography. Probably, a buried fault scarp provides the best interpretation of the contact in this area.

The wedge shape of the marginal fan complexes (Figs 2 and 4) apparently records progressive eastwards tilting of the hangingwall of the detachment zone during deposition. The syndepositional rotation of the basin on the fault as deduced from fanning dips in the Devonian strata is  $20^\circ$ . The total amount of rotation in the hangingwall from the onset of sedimentation is  $\approx 30^\circ$  ( $20^\circ$  syndepositional rotation +  $\approx 10^\circ$  dip recorded by the uppermost Devonian strata). Across the Instelva fault, the eastwards dip of the basal unconformity is reduced to  $\approx 20^\circ$ . The reduction in dip is accompanied by a thickness decrease in the lower part of the southern margin fan complex, from more than 1 km in the footwall to  $\approx 500$  m in the hangingwall. Westwards, thickness increases gradually. In the hangingwall of the Instelva fault, a floodplain unit onlaps or interfingers with the lower part of the southern margin fan complex. Apparently, the southern margin fan complex dipped to the west at the time of deposition of the fine-grained units immediately overlying it. At the same stratigraphic level, the conglomerates of the northern margin fan complex display an eastwards onlap onto the basal unconformity. If bedding immediately above the basal unconformity is restored to a horizontal position (Fig. 10a), the basal unconformity displays a westwards dip. A change in the direction of onlap takes place across the faulted area between the Instelva and Grunnevatn faults. West of this area, onlap is towards the east. East of the Instelva fault onlap is towards the west, as displayed by the wedge geometry of the marginal fan complexes. The above observations indicate that a large-scale, rollover anticline-syncline pair developed in the hangingwall of the detachment zone during basin deposition (Fig. 17). In Fig. 4 an anticlinal geometry is evident also at high stratigraphic levels in the easternmost parts of the basin. The anticline is associated with a fanning wedge geometry displayed by the Devonian strata. The fanning wedge geometry indicates that the migration of fluvial channel sandstones and fine-grained heterolithic units towards the east and stratigraphically upwards was related to the progressive eastwards tilting of the basin floor. We infer that the rollover migrated through the basin with time, much in the way modelled by McClay & Scott (1991). A migrating rollover structure explains some of the onlap onto the unconformable basin margins, and is in accordance with large-scale extensional displacements along a W- or NW-dipping detachment. The southwards component of dip inferred from onlap relationships at low stratigraphic levels does, together with the basic asymmetry in sedimentary facies configuration, suggest that the boundary

conditions in terms of tectonic control changed from early to late stages of basin deposition. This opens the possibility that the Kvamshesten Basin is a polyhistory basin, or that the fundamental basin-forming mechanism itself induced a change in the strain field during sedimentation.

**Syndepositional extensional faults**

Our observations strongly suggest a syndepositional origin for a number of the oblique faults described earlier. Evidence for syndepositional fault activity includes thickness variations across faults, rapid termination of fault displacement upwards in the stratigraphy and wedges of coarse sediment that thin away from the fault planes and intercalate with sandstones distally. We infer the offsets of the basal unconformity to represent synsedimentary basin floor topography. Also, we infer the climbs of stratigraphic boundaries associated with the Selsvatn fault system to reflect synsedimentary fault activity. To reveal the synsedimentary orientations of the faults, the basin margin must be restored to its syndepositional orientation (Fig. 11c,d). This is achieved by rotating the faults with bedding around the axis of the basinal synform, followed by rotation around a N-S axis to compensate for the eastwards tilt of the basin upon the detachment zone. The apparent strike-parallel separation observed for many of the faults in map view changes to mainly normal separation when the flank of the basinal syncline is restored. Restoration of the NE-dipping south-western basin margin to its syndepositional orientation leaves most of the faults with dips between  $60^\circ$  and  $80^\circ$ . Some are rotated to a reverse position. The steep dips of some of the faults, together with their generally high cutoff angles with bedding, indicate that the faults originated as tension fractures that started to accommodate displacement as the basin rotated upon the detachment zone. Thus, some of the intrabasinal faults may be regarded as second- or third-order faults in the terminology of Angelier & Coletta (1983). The inferred presence of a hangingwall anticline-syncline pair indicates that the basin-bounding fault had a ramp-flat geometry. McClay & Scott (1991) showed that reverse faults may develop in a basin as it passes the ramp. The faults that display reverse positions after restoration may have formed in this way. The lack of lineations from most of the faults along the south-western margin does not allow for any accurate determination of extension direction.

Restoration of the Selsvatn fault system (Fig. 11d) in a similar manner reveals four sets of syndepositional faults, apparently conjugate to each other. The displacements accommodated by the faults must have been mainly normal to provide accommodation for the excess stratigraphy preserved in their hangingwalls. The long-waved ( $>1$  km) deflection of bedding associated with some of the faults in the Selsvatn fault system are interpreted by us as rollover anticlines, superposed on the larger-scale anticline evident in Fig. 4. As activity on the four main faults in the area must have partly

P. T. Osmundsen et al.

overlapped in time, the faults would define an orthorhombic fault pattern with NE- and NW-striking faults, respectively, on the synsedimentary surface. An orthorhombic fault pattern (Reches & Dieterich, 1983, Krantz, 1988) comprises four mutually conjugate sets of faults and are interpreted as the product of a three-dimensional strain field. The orientations of fault planes can be used to determine the directions and signs of the principal strain axes. In the odd-axis model of Krantz (1988) the 'odd' strain axis is defined as the axis with a sign of elongation that is opposite to the other two. Correspondingly, the 'similar' axes have signs of elongation that are similar to each other, but different from that of the 'odd' axis. The intermediate strain axis and the axis which is similar to it bisect the acute and obtuse angles, respectively, between the strikes of the fault sets. The axes of symmetry that can be extracted from Fig. 11(d) are orientated approximately E–W and N–S, respectively. Thus, the Selsvatn fault system formed in a strain field characterized by E–W and N–S extension. The axis of maximum elongation was approximately E–W, parallel to the ductile lineation in the extensional mylonites below the basin. The strain field deduced from the restored Selsvatn fault system thus provides a kinematic link between synsedimentary faults in the Devonian basin and the Devonian extensional shear zone below it. In the present conception of the syndepositional tectonic framework, eastwards migration of the depocentre can be related to the progressive eastwards tilting of the basin upon the detachment zone. The stratigraphic climbs displayed by the lower boundary of the green sandstones adjacent to the Mariefjellet and Berge faults indicate that the faults affected the (south) eastwards migration of the sandy fluvial belt. Apparently, the sandy fluvial belt was trapped temporarily in the hangingwalls of the intrabasinal faults. The intrabasinal faults described above affect and are draped by progressively higher stratigraphic levels eastwards in the basin. We infer that intrabasinal fault activity migrated eastwards through the basin during the course of its deposition. Experimental work by Xiao *et al.* (1991) indicates that intrahangingwall faults within extensional wedges migrate towards the footwall with time. In the case of a ramp–flat extensional detachment, the crestal collapse of a hangingwall rollover anticline tends to migrate stratigraphically upwards and towards the detachment breakaway (McClay & Scott, 1991). We suggest that this was the case in the Kvamshesten Basin.

### North–south shortening

The N–S shortening of the Kvamshesten Basin was accommodated by folding, reverse faulting and re-activation of earlier extensional faults. To the west and east of the Instelva and Blegjeskardet faults, respectively, fold trains an order of magnitude smaller than the basinal syncline are common. In the trapezoidal fault block that constitutes the footwall of the Instelva, Blegjeskardet and Kringlefjellet faults, folds of this amplitude and wavelength are generally not recognized. The

axis of the basinal syncline is apparently displaced with a sinistral and dextral sense, respectively, across the Instelva and Blegjeskardet faults. We interpret the Instelva and Blegjeskardet faults to have acted as transfer faults during N–S shortening, in the way that they separated the area dominated by thrusting on the Kringlefjellet reverse fault from areas where shortening was taken up by other combinations of faulting and folding. Theoretically, conjugate sets of NE- and NW-striking extensional faults would have orientations that were favourable for strike-slip reactivation during N–S shortening. Moreover, rotation of the faults towards steeper orientations during formation of the basinal syncline would enhance the potential for re-activation. The strike-slip movements accommodated by the Blegjeskardet and Instelva faults may be explained in this way. The steep, NE- and NW-striking shear fractures reported from the basin as well as from the depositional substrate (Markussen, 1994; Osmundsen, 1996) may have formed during continued shortening, as suggested by Skjerlie (1971). Across the Instelva fault, the trend of the basinal syncline changes by  $\approx 10^\circ$  in a clockwise direction (Fig. 13). Correspondingly, in the westernmost part of the basin, a number of folds and reverse faults have a north–west trend. This may be explained by rotation about a vertical axis during sinistral slip on the Instelva fault. Alternatively, the stratigraphic levels in the western parts of the basin record a NE-directed shortening that was not experienced by higher stratigraphic levels. The relationship between N–S shortening and sedimentation in the Kvamshesten Basin is, however, not unambiguous. Seranne *et al.* (1989) followed by Chauvet & Seranne (1994) inferred that the northward onlap relationship observed along the northern basin margin was produced by syndepositional N–S shortening. This interpretation requires a syndepositional, southwards dip of the basal unconformity along the northern margin. The southern margin would, in this scenario, be characterized by southwards onlap onto basement. A north- to north-eastwards component of onlap is inferred for the entire westernmost part of the basin including the southern flank of the basinal synform. Thus, the observed onlap onto basement does not seem to reflect the present synformal shape of the Devonian strata. Our profiles in Fig. 5 do not reveal any significant difference in the degree of shortening between low and high stratigraphic levels. At high stratigraphic levels in the basin, bedding is overturned in the hangingwall of a large reverse fault (see also Braathen, 1997) that crops out along the present northern basin margin. Thus, considerable shortening took place at a relatively late stage, probably after deposition of the preserved stratigraphy. Some unconformities are re-interpreted as related to rollover formation rather than to syndepositional N–S shortening (Osmundsen, 1996). In the Hornelen Basin, discontinuities interpreted as internal unconformities were rejected by Wilks & Cuthbert (1994). In the Kvamshesten Basin, interpretation of discontinuities in the Devonian stratigraphy that would conform to the

## Tectonics and sedimentation, Devonian, western Norway

internal unconformities suggested by Chauvet & Seranne (1994) is generally ambiguous. Some of the proposed unconformities have been rejected (Osmundsen, 1996). Thus, some doubt exists whether shortening commenced during deposition. The syndepositional Selsvatn Fault System represents a strain field that was characterized by E–W and N–S extension. Thus, if shortening commenced during basin deposition, it cannot have been continuous throughout the basin history.

## DISCUSSION

## Models for Devonian basin formation in western Norway

Steel (1976) ruled out climate and source rock variation as major controls in the western Norwegian Devonian basins. Thus, the facies architecture of individual basins should closely reflect the tectonics during deposition. With respect to the general facies architecture, the Kvamshesten Basin shows similarities with the Hornelen (cf. Steel & Aasheim, 1978; Steel & Gloppen, 1980) and Solund (Nilsen, 1968; Steel *et al.*, 1985; Seranne, 1988) basins. All three basins display large, streamflow-dominated fan complexes along their southern margins, whereas the northern basin margins have variably been the locus of mass-flow type deposition (Steel *et al.*, 1985; this work) on smaller fans. In the model for the Hornelen Basin by Steel & Gloppen (1980), the southern and northern basin margins were principally different in nature, and dominated by normal and strike-slip faulting, respectively. Following the identification of the low-angle normal faults (Hossack, 1984; Norton, 1986), it was argued that the detachment faults that controlled Devonian basin sedimentation were scoop-shaped (Hossack, 1984; Seranne *et al.*, 1989; Chauvet & Seranne, 1994; Wilks & Cuthbert, 1994). In these interpretations, the scoop-shaped detachment faults were characterized by a normal slip eastern segment, giving way to strike slip segments at the northern and southern margins, respectively (Hossack, 1984). This would explain the marginal conglomerates and the central belt of fluvial sandstones observed in the Hornelen Basin as well as the Kvamshesten Basin and also the lateral stacking of fanglomerates along the basin margins (Steel & Gloppen, 1980). However, a problem with these models is the consistent asymmetry of the Devonian basins, in particular the Kvamshesten and Solund basins. In the models by Hossack (1984) and Wilks & Cuthbert (1994) both the southern and the northern basin margins were bordered by strike-slip fault segments from the onset of deposition. Thus, there would be no principal difference between the northern and southern basin margins except in the sense of displacement. Our data from the Kvamshesten Basin indicate that a principal difference did exist between the northern and southern basin margins, at least at an early stage. This suggests that a change in boundary conditions took place during sedimentation. Either there was a re-arrangement in the pattern of basin-bounding

faults during sedimentation or the kinematics of the basin-bounding faults changed, or both.

The inferred scoop shape was given different explanations by the various authors. Hossack's (1984) model was based mainly on the present basin margins and interpreted the basin bounding fault as a re-activated thrust where the strike-slip segments were lateral ramps inherited from the original thrust geometry. Milnes *et al.* (1988) showed, however, that the Nordfjord–Sogn detachment zone cross-cuts the Caledonian tectonostratigraphy. Wilks & Cuthbert (1994) argued for a basin-bounding fault that had a primary scoop-shape, analogous to corrugated detachments described from the Basin and Range Province (see Friedman & Burbank, 1995). Chauvet & Seranne (1994) argued that the basin-bounding faults acquired their scoop shape through progressive, synsedimentary folding around E–W trending axes. They presented a model that attempted to explain the parallelism between the mylonitic lineation and fold axes in the footwall of the detachment zone as well as the proposed unconformities in the Devonian basin fill. Chauvet & Seranne (1994) suggested that during Devonian basin formation, the axes of maximum and intermediate compressive stress had values close to each other, i.e. they were both compressive, and orientated vertically and N–S, respectively.  $\sigma_3$  was horizontal, extensional and orientated in an E–W direction. The basin-controlling fault would be folded around a fold axis parallel to the W-plunging mylonitic lineation in the WGR. The implication would be a basin that was symmetric with respect to the mylonitic lineation as well as with respect to the basinal syncline. Our profiles in Fig. 5 are constructed normal to the basinal synform. The profiles show both a pronounced asymmetry in the organization of sedimentary facies units as well as a marked diachronism between the northern and southern basin margins. Thus, in our view, the basinal synform axis does not represent an axis of symmetry. Rather, the asymmetry of sedimentary facies indicates that the early basin history did not conform to a symmetric tectonic model.

Hartz & Andresen (1997) argue that the Hornelen Basin initiated as an E–W-trending graben, analogous to the orogen-normal grabens of the Tibetan Plateau. In their model, the earliest stages of basin formation was controlled by N–S extension parallel to the orogenic front. The orogen-parallel extension was followed by gradual E–W and N–S extension, as a function of stress axis permutation when crustal thickening was relieved by orogenic collapse. After deposition, N–S shortening commenced due to sinistral plate movements between Baltica and Laurentia. Theoretically, the southwards component of tilt of the floor of the Kvamshesten Basin could be related to an E–W- or NW-trending, asymmetric graben formed normal to the orogenic front. Several NW-striking faults in the vicinity of the basin are cut and displaced by NE-trending synsedimentary faults (Osmundsen, 1996). As their relations to the Devonian unconformity are generally indeterminable, they may

P. T. Osmundsen *et al.*

pre-date deposition in the Kvamshesten Basin. The southern margin fan complex remained a major depositional system through the preserved stratigraphy. If the fan complex was controlled by a W- or NW-striking fault at an early stage, this fault should theoretically have developed into a transfer fault at the onset of top-to-the-west extension. Such a fault would cut the Caledonian tectonostratigraphy south-west of the basin and produce displacements comparable to the length of the basin. This does not appear to be the case. Thus, a model like that of Hartz & Andresen (1997) cannot readily be adapted for the Kvamshesten Basin.

### A model for the Kvamshesten Basin

In our discussion of a model for the Kvamshesten and other Devonian basins we focus on basinal asymmetry with respect to the mylonitic lineation below the basin, as well as with respect to the main synclinal axis. In the Kvamshesten Basin, the southern margin fan complex is clearly the thickest of the two marginal fan complexes, and our profiles (Fig. 5) indicate a significant southwards component of tilt during early stages of deposition. The geometries of fans at high stratigraphic levels indicate a bulk transport direction from the south-east towards the north-west on the southern basin margin. The southwards component of rotation accommodated by the Kvamshesten Basin provided accommodation for the lower part of the southern margin fan complex at a time when the northern margin was in an updip position characterized by bypass or erosion (Fig. 17). As the northern basin margin was draped with sediment, the northern margin fan complex developed as a sedimentary wedge similar to the southern margin fan complex. We suggest (Fig. 17) that sedimentation in the northern margin fan complex was triggered by the formation of a NW-trending transfer fault. From this stage, the basin had a 'scoop' shape and coarse debris was transported into the basin from both sides. The northern and southern basin margins would be principally different because the dip of the NW-trending transfer fault would be steeper than the dip of the normal fault bounding the basin in the south-east. A steeper fault on the northern margin would account for the abundant debris flow deposits (Steel *et al.*, 1985) encountered in the northern margin fan complex. The northern margin fan complex probably remained subordinate in thickness compared to the southern margin fan complex, as the latter continued to be a major depositional system throughout the preserved basin stratigraphy. The E-W direction of maximum elongation inferred from the Selsvatn fault system is in accordance with an eastwards rotation of the basin. Thus, the stratigraphy at medium stratigraphic levels must record a change in subsidence pattern from a half graben that accommodated a significant component of southwards rotation to a half graben that rotated mainly towards the east (Fig. 17). The stratigraphic interval in question records firstly the apparent shift in the locus of floodplain deposition from a relatively widespread con-

figuration in the (preserved) basin to a position restricted to the northern margin. Second, it records the progradation of coarse-grained fans from both basin margins towards the central areas. The shift of the locus of floodplain deposition has been thought to reflect episodes of subsidence in extensional basins (Alexander & Leeder, 1987; Leeder & Gawthorpe, 1987). Floodplains as well as channel belts will have a tendency to migrate towards the area of maximum subsidence. Tentatively, the shift in position of the floodplain referred to above can be explained by the change in slip directions on the basin-bounding faults. If the direction of extension changed from north-west to west, slip on the relatively steep northern margin fault would change from dominantly dextral to oblique normal. The northern basin margin would thus experience an increase in subsidence relative to the southern margin. This may have caused the migration of the floodplain towards the northern margin. Eventually, the increased subsidence would allow increased fan progradation from the northern margin. The stratigraphic interval referred to above suggests a major period of subsidence in the entire basin, as major fan segments prograded from the northern as well as the southern basin margins following the northwards shift of the floodplain. At high stratigraphic levels, the basin was extending in E-W as well as N-S directions. At this stage (Fig. 17d), the basin experienced top-to-the-west displacement and eastwards rotation. The locus of floodplain deposition had apparently shifted again to be located mainly along the south-eastern basin margin. This shift cannot be explained by a line of argument like that above, as the fault on the south-eastern margin must have undergone a change from mainly normal to sinistral/normal. Thus, the southern margin would have undergone a decrease in subsidence per unit of extension. Possibly, the locus of floodplain deposition was controlled by the intrabasinal faults at this stage.

Most of the shortening experienced by the Kvamshesten Basin took place after deposition of the preserved stratigraphy. This is evident by the rotation of bedding at high stratigraphic levels on the southern margin to dips of 45° and more, and by the inversion of bedding at high stratigraphic levels on the northern margin. Thus, the basinal syncline represents the relatively late stages of contraction responsible for most of the shortening in the Kvamshesten Basin. Within the model framework outlined above, the lack of symmetry in sections normal to the basinal syncline is explained by the oblique relationship between the originally NW-dipping basin-bounding fault and the E-plunging fold axis.

The Dalsfjord fault sharply truncates already folded Devonian strata. The cross-cutting relationships between the Dalsfjord fault and the Devonian basin added further asymmetry to the structural section, as the syndimentary basin margins had rotated out of their original orientation by folding prior to slip on the Dalsfjord fault. The age of incipient displacement along the Dalsfjord fault is unknown. The W-plunging scoop shape of the

## Tectonics and sedimentation, Devonian, western Norway

fault indicates that it experienced N–S shortening, although less than the Devonian basin (see also Torsvik *et al.*, 1986). Juxtaposition of Devonian rocks with detachment mylonites was completed during late slip along the Dalsfjord fault. The amount of late slip is uncertain due to unknown amounts of juxtaposition at depth during synsedimentary slip on the original basin-bounding fault. It is possible, however, that the entire juxtaposition is due to slip on the Dalsfjord fault, in which case more than 13 km of displacement post-dated the preserved basin stratigraphy. Tentatively, slip on the Dalsfjord fault may have commenced in the late Devonian/early Carboniferous, prior to complete cessation of N–S shortening. Permian and Mesozoic movements along the fault (Torsvik *et al.*, 1992; Eide *et al.*, 1997) show that movement continued past the time-window represented by the Devonian basins.

### The Devonian basins of western Norway: products of combined extension and strike-slip?

The Hornelen Basin does not display the kilometre-thick fan complexes that are prominent in the southern basins. The exposed levels of the basin thus display a more symmetrical facies configuration with conglomerate fringes along the basin margins and a large central area occupied by sandstones. The geometry of the basin at depth is largely unknown, although low stratigraphic levels are preserved on skerries and islands along the basin's unconformable western margin (see Hartz & Andresen, 1997). Palaeocurrent directions in the Hornelen Basin are generally westwards in the central basin area, and towards the central basin area from the southern and northern margins (Steel & Gloppen, 1980). In summary, the Hornelen Basin is more symmetric about the W-plunging lineation in the ductilely deformed rocks below the basin than are the southern basins. In the Solund basin, the conglomerate complex of the basin's south-eastern margin is banked against the NW-dipping Solund fault. Palaeocurrents in the conglomerates as well as in minor sandstone bodies were mainly towards the NW, consistent with transverse drainage and deposition away from a NW-dipping fault (Nilsen, 1968). Apparently, the thickest and coarsest conglomerate units in both the Solund and Kvamshesten Basins were sourced from drainage basins located on the SE side of the basins, developed in the footwalls of low- to moderate-angle, NW-dipping faults. The original basin-controlling faults were thus oblique to the W- to WNW-plunging lineation observed in the detachment mylonites directly below the basins. Therefore, on a regional scale (Fig. 1), intrabasin asymmetry apparently increases from the Hornelen Basin in the north to the Solund Basin in the south. If tectonics was the main control on basin formation (Steel, 1976), this points towards a variation in the geometry and/or slip directions of the basin-controlling faults.

The ductile lineations in the mylonites of the Nordfjord–Sogn Detachment Zone are oblique to the

NE-trending enveloping surface of the shear zone on a regional scale. Thus, displacement in the detachment zone was transtensional rather than dip-slip extensional (Krabbendam & Dewey, in press). Moreover, the azimuth of the ductile lineation swings from a WNW orientation east of the Solund Basin to a WSW orientation north of the Hornelen Basin close to the Møre–Trøndelag Fault Zone (MTFZ) (Seranne *et al.*, 1991; Chauvet & Seranne, 1994; Krabbendam & Dewey, in press). North of the Møre–Trøndelag fault, it swings back to a north-west plunge in the Roan Window area (Krabbendam & Dewey, in press). They concluded that the MTFZ was active as a sinistral shear zone during detachment faulting and exhumation of the Caledonian eclogites of the WGR. A critical point is whether sinistral shearing was contemporaneous with Devonian sedimentation, or occurred at a later stage. Recent low-temperature Ar–Ar geochronology and thermal modelling on feldspars indicate that the rocks of the WGR cooled from  $\approx 285^\circ\text{C}$  to below  $150^\circ\text{C}$  prior to 350 Ma (Eide *et al.*, 1998). The anticlockwise deflection of the extensional lineation as well as the folding about E–W axes should therefore pre-date 350 Ma. The change in syndepositional tilt direction inferred by us from the Kvamshesten Basin suggests a rotation of the direction of maximum elongation from north-west to west during basin formation. The hangingwall of the detachment zone experienced a minimum of 50–100 km of north-west to west translation in the Devonian. Thus, the initial NW-directed extension direction apparently recorded by the Kvamshesten Basin represents deformation that took place when the basin was in a position tens of kilometres to the south-east of its present location. Thus, the anticlockwise change in tilt direction displayed by the basin may reflect the same strain gradient as the anticlockwise rotation displayed by the ductile lineation in the detachment zone and WGR. Both relations are compatible with sinistral shearing along the MTFZ. If the basin-controlling faults formed with orientations approximately perpendicular to the local direction of maximum elongation, then the array of basin-forming faults would display north-west dips in the Solund and Kvamshesten areas, and west to south-west dips in the Hornelen and Møre–Trøndelag areas (Fig. 18). For the Kvamshesten Basin, this would imply an early phase of north-westwards extension, gradually taken over by west-northwest extension as the basins moved closer to the MTFZ. An early south-eastwards tilt of the basin floor would correspondingly be taken over by tilting towards the east-southeast and by a change in movement direction for the basin-bounding faults. The marginal fan complexes in the individual basins would thus be thicker in the south-east for both the Solund and Kvamshesten basins. Tentatively, the generally NE-trending faults that dominate in the basin's depositional substrate and that were synsedimentary at low stratigraphic levels may represent an early strain field dominated by north-west extension. Correspondingly, the orthorhombic Selsvatn fault system may reflect the E–W extension experienced by the basin at a later stage,

P. T. Osmundsen et al.

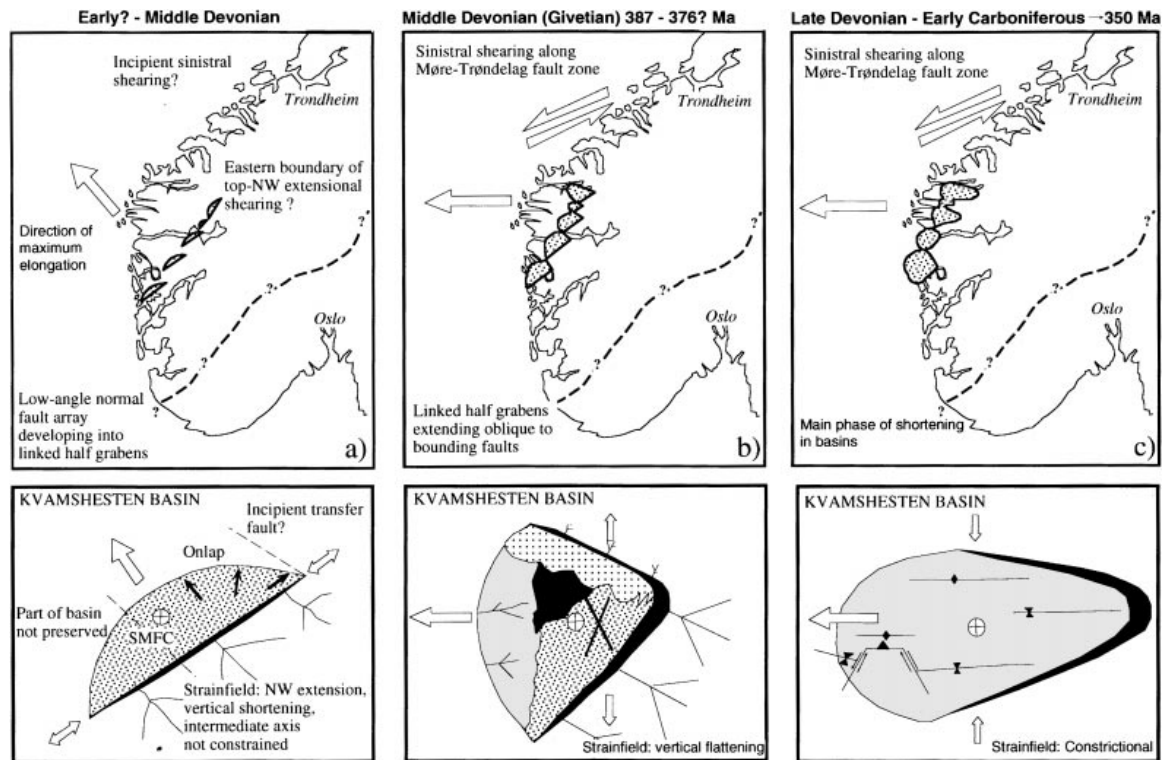


Fig. 18. Tentative model for Devonian basin development in western Norway. The model involves strain partitioning between the mainly extensional Nordfjord–Sogn Detachment Zone and the mainly sinistral Møre–Trøndelag Fault Zone. The model is based on observations presented in this paper, as well as on regional data and inferences by Chauvet & Seranne (1994) and by Krabbendam & Dewey (in press). (a) Initial configuration of basin-bounding faults. The direction of maximum elongation was north–west for the southernmost basin area. Correspondingly, basin-bounding faults were NE–striking in the Solund and Kvamshesten areas. It is not obvious whether any extension–normal shortening affected the basins at this stage. In the Kvamshesten Basin, this stage corresponds to stage (a) of Fig. 17. (b) The basins were transported closer to the principal zone of orogen-parallel sinistral shearing. The direction of maximum elongation changed to a more westward orientation, as evidenced by the present W-plunging lineation in the footwall of the detachment zone, as well as by intrabasinal extensional faults (Selvatn fault system). Intermediate elongation was positive and north–south, contrary to the continuous, negative north–south elongations suggested by previous authors (Chauvet & Seranne, 1994; Krabbendam & Dewey, in press). We suggest that the strain fields experienced by the basins may not have been entirely identical to the strain fields experienced by the footwall of the detachment zone (see text). In the Kvamshesten Basin, this stage corresponds to stage (d), possibly also to stage (c) in Fig. 17. (c) The main phase of north–south shortening affected the basin after deposition of the preserved stratigraphy, as the basins were transported closer to the Møre–Trøndelag Fault Zone. The basin was still extending in an east–west direction.

as the basin was transported into areas closer to the principal sinistral shear zone. Eventually, the basins would be juxtaposed with extensional mylonites that recorded the later stages of transport. The configuration of sedimentary facies in the basins would, however, preserve a record of the tectonic development from the onset of sedimentation. Among the preserved basins, the Solund Basin displays a geometry and facies distribution that corresponds most closely to the earliest stage of basin formation outlined above (Fig. 18a). The Kvamshesten Basin records both early, NW- and later W-directed extension (stage a and b in Fig. 18). The Hornelen Basin is apparently more symmetric about the lineation in the footwall and may record mainly stage (b). The sedimentary facies configuration in the preserved basins are therefore interpreted to reflect their position

with respect to the MTFZ, and thus a strain gradient related to sinistral shearing along the orogen.

The transtensional model by Krabbendam & Dewey (in press) predicts plane strain followed by constrictional strain. From our data, it is not obvious whether the basin experienced early, syndepositional shortening. At a high stratigraphic level, the strain field was three-dimensional (Fig. 11d), characterized by positive elongation both in the *X* and *Y* directions (Osmundsen, 1996). A synsedimentary strain field characterized by vertical flattening has recently been documented also from low stratigraphic levels in the Hornelen Basin (Hartz & Andresen, 1997). Thus, E–W and N–S elongation accompanied basin formation on a regional scale. This is not compatible with models that predict continuous N–S shortening of the basins during sedimentation. In the hangingwall of

## Tectonics and sedimentation, Devonian, western Norway

the detachment zone, N–S shortening must either have occurred in pulses separated by periods of N–S extension or it must entirely post-date basin formation. This points towards a strong partitioning between extensional and strike-slip deformation or a time lag between the onset of north-westwards extension and the onset of sinistral shearing. Also, while the WGR was being unloaded by extension, the basin areas were increasing their load by receiving large amounts of sediment. Thus, the local strain field in the hangingwall of the detachment zone may not have constituted a blueprint of the strain field in the footwall, that was undergoing contemporaneous unloading. A model involving a large-scale sinistral component of deformation rather than continuous dip-slip extension explains several of our observations in the Kvamshesten Basin, and is compatible with observations on a regional scale. In particular, it provides a better explanation for the asymmetry of individual basins, the regional variation in asymmetry between the basins, and the oblique relationship between the basinal fold axis and the sedimentary facies distribution.

## ACKNOWLEDGEMENTS

We thank Maarteen Krabbendam for discussions. Ebbe Hartz commented on an earlier version of the manuscript. The present study was funded by the Norwegian Research Council (NFR), grants ABC/LR 440.92.002 & 007, and by NORSK AGIP a.s.

## REFERENCES

- ALEXANDER, J.A. & LEEDER, M.R. (1987) Active tectonic control on fluvial architecture. In: *Fluvial Sedimentology* (Ed. by F.G. Etheridge and, R.M. Flores), *Soc. Econ. Mineralogists Petrol.*, **39**, 243–252.
- ANDERSEN, T.B. & JAMTVEIT, B. (1990) Uplift of deep crust during orogenic extensional collapse: A model based on field studies in the Sogn-Sunnfjord region of Western Norway. *Tectonics*, **9**, 1097–1111.
- ANDERSEN, T.B., OSMUNDSEN, P.T. & BERRY, H. (1997) Multi-level extensional detachment systems in western Norway (abstract) *Geonytt*, **1**, 19.
- ANDERSEN, T.B., OSMUNDSEN, P.T. & JOLIVET, L. (1994) Deep crustal fabrics and a model for the extensional collapse of the southwest Norwegian Caledonides. *J. struct. Geol.*, **16**, 1191–1203.
- ANGELIER, J. & COLETTA, B. (1983) Tension fractures and extensional tectonics. *Nature*, **301**, 49–51.
- ASPHAUG, E.J. (1975) *Sedimentologi og stratigrafi i vestlige deler av Kvamshesten Devonbasseng*. Cand. real thesis, University of Bergen, Bergen.
- BERRY, H.N., LUX, D.R., ANDRESEN, A. & ANDERSEN, T.B. (1995) Progressive exhumation during orogenic collapse as indicated by 40 Ar/39 Ar cooling ages from different structural levels, southwest Norway (abstract). *Geonytt*, **22**, 20–21.
- BJØRLYKKE, K. (1983) Subsidence and tectonics in late Precambrian and Paleozoic sedimentary basins of southern Norway. *Nor. Geol. Unders. Bull.*, **380**, 159–172.
- BRAATHEN, A. (1997) Post-Devonske forkastningssystemer i Sunnfjord, Vest-Norge. *Geonytt*, **24**, 127.
- BRYHNI, I. (1964a) Migrating basins on the Old Red Continent. *Nature*, **202**, 284–285.
- BRYHNI, I. (1964b) Relasjonen mellom senkaledonisk tektonikk og sedimentasjon ved Hornelens og Håsteinens Devon. *Nor. Geol. Unders. Bull.*, **223**, 10–25.
- BRYHNI, I. (1975) ‘Gabbro’ in the Solund conglomerates: a Devonian debris flow deposit? *Nor. Geol. Tidsskr.*, **56**, 95–102.
- BRYHNI, I. & SKJERLIE, F. (1975) Syn-depositional tectonism in the Kvamshesten district (Old Red Sandstone), western Norway. *Geol. Mag.*, **112**, 593–600.
- BUCK, W.R. (1988) Flexural rotation of normal faults. *Tectonics*, **7**, 959–973.
- BURCHFIEL, B.C. & ROYDEN, R.H. (1985) North–south extension within the convergent Himalayan region. *Geology*, **13**, 679–682.
- CHAUVET, A., KIENAST, J.R., PINARDEN, J.L. & BRUNEL, M. (1992) Petrological constraints and PT path of Devonian collapse tectonics within the Scandinavian mountainbelt (Western Gneiss Region, Norway). *J. Geol. Soc. London*, **149**, 383–400.
- CHAUVET, A. & SERANNE, M. (1994) Extension-parallel folding in the Scandinavian Caledonides: implications for late-orogenic processes. *Tectonophysics*, **238**, 31–54.
- CUTHBERT, S.J. (1991) Evolution of the Devonian Hornelen Basin, Western Norway: new constraints from petrological studies of metamorphic clasts. In: *1991, Developments in Sedimentary Provenance Studies* (Ed. by A.C. Morton, S. P Todd and P.D.W. Haughton), *Spec. Publ. Geol. Soc. London*, **57**, 343–360.
- DEWEY, J.F. (1988) Extensional collapse of orogens. *Tectonics*, **7**, 1123–1139.
- DEWEY, J.F., RYAN, P.D. & ANDERSEN, T.B. (1993) Orogenic uplift and collapse, crustal thickness, fabrics and metamorphic phase changes: the role of eclogites. *Spec. Publ. Geol. Soc. London*, **76**, 325–343.
- EIDE, E.A., TORSVIK, T.H. & ANDERSEN, T.B. (1997) Ar–Ar geochronologic and paleomagnetic dating of fault breccias; characterization of late Paleozoic and early Cretaceous fault reactivation in Western Norway. *Terra Nova*, **9**, 135–139.
- EIDE, E.A., TORSVIK, T.H., ANDERSEN, T.B. & ARNAUD, N.O. (1998) Early Carboniferous unroofing in western Norway and alkali feldspar thermochronology. *J. Geol. Soc. London*.
- FLETCHER, J.M. & BARTLEY, J.M. (1994) Constrictional strain in a non-coaxial shear zone: implications for fold and rock fabric development, Central Mojave metamorphic core complex. *California. J. struct. Geol.*, **16**, 555–570.
- FRIEDMANN, S.J. & BURBANK, D.W. (1995) Rift basins and supra-detachment basins: Intracontinental extensional end-members. *Basin Res.*, **7**, 109–127.
- HARTZ, E.H. & ANDRESEN, A. (1995) The Caledonian sole thrust of East Greenland: a crustal scale Devonian extensional detachment? *Geology*, **23**, 637–640.
- HARTZ, E.H. & ANDRESEN, A. (1997) From collision to collapse: complex strain permutations in the hinterland of the Scandinavian Caledonides. *J. geophys. Res.*, **102** (B11), 24697–24711.
- HOSSACK, J.R. (1984) The geometry of listric normal faults in the Devonian basins of Sunnfjord, W. Norway. *J. Geol. Soc. London*, **141**, 629–637.
- HVEDING, B.S. (1992) *En strukturgeologisk undersøkelse av mylonittsonen under Dalsfjordforkastningen i Atloy-Åskvoll området Sunnfjord*. Cand. scient thesis, University of Oslo, Oslo.
- JACKSON, J.A. (1987) Active normal faulting and crustal extension. In: *Continental Extensional Tectonics* (Ed. by

P. T. Osmundsen et al.

- M.P. Coward, J.F. Dewey and P.L. Hancock), *Geol. Soc. London Spec. Publ.*, **28**, 3–17.
- JARVIK, E. (1949) *On the Middle Devonian Crossopterygians from the Hornelen field in western Norway*. University of i Bergen Aarb., Nat. vitensk. Rekke, 8.
- JOLIVET, L., DANIEL, J.M., TRUFFERT, C. & GOFFE, B. (1994) Exhumation of deep crustal metamorphic rocks and crustal extension in arc and back-arc regions. *Lithos*, **33**, 3–30.
- KILDAL, E.S. (1970) Geologisk kart over Norge, Berggrunnskart, 1: 250,000 Måløy. Nor. Geol. Unders. 1915–16, Nat.vitenskapelig række.
- KOLDERUP, C.F. (1916) Solunds devonfelt. Berg. Mus. Aarb. 1915–16, Nat.vitenskapelig række.
- KOLDERUP, C.F. (1921) Kvamshestens devonfelt. Berg. Mus. Aarb. 1920–21, Nat. vidensk. række, 4.
- KRABBENDAM, M. & DEWEY, J.F. (in press) Exhumation of UHP rocks by transtensionion in the Western Gneiss Region, Scandinavian Caledonides. In: *Transpression and Transtension*, *Geol. Soc. London Spec. Publ.*
- KRANTZ, R.W. (1988) Multiple fault sets and three-dimensional strain: theory and application. *J. struct. Geol.*, **10**, 225–237.
- KULLERUD, L., TRUDBAKKEN, B.O. & ILEBEKK, S. (1986) A compilation of radiometric age determinations from Western Gneiss Region, South Norway. *Nor. Geol. Unders., Bull.*, **406**, 17–42.
- LEEDER, M.R. & GAWTHORPE, R.L. (1987) Sedimentary models for extensional tilt- block/half-graben basins. In: *Continental Extensional Tectonics* (Ed. by M.P., Coward, J.F. Dewey and P.L. Hancock), *Spec. Publ. Geol. Soc. London*, **28**, 139–152.
- MANKTELOW, N.S. & PAVLIS, T.L. (1994) Fold-fault relationships in low-angle detachment systems. *Tectonics*, **13**, 668–685.
- MARKUSSEN, S. (1994) *Strukturgeologi og strukturell kontroll på sedimentasjonen innen Kvamshesten Devonbasseng mellom Grunnevatn og Instelforkastningene, Sunnfjord, vest-Norge*. Cand. Scient. Thesis, University of Oslo, Oslo.
- MCCLAY, K.R. & SCOTT, A.D. (1991) Experimental models of hangingwall deformation in ramp-flat listric extensional detachment systems. *Tectonophysics*, **188**, 85–96.
- MILNES, A.G., DIETLER, T.N. & KOESTLER, A.G. (1988) The Sognefjord north shore log – a 25 km depth section through Caledonized basement in western Norway. *Nor. Geol. Unders. Spec. Publ.*, **3**, 114–121.
- NILSEN, T.H. (1968) The relationship of sedimentation to tectonics in the Solund Devonian District of southwestern Norway. *Bull. Nor. Geol. Unders.*, **259**, 1–108.
- NORTON, M.G. (1986) Late Caledonian extension in western Norway: a response to extreme crustal thickening. *Tectonics*, **5**, 195–204.
- NORTON, M.G. (1987) The Nordfjord-Sogn detachment, W. Norway. *Nor. Geol. Tidsskr.*, **67**, 93–106.
- OSMUNDSEN, P.T. (1996) *Late-orogenic structural geology and Devonian basin formation in Western Norway: a study from the hanging wall of the Nordfjord-Sogn Detachment in the Sunnfjord region*. Dr. Scient thesis, University of Oslo, Oslo.
- PLATT, J.P. & VISSERS, R.L.M. (1989) Extensional collapse of thickened continental lithosphere: a working hypothesis for the Alboran Sea and Gibraltar Arc. *Geology*, **17**, 540–543.
- RECHES, Z. & DIETERICH, J.H. (1983) Faulting of rocks in three-dimensional strain fields Failure of rocks in polyaxial, servo-controlled experiments. *Tectonophysics*, **95**, 111–132.
- ROBERTS, D. (1983) Devonian tectonic deformation in the Norwegian Caledonides and its regional perspectives. *Bull. Nor. Geol. Unders.*, **380**, 85–96.
- SEGURET, M., SERANNE, M., CHAUVET, A. & BRUNEL, M. (1989) Collapse basins: a new type of extensional sedimentary basin from the Devonian of Norway. *Geology*, **17**, 127–130.
- SERANNE, M. (1988) *Tectonique des bassins de Norvege: mise en evidence de bassins sedimentaires en extension lormes par amincissement d'ruve crouette orogenique e'paisse*. These Doct., Universite Montpellier.
- SERANNE, M., CHAUVET, A. & FAURE, J.-L. (1991) Cinematique de l'extension tardi- orogenique (Dévonien) dans les Caledonides Scandinaves et Britanniques. *C.R. Acad. Sci. Paris*, **313**, Serie II, 1305–1312.
- SERANNE, M., CHAUVET, A., SEGURET, M. & BRUNEL, M. (1989) Tectonics of the Devonian collapse-basins of western Norway. *Bull. Soc. Geol. France*, **8**, 489–499.
- SÉRANNE, M. & SÉGURET, M. (1987) The Devonian basins of western Norway: tectonics and kinematics of an extending crust. In: *Continental Extensional Tectonics* (Ed. by M.P., Coward, J.F. Dewey and P.L. Hancock), *Spec. Publ. Geol. Soc. London*, **28**, 537–548.
- SKJERLIE, F.J. (1971) Sedimentasjon og tektonisk utvikling i Kvamshesten devonfelt. *Vestlandet. Bull. Nor. Geol. Unders.*, **270**, 77–108.
- STEEL, R.J. (1976) Devonian basins of western Norway—sedimentary response to tectonism and varying tectonic context. *Tectonophysics*, **36**, 207–224.
- STEEL, R.J. & AASHEIM, S. (1978) Alluvial sand deposition in a rapidly subsiding basin (Devonian, Norway). In: *Fluvial Sedimentology* (Ed. by A.D. Miall), *Mem. Can. Soc. Petrol. Geol.*, **5**, 385–413.
- STEEL, R.J. & GLOPPEN, T.G. (1980) Late Caledonian Devonian basin formation, western Norway: signs of strike-slip tectonics during infilling. *Spec. Pub. Intern. Assoc. Sediment.*, **4**, 79–103.
- STEEL, R.J., MÆHLE, S., NILSEN, H., RE, S.L. & SPINNANGR, Å. (1977) Coarsening-upwards cycles in the alluvium of Hornelen Basin (Devonian), Norway: sedimentary response to tectonic events. *Bull. Geol. Soc. Am.*, **88**, 1124–1134.
- STEEL, R.J., SIEDLECKA, A. & ROBERTS, D. (1985) The Old Red Sandstone basins of Norway and their deformation: a review. In: *The Caledonian Orogen—Scandinavia and Related Areas* (Ed. by D.G. Gee & B.A. Sturt), pp. 293–315. John Wiley, Chichester.
- TORSVIK, T.H., STURT, B.A., RAMSAY, D.M., BERING, D. & FLUGE, P.R. (1988) Hornelen Paleomagnetism, magnetic fabrics and the structural style of the Hornelen Old Red Sandstone, western Norway. *J. Geol. Soc. London*, **145**, 413–430.
- TORSVIK, T.H., STURT, B.A., RAMSAY, D.M., KISCH, H.J. & BERING, D. (1986) The tectonic implications of Solundian (Upper Devonian) magnetization of the Devonian rocks of Kvamshesten, western Norway. *Earth planet. Sci. Lett.*, **80**, 337–347.
- TORSVIK, T.H., STURT, B.A., SWENSSON, E., ANDERSEN, T.B. & DEWEY, J.F. (1992) Palaeomagnetic dating of fault rocks: evidence for Permian and Mesozoic movements and brittle deformation along the extensional Dalsfjord fault, western Norway. *Geophys. J. Intern.*, **109**, 565–580.
- WILKS, W.H. & CUTHBERT, S.J. (1994) The evolution of the Hornelen Basin detachment system, western Norway: implications for the style of late-orogenic extension in the southern Scandinavian Caledonides. *Tectonophysics*, **238**, 1–30.
- XIAO, H.B., DAHLEN, F.A. & SUPPE, J. (1991) Mechanics of extensional wedges. *J. geophys. Res.*, **96** (B)6, 10301–10318.

Received 13 May 1996; revision accepted 23 March 1998.

# Cold subduction and the formation of lawsonite eclogite – constraints from prograde evolution of eclogitized pillow lava from Corsica

E. J. K. RAVNA,<sup>1</sup> T. B. ANDERSEN,<sup>2</sup> L. JOLIVET<sup>3</sup> AND C. DE CAPITANI<sup>4</sup>

<sup>1</sup>Department of Geology, University of Tromsø, N-9037 Tromsø, Norway (erling.ravna@uit.no)

<sup>2</sup>Department of Geosciences and PGP, University of Oslo, PO Box 1047, Blindern, 0316 Oslo, Norway

<sup>3</sup>ISTO, UMR 6113, Université d'Orléans, 1A Rue de la Férollerie, 45071 Orléans, Cedex 2, France

<sup>4</sup>Mineralogisch-Petrographisches Institut, Universität Basel, Bernoullistrasse 30, 4056 Basel, Switzerland

**ABSTRACT** A new discovery of lawsonite eclogite is presented from the Lancône glaucophanites within the Schistes Lustrés nappe at Défilé du Lancône in Alpine Corsica. The fine-grained eclogitized pillow lava and inter-pillow matrix are extremely fresh, showing very little evidence of retrograde alteration. Peak assemblages in both the massive pillows and weakly foliated inter-pillow matrix consist of zoned idiomorphic Mg-poor (<0.8 wt% MgO) garnet + omphacite + lawsonite + chlorite + titanite. A local overprint by the lower grade assemblage glaucophane + albite with partial resorption of omphacite and garnet is locally observed. Garnet porphyroblasts in the massive pillows are Mn rich, and show a regular prograde growth-type zoning with a Mn-rich core. In the inter-pillow matrix garnet is less manganiferous, and shows a mutual variation in Ca and Fe with Fe enrichment toward the rim. Some garnet from this rock type shows complex zoning patterns indicating a coalescence of several smaller crystallites. Matrix omphacite in both rock types is zoned with a rimward increase in  $X_{\text{Jd}}$ , locally with cores of relict augite. Numerous inclusions of clinopyroxene, lawsonite, chlorite and titanite are encapsulated within garnet in both rock types, and albite, quartz and hornblende are also found included in garnet from the inter-pillow matrix. Inclusions of clinopyroxene commonly have augitic cores and omphacitic rims. The inter-pillow matrix contains cross-cutting omphacite-rich veinlets with zoned omphacite, Si-rich phengite ( $\text{Si} = 3.54$  apfu), ferroglaucophane, actinolite and hematite. These veinlets are seen fracturing idiomorphic garnet, apparently without any secondary effects. Pseudosections of matrix compositions for the massive pillows, the inter-pillow matrix and the cross-cutting veinlets indicate similar  $P$ – $T$  conditions with maximum pressures of 1.9–2.6 GPa at temperatures of 335–420 °C. The inclusion suite found in garnet from the inter-pillow matrix apparently formed at pressures below 0.6–0.7 GPa. Retrogression during initial decompression of the studied rocks is only very local. Late veinlets of albite + glaucophane, without breakdown of lawsonite, indicate that the rocks remained in a cold environment during exhumation, resulting in a hairpin-shaped  $P$ – $T$  path.

**Key words:** Alpine orogeny; cold subduction; Corsica; lawsonite eclogite.

## INTRODUCTION

Lawsonite eclogite and blueschist are expected to be the dominant lithologies forming during subduction of oceanic crust and should therefore be fairly abundant within the Earth's crust and particularly common in exhumed subduction complexes. However, lawsonite eclogite is rare and has been described only from a few localities worldwide (e.g. McBirney *et al.*, 1967; Watson & Morton, 1969; Krogh, 1982; Caron & Péquignot, 1986; Oh *et al.*, 1991; Ghent *et al.*, 1993, 2009; Shibakusa & Maekawa, 1997; Parkinson *et al.*, 1998; Carswell *et al.*, 2003; Och *et al.*, 2003; Usui *et al.*, 2003, 2006; Altherr *et al.*, 2004; Harlow *et al.*, 2004; Mattinson *et al.*, 2004; Tsujimori *et al.*, 2005, 2006a,b; Davis & Whitney, 2006; Zhang & Meng, 2006; Zhang *et al.*, 2007). Altherr *et al.* (2004) and

Zack *et al.* (2004) discussed the paucity of known lawsonite eclogite complexes, which they related to the following two factors: (i) in 'normal' subduction settings lawsonite eclogite enters the subduction factory and hence is usually not exhumed (Agard *et al.*, 2002), and (ii) in accretionary wedges where the  $P$ – $T$  path leaves the stability field of lawsonite eclogite due to heating, lawsonite eclogite is only preserved if the exhumation path is constrained to a narrow window where the terminal stability of lawsonite is not crossed. Whitney & Davis (2006) suggested, based on observations from Sivrihisar, Turkey, that pristine lawsonite eclogite pods may represent rocks that were not deformed during exhumation. Tsujimori *et al.* (2006c) have used changes in inclusion mineralogy within garnet to distinguish between two types of lawsonite eclogite: L-type and E-type. L-type lawsonite eclogite

contains garnet porphyroblasts that grew only within the lawsonite stability field, whereas the E-type lawsonite eclogite records maximum temperatures in the epidote stability field (Tsuji-mori *et al.*, 2006c).

This paper presents data on eclogitized pillow lava and inter-pillow matrix from a new lawsonite eclogite locality in Corsica – Défilé du Lancône – showing evidence of very cold subduction-related prograde metamorphism.

**GEOLOGICAL SETTING**

The island of Corsica was isolated from the main European continent and from Italy during the opening of the Liguro-Provençal basin and the northern Tyr-

renian Sea, two back-arc basins of the central Mediterranean (Rehault *et al.*, 1984; Sartori *et al.*, 1987; Jolivet *et al.*, 1998). Despite significant deformation during this Oligocene extensional episode (Jolivet *et al.*, 1991), evidence for early Alpine evolution that started in the Late Cretaceous and ended in the Early Oligocene is well preserved (Mattaueer *et al.*, 1981; Durand Delga, 1984; Fournier *et al.*, 1991; Caron, 1994; Brunet *et al.*, 2000). The north-eastern part of Corsica (Figs 1 & 2) is mainly made up of “Schistes Lustrés”, which have undergone an Alpine HPLT metamorphism of glaucophane–lawsonite type (Caron & Péquignot, 1986). The Schistes Lustrés nappe complex consists of several thrust sheets folded and faulted in the late Cap Corse-Castagniccia antiform (Figs 1 & 2). Eclogite and

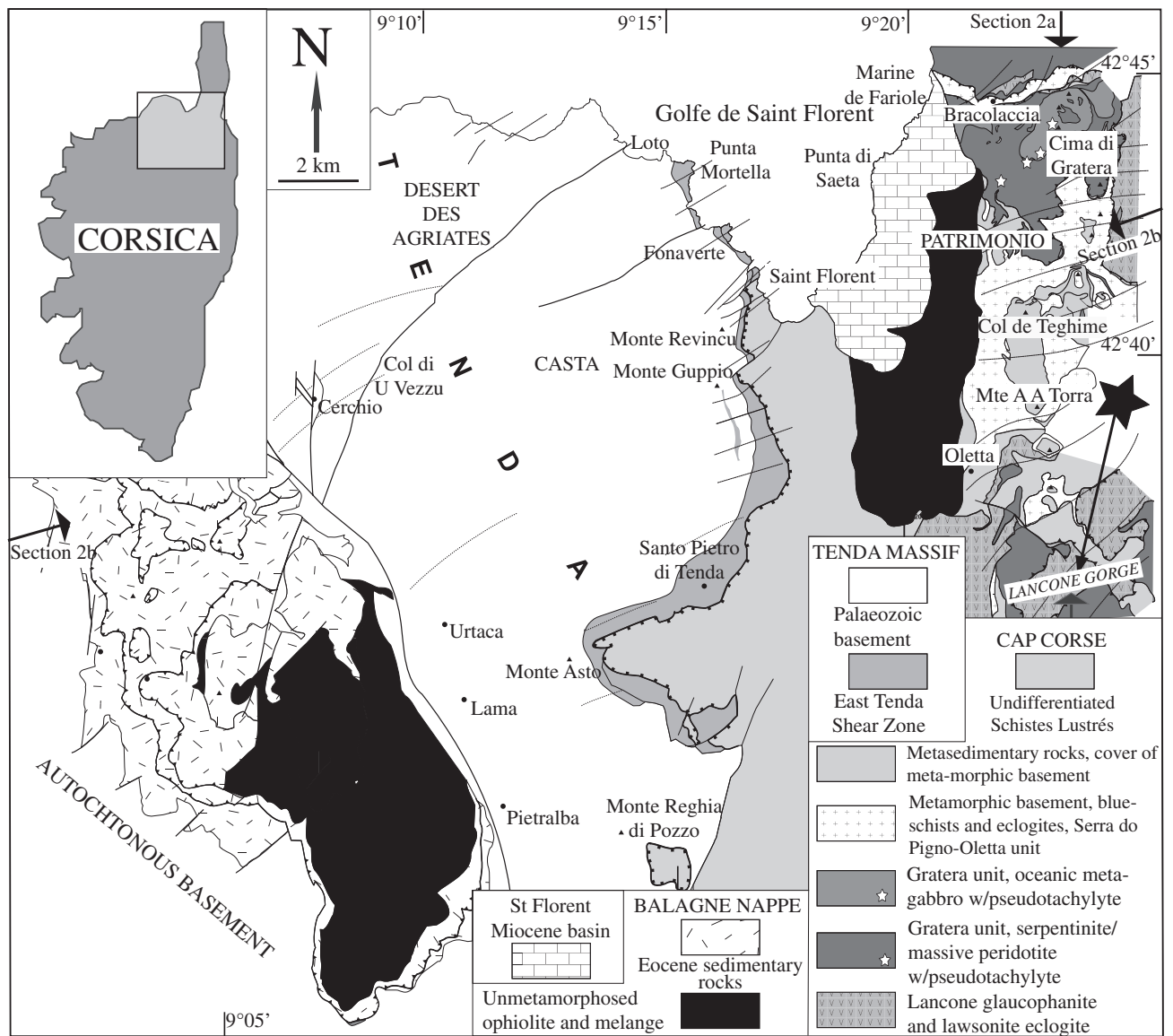


**Fig. 1.** Geological map of northern Corsica (see inset map for location) showing the main Alpine tectonic units and location of the new lawsonite eclogite locality in Défilé du Lancône (marked with star). Notice the location of subduction-related pseudotachylites north of Patrimonio.

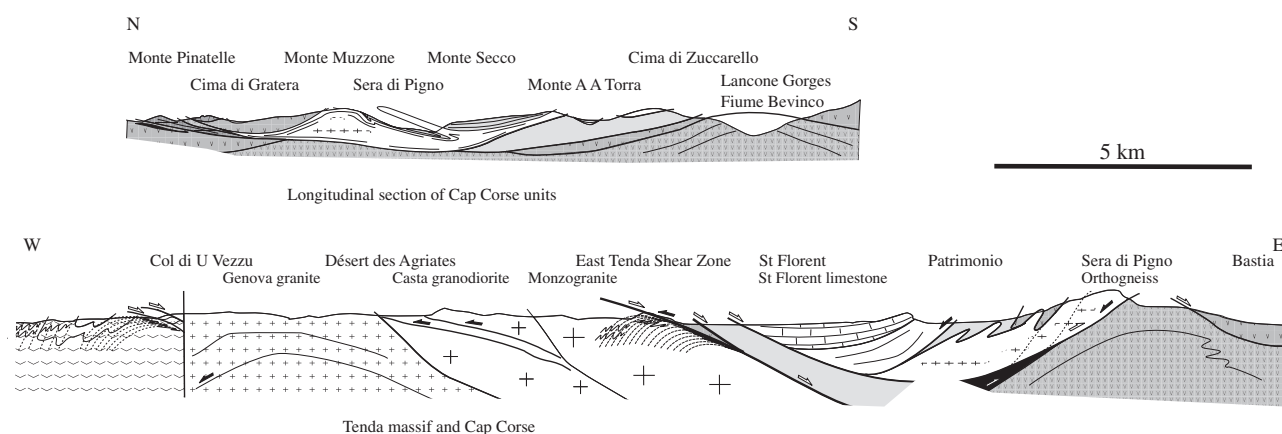


**Fig. 2.** N–S (a) and E–W (b) cross-sections of northern Corsica (modified from Jolivet *et al.*, 1998) showing the main tectonic units and the locations of blueschist to eclogite facies pseudotachylites and the eclogite facies rocks in the area. Notice that the Défilé du Lancône lawsonite eclogite locality is positioned at a low structural level.

blueschist occur within both the lower ophiolitic unit and within nappes originating from the Hercynian continental basement (Lahondere, 1988). The Schistes Lustrés nappe is thrust on a large sheet of metamorphosed continental basement, the Tenda massif, where intermediate pressure blueschist parageneses have been described (Tribuzio & Giacomini, 2002; Molli *et al.*, 2006). All syn-high-pressure kinematic indicators show a top-to-the-west shear sense compatible with the underthrusting of the European basement below the oceanic nappes (Mattauer *et al.*, 1981; Fournier *et al.*, 1991). The age of the HPLT metamorphism is controversial, but  $^{40}\text{Ar}/^{39}\text{Ar}$  dating of phengite indicates *c.* 65 Ma for the eclogitic stage and a subsequent major blueschist event from  $\sim 45$  Ma until 37–35 Ma in the Cap Corse and Tenda massif (Brunet *et al.*, 2000). Older ages, between 80 and 60 Ma, are associated with the eclogitic stage (Brunet *et al.*, 2000). The overall history of HPLT metamorphism in Corsica is thus quite similar to that of the Alps both in terms of *P–T* conditions and timing (Agard *et al.*, 2002).

The Balagne nappe is the uppermost tectonic unit of the metamorphic complex and also overlies the autochthonous Hercynian basement and its cover (Fig. 1). The nappe, which occurs as two klippen, comprises a large sheet of pillow lavas in the west (Balagne ophiolite) and a *mélange* correlated with the Ligurian domain south of St Florent. Both of these klippen lack HPLT metamorphic rocks. The Balagne nappe was emplaced during the Eocene as attested by the presence of olistoliths in the Eocene foreland basin occurring just below the basalts (Egal, 1992).

Lawsonite eclogite has previously been described from Corsica in the Monte San Petrone Complex, further south in the Castagniccia antiform, within a meta-ophiolitic thrust-sheet consisting of serpentinized peridotite, Fe–Ti-rich and Mg–Cr-rich metagabbro, tholeiitic metabasalt and metasedimentary rocks including manganiferous metachert (Lardeaux *et al.*, 1986). In the field, the Monte San Petrone eclogite

occurs as lenses within a glaucophane schist matrix (Péquignot *et al.*, 1984). The eclogite consists of almandine-rich garnet + omphacite + phengite + glaucophane + lawsonite + quartz + titanite + opaques (Caron *et al.*, 1981; Caron & Péquignot, 1986; Lardeaux *et al.*, 1986), and a temperature of 400–450 °C at 1.0 GPa was estimated by Lardeaux *et al.* (1986). However, a recalculation of the garnet–clinopyroxene–phengite data of Caron & Péquignot (1986) using the garnet–clinopyroxene thermometer (Ravna, 2000) and the garnet–clinopyroxene–phengite barometer (Ravna & Terry, 2004) gives  $\sim 390$  °C at 2.05 GPa.

In Défilé du Lancône (Fig. 1) blueschist of the Lower Ophiolitic unit outcrops (Fournier *et al.*, 1991). This is the best-exposed section through the lower glaucophanite unit, which is composed of several sheets of massive basalt, pillow breccia and pillow lava. The main foliation is folded in a broad antiform, and a NE–SW-stretching lineation defined by the elongation of pillows and pillow fragments is observed throughout the section. Syn-high-pressure kinematic indicators consistently indicate top-to-the-SW shear during the formation of the blueschist foliation that, until the discovery of the lawsonite eclogite, was thought to represent peak pressure conditions (Jolivet *et al.*, 1991). At this locality, variably deformed pillow lava and hyaloclastite breccia consisting of glaucophane + epidote + titanite  $\pm$  garnet  $\pm$  lawsonite is common within a late foliation of chlorite + albite  $\pm$  actinolite  $\pm$  quartz (Fournier *et al.*, 1991), who estimated a minimum *P–T* of 1.1 GPa and 400 °C for the glaucophane assemblage.

Well-preserved pillow breccia and pillow lava, the latter locally with preserved drain-out cavities, occur along the riverbed in Défilé du Lancône, immediately downstream from the water reservoir (Fig. 3a). Massive green-coloured fine-grained cores of the pillows are metamorphosed to low-temperature eclogite. The longest dimension of the eclogitized pillows ranges from 10 to 40 cm (Fig. 3a), and they consist of a green,

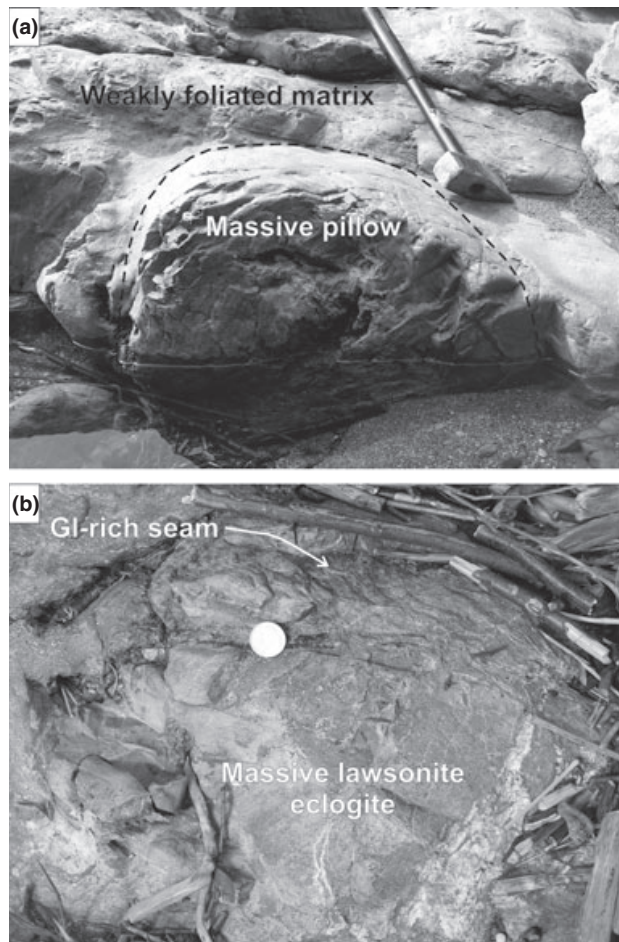


**Fig. 3.** Eclogitized pillow lava along the riverbed of Défilé du Lancône. (a) A well-preserved pillow with internal drain-out, convex upward cavity. Notice that the pillows have blue outer margins due to the superimposed blueschist facies metamorphism. (b) Details of a massive eclogitized pillow with a thin seam of glaucophane.

very fine-grained massive rock with tiny euhedral garnet evenly distributed throughout. Locally, somewhat coarser grained, weakly foliated zones with aggregates of white mica form matrix material between pillows and pillow fragments. Seams of glaucophane-rich material are locally present, especially in the deformed pillows and meta-hyaloclastite, the latter occurring between the pillows and fragmented pillows and along pillow margins (Fig. 3b).

#### ANALYTICAL PROCEDURES

Mineral analyses were performed by electron microprobe (Cameca SX-100) at Dionýz Štúr Institute of Geology in Bratislava. Analytical conditions for the EMPA were 15 kV accelerating voltage and 20 nA beam current, with a peak counting time of 20 s and a beam diameter of 2–10  $\mu\text{m}$ . Raw counts were corrected using a PAP routine. Mineral standards (Si, Ca: wollastonite; Na: albite; K: orthoclase; Fe: fayalite, Mn:

**Table 1.** Selected garnet analyses.

	Sample					
	COR-1		COR-1'		COR-4	
	Core	Rim	Core	Rim	Core	Rim
SiO <sub>2</sub>	37.83	37.94	37.71	38.22	38.11	37.53
Al <sub>2</sub> O <sub>3</sub>	20.49	20.95	20.63	20.82	21.00	20.40
TiO <sub>2</sub>	0.32	0.12	0.24	0.17	0.10	0.12
Cr <sub>2</sub> O <sub>3</sub>	0.08	0.07	0.04	0.05	0.04	0.01
FeO	19.15	22.53	20.38	22.48	22.72	26.59
MnO	12.06	6.78	9.87	4.97	2.64	3.56
MgO	0.60	0.80	0.56	0.72	0.40	0.51
CaO	10.55	11.61	11.10	13.53	15.93	11.16
	101.07	100.81	100.53	100.96	100.94	99.89
12 oxygen						
Si	3.01	3.01	3.01	3.01	3.00	3.02
Al	1.92	1.96	1.94	1.94	1.95	1.93
Ti	0.02	0.01	0.01	0.01	0.01	0.01
Cr	0.01	0.00	0.00	0.00	0.00	0.00
Fe	1.27	1.49	1.36	1.48	1.50	1.79
Mn	0.81	0.46	0.67	0.33	0.18	0.24
Mg	0.07	0.09	0.07	0.08	0.05	0.06
Ca	0.90	0.99	0.95	1.14	1.34	0.96
Cations	8.01	8.00	8.01	8.01	8.02	8.01
$X_{\text{Ca}}$	0.29	0.33	0.31	0.38	0.44	0.32
$X_{\text{Mn}}$	0.27	0.15	0.22	0.11	0.06	0.08
$X_{\text{Fe}}$	0.42	0.49	0.45	0.49	0.49	0.59
$X_{\text{Mg}}$	0.02	0.03	0.02	0.03	0.02	0.02

rhodonite), pure element oxides (TiO<sub>2</sub>, Al<sub>2</sub>O<sub>3</sub>, Cr<sub>2</sub>O<sub>3</sub> and MgO) were used for calibration. Supplementary analyses were performed using a JEOL-840 Scanning Electron Microscope with an EDAX unit at the Department of Medical Biology, University of Tromsø. The ZAF matrix correction and optimized SEC factors using various natural standards were used. Counting time was 200 s with an accelerating voltage of 20 kV and a sample current of 6 nA. Totals of anhydrous minerals are normalized to 100.0 wt%, amphibole to 98.0% and chlorite to 86.0 wt%.

Garnet formulae are normalized to 12 oxygen and clinopyroxene to four cations, with Fe<sup>3+</sup> calculated by charge balance (Droop, 1987). Phengite is normalized to 11 oxygen, chlorite to 28 oxygen, and lawsonite and titanite to eight and five oxygen respectively. Amphibole analyses were normalized according to the scheme recommended by the IMA (Leake *et al.*, 1997), using the spreadsheet AMPH-CLASS (Esawi, 2004). Selected mineral analyses are given in Tables 1–3.

#### PETROGRAPHY AND MINERAL CHEMISTRY

The massive pillows generally consist of very fine-grained eclogite (Fig. 3). Of 10 samples, three representative samples were chosen for our investigation. Samples from massive pillows and the weakly foliated phengite-bearing layers are described, and mineral analyses of principal minerals from three samples are presented. Samples COR-1 and COR-1' are from a massive pillow fragment, whereas samples COR-4 are from the weakly foliated variety. Sample COR-1 is from the core and COR-1' from the faint bluish margin of the same pillow fragment.

**Table 2.** Selected clinopyroxene analyses.

	COR-1			COR-1'			COR-4								
	Incl		Matrix	Inc		Matrix	Incl			Matrix		Vein			
	Core	Mantle	Rim	Rim	Core	Rim	Rim	Core	Mantle	Rim	Core	Rim	Core	Mantle	Rim
SiO <sub>2</sub>	48.71	55.09	55.28	55.34	48.59	56.24	55.99	46.10	51.39	54.85	50.08	55.46	53.78	53.25	52.62
Al <sub>2</sub> O <sub>3</sub>	3.84	6.19	6.76	8.52	4.43	6.99	8.75	4.58	1.33	5.67	2.55	7.05	5.48	3.62	2.36
TiO <sub>2</sub>	1.99	0.05	0.11	0.01	2.78	0.02	0.08	3.95	0.37	0.07	1.69	0.03	0.04	0.03	0.02
Cr <sub>2</sub> O <sub>3</sub>	0.14	0.08	0.11	0.09	0.09	0.13	0.01	0.18	0.00	0.05	0.02	0.00	0.00	0.04	0.03
FeO	12.29	8.51	8.44	7.69	11.44	7.86	7.26	14.50	13.86	11.92	13.73	10.45	14.60	16.29	17.01
MnO	0.50	0.47	0.53	0.20	0.54	0.48	0.29	0.36	0.46	0.17	0.40	0.11	0.07	0.10	0.14
MgO	11.85	9.02	8.71	7.68	12.53	8.73	8.01	9.34	9.04	7.33	11.48	6.83	5.44	5.79	6.17
CaO	20.82	16.29	15.60	13.84	19.48	15.19	13.81	20.68	21.12	15.04	19.29	13.70	14.18	16.32	18.34
Na <sub>2</sub> O	0.45	5.07	5.49	6.88	0.68	5.92	6.97	0.76	2.29	5.76	0.84	6.79	6.17	4.62	3.40
	100.59	100.77	101.02	100.25	100.56	101.57	100.17	100.44	99.86	100.86	100.09	100.42	99.77	100.05	100.08
4 cations, 6 oxygen															
Si	1.83	1.99	1.99	1.98	1.82	2.00	1.98	1.76	1.94	2.00	1.90	2.00	2.00	2.00	2.00
Al	0.17	0.26	0.29	0.36	0.20	0.29	0.37	0.21	0.06	0.24	0.11	0.30	0.24	0.16	0.11
Ti	0.06	0.00	0.00	0.00	0.08	0.00	0.00	0.11	0.01	0.00	0.05	0.00	0.00	0.00	0.00
Cr	0.00	0.00	0.00	0.00	0.00	0.00	0.00	0.01	0.00	0.00	0.00	0.00	0.00	0.00	0.00
Fe <sup>3+</sup>	0.08	0.11	0.11	0.15	0.06	0.11	0.14	0.09	0.20	0.17	0.06	0.16	0.21	0.17	0.14
Fe <sup>2+</sup>	0.30	0.15	0.14	0.08	0.30	0.13	0.07	0.37	0.24	0.20	0.38	0.15	0.24	0.34	0.40
Mn	0.02	0.01	0.02	0.01	0.02	0.01	0.01	0.01	0.01	0.01	0.01	0.00	0.00	0.00	0.00
Mg	0.66	0.49	0.47	0.41	0.70	0.46	0.42	0.53	0.51	0.40	0.65	0.37	0.30	0.32	0.35
Ca	0.84	0.63	0.60	0.53	0.78	0.58	0.52	0.85	0.86	0.59	0.78	0.53	0.56	0.66	0.75
Na	0.03	0.35	0.38	0.48	0.05	0.41	0.48	0.06	0.17	0.41	0.06	0.48	0.44	0.34	0.25
∑Cat	4.00	4.00	4.00	4.00	4.00	4.00	4.00	4.00	4.00	4.00	4.00	4.00	4.00	4.00	4.00
Mg#	68.7	76.3	76.8	83.8	69.9	78.4	85.4	58.8	68.2	67.1	63.2	70.8	55.4	48.5	46.7
Jd	0	25	27	33	0	30	34	0	0	24	0	31	23	17	11
Ac	8	11	11	15	6	11	14	9	20	17	6	16	21	17	14
Ca-px	92	65	62	52	94	59	52	91	80	59	94	52	55	66	75

**Table 3.** Selected analyses of lawsonite, chlorite, phengite, amphibole, albite and titanite.

	Sample													
	COR-1			COR-1'			COR-4							
	Lws	Lws	Chl	Chl	Ttn	Lws	Glc	Ab	Hbl <sup>EDS</sup>	Ab <sup>EDS</sup>	Lws	Chl <sup>EDS</sup>	Phn	Fe-Glc
	In	Matrix	In	Matrix	Matrix	In	Sec	Sec	In	In	Matrix	Matrix	Vein	Vein
SiO <sub>2</sub>	38.41	37.84	28.98	28.98	30.79	38.33	58.15	69.31	45.30	67.15	38.28	26.42	52.80	57.04
Al <sub>2</sub> O <sub>3</sub>	31.79	31.11	18.32	18.98	1.01	31.52	11.08	19.66	12.79	20.03	31.21	19.19	23.52	8.17
TiO <sub>2</sub>	0.09	0.07	0.33	0.48	38.45	0.20	0.06	0.00	0.77	0.00	0.13	0.00	0.05	0.00
Cr <sub>2</sub> O <sub>3</sub>	0.00	0.00	0.12	0.17	0.00	0.00	0.04	0.00	0.00	0.00	0.00	0.00	0.04	0.00
FeO	0.94*	1.09*	18.66	17.74	0.47	0.50*	10.68	0.17*	14.75	0.57*	1.18*	25.54	3.66	17.06
MnO	0.18	0.35	0.51	0.52	0.04	0.03	0.11	0.00	0.06	0.00	0.03	0.33	0.04	0.09
MgO	0.00	0.00	19.76	21.09	0.02	0.00	9.55	0.00	10.54	0.00	0.00	14.52	4.05	7.54
CaO	17.78	17.86	0.02	0.57	28.44	17.79	1.32	0.09	10.86	0.83	17.76	0.00	0.06	1.54
Na <sub>2</sub> O	0.00	0.00	0.00	0.00	0.06	0.00	7.30	11.67	2.66	11.42	0.00	0.00	0.10	6.49
K <sub>2</sub> O	0.00	0.00	0.00	0.00	0.00	0.00	0.04	0.02	0.28	0.04	0.00	0.00	11.26	0.03
Total	89.19	88.32	86.70	88.53	99.28	88.37	98.33	100.91	98.00	100.00	88.59	86.00	95.21	97.96
Oxygen	8	8	28	28	5	8	23	8	23	8	8	28	11	23
Si	2.00	2.00	5.94	5.81	1.01	2.01	8.00	3.00	6.61	2.95	2.01	5.69	3.56	8.04
Al	1.95	1.94	4.43	4.48	0.04	1.95	1.78	1.00	2.20	1.04	1.93	4.87	1.84	1.36
Ti	0.00	0.00	0.05	0.07	0.95	0.01	0.00	0.00	0.09	0.00	0.01	0.00	0.00	0.00
Cr	0.00	0.00	0.02	0.03	0.00		0.01							
Fe <sup>3+</sup>	0.04	0.04			0.02	0.00	0.00	0.01	0.25	0.02	0.05			0.33
Fe <sup>2+</sup>	0.00	0.00	3.20	2.97	0.01	1.23	1.23	0.01	1.56	0.02		4.60	0.21	1.70
Mn	0.01	0.02	0.09	0.09	0.00	0.00	0.02	0.00	0.01	0.00	0.00	0.06	0.00	0.01
Mg	0.00	0.00	6.04	6.30	0.00	0.00	1.96	0.00	2.29	0.00	0.00	4.66	0.41	1.58
Ca	0.99	1.01	0.00	0.12	1.00	1.00	0.18	0.00	1.70	0.04	1.00	0.00	0.00	0.23
Na	0.00	0.00	0.00	0.00	0.00	0.00	1.98	0.98	0.75	0.97	0.00	0.00	0.01	1.77
K	0.00	0.00	0.00	0.00	0.00	0.00	0.00	0.00	0.05	0.00	0.00	0.00	0.97	0.01
∑Cat	5.00	5.01	19.78	19.87	3.02	4.99	15.16	4.99	15.51	5.01	5.00	19.88	7.01	15.03
Mg#			65	68			61		60			50	66	48
X <sub>Fe<sup>3+</sup></sub>							0.00		0.24					0.20

X<sub>Fe<sup>3+</sup></sub> = Fe<sup>3+</sup> / (Fe<sup>3+</sup> + Al).  
 \*Fe<sub>2</sub>O<sub>3</sub>.

Both the massive eclogite (Fig. 4a) and the foliated variety (Fig. 4b) have small idiomorphic garnet (5 modal %; up to 200  $\mu\text{m}$  across) set in a matrix of omphacite (55–60 modal %; up to  $70 \times 200 \mu\text{m}$  across), lathlike lawsonite (20–30 modal %; up to  $20 \times 300 \mu\text{m}^2$  across), chlorite (7–15%) and titanite (3–5%). Calcite occurs in tiny veinlets. In the foliated inter-pillow matrix, cross-cutting veinlets consisting of omphacite (80%), phengite (15%) with minor glaucophane (< 5%) and hematite is common (Fig. 4d–g). Locally, these veinlets also cross-cut fractured garnet (Fig. 4f), but there does not seem to be any resorption of garnet in contact with the veins. Garnet commonly contains numerous solid inclusions. Inclusions of lawsonite, chlorite, titanite and clinopyroxene are present in all samples (Fig. 4a–c). In addition, inclusions of albite, hornblende and quartz are found in garnet in the foliated rock. Glaucophane has been found as a secondary matrix phase in the marginal part of the massive pillow fragment (sample COR-1') where it occurs together with albite against slightly resorbed garnet (Fig. 4g). In the massive eclogite, omphacite and lawsonite are randomly oriented (Fig. 4a). In foliated eclogite matrix omphacite and lawsonite show a weak preferred orientation.

#### Garnet

Garnet is rich in almandine, grossular and spessartine, and low in pyrope (Table 1), similar to that described by Caron *et al.* (1981). It is chemically zoned, in sample COR-1 ranging from  $\text{Gr}_{29}\text{Sp}_{27}\text{Alm}_{42}\text{Py}_2$  (core) to  $\text{Gr}_{33}\text{Sp}_{15}\text{Alm}_{49}\text{Py}_3$  (rim). Garnet in sample COR-4 is more Ca- and Fe-rich and lower in Mn, ranging from  $\text{Gr}_{44}\text{Sp}_6\text{Alm}_{49}\text{Py}_2$  (core) to  $\text{Gr}_{32}\text{Sp}_8\text{Alm}_{59}\text{Py}_2$  (rim). Zoning profiles appear to be continuous in both samples (Fig. 5a,b), except for some irregularly zoned garnet from COR-4 (Fig. 4b).

#### Clinopyroxene

Clinopyroxene analyses are recalculated to four cations and six oxygen with estimation of  $\text{Fe}^{3+}$  by charge balance (Droop, 1987). Clinopyroxene in the studied samples shows a large compositional variation (Table 2; Fig. 6). Generally, clinopyroxene inclusions in garnet are less sodic than the matrix omphacite in all samples. Low-Na and Al–Ti-rich clinopyroxene (augite) with up to 4.6 wt%  $\text{Al}_2\text{O}_3$  and 3.95 wt%  $\text{TiO}_2$  occurs as cores of inclusions in all samples, commonly

mantled and rimmed by successively more jadeite-rich omphacite (Fig. 4c; Table 2). Matrix clinopyroxene is also zoned with augitic cores and increasing jadeite content toward the rim. Omphacite in the cross-cutting veinlets in sample COR-4 have distinctly lower Mg # (46.7–55.4) than those in the matrix (63.2–70.8). They also show an opposite rimward zoning from  $\text{Jd}_{23}\text{Aeg}_{21}$  (Mg# = 55) to  $\text{Jd}_{11}\text{Aeg}_{14}$  (Mg# = 47).

#### Other minerals

Phengite in the cross-cutting veins of sample COR-4 is virtually unzoned, with a Si-content of 3.56 apfu based on 11 oxygen and Mg# = 66 assuming all Fe as  $\text{Fe}^{2+}$  (Table 3). Lawsonite has  $\text{Fe}_2\text{O}_3$  content in the range 0.50–1.18%, inclusions in garnet having the lower values. Chlorite is present as inclusions in garnet and as a matrix phase, with Mg# ranging from 65 (inclusion in garnet) to 68 (matrix) in COR-1, and Mg# = 50 in COR-4. Titanite is relatively Al-poor ( $X_{\text{Al}} = 0.04$ ). Albite included in garnet in sample COR-4 and as a secondary matrix phase in sample COR-1' is relatively pure ( $\text{Ab}_{97}$  and  $\text{Ab}_{100}$  respectively). Small inclusions of edenitic hornblende with  $\text{Ca}_B = 1.70$ ,  $(\text{Na} + \text{K})_A = 0.51$ ,  $\text{Fe}^{3+}/(\text{Fe}^{3+} + \text{Al}) = 0.24$  and Mg# = 60 were identified in the core of a garnet in sample COR-4. Blue amphibole occurring in the omphacite-rich veins in sample COR-4 has  $\text{Fe}^{3+}/(\text{Fe}^{3+} + \text{Al}) = 0.21$  and Mg# = 48, and is classified as ferroglaucophane. Secondary blue amphibole associated with albite in sample COR-1' is glaucophane with  $\text{Fe}^{3+}/(\text{Fe}^{3+} + \text{Al}) = 0.00$  and Mg# = 62.

### METAMORPHIC EVOLUTION AND CONDITIONS

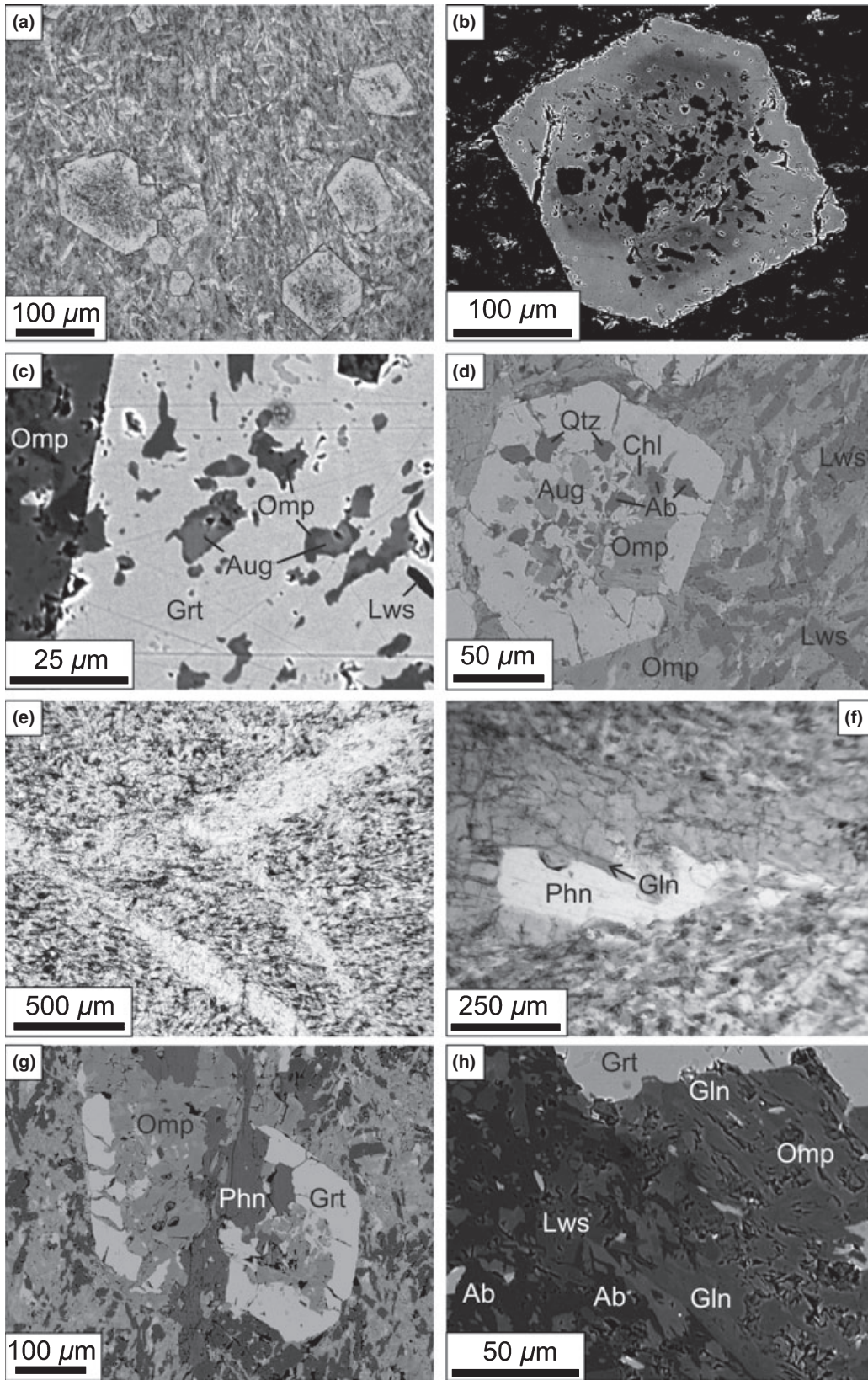
#### Pre-metamorphic relics (0)

Ca–Al–Ti-rich cores (augite) of clinopyroxene inclusions in garnet and in the matrix most likely represent relict magmatic pyroxene crystallized from the basaltic precursor. Similar compositions are reported from relict magmatic cores of porphyroblastic Na-pyroxene in eclogitic metabasites from Sivrihisar in the Tavsanlı Zone, Turkey (Çetinkaplan *et al.*, 2008).

#### Pre-eclogitic metamorphic stages (I)

The earliest metamorphic minerals recorded in the lawsonite eclogite from Défilé du Lancône are found as

**Fig. 4.** (a) Massive lawsonite eclogite with euhedral garnet in a matrix of randomly oriented omphacite and lawsonite (light grey laths). Sample COR-1. (b) BSE image of euhedral garnet showing complex compositional variation due to reciprocal concentrations of Fe and Ca. Areas with dark grey colour have lower Fe/Ca ratio. Dark inclusions are mainly omphacite and lawsonite. Sample COR-4. (c) BSE image of euhedral garnet with numerous inclusions of augite, omphacite, albite, chlorite and quartz. Matrix consists of omphacite, lawsonite and minor titanite. Sample COR-4. (d) BSE image of euhedral garnet with inclusions of lawsonite and augite overgrown by omphacite. Matrix consists of omphacite, lawsonite and minor titanite. Sample COR-1. (e) Veinlets of omphacite + phengite + minor glaucophane cross-cutting the weakly foliated matrix of sample COR-4. (f) Details of omphacite-rich veinlet with phengite and glaucophane. Sample COR-4. (g) Omphacite-rich veinlet cross-cutting a fractured garnet. Sample COR-4. (f) Incipient retrogression with secondary glaucophane and albite and partly resorption of garnet. Sample COR-1'.



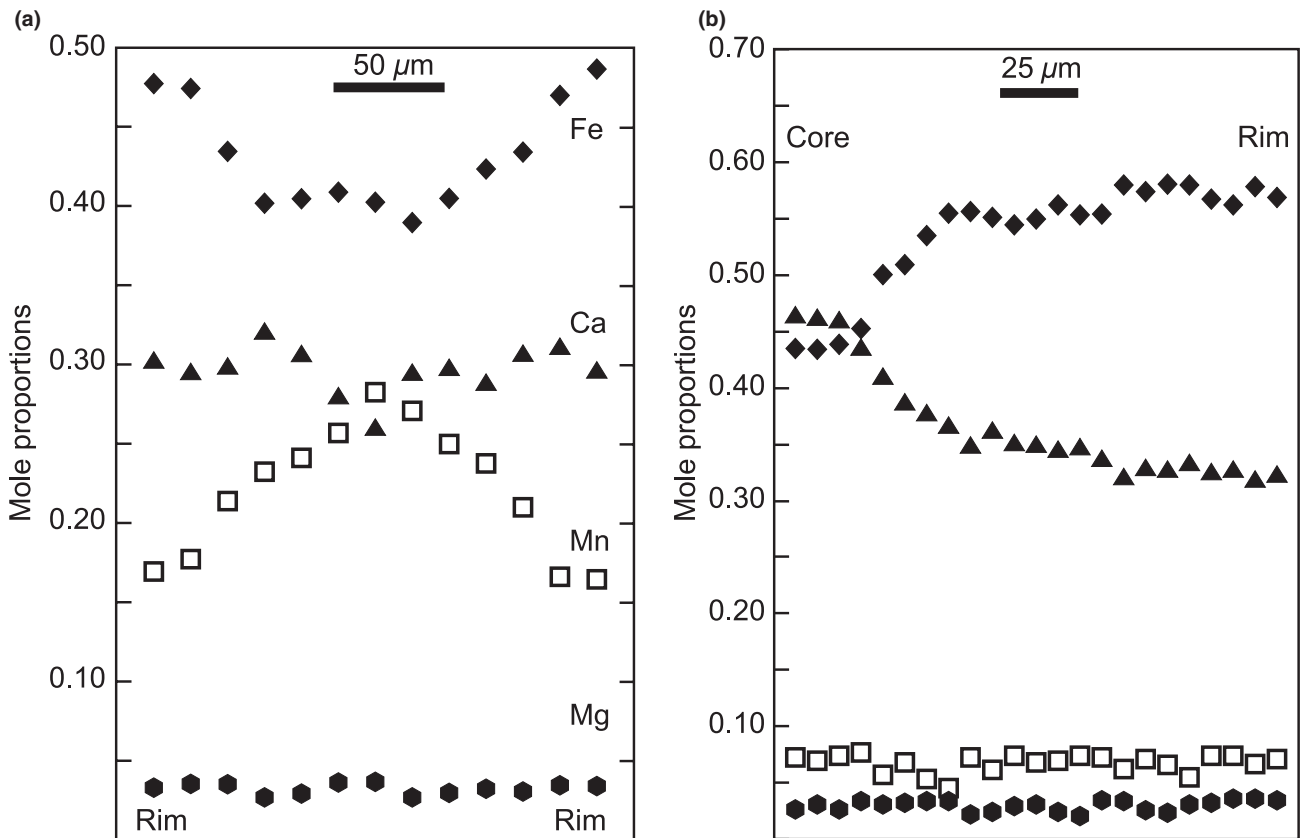


Fig. 5. Zoning profile across euhedral garnet in sample COR-1 (a) and COR-4 (b). The garnet from the latter sample did not show any evidence of coalescence of several smaller garnet as that shown in Fig. 4c.

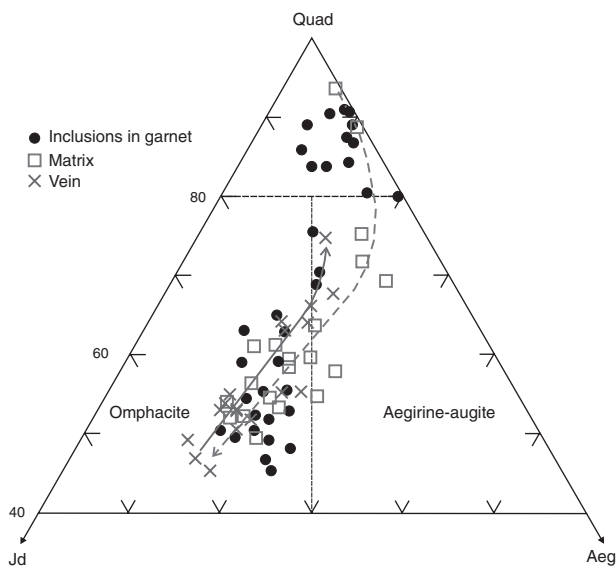
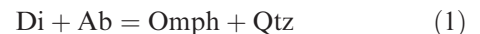


Fig. 6. Compositional variations of clinopyroxene from sample COR-4. Quad = quadrilateral components (Ca, Mg and Fe) in clinopyroxene. Stippled and solid arrows indicate compositional evolution of matrix and vein clinopyroxenes respectively.

inclusions within garnet and as low-jadeite cores of matrix clinopyroxene. Inclusions of Ca-rich and TiO<sub>2</sub>-poor clinopyroxene, hornblende, chlorite, albite and

titanite probably represent early (low-*P*) metamorphic phases. Overgrowths of successively more sodic pyroxene on Na-poor pyroxene indicate that the continuous reaction



produced more omphacitic pyroxene by consumption of albite during increasing pressure. The observed zoning in matrix omphacite in the same sample supports this interpretation. The zoning patterns of garnet from the two different lithologies studied here, with cores strongly enriched in Mn (COR-1) or Ca (COR-4) are also consistent with initial growth at low *P-T* conditions. Thus, the observed inclusion suite of albite, quartz, hornblende and low- to high-Na clinopyroxene in garnet in sample COR-4 apparently represents different transient *P-T* conditions during early subduction. A true equilibrium assemblage among these phases is therefore difficult to suggest. The irregular zoning pattern observed in some garnet in sample COR-4 apparently indicates that they formed by coalescence and overgrowth of several smaller garnet during increasing *P-T*.

A precise estimate of *P-T* for these early stages of subduction is not straight forward. Reaction (1) is likely to have proceeded during this time until albite was entirely consumed. The low modal content and

Mn- and Ca-rich and Mg-poor composition of garnet points to very low temperatures.

#### Lawsonite eclogite stage (II)

The Fe–Mg distribution among garnet and omphacite is commonly used as a temperature monitor, and the garnet–clinopyroxene Fe–Mg exchange thermometer (Ravna, 2000) gives temperatures in the range of 350–400 °C at a nominal pressure of 2.0 GPa, using rim compositions of garnet and matrix omphacite.

The cross-cutting omphacite-rich veinlets with phengite, ferroglaucofane and hematite in sample COR-4 were obviously emplaced as a result of influx of Na-rich fluids along fractures after the growth of garnet (Fig. 4f), but at still high-*P* conditions as evidenced by high jadeite content of omphacite, stability of ferro-glaucophane and the high Si-content of phengite. The zoning of vein omphacite with decreasing jadeite content from core to rim suggests that the fluid influx continued at decreasing pressure conditions or, alternatively, at changing composition of the fluid. The significantly lower Mg number of the vein clinopyroxene compared with the matrix pyroxene clearly indicates different origins.

#### Lawsonite blueschist stage (III)

The assemblage glaucophane + albite, observed very locally in sample COR-1', post-dates the lawsonite eclogite stage and constrains the metamorphic conditions to <450 °C and <1.5 GPa according to the metamorphic facies grid of Bousquet *et al.* (1997).

#### Post-blueschist stages

As no greenschist overprint was observed in the samples reference is made to Miller & Cartwright (2006) who presented data on greenschist facies metamorphism and almost monomineralic albite veins from the same locality at Défilé du Lancône. They estimated that the greenschist assemblages formed at 510 °C and 0.6 GPa, whereas they concluded that the albite veins were formed at  $478 \pm 31$  °C and  $0.37 \pm 0.14$  GPa after the regional greenschist facies retrogression.

#### *P–T* estimates from isochemical phase diagrams

To further constrain the metamorphic evolution and *P–T* conditions for the Défilé du Lancône lawsonite eclogites isochemical *P–T* phase diagrams were constructed for three bulk compositions. The bulk compositions (Figs 7–9) were obtained by EDS area scans of the matrix of samples COR-1 and COR-4, respectively, as well as of the omphacite-rich veinlets in sample COR-4.

For the first two compositions the system  $\text{SiO}_2\text{–TiO}_2\text{–Al}_2\text{O}_3\text{–FeO–MgO–CaO–Na}_2\text{O}$  and for the veinlets the system  $\text{SiO}_2\text{–Al}_2\text{O}_3\text{–FeO–MgO–CaO–}$

$\text{Na}_2\text{O–K}_2\text{O–O}_2$ , all with excess  $\text{H}_2\text{O}$  were investigated. Clarke *et al.* (2006) pointed out that unusually high water contents are demanded by lawsonite assemblages. The program Theriak–Domino (de Capitani & Brown, 1987) with the Berman database JUN92.bs and the activity models therein were used. The modelling does not include Mn, which principally will be partitioned into garnet and thus increase the stability field of garnet to lower temperatures and pressures.

For sample COR-1 the calculated stability field of the matrix assemblage garnet–omphacite–lawsonite–chlorite–titanite within a wedge-shaped field occurs between ~1.9 and 2.75 GPa at 350 °C with a maximum thermal stability of ~470 °C at 2.3 GPa (Fig. 7). At lower pressures amphibole is stable, and at higher pressures ilmenite becomes an additional phase. Neither of these phases has been observed. Albite is stable in this composition only up to ~0.6 GPa, garnet (Ca-rich) appears at pressures slightly below 0.5 GPa and lawsonite appears at ~1.1 GPa, all at 400 °C.

Sample COR-4 has the same matrix assemblage, which is stable within a relatively large field ranging from ~340 °C and 1.3–2.6 GPa to a thermal maximum of 490–500 °C at 2.0–2.1 GPa (Fig. 8). In this composition garnet is stable over most of the diagram. Lawsonite appears at ~1.1 GPa and albite disappears at ~0.7 GPa at 400 °C. The assemblage albite + Ca-clinopyroxene + hornblende + titanite, which is included in garnet cores, is stable together with garnet and paragonite (not observed) at pressures below ~0.7 GPa at 400 °C.

The omphacite-rich veinlets consisting of omphacite + phengite + glaucophane + hematite + quartz are stable between 1.05–2.4 GPa at 330 °C and 1.9–2.5 GPa, 410–420 °C (Fig. 9). The assemblage omphacite + phengite + glaucophane + hematite may also coexist with coesite at pressures above 2.4–2.5 GPa. Quartz/coesite has not been observed, but the estimated content of free silica in our calculations is less than 2%.

To summarize, the results of the thermodynamic modelling of the three different bulk compositions indicate that the observed peak mineral assemblages were all stable within a wedge-shaped window ranging from ~340 °C and 1.9–2.6 GPa to 415 °C and 2.2 GPa.

#### DISCUSSION

The lawsonite eclogite from Défilé du Lancône shows evidence of extremely low temperatures, as exemplified by low modal content of garnet, typical low-*T* composition of garnet (low Mg, high Mn and Ca), large compositional variations of clinopyroxene and garnet. These features may also be indicative of rapid subduction. There is no evidence of breakdown of lawsonite during decompression, clearly indicating that the terminal stability limit of lawsonite was not crossed, and that the low *P/T* persisted during exhumation.

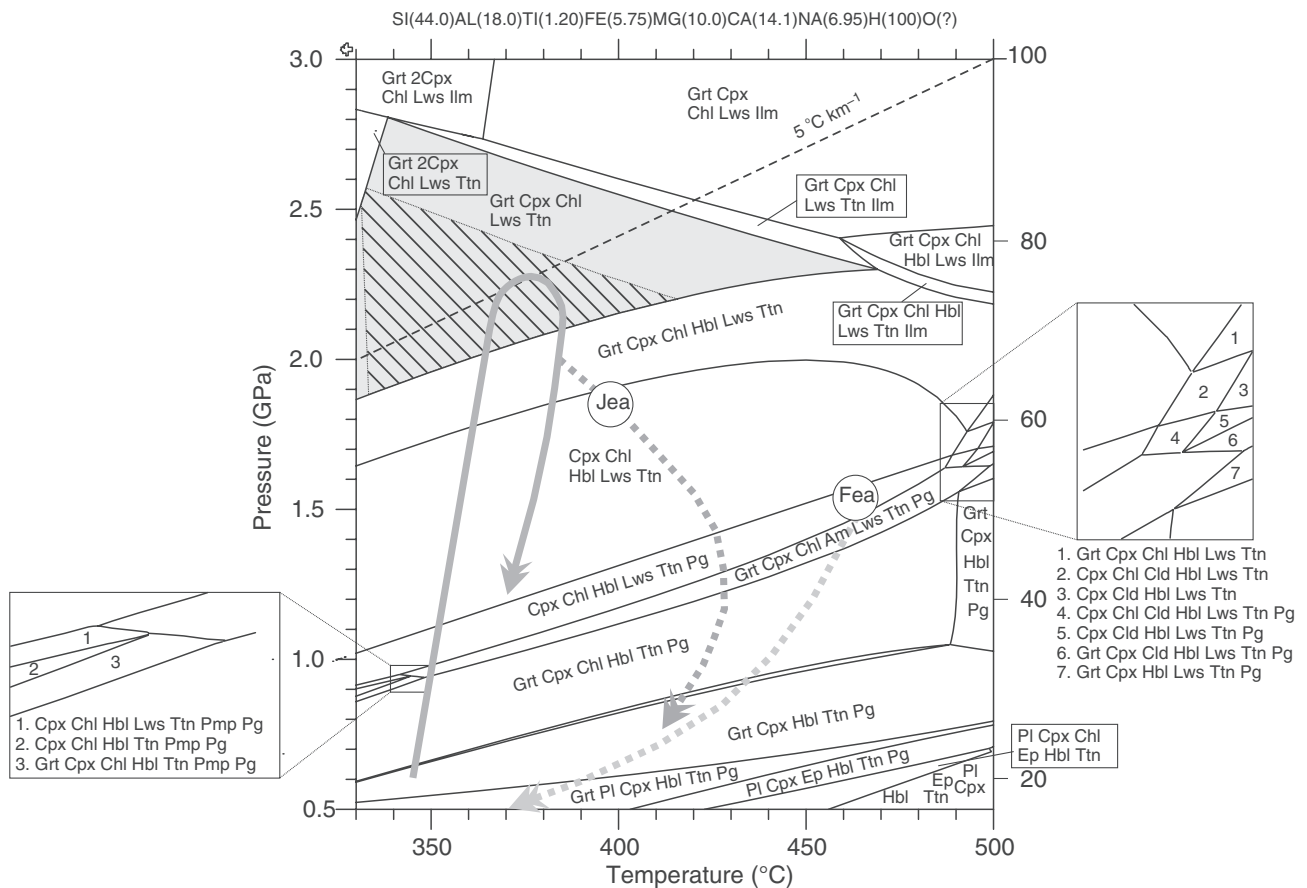


**Fig. 7.** Isochemical  $P$ - $T$  phase diagram showing the stability fields for mineral assemblages in sample COR-1, calculated using Theriak–Domino. See text for discussion. Hatched area marks overlapping  $P$ - $T$  conditions for peak assemblages in all three bulk compositions. Note that in the upper left corner are two small fields with two coexisting clinopyroxenes. A tentative  $P$ - $T$  path of the Défilé du Lancône lawsonite eclogite based on textural observations and thermodynamic modelling is shown (solid hairpin arrow). Alternative retrograde  $P$ - $T$  paths are taken from Fournier *et al.*, 1991 (Fea) and Jolivet *et al.*, 1998 (Jea).

The earliest observed phase occurring as inclusions in garnet and as cores of matrix clinopyroxene is Ti–Al-rich augite assumed to represent relicts of the magmatic stage. During the early stages of subduction Ca- and Mn-rich garnet, diopsidic clinopyroxene, Ca-amphibole, chlorite, albite, titanite and probably epidote and paragonite (not observed) became stable at pressures below  $\sim 0.7$  GPa, probably at temperatures of  $\sim 350$  °C. Continued subduction resulted in the consumption of the lower pressure assemblages, giving rise to the peak assemblage garnet–omphacite–lawsonite–chlorite–titanite, representing lawsonite eclogite facies. The thermodynamic modelling using Theriak–Domino constrains the peak  $P$ - $T$  conditions to 340–415 °C and 1.9–2.6 GPa, which actually is in agreement with the garnet–clinopyroxene Fe–Mg thermometric estimates. These peak conditions are close to, and even enter, the coesite stability field and the so-called “forbidden zone” of Liou *et al.* (2000), which indicates a regime of rapid subduction. Rapid subduction and burial of the HPLT rocks in Corsica is further supported by the evidence of subduction-related seismic activity recorded by blueschist facies

pseudotachylites found in both gabbro and spinel-peridotite in the Cima di Gratera area (see Fig. 1; Austrheim & Andersen, 2004; Andersen & Austrheim, 2006). These rocks preserve evidence of high strength during subduction, another argument for the very cold geotherm (Andersen *et al.*, 2008).

It is, however, important to stress that the accuracy of the  $P$ - $T$  estimates obtained here are hampered by large uncertainties. In the present samples the pyrope content of garnet is very low and far outside the range used for the calibration of the garnet–clinopyroxene Fe–Mg thermometer, and the obtained temperatures are at least 200 °C lower than the lowermost temperature (600 °C) used for this calibration (Ravna, 2000). Thus, these temperature estimates obtained here should only be regarded as indicative of very low temperatures. Likewise, in the thermodynamic modelling Mn as a major component in garnet has been omitted, and the results are also strongly dependent on the quality of the thermodynamic data at such low temperatures. In addition, the observed incomplete reactions of even pre-metamorphic phases will probably have some influence on the effective bulk

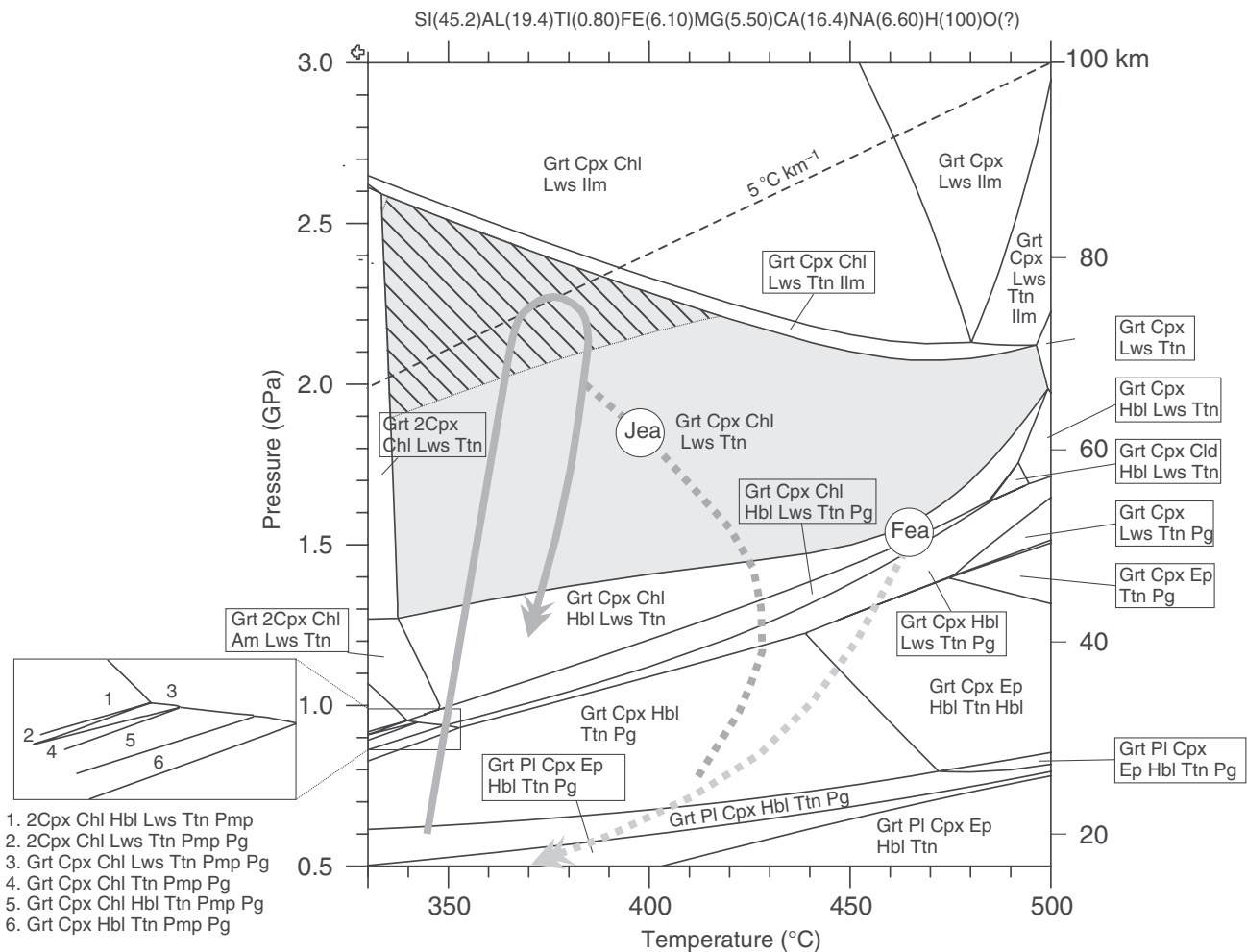


**Fig. 8.** Isochemical  $P$ - $T$  phase diagram showing the stability fields for mineral assemblages in sample COR-4 matrix, calculated using Theriak-Domino. See text for discussion. Note that at 0.9–2.6 GPa and  $<340$  °C two coexisting clinopyroxenes can be stable.

composition, and thus the final output. Nevertheless, the obtained results are not unrealistic. More important than the 'absolute'  $P$ - $T$  conditions is the sequential metamorphic evolution which clearly demonstrates a cold regime during subduction as well as initial exhumation. If these rocks ever entered the area defined as the 'forbidden zone', or were subjected to coesite stability conditions cannot be evaluated here.

The prograde metamorphic evolution of the Défilé du Lancône lawsonite eclogite bears similarities to lawsonite eclogite described from the Motagua fault zone, Guatemala (Harlow *et al.*, 2004; Tsujimori *et al.*, 2005, 2006b), where the basalt-eclogite transformation may have occurred at temperatures as low as  $\sim 300$  °C in a cold subduction zone with the apparent direct formation of lawsonite eclogite without passing through the blueschist facies. These authors suggested that dehydration of chlorite + albite + lawsonite  $\pm$  pumpellyite to form garnet + omphacite within the lawsonite field may be more effective than the glaucophane-forming reaction during subduction. In our samples, however, the thermodynamic model-

ling indicates that glaucophane was not a stable phase at any  $P$ - $T$  conditions due to bulk compositional constraints. Glaucophane was only stabilized in the extreme Na-rich composition of the omphacite-rich veinlets of sample COR-4, and in the very local domains of retrograde glaucophane + albite.

The preservation of lawsonite indicates that the low geothermal gradient prevailed during at least the initial stages of exhumation, following more or less the same path as during subduction, similar to the path proposed by Çetinkaplan *et al.* (2008) for the lawsonite eclogite in Sivrihisar, Tavşanlı Zone in Turkey. This suggests that material flowing up along the subduction channel was refrigerated by continued subduction of cold material. The estimated peak pressures of 1.9–2.6 GPa are much higher than those recorded for the main lawsonite blueschist facies (top-to-the-south-west shear) event, which is well developed elsewhere in the area and most probably related to retrogression during exhumation. The main thrusting phase was thus contemporaneous with the upward motion of the HP units within the subduction complex. This shows that

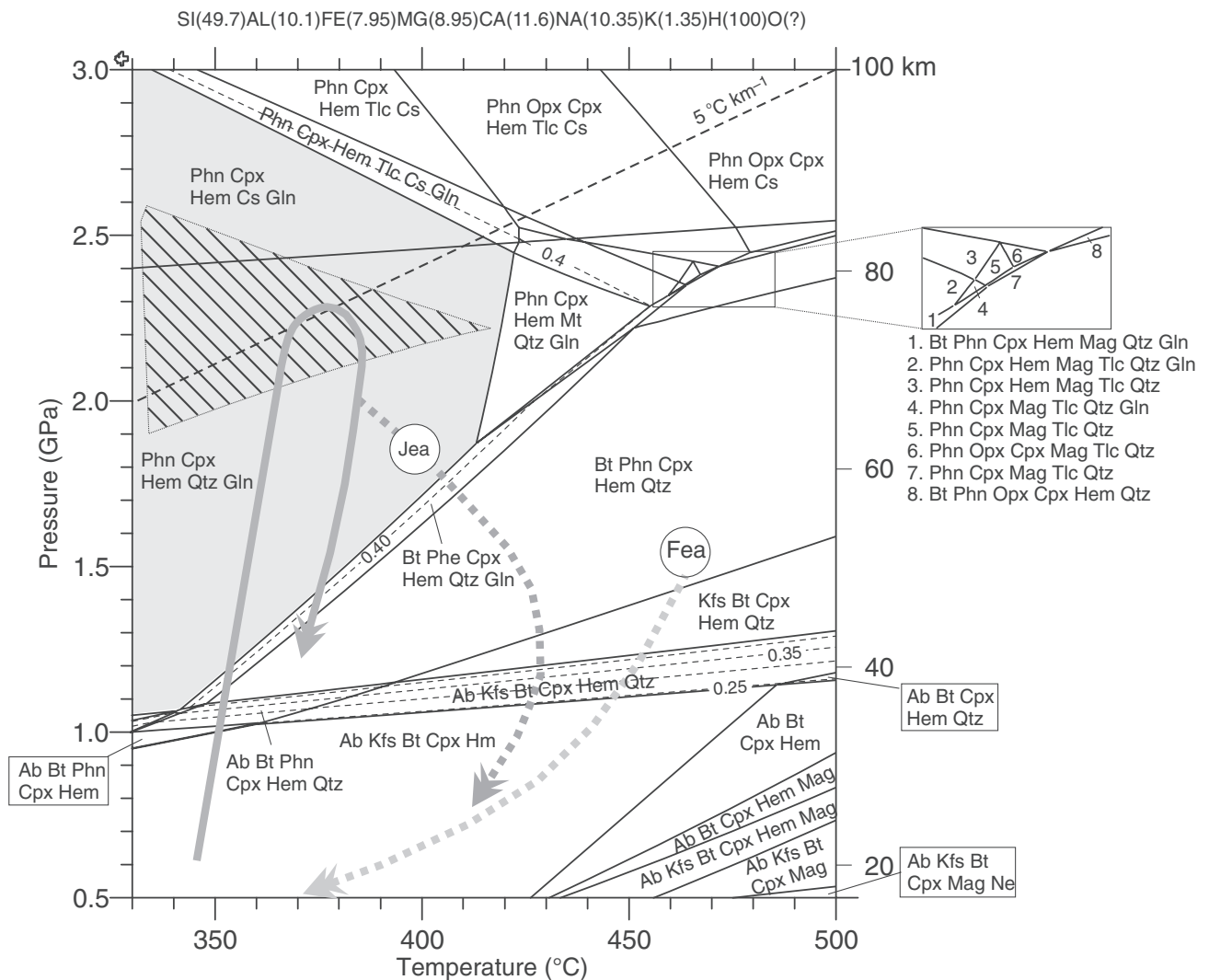


**Fig. 9.** Isochemical  $P$ - $T$  phase diagram showing the stability fields for mineral assemblages in omphacite-rich veins, sample COR-4, using Theriak-Domino. Contours for jadeite content of clinopyroxene are shown as stippled lines. See text for discussion.

the Lancône ophiolitic material was not significantly deformed until after it reached its maximum depth and that the first deformation was associated with exhumation. Continued retrogression into greenschist facies conditions has been thoroughly studied (Fournier *et al.*, 1991; Jolivet *et al.*, 1998; Miller & Cartwright, 2006) and the suggested retrograde  $P$ - $T$  paths from Fournier *et al.* (1991) and Jolivet *et al.* (1998) are shown in Fig. 10. The latter part of exhumation has been attributed to the post-orogenic extension that started at *c.* 33–32 Ma and led to the opening of the Liguro-Provençal Basin and the Tyrrhenian Sea (Jolivet *et al.*, 1991; Brunet *et al.*, 2000). Miller & Cartwright (2006) suggested estimates of 510 °C at 0.6 GPa for the greenschist facies overprint, which requires a late thermal pulse. However, their estimate may be too high for greenschist facies.

In the model presented here we assume, supported by the numerical modelling of  $P$ - $T$ -depth conditions

in subduction channels (Gerya *et al.*, 2002; Yamato *et al.*, 2007), that pressure can be converted to depth according to  $P \pm 10\% = \rho gh$  ( $\rho$ , density;  $g$ , gravitational acceleration;  $h$ , burial depth).

Finally, we propose a possible exhumation scenario (Fig. 10). The finding of very high pressure in Défilé du Lancône forces us to reconsider previously proposed schemes (Fournier *et al.*, 1991), that did not have to accommodate such large depths of burial. Our reconstruction starts in the latest Cretaceous when Ligurian oceanic crust and perhaps also the leading edge of the European continental margin (the youngest oceanic sediments date to late Cretaceous) had entered the subduction zone, and an accretionary complex had already developed above it at the expense of Ligurian oceanic domain. At this time a piece of partly eclogitized oceanic crust detached from the subducting lithosphere at  $\sim 80$  km depth and began its exhumation path along the subduction channel. The

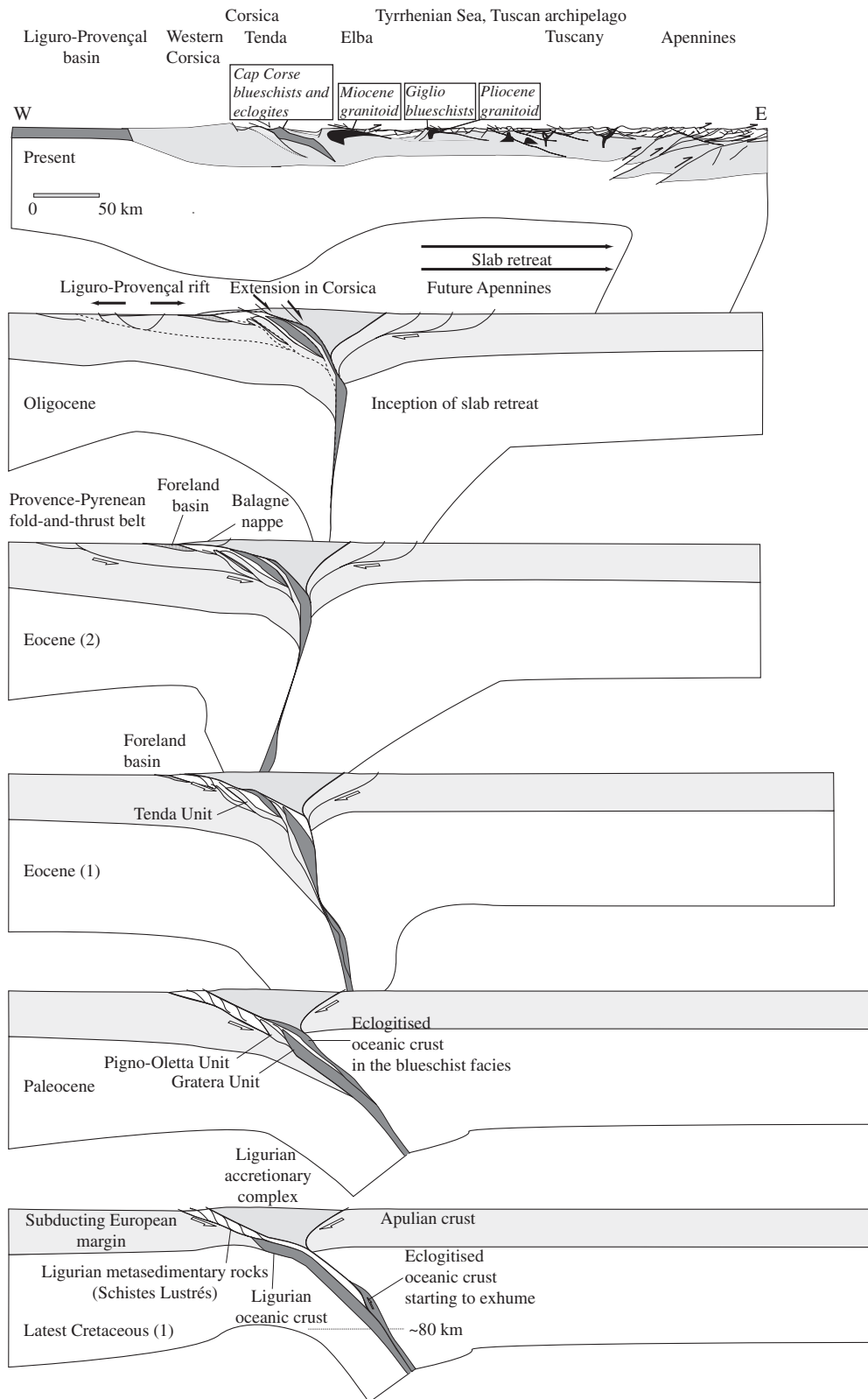


**Fig. 10.** Model of tectonic evolution of the Alpine LTHP metamorphic complexes Corsica (modified from Jolivet *et al.*, 1998), where the new *P-T* data from lawsonite eclogites in Défilé du Lancône have been incorporated. See text for discussion and details.

main top-to-the-west deformation recorded in the eclogite dates from the Palaeocene and Eocene when it had reached the blueschist domain. From the Eocene onward the Adria plate to the east started subducting and a progressive reorganization of the subduction polarity ensued orogen-parallel extension and arc bending forced by slab tearing and toroidal flow at the junction between the Alps and Apennines (Vignaroli *et al.*, 2008). This situation developed during the Eocene and culminated in the middle Eocene with the emplacement of superficial parts of the accretionary complex onto the foreland basin to the west. Units undergoing exhumation continued their way up in the subduction channel and eventually reached the accretionary complex, the last units to be involved in thrusting being the Tenda massif and Corte slices. At 33 Ma the regime of subduction changed in the Mediterranean region as a whole and slab retreat started (Jolivet & Faccenna, 2000), leading to the reactivation of major thrusts as extensional shear zones and normal faults that completed the exhumation of the metamorphic domain. Finally, the extensional deformation migrated eastward and Corsica became more or less stable.

#### ACKNOWLEDGEMENTS

Grants covering the analytical expenses of E. Krogh Ravna were received from the Norwegian Academy of Science and Letters through 'Nansenfondet og dermed forbundne fond'. A Centre of Excellence grant from the Norwegian Research Council to the PGP financed T.B. Andersen. The technical support by T.I. Eilertsen at the Electron Microscopy Lab, Department of Medical Biology, University of Tromsø, and the staff at the Electron Microprobe Lab at Dionýz Štúr Institute of Geology in Bratislava are much appreciated. Thorough reviews by T. Rivers and J.X. Zhang greatly improved the paper.

#### REFERENCES

- Agard, P., Monie, P., Jolivet, L. & Goffé, B., 2002. Exhumation of the Schistes Lustrés complex: *in situ* laser probe  $^{40}\text{Ar}/^{39}\text{Ar}$  constraints and implications for the Western Alps. *Journal of Metamorphic Geology*, **20**, 599–618.
- Altherr, R., Topuz, G., Marschall, H., Zack, T. & Ludwig, T., 2004. Evolution of a tourmaline-bearing lawsonite eclogite from the Elekdag area (Central Pontides, N Turkey): evidence for infiltration of slab-derived B-rich fluids during exhumation. *Contributions to Mineralogy and Petrology*, **148**, 409–425.
- Andersen, T.B. & Austrheim, H., 2006. Fossil earthquakes recorded by pseudotachylytes in mantle peridotite from the Alpine subduction complex of Corsica. *Earth and Planetary Science Letters*, **242**, 1–2.
- Andersen, T.B., Mair, K., Austrheim, H., Podladchikov, Y.Y. & Vrijmoed, J.C., 2008. Stress-release in exhumed intermediate-deep earthquakes determined from ultramafic pseudotachylyte. *Geology*, **36**, 995–998.
- Austrheim, H. & Andersen, T. B., 2004. Pseudotachylytes from Corsica: fossil earthquakes from a subduction complex. *Terra Nova*, **16**, 193–197.
- Bousquet, R., Goffé, B., Henry, P., Le Pichon, X. & Chopin, C., 1997. Kinematic, thermal and petrological model of the Central Alps: leontine metamorphism in the upper crust and eclogitization of the lower crust. *Tectonophysics*, **273**, 105–127.
- Brunet, C., Monie, P., Jolivet, L. & Cadet, J.P., 2000. Migration of compression and extension in the Tyrrhenian Sea, insights from  $^{40}\text{Ar}/^{39}\text{Ar}$  ages on micas along a transect from Corsica to Tuscany. *Tectonophysics*, **321**, 127–155.
- de Capitani, C. & Brown, T.H., 1987. The computation of chemical equilibria in complex systems containing non-ideal solutions. *Geochimica et Cosmochimica Acta*, **51**, 2639–2652.
- Caron, J.M., 1994. Metamorphism and deformation in Alpine Corsica. *Schweizerische Mineralogische und Petrographische Mitteilungen*, **74**, 105–114.
- Caron, J.M. & Péquignot, G., 1986. The transition between blueschists and lawsonite-bearing eclogites based on observations from Corsican metabasalts. *Lithos*, **19**, 205–218.
- Caron, J.M., Kienast, J.R. & Triboulet, C., 1981. High-pressure–low-temperature metamorphism and polyphase Alpine deformation at Sant'Andrea di Cotone (Eastern Corsica, France). *Tectonophysics*, **78**, 419–451.
- Carswell, D.A., Tucker, R.D., O'Brien, P.J. & Krogh, T.E., 2003. Coesite micro-inclusions and the U/Pb age of zircons from the Hareidland eclogite in the Western Gneiss Region of Norway. *Lithos*, **67**, 181–190.
- Çetinkaplan, M., Candan, O., Oberhänsli, R. & Bousquet, R., 2008. Pressure–temperature evolution of lawsonite eclogite in Sivrihisar; Tavşanlı Zone – Turkey. *Lithos*, **104**, 12–32, doi: 10.1016/j.lithos.2007.11.007
- Clarke, G.L., Powell, R. & Fitzherbert, J.A., 2006. The lawsonite paradox: a comparison of field evidence and mineral equilibria modeling. *Journal of Metamorphic Geology*, **24**, 715–725, doi: 10.1111/j.1525-1314.2006.00664.x.
- Davis, P.B. & Whitney, D.L., 2006. Petrogenesis of lawsonite and epidote eclogite and blueschist, Sivrihisar, Turkey. *Journal of Metamorphic Geology*, **24**, 823–849, doi: 10.1111/j.1525-1314.2006.00671.x.
- Droop, G.T.R., 1987. A general equation for estimating  $\text{Fe}^{3+}$  concentrations in ferromagnesian silicates and oxides from microprobe analyses using stoichiometric criteria. *Mineralogical Magazine*, **51**, 431–435.
- Durand Delga, M., 1984. Principaux traits de la Corse alpine et corrélation avec les Alpes ligures. *Memorie della Società Geologica Italiana*, **28**, 285–329.
- Egal, E., 1992. Structures and tectonic evolution of the External Zone of Alpine Corsica. *Journal of Structural Geology*, **14**, 1215–1228.
- Esawi, E.K., 2004. AMPH-CLASS: an Excel spreadsheet for the classification and nomenclature of amphiboles based on the 1997 recommendations of the International Mineralogical Association. *Computers & Geosciences*, **30**, 753–760.
- Fournier, M., Jolivet, L., Goffé, B. & Dubois, R., 1991. The Alpine Corsica metamorphic core complex. *Tectonics*, **10**, 1173–1186.
- Gerya, T.V., Stöckhert, B. & Perchuk, A.L., 2002. Exhumation of high-pressure metamorphic rocks in a subduction channel: a numerical simulation. *Tectonics*, **21**, 1–15.
- Ghent, E.D., Stout, M.Z. & Erdmer, P., 1993. Pressure–temperature evolution of lawsonite-bearing eclogites, Pinchi Lake, British Columbia. *Journal of Metamorphic Geology*, **11**, 279–290.
- Ghent, E.D., Tinkham, D. & Marr, R., 2009. Lawsonite eclogites from the Pinchi Lake area, British Columbia – new *P–T* estimates and interpretation. *Lithos*, **109**, 248–253, doi: 10.1016/j.lithos.2008.06.018.
- Harlow, G.E., Hemming, S.R., Avé Lallemand, H.G., Sisson, V.B. & Sorensen, S.S., 2004. Two high-pressure–low-temperature serpentinite-matrix melange belts, Motagua fault zone, Guatemala: a record of Aptian and Maastrichtian collisions. *Geology*, **32**, 17–20.
- Jolivet, L. & Faccenna, C., 2000. Mediterranean extension and the Africa–Eurasia collision. *Tectonics*, **19**, 1095–1106.

- Jolivet, L., Daniel, J.M. & Fournier, M., 1991. Geometry and kinematics of extension in Alpine Corsica. *Earth and Planetary Science Letters*, **104**, 278–291.
- Jolivet, L., Faccenna, C., Goffé, B. *et al.*, 1998. Midcrustal shear zones in postorogenic extension: example from the northern Tyrrhenian Sea. *Journal of Geophysical Research*, **103**, 12123–12160.
- Krogh, E.J., 1982. Metamorphic evolution of Norwegian country-rock eclogites, as deduced from mineral inclusions and compositional zoning in garnets. *Lithos*, **15**, 305–321.
- Lahondere, D., 1988. Eclogitic Metamorphism in Farinoles orthogneisses and ophiolitic metabasites (Northern Corsica, France). *Bulletin de la Société Géologique de France*, **4**, 579–585.
- Lardeaux, J.-M., Caron, J.-M., Nisio, P., Péquignot, G. & Boudeulle, M., 1986. Microstructural criteria for reliable thermometry in low-temperature eclogites. *Lithos*, **19**, 187–203.
- Leake, B.E., Woolley, A.R., Arps, C.E.S. *et al.*, 1997. Nomenclature of Amphiboles: report of the subcommittee on amphiboles of the International Mineralogical Association, commission on new minerals and mineral names. *Canadian Mineralogist*, **35**, 219–246.
- Liou, J.G., Hacker, B.R. & Zhang, R.Y., 2000. Into the forbidden zone. *Science*, **287**, 1215–1216, doi: 10.1126/science.287.5456.1215.
- Mattauer, M., Faure, M. & Malavieille, J., 1981. Transverse lineation and large-scale structures related to Alpine obduction in Corsica. *Journal of Structural Geology*, **3**, 401–409.
- Mattinson, C.G., Zhang, R.Y., Tsujimori, T. & Liou, J.G., 2004. Epidote-rich talc-kyanite-phengite eclogites, Sulu terrane, eastern China: *P-T-t*( $O_2$ ) estimates and the significance of the epidote-talc assemblage in eclogite. *American Mineralogist*, **89**, 1772–1783.
- McBirney, A., Aoki, K.I. & Bass, M.N., 1967. Eclogites and jadeite from Motagua Fault Zone Guatemala. *American Mineralogist*, **52**, 908–918.
- Miller, J.A. & Cartwright, I., 2006. Albite vein formation during exhumation of high-pressure terranes: a case study from Alpine Corsica. *Journal of Metamorphic Geology*, **24**, 409–428.
- Molli, G., Tribuzio, R. & Marquer, D., 2006. Deformation and metamorphism at the eastern border of the Tenda Massif (NE Corsica): a record of subduction and exhumation of continental crust. *Journal of Structural Geology*, **28**, 1748–1766.
- Och, D.J., Leitch, E.C., Caprarelli, G. & Watanabe, T., 2003. Blueschist and eclogite in tectonic melange, Port Macquarie, New South Wales, Australia. *Mineralogical Magazine*, **67**, 609–624.
- Oh, C.W., Liou, J.G. & Maruyama, S., 1991. Low-temperature eclogites and eclogitic schists in Mn-rich metabasites in Ward Creek, California – Mn and Fe effects on the transition between blueschist and eclogite. *Journal of Petrology*, **32**, 275–302.
- Parkinson, C.D., Miyazaki, K., Wakita, K., Barber, A.J. & Carswell, D.A., 1998. An overview and tectonic synthesis of the pre-Tertiary very-high-pressure metamorphic and associated rocks of Java, Sulawesi and Kalimantan, Indonesia. *Island Arc*, **7**, 184–200.
- Péquignot, G., Lardeaux, J.M. & Caron, J.M., 1984. Recristallisation d'éclogites de basse température dans les metabasites corses. *C.R. Académie des Sciences Paris*, **299 II** (13), 871–874.
- Ravna, E.K., 2000. The garnet-clinopyroxene  $Fe^{2+}$ -Mg geothermometer: an updated calibration. *Journal of Metamorphic Geology*, **18**, 211–219.
- Ravna, E.J.K. & Terry, M.P., 2004. Geothermobarometry of UHP and HP eclogites and schists – an evaluation of equilibria among garnet-clinopyroxene-kyanite-phengite-coesite/quartz. *Journal of Metamorphic Geology*, **22**, 579–592.
- Rehault, J.P., Boillot, G. & Mauffret, A., 1984. The western Mediterranean Basin geological evolution. *Marine Geology*, **55**, 447–477.
- Sartori, R., Mascle, G. & Amaudric du Chaffaut, S., 1987. A review of circum-Tyrrhenian regional geology. *Proceedings Initial Reports Ocean Drilling Program (Part A)*, **107**, 37–63.
- Shibakusa, H. & Maekawa, H., 1997. Lawsonite-bearing eclogitic metabasites in the Cazadero area, northern California. *Mineralogy and Petrology*, **61**, 163–180.
- Tribuzio, R. & Giacomini, F., 2002. Blueschist facies metamorphism of peralkaline rhyolites from the Tenda crystalline massif (northern Corsica): evidence for involvement in the Alpine subduction event? *Journal of Metamorphic Geology*, **20**, 513–526.
- Tsujimori, T., Liou, J.G., & Coleman, R.G., 2005. Coexisting retrograde jadeite and Omphacite in a jadeite-bearing lawsonite eclogite from the Motagua Fault Zone, Guatemala. *American Mineralogist*, **90**, 836–842.
- Tsujimori, T., Matsumoto, K., Wakabayashi, J. & Liou, J.G., 2006a. Franciscan eclogite revisited: reevaluation of the P-T evolution of tectonic blocks from Tiburon Peninsula, California, USA. *Mineralogy and Petrology*, **88**, 243–267.
- Tsujimori, T., Sisson, V.B., Liou, J.G., Harlow, G.E. & Sorensen, S.S., 2006b. Petrologic characterization of Guatemalan lawsonite eclogite: Eclogitization of subducted oceanic crust in a cold subduction zone. Ultrahigh-Pressure Metamorphism: Deep continental subduction. *Geological Society of America Special Papers* **403**, pp.147–168 (eds Hacker, B.R., McClelland, W.C. & Liou, J.G.).
- Tsujimori, T., Sisson, V.B., Liou, J.G., Harlow, G.E. & Sorensen, S.S., 2006c. Very-low-temperature record of the subduction process: a review of worldwide lawsonite eclogites. *Lithos*, **92**, 609–624.
- Usui, T., Nakamura, E., Kobayashi, K., Maruyama, S. & Helmstaedt, H., 2003. Fate of the subducted Farallon plate inferred from eclogite xenoliths in the Colorado Plateau. *Geochimica et Cosmochimica Acta*, **67**, A505.
- Usui, T., Nakamura, E. & Helmstaedt, H., 2006. Petrology and geochemistry of eclogite xenoliths from the Colorado Plateau: implications for the evolution of subducted oceanic crust. *Journal of Petrology*, **47**, 929–964.
- Vignaroli, G., Faccenna, C., Jolivet, L., Piromallo, C. & Rossetti, F., 2008. Subduction polarity reversal at the junction between the Western Alps and the Northern Apennines, Italy. *Tectonophysics* **450**, 34–50, doi: 10.1016/j.tecto.2007.12.012
- Watson, K.D. & Morton, D.M., 1969. Eclogite inclusions in kimberlite pipes at Garnet Ridge, northeastern Arizona. *American Mineralogist*, **54**, 267–285.
- Whitney, D.L. & Davis, P.B., 2006. Why is lawsonite eclogite so rare? Metamorphism and preservation of lawsonite eclogite, Sivrihisar, Turkey. *Geology*, **34**, 473–476, doi: 10.1130/G22259.1.
- Yamato, P., Agard, P., Burov, E., Le Pourhiet, L., Jolivet, L. & Tiberi, C., 2007. Burial and exhumation in subduction wedge: mutual constraints from thermo-mechanical modelling and natural *P-T-t* data (Schistes Lustrés, W. Alps). *Journal of Geophysical Research – Solid Earth*, **112**, B07410, doi:10.1029/2006JB004441.
- Zack, T., Rivers, T., Brumm, R. & Kronz, A., 2004. Cold subduction of oceanic crust: implications from a lawsonite eclogite from the Dominican Republic. *European Journal of Mineralogy*, **16**, 909–916.
- Zhang, J.X. & Meng, F.C., 2006. Lawsonite-bearing eclogites in the north Qilian and north Altyn Tagh: evidence for cold subduction of oceanic crust. *Chinese Science Bulletin*, **51**, 1238–1244.
- Zhang, J.X., Meng, F.C. & Wan, Y.S., 2007. A cold Early Palaeozoic subduction zone in the North Qilian Mountains, NW China: petrological and U-Pb geochronological constraints. *Journal of Metamorphic Geology*, **25**, 285–304.

Received 1 September 2009; revision accepted 27 January 2010.

## The age and tectonic significance of dolerite dykes in western Norway

TROND H. TORSVIK<sup>1,3</sup>, TORGEIR B. ANDERSEN<sup>2</sup>, ELIZABETH A. EIDE<sup>1</sup> & HARALD J. WALDERHAUG<sup>3</sup>

<sup>1</sup>Geological Survey of Norway, PB 3006 Lade, N-7002 Trondheim, Norway

<sup>2</sup>Department of Geology, University of Oslo, PO Box 1047, 0316 Blindern, Oslo 3, Norway

<sup>3</sup>Institute of Solid Earth Physics, University of Bergen, Allegt. 41, N-5007 Bergen, Norway

**Abstract:** Coast-parallel dykes in SW Norway, primarily of Permo-Triassic age, have been linked regionally to the early tectonic evolution of the Norwegian continental shelf. We demonstrate from palaeomagnetic data (mean declination=206.1°, inclination=−30.1°,  $\alpha_{95}$ =11.8°) that dolerite dykes in the coastal Sunnfjord region of Western Norway and immediately west of the Devonian Basins are also of Permian (c. 250–270 Ma) age, and not lower- or pre-Devonian as previously advocated. The Sunnfjord dykes appear to be contemporaneous with dykes from SW Norway at Sotra (262 ± 6 Ma) and the oldest dykes from Sunnhordland (260–280 Ma), and geochemical data attest to a transition from sub-alkaline to alkaline magmatism at the dawn of the Mesozoic.

The Sunnfjord dykes are not simple records of E–W extension and magma intrusion, but instead represent significant mid–late Permian time markers within a complex zone of fault activation and rejuvenation. Late Mesozoic–Cenozoic magnetic overprinting (mean declination=348.6°, inclination=+68.9°,  $\alpha_{95}$ =12°) and metamorphic alteration documented by these dykes are directly dependent upon proximity to major E–W brittle faults south of the Hornelen Devonian Basin, hence some motion and related fluid activity do post-date dyke intrusion. The E–W high-angle normal or oblique-slip faults can be regionally traced offshore to the Øygarden Fault Zone. Onshore, these faults truncate the Hornelen low-angle detachment, which in turn cuts folded Devonian strata. These observations, along with evidence for Permian and Late Jurassic–Cretaceous extension from the nearby Dalsfjord region, demonstrate important reactivation of a Late to post-Caledonian detachment and high-angle fault system in Western Norway.

**Keywords:** Norway, Permian, dykes, faults, reactivation.

Recent interpretation of seismic reflection data from offshore Western Norway (Fig. 1a) indicates that Permian extension was significantly greater and more regionally important than the Mesozoic (Jurassic–early Cretaceous) extension (Christiansson *et al.* 1995; Færseth *et al.* 1995). In onshore areas, Permian low-angle fault-rejuvenation in western Norway (Torsvik *et al.* 1992; Osmundsen 1996; Eide *et al.* 1997) and coast-parallel Permo-Triassic dykes in Southwest Norway (Færseth *et al.* 1976; Løvlie & Mitchell 1982) further attest to the importance of Late Palaeozoic rifting in the region (Fig. 1a).

Relatively abundant, coast-parallel, predominantly N–S-trending dykes, from the Sunnfjord area of Western Norway have also been noted since early mapping in the area commenced (Reusch 1881), but their age(s) and tectonic significance were never thoroughly investigated. The majority of these dykes were affected by E–W high-angle faults south of the Hornelen Devonian Basin (Fig. 1b); thus, Skjervlie & Tysseland (1981) interpreted the dykes as Lower Devonian or older because the faults were traditionally and regionally interpreted as primary controlling elements of Devonian sedimentation (Steel 1976; Norton 1986; Seranne & Seguret 1987). However, in more recent studies, these faults have been found to contain Late Palaeozoic and Mesozoic rejuvenation components (Torsvik *et al.* 1988, 1992; Wilks & Cuthbert 1994). The importance of establishing the age of the Sunnfjord dolerite dykes is therefore two-fold. First, they represent an important coast-parallel magmatic event which probably ties to the offshore tectonic development (pre-syn-rift?). Second,

the dyke ages provide an important time-marker for subsequent faulting or rejuvenation of E–W high-angle structures in Western Norway.

### Regional setting

The west Norwegian geological infrastructure is largely a product of the Scandian Orogeny that resulted from continental collision between Baltica and Laurentia and subsequent, extensional post-orogenic tectonics. In the Sunnfjord area, the continental collision can be accurately timed to the Mid-Silurian by the stratigraphic and deformational history of the Herland Group on Atløy (Fig. 1b) (Andersen *et al.* 1990). The collision hallmarks included high, pre-collision plate velocities (Torsvik *et al.* 1996), whole-scale subduction of Baltic continental crust and ensuing rapid Late Silurian–Lower Devonian exhumation of an orogen that contains high- and ultra-high pressure (HP–UHP) metamorphic rocks (Andersen *et al.* 1991, 1994; Dewey *et al.* 1993; Dobrzhinetskaya *et al.* 1995; Eide & Torsvik 1996). Extensional and erosional unroofing along the central parts of the orogen eventually resulted in formation of high-angle faults in the exhumed middle and upper crustal complexes. These faults subsequently controlled the formation of the Devonian Old Red Basins of Western Norway (Osmundsen & Andersen 1994) and were rooted in an array of lower-angle, extensional detachments that presently floor the eastern margins of the Devonian Basins (Andersen & Jamtveit 1990). The principal Nordfjord–Sogn Detachment

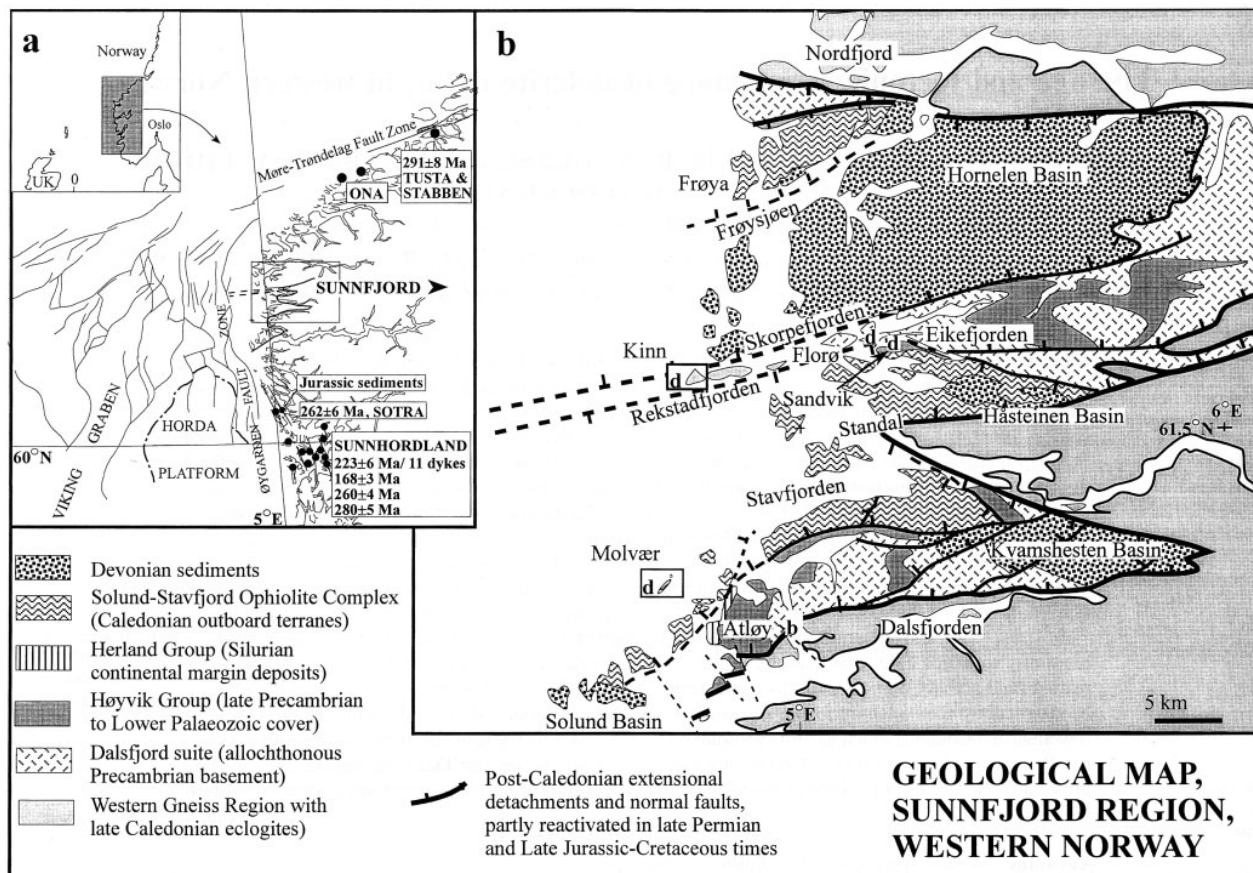


**Fig. 1.** (a) Sketch map of western Norway (see inset map for location in Norway), principal offshore structural elements and location of Permo-Triassic coast-parallel dykes. (b) Geological map of the Sunnfjord region, western Norway (see inset in a) and Sunnfjord dyke sampling localities (marked d). Fault-rock localities (Dalsfjord Fault) from the Atløy-Askvoll region (see text) are marked b.

(Norton 1986) juxtaposes the late-Caledonian HP rocks of the Lower Plate and low- to medium-grade Precambrian to Silurian allochthonous units of the Upper Plate (Fig. 1b) (Dewey *et al.* 1993; Andersen *et al.* 1994).

With the exception of the Håsteimen Basin which is mostly unconformable on its substrate, the Devonian Basins in western Norway are presently bounded by low-angle detachments to the east, reactivated faults along their northern and southern margins, and depositional unconformities to the west (Fig. 1b). Within the detachments and other major shear zones, kinematic indicators demonstrate top-west displacement; associated stretching lineations and magnetic fabrics have an E–W orientation (Chauvet & Seranne 1989; Swensson & Andersen 1991; Torsvik *et al.* 1992). Most of the penetrative deformation in the hanging- and footwalls of the detachments have been traditionally explained as syn-kinematic features related to post-orogenic extensional collapse (Seranne & Seguret 1987; Seguret *et al.* 1989). However, the structure of Devonian Basins, as well as their Upper and Lower Plate substrates, are dominated by inversion and E–W folding; these structures are arguably related to a phase of N–S shortening. Based on palaeomagnetic studies, Torsvik *et al.* (1988) demonstrated that N–S shortening continued into the Late Devonian and possible Early Carboniferous, although detailed structural studies in the footwall of the main detachment indicate that N–S shortening may have been related to sinistral transtensional deformation that had already begun in the Devonian (Krabbendam pers. com. 1996).

sional deformation that had already begun in the Devonian (Krabbendam pers. com. 1996).

### Sunnfjord dykes

The Sunnfjord dykes (Reusch 1881; Kolderup 1928; Kildal 1969; Skjerlie & Tysseland 1981) intrude the Late Precambrian and early Palaeozoic sequences of the basement and allochthons, but have not been observed to cut the Devonian Basins. Dykes trend 350°–060° (but mostly N–S) with steep WNW or vertical dips and vary in thickness from 0.1 to 10 m (Skjerlie & Tysseland 1981). Detailed sampling profiles from eight dykes and contacts at Molvær (Fig. 2a) and Kinn (Fig. 2b) were drilled in the field, whereas two dykes at Florø and Sandvik (Fig. 1b) were hand-sampled for logistic and archaeological reasons.

The Sunnfjord dykes have chemical compositions similar to continental tholeiites (Skjerlie & Tysseland 1981), but exhibit variable primary igneous textures and degrees of secondary alteration. Primary igneous textures appear to be logically correlated with dyke width and corollary differences in intrusive cooling rates, whilst secondary alteration depends upon the proximity of the dykes to the E–W Skorpe- and Rekstadfjorden Faults (Fig. 1b).

The least altered dykes occur on the Molvær isles (Figs 1b & 2a) where they intrude a highly deformed sequence of

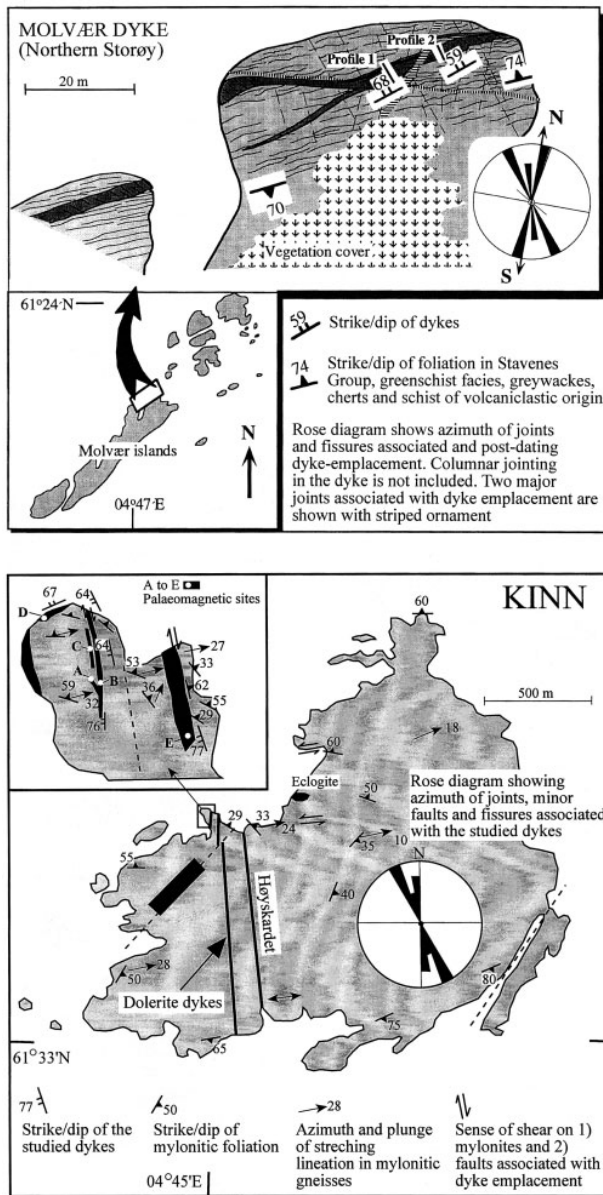


Fig. 2. Geological sketch map from (a) the Molvær isles and (b) Kinn (see Fig. 1b). Structural data from central and southern Kinn from Lutro (1991).

greenschist-facies schists, including meta-greywackes, graphitic schists, meta-cherts and meta-tuffaceous rocks of the Stavnes Group. The latter represents the volcano-sedimentary cover to the late Ordovician Solund–Stavfjord Ophiolite Complex (Furnes *et al.* 1990) both of which were obducted onto the Middle Silurian Herland Group during the initial stages of the Scandian orogeny (Andersen *et al.* 1990). The relationships between the Molvær dykes and the wall-rock structure indicate that dyke emplacement was partly controlled by the orientation of the main foliation of the Stavnes Group and a NNE-trending joint system that at least locally predates the Molvær dykes. A pre-existing, roughly E–W trending (0.1–0.5 m wide) zone of cataclastic brecciation controlled a 15 m long, E–W segment of the dyke (Fig. 2a). A separate set

of NW-trending fractures apparently post-date the dykes at Molvær.

Except for jointing, the Molvær dykes are essentially unmetamorphosed and display glassy chilled margins and columnar jointing; both features indicate shallow intrusion levels and rapid cooling against the wall-rock. The dykes are hypocrystalline basalts with phenocrysts of plagioclase, clinopyroxene, and oxides in a groundmass that largely comprises grey-green, fresh glass. The opaque phases comprise abundant titanomagnetite and some accessory pyrite. Titanomagnetite grains range in size from the limit of optical resolution up to several hundred microns. Grain are elongated and often skeletal, indicative of fairly rapid cooling. Close inspection of the grains (Fig. 3a) shows that ilmenite lamellae are present on a very fine scale, indicating high-temperature oxidation to class II of Ade-Hall *et al.* (1971). The lamellae are closely spaced and always less than 1 µm in width, causing a partitioning which should have a marked effect on the domain state of the larger grains.

A basaltic dyke at Sandvik, just south of the Rekstadvjorden Fault (Fig. 1b), intrudes Late Precambrian quartzites and appears fresh in hand-specimen, but has undergone some low-grade metamorphic alteration. Plagioclase is pervasively pseudomorphed by sericite, while clinopyroxene is generally unaltered or may have minor epidote, biotite or amphibole replacement products. The dominant opaque phase is abundant class II titanomagnetite (Fig. 3b) with accessory pyrite. Slight to moderate low-temperature oxidation, with granulation and some replacement of opaque phases along grain edges is evident.

The Kinn dykes (Figs 1b & 2b) intrude highly deformed orthogneisses which locally preserve eclogite facies assemblages correlated with the Western Gneiss Region. Dyke margins are variably brecciated and in outcrop, these dykes are part of an intrusive network that comprises a large, coarse-grained gabbroic dyke- or sill-like mass with numerous, associated, narrow, branching aphanitic to porphyritic basaltic dykes. The main gabbro body (Site E in Fig. 2b) has a coarse-grained, subophitic texture, although clinopyroxene now occurs as sub- to euhedral grains with preserved cores replaced progressively or completely by amphibole. Coarse-grained opaque grains are typically up to several hundred microns in size. Titanomagnetite of high-temperature oxidation class II is again the dominant phase (Fig. 3c). The grains exhibit coarse ilmenite lamellae, and often contain smaller inclusions of pyrite. Low temperature alteration of individual titanomagnetite grains varies from slight to heavy, with replacement of oxides by non-opaque phases resulting in many cases. Fine-grained oxides occur on pseudomorph amphibole.

The thinner basaltic Kinn dykes probably once had a texture similar to that of Molvær, but are now completely altered to lower greenschist facies. A glassy groundmass comprises amphibole and chlorite, in addition to amphibole pseudomorphs after clinopyroxene. Two distinct generations of oxides are present: (1) Primary titanomagnetite grains with maximum sizes in excess of 100 µm with well-developed ilmenite lamellae indicating high-temperature oxidation to class II (Fig. 3d). The lamellae pattern is on a coarser scale than e.g. the Molvær dykes. (2) A pervasive cross-hatched pattern of elongate magnetite particles, apparently formed during secondary metamorphism of the rock (Fig. 3e). The pattern is best seen in transmitted light (Fig. 3f), and secondary magnetite appears to follow microfractures.

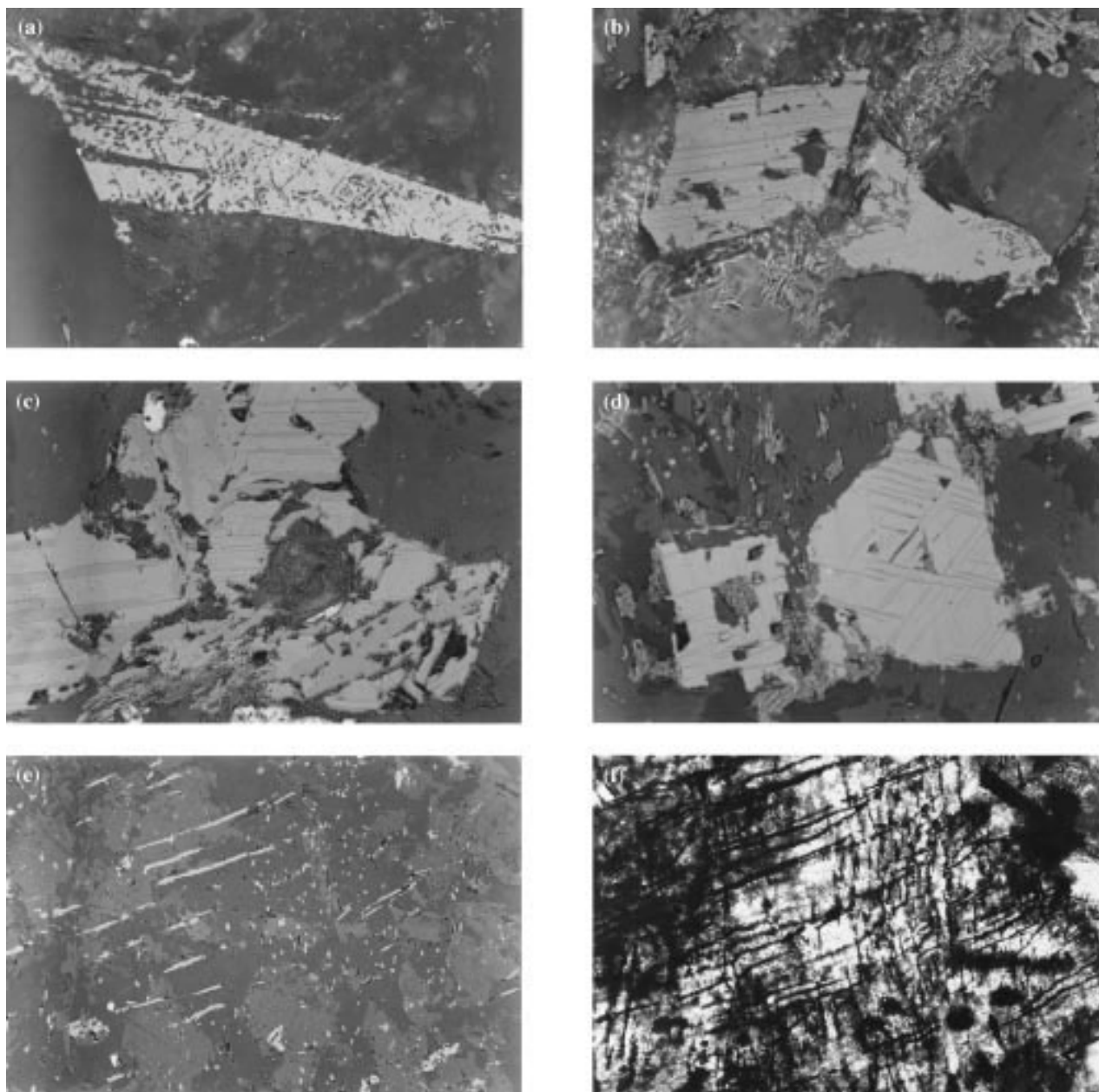


**Fig. 3.** Reflected light (a–e) and transmitted light (f) photomicrographs of opaque grains. See text for further descriptions. (a) Molvær dyke titanomagnetite (TM) grain. Frame width = 130  $\mu\text{m}$ . Note very fine-scale ilmenite lamellae. (b) Sandvik dyke TM grain. Frame width = 130  $\mu\text{m}$ . (c) Broad Kinn dyke TM grain (location E). Frame width = 325  $\mu\text{m}$ . (d) Thinner Kinn dyke TM grain (location A). Frame width = 130  $\mu\text{m}$ . (e, f) From same micrograph as (d) viewed in reflected and transmitted light, respectively, showing cross-hatched pattern of secondary magnetite. Frame width = 325  $\mu\text{m}$ .

### Palaeomagnetic experiments

The natural remanent magnetization (NRM) was measured with a JR5A magnetometer and remanence stability was tested by thermal and two-axis tumbler alternating field (AF) demagnetization. Characteristic remanence components were calculated using least squares analysis. NRM intensities and bulk-susceptibilities are listed in Table 1.

Thermo-magnetic analysis was performed on a horizontal translation balance, and all tested samples, independent of

dyke alteration state or location within a single dyke, yield Curie-temperatures of 580°C, i.e. titanium-poor titanomagnetite or almost pure magnetite (Fig. 4a). Heating and cooling curves are practically identical and indicate minimal thermochemical alterations during the experiments.

Isothermal remanent magnetization (IRM) acquisition curves are dominated by magnetic phases which saturate in fields of 150–300 mT, and remanence coercive forces ( $H_{cr}$ ) vary from 15 to 40 mT. High  $H_{cr}$  and probable pseudo-single domain (PSD) magnetite are observed from the pristine

## DOLERITE DYKES IN WESTERN NORWAY

965

**Table 1.** Sampling details, mean NRM intensity and susceptibility and characteristic remanence components for the Sunnfjord dykes (mean sampling coordinates: 61.5°N and 4.8°E)

	Strike/dip	Width (m)	NRM	Sus	Dec°	Inc°	N	$\alpha_{95}$	k	Component
Molvær dykes										
Dyke A	232°/59°	2.0	495 ± 247	45 949 ± 4873	355.8	63.2	12	7.6	33.8	M-C
					220.1	-36.5	18	4.6	57.8	P
Dyke B	232°/59°	0.4	562 ± 97	35 281 ± 1837	329.8	73.8	3	17.5	50.8	M-C
					220.4	-20.6	6	23.7	8.4	P
Dyke C	232°/68°	0.6	1070 ± 388	36 019 ± 4259	213.3	-36.0	7	3.3	345.5	P
Contact schist			1.4 ± 0.9	529 ± 24	204.0	-28.6	6	2.9	550.0	P
Sandvik dyke										
	036°/90°	1.5	1507 ± 67	77 868 ± 5535	342.6	+73.2	13	10.1	17.8	M-C
					191.5	-32.8	8	8.2	46.7	P
Kinn dykes										
Dyke A	267°/63°	0.2	721 ± 250	55 862 ± 5117	069.0	+84.2	8	10.3	29.6	M-C
Dyke B	175°/64°	1.4	784 ± 219	53 927 ± 4699	030.4	+68.8	8	16.2	12.7	M-C
Dyke C	158°/70°	0.25	825 ± 227	57 577 ± 2738	038.7	+69.4	2	(38.4)	(44.4)	M-C
					188.3	-22.8	3	(56)	(5.9)	P
Dyke D	240°/67°	3.5+	792 ± 129	52 754 ± 5220						
Dyke E	170°/77°	9.0	854 ± 109	59 868 ± 7297	342.8	+53.1	3	26.3	23.1	M-C
Contact gneiss			260 ± 118	13 162 ± 9706	357.0	+60.2	3	28.5	19.7	M-C
Florø dyke										
	010°/90°	2.3	4889 ± 695	81 331 ± 4361	299.7	+42.3	5	8.5	82.2	M-C
Combined					348.6	+68.9	9*	12.0	19.4	M-C
					206.1	-30.1	6*	11.8	33.3	P

NRM=natural remanent magnetization (mA/M); Sus=susceptibility ( $10^{-6}$  SI); Dec°, Inc°=mean declination and inclination; n=number of samples/sites\*;  $\alpha_{95}$ =95% cone of confidence; k=precision parameter; component interpretation: M-C, Mesozoic-Cenozoic; P, Permian.

Molvær dykes whilst the altered Kinn and Florø dykes show minimum values. This may partly indicate magnetite 'softening' with increased alteration, but properties of the magnetically harder Molvær dykes are clearly the result of smaller grains and finer lamella structure, i.e. due to primary mineralogical difference. Hysteresis analysis and saturation remanence to saturation magnetization ( $J_{rs}/J_s$ ) and coercivity ( $H_{cr}/H_c$ ) ratios show a clear trend towards a multidomain (MD) state from Molvær to Kinn dykes (Fig. 4b).  $J_{rs}/J_s$  is normally regarded as the best measure of grain size ranges, from 0.5 for uniaxial SD grains down to <0.02 for true MD magnetite (Dunlop 1986). Increasing titanium content raises the MS/PSD transition to 0.1.  $H_{cr}/H_c$  is theoretically between 1 and 2 for SD grains and increases with grain size. In practice true SD values for  $J_{rs}/J_s$  are very rare and in the Day diagram (Fig. 4b, Day *et al.* 1977), values most commonly fall in the PSD range.  $J_s$  values are around  $1 \text{ Am}^2 \text{ kg}^{-1}$  for the Kinn, Florø and Molvær dykes and just below  $2 \text{ Am}^2 \text{ kg}^{-1}$  for the Sandvik dyke, indicative of magnetite contents of *c.* 1% and 2% respectively.

### Molvær dykes

The pristine Molvær dykes (Fig. 2) are characterized by two remanence components: (1) a low to intermediate unblocking component (denoted M-C) with northerly declinations and steep positive inclinations and, (2) a high unblocking component (denoted P) with SW declinations and negative inclinations (Fig. 5a; Table 1). Component P is characterized by discrete thermal unblocking between 560 and 580°C or by isolation in AF fields above 15–19 mT (Fig. 5b). Median destructive ( $M_{1/2}$ ) AF fields range between 12 and 20 mT. In many instances the M-C component is not randomized before 550°C (Fig. 5a), but dyke margin samples and the baked contact schist (Fig. 5c) are less influenced by the M-C component. Maximum susceptibilities are recorded in the widest

dyke A (Fig. 5d) and marginal samples show lower values than the interior and centre, which may attest to grain-size contrasts. However, titanomagnetite concentration and degree of high-temperature titanomagnetite oxidation are important

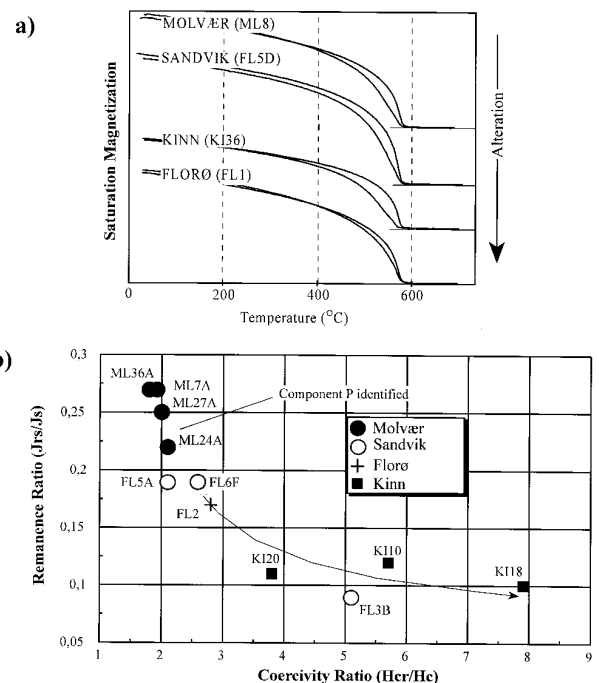


**Fig. 4.** (a) Thermomagnetic curves from the Sunnfjord dykes which are all identical with  $T_c \approx 580^\circ\text{C}$  and reversible heating and cooling curves (b)  $J_{rs}/J_s$  and  $H_{cr}/H_c$  ratios. In the Day diagram, only the encircled samples with high  $J_{rs}/J_s$  and low  $H_{cr}/H_c$  reveal the P-component (probably primary Permian).

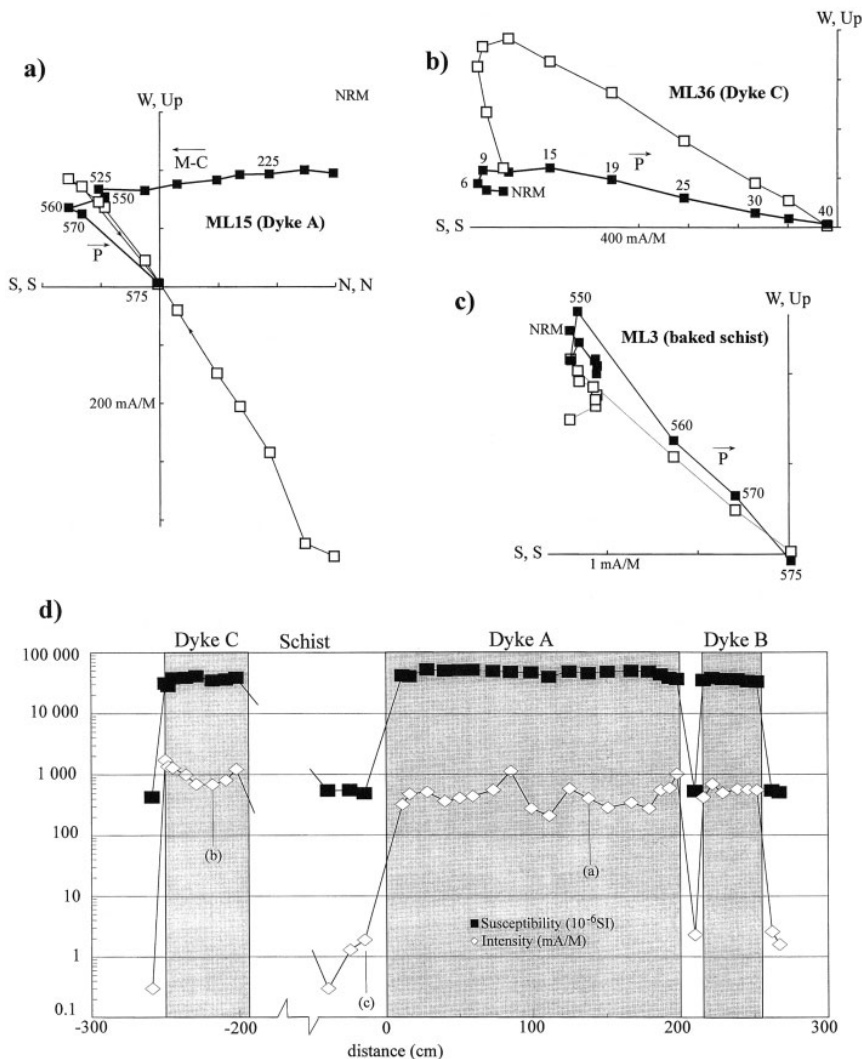


**Fig. 5.** Thermal (a) and alternating field (b) demagnetization of Molværdyke samples and (c) thermal demagnetization of a baked contact sample. (d) Intensity and susceptibility profile (note logarithmic scale) through the tested dykes and contact (distance in centimetres). In orthogonal vector plots, solid (open) symbols represent projections onto the horizontal (vertical) plane.

factors. NRM intensities are also clearly influenced by overprints (M-C), but the narrow dyke C (Profile 2 in Fig. 2a), which is least affected by the M-C component, exhibits a pattern of high NRM with low susceptibility along the margins. This probably reflects a relatively undisturbed primary cooling pattern of a fine-grained margin and coarser-grained interior. The P component in the contact schist closely corresponds to the dyke components but schists sampled outside the baked region did not yield sensible palaeomagnetic results due to low intensity and viscous directional behaviour.

#### Sandvik dyke

The Sandvik dyke (Fig. 1b) is directionally more complex than the Molværdykes. Most commonly the M-C component is identifiable whereas the P component is not isolated. Southerly directional trends show that the high unblocking component P is always present (identified in Fig. 6a), but 'stable end-directions' are often difficult to observe (Fig. 6b) due to the combined effect of overlapping unblocking-spectra and the fact that the P component often resides within an extremely narrow temperature interval (570–580°C).  $M_{1/2}$  is considerably

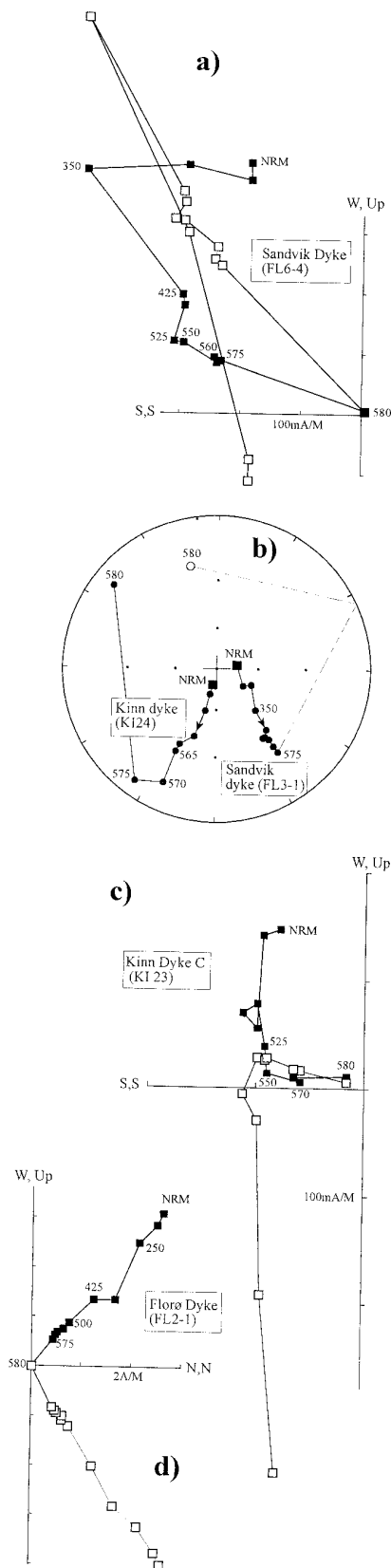
lower than the Molværdykes, generally 1–5 mT, except in a subordinate number of samples where the P component was identified and  $M_{1/2}$  was 10–12 mT.

#### Kinn dykes

These dykes were tested in considerable detail due to their relatively complex textural characteristics (Fig. 3), but demagnetization behaviour is similar to, but less stable than those from Sandvik. All samples show pronounced southerly directional movement during demagnetization (Fig. 6b), but the high unblocking P component is difficult to isolate and only poorly identified in three samples from one dyke at temperatures above 550–570°C (Fig. 6c, Table 1). Low  $M_{1/2}$  (2–4 mT) prevails, and the low to intermediate M-C components are comparable to those from Molværdykes and Sandvik (Fig. 7a).

#### Florø dyke

The Florø dyke has significantly higher NRM intensity (Table 1) and only M-C components are identified. A few



samples from this strongly altered dyke were thermally tested; they all show identical and almost uni-vectorial directional behaviour (Fig. 6d), but with somewhat more westerly declinations than M-C components from the other dykes (Fig. 7a).

### Magnetic interpretation

Palaeomagnetic results from Sunnfjord dykes reveal a high unblocking component (P) with SSW declinations and negative inclinations, which is partially or entirely (Florø) overprinted by components (M-C) with N or NNW declinations and positive inclinations (Fig. 7a). Component P can be interpreted as mid-late Permian (*c.* 250–270 Ma) with a late Mesozoic–Cenozoic (M-C), probably Cretaceous or younger, overprint (Fig. 7a). The Sunnfjord dyke pole (P) is almost identical to fault-rocks ('green breccia' of Torsvik *et al.* 1992) from Atløy (Fig. 8), formed during low-angle faulting on the Dalsfjord Fault (Fig. 1b), and isotopically dated to 250–260 Ma (Eide *et al.* 1997). The Permian magnetic signature in the Sunnfjord dykes represents either a primary intrusion age or a regional overprint. We prefer the former explanation because extensive palaeomagnetic studies of the Devonian Basins and substrate (including an anorthosite locality 200 m from the Sandvik dyke; Site 25 in Torsvik *et al.* 1988) in the Sunnfjord area essentially yield pre-Permian magnetic ages.

Alteration and magnetic resetting of the Sunnfjord dykes is clearly related to movements along the prominent E–W faults south of the Hornelen Devonian Basin (Fig. 1b). Just south of the Rekstadjorden Fault, at Sandvik, Permian directions are partially recovered whereas within the fault-zone, remagnetization prevails (Kinn), and at Florø (Fig. 1b) the Permian direction is entirely obliterated. These magnetic characteristics are represented by respective differences in mineralogy and degree of metamorphism, manifested first by primary igneous textural characteristics and grain sizes, and second, by the effects of subsequent metamorphic (hydrothermal) alteration on the magnetomineralogy. The M-C overprint plots near the present earth's magnetic field direction and may partly have a viscous and recent origin.

The Sunnfjord dykes all share a similar primary magnetic phase, i.e. abundant titanomagnetite of oxidation class II (Fig. 3) which explains the high Curie temperatures and unblocking temperatures. Differences in magnetic hardness partly arise from differences in grain-size and coarseness of the lamellae. The Molvær dykes show signs of fairly rapid cooling with commonly skeletal and very fine scale lamellae, while the broadest Kinn dyke (Dyke E) has the largest grains and coarsest lamellae. Varying degrees of low-temperature alteration of the primary titanomagnetite phase are evident in all dykes, and the thinner Kinn dykes (and Florø dyke) have a second significant magnetic phase (magnetite), clearly associated with later, lower greenschist-facies metamorphism (Fig. 3e & f).

### A regional dyke perspective

Permo-Trassic dykes are observed in several areas in coastal western Norway, and the oldest dated dykes are located at

**Fig. 6.** Thermal demagnetization samples from the Sandvik (a, b), Kinn (b, c) and Florø dykes (d). In the stereonet, closed (open) symbols denote positive (negative) inclination. See Fig. 5 for further legend.

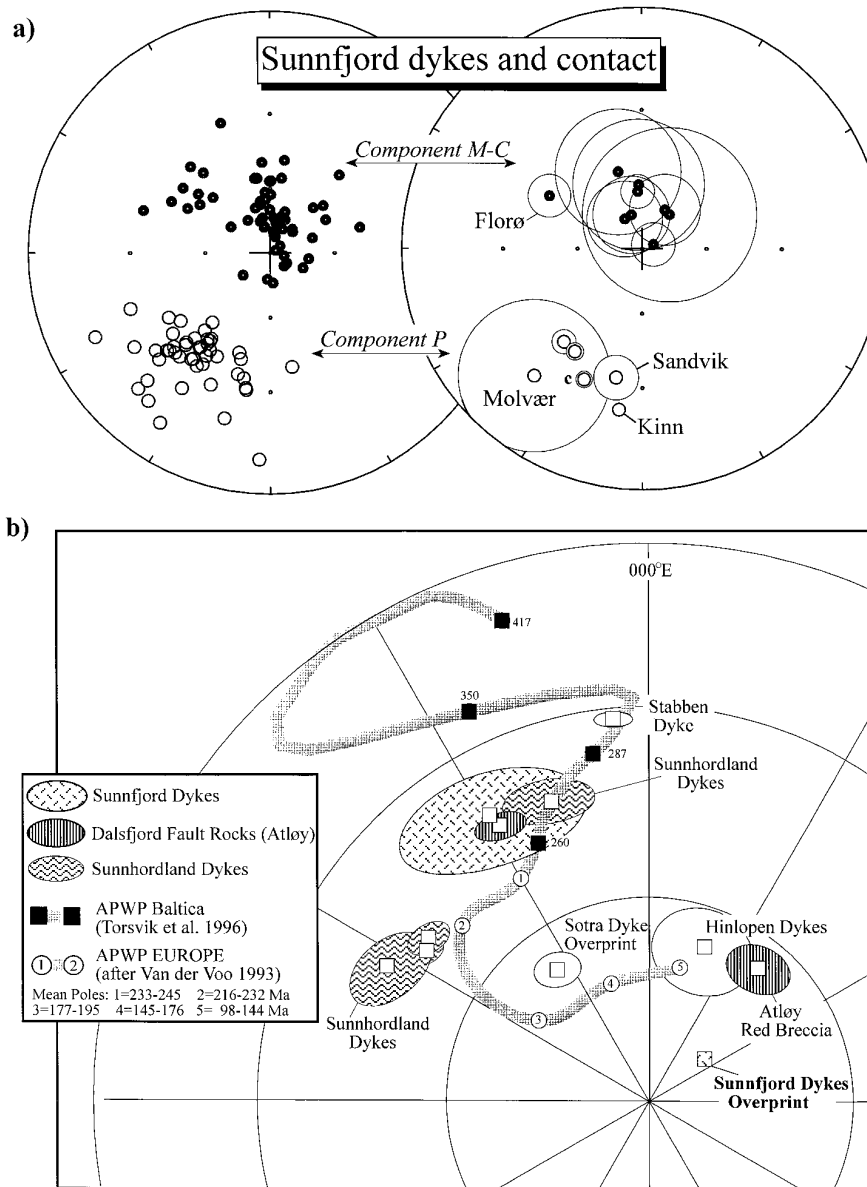


**Fig. 7.** (a) Characteristic remanence components from the Sunnfjord dykes, sample (left) and dyke-contact mean directions (right diagram with  $\alpha_{95}$  confidence circles), respectively. (b) Apparent polar wander paths (APWP) for Baltica and Europe, selected poles from Western Norway (Table 2) and the Sunnfjord mean poles (component P and M-C, Tables 1–2). Sunnfjord M-C pole is shown without error confidence ellipses ( $dp/dm$ ). For comparison, we also include a pole from the c. 145 Ma Hinlopen dolerites (Halvorsen 1989). Equal area polar projection.

Tustna-Stabben (Fig. 1a) and within the eastern part of the Møre Trøndelag Fault Zone. The palaeomagnetic pole from the E–W Stabben syenitic dykes (Sturt & Torsvik 1987) plots at the Lower Permian part of the Baltica APWP (Fig. 7b) and a Rb–Sr age of  $291 \pm 8$  Ma obtained from the nearby island of Tustna (Råheim 1974) fits well with the magnetic age estimate. South of the Møre Trøndelag Fault Zone, N–S-trending basaltic dykes are observed on the island of Ona (Fig. 1a; Robinson pers. comm. 1995) but presently lack isotopic age constraints.

Isotopic age data are not yet available for the Sunnfjord dykes, but the palaeomagnetic data strongly suggest a mid-late Permian age (c. 250–270 Ma; Fig. 7a). Two ultrapotassic dykes from the same region (Dalsfjord area) are dated between 256–262 Ma (K/Ar whole rock; Furnes *et al.* 1982). These dykes, however, are highly altered with a strong magnetic fabric, and palaeomagnetic testing proved unsuccessful

(Torsvik unpublished data 1992). Their unusual strike (E–W) and geochemistry are also markedly different from the subalkaline tholeiitic Sunnfjord dykes (Fig. 8b). Following Furnes *et al.* (1982) we regard it reasonable to conclude that the K/Ar whole rock ages from these dykes relate to strong hydrothermal alteration, probably linked to movement along the Dalsfjord Fault. The exact intrusion-crystallization age of these dykes is therefore uncertain.

Further southward along the coast, six concordant ages from two dykes on the island of Sotra (west of Bergen; Fig. 1a) yield a mean age of  $262 \pm 6$  Ma (Fig. 8a; Løvlie & Mitchell 1982). Unpublished geochemical data suggest a continental tholeiitic affinity, conceivably similar to the Permian-aged Sunnfjord dykes (Furnes pers. comm. 1996). The palaeomagnetic data from the Sotra dykes, however, are clearly discordant with the Permian isotopic ages (Fig. 7b). The Sotra dykes are located along a major NNW–SSE lineament and the

## DOLERITE DYKES IN WESTERN NORWAY

Table 2. Post-Carboniferous palaeomagnetic data from Western Norway (Figs 1 and 7b) that are discussed in the text

Site	Rock Unit (Geo.Lat., Geo.Long.)	Dec°	Inc°	$\alpha_{95}$	Pole		dp	dm	Isotopic age	Magnetic age estimate	Ref.
					Lat.	Long					
NW Norway											
Stabben Dykes	(63.3°N, 8.5°E)	192.0	-12.0	2.4	-32.1	354.4	1.0	2.0	291 ± 8 Ma (Rb/Sr)	Early Permian	1, 2
Central western Norway											
Sunnifjord Dykes	(61.5°N, 4.8°E)	206.1	-30.1	11.8	-41.0	330.7	7.3	13.1		Mid-late Permian (Component P)	3
Sunnifjord Dykes	(61.5°N, 4.8°E)	348.6	+68.9	12.9	-79.0	053.9	17.3	20.4		<Cretaceous (Component M-C)	3
Atløy 'green breccia'	(61.3°N, 5°E)	205.0	-33.0	3.2	-43.2	331.5	2.0	4.0	253 ± 5 Ma ( <sup>40</sup> Ar/ <sup>39</sup> Ar)	Mid-Late Permian	4, 5
Atløy 'red breccia'	(61.3°N, 5°E)	342.0	+58.0	3.2	-64.8	039.5	3.0	5.0	<130 Ma ( <sup>40</sup> Ar/ <sup>39</sup> Ar)	L. Jurrassic-E. Cretaceous	4, 5
SW Norway											
Sotra Dykes	(60.0°N, 5°E)	019.5	+59.1	2.3	-66.0	325.0			262 ± 6 Ma (K/Ar)	Jurrassic ?	6
Sunnhordland Dykes	(59.8°N, 5.5°E)	198.0	-27.0	5.8	-43.0	342.0			280-164 Ma (K/Ar)	Permian	7, 8
Sunnhordland Dykes	(59.8°N, 5.5°E)	047.8	+48.9	5.0	-46.0	297.0				Triassic	7
Sunnhordland Dyke-UH	(59.8°N, 5.5°E)	040.0	+48.0	2.5	-49.2	306.3			280 ± 5 Ma (K/Ar)	Triassic	9, 8
Sunnhordland Dyke-SA	(59.8°N, 5.5°E)	041.0	+50.0	1.9	-50.2	303.8			223 ± 6 Ma (K/Ar)	Triassic	9, 8

Ref, References: 1, Sturt & Torsvik (1987); 2, Råheim (1974)-recalculated age from the Tustna dyke; 3, this study (Table 1); 4, Torsvik *et al.* (1992); 5, Eide *et al.* (1997); 6, Lovlie & Mitchell (1982); 7, Lovlie (1981); 8, Frereth *et al.* 1976-recalculated ages; 9, Walderhaug (1993).

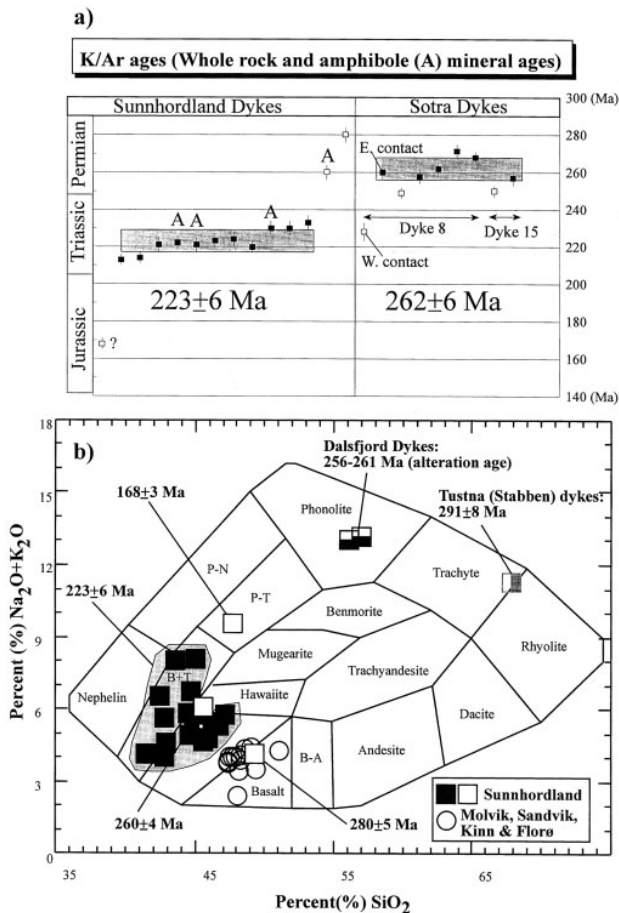


**Fig. 8.** (a) Recalculated K/Ar ages from 14 Sunnhordland dykes, Western Norway (after Færseth *et al.* 1976). Also included are K/Ar data from dykes (two profiles) from Sotra (Løvlie & Mitchell 1982). Concordant ages (with errors) are shaded. (b) Alkali-silica discrimination plot for the sub-alkaline Sunnfjord dykes (Molvær, Sandvik, Kinn & Florø; data from Skjerlie & Tysseland 1981), Sunnhordland dykes (mainly alkaline signature; data from Færseth *et al.* 1976). Also included for comparison, data from the Dalsfjord (Furnes *et al.* 1982) and Tustna dykes (Råheim 1974). B - A, basaltic andesite; B + T, basanite/tephrite; P - T, phonolitic tephrite; P - N, phonolitic nephelinite

palaeomagnetic pole probably represents a Jurassic remagnetization. In this respect it is important to note that faulted and fractured Jurassic sediments have recently been discovered in a fjord close to these dykes (Fossen 1997).

In the Sunnhordland region (Fig. 1b), Færseth *et al.* (1976) obtained 11 concordant K/Ar whole-rock and amphibole ages from alkaline-basaltic dykes that yielded a mean age of  $223 \pm 6$  Ma (recalculated ages, this study; Fig. 8a). With the addition of a few 'outlying' ages ( $280 \pm 5$ ,  $260 \pm 4$  and  $168 \pm 3$  Ma), they argued for three intrusive events, i.e. Permian, Mid-Triassic and Jurassic. In our opinion, the composite  $223 \pm 6$  Ma isotopic age fits with the bulk palaeomagnetic poles from these dykes (Løvlie 1981, Walderhaug 1993) since they plot near the 216–232 Ma mean pole for Europe (Van der Voo 1993; Fig. 7b). From some dykes, Løvlie (1981), found a poorly defined Permian direction (see pole in Fig. 7b) and this may validate the 260–280 Ma K/Ar ages.

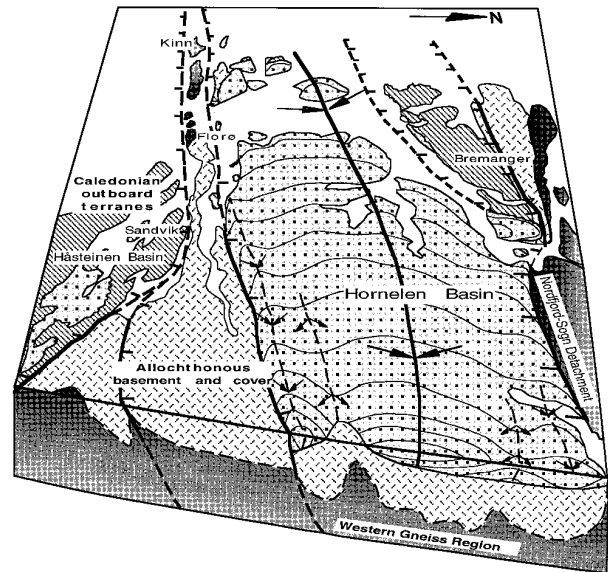


**Fig. 9.** Block diagram of the Hornelen Basin and substrate. The NNE-SSW section demonstrates age relationships between the basin-margin faults, Devonian basin fill, detachments and the regional east-west-trending folds in western Norway. Notice that the Nordfjord-Sogn Detachment capping the Western Gneiss Region is more intensely folded than the Hornelen Detachment. The low-angle and gently folded Hornelen Detachment truncates already folded Devonian sediments. The south-margin fault of the basin truncates all the other main structural elements in the area.

Færseth *et al.* (1976) noted that the  $280 \pm 5$  Ma dyke differs in bulk- and rare earth element geochemistry from other Sunnhordland dykes; its sub-alkalic signature is comparable with the Sunnfjord dykes (Fig. 8b) and probably also to the Permian Sotra dykes. This argues for a Permian origin for some Sunnhordland dykes, although the 260 Ma Sunnhordland dyke does not follow the same chemical trend. The 168 Ma dyke age is troublesome since palaeomagnetic data from this dyke are similar to the 223 Ma dykes (Løvlie 1981; Walderhaug 1993) and new isotopic age data are clearly necessary to clarify the incongruities. On balance, available palaeomagnetic, isotopic and geochemical data from the entire group of dykes in Western Norway indicate probably two (mid-late Permian and mid-Triassic) intrusive events with subtle different magmatic signatures.

## Conclusions

Palaeomagnetic data from the Sunnfjord dykes in coastal western Norway suggest a mid-late Permian (250–270 Ma) age and not Early Devonian or older age as argued by earlier workers. The primary remanent signature is carried by deuterically oxidized titanomagnetite (class II); the documented strong Late Mesozoic-Cenozoic overprinting and metamorphic alteration up to lower greenschist facies relate to proximity to major E-W shear zones and faults south of the Hornelen Devonian Basin. This leads to the conclusion that some of the motion and related hydrothermal fluid flow along the faults post-date dyke intrusion. The Sunnfjord dykes are thus not simple records of E-W extension and magma intrusion, but rather represent significant time markers within a complex zone of fault activation and rejuvenation. Mapping

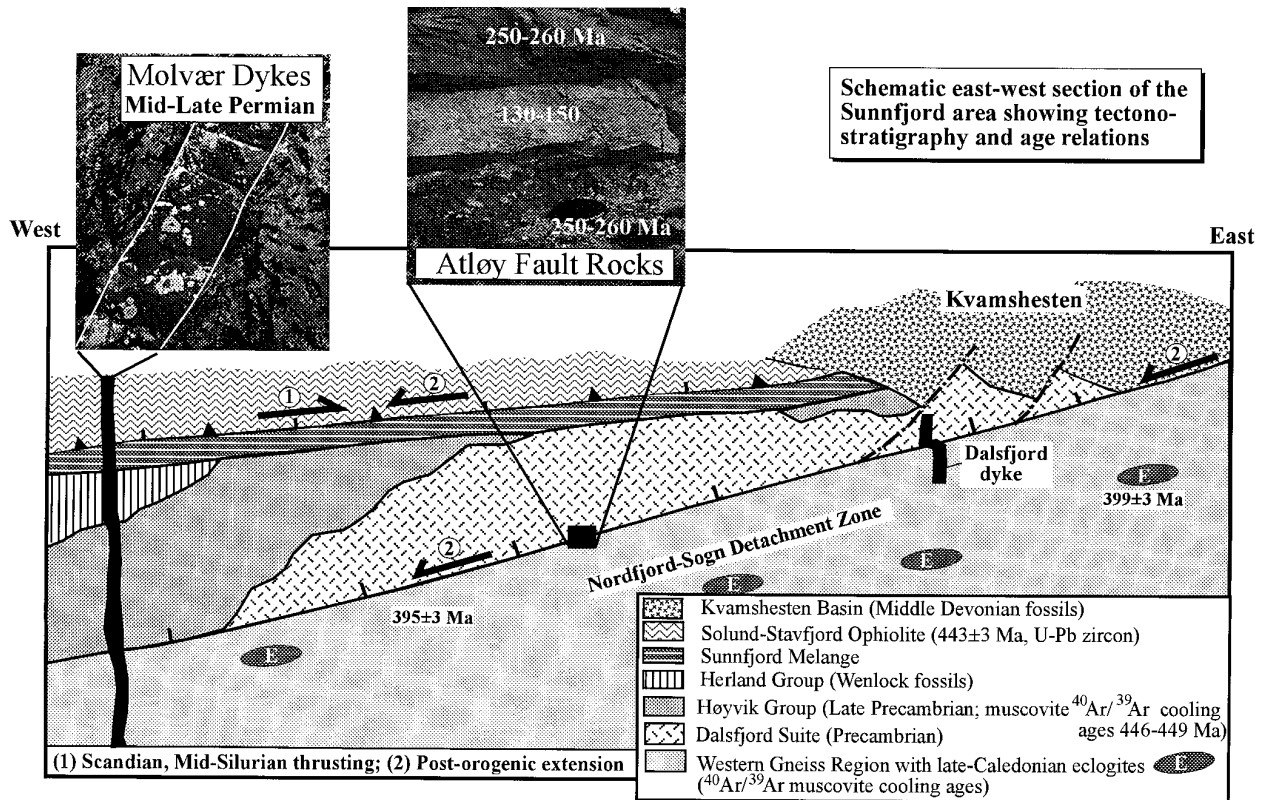


**Fig. 10.** Schematic (not to scale) east-west section of the Kvamshesten Devonian Basin and substrate. The profile illustrates the tectono-stratigraphy and the approximate position of the Molvær and Dalsfjord dykes. Notice that syn-depositional Devonian faults are truncated by the reactivated Nordfjord-Sogn Detachment, and that the Dalsfjord dyke is deformed by the fault. The relationship between the Molvær dykes and the main detachment can only be inferred from the relationships at Kinn, Florø and Sandvik. <sup>40</sup>Ar/<sup>39</sup>Ar cooling ages of white micas are from Berry *et al.* (1993), Andersen *et al.* (1997) and Eide *et al.* (1997).

along the southern and eastern margin of the Hornelen Basin also shows that the south-margin fault of the basin truncates the east margin low-angle detachment, which in turn truncates the already folded youngest Devonian strata in the Hornelen Basin (Fig. 9). These observations of polyphase normal faulting reinforce previous analyses (Torsvik *et al.* 1988, 1992; Wilks & Cutbert 1994) and support the new palaeomagnetic data which demonstrate important reactivation of the Late to Post-Caledonian detachment and high-angle fault system in Western Norway. It is also noteworthy that the provenance for the Hornelen Devonian sediments is entirely from the Upper Plate lithologies (Nilsen 1968; Cuthbert 1991) and thus clearly demonstrates post-depositional rejuvenation of the main detachments and faults that presently bound the basins.

The importance of contractional and extensional rejuvenation of the Devonian on-shore structures in western Norway for the Late Palaeozoic and Mesozoic tectonic development of the offshore Horda Platform and the Viking Graben (Fig. 1a) is equivocal since correlation and integrated interpretation of the on- and off-shore structural features have hitherto been few and preliminary. Nonetheless, onshore tectonic models do serve as templates for understanding offshore structural geometries, and in our opinion the following sequence of Late Palaeozoic-Mesozoic events can be deduced from the onshore information.

(1) The Sunnfjord dykes are mid-late Permian in age and probably contemporaneous with the geochemically similar

Sotra dykes (262 ± 6 Ma) and the oldest phase of magmatism in the Sunnhordland area (260–280 Ma). Collectively they attest to major Permo-Triassic rifting and a change from sub-alkaline (Permian) to alkaline (Triassic) magmatism.

(2) The Hornelen Basin is bounded by a shallow westward dipping detachment in the east and to the north and south by steep brittle E-W faults which cut the detachment (Fig. 9). These are post-depositional structures, although they probably lie close to the syn-sedimentary Devonian bounding faults. The E-W faults clearly affect the Permian aged Sunnfjord dykes and therefore record a protracted rejuvenation history and magnetic resetting during the Mesozoic-Cenozoic. Indeed, these faults are still seismically active.

(3) The E-W brittle faults can clearly be traced offshore to the Øygarden Fault Zone (Fig. 1a), the most extensive N-S structural element in offshore Norway, and probably representative of the main basin margin during Permo-Triassic and Jurassic extension (Færseth *et al.* 1995). Detailed offshore aeromagnetic studies which are underway will delineate if these E-W faults cut, or terminate at, the Øygarden Fault Zone.

(4) In the Dalsfjord region (Atløyst, Fig. 1b) there is blatant onshore evidence for reactivation of the Nordfjord-Sogn Detachment (Fig. 10). Well-dated fault-rocks indicate that the Dalsfjord Fault, now flooring the Kvamshesten Devonian Basin, underwent periods of brittle low-angle (<15°) extensional reactivation during Permian and Upper Jurassic/Lower Cretaceous times (Torsvik *et al.* 1992; Eide *et al.* 1997).

Palaeomagnetic data from the oldest brittle fault rocks at Atløy (250–260 Ma) match the Sunnfjord dykes (Figs 7a & 8), and it thus appears that sub-alkaline magmatism and low-angle faulting were fairly contemporaneous, and in a predominantly E–W-oriented extensional stress field.

(5) South of the Solund Devonian Basin (Fig. 1), Færseth *et al.* (1995) argue that the Solund Fault (part of the Nordfjord-Sogn Detachment) continues offshore and represents a major structural barrier with opposing blocktilts. Although they find no direct evidence of post-Devonian faulting or reactivation, we observe that the Dalsfjord and probably also Solund Faults are ‘young’ tectonic features and the most important onshore faulting took place during the mid–late Permian times.

Financial support by the Geological Survey of Norway–Mobil Norway–Norwegian Research Council–Phillips–Statoil a.s. (T.H.T. & E.A.E.) and Norsk Agip–Norwegian Research Council (T.B.A.). ONOFF contribution no. 1.

## References

- ADE-HALL, J.M., PALMER, H.C. & HUBBARD, T.P. 1971. The magnetic and opaque petrological response of basalts to regional hydrothermal alteration. *Geophysical Journal of the Royal Astronomical Society*, **24**, 137–174.
- ANDERSEN, T.B. & JAMTVEIT, B. 1990. Uplift of deep crust during orogenic extensional collapse: A model based on field studies in the Sogn-Sunnfjord region, W. Norway. *Tectonics*, **9**, 1097–1111.
- , BERRY, H.N., LUX, D.R. & ANDRESEN, A. 1997. The tectonic significance of pre-Scandian  $^{40}\text{Ar}/^{39}\text{Ar}$  phengite cooling ages in the Caledonides of western Norway. *Journal Geological Society, London*, in press.
- , JAMTVEIT, B., DEWEY, J.F. & SWENSSON, E. 1991. Subduction and exduction of continental crust: major mechanisms during continent-continent collision and orogenic extensional collapse, a model based on the south Norwegian Caledonides. *Terra Nova*, **3**, 303–310.
- , OSMUNDSEN, P.T. & JOLIVET, L. 1994. Deep crustal fabrics and a model for the extensional collapse of the southwest Norwegian Caledonides. *Journal of Structural Geology*, **16**, 1191–1204.
- , SKJERLIE, K.P. & FURNES, H. 1990. The Sunnfjord Melange, evidence of Silurian ophiolite accretion in the West Norwegian Caledonides. *Journal of the Geological Society, London*, **147**, 59–68.
- BERRY, H.N., LUX, D.R., ANDRESEN, A. & ANDERSEN, T.B. 1993.  $^{40}\text{Ar}/^{39}\text{Ar}$  dating of rapidly uplifted high-pressure rocks during late-orogenic extension in southwest Norway. *Abstract volume, GSA-Annual meeting, Boston*.
- CHAUVET, A. & SERANNE, M. 1989. Microtectonic evidence of Devonian extensional westward shearing in Southwest Norway. In: GAYER, R.A. (ed.) *The Caledonide Geology of Scandinavia*. Graham & Trotman, London, 245–254.
- CHRISTIANSSON, P., ODINSEN, T., BERGE, A.M., FALEIDE, J.I. & GABRIELSEN, R.H. 1995. Crustal structure from deep seismic data in the northern north sea. *Terra Nova, abstracts supplement No. 1*, 7, 55.
- CUTHBERT, S. 1991. Evolution of the Hornelen Basin, west Norway: new constraints from petrological studies of metamorphic clasts. In: MORTON, A., TODD, S.P. & HAUGHTON, P.D.W. (eds) *Developments in Sedimentary Provenance Studies*. Geological Society, London, Special Publications, **57**, 343–360.
- DAY, R., FULLER, M. & SCHMIDT, V.A. 1977. Hysteresis properties of titanomagnetite: grain size and compositional dependence. *Physics of the Earth and Planetary Interiors*, **13**, 260–267.
- DEWEY, J.F., RYAN, P.D. & ANDERSEN, T.B. 1993. Orogenic uplift and collapse, crustal thickness, fabrics and metamorphic phase changes: the role of eclogites. In: PRICHARD, H.M., ALABASTER, T., HARRIS, N.B.W. & NEARY, C.R. (eds) *Magmatic Processes and Plate Tectonics*. Geological Society, London, Special Publications, **76**, 325–343.
- DOBZHINETSAYA, L.F., EIDE, E.A., LARSEN, R.B., STURT, B.A., TRØNNES, R.G., SMITH, D.C., TAYLOR, W.R. & POSUKHOVA, T.V. 1995. Microdiamond in high-grade metamorphic rocks of the Western Gneiss Region, Norway. *Geology*, **23**, 597–600.
- DUNLOP, D.J. 1986. Hysteresis properties and their dependence on particle size: A test of Pseudo-Single-Domain remanence models. *Journal of Geophysical Research*, **91**, 9569–9584.
- EIDE, E.A. & TORSVIK, T.H. 1996. Paleozoic Supercontinent assembly, Mantle flushing and genesis of the Kiaman Superchron. *Earth and Planetary Science Letters*, **144**, 389–402.
- , — & ANDERSEN, T.B. 1997.  $^{40}\text{Ar}/^{39}\text{Ar}$  geochronologic and paleomagnetic dating of fault breccias; characterization of Late Palaeozoic and early Cretaceous fault reactivation in Western Norway. *Terra Nova*, in press.
- FOSSEN, H. 1997. Advances in understanding the post Caledonian structural evolution of the Bergen area, West Norway. *Norsk Geologisk Tidsskrift*, in press.
- FURNES, H., MITCHELL, J.G., RYAN, P. & SKJERLIE, F.J. 1982. Petrography and geochemistry of peralkaline, ultrapotassic syenite dykes of Middle Permian age, Sunnfjord, West Norway. *Norsk Geologisk Tidsskrift*, **62**, 147–159.
- , SKJERLIE, K.P., PEDERSEN, R.B., ANDERSEN, T.B., STILLMAN, C.J., SUTHREN, R., TYSSELAND, M. & GARMANN, L.B. 1990. The Solund-Stavfjord Ophiolite Complex and associated rocks, west Norwegian Caledonides: Geology, geochemistry and tectonic environment. *Geological Magazine*, **28**, 209–224.
- FÆRSETH, R.B., MACINTYRE, R.M. & NATERSTAD, J. 1976. Mesozoic alkaline dykes in the Sunnhordland region, western Norway: ages, geochemistry and regional significance. *Lithos*, **9**, 331–345.
- , GABRIELSEN, R.H. & HURICH, C.A. 1995. Influence of basement in structuring of the North Sea basin, offshore southwest Norway. *Norsk Geologisk Tidsskrift*, **75**, 105–119.
- HALVORSEN, E. 1989. A palaeomagnetic pole position of Late Jurassic/Early Cretaceous dolerites from Hinlopenstretet, Svalbard, and its tectonic implications. *Earth and Planetary Science Letters*, **94**, 398–408.
- KILDAL, E.S. 1969. *Geological map of Norway, bedrock Måløy*, map-sheet 20, 1:250 000. Geological Survey Norway.
- KOLDERUP, N.H. 1928. *Fjellbygningen i kyststroket mellom Nordfjord og Sognefjord*. Bergens Museums Arbok Naturvitenskaplig. Rekke, **1**.
- LUTRO, O. 1991. *Preliminary bedrock map of Florø*. Geological Survey of Norway.
- LØVLIE, R. 1981. Palaeomagnetism of coast-parallel alkaline dykes from western Norway: ages of magmatism and evidence for crustal uplift and collapse. *Geophysical Journal of the Royal Astronomical Society*, **66**, 417–426.
- & MITCHELL, J.G. 1982. Complete remagnetization of some Permian dykes from western Norway induced during burial/uplift. *Physics of the Earth and Planetary Interiors*, **30**, 415–421.
- NILSEN, T. 1968. The relationship of sedimentation to tectonics in the Solund Devonian District of southwestern Norway. *Norges Geologiske Undersøkelse Bulletin*, **259**, 1–108.
- NORTON, M. 1986. Late Caledonian extension in western Norway: A response to extreme crustal thickening. *Tectonics*, **5**, 195–204.
- OSMUNDSEN, P.-T. 1996. *Late-orogenic structural geology and Devonian basin formation in Western Norway: A study from the hanging wall of the Nordfjord–Sogn Detachment in the Sunnfjord Region*. Dr. Scient thesis, University of Oslo, Norway.
- & ANDERSEN, T.B. 1994. Caledonian compressional and late-orogenic extensional deformation in the Staveneset area, Sunnfjord, Western Norway. *Journal of Structural Geology*, **16**, 1385–1401.
- REUSCH, H. 1881. Konglomerat-sandsteinsfelterne i Nordfjord, Søndfjord og Sogn. *Nyt. Magazin for Naturvidenskaberne*, **26**, 93–170.
- RÅHEIM, A. 1974. A Post Caledonian syenite porphyry dyke in the Western Gneiss Region, Tustna, Central Norway. *Norsk Geologisk Tidsskrift*, **54**, 139–147.
- SEGURET, M., SERANNE, M., CHAUVET, A. & BRUNEL, M. 1989. Collapse basins: A new type of extensional sedimentary basin from the Devonian of Norway. *Geology*, **17**, 127–130.
- SERANNE, M. & SEGURET, M. 1987. The Devonian basins of western Norway: tectonics and kinematics of an extending crust. In: COWARD, M.P., DEWEY, J.F. & HANCOCK, P.L. (eds) *Continental Extensional Tectonics*. Geological Society, London, Special Publications, **28**, 537–548.
- SKJERLIE, F.J. & TYSSELAND, M. 1981. Geochemistry and petrology of dolerite dykes of probably Late Caledonian age from the outer Sunnfjord region, West Norway. *Norges Geologiske Bulletin*, **363**, 25–43.
- STEEL, R.J. 1976. Devonian basins of western Norway – sedimentary response to tectonism and to varying tectonic context. *Tectonophysics*, **36**, 207–224.
- STURT, B.A. & TORSVIK, T.H. 1987. A Late Carboniferous palaeomagnetic pole recorded from a syenite sill, Stabben, Central Norway. *Physics Earth Planetary Interior*, **49**, 350–359.
- SWENSSON, E. & ANDERSEN, T.B. 1991. Contact relationships between the Askvoll group and basement gneisses of the Western Gneiss Region (WGR), Sunnfjord, W. Norway. *Norsk Geologisk Tidsskrift*, **71**, 15–27.
- TORSVIK, T.H., STURT, B.A., RAMSAY, D.M., BERING, D. & FLUGE, P.R. 1988. Palaeomagnetism, magnetic fabrics and the structural style of the Hornelen

DOLERITE DYKES IN WESTERN NORWAY

973

- Old Red Sandstone, Western Norway. *Journal of the Geological Society, London*, **145**, 413–430.
- , —, SWENSSON, E., ANDERSEN, T.B. & DEWEY, J.F. 1992. Palaeomagnetic dating of fault rocks: Evidence for Permian and Mesozoic movements and brittle deformation along the extensional Dalsfjord Fault, western Norway. *Geophysical Journal International*, **109**, 565–580.
- , SMETHURST, M.A., MEERT, J.G., VAN DER VOO, R., MCKERROW, W.S., BRASIER, M.D., STURT, B.A. & WALDERHAUG, H.J. 1996. Continental break-up and collision in the Neoproterozoic and Palaeozoic: A tale of Baltica and Laurentia. *Earth Science Review*, **40**, 229–258.
- VAN DER VOO, R. 1993. *Paleomagnetism of the Atlantic, Tethys and Iapetus Oceans*. Cambridge University Press, Cambridge.
- WALDERHAUG, H. 1993. Rock magnetic and magnetic fabric variations across three thin alkaline dykes from Sunnhordland, Western Norway: influence of initial mineralogy and secondary alterations. *Geophysical Journal International*, **115**, 97–108.
- WILKS, W.J. & CUTBERT, S.J. 1994. The evolution of the Hornelen Basin detachment system, western Norway: implications for the style of late orogenic extension in the southern Scandinavian Caledonides. *Tectonophysics*, **238**, 1–30.

Received 20 January 1997; revised typescript accepted 7 April 1997.  
Scientific editing by David Snyder